frontiers | Research Topics

# From classical breeding to modern biotechnological advancement in horticultural crops - trait improvement and stress resilience

**Edited by**
Mohammad Irfan, Pankaj Kumar, Mohammed Wasim Siddiqui, Radhakrishnan T. and Weibiao Liao

**Published in**
Frontiers in Plant Science

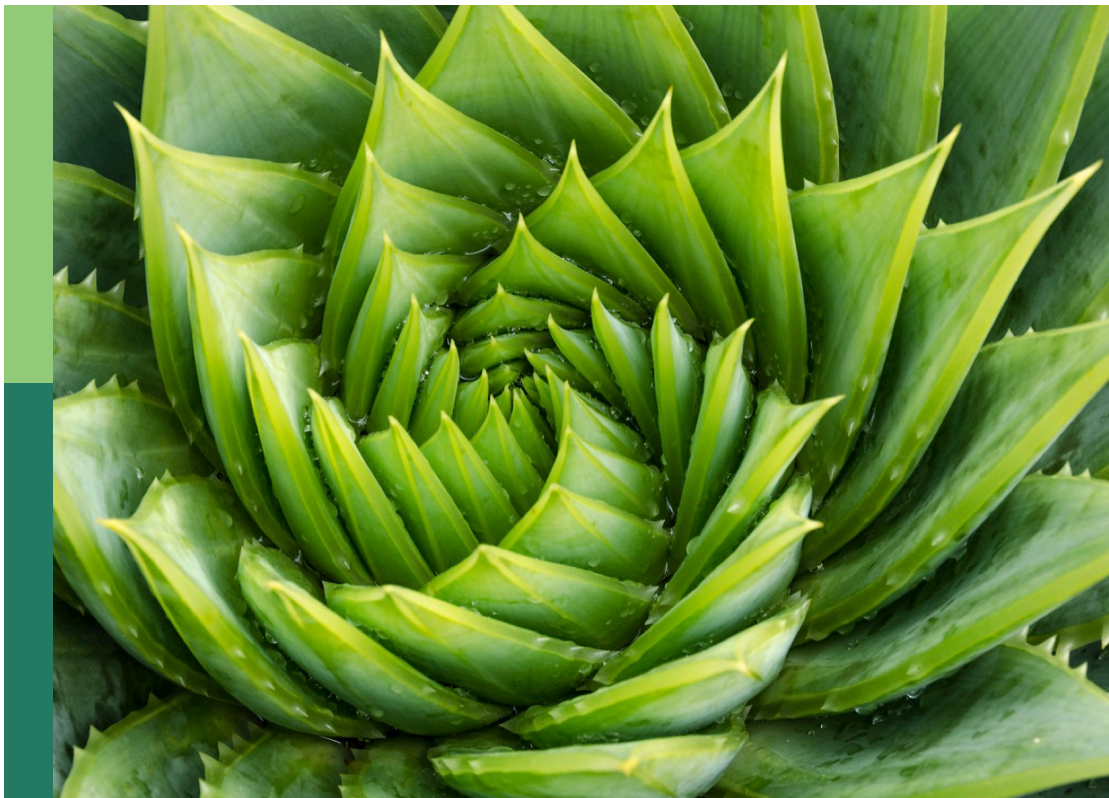

ISSN 1664-8714
ISBN 978-2-8325-3787-9
DOI 10.3389/978-2-8325-3787-9

## About Frontiers

Frontiers is more than just an open access publisher of scholarly articles: it is a pioneering approach to the world of academia, radically improving the way scholarly research is managed. The grand vision of Frontiers is a world where all people have an equal opportunity to seek, share and generate knowledge. Frontiers provides immediate and permanent online open access to all its publications, but this alone is not enough to realize our grand goals.

## Frontiers journal series

The Frontiers journal series is a multi-tier and interdisciplinary set of open-access, online journals, promising a paradigm shift from the current review, selection and dissemination processes in academic publishing. All Frontiers journals are driven by researchers for researchers; therefore, they constitute a service to the scholarly community. At the same time, the *Frontiers journal series* operates on a revolutionary invention, the tiered publishing system, initially addressing specific communities of scholars, and gradually climbing up to broader public understanding, thus serving the interests of the lay society, too.

## Dedication to quality

Each Frontiers article is a landmark of the highest quality, thanks to genuinely collaborative interactions between authors and review editors, who include some of the world's best academicians. Research must be certified by peers before entering a stream of knowledge that may eventually reach the public - and shape society; therefore, Frontiers only applies the most rigorous and unbiased reviews. Frontiers revolutionizes research publishing by freely delivering the most outstanding research, evaluated with no bias from both the academic and social point of view. By applying the most advanced information technologies, Frontiers is catapulting scholarly publishing into a new generation.

## What are Frontiers Research Topics?

Frontiers Research Topics are very popular trademarks of the *Frontiers journals series*: they are collections of at least ten articles, all centered on a particular subject. With their unique mix of varied contributions from Original Research to Review Articles, Frontiers Research Topics unify the most influential researchers, the latest key findings and historical advances in a hot research area.

Find out more on how to host your own Frontiers Research Topic or contribute to one as an author by contacting the Frontiers editorial office: frontiersin.org/about/contact

# From classical breeding to modern biotechnological advancement in horticultural crops - trait improvement and stress resilience

**Topic editors**

Mohammad Irfan — Cornell University, United States

Pankaj Kumar — Dr. Yashwant Singh Parmar University of Horticulture and Forestry, India

Mohammed Wasim Siddiqui — Bihar Agricultural University, India

Radhakrishnan T. — Directorate of Groundnut Research (ICAR-DGR), India

Weibiao Liao — Gansu Agricultural University, China

**Citation**

Irfan, M., Kumar, P., Siddiqui, M. W., Radhakrishnan, T., Liao, W., eds. (2023). *From classical breeding to modern biotechnological advancement in horticultural crops - trait improvement and stress resilience*. Lausanne: Frontiers Media SA. doi: 10.3389/978-2-8325-3787-9

# Table of contents

05 Editorial: From classical breeding to modern biotechnological advancement in horticultural crops - trait improvement and stress resilience
Pankaj Kumar, Mohammad Irfan, Mohammed Wasim Siddiqui, Radhakrishnan T and Weibiao Liao

08 Synergistic effect of graphene oxide and silver nanoparticles as biostimulant improves the postharvest life of cut flower bird of paradise (Strelitzia reginae L.)
Meenakshi Thakur, Anjali Chandel, Shweta Guleria, Vipasha Verma, Raghawendra Kumar, Gurpreet Singh, Anjali Rakwal, Diksha Sharma and Bhavya Bhargava

22 Sugar and acid profile of loquat (*Eriobotrya japonica* Lindl.), enzymes assay and expression profiling of their metabolism-related genes as influenced by exogenously applied boron
Muhammad Moaaz Ali, Raheel Anwar, Rana Naveed Ur Rehman, Shaghef Ejaz, Sajid Ali, Ahmed F. Yousef, Sezai Ercisli, Xiaobo Hu, Youming Hou and Faxing Chen

40 Identification and comprehensive analysis of MIPSs in Rosaceae and their expression under abiotic stresses in rose (*Rosa chinensis*)
Himanshi Gangwar, Priya Kumari, Vijay Gahlaut, Sanjay Kumar and Vandana Jaiswal

53 Use of stability statistics in the selection of *Clausena heptaphylla* (Roxb.) Wight & Arn for novel anethole rich strain (Jor Lab CH-2)
Mohan Lal, Sunita Munda, Anindita Gogoi, Twahira Begum, Joyashree Baruah, Sanjoy K. Chanda and Himangshu Lekhak

64 Global whole-genome comparison and analysis to classify subpopulations and identify resistance genes in weedy rice relevant for improving crops
Zhenyun Han, Fei Li, Weihua Qiao, Xiaoming Zheng, Yunlian Cheng, Lifang Zhang, Jingfen Huang, Yanyan Wang, Danjing Lou, Meng Xing, Weiya Fan, Yamin Nie, Wenlong Guo, Shizhuang Wang, Ziran Liu and Qingwen Yang

75 Advances in genomics for diversity studies and trait improvement in temperate fruit and nut crops under changing climatic scenarios
Ikra Manzoor, Kajal Samantara, Momin Showkat Bhat, Iqra Farooq, Khalid Mushtaq Bhat, Mohammad Amin Mir and Shabir Hussain Wani

93 Nitric oxide promotes adventitious root formation in cucumber under cadmium stress through improving antioxidant system, regulating glycolysis pathway and polyamine homeostasis
Lijuan Niu, Yunlai Tang, Bo Zhu, Zhenfu Huang, Dan Wang, Qiyang Chen and Jian Yu

107 Stability estimation through multivariate approach among solasodine-rich lines of *Solanum khasianum* (C.B. Clarke): an important industrial plant
Twahira Begum, Sunita Munda, Tanmita Gupta, Roktim Gogoi, Vikash Kumar Choubey, Sanjoy K. Chanda, Himangshu Lekhak, G. N. Sastry and Mohan Lal

125 ISSR molecular markers and anatomical structures can assist in rapid and directional screening of cold-tolerant seedling mutants of medicinal and ornamental plant in *Plumbago indica* L.
Yirui Li, Xu Cheng, Junlin Lai, Yunzhu Zhou, Ting Lei, Lijuan Yang, Jiani Li, Xiaofang Yu and Suping Gao

146 Comparative transcriptome analysis reveals the involvement of an MYB transcriptional activator, *SmMYB108*, in anther dehiscence in eggplant
Ruolin Hu, Jiali Wang, Huiqing Yang, Dayong Wei, Qinglin Tang, Yang Yang, Shibing Tian and Zhimin Wang

157 Volatile profiling as a potential biochemical marker for validation of gamma irradiation derived putative mutants in polyembryonic genotypes of mango (*Mangifera indica* L.)
Nusrat Perveen, M. R. Dinesh, M. Sankaran, K. S. Shivashankara, K. V. Ravishankar, R. Venugopal and Hidayatullah Mir

frontiers | Frontiers in Plant Science

TYPE Editorial
PUBLISHED 11 October 2023
DOI 10.3389/fpls.2023.1293682



OPEN ACCESS

EDITED AND REVIEWED BY
Anna Maria Mastrangelo,
Council for Agricultural and Economics Research (CREA), Italy

*CORRESPONDENCE
Mohammad Irfan
mi239@cornell.edu
Pankaj Kumar
pksharmabiotech@gmail.com

RECEIVED 13 September 2023
ACCEPTED 27 September 2023
PUBLISHED 11 October 2023

CITATION
Kumar P, Irfan M, Siddiqui MW, T R and Liao W (2023) Editorial: From classical breeding to modern biotechnological advancement in horticultural crops - trait improvement and stress resilience. *Front. Plant Sci.* 14:1293682. doi: 10.3389/fpls.2023.1293682



# Editorial: From classical breeding to modern biotechnological advancement in horticultural crops - trait improvement and stress resilience

Pankaj Kumar[1]*, Mohammad Irfan[2]*, Mohammed Wasim Siddiqui[3], Radhakrishnan T[4] and Weibiao Liao[5]

[1]Department of Biotechnology, Dr. Yashwant Singh Parmar University of Horticulture and Forestry, Nauni, Solan, India, [2]Plant Biology Section, School of Integrative Plant Science, Cornell University, Ithaca, NY, United States, [3]Department of Food Science and Postharvest Technology, Bihar Agricultural University, Bhagalpur, India, [4]Indian Council of Agricultural Research-Directorate of Groundnut Research (ICAR-DGR), Junagadh, India, [5]College of Horticulture, Gansu Agricultural University, Lanzhou, China

KEYWORDS

**fruit, vegetable, medicinal plant, horticulture, ornamental plant, antioxidants, stress resilience, biotechnology**

Editorial on the Research Topic
From classical breeding to modern biotechnological advancement in horticultural crops - trait improvement and stress resilience

Horticultural crops including fruits, vegetables, medicinal, aromatic, and ornamental plants, play a crucial role in enhancing human nutrition and our living environment. Fruits and vegetables are rich sources of essential nutrients, while ornamental plants contribute to aesthetic value. However, losses in quantity and quality during pre and post-harvest stages, as well as the impact of environmental stresses, limit their potential (Irfan et al., 2023). Therefore, developing strategies to improve crop quality and resilience is vital for sustainable production. Traditional breeding methods such as hybridization and mutation breeding have been employed for horticultural crop improvement, but they are time-consuming and labor-intensive, hindering their global adoption in sustainable agriculture. The emergence of molecular genetics has opened doors to modern biotechnological tools for enhancing horticultural crops. In recent decades, genetic engineering and molecular breeding technologies have been extensively used to create horticultural varieties with improved traits (Kumari et al., 2020).

The primary objective of this Research Topic was to offer the most up-to-date research in this field, achieved by gathering contributions from leading experts. This Research Topic comprises 11 papers, consisting of 10 research articles and one review article, collectively exploring various facets of the research theme. To better understand their distinct research trajectories, these articles have been meticulously summarized.

The evolution of horticultural crop improvement has undergone a remarkable transformation, transitioning from classical breeding methods to cutting-edge biotechnological advancements. This progression has paved the way for enhancing traits and stress resilience in these crops. One avenue of advancement lies in the application of biostimulants, which have proven effective in extending the post-harvest longevity of the magnificent bird of paradise cut flower. Thakur et al. investigated the use of graphene oxide (GO) and silver nanoparticles (SNPs) as biostimulants to enhance the post-harvest longevity of bird of paradise (*Strelitzia reginae* L.) cut flowers. The combination of GO and SNPs at a concentration of 1.0 μL $L^{-1}$ significantly extended the vase life of the flowers by six days compared to the control. This improvement was attributed to better water uptake, reduced microbial density, delayed stem blockage, decreased electrolyte leakage, and enhanced antioxidant enzyme activity. These findings suggest that biologically synthesized nanoparticles have potential as a novel post-harvest technology, which holds promise for widespread commercial implementation within the cut flower industry.

Modern biotechnology has also enabled a deeper exploration of the regulatory genes/transcription factors, employing advanced bioinformatics strategies to unravel their biological functions. Gangwar et al. conducted a study on myo-inositol-1-phosphate synthase (MIPS) genes in Rosaceae plants, revealing their importance in various plant processes like signal transduction, stress tolerance, and growth. They identified 51 MIPS genes in 26 Rosaceae species and found them to be conserved in structure and function. The study highlighted the involvement of the *RcMIPS* gene in plant development and its response to abiotic stresses like drought and heat, providing valuable insights for future functional studies in this plant family. Additionally, Ali et al. investigated the impact of boron application on sugar and acid profiles in loquat fruits. This research delves into the intricate physiological, biochemical, and molecular mechanisms that govern the biosynthesis of soluble sugars and malic acid in loquats, with potential applications for fruit quality improvement.

Another noteworthy accomplishment in this realm involves the identification of a naturally anethole-rich strain of *Clausena heptaphylla* through rigorous selection processes, subsequently confirmed *via* multi-location trials (Lal et al.). Twenty-three accessions of anethole were evaluated which ultimately resulted in identifying a superior strain (Jor Lab CH-2) with consistent performance across multiple locations. This strain exhibited an average herbage yield of 1.2 Kg/plant/cutting and an essential oil yield of 1.22%, with trans-anethole as the major constituent (93.25%). This offers a novel and cost-effective alternative for anethole production, expanding industry possibilities. Expanding the horizon, global whole-genome comparisons and analysis have been instrumental in categorizing sub-populations and pinpointing resistance genes within weedy rice, thereby contributing to crop enhancement endeavors. Among the notable findings is the presence of the *RPW8* domain in ORUFILM12g000772, holding potential for plant resistance to pathogens and its applicability in rice breeding programs (Han et al.).

Furthermore, the mechanism underlying nitric oxide-induced adventitious root development under cadmium stress has been thoroughly investigated, shedding light on strategies for stress resilience (Niu et al.). It was reported that nitric oxide (NO), supplied through a donor sodium nitroprusside (SNP), significantly increased the number and length of adventitious roots while also boosting endogenous NO levels. Additionally, NO-enhanced antioxidant defenses reduced oxidative damage, and upregulated the glycolysis and polyamine-related genes. However, the inhibitory effects of NO scavenger and inhibitor suggested a direct link between NO and adventitious root development under Cd stress (Niu et al.). Further studies have explored diverse germplasm lines (186 lines) of *Solanum khasianum* for stability in economically important traits such as solasodine content and fruit yield. These findings have a pivotal role in advancing breeding programs aimed at improving crop quality and yield (Begum et al.).

Li et al. employed inter simple sequence repeats (ISSR) molecular markers and anatomical analysis to screen cold-tolerant mutants of *Plumbago indica* L., a valuable ornamental and medicinal plant. Through tissue culture, chemical treatment, and low-temperature stress induction, a total of nine mutants were identified with altered DNA profiles. These mutants exhibited modified anatomical structures and increased plumbagin content, with four mutants showing enhanced cold resistance. The mutants also demonstrated traits consistent with cold-resistance plants and displayed delayed flowering and senescence. This innovative approach offers promising prospects for the development of cold-resistant varieties in this species. Moreover, Hu et al. have elucidated the role of an R2R3-MYB transcription factor gene (*SmMYB108*) as a transcriptional activator regulating anther development in eggplants. Differentially expressed gene *SmMYB108* in the fertile line F142 across various anther developmental stages has provided profound insights into the molecular mechanisms governing anther development.

The utilization of volatile profiling as a potential biochemical marker has shown promise in validating gamma irradiation-derived putative mutants in polyembryonic genotypes of mango, underscoring its significance in crop improvement strategies (Perveen et al.). It has been reported that volatile profiling *via* headspace-solid phase micro-extraction (HS SPME) method coupled with gas chromatography–mass spectrometry (GC-MS MS) analysis revealed significant differences in major volatile compounds between mutants, control seedlings, and mother plants. Simple sequence repeat (SSR) markers confirmed genetic diversity in the putative mutants, with clustering indicating distinct genetic profiles. This research highlighted the potential of volatile profiling and SSR markers for validating mutations and detecting genetic variation in polyembryonic mango genotypes, particularly when nucellar seedlings closely resemble mother plants (Perveen et al.).

Lastly, the review article by Manzoor et al. emphasizes the limitations of conventional breeding methods for temperate fruit and nut crops, citing factors like long juvenile periods and genetic complexities. They contended that integrating advanced biotechnological tools, such as molecular markers like single-nucleotide polymorphism (SNP), and Diversity Arrays Technology (DArT) markers, can enhance the precision and efficiency of plant selection based on genotypes. These markers enabled the direct targeting of genomic regions governing desired traits, like quality and resistance, saving time and space. Overall, the review highlighted the potential of molecular marker approaches to improve adaptability and stress resistance in temperate fruit and nut species through genome sequencing and cultivar selection.

In summary, the papers published on the aforementioned Research Topic showcase the latest breakthroughs in research. The transition from traditional breeding methods to cutting-edge biotechnological innovations in the realm of horticultural crops has resulted in a treasure trove of knowledge and inventive techniques. These endeavors are all geared towards enhancing characteristics and bolstering stress resistance in these valuable crops. These multifaceted approaches point the way forward for the improvement of horticultural crops, promising heightened sustainability and productivity.

## Author contributions

PK: Writing – original draft, Writing – review & editing. MI: Writing – original draft, Writing – review & editing. MS: Writing – review & editing. RT: Writing – review & editing. WL: Writing – review & editing.

## Acknowledgments

We thank all the contributors and reviewers for their contributions and valuable comments.

## Conflict of interest

The authors declare that the research was conducted in the absence of any commercial or financial relationships that could be construed as a potential conflict of interest.

The author(s) declared that they were an editorial board member of Frontiers, at the time of submission. This had no impact on the peer review process and the final decision

## Publisher's note



## References

Irfan, M., Kumar, P., Ahmad, M. F., and Siddiqui, M. W. (2023). Biotechnological interventions in reducing losses of tropical fruits and vegetables. *Curr. Opin. Biotechnol.* 79, 102850. doi: 10.1016/j.copbio.2022.102850

Kumari, C., Sharma, M., Kumar, V., Sharma, R., Kumar, V., Sharma, P., et al. (2022). Genome editing technology for genetic amelioration of fruits and vegetables for alleviating post-harvest loss. *Bioengineering* 9 (4), 176. doi: 10.3390/bioengineering9040176

frontiers | Frontiers in Plant Science

TYPE Original Research
PUBLISHED 29 September 2022
DOI 10.3389/fpls.2022.1006168



OPEN ACCESS

EDITED BY
Mohammed Wasim Siddiqui,
Bihar Agricultural University, India

REVIEWED BY
Mohamed Farag Mohamed Ibrahim,
Ain Shams University, Egypt
Vikas Kumar,
Punjab Agricultural University, India
Ghan Shyam Abrol,
Rani Lakshmi Bai Central Agricultural University, India

*CORRESPONDENCE
Bhavya Bhargava
bhavya@ihbt.res.in

SPECIALTY SECTION
This article was submitted to Plant Biotechnology, a section of the journal Frontiers in Plant Science

RECEIVED 29 July 2022
ACCEPTED 01 September 2022
PUBLISHED 29 September 2022

CITATION
Thakur M, Chandel A, Guleria S, Verma V, Kumar R, Singh G, Rakwal A, Sharma D and Bhargava B (2022) Synergistic effect of graphene oxide and silver nanoparticles as biostimulant improves the postharvest life of cut flower bird of paradise (Strelitzia reginae L.). *Front. Plant Sci.* 13:1006168. doi: 10.3389/fpls.2022.1006168



# Synergistic effect of graphene oxide and silver nanoparticles as biostimulant improves the postharvest life of cut flower bird of paradise (Strelitzia reginae L.)

Meenakshi Thakur[1], Anjali Chandel[1,2], Shweta Guleria[3], Vipasha Verma[1], Raghawendra Kumar[1], Gurpreet Singh[1], Anjali Rakwal[1], Diksha Sharma[1] and Bhavya Bhargava[1,2]*

[1]Floriculture Laboratory, Agrotechnology Division, Institute of Himalayan Bioresource Technology-Council of Scientific and Industrial Research, Palampur (HP), India, [2] Academy of Scientific and Innovative Research, Ghaziabad, Uttar Pradesh, India, [3]Biotechnology Division, Institute of Himalayan Bioresource Technology-Council of Scientific and Industrial Research, Palampur (HP), India

The bird of paradise (*Strelitzia reginae* L.) is one of the important tropical cut flowers. Generally, flowers like bird of paradise (BOP) grown for the commercial ornamental market must be of high pre and postharvest quality. Thus, to improve the postharvest longevity and increase marketability, the relative efficacy of two different biologically synthesized nanoparticles (NPs) was evaluated. The novel proprietary stimulants were graphene oxide (GO) and silver nanoparticles (SNPs). The NP treatments were applied as a vase (lower concentrations) solutions. Among all the applied treatments, the synergistic effect of GO + SNPs at 1 µL $L^{-1}$ vase solution significantly ($p$ =0.05) prolongs the post-harvest life of cut flowers of BOP. Increased vase life over the deionized water (DI) control was associated with better maintenance of relative water uptake, relative fresh weight, suppressed microbial density at stem-end and delay of stem blockage, reduced electrolyte leakage, malondialdehyde (MDA), SOD, and POD activity. In contrast to control, administration of NPs gave better results for all analyzed parameters. Application of biologically synthesized NPs in combination (GO + SNPs at 1 µL $L^{-1}$) extended the vase life of cut flowers by 6 days compared with control flowers, and overall, showed better results than the control. The findings of the studies revealed that the standardized NPs could have more potential in prolonging the postharvest life of cut flowers in BOP. Thus, this technique can be used as a novel postharvest technology for commercial application in cut flowers.

KEYWORDS

**antioxidant, cut flower, enzymes, nanoparticles, senescence, vase life**

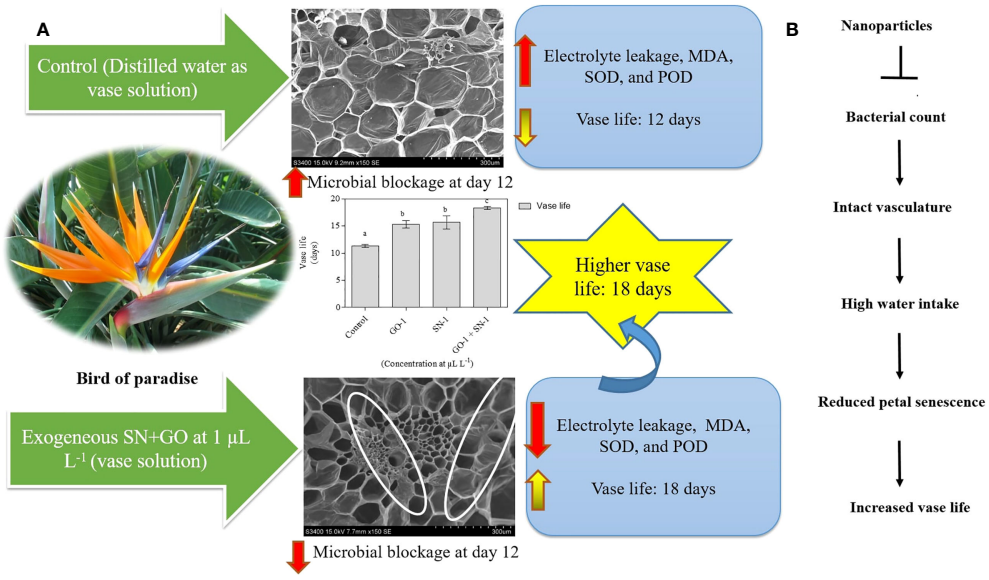


GRAPHICAL ABSTRACT
Exogenous application of NPs increased the postharvest life of bird of paradise.

## Introduction

The bird of paradise (*Strelitzia reginae* L.) of the Strelitziaceae family is an evergreen, monocotyledonous, perennial herbaceous flowering plant (Rai et al., 2021). It is commonly referred to as the crane flower, which plays a significant role in floral arrangements due to its exotic specialty, the combination of orange and purple colored flower clusters, and the unique shape of the crested head of a bird (Sane et al., 2020; Pereira et al., 2021). Conventionally, this plant is propagated through seeds and rhizomes and has a long gestation period of about 4–7 years (Navyashree et al., 2017; Sane et al., 2020). Its commercial cultivation occurs in North America, California, Israel, South Africa, Netherlands, Poland, China, and Japan (Pereira et al., 2021). Previous studies reported that the postharvest life of BOP ranged between 6–16 days (d) and 38.5 d (El-Saka et al., 1995). However, more commonly, the postharvest life varies from 6 to 16 d (El-Saka et al., 1995; Bayogan et al., 2008). Growing conditions, harvest stage, different holding conditions, and criteria used for evaluating inflorescence postharvest life, and conventional methods *viz.*, cold storage or low temperature, and preservative solutions, could all contribute to extending the vase life of horticulture crops (Kumari et al., 2022; Tayal et al., 2022).

In plants, the water content is absorbed by the xylem vessels of the stem ends, which helps maintain the petal turgor and flower freshness (He et al., 2018). Microbial blockage, on the other hand, reduces the water uptake, resulting in water loss even when the stem is dipped in water and eventually causing a water metabolism imbalance (Jaroenkit and Paull, 2003; He et al., 2018). Additionally, the depletion of carbohydrates also contributes to reducing the postharvest life of cut flowers (Carrillo-Lopez et al., 2016). The longevity of cut flowers can be greatly influenced by the inclusion of various chemicals in the vase solution, such as biocides and growth regulators, which prevent the proliferation of microbes and extend the vase life of cut flowers (Edrisi et al., 2015). Commercial flower preservatives, on the other hand, have yet to be proven to be consistent in the extension of the postharvest life of cut flowers (Jaroenkit and Paull, 2003). Many studies have recently reported that nanoparticles (NPs) can extend the vase life of cut flowers such as gladiolus, roses, BOP, and gerbera by inhibiting bacterial colonization (Hassan et al., 2014; Li et al., 2017; Naing et al., 2017; Azarhoosh et al., 2021).

NPs are new compounds that are widely used for their antimicrobial properties, thermal conductivity, chemical stability, and catalytic activity (Hassan et al., 2014; Yan and Chen, 2019; Sharma et al., 2022; Zafar et al., 2022). Silver nanoparticles (SNPs) have a high surface-to-volume ratio and have a specific ability to get oxidized, which strongly inhibits microbial growth (Basiri et al., 2011; Rafi and Ramezanian, 2013). Furthermore, these NPs interact with the phosphate (DNA), sulfur (proteins), and thiol groups (enzymes) of the biomolecules and interfere with the microbial metabolism, ultimately preventing microbial growth (Prabhu and Poulose, 2012; Yin et al., 2020). Another NP, graphene oxide (GO), is

known for excellent antimicrobial properties by inducing the degradation of inner and outer cell membranes of various microbes, which reduces their viability (Xu et al., 2017; He et al., 2018). GO as an effective antimicrobial agent is expected to improve plant growth and extend the life of cut flowers after harvest.

Therefore, the vase life can be extended by placing cut stems in a preservative solution and providing them with a suitable environment for delaying senescence (Langroudi et al., 2019). Because of its global popularity, SNPs and GO were used as novel antimicrobial agents for the longevity of BOP in the current study. The rationale for the study approach is water metabolism in BOP and protection of stem ends from bacterial blockage by using NPs. To date, there has been no report on the use of NPs to extend vase life in BOP. Therefore, the present study hypothesized that use of an optimal dose of SNPs, GO and its synergistic effect can effectively prevent microbial colonization and ensure the proper water uptake through the xylem vessel, which ultimately increases the vase life of cut flowers of BOP.

# Materials and methods

## Plant material

The cut spike of BOP was harvested in October 2021 from the eight-year-old plantation of BOP cultivated under the shade net house of the Floriculture Farm of the Agrotechnology Division, Council of Scientific and Industrial Research-Institute of Himalayan Bioresource Technology, Palampur, Himachal Pradesh, India. These cut spikes were harvested at the commercial stage when the spike had an unopened bract on the upper side and a prominent orange knuckle. Within 1 h, the stems were placed upright in a bucket partially filled with tap water and transported to the laboratory (Liu et al., 2021). Prior to the experiment, stems were uniformly sorted and recut to a length of 50 cm under distilled water to avoid air embolism (Liao et al., 2012).

## Experimental details

The experiment was carried out at a temperature of 20.7–25.2°C with a relative humidity of 46.7–61.9% and a photoperiod of 12 h at an intensity of 15 μM $m^{-2}s^{-1}$. Prior to the experiment, the glass vases were surface sterilized with ethanol. To determine the concentrations of NPs, trial screening on phenological studies of cut spikes of BOP was performed by using different concentrations of NPs *viz*., $T_1$: Control (distilled water), $T_2$: GO at 0.5 μL $L^{-1}$, $T_3$: GO at 1 μL $L^{-1}$, $T_4$: GO at 3 μL $L^{-1}$, $T_5$: SNP at 0.5 μL $L^{-1}$, $T_6$: SNP at 1 μL $L^{-1}$, $T_7$: SNP at 3 μL $L^{-1}$ and $T_8$: GO + SNPs at 1 μL $L^{-1}$. Based on preliminary observations, the following treatments, *viz*., $T_1$: Control (distilled water); $T_2$: GO at 1 μL $L^{-1}$; $T_3$: SNP at 1 μL $L^{-1}$ and $T_4$: GO + SNPs at 1 μL $L^{-1}$ (a synergistic effect of NPs) were selected and analyzed at 0, 6, 12, and 18 d. Nanoparticles *viz*., SNP and GO solutions were purchased from Sigma Aldrich as silver dispersion nanoparticles, with a 10 nm particle size (TEM), 0.02 mg $mL^{-1}$ in aqueous buffer (Code:1003234773) and graphene oxide, 2 mg $mL^{-1}$, dispersed in water (Code:1003039080). These solutions were freshly prepared before the execution of experiments by dissolving dimethyl sulfoxide (DMSO) with SNP and GO solution. Each cut spike was individually placed in a 500 mL vase solution. To prevent evaporation and microbial contamination of preservative solutions, the tops of the vases were covered with thermocol. The solutions were only prepared and placed in the various vases on the first day, and they were not renewed during the storage period. This experiment was executed in a completely randomized block design. In total, 18 spikes from each treatment in three replications (six spikes in each replication) were taken for the experimental study.

## Water uptake, relative fresh weight, and floret opening

Water uptake was measured at regular intervals (mL) by weighing the vases without flowers and individual flowers separately, then combining the results at the end of the vase life assessment (Li et al., 2012; Liao et al., 2013). After harvest, the initial fresh weight of cut flower stems was measured immediately before placing them in a vase solution. In all the treatments, fresh weight was recorded at 0, 6, 12, and 18 d and the relative fresh weight of each stem was calculated as the percentage on the basis of the initial fresh weight (Singh et al., 2008).

## Flower diameter and vase life

The diameter of each flower was measured at 0, 6, 12, and 18 d using a Vernier calliper. For each treatment, six cut flowers were selected for calculation, and their mean was taken as the final value. The vase life of each flower was determined by the time it took for one-third of its petals to show inward rolling, browning, discoloration, wilt, and loss of turgidity after being placed in various vase solutions (Liao et al., 2013; Lin et al., 2019).

## Microbial analysis

The bacterial isolation was carried out from a 12-d-old spike using the method described by Balestra et al. (2005) and Li et al. (2012), with some modifications. Specifically, the proximal end of the BOP spike was cut with sterile scalpel blades that had been

surface sterilized with 70% ethanol (Liu et al., 2021) and then cut up into small pieces. These pieces were placed in sterile tubes with 1 mL of sterile 0.9% normal saline solution (Li et al., 2012). Bacteria were dislodged by using a sterile motor pestle to crush the small pieces. The serial dilution was done with a sterile 0.9% normal saline solution, from which 0.1 mL of liquid extract was spread onto nutrient agar plates and incubated for 24 h at 37°C.

## Analysis of xylem blockage by scanning electron microscopy (SEM)

The existence of bacteria in the xylem vessel at the stem end of the cut flower was analyzed by using scanning electron microscopy (SEM) (JEOL, Japan). The samples of the cut spike from the end were collected and analyzed on day 12 of the vase period. Using fresh surgical blades, 1 cm-long stem-end segments were excised from the base of each spike. The samples were examined using SEM, which works on the principle of focusing a beam of electrons (0.2–20 KeV) from a tungsten filament on the specimen (Thakur and Kumar, 2021). On an aluminum stub, the samples were mounted with double-sided carbon tape. Samples were coated with a thin layer of gold using a sputter-coater at a vacuum of 10 Pa for 10 s to provide electrical conductivity. At a 30 kV accelerating filament voltage, the images were captured at the desired magnification (Thakur and Kumar, 2021).

## Electrolyte leakage

The electrolyte leakage was evaluated by following the procedure given by Danish and Zafar-ul-Hye (2019). Briefly, 12-day-old petals were collected and washed with deionized water and punched using a cork borer having a diameter of 1 cm, in triplicate. Petal pieces of uniform size were immersed in a test tube containing 10 mL of deionized water and incubated for 24 h at 25°C. A pre-calibrated electrical conductivity meter (PC 700, Eutech Instruments, Singapore) was used to determine the solution's initial electrical conductivity (EC1). The solution was heated in an autoclave at 120°C for 20 min, and conductivity (EC2) was measured again after cooling at room temperature, and electrolyte leakage (EL) was calculated by using the formula: EL = EC1/EC2 × 100 (Kaya et al., 2002).

## Enzymatic activity

The petals were collected on day 12 for enzymatic activity assays.

## Extraction of total soluble proteins and quantification

The tissue of 200 mg was ground in liquid nitrogen and dissolved in 5 mL of 50 mM potassium phosphate buffer at pH 7.8, followed by the addition of 2% polyvinylpolypyrrolidone. The homogenized solution was centrifuged at 8,000×*g* for 20 min and the supernatant was used for superoxide dismutase and peroxidase activity. Protein was quantified according to the protocol given by Bradford (Bradford, 1976). As a standard, bovine serum albumin was used.

## Superoxide dismutase and peroxidase assay

In a 96-well plate, an enzymatic assay for superoxide dismutase (SOD) activity was performed using the nitro blue tetrazolium (NBT) reduction assay as described by Sahoo et al. (2001) for day 12 old petals. In brief, to a final volume of 200 µL, 50 mM potassium phosphate buffer (pH 7.8), 20 µL of total protein, $5.7 \times 10^{-5}$ M NBT, $9.9 \times 10^{-3}$ M methionine, $1.17 \times 10^{-6}$ M riboflavin, and 0.025% Triton X-100 were added. For the assay control, total protein was replaced with an equal volume of 50 mM phosphate buffer (pH 7.8). At room temperature, the reaction mixture was illuminated with white light for 10 min. The absorbance was taken at 560 nm by using a microtiter plate reader (Synergy HT, BioTek, USA) (Chafik et al., 2019; Guleria et al., 2021). SOD activity was measured in units per mg of protein. One unit of the activity of an enzyme is the amount of enzyme required to suppress NBT reduction by 50% at room temperature in 10 min as per the following formula: Percent inhibition = $[(A_{560}$ control $- A_{560}$ sample$)/A_{560}$ control$] \times 100$ (Kumar et al., 2016).

The peroxidase activity was measured by quantifying the amount of purpurogallin formed in 12-d-old petals. The peroxidase activity was carried out using the protocol of Kar and Mishra (1976) with a minor modification. To the 10 µL of crude enzyme, 165 µL of potassium phosphate buffer (50 mM, pH 7.8), 20 µL of pyrogallol (0.5 M), and 5 µL of $H_2O_2$ (0.2 M) were added to a total volume of 200 µL. The amount of purpurogallin formed during the reaction was evaluated by recording absorbance at 420 nm for 5 min. Enzyme activity was measured in unit $g^{-1}$ of fresh weight and calculated using the following formula: ($\Delta A_{420}$/20 s test sample − $\Delta A_{420}$/20 s Blank) (volume of the assay) (dilution factor)/(12) (volume of enzyme used) (Kwak et al., 1995; Zhu et al., 2019).

## Lipid peroxidation assay

Lipid peroxidation was measured by quantifying malondialdehyde (MDA) content in 12 d-old petals. A petal sample of 200 mg was homogenized by using 2 mL of 50 mM Tris-Cl, pH 8.0 solution containing 0.5% (w/v) thiobarbituric acid, 20% (v/v) trichloroacetic acid, and 0.25 mL of 175 mM NaCl. The mixture was boiled for 5 min at 100°C, then cooled in an ice bath for 5 min (Dangol et al., 2021). The solution was

centrifuged at 14,000×*g* for 5 min at 4°C, and the absorbance of the resulting supernatant was measured at 450, 532, and 600 nm. MDA content (C) was calculated as μmol $g^{-1}$ of fresh weight using the formula: C = 6.45 ($A_{532}$ − $A_{600}$) − (0.56 $A_{450}$).

## Statistical analysis

The results of the experiment were analyzed using the analysis of variance (ANOVA) method. Within each treatment, there were six inflorescences. Here we have presented significant data for GO at 1 μL $L^{-1}$, SNPs at 1 μL $L^{-1}$, and a combination of GO + SNPs at 1 μL $L^{-1}$ at 6, 12, and 18 d. The Waller–Duncan multiple range test was used to compare means, and for statistical analysis, the SAS statistical package (SAS Institute Inc., Cary, NC) was used. The least significant difference test was used to compare means at the 0.05 probability level (Li et al., 2017). The data have been presented as means ± standard errors.

# Results

## Relative water uptake (mL)

Cut spikes treated with distilled water recorded efficient water uptake (37.0 mL) followed by SNP at 1 μL $L^{-1}$ (23.0 mL) and GO at 1 μL $L^{-1}$ (22.3 mL) along with GO + SNP at 1 μL $L^{-1}$ (18.7 mL). These cut spikes survived until day 6 without showing any signs of senescence (Figure 1A). Relative water uptake was reduced significantly on day 12 in all the treatments and reached up to 5.7 to 9.7 mL only. A significant reduction was observed in control and it exhibited petal senescence (Figure 1A), whereas significantly higher water uptake was recorded in cut spikes placed in GO + SNP at 1 μL $L^{-1}$ (9.7 mL). Flowers treated with combinations of NPs showed no senescence symptoms until 6 d. Relative water uptake decreased with the increase in the number of days, and was found to be significantly less in all the treatments at 18 d (3.0 to 6.2 mL). While comparing treatments, cut spikes placed under control showed significantly lower water uptake (3.3 mL) as they exhibited senescence on day 12. Relative water uptake was significantly higher in cut spikes placed along with the NPs, i.e., GO + SNP at 1 μL $L^{-1}$ (6.2 mL), which was not statistically different from treated SNP at 1 μL $L^{-1}$ (Figure 1A).

## Petal length and petal width (cm)

Petal length and petal width were significantly affected by different vase solutions and the number of days (Figures 1B, C). Petal length decreases with an increase in the number of days in all the treatments except for GO + SNP. On day 6, petal length ranged from 9.3 to 9.9 cm. However, no such statistical difference was observed within the treatments. Significantly higher petal length was recorded in the cut spikes placed along with two different NPs, i.e., GO + SN at 1 μL $L^{-1}$ (11.0 cm) compared with control (9.2 cm), while, the latter one was statistically at par with the individual solutions of GO (10.0 cm) and SN (9.9 cm) at 1 μL $L^{-1}$ concentration in 12 d. Petal length on day 18 was reduced significantly in all the vase solutions. However, it was observed significantly higher for cut spikes placed in GO + SNP at 1 μL $L^{-1}$ solution (10.8 cm) compared to the control. Petal length under control (8.9 cm) was not statistically different from the rest of the other treatments (Figure 1B).

Petal width decreased significantly with an increase in the number of days, and it was observed to be significantly higher on day 6. Among treatments, the significantly lowest petal width was recorded in cut spikes treated with the combined effect of GO + SNP at 1 μL $L^{-1}$ solution (2.4 cm) (Figure 1C). However, the rest of the treatments were statistically at par with each other and showed higher petal width on 6 d. A reduction in petal width was observed in control (1.4 cm) on day 12, while it was significantly higher in GO + SNP at 1 μL $L^{-1}$ solution (1.8 cm). The lowest petal width was observed on day 18 in all the treatments, and it was significantly lower in the absence of treated cut spikes (1.0 cm) as compared with the combination of GO + SNP at 1 μL $L^{-1}$ solution (1.5 cm). Control-treated cut spikes were statistically at par with GO (1.0 cm) and SNP at 1 μL $L^{-1}$ (1.1 cm) (Figure 1C).

## Floret opening, relative fresh weight (RFW), and vase life

Floret opening rate was significantly affected by different treatments, with an increase in the number of days (Figure 1D). At day 6 floret opening rate was observed significantly lowest in all the cut spikes and when we compared different treatments, it was recorded significantly higher in control (52.4%) followed by GO at 1 μL $L^{-1}$ (41.1%), SNP at 1 μL $L^{-1}$ (39.9%) and GO + SNP at 1 μL $L^{-1}$ (36.1%). Floret opening rate increased significantly on day 12 in all the treatments, which was recorded significantly higher in cut spikes placed in control (87.9%) and lowest with the combinations of NPs, *viz.*, GO + SNP at 1 μL $L^{-1}$ (57.4%). On day 18, the floret opening rate starts decreasing significantly in control (71.9%). However, a significant increment was observed in cut spikes treated with NPs alone and in combination with each other. Floret opening rate was recorded significantly higher till 18 d in GO + SNP at 1 μL $L^{-1}$ (88.7%) cut spikes which were not statistically different from GO at 1 μL $L^{-1}$ (82.5%) and SNP at 1 μL $L^{-1}$ (82.9%) treated cut spikes (Figure 1D).

Relative fresh weight (RFW) was significantly influenced by different treatments, with an increase in the number of days (Figure 1E). On day 6, RFW was observed to be significantly higher in cut spikes placed in control (137.2%) as compared to GO at 1 μL $L^{-1}$ (123.7%), SNP at 1 μL $L^{-1}$ (119.9%) and GO + SNP at 1 μL $L^{-1}$ solution (113.4%). RFW was reduced significantly with an increase in the number of days between

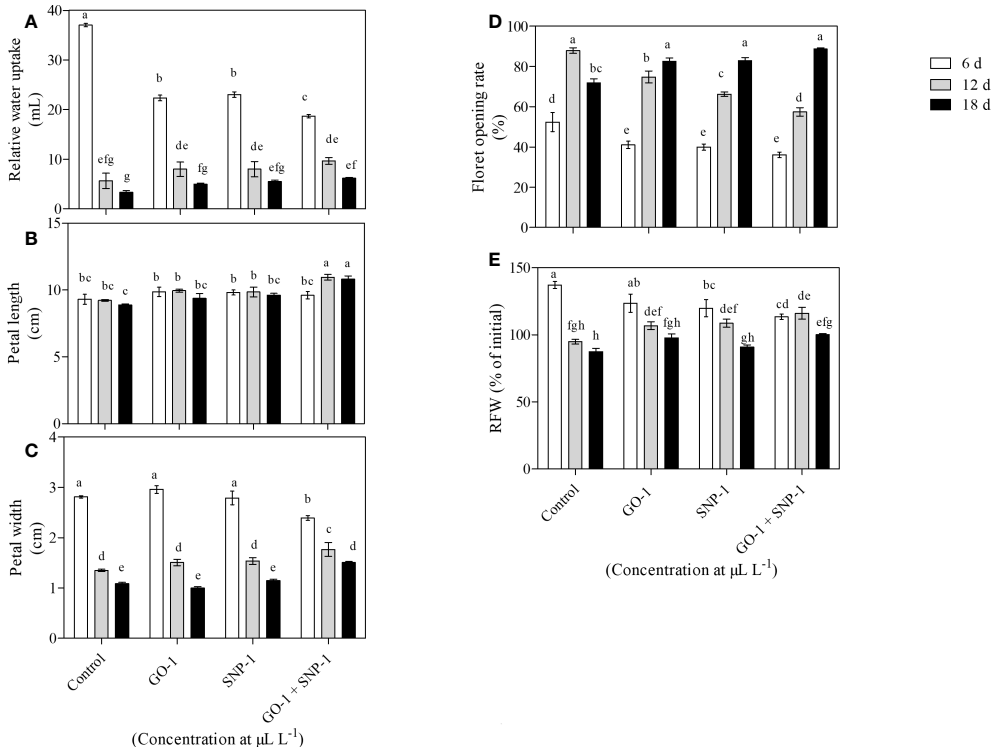


FIGURE 1
Effect of NPs, *viz*., control, GO, SNP and GO + SNP at 1 µL $L^{-1}$ on various morpho-physiological parameters such as **(A)** relative water uptake, **(B)** petal length, **(C)** petal width, **(D)** floret opening, and **(E)** RFW. Results are shown as mean ± SE of three replicates. Means with different letters are significantly different (Duncan's multiple range test, $p = 0.05$).

12 and 18 d. Flowers placed in control produced significantly lower RFW. However, the combination of GO + SNP at 1 µL $L^{-1}$ vase solution produced significantly higher RFW (116.1%) at 12 d. The cut spikes treated with GO (106.8%) and SNP at 1 µL $L^{-1}$ solutions (108.7%) were not statistically different from each other, but these treatments produced significantly higher RFW in comparison to control. On day 18, RFW reduced significantly in all the treated cut spikes, while it was observed to be significantly higher in spikes treated with GO + SNP at 1 µL $L^{-1}$ vase solution (100.2%) as compared to other treatments (Figure 1E).

The vase life of BOP significantly influenced by different treatments of NPs. Plants treated with the combination of GO + SNP at 1 µL $L^{-1}$ produced significantly longer vase life up to day 18 in comparison to control (Figure 2A). The cut spikes placed in an individual solution of GO and SNP at 1 µL $L^{-1}$ did not differ from each other for the duration of the vase period up to day 18 (Figures 2A, B). Cut spikes of BOP placed in different treatments were captured at 0, 6, 12, and 18 d (Figure 2B). This shows the variability of growth in cut spikes of BOP with an increase in the number of days. On day 6, all the cut spikes of BOP placed in different treatments showed a significant increase in the floret opening. On day 12, cut spikes placed under control exhibited different symptoms of senescence and showed more loss of visual quality than other treatments. Spikes placed in GO + SNP at 1 µL $L^{-1}$ solution produced a significantly higher floret opening rate till day 18, as presented in Figure 2B.

## SEM observation and microbial analysis

The relationship between microbes and the longevity of cut spike is shown by the density of bacteria present in the stem end segments. The SEM images in Figure 3 showed that on day 12, the stem ends of cut spikes were completely filled with a high density of bacteria under control conditions, which showed a reduction in the water-uptake channel. The cut spikes treated with GO at 1 µL $L^{-1}$ solution reduced the bacterial colonization, followed by SNP at 1 µL $L^{-1}$ and GO + SNP at 1 µL $L^{-1}$ solution. In comparison to all the treatments, lower bacterial density was recorded with the combined solution of GO + SNP at 1 µL $L^{-1}$ (Figure 3).

Microbes in the GO, SNP, and GO + SNP solutions were counted on the same day of SEM observation to further prove

the antimicrobial activity of NPs. In the current experiment, we analyzed bacterial density at day 12 when most of the petals were opened and few were in senescence due to the reduction of water uptake. The distilled water group (control) had a significantly higher number of bacteria, with $37 \times 10^{-5}$ colony forming units (cfu) per mL (about equal to bacteria per mL) (Figure 4). As for the cut spikes treated with GO at 1 μL $L^{-1}$ concentration, the bacterial density was recorded up to $14 \times 10^{-5}$ cfu $mL^{-1}$ (Figure 4). The spikes treated with SNP at 1 μL $L^{-1}$ solution produced a bacterial density of $7 \times 10^{-5}$ cfu $mL^{-1}$. The stem ends dipped under the combination of GO + SNP at 1 μL $L^{-1}$ had a lower bacterial density ($4 \times 10^{-5}$ cfu $mL^{-1}$) (Figure 4). Based on the phenotype, we have analyzed that only a single type of bacteria was found in the cut spike of BOP.

## Electrolyte leakage measurement

Changes in electrolyte leakage were observed in petals corresponding to changes in membrane permeability. The least ion leakage was observed in florets kept in a solution containing GO at 1 μL $L^{-1}$ and SNP at 1 μL $L^{-1}$ solution. This was significantly ($p$ = 0.05) lower than the control and other treatments (Figure 5A), confirming the integrity of the cellular membrane.

## Malondialdehyde content (MDA)

A significant ($p$ = 0.05) accumulation of MDA was observed in the untreated flower stalk (control), which accounts for more lipid peroxidation. However, treatment with GO at 1 μL $L^{-1}$ and SNP at 1 μL $L^{-1}$, both separately and in combination, significantly ($p$ = 0.05) reduced the accumulation of MDA when compared with untreated cut spikes (Figure 5B).

## Superoxide dismutase (SOD) and peroxidase assay (POD)

SOD activity decreases significantly ($p$ = 0.05) on day 12 for florets kept in SNP at 1 μL $L^{-1}$, solitary and in combination with GO at 1 μL $L^{-1}$, compared to the control. While there was no significant ($p$ = 0.05) difference in SOD activity in florets kept in GO at 1 μL $L^{-1}$ vase solution as compared to the control (Figure 5C). POD activity increases significantly ($p$ = 0.05) in day 12 florets kept in SNP at 1 μL $L^{-1}$ solution in comparison to the control. However, when florets were kept in GO at 1 μL $L^{-1}$ solution alone or in combination with SNP at 1 μL $L^{-1}$ solution, a significant ($p$ = 0.05) decrease was observed, while no significant ($p$ = 0.05) effect on POD activity was observed, respectively, as compared with cut spikes placed in distilled water (Figure 5D).

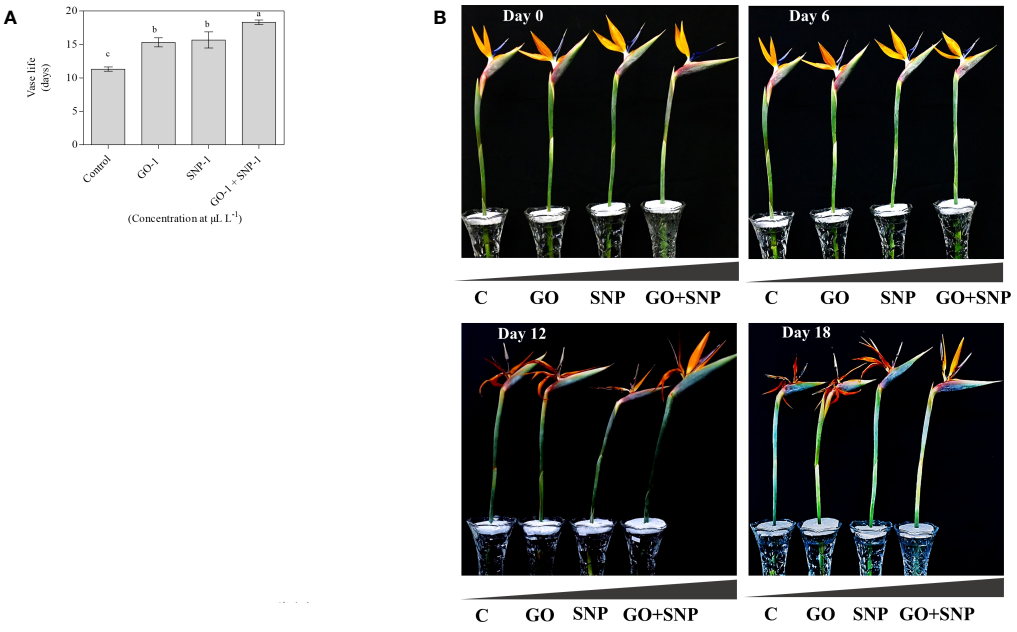


FIGURE 2
Effect of NPs (C, GO, SNP and GO + SNP at 1 μL $L^{-1}$ on **(A)** vase life and **(B)** vase performance on cut spikes of bird of paradise. Means with different letters are significantly different from each other (Duncan's multiple range test, p = 0.05).

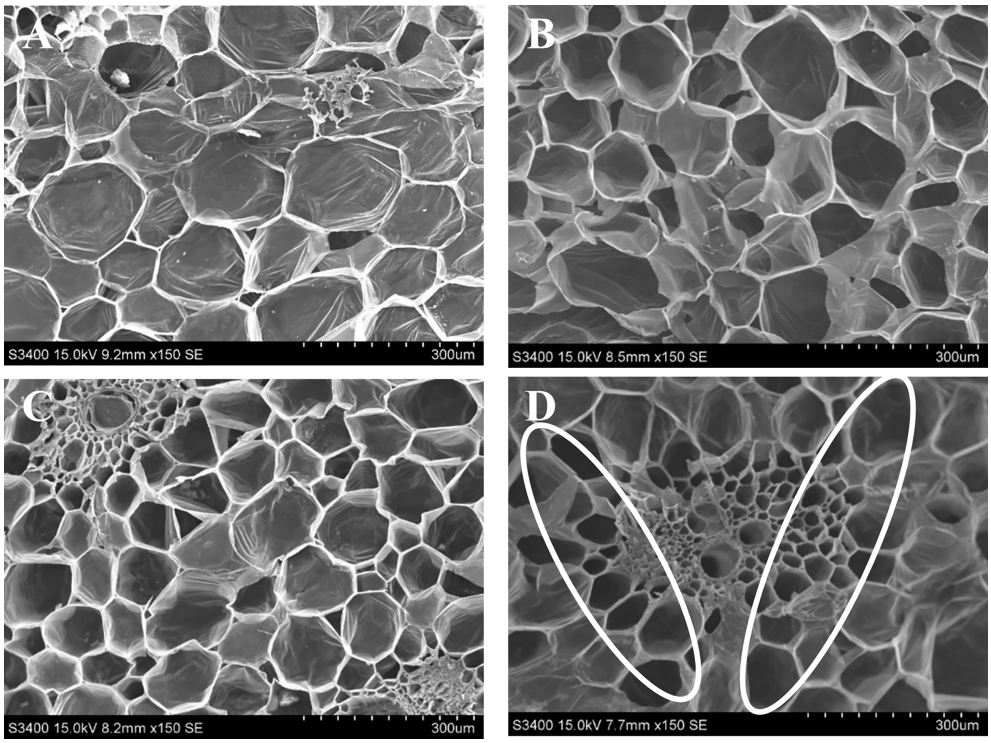


FIGURE 3
SEM characterization of stem ends of bird of paradise treated with **(A)** Control, **(B)** GO at 1 µL $L^{-1}$, **(C)** SNP at 1 µL $L^{-1}$, and **(D)** GO + SNP at 1 µL $L^{-1}$ at 12 **(D)** Scale bars: 300 µm.

## Discussion

Multi-colored BOP flowers are very showy, thus have a great global demand as cut flower. Cut spikes usually suffer water stress when they are detached from the mother plant (Halevy and Mayak, 1981), which results in irregular floret opening, quick loss of chlorophyll, proteolysis, and enhanced membrane permeability, and premature wilting premature wilting, which ultimately reduces the postharvest life of flowers. The senescence of cut spike cannot be eliminated. However, it can be regulated by various postharvest techniques (van Doorn, 2012; Rabiza-Swider et al., 2020). Therefore, microbial blockage at the stem end is considered to be the major key factor for reducing the vase life of cut flowers. In addition, proper water uptake, transport, and prevention of microbial blockage are effectively utilized for the development of buds to bloom and to boost the postharvest life of cut flowers (Solgi et al., 2009; Lu et al., 2010; Naing and Kim, 2020). The use of toxic chemicals results in environmental pollution, which will eventually affect human health. NPs at low concentration have been reported to be a safe biocide capable of extending the postharvest life of cut flowers (Zhao et al., 2018; Rabiza-Swider et al., 2020). As a result, the current study was carried out to assess the effect of NPs in increasing the postharvest life of cut spikes of the BOP. NPs are made up of small particles that appear to extend the postharvest life of cut flowers by inhibiting their antibacterial properties (Williamson et al., 2011; Liu et al., 2012).

Water uptake is a crucial factor in improving the vase life and quality of cut flowers (Reid and Evans, 1985; Naing et al., 2017) and depends on water storage, hydraulic conductivity, salinity, and water potential (Solgi et al., 2009; Naing and Kim, 2020). The proliferation of bacterial growth in the xylem vessels is the primary cause of water transport to cut flowers, so bacterial growth in the xylem vessels can obstruct water uptake in the vase (Park et al., 2017; Xia et al., 2017; Naing and Kim, 2020). The current applications of NPs have demonstrated stronger antimicrobial properties that extend the postharvest life of cut flowers, but these studies have not been widely popularized (Ahmed et al., 2016). SNPs and GO also interact with cytoplasmic and nucleic acid components, inhibiting respiratory chain enzymes and interfering with membrane permeability (Lok et al., 2007; He et al., 2018). In the current study, water uptake increased slowly but steadily up to day 18 when cut spikes were placed in combination with GO + SNP at 1 µL $L^{-1}$ solution (Figure 1A). The application of NP mostly inhibits gram-positive bacteria and bacterial DNA replication,

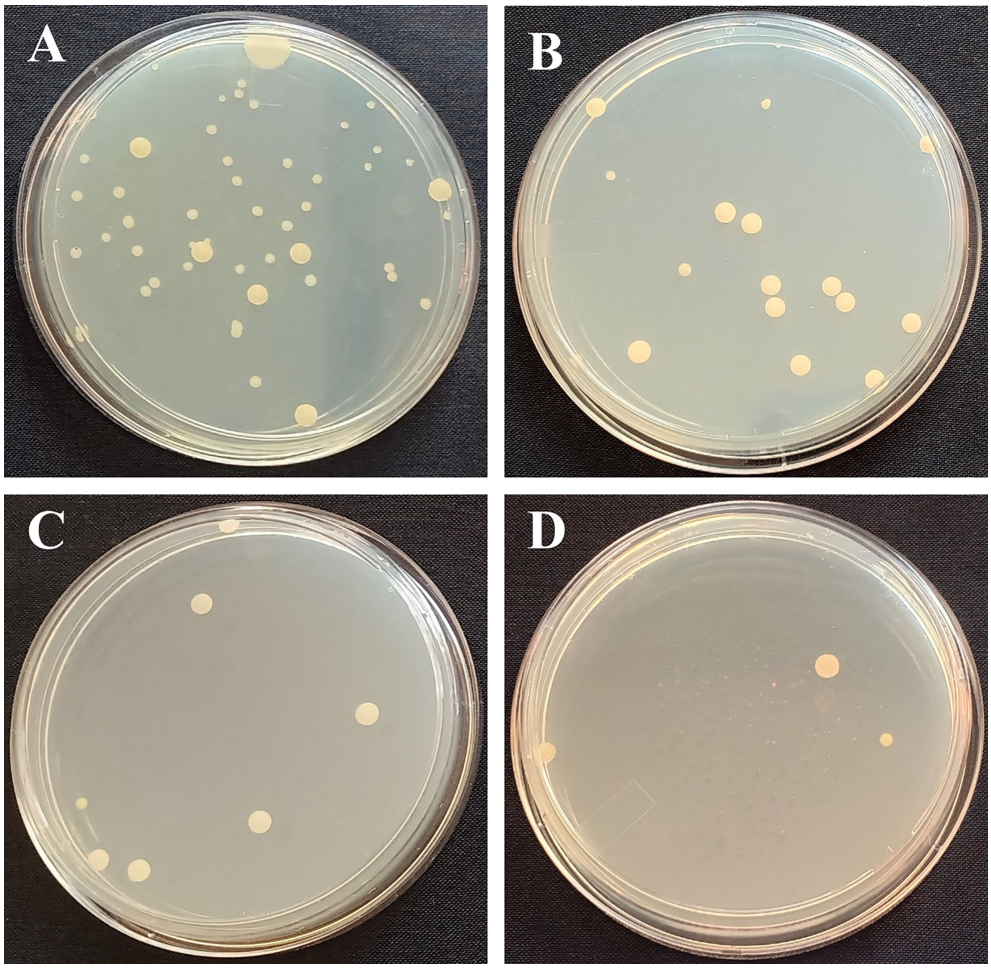


FIGURE 4
Photographs of petri dishes of **(A)** Control, **(B)** GO at 1 μL $L^{-1}$, **(C)** SNP 1 μL $L^{-1}$, and **(D)** GO + SNP 1 μL $L^{-1}$.

resulting in increased water absorption in cut flowers (Sondi and Salopek-Sondi, 2004). NPs alone showed significant variation for water uptake in comparison to control. However, the synergistic effect of GO + SNPs showed significant variations. The microbes were effectively killed by the concentration of GO, SNP, and GO + SNP at 1 μL $L^{-1}$ which resulted in clear xylem vessels for water uptake. Relative water uptake decreases with an increase in the number of days in control, which could be attributed to the blockage of water-conducting tissues, particularly xylem vessels, by the accumulation of microbes (bacteria) (van Doorn, 2012). Previous studies reported similar findings on the positive effect of NPs on cut flowers, including carnations, cut roses, lisianthus, tuberose, gladiolus, and lily (Hatami et al., 2013; Bahremand et al., 2014; Hajizadeh-Oghaz et al., 2016; Park et al., 2017; He et al., 2018; Lin et al., 2019; Maity et al., 2019; Naing and Kim, 2020). Besides these studies, no synergistic effect has been reported yet with the combined applications of two different NPs like GO and SNPs. In current studies, petal length and width significantly increased slowly but steadily after day 6 to day 12 when cut spikes were treated with the individual NPs. However, combined GO + SNPs at 1 μL $L^{-1}$ showed the highest petal length and width (Figures 1B, C). This could be due to the proper uptake of water (GO + SNPs), which is translocated to the petals, resulting in carbohydrate accumulation and increased petal length and width overall (Rabiza-Swider et al., 2020).

Exposure of cut spikes under control conditions inhibited the floret opening percentage after day 12 (Figure 1D), resulting in premature wilting of petals. However, the combination of GO and SNP promoted the flower opening (Figure 1D) and it maintained high RFW during the vase period, which ultimately increased the postharvest life of BOP cut flowers till 18 d. Moreover, the GO and SNPs alone had similar effects in enhancing the flower opening, while the synergistic effect of both these NPs was more pronounced. It might be because NP accumulated in stem-ends, and transported

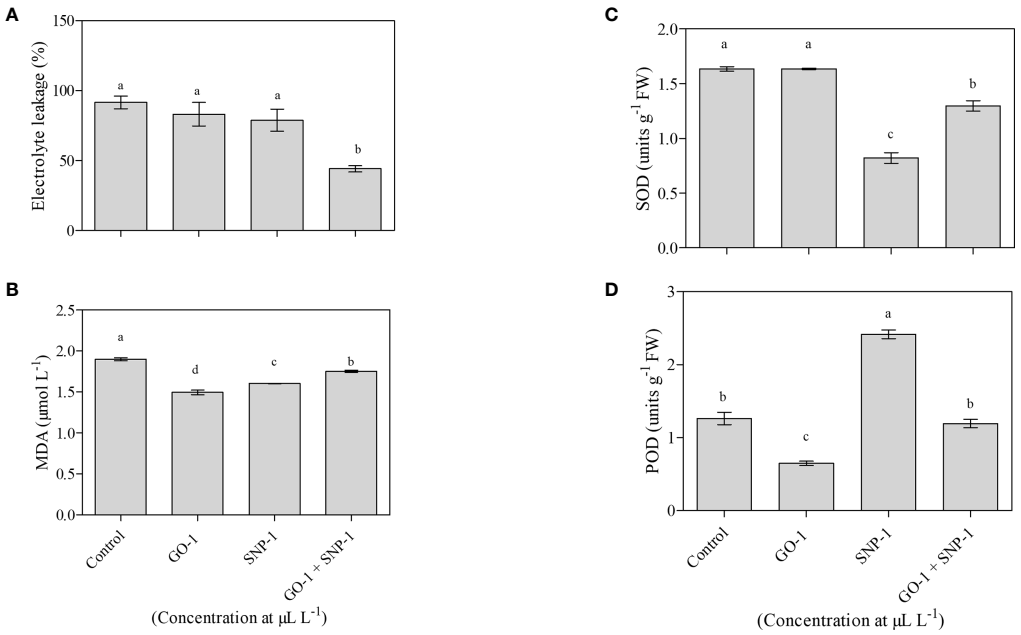


FIGURE 5
Effect of NPs **(A)** Control, **(B)** GO at 1 μL $L^{-1}$, **(C)** SNP 1 μL $L^{-1}$, and **(D)** GO + SNP 1 μL $L^{-1}$ on **(A)** Electrolyte leakage, **(B)** MDA, **(C)** SOD activity, and **(D)** POD activity in the petals of bird of paradise cut flowers. The samples were collected at day 12. Each data point indicates mean of three independent biological replicates. Error bars indicate SE of mean. Means with different letters are significantly different (Duncan's multiple range test, $p = 0.05$).

up to the receptacle, calyx, and petal tissues (Liu et al., 2018). These findings were synonymous with the findings of Lu et al. (2010) in cut rose flowers. Initially, there was a significant increase in RFW till day 6, after that it started decreasing in all the treatments during the vase life of BOP (Figure 1E). RFW and rate of senescence were reduced comparatively with an increase in the number of days in cut spikes treated under control conditions (Figure 1E). This might be because of lesser absorption of water uptake, increased respiration rate and ion leakage from petals lead to the damage cell membrane (Singh and Jegadheesan, 2003). Similar findings were reported in petunias, daylilys, roses, and gladiolus (Bieleski and Reid, 1992; Ezhilmathi et al., 2007; Seyf et al., 2012; Ha et al., 2019). Studies reported that NPs treatment in cut roses, gerberas, anthuriums, and carnations increased water uptake rate and RFW by limiting bacterial growth, transpiration rate, and stomatal conductance (Ansari et al., 2011; Rafi and Ramezanian, 2013; Liu et al., 2014; Abdel-Kader et al., 2017; Amin, 2017).

The relationship between flower senescence and protein degradation has been observed in several cut flowers, including carnation, sword lily, daylily, and dendrobium (Vierstra, 1996; Stephenson and Rubinstein, 1998; Sugawara et al., 2002; Azeez et al., 2007; Lerslerwong et al., 2009; Rabiza-Swider et al., 2020). Biofilms play a crucial role in creating a protective microhabitat against environmental stress (Ratnayake et al., 2012; Sharma et al., 2022). The accumulation of MDA is an indicator of the free radical induced peroxidation of the cell membrane, which impairs the function of the lipid membrane (Leverentz et al., 2002; Irfan et al., 2021; Sharma et al., 2021; Kapoor et al., 2022). In current findings, MDA decreases with NP treatments on day 12 (Figure 5B), which extends vase life over the control group. Antioxidant enzyme activity is thought to play an important role in cellular defense against oxidative stress (Sevillano et al., 2009; Hassan et al., 2014; Khan et al., 2021). Their activity increases in the presence of high levels of free radicals (Nair and Chung, 2015). Cut spikes treated with GO alone and in combination with GO + SNP at 1 μL $L^{-1}$ had lower levels of SOD and POD activities, which was most likely due to less oxidative stress experienced by cut flowers on day 12 (Figures 5C, D). The extended vase life with NPs is associated with the increment of the absorption of relative water uptake (Figure 1A), improved water balance, reduction in electrolyte leakage (Figure 5A), and integrity of the phospholipid membrane (Figure 5B), which inhibited the progress of senescence and resulted in the extension of vase life (Seyf et al., 2012). These results are accompanied by the effect of NPs as an antimicrobial agent, thus increasing the relative water uptake, petal length, width, and floret opening, which increases the RFW and extends the postharvest life of cut flowers of BOP as compared with control (Figure 2). The combined application of NPs as preservative vase solutions for cut flower longevity has not been studied yet, thus the current findings are reported for the first time with the synergistic effect of GO + SNP on post-harvest life of cut flowers. Our results confirm the efficacy of SNP in extending the vase-life of BOP cut

flowers. NPs are potent ethylene blockers, which may have an additive effect in extending the postharvest life of cut flowers such as cut lily, rose, and carnation (Kim et al., 2005; He et al., 2018; Liu et al., 2018; Lin et al., 2019).

Microbial growth at the stem end is the primary cause of xylem vessel blockage, which prevents water uptake and, as a result, reduces cut flower longevity (Balestra et al., 2005). Stem blockage initially occurs at the stem ends, up to 2 cm (van Doorn and Vaslier, 2002). The NP has antimicrobial properties which have been proved to conserve the postharvest life of cut flowers (Naing and Kim, 2020; Liu et al., 2021). As per SEM observations, cut spikes treated with NPs alone or in combination reduced the density of bacteria in the vase solution (Figure 3), which probably improved the water uptake, floret opening, and RFW, resulting in an increased postharvest life of BOP as compared with the cut spikes placed in distilled water. After exposure of treatments to cut spikes, NPs not only inhibit the microbial growth at stem-ends (Figure 4) but also enters the xylem to inhibit the bacterial proliferation, and are translocated to flower parts, *viz*., petals and gynoecium leading to a higher uptake of water, floret opening, and RFW which ultimately increase the longevity of cut flowers (Hassan et al., 2014; Naing et al., 2017). Similarly, the reduction of vase solution uptake was related to bacterial density in the stem-ends of cut roses (Li et al., 2012). Furthermore, several studies have reported that NPs have a bactericidal effect, which has an impact on the ability of the cut flower to absorb water (Rai et al., 2009; Lu et al., 2010). In the current studies, bacterial density was observed to be significantly higher in control as presented by SEM images (Figure 3), which probably caused microbial blockage at the stem end, resulting in water deficit and inhibiting the vase life of cut flowers (van Doorn and De Witte, 1997). Due to reduced bacterial populations in solutions of NPs, there was a significant increase in the vase life of lily, tuberose, chrysanthemum, and tulip (Nemati et al., 2013; Bahremand et al., 2014; Byczynska and Salachna, 2017). GO has effective antimicrobial properties as it can attach to the cell membranes and penetrate bacteria cells by disrupting the metabolic processes leading to reduce the microbial viability (Tu et al., 2013). However, no such studies have been reported in most of the cut flower crops with the GO and its effectiveness depends on the dosage since excessive concentration clogged vascular tissues and induced oxidative stress that accelerated flower senescence.

## Conclusion

NPs were evaluated as a novel antimicrobial agent for increasing the postharvest life of cut flowers after harvest. In the current study, cut spikes of BOP were treated with various concentrations of NPs and characterized by using various parameters, demonstrating that NPs could extend the vase life of BOP. Cut spikes treated with NPs effectively prevented microbial proliferation, increased the relative water uptake, and led to improve the water relation of cut spikes of the BOP. The synergistic effect of GO + SNP at 1 μL $L^{-1}$ was most effective in preventing the microbial density, increasing relative water uptake, floret opening, RFW, preserving proteins, decreasing MDA accumulation, and boosting the antioxidant enzyme activity. Therefore, the combined application of GO + SNPs can be recommended as the most appropriate vase solution to extend the postharvest life of cut flowers of BOP up to day 18 due to its excellent antimicrobial property, which has great potential in the agriculture sector. Although this is the first study we have reported of cut flowers of BOP, the developed technology could be routinely used to enhance the postharvest life of cut flowers in the commercial sector worldwide. Thus, more future studies are required with appropriate controlled conditions, different concentrations, and combinations with other chemicals and sugars to establish the superiority of NPs.

## Data availability statement

The original contributions presented in the study are included in the article/Supplementary Material. Further inquiries can be directed to the corresponding author.

## Author contributions

MT initiated experimental planning, execution, statistical analysis, data compilation, data curation, data presentation literature search and manuscript writing. AC helped to execute experiments, data observation, SEM observation. SG contributed to biochemical analysis and manuscript writing. VV edit the manuscript and data presentation. RK and DS helped in microbial analysis. AR and GS helped in SEM analysis, data recording and data compilation. BB supervised the research, funding acquisition, project administration, and manuscript editing. All authors contributed to the article and approved the submitted version.

## Funding

The project was funded by the Council of Scientific and Industrial Research (CSIR), Government of India, under CSIR-Floriculture Mission (Project Number: HCP-0037).

## Acknowledgments

The authors are grateful to the Director, CSIR-IHBT, Palampur, (HP), India for providing necessary facilities during study. We are very thankful to Dr. Amitabha Acharya and Mr. Akib Iqbal Dar for helping in the measurement of zeta potential of nanoparticles. Mr. Vikas and Mr. Balwant Raj are also

acknowledged for their technical support. This is CSIR-IHBT publication number 5146.

## Conflict of interest

The authors declare that the research was conducted in the absence of any commercial or financial relationships that could be construed as a potential conflict of interest.

## Publisher's note



## References

Abdel-Kader, H. H., Hamza, A. M., Elbaz, T. T., and Eissa, S. M. (2017). Effects of some chemicals on vase life of some cut flowers i. effect of 8-hydroxyquinoline sulfate, silver nitrate, silver nano particles and chitosan on vase life and quality of cut rose flowers (*Rosa hybrida.* cv. "Black magic"). *J. Plant Production.* 8 (1), 49–53. doi: 10.21608/JPP.2017.37812

Ahmed, S., Ahmad, M., Swami, B. L., and Ikram, S. (2016). Green synthesis of silver nanoparticles using *Azadirachta indica* aqueous leaf extract. *J. Radiat. Res. Appl. Sci.* 9 (1), 1–7. doi: 10.1016/j.jrras.2015.06.006

Amin, O. A. (2017). Influence of nanosilver and stevia extract on cut *Anthurium* inflorescences. *Middle East J. Appl. Sci.* 7 (2), 299–313. doi: 10.22271/chemi.2021.v9.i1ah.11594

Ansari, S., Hadavi, E., Salehi, M., and Moradi, P. (2011). Application of microorganisms compared with nanoparticles of silver, humic acid and gibberellic acid on vase life of cut gerbera good timming. *J. Ornamental Plants* 1 (1), 27–33.

Azarhoosh, J., Hashemabadi, D., Asadpour, L., and Kaviani, B. (2021). The effect of vase solutions containing cobalt, cerium, and silver nanoparticles on postharvest life and quality of cut birds of paradise (*Strelitzia reginae*). *J. Ornamental Plants.* 11 (4), 297–312. doi: 20.1001.1.22516433.2021.11.4.5.8.

Azeez, A., Sane, A. P., Bhatnagar, D., and Nath, P. (2007). Enhanced expression of serine proteases during floral senescence in gladiolus. *Phytochemistry* 68 (10), 1352–1357. doi: 10.1016/j.phytochem.2007.02.027

Bahremand, S., Razmjoo, J., and Farahmand, H. (2014). Effects of nano-silver and sucrose applications on cut flower longevity and quality of tuberose (*Polianthus tuberosa*). *Int. J. Hortic. Sci. Tech.* 1 (1), 67–77. doi: 10.22059/IJHST.2014.50519

Balestra, G. M., Agostini, R., Varvaro, L., Mencarelli, F., and Bellincontro, A. (2005). Bacterial populations related to gerbera ("*Gerbera jamesonii*" l.) stem break. *Phytopathologia Mediterranea.* 44, 1000–1009, 291–299. doi: 10.1400/14693.

Basiri, Y., Zarei, H., and Mashayekhi, K. (2011). Effects of nano-silver treatments on vase life of cut flowers of carnation (*Dianthus caryophyllus* cv. 'White liberty'). *J. Advanced Lab. Res. Biol.* 2 (2), 49–55. doi: 10.32404/rean.v6i2.2366

Bayogan, E. R. V., Jaroenkit, T., and Paull, R. E. (2008). Postharvest life of bird-of-Paradise inflorescences. *Postharvest Biol. Tech.* 48 (2), 259–263. doi: 10.1016/j.postharvbio.2007.10.010

Bieleski, R. L., and Reid, M. S. (1992). Physiological changes accompanying senescence in the ephemeral daylily flower. *Plant Physiol.* 98 (3), 1042–1049. doi: 10.1104/pp.98.3.1042

Bradford, M. M. (1976). A rapid and sensitive method for the quantitation of microgram quantities of protein utilizing the principle of protein-dye binding. *Analytical Biochem.* 72 (1-2), 248–254. doi: 10.1006/abio.1976.9999

Byczynska, A., and Salachna, P. (2017). Effects of colloidal silver on vase life of cut chrysanthemum. *World Sci. News.* 69, 239–243. doi: 10.52878/ipsci.2021.1.1.1

Carrillo-Lopez, L. M., Morgado-Gonzalez, A., and Morgado-González, A. (2016). Biosynthesized silver nanoparticles used in preservative solutions for chrysanthemum cv. puma. *J. Nanomaterials.* 1769250, 1–10. doi: 10.1155/2016/1769250

Chafik, A., Essamadi, A., Çelik, S. Y., and Mavi, A. (2019). Purification and biochemical characterization of a novel copper, zinc superoxide dismutase from liver of camel (*Camelus dromedarius*): An antioxidant enzyme with unique properties. *Bioorganic Chem.* 86, 428–436. doi: 10.1016/j.bioorg.2019.02.024

Dangol, S., Nguyen, N. K., Singh, R., Chen, Y., Wang, J., Lee, H. G., et al. (2021). Mitogen-activated protein kinase OsMEK2 and OsMPK1 signaling is required for ferroptotic cell death in rice–*Magnaporthe oryzae* interactions. *Front. Plant Sci.* 12, 1–22. doi: 10.3389/fpls.2021.710794

Danish, S., and Zafar-ul-Hye, M. (2019). Co-Application of ACC-deaminase producing PGPR and timber-waste biochar improves pigments formation, growth and yield of wheat under drought stress. *Sci. Rep.* 9 (1), 1–13. doi: 10.1038/s41598-019-42374-9

Edrisi, B., Sadrpoor, A., and Saffari, V. R. (2015). Effects of chemicals on vase life of cut carnation (*Dianthus caryophyllus* L.'Delphi') and microorganisms' population in solution. *J. Ornamental Plants.* 2 (1), 1–11.

El-Saka, M., Fahmy, B., Awad, A. E., and Dowh, A. K. (1995). Trials to improve the quality of Strelitzia reginae. Ait. flowers after cutting. In *Proceeding of the international symposium on postharvest physiology, pathology and technologies for horticultural commodities*, Institut Agronomique et Veterinaire Hassan 2, Agadir (Maroc). Complexe Horticole d'Agadir.- Agadir (Maroc): IAV Hassan 2, 1995. p. 480–488

Ezhilmathi, K., Singh, V. P., Arora, A., and Sairam, R. K. (2007). Effect of 5-sulfosalicylic acid on antioxidant activity in relation to vase life of gladiolus cut flowers. *Plant Growth Regulation.* 51 (2), 99–108. doi: 10.1007/s10725-006-9142-2

Guleria, S., Jain, R., Singh, D., and Kumar, S. (2021). A thermostable Fe/Mn SOD of geobacillus sp. PCH100 isolated from glacial soil of Indian trans-himalaya exhibits activity in the presence of common inhibitors. *Int. J. Biol. Macromolecules.* 179, 576–585.

Hajizadeh-Oghaz, M., Razavi, R. S., Barekat, M., Naderi, M., Malekzadeh, S., and Rezazadeh, M. (2016). Synthesis and characterization of Y2O3 nanoparticles by sol–gel process for transparent ceramics applications. *J. Sol-Gel Sci. Tech.* 78 (3), 682–691. doi: 10.1007/s10971-016-3986-3

Halevy, A. H., and Mayak, S. (1981). Senescence and postharvest physiology of cut flowers. part. 2. *Hortic. Rev.* 3, 59–143. doi: 10.1016/j.ijbiomac.2021.03.019

Ha, S. T., Lim, J. H., and In, B. C. (2019). Extension of the vase life of cut roses by both improving water relations and repressing ethylene responses. *Hortic. Sci. Technol.* 37(1), 65–77. doi: 10.12972/kjhst.20190007

Hassan, F. A. S., Ali, E. F., and El-Deeb, B. (2014). Improvement of postharvest quality of cut rose cv.'First red'by biologically synthesized silver nanoparticles. *Scientia Horticulturae.* 179, 340–348. doi: 10.1016/j.scienta.2014.09.053

Hatami, M., Hatamzadeh, A., Ghasemnezhad, M., and Ghorbanpour, M. (2013). The comparison of antimicrobial effects of silver nanoparticles (SNP) and silver nitrate (AgNO3) to extend the vase life of 'Red ribbon'cut rose flowers. *Trakia J. Sci.* 2, 144–151.

He, Y., Qian, L., Liu, X., Hu, R., Huang, M., Liu, Y., et al. (2018). Graphene oxide as an antimicrobial agent can extend the vase life of cut flowers. *Nano Res.* 11 (11), 6010–6022. doi: 10.1007/s12274-018-2115-8

Irfan, M., Kumar, P., Ahmad, I., and Datta, A. (2021). Unraveling the role of tomato bcl-2-associated athanogene (BAG) proteins during abiotic stress response and fruit ripening. *Sci. Rep.* 11 (1), 1–15. doi: 10.1038/s41598-021-01185-7

Jaroenkit, T., and Paull, R. E. (2003). Postharvest handling of heliconia, red ginger, and bird-of-paradise. *HortTechnology* 13, 2, 259–2, 266. doi: 10.21273/horttech.13.2.0259

Kapoor, B., Kumar, P., Gill, N. S., Sharma, R., Thakur, N., and Irfan, M. (2022). Molecular mechanisms underpinning the silicon-selenium (Si-Se) interactome and cross-talk in stress-induced plant responses. *Plant Soil.*, 1–24. doi: 10.1007/s11104-022-05482-6

Kar, M., and Mishra, D. (1976). Catalase, peroxidase, and polyphenoloxidase activities during rice leaf senescence. *Plant Physiol.* 57 (2), 315–319. doi: 10.1104/pp.57.2.315

Kaya, C., Higgs, D., Saltali, K., and Gezerel, O. (2002). Response of strawberry grown at high salinity and alkalinity to supplementary potassium. *J. Plant Nutr.* 25 (7), 1415–1427. doi: 10.1081/PLN-120005399

Khan, M. I. R., Jahan, B., AlAjmi, M. F., Rehman, M. T., Iqbal, N., Irfan, M., et al. (2021). Crosstalk of plant growth regulators protects photosynthetic performance from arsenic damage by modulating defense systems in rice. *Ecotoxicol. Environ. Safety*. 222, 112535. doi: 10.1016/j.ecoenv.2021.112535

Kim, J. H., Lee, A. K., and Suh, J. K. (2005). Effect of certain pre-treatment substances on vase life and physiological characters in Lilium spp. *Acta Horticulturae*. 673, 307–314. doi: 10.17660/ActaHortic.2005.673.39

Kumari, C., Sharma, M., Kumar, V., Sharma, R., Kumar, V., Sharma, P., et al. (2022). Genome editing technology for genetic amelioration of fruits and vegetables for alleviating post-harvest loss. *Bioengineering* 9 (4), 176. doi: 10.3390/bioengineering9040176

Kumar, A., Sharma, M., Bhardwaj, P. K., Vats, S. K., Singh, D., and Kumar, S. (2016). Copper, zinc superoxide dismutase from caragana jubata: A thermostable enzyme that functions under a broad pH and temperature window. *Process Biochem.* 51 (10), 1434–1444. doi: 10.1016/j.procbio.2016.06.025

Kwak, S. S., Kim, S. K., Lee, M. S., Jung, K. H., Park, I. H., and Liu, J. R. (1995). Acidic peroxidases from suspension-cultures of sweet potato. *Phytochemistry* 39 (5), 981–984. doi: 10.1016/0031-9422(95)00098-R

Langroudi, M. E., Hashemabadi, D., Kalatejari, S., and Asadpour, L. (2019). Effect of silver nanoparticles, spermine, salicylic acid and essential oils on vase life of alstroemeria. *Rev. Agricultura Neotropical*. 6 (2), 100–108. doi: 10.32404/rean.v6i2.2366

Lerslerwong, L., Ketsa, S., and van Doorn, W. G. (2009). Protein degradation and peptidase activity during petal senescence in dendrobium cv. khao sanan. *Postharvest Biol. Tech.* 52 (1), 84–90. doi: 10.1016/j.postharvbio.2008.09.009

Leverentz, M. K., Wagstaff, C., Rogers, H. J., Stead, A. D., Chanasut, U., Silkowski, H., et al. (2002). Characterization of a novel lipoxygenase-independent senescence mechanism in alstroemeria peruviana floral tissue. *Plant Physiol.* 130 (1), 273–283. doi: 10.1104/pp.000919

Liao, W. B., Zhang, M. L., Huang, G. B., and Yu, J. H. (2012). Hydrogen peroxide in the vase solution increases vase life and keeping quality of cut oriental× trumpet hybrid lily 'Manissa'. *Scientia Horticulturae*. 139, 32–38. doi: 10.1016/j.scienta.2012.02.040

Liao, W. B., Zhang, M. L., and Yu, J. H. (2013). Role of nitric oxide in delaying senescence of cut rose flowers and its interaction with ethylene. *Scientia Horticulturae*. 155, 30–38. doi: 10.1016/j.scienta.2013.03.005

Li, H., Huang, X., Li, J., Liu, J., Joyce, D., and He, S. (2012). Efficacy of nano-silver in alleviating bacteria-related blockage in cut rose cv. movie star stems. *Postharvest Biol. Tech.* 74, 36–41. doi: 10.1016/j.postharvbio.2012.06.013

Li, H., Li, H., Liu, J., Luo, Z., Joyce, D., and He, S. (2017). Nano-silver treatments reduced bacterial colonization and biofilm formation at the stem-ends of cut gladiolus '*Eerde*' spikes. *Postharvest Biol. Tech*. 123, 102–111. doi: 10.1016/j.postharvbio.2016.08.01

Lin, X., Li, H., Lin, S., Xu, M., Liu, J., Li, Y., et al. (2019). Improving the postharvest performance of cut spray 'Prince' carnations by vase treatments with nano-silver and sucrose. *J. Hortic. Sci. Biotechnol.* 94 (4), 513–521. doi: 10.1080/14620316.2019.1572461

Liu, J., Lai, L., Liu, H., Li, H., Yu, G., Sun, Y., et al. (2021). Nano-silver treatment reduces bacterial proliferation and stem bending in cut gerbera flowers: An *in vitro* and *in vivo* evaluation. *Postharvest Biol. Tech.* 180, 111595. doi: 10.1016/j.postharvbio.2021.111595

Liu, J., Ratnayake, K., Joyce, D. C., He, S., and Zhang, Z. (2012). Effects of three different nano-silver formulations on cut *Acacia holosericea* vase life. *Postharvest Biol. Tech.* 66, 8–15. doi: 10.1016/j.postharvbio.2011.11.005

Liu, D., Sui, S., Ma, J., Li, Z., Guo, Y., Luo, D., et al. (2014). Transcriptomic analysis of flower development in wintersweet (*Chimonanthus praecox*). *PloS One* 9 (1), e86976. doi: 10.1371/journal.pone.0086976

Liu, J., Zhang, Z., Li, H., Lin, X., Lin, S., Joyce, D. C., et al. (2018). Alleviation of effects of exogenous ethylene on cut 'Master'carnation flowers with nano-silver and silver thiosulfate. *Postharvest Biol. Tech.* 143, 86–91. doi: 10.1016/j.postharvbio.2018.04.017

Lok, C. N., Ho, C. M., Chen, R., He, Q. Y., Yu, W. Y., Sun, H., et al. (2007). Silver nanoparticles: Partial oxidation and antibacterial activities. *JBIC J. Biol. Inorganic Chem.* 12 (4), 527–534. doi: 10.1007/s00775-007-0208-z

Lu, P., Cao, J., He, S., Liu, J., Li, H., Cheng, G., et al. (2010). Nano-silver pulse treatments improve water relations of cut rose cv. movie star flowers. *Postharvest Biol. Tech.* 57 (3), 196–202. doi: 10.1016/j.postharvbio.2010.04.003

Maity, D., Minitha, C. R., and RT, R. K. (2019). Glucose oxidase immobilized amine terminated multiwall carbon nanotubes/reduced graphene oxide/polyaniline/gold nanoparticles modified screen-printed carbon electrode for highly sensitive amperometric glucose detection. *Materials Sci. Eng.: C.* 105, 110075. doi: 10.1016/j.msec.2019.110075

Naing, A. H., and Kim, C. K. (2020). Application of nano-silver particles to control the postharvest biology of cut flowers: A review. *Scientia Horticulturae*. 270, 109463. doi: 10.1016/j.scienta.2020.109463

Naing, A. H., Win, N. M., Han, J. S., Lim, K. B., and Kim, C. K. (2017). Role of nano-silver and the bacterial strain enterobacter cloacae in increasing vase life of cut carnation 'Omea'. *Front. Plant Sci.* 8. doi: 10.3389/fpls.2017.01590

Nair, P. M. G., and Chung, I. M. (2015). The responses of germinating seedlings of green peas to copper oxide nanoparticles. *Biol. Plantarum.* 59 (3), 591–595. doi: 10.1007/s10535-015-0494-1

Navyashree, M., Munikrishnappa, P. M., Seetharamu, G. K., Krishna, H. C., Kumar, S. A., and Dayamani, K. J. (2017). Effect of NPK and micronutrients on vegetative growth and flower quality parameters of bird of paradise (*Strelitzia reginae* l.). *Environ. Ecol.* 35 (3B), 2194–2198.

Nemati, S. H., Tehranifar, A., Esfandiari, B., and Rezaei, A. (2013). Improvement of vase life and postharvest factors of *Lilium orientalis* 'Bouquet' by silver nano particles. *Notulae Scientia Biologicae* 5 (4), 490–493. doi: 10.15835/nsb549135

Park, D. Y., Naing, A. H., Ai, T. N., Han, J. S., Kang, I. K., and Kim, C. K. (2017). Synergistic effect of nano-sliver with sucrose on extending vase life of the carnation cv. edun. *Front. Plant Sci.* 8. doi: 10.3389/fpls.2017.01601

Pereira, A. M., Gomes, M. D. P., Gonçalves, D. N., Guimaraes, M. E. D. S., Freire, A. I., and Finger, F. L. (2021). Use of methyl jasmonate in bird of paradise. *Rev. Ceres.* 68, 396–400. doi: 10.1590/0034-737x202168050004

Prabhu, S., and Poulose, E. K. (2012). Silver nanoparticles: mechanism of antimicrobial action, synthesis, medical applications, and toxicity effects. *Int. Nano Letters.* 2 (1), 1–10. doi: 10.1186/2228-5326-2-32

Rabiza-Swider, J., Skutnik, E., Jędrzejuk, A., and Rochala-Wojciechowska, J. (2020). Nanosilver and sucrose delay the senescence of cut snapdragon flowers. *Postharvest Biol. Tech.* 165, 111165. doi: 10.1016/j.postharvbio.2020.111165

Rafi, Z. N., and Ramezanian, A. (2013). Vase life of cut rose cultivars 'Avalanche'and 'Fiesta'as affected by nano-silver and s-carvone treatments. *South Afr. J. Botany.* 86, 68–72. doi: 10.1016/j.sajb.2013.02.167

Rai, O., Rana, M., and Bag, N. (2021). Micropropagation of bird of paradise (*Strelitzia reginae* ait.). *Natl. Acad. Sci. Letters.* 44 (5), 447–451. doi: 10.1007/s40009-020-01023-w

Rai, M., Yadav, A., and Gade, A. (2009). Silver nanoparticles as a new generation of antimicrobials. *Biotechnol. Adv.* 27 (1), 76–83. doi: 10.1016/j.biotechadv.2008.09.002

Ratnayake, K., Joyce, D. C., and Webb, R. I. (2012). A convenient sample preparation protocol for scanning electron microscope examination of xylem-occluding bacterial biofilm on cut flowers and foliage. *Scientia Horticulturae.* 140, 12–18. doi: 10.1016/j.scienta.2012.03.012

Reid, M. S., and Evans, R. Y. (1985). Control of cut flower opening. In *III International Symposium on Postharvest Physiology of Ornamentals*. Noordwijkerhout, Netherlands 181, 45–54.

Sahoo, R., Kumar, S., and Ahuja, P. S. (2001). Induction of a new isozyme of superoxide dismutase at low temperature in *Potentilla astrisanguinea* lodd. variety *argyrophylla* (Wall. ex. lehm) griers. *J. Plant Physiol.* 158 (8), 1093–1097. doi: 10.1078/0176-1617-00224

Sane, A., Sujatha, S., Shilpa, K. N., Laxman, R. H., and Shivashankara, K. S. (2020). Growth, yield, physiological and biochemical traits of different accessions of bird of paradise (*Strelitzia reginae* l.). *Ind. Crops Products.* 151, 112477. doi: 10.1016/j.indcrop.2020.112477

Sevillano, L., Sanchez-Ballesta, M. T., Romojaro, F., and Flores, F. B. (2009). Physiological, hormonal and molecular mechanisms regulating chilling injury in horticultural species. postharvest technologies applied to reduce its impact. *J. Sci. Food Agriculture.* 89 (4), 555–573. doi: 10.1002/jsfa.3468

Seyf, M., Khalighi, A., Mostofi, Y., and Naderi, R. (2012). Study on the effect of aluminum sulfate treatment on postharvest life of the cut rose 'Boeing' (*Rosa hybrida* cv. Boeing). *J. Horticulture Forestry Biotechnol.* 16 (3), 128–132.

Sharma, M., Irfan, M., Kumar, A., Kumar, P., and Datta, A. (2021). Recent insights into plant circadian clock response against abiotic stress. *J. Plant Growth Regul.*, 1–14. doi: 10.1007/s00344-021-10531-y

Sharma, M., Kumar, P., Verma, V., Sharma, R., Bhargava, B., and Irfan, M. (2022). Understanding plant stress memory response for abiotic stress resilience: Molecular insights and prospects. *Plant Physiol. Biochem.* 179, 10–24. doi: 10.1016/j.plaphy.2022.03.004

Singh, V. P., and Jegadheesan, A. (2003). Effect of alpha lipoic acid on senescence in gladiolus flowers. *Indian J. Plant Physiol.* 1, 516–521.

Singh, A., Kumar, J., and Kumar, P. (2008). Effects of plant growth regulators and sucrose on post-harvest physiology, membrane stability and vase life of cut spikes of gladiolus. *Plant Growth Regul.* 55 (3), 221–229. doi: 10.1007/s10725-008-9278-3

Solgi, M., Kafi, M., Taghavi, T. S., and Naderi, R. (2009). Essential oils and silver nanoparticles (SNP) as novel agents to extend vase-life of gerbera (*Gerbera jamesonii* cv.'Dune') flowers. *Postharvest Biol. Tech.* 53 (3), 155–158. doi: 10.1016/j.postharvbio.2009.04.003

Sondi, I., and Salopek-Sondi, B. (2004). Silver nanoparticles as antimicrobial agent: a case study on *E. coli* as a model for gram-negative bacteria. *J. Colloid Interface Sci.* 275 (1), 177–182. doi: 10.1016/j.jcis.2004.02.012

Stephenson, P., and Rubinstein, B. (1998). Characterization of proteolytic activity during senescence in daylilies. *Physiologia Plantarum* 104 (3), 463–473. doi: 10.1034/j.1399-3054.1998.1040323.x

Sugawara, H., Shibuya, K., Yoshioka, T., Hashiba, T., and Satoh, S. (2002). Is a cysteine proteinase inhibitor involved in the regulation of petal wilting in senescing carnation (*Dianthus caryophyllus* l.) flowers? *J. Exp. Botany.* 53 (368), 407–413. doi: 10.1093/jexbot/53.368.407

Tayal, R., Kumar, V., and Irfan, M. (2022). Harnessing the power of hydrogen sulphide ($H_2S$) for improving fruit quality traits. *Plant Biol.* 24 (4), 594–601. doi: 10.1111/plb.13372

Thakur, M., and Kumar, R. (2021). Light conditions and mulch modulate the damask rose (*Rosa damascena* mill.) yield, quality, and soil environment under mid hill conditions of the western himalaya. *Ind. Crops Products.* 163, 113317. doi: 10.1016/j.indcrop.2021.113317

Tu, Y. S., Lv, M., Xiu, P., Huynh, T., Zhang, M., Castelli, M., et al. (2013). Destructive extraction of phospholipids from *Escherichia coli* membranes by graphene nanosheets. *Nat. Nanotechnol.* 8, 594–601. doi: 10.1038/nnano.2013.125

van Doorn, W. G. (2012). Water relations of cut flowers: an update. *Hortic. Rev.* 40, 55–106. doi: 10.1002/9781118351871.ch2

van Doorn, W. G., and Vaslier, N. (2002). Wounding-induced xylem occlusion in stems of cut chrysanthemum flowers: roles of peroxidase and cathechol oxidase. *Postharvest Biol. Tech.* 26 (3), 263–266. doi: 10.1016/S0925-5214(02)00039-X

Van Doorn, W. G., and De Witte, Y. (1997). Sources of the bacteria involved in vascular occlusion of cut rose flowers. *J. Am. Soc. Hortic. Sci.* 122 (2), 263–266.

Vierstra, R. D. (1996). Proteolysis in plants: Mechanisms and functions. Post-Transcriptional Control of Gene Expression in Plants. *Plant Mol. Biol.* 32, 275–302. doi: 10.1007/978-94-009-0353-1_12

Williamson, P. A., Blower, P. J., and Green, M. A. (2011). Synthesis of porous hollow silica nanostructures using hydroxyapatite nanoparticle templates. *Chem. Commun.* 47 (5), 1568–1570. doi: 10.14356/kona.2013009

Xia, Q. H., Zheng, L. P., Zhao, P. F., and Wang, J. W. (2017). Biosynthesis of silver nanoparticles using artemisia annua callus for inhibiting stem-end bacteria in cut carnation flowers. *IET Nanobiotech.* 11 (2), 185–192. doi: 10.1049/iet-nbt.2015.0125

Xu, W., Xie, W., Huang, X., Chen, X., Huang, N., Wang, X., et al. (2017). The graphene oxide and chitosan biopolymer loads TiO2 for antibacterial and preservative research. *Food Chem.* 221, 267–277. doi: 10.1016/j.foodchem.2016.10.054

Yan, A., and Chen, Z. (2019). Impacts of silver nanoparticles on plants: A focus on the phytotoxicity and underlying mechanism. *Int. J. Mol. Sci.* 20 (5), 1003. doi: 10.3390/ijms20051003

Yin, I. X., Zhang, J., Zhao, I. S., Mei, M. L., Li, Q., and Chu, C. H. (2020). The antibacterial mechanism of silver nanoparticles and its application in dentistry. *Int. J. Nanomed.* 15, 2555. doi: 10.2147/IJN.S246764

Zafar, S., Perveen, S., Kamran Khan, M., Shaheen, M. R., Hussain, R., Sarwar, N., et al. (2022). Effect of zinc nanoparticles seed priming and foliar application on the growth and physio-biochemical indices of spinach (*Spinacia oleracea* l.) under salt stress. *PloS One* 17 (2), e0263194. doi: 10.1371/journal.pone.0263194

Zhao, D., Cheng, M., Tang, W., Liu, D., Zhou, S., Meng, J., et al. (2018). Nano-silver modifies the vase life of cut herbaceous peony (*Paeonia lactiflora* pall.) flowers. *Protoplasma* 255 (4), 1001–1013. doi: 10.1007/s00709-018-1209-1

Zhu, Y., Zou, X., Dean, A. E., Brien, J. O., Gao, Y., Tran, E. L., et al. (2019). Lysine 68 acetylation directs MnSOD as a tetrameric detoxification complex versus a monomeric tumor promoter. *Nat. Commun.* 10 (1), 1–15. doi: 10.1038/s41467-019-10352-4

frontiers | Frontiers in Plant Science

TYPE Original Research
PUBLISHED 20 October 2022
DOI 10.3389/fpls.2022.1039360



OPEN ACCESS

EDITED BY
Pankaj Kumar,
Dr. Yashwant Singh Parmar University of Horticulture and Forestry, India

REVIEWED BY
Ilian Badjakov,
Agrobioinstitute (CAB), Bulgaria
Ahmad Latif Virk,
China Agricultural University, China
Behiye Banu Bilgen,
Namik Kemal University, Turkey

*CORRESPONDENCE
Youming Hou
ymhou@fafu.edu.cn
Faxing Chen
fxchen@fafu.edu.cn

SPECIALTY SECTION
This article was submitted to Plant Biotechnology, a section of the journal Frontiers in Plant Science

RECEIVED 08 September 2022
ACCEPTED 03 October 2022
PUBLISHED 20 October 2022

CITATION
Ali MM, Anwar R, Rehman RNU, Ejaz S, Ali S, Yousef AF, Ercisli S, Hu X, Hou Y and Chen F (2022) Sugar and acid profile of loquat (*Eriobotrya japonica* Lindl.), enzymes assay and expression profiling of their metabolism-related genes as influenced by exogenously applied boron. *Front. Plant Sci.* 13:1039360. doi: 10.3389/fpls.2022.1039360



# Sugar and acid profile of loquat (*Eriobotrya japonica* Lindl.), enzymes assay and expression profiling of their metabolism-related genes as influenced by exogenously applied boron

Muhammad Moaaz Ali[1,2], Raheel Anwar[3], Rana Naveed Ur Rehman[4], Shaghef Ejaz[5], Sajid Ali[5], Ahmed F. Yousef[6], Sezai Ercisli[7], Xiaobo Hu[1,2], Youming Hou[1]* and Faxing Chen[1,2]*

[1]State Key Laboratory of Ecological Pest Control for Fujian and Taiwan Crops, College of Plant Protection, Fujian Agriculture and Forestry University, Fuzhou, China, [2]Institute of Subtropical Fruits, Fujian Agriculture and Forestry University, Fuzhou, China, [3]Institute of Horticultural Sciences, University of Agriculture, Faisalabad, Pakistan, [4]Department of Horticulture, Faculty of Food and Crop Science, Pir Mehr Ali Shah (PMAS)-Arid Agriculture University, Rawalpindi, Pakistan, [5]Department of Horticulture, Faculty of Agricultural Sciences and Technology, Bahauddin Zakariya University, Multan, Pakistan, [6]Department of Horticulture, College of Agriculture, University of Al-Azhar (Branch Assiut), Assiut, Egypt, [7]Department of Horticulture, Agricultural Faculty, Ataturk University, Erzurum, Turkey

Soluble sugars and organic acids are the most abundant components in ripe fruits, and they play critical roles in the development of fruit flavor and taste. Some loquat cultivars have high acid content which seriously affect the quality of fruit and reduce the value of commodity. Consequently, studying the physiological mechanism of sugar-acid metabolism in loquat can clarify the mechanism of their formation, accumulation and degradation in the fruit. Minerals application has been reported as a promising way to improve sugar-acid balance of the fruits. In this study, loquat trees were foliar sprayed with 0.1, 0.2 and 0.3% borax, and changes in soluble sugars and organic acids were recorded. The contents of soluble sugars and organic acids were determined using HPLC-RID and UPLC-MS, respectively. The activities of enzymes responsible for the metabolism of sugars and acids were quantified and expressions of related genes were determined using quantitative real-time PCR. The results revealed that 0.2% borax was a promising treatment among other B applications for the increased levels of soluble sugars and decreased acid contents in loquats. Correlation analysis showed that the enzymes i.e., SPS, SS, FK, and HK were may be involved in the regulation of fructose and glucose metabolism in the fruit pulp of loquat. While the activity of NADP-ME showed negative and NAD-MDH showed a positive correlation with malic acid content. Meanwhile, *EjSPS1*, *EjSPS3*, *EjSS3*, *EjHK1*, *EjHK3*, *EjFK1*, *EjFK2*, *EjFK5*, and *EjFK6* may play an important role in soluble sugars metabolism in fruit pulp of loquat. Similarly,

*EjPEPC2*, *EjPEPC3*, *EjNAD-ME1*, *EjNAD-MDH1*, *EjNAD-MDH5-8*, *EjNAD-MDH10*, and *EjNAD-MDH13* may have a vital contribution to malic acid biosynthesis in loquat fruits. This study provides new insights for future elucidation of key mechanisms regulating soluble sugars and malic acid biosynthesis in loquats.

KEYWORDS

malic acid, PEPC, fruit quality, malate dehydrogenase, borax, fructokinase, sucrose, liquid chromatography

## Introduction

Fruits have their own biochemical and nutritional features over the course of their growth, which eventually results in their distinct fruit quality (Bermejo and Cano, 2012; Ren et al., 2015; Zhang et al., 2021). This process promotes the development of sugar and organic acid metabolites, which are important for the development of fruit flavor since the growth of fruit is usually accompanied by the accumulation and degradation of sugars and organic acids (; Zhang et al., 2014: 2021). The balance between the sugar-acid production, breakdown, and vacuole storage determines their ultimate content in ripe fruits (Ruffner et al., 1984; Pan et al., 2021). Fruits are categorised into three major categories based on the amount of organic acid they contain: malic acid, citric acid, and tartaric acid (Batista-Silva et al., 2018). Malic acid is the primary organic acid type in loquat (Li et al., 2015b; Ali et al., 2021a).

Loquat (*Eriobotrya japonica* Lindl.) is an evergreen fruit tree native to China (Ali et al., 2021b). It is a member of family Rosaceae, subfamily Maloideae (Ali et al., 2021c). Vitamin A, vitamin B6, potassium, magnesium, and dietary fibre are all abundant in this fruit (Badenes et al., 2003). It is an orange-colored fruit with a mildly sweet flavor (Zhi et al., 2021). Loquat fruit cannot be preserved for lengthy periods of time due to its soft and juicy flesh and thin peel (Tian et al., 2011). Besides its utilization as fruit, it is a good source of honey. Its flowers are much attractive to honey bees, especially white-colored flowers (Karadeniz et al., 2012). Japan, Korea, India, Pakistan, and China's south-central area are the main producers of loquat (Ali et al., 2021d). In California, it's also cultivated as an ornamental shrub (LaRue, 2020). Loquat is grown on more than 130 thousand hectares in China, making it the world's biggest producer and exporter. China produces 650 thousand tonnes of loquats each year (Zheng et al., 2019). High fruit acidity and low sugars have been major factors lowering fruit quality and commodity value in commercial loquat production (Chen et al., 2009).

The mineral elements are absorbed to variable degrees and play important roles in fruit quality, since many of them are required for photosynthesis, respiration, energy metabolism, and cell structure (Broadley et al., 2012; Engels et al., 2012; Wiesler, 2012; Ali et al., 2021d). In comparison to soil application, foliar application of nutrients has a 10-20 percent greater influence (Zaman and Schumann, 2006; Ali et al., 2021b). Boron (B) is involved in a variety of metabolic functions, such as sugar transport and respiration (Ali et al., 2019), cell wall formation (Brown et al., 2002), cell division and elongation (Goldbach et al., 2001; de Oliveira et al., 2006), membrane stability, carbohydrate metabolism and $Ca^{2+}$ uptake, hormone activation, root development, water translocation (Zhao and Oosterhuis, 2002; Sheng et al., 2009), and the activation of dehydrogenase enzymes (Marschner, 1995; El-Sheikh et al., 2007). However, the physiological and molecular functions of boron in regulating sugar-acid metabolism are not fully known at this time, and more research is required to clarify this.

Here, in this study, loquat trees were foliar sprayed with 0.1, 0.2 and 0.3% borax, and changes in soluble sugars and organic acids were recorded. Soluble sugars (fructose, glucose and sucrose) and organic acids (fumaric acid, ascorbic acid, malic acid, *cis*-aconitic acid and acetic acid) were quantified using HPLC and UPLC, respectively. The HPLC method can directly determine oligosaccharide with a simple sample preparation. It is one of the most promising methods for sugar analysis, due to its universality, time efficiency, accuracy, and selectivity for the quantification of carbohydrates (Kakita et al., 2002). Similarly, UPLC method is used to determine organic acid content of fruits, because of its simplicity, speed and stability (Fedorova et al., 2020). We not only investigated the effect of different concentrations of B on yet unexplored aspects of loquat sugar-acid metabolism but also segregated concentration-dependent variations in activities of related enzymes and relative expression of their biosynthesis-related genes.

## Materials and methods

### Plant material, experimental design and treatments

The young loquat trees (Cv. Jiefangzhong), growing in an orchard located in the subtropical area of Fujian province

(Fuqing) (25°47'26.0"N 119°20'31.0"E), were selected for this study. The loquat trees ranged in height from 4 to 5.5 m and had a canopy diameter of 4 to 5 m. The spacing between each tree in the planting was roughly 6 × 6 m. Throughout the last three growing seasons, loquat trees have been subjected to methodical pruning and thinning, as well as fertilization with nitrogen (N), phosphorus (P) and potassium (K) (15:15:15) at a rate of 5 kg per plant every season. A randomized block design was used to allocate the distribution of plants for various treatments (RCBD). Each treatment had a total of four replications, or blocks, allocated to it, and each individual tree was counted as a single replicate for each treatment. Standard agricultural procedures were used throughout the production of loquats. These activities included drip irrigation, mineral supplementation, weed management, and the management of insects/pests and diseases. The experiment consisted of four separate treatments, the control (water spray), 0.1% borax, 0.2% borax, and 0.3% borax respectively. These foliar concentrations were chosen after an earlier study about phyto-nutritional composition of loquat (Ali et al., 2021b). The foliar treatment was done twice during the full bloom stage (the first week of January, 2020), with a three-week break in between each application. Early in the morning, a foliar spray of B was applied to loquat trees using an electronic sprayer with a capacity of 5 L that was set at a constant pace. Fully ripened fruits were sampled from the sun-exposed tree canopy (Ali et al., 2021c; Ali et al., 2021b), at about 1.5–2.5 m height, 90 days after first foliar spray, and brought back immediately to the laboratory (Institute of Tropical and Subtropical Fruits, FAFU).

## Fruit weight and size

The average fresh weight, length (from the tallest point), and width (from the widest point) of the fruit were determined by averaging five batches of fruit, each of which consisted of 10 loquats from the same treatment. The fruit's weight was measured using a digital weighing balance (MJ-W176P, Panasonic, Japan), and its length and diameter were gauged with digital Vernier callipers (DR-MV0100NG, Ningbo Dongrun Imp. & Exp. Co., Ltd., China). The length-to-width ratio, hereafter referred to as the fruit shape index, was determined by dividing each fruit's length by its diameter.

## Soluble solids, titratable acids, sugar-acid ratio and fruit juice pH

Using a titrimetric approach based on NaOH (Hortwitz, 1960), the total titratable acids were calculated and shown as a percentage of citric acid. A portable digital refractometer was used to calculate the total soluble solids (Atago, Hybrid PAL-BXIACID F5, Japan). Total soluble solids in the sample were divided by total titratable acids to get the sugar-acid ratio. The acidity level of fruit juice was measured using a digital pH meter (Hanna, HI-98107, Mauritius).

## Soluble sugars determination through HPLC-RID

The contents of soluble sugars were determined through high-performance liquid chromatography – refractive index detection (HPLC-RID) as earlier described by Yu et al. (2021). Fruit samples (pulp stored at -80°C) were ground up in liquid nitrogen, and the resulting 2 g of fine powder was mixed with a modest quantity of polyvinylpyrrolidone in 10 mL of 95% methanol. The supernatant fluid was collected after ultra-sonification at 40°C for 30 min and centrifugation at 1000 rpm for 10 min. With 8 mL of ultrapure water, the procedure was repeated using the leftover residue. A 0.22 m syringe filter was then used to filter the clear liquid (ANPEL, China). A Waters 2695 autosampler system was used for HPLC-RID analysis. Ellistat Supersil $NH_2$ column (4.6 mm × 250 mm, 5 µm particle size) (Waters Inc, Zellik, Belgium) was used to separate soluble sugars, operated at 40°C. The mobile phases consisted of 82% acetonitrile and 18% ultrapure water solution mixture. The amount of the injection was 20 µL, and the flow rate was 1.2 mL per min. In the end, the concentration of each and every solitary soluble sugar was determined by using the calibration curve of the standard that corresponded to it. The standards of fructose (99%), glucose (99.5%)) and sucrose (99.5%) were obtained from Sigma-Aldrich, USA. Every single one of the assays for soluble sugars was carried out using three separate samples. The output was given in milligrams per milliliter, which was denoted with the notation $mg{\cdot}ml^{-1}$.

## Organic acids determination through UPLC-MS

The extraction of organic acids was carried out using the method outlined by Nour et al. (2010), although with minor adjustments. In order to extract juice from the loquat fruits, they were first halved and then pressed. After going through three layers of gauze material, the pulp was removed. Following centrifugation of the juice at 4000 rpm for 15 min, the supernatant was diluted 25 times and passed through an MF-Millipore™ Membrane Filter with a pore size of 0.22 µm in diameter. The ultra-performance liquid chromatography – mass

spectrometry (UPLC-MS) technique was used in order to investigate organic acids. A sample of 10 µL of eluate was injected into an Acquity UPLC HSS T3 column (1.8 µm particle size, 2.1 mm × 100 mm). When employing a solution containing 0.025% $H_3PO_4$ as the solvent, the flow rate was 0.2 mL per min. Organic acids were detected at 210 nm, while column temperature was 30°C. A Waters 2996 diode array detector (Waters Corporation, USA) was used to detected the eluted peaks. Using the calibration curve of the relevant standard, the contents of the various organic acids were able to be determined and computed. The standards of fumaric acid (99%), ascorbic acid (99%), malic acid (99%), *cis*-aconitic acid (98%) and acetic acid (99.7%) were obtained from Sigma-Aldrich, USA. Every one of the assays for organic acids was carried out using three separate samples. The output was reported in milligrams per milliliter of fresh juice, which is abbreviated as $mg{\cdot}ml^{-1}$ juice.

Limits of detection and quantification were included as parts of the HPLC-RID and UPLC-MS procedures' validation parameters (Ribani et al., 2004). The peaks were identified by their retention times, comparing the UV–Visible spectra and spiking with standards. Quantification has been done using an external standard curve with five points (Table 1; Figures S1, S2).

## Enzymes extraction and activity assay

The enzymes responsible for sugar [sucrose-phosphate synthase (SPS), sucrose synthase (SS), hexokinase (HK) and fructokinase (FK)] and acid metabolism [phospho*enol*pyruvate carboxylase (PEPC), NADP – dependent malic enzyme (NADP-ME) and NAD – malate dehydrogenase (NAD-MDH)] were extracted and measured using the Solarbio enzyme activity kits (Solarbio Life Sciences, Beijing, China) according to the manufacturer's instructions (Zhang et al., 2021). The extraction kits were based on the earlier determined methods for SPS (Schrader and Sauter, 2002), SS (Schrader and Sauter, 2002), HK (Pancera et al., 2006), FK (Papagianni and Avramidis, 2011), PEPC (Zhang et al., 2008), NADP-ME (Spampinato et al., 1994), and NAD-MDH (Yao et al., 2011).

## RNA extraction and real-time quantitative PCR

Total RNA was extracted from loquat fruit pulp using a Total RNA kit (TianGen Biotech, Beijing, P.R. China). NanoDrop N-1000 spectrophotometer (NanoDrop technologies, Wilmington, DE, USA) was used to analyze RNA concentration and purity. First-strand cDNA was synthesized from 1 µg of total RNA using the Prime Script RT Reagent Kit with a gDNA Eraser (TaKaRa, Dalian, China). High-performance real-time PCR (LightCycler® 96, Roche Applied Science, Penzberg, Germany) was used for the qPCR analysis. Primers used in quantitative real-time polymerase chain reaction (qRT-PCR) are included in Table S1, which were designed using Primer-blast.

The reaction mixture contained 10 µL 2×RealStar Green Fast Mixture (GenStar, Bejing, China), 1 µL cDNA, 0.25 µM of each primer and water was added to make a final volume of 20 µL. The qRT-PCR protocol started with a 5 min "preincubation" at 95°C, then 40 cycles at 95°C for 10 s and 60°C for 30 s, a "melting" step at 95°C for 10 s, 65°C for 1 min, and 97°C for 1 s, and a "cooling" phase at 37°C for 30 s. The $2^{-\Delta\Delta ct}$ approach (Munhoz et al., 2015) was used to determine relative gene expression, with the actin protein (EVM0004523.1) serving as the internal control (Gan et al., 2020). The validation of $2^{-\Delta\Delta Ct}$ method was carried out by ΔCt variation analysis at different template concentrations (Livak and Schmittgen, 2001; Xu et al., 2017; De Rossi et al., 2021). Each sample was analysed using three biological replicates.

## Statistical analysis

The collected data was analyzed using an ANOVA with the help of the statistical programme "Statistix 8.1" (https://www.

TABLE 1 Validation parameters for HPLC/UPLC method.

| Sugar/Acid type | Linearity ($R^2$) | Standard deviation (SD) | Slope (y) | Response (Sy) | Sy/y | LOD* ($mg{\cdot}ml^{-1}$) | LOQ** ($mg{\cdot}ml^{-1}$) |
|---|---|---|---|---|---|---|---|
| Fructose | 0.9767 | 1.5811 | 6544.8 | 1845.64 | 0.28 | 0.93 | 2.82 |
| Glucose | 0.9864 | 1.5811 | 5743.4 | 1231.92 | 0.21 | 0.71 | 2.15 |
| Sucrose | 0.9799 | 1.5811 | 4413.2 | 1154.19 | 0.26 | 0.86 | 2.62 |
| Fumaric acid | 0.9713 | 0.0016 | 1814350 | 381.7 | 0.0002 | 0.0006 | 0.0021 |
| Ascorbic acid | 0.9804 | 0.0174 | 232772.1 | 1303.62 | 0.0056 | 0.0184 | 0.056 |
| Malic acid | 0.9998 | 0.3488 | 31444.57 | 626.07 | 0.0199 | 0.0657 | 0.1991 |
| *Cis*-aconitic acid | 0.9777 | 0.0014 | 669100 | 228.85 | 0.0003 | 0.0011 | 0.0034 |
| Acetic acid | 0.9771 | 0.3488 | 14109.31 | 820.78 | 0.0581 | 0.1919 | 0.5817 |

*Limit of detection; **Limit of quantification

statistix.com/). Means of replicated data from each treatment were compared using Fisher's least significant difference (LSD) method, when $p \leq 0.05$. The Pearson (n) approach was used in 'Statistix 8.1' to calculate the correlation coefficient values, and "TBtools ver. 0.6655" (https://github.com/CJ-Chen/TBtools) was used to depict the data as a heat map. Principle component analysis (PCA) of treatments and tested variable was done through Pearson (*n*) method using "XLSTAT ver. 2019" (https://www.xlstat.com/en/).

# Results

## Fruit weight and size

Loquat plants treated with foliar supplied B exhibited a significant increase ($p \leq 0.05$) in fruit weight and size (fruit length, width, and fruit shape index) as compared to untreated plants. The plants receiving 0.2% borax exhibited maximum fruit weight (57.95 g), which was 18.19% higher than that of untreated plants (Figure 1A). Regardless of concentration, B improved the loquat fruit length by 8-18% as compared to control (Figure 1B). The maximum fruit width (43.52 mm) was recorded in the plants treated with 0.2% borax followed by the plants receiving 0.1% (40.88 mm) and 0.3% borax (39.11 mm) (Figure 1C). Boron application reduced fruit shape index regardless of concentration applied, indicating its possible role in improving fruit size in terms of diameter. The minimum fruit shaped index (1.25) was recorded in the plants treated with 0.1-0.2% borax, which was 8% less as compared to that of untreated plants (Figure 1D).

## Soluble solids, titratable acids, sugar-acid ratio and fruit juice pH

Total soluble solids (TSS) and titratable acidity (TTA) of loquat fruits showed reciprocal responses to each other. Foliar application of 0.2% borax enhanced TSS by 36.86%, while reduced the TTA by 61.90% comparing with control (Figures 2A, B). The plants receiving foliar application of 0.2% B exhibited 3.60-fold increase in sugar-acid ratio, as compared to control. The increased sugar-acid ratio and fruit juice pH indicates the positive influence of applied treatments on sugars accumulation in loquat fruits (Figures 2C, D).

## Soluble sugars

Three soluble sugars i.e., fructose, glucose and sucrose were quantified in the fruit pulp of B-treated loquat fruits through HPLC (Figure 3). The results revealed that fructose and glucose

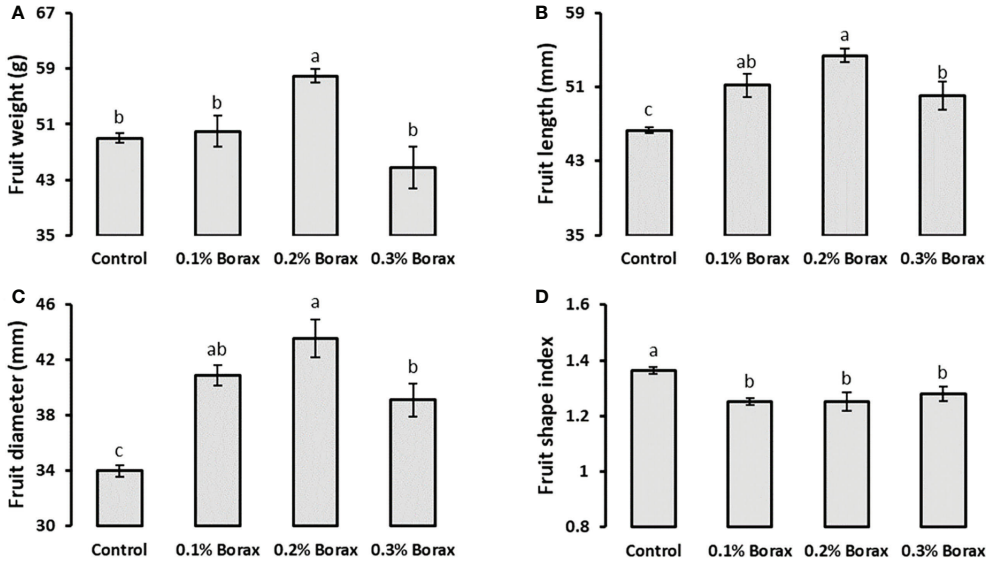


FIGURE 1
Effect of foliar application of B on weight **(A)**, length **(B)**, diameter **(C)**, and shape index **(D)** of loquat fruits. Loquat plants were foliar sprayed with B twice at blooming stage. Same letters indicate non-significant difference among treatments according to Fisher's least significant difference (LSD) test, when $p \leq 0.05$. Vertical bars indicate mean ± standard error (n=4, 4-block RCBD arrangement).

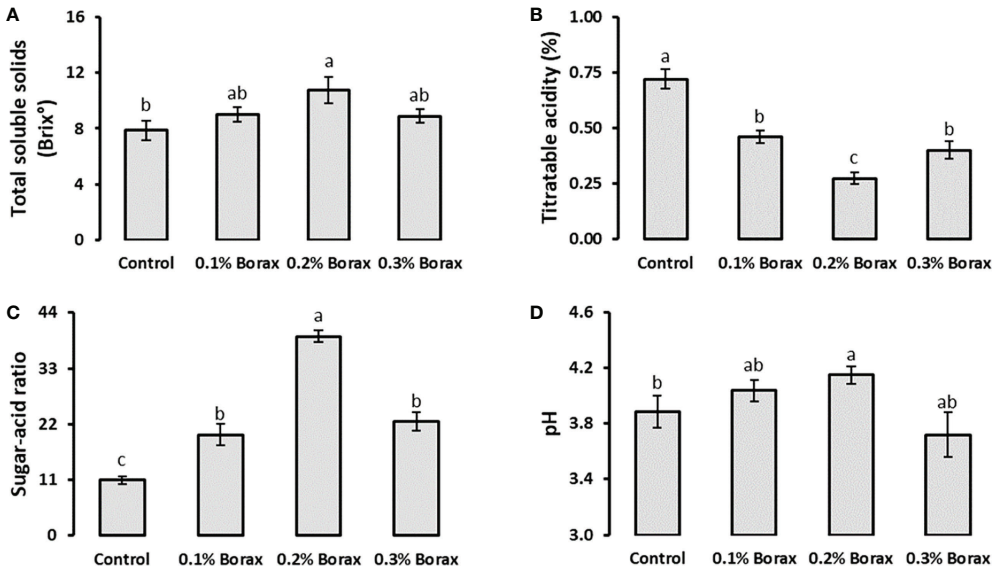


FIGURE 2
Effect of foliar application of B on total soluble solids **(A)**, titratable acidity **(B)**, sugar-acid ratio **(C)**, and pH **(D)** of loquat fruits. Same letters indicate non-significant difference among treatments according to Fisher's least significant difference (LSD) test, when $p \leq 0.05$. Vertical bars indicate mean ± standard error (n=4, 4-block RCBD arrangement).

were the abundant soluble sugars in loquat pulp as compared to sucrose contributing 45.31%, 41.95% and 12.74%, respectively. The fructose and glucose accumulation in loquat fruits showed same pattern with respect to applied treatments. The plants receiving exogenous application of 0.2% borax exhibited maximum fruit fructose level (8.91 mg·ml$^{-1}$) among all other treatments, which was 1.34-times higher (33.89%) than that of untreated plants (Figure 3A). Among B treatments, 0.2% borax

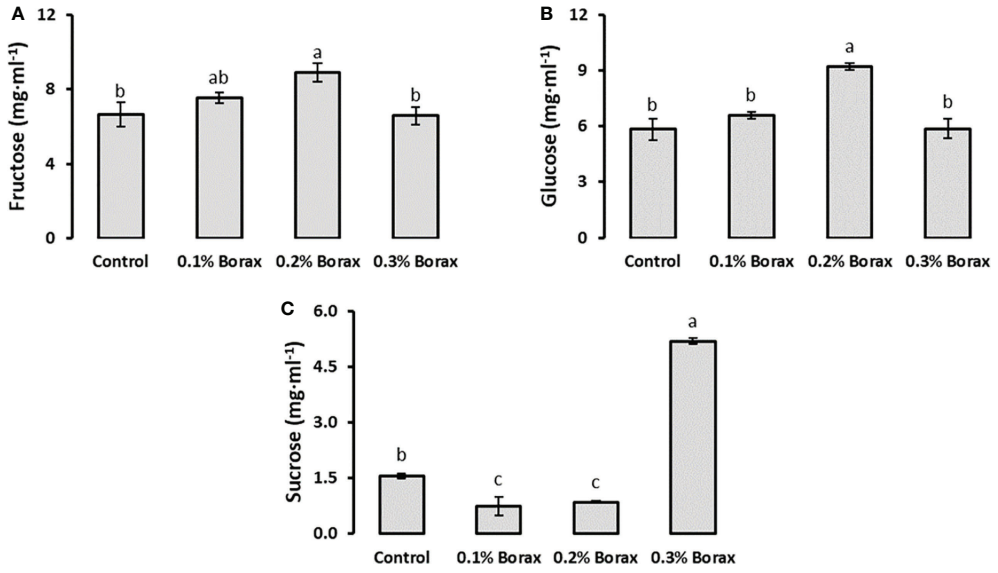


FIGURE 3
Effect of foliar application of B on soluble sugars i.e., fructose **(A)**, glucose **(B)**, and sucrose **(C)** content of loquat fruits. Same letters indicate non-significant difference among treatments according to Fisher's least significant difference (LSD) test, when $p \leq 0.05$. Vertical bars indicate mean ± standard error (n=4, 4-block RCBD arrangement).

improved fruit glucose level by 58.21%, as compared to the fruit glucose level of untreated plants (Figure 3B). In case of fruit sucrose, plants receiving 0.3% borax showed a significant ($p \leq 0.05$) improvement in sucrose level, which was recorded as 3.31-fold higher than control (Figure 3C).

## Organic acids

Five organic acids i.e., fumaric acid, ascorbic acid, malic acid, *cis*-aconitic acid and acetic acid were quantified in the fruit pulp of B-treated loquat fruits through UPLC. The results revealed that malic acid was the most abundant organic acid in loquat pulp followed by acetic acid contributing 81.12% and 18.21%, respectively. The proportion of fumaric acid, ascorbic acid and *cis*-aconitic acid was less than 1% among tested organic acids (Figures 4A, B, E). The exogenous application of B significantly reduced the malic acid concentration as compared to control, ultimately reduced overall acidity of the fruits. The plants receiving 0.2% borax exhibited minimum fruit malic acid level (1.31 mg·ml$^{-1}$) among all other treatments, which was 1.56-times (36.07%) lower than that of untreated plants (Figure 4C). In case of acetic acid content, it was observed that B treatments reduced the acetic acid content in dose-dependent manner (Figure 4D).

## Key enzymes involved in soluble sugars metabolism

The SPS activity in the fruit pulp of loquat significantly ($p \leq 0.05$) increased with B application. The maximum SPS activity was detected in the fruit pulp of the plants treated with 0.2% borax (3237.07 U·g$^{-1}$ protein) (Figure 5A). Interestingly, the SS activity was found decreased with the foliar application of

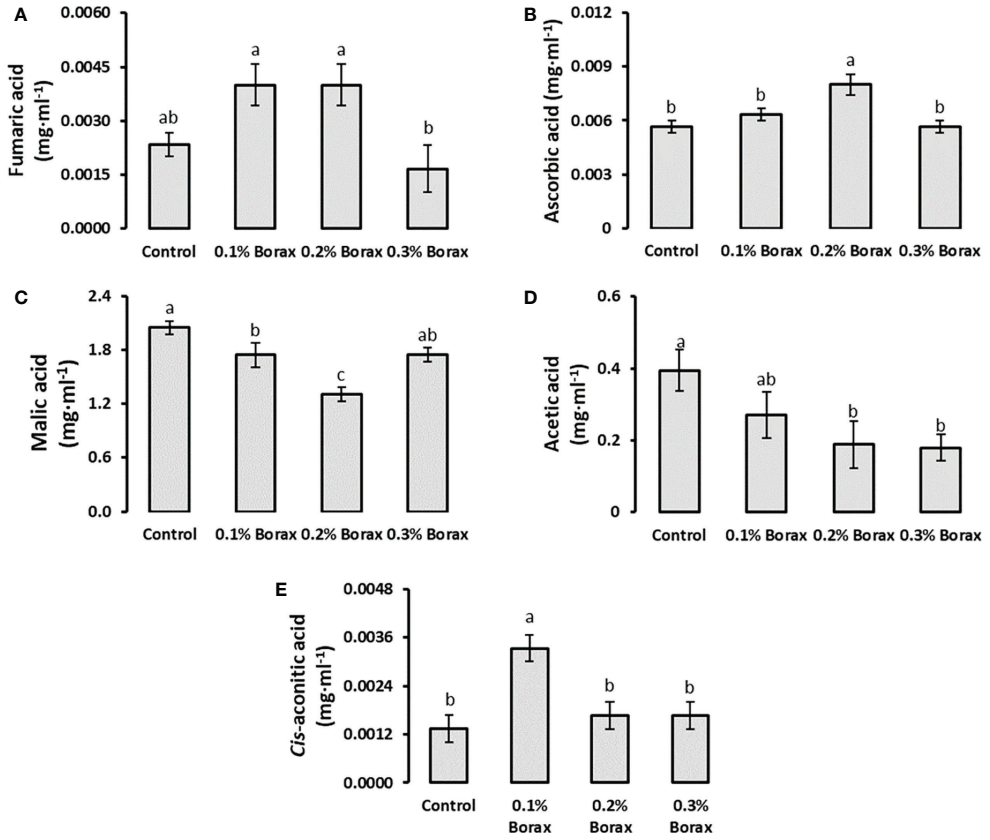


FIGURE 4
Effect of foliar application of B on the level of organic acids i.e., fumaric acid **(A)**, ascorbic acid **(B)**, malic acid Ali et al.,, acetic acid **(D)**, and *cis*-aconitic acid **(E)** in loquat fruits. Same letters indicate non-significant difference among treatments according to Fisher's least significant difference (LSD) test, when $p \leq 0.05$. Vertical bars indicate mean ± standard error (n=4, 4-block RCBD arrangement).

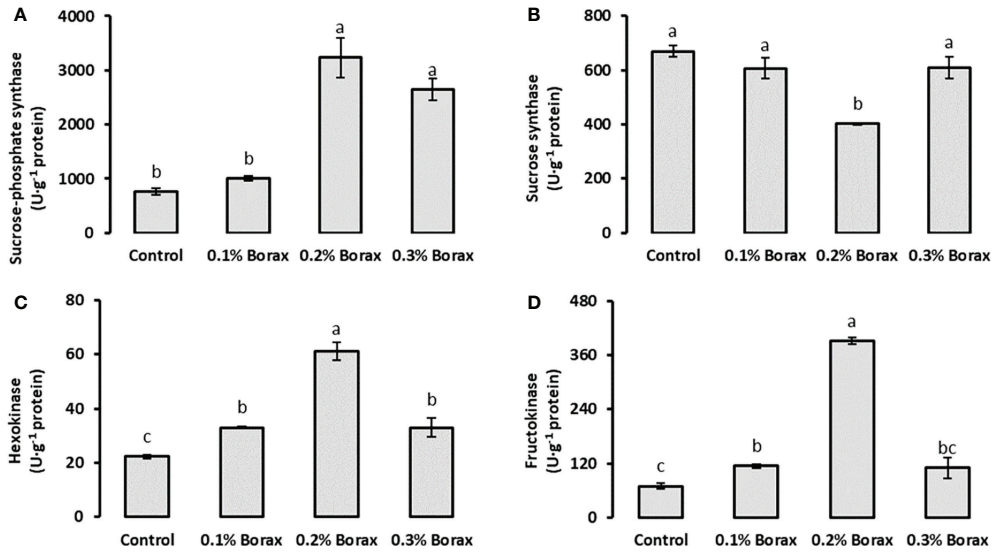


FIGURE 5
Effect of foliar application of B on the activities of key enzymes involved in soluble sugars metabolism i.e., sucrose-phosphate synthase **(A)**, sucrose synthase **(B)**, hexokinase **(C)** and fructokinase **(D)** of loquat fruits. Same letters indicate non-significant difference among treatments according to Fisher's least significant difference (LSD) test, when $p \leq 0.05$. Vertical bars indicate mean ± standard error (n=4, 4-block RCBD arrangement).

0.2% borax (401.97 U·g$^{-1}$ protein) as compared to control (669.69 U·g$^{-1}$ protein), which was 39.98% reduced as compared to control (Figure 5B). Unlike SS, HK and FK activities were recorded improved in fruit pulp of loquat with all preharvest treatments of B. The maximum HK activity (61.22 U·g$^{-1}$ protein) was measured in the fruit pulp of the plants treated with 0.2% borax (Figure 5C). Similarly, maximum FK activity was recorded in fruit pulp of the loquat plants receiving

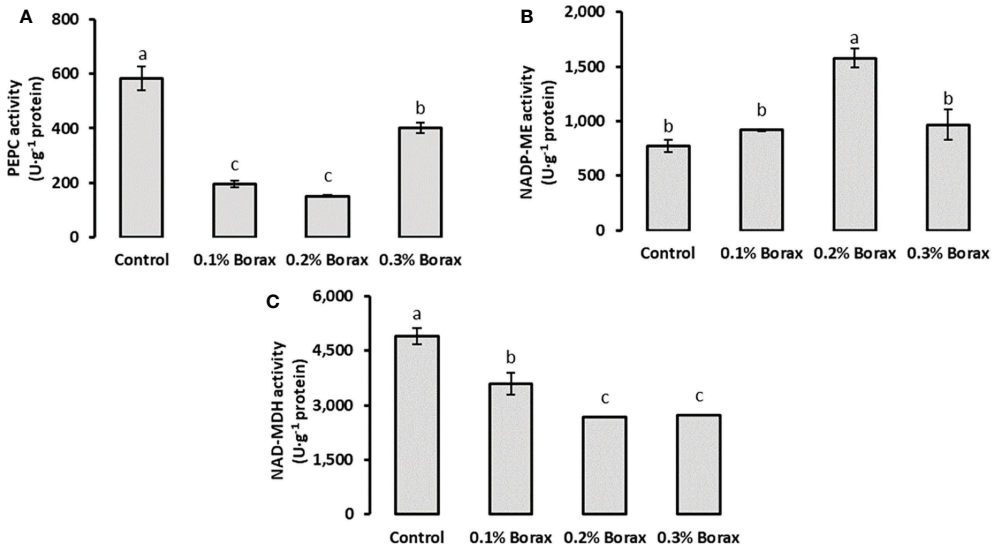


FIGURE 6
Effect of foliar application of B on the activities of key enzymes involved in malic acid metabolism i.e., PEPC **(A)**, NADP-ME **(B)**, and NAD-MDH **(C)** of loquat fruits. Same letters indicate non-significant difference among treatments according to Fisher's least significant difference (LSD) test, when $p \leq 0.05$. Vertical bars indicate mean ± standard error (n=4, 4-block RCBD arrangement).

10.3389/fpls.2022.1039360

foliar application of 0.2% borax (391.50 U·g$^{-1}$ protein), which was 5.61-fold higher than that of untreated plants (Figure 5D).

## Key enzymes involved in malic acid metabolism

The PEPC activity in the fruit pulp of loquat significantly ($p \leq 0.05$) reduced with B application. The minimum PEPC activity was detected in the fruit pulp of the plants treated with 0.2% borax (150.87 U·g$^{-1}$ protein) (Figure 6A). Interestingly, the NADP-ME activity was found increased with the foliar application of B at the concentration of 0.2%. The maximum NADP-ME activity was recorded in the fruit pulp of loquats receiving 0.2% borax (1578.76 U·g$^{-1}$ protein) in comparison with control (771.68 U·g$^{-1}$ protein), which were 2.04-fold higher that of untreated plants, respectively (Figure 6B). Conversely, the exogenous application of B significantly reduced the activity of NAD-MDH as compared to control. Among B treatments, the minimum NAD-MDH activity level was recorded in the loquats treated with 0.20-0.30% borax (2668.87-2733.18 U·g$^{-1}$ protein) (Figure 6C).

## Expression profiling of soluble sugars metabolism-related genes

The expression patterns of core genes i.e., *EjSPS1-4*, *EjSS1-5*, *EjHK1-3*, and *EjHK1-6* encoding key enzymes i.e., SPS, SS, HK and FK responsible for the metabolism of soluble sugars in fruit pulp of loquat were studied (Figure 7). The expression patterns of *EjSPS1-4* genes increased with the foliar application of B. Briefly, the relative expression of *EjSPS1* was recorded maximum in the fruit pulp of loquat when treated with 0.2% borax. Similarly, *EjSPS2* was maximally expressed under the influence of 0.2% borax, which was 2.14-fold higher than that of control. The *EjSPS3* and *EjSPS4* exhibited maximum upregulation under the influence of 0.1-0.2% and 0.2-0.3% borax, respectively.

The *EjSS3* and *EjSS5* were maximally expressed under the influence of 0.2% borax. Specifically, *EjSS1* was significantly ($p \leq 0.05$) down-regulated by aforementioned treatment, while showed non-significant ($p \leq 0.05$) variation under the influence of 0.1 and 0.3% borax. The *EjSS2* significantly ($p \leq 0.05$) upregulated under the influence of 0.1% borax by 2.14-fold. The maximum expression of *EjSS3* was recorded in the loquats treated with 0.2% borax. Foliar application of B significantly ($p \leq$

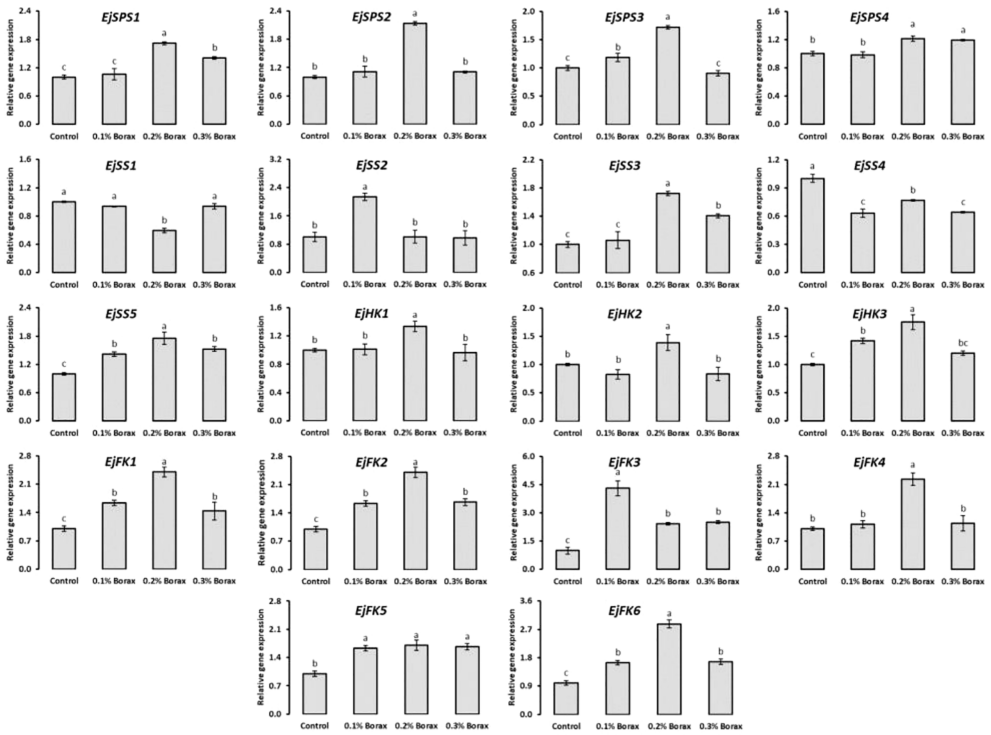


FIGURE 7
The expression profiling of core genes involved in soluble sugars metabolism of loquat as influenced by the foliar application of B Same letters indicate non-significant difference among treatments according to Fisher's least significant difference (LSD) test, when $p \leq 0.05$. Vertical bars indicate mean ± standard error (4 biological and 3 technical replicates).

*0.05*) reduced the expression of *EjSS4* as compared to control. Conversely, *EjSS5* was found upregulated under the influence of B. The maximum relative expression of *EjSS5* was recorded in the loquat treated with 0.2% borax.

Among B treatments, 0.2% borax significantly ($p \leq 0.05$) upregulated the expressions of *EjHK1-3*. The expressions of *EjHK1* and *EjHK2* remained unchanged with B treatments except when loquats received 0.20% borax. While, in the case of *EjHK3*, 0.1% borax also upregulated the expression by 41.9%.

The relative expression level of *EjFK1* was significantly ($p \leq 0.05$) increased with the foliar application of B. The *EjFK1* was maximally upregulated under the influence of 0.2% borax (by 2.41-fold). Similarly, in the case of *EjFK2*, the maximum transcript level was observed in the loquats treated with 0.2% borax (3.43). The borax application significantly ($p \leq 0.05$) upregulated *EjFK3* when applied at the concentration of 0.10% and reduced with increase in its concentration. Among B treatments, 0.2% borax maximally upregulated the *EjFK4* by 2.23-fold. Although the maximum expressions of *EjFK5* and *EjFK6* were recorded in the loquats treated with 0.2% borax, their levels remained upregulated with all B treatments (Figure 7).

## Expression profiling of malic acid metabolism-related genes

The expression patterns of core genes i.e., *EjPEPC*, *EjNAD(P)ME* and *EjNAD-MDH* encoding key enzymes i.e., PEPC, NADP-ME and NAD-MDP responsible for the malic acid metabolism in fruit pulp of loquat were studied (Figure 8). The expression of *EjPEPC1* found significantly decreased with the foliar application of 0.2-0.3% borax. The loquats treated with 0.1-0.2% borax exhibited downregulated expression of *EjPEPC2*. *EjPEPC2* was minimally expressed under the influence of 0.1 and 0.2% borax, which was ≥40% lower than that of control. The *EjPEPC3* also exhibited maximum downregulation under the influence of 0.2% borax.

The relative expression patterns of *EjNAD(P)-ME* genes increased with the foliar application of B. Among B treatments, 0.1-0.2% borax significantly ($p \leq 0.05$) upregulated the expressions of *EjNAD-ME1*. Specifically, the maximum expression of *EjNAD-ME1* was recorded in the loquats treated with 0.2% borax, which were 1.56-fold higher than that of untreated loquats. Similarly, 0.1-0.3% borax significantly ($p \leq$

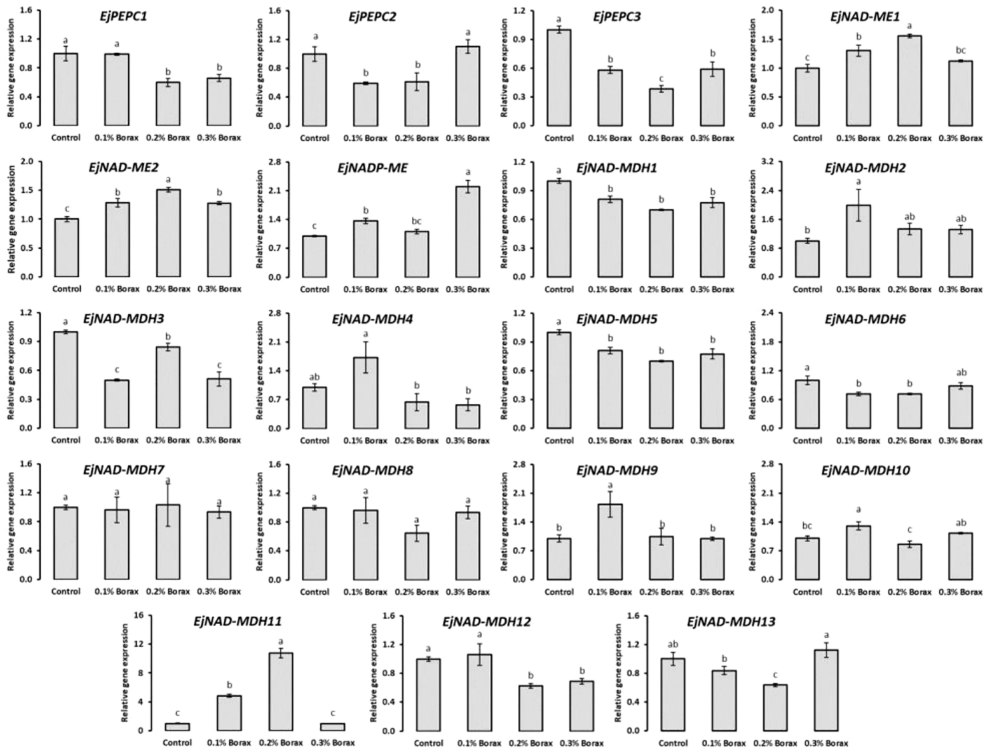


FIGURE 8
The expression profiling of core genes involved in malic acid metabolism of loquat as influenced by the foliar application of B. Same letters indicate non-significant difference among treatments according to Fisher's least significant difference (LSD) test, when $p \leq 0.05$. Vertical bars indicate mean ± standard error (4 biological and 3 technical replicates).

*0.05*) improved the expression of *EjNAD-ME2* in fruit pulp. The expression of *EjNADP-ME* remained unchanged with B treatments except when loquats received 0.1 and 0.3% borax. Its maximum expression was recorded under the influence of 0.3% borax which was 2.20-fold higher than that of control loquats.

The expression of *EjNAD-MDH1* decreased with the application of borax, regardless of its concentration. The lowest *EjNAD-MDH1* transcript was recorded in the loquats treated with 0.2% borax. *EjNAD-MDH2* was maximally expressed under the influence of 0.1% borax, which was 2-fold higher than that of control. The *EjNAD-MDH3* exhibited downregulation under the influence of 0.1-0.3% borax. The relative expression pattern of *EjNAD-MDH4* comparatively increased with the foliar application of 0.1% borax, while remained unchanged under the influence of other treatments. The expression of *EjNAD-MDH5* significantly reduced with the foliar application of B, regardless of its concentration applied. The expression of *EjNAD-MDH6* reduced with the application of 0.1-0.2% borax. The minimum expression of *EjNAD-MDH6* was observed in the loquats treated with 0.2% borax, which was 29% less than that of control. The relative expression pattern of *EjNAD-MDH7* and *EjNAD-MDH8* remained unchanged under the influence of B treatments. The *EjNAD-MDH9* and *EjNAD-MDH10* exhibited its upregulated expression only under the influence of 0.1% borax. The 0.1-0.2% borax significantly ($p \leq 0.05$) improved the expressions of *EjNAD-MDH11*. Its maximum expression level was recorded in the loquats treated with 0.2% borax, which was 10.75-fold higher than control. The expression of *EjNAD-MDH12* significantly ($p \leq 0.05$) reduced under the influence of 0.2-0.3% borax. The *EjNAD-MDH13* was significantly downregulated in fruit pulp of loquat with the foliar application of 0.2% borax (Figure 8).

## Correlation analysis

Principal component analysis (PCA) was conducted to delineate concentration-dependent effects of B on basic fruit quality variables (i.e., fruit weight, size, total soluble solids, total titratable acidity and fruit juice pH), soluble sugars (i.e., fructose, glucose and sucrose), organic acids (i.e., fumaric acid, ascorbic acid, malic acid, *cis*-aconitic acid and acetic acid), key enzymes related to soluble sugars (i.e., SPS, SS, HK and FK) and malic acid metabolism (i.e., PEPC, NADP-ME and NAD-MDH), and relative expression levels of sugar-acid metabolic pathway genes (Figure 9A). Based on the highest squared cosine values corresponding to factors F1 or F2, measured attributes were clustered around B treatments. Factor F1, covering 64.18% variability in data (eigenvalue 38.51), showed clustering of fruit weight, fruit length, fruit diameter, total soluble solids, sugar-acid ratio, fruit fructose, fruit glucose, ascorbic acid, activity of SPS, HK, FK, NADP-ME, expression of *EjSPS1-4*, *EjSS3*, *EjHK1-3*, *EjFK1*, *EjFK2*, *EjFK4*, *EjFK6*, *EjNAD-MDH11*, and *EjNAD-MDH13* with 0.2% borax suggesting its positive influence on these parameters. While, the clustering in opposite quadrant exhibited negative association of 0.2% borax with aforementioned variables. Second factor, covering 19.28%

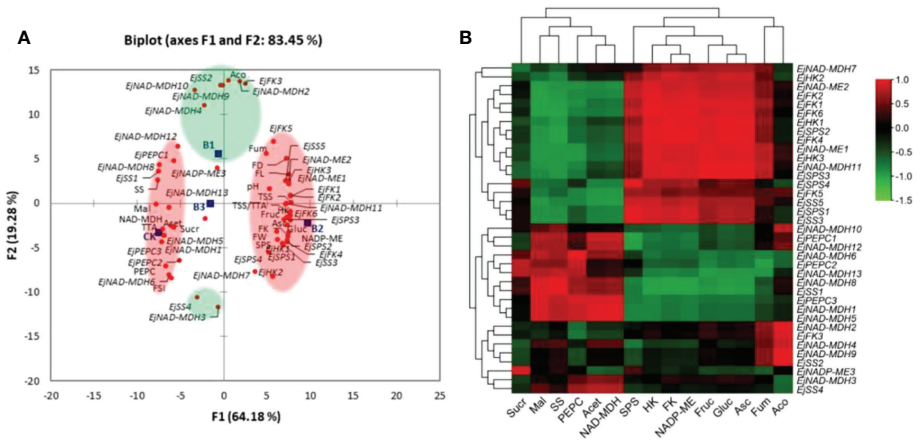


FIGURE 9
**(A)** Principal component analysis (PCA)among B treatments and sugar-acid attributes of loquat. Clustering of B treatments and measured attributes into groups (coloured circles) is based on their highest squared cosine values corresponding to the factor, F1 (red) or F2 (green). **(B)** Pearson (*n*) correlation analysis between "sugar-acid profile and key enzymes involved in their metabolism" and "relative expressions of related genes" in fruit pulp of loquat. CK, control; B1, 0.1% borax; B2, 0.2% borax; B3, 0.3% borax; FW, fruit weight; FL, fruit length; FD, fruit diameter; FSI, fruit shape index; TSS, soluble solid contents; TTA, total titratable acidity; TSS/TTA, sugar-acid ratio; pH, fruit juice pH; Fruc, fruit fructose; Gluc, fruit glucose; Sucr, fruit sucrose; SPS, sucrose-phosphate synthase; SS, sucrose synthase; HK, Hexokinase; FK, fructokinase.

variability in data (eigenvalue 11.566), showed clustering of *cis*-aconitic acid, *EjNAD-MDH2*, *EjNAD-MDH4*, *EjNAD-MDH9*, *EjNAD-MDH10*, *EjSS2*, and *EjFK3* with 0.1% borax. The presence of *EjSS4* and *EjNAD-MDH3* in opposite quadrant indicated the negative association of 0.1% borax with these parameters. Third factor of PCA (not shown), covering 16.55% variability in data (eigenvalue 9.927), showed clustering of pH, fruit sucrose, fumaric acid, *EjNADP-ME*, and *EjNAD-MDH7* with 0.3% borax. Thus, principal component analysis helped to delineate individual roles of B concentrations in regulating sugar-acid metabolism of loquat (Figure 9A).

The correlation between "relative expression levels of sugar-acid metabolism-related genes" and "sugar-acid profile and key enzymes related to their metabolism" was analysed (Figure 9B). The fructose and glucose were positively correlated with *EjSPS1-4*, *EjSS5*, *EjHK1-3*, *EjFK1,2,4-6, EjNAD-ME1,2*, and *NAD-MDH7,11*. The fruit sucrose content was negatively correlated with most of the studied genes except *EjSPS4*, *EjPEPC2, EjNAD-ME3*, and *EjNAD-MDH6,12*. The ascorbic acid was significantly ($p \leq 0.05$) positively correlated with *EjSPS1-3*, *EjSS5*, *EjHK1-3*, *EjFK1,2,4,6, EjNAD-ME1,2*, and *NAD-MDH7,11*. The fruit malic acid content was significantly ($p \leq 0.05$) positively correlated with *EjSS1*, *EjPEPC3*, *EjNAD-MDH1*, *EjNAD-MDH5*, *EjNAD-MDH8* and *EjNAD-MDH13*, while significantly ($p \leq 0.05$) negatively correlated with *EjSPS1-3*, *EjSS5*, *EjHK1,3*, *EjFK1,2,4, EjNAD-ME1,2*, and *NAD-MDH11*. The negative association of *cis*-aconitic acid was observed with the expression of *EjSS4* and *EjNAD-MDH3*. A positive correlation was also found between acetic acid and *EjPEPC3*, *EjNAD-MDH1* and *EjNAD-MDH5*. The enzymatic activity of SPS was positively correlated with *EjSPS1-4*, *EjSS5*, *EjHK1-3*, *EjFK1,2,4-6, EjNAD-ME1,2*, and *NAD-MDH7,11*, while SS only found significantly ($p \leq 0.01$) and positively associated with *EjSS1* and *EjNAD-MDH8*. The HK and FK activity significantly ($p \leq 0.05$) and positively correlated with *EjSPS1-4*, *EjSS5*, *EjHK1-3*, *EjFK1,2,4-6, EjNAD-ME1,2*, and *NAD-MDH7,11*. The enzymatic activity of PEPC was positively correlated with *EjSS1*, *EjPEPC2,3* and *EjNAD-MDH1,5,6,8,13*. The NADP-ME activity was found significantly ($p \leq 0.05$) positively associated with *EjSPS1-3*, *EjHK1*, *EjFK1,2,4,6* and *NAD-MDH11*, while negatively correlated with *EjSS1* and *EjNAD-MDH8*. The NAD-MDH activity positively correlated with *EjPEPC3*, *EjNAD-MDH1*, *EjNAD-MDH5* and *EjNAD-MDH6* (Figure 9B).

# Discussion

## Soluble sugars

The quality of fruit is heavily influenced by soluble sugars and organic acids, the two main components of fruit flavor (Borsani et al., 2009). At the ripe fruit stage, the soluble sugar content of 'Jiefangzhong' loquat was increased to a maximum of 19 mg·ml$^{-1}$ in the current investigation. Previous research has shown that the primary sugars that may be found in loquat fruits are sucrose, glucose, and fructose (Toker et al., 2013; Wei et al., 2017). When it comes to the amount of sugar that they contain, various loquat cultivars have varying degrees of variation. The majority of cultivars have a high concentration of sucrose, followed by fructose and glucose, although wild species do not have any sucrose (Liu et al., 2016). According to the findings of our study, the fructose level was found to be the highest among the soluble sugars that were examined.

In the present study, maximum fructose and glucose were recorded in the loquats treated with 0.2% borax. In a previously reported study, foliar spraying of B alone or in combination with Zn led to a large rise in the concentration of non-reducing sugar in fruit juice. On the other hand, these sprays led to a significant reduction in the concentration of reducing sugar and total sugar in pomegranate (Maity et al., 2021). After being sprayed with B, it was found that the content of sugar in papaya, mandarin orange, mango, and pomegranate fruits increased (Babu and Yadav, 2005; Anees et al., 2011; Davarpanah et al., 2016; Subedi et al., 2019). The effect of B on sugar concentration could be attributed to its role in photosynthesis, starch and nucleic acid metabolism, the transport of sugars, and carbohydrate metabolism (Maity et al., 2021).

During soluble sugars metabolism in plant cell, sucrose is cleaved into UDG-glucose and fructose by sucrose synthase (SS), or can be cleaved into glucose and fructose by invertases (Ghosh et al., 2013; Irfan et al., 2014; Chen et al., 2017). Fructokinases (FKs) and hexokinases (HKs) can phosphorylate free fructose with high substrate specificity and affinity (Renz and Stitt, 1993; Irfan et al., 2016; 2021; 2022). The cleavage of sucrose and the metabolism of sugar are crucial processes in the formation of healthy vascular tissue, and hence it is thought that fructose phosphorylation by FKs and HKs is required for these processes to take place German et al., 2003; Damari-Weissler et al., 2009; Kumar et al., 2016; 2019; Kumari et al., 2022). Both sucrose phosphate synthase (SPS) and sucrose synthase (SS) are important prerequisites in the biochemical process that results in the formation of sucrose. The synthesis of 6-phosphate sucrose from UDP-glucose and 6-phosphate fructose is facilitated by the presence of SPS (Stein and Granot, 2019), whereas SS converts sucrose into UDP-glucose and fructose (Ruan, 2014) (Figure 10A). The majority of the SS proteins may be found in either the cytosol or the plasma membrane, but some can be localized in the vacuole, the cell wall, or the mitochondria (Stein and Granot, 2019). In *Arabidopsis thaliana* and *Malus domestica*, there are 4 and 6 *SPS* genes, respectively (Langenkämper et al., 2002; Li et al., 2012). The number of *SS* genes varies greatly among plant species. There are 6, 8, 12, and 14 *SS* genes in Arabidopsis, carrot (*Daucus carota*), soybean (*Glycine max*) and tobacco (*Nicotiana tabacum*), respectively (Wang et al., 2015; Xu et al., 2019). In Chinese

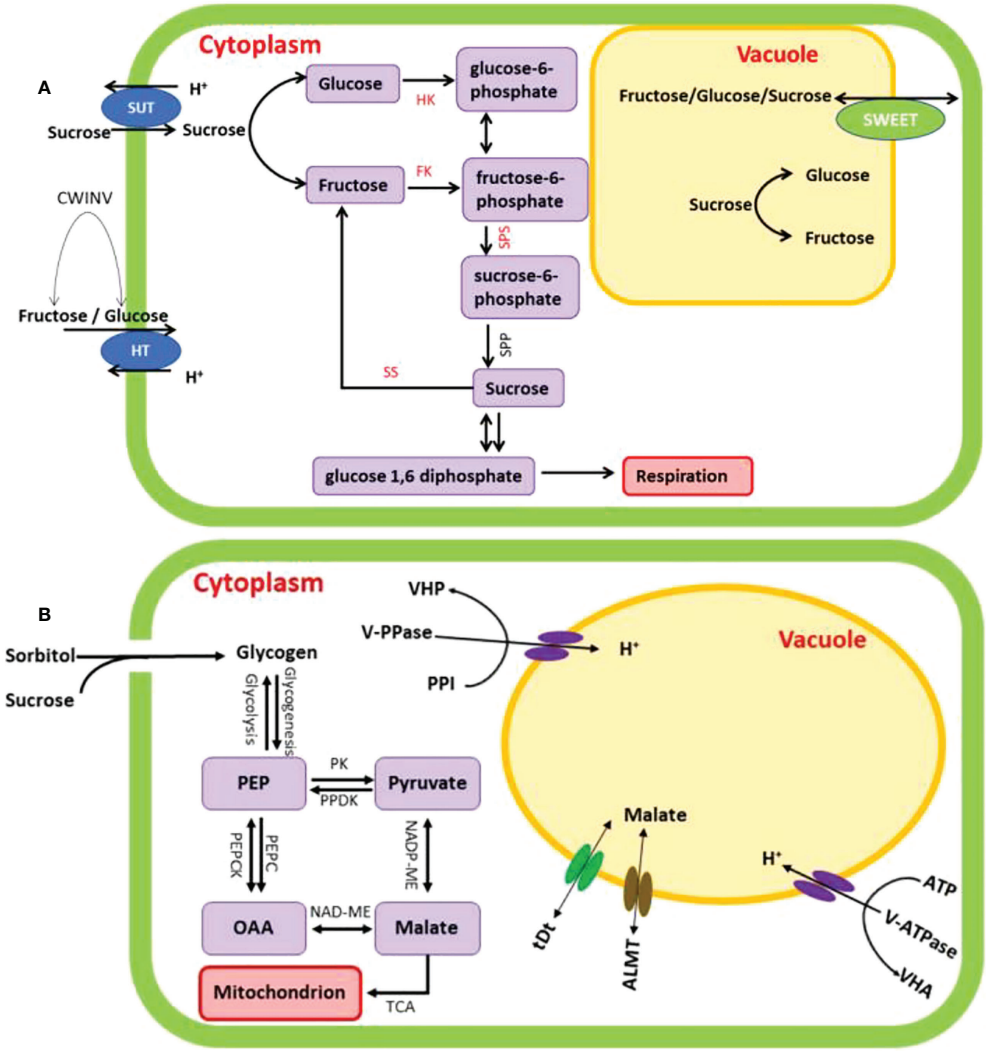


FIGURE 10
Proposed schematic representation of soluble sugars **(A)** and malic acid **(B)** metabolic pathway in fruit cell. SUT, sucrose transporters; CWINT, cell wall invertase; HT - hexose transporters; HK, hexokinase; FK, fructokinase; SPS, sucrose phosphate synthase; SS, sucrose synthase; SPP, sucrose-phosphate phosphatase; SWEET, sugars will eventually be exported transporter; PK, phosphokinase; PPDK, pyruvate phosphate dikinase; PEPC, phospho*enol*pyruvate carboxylase; NADP-ME, NADP-dependent malic enzyme; NAD-MDH, NAD-malate dehydrogenase; ALMT, aluminium activated malate transporter; tDt, terminal deoxynucleotidyl transferase.

pear, it is reported that there were thirty SS genes (Abdullah et al., 2018).

The expressions of most important genes involved in sugar metabolism and accumulation were studied under the influence of B treatments. The SPS genes showed relative high expression level, while sucrose content was very low. The high transcript level, indicated a negative correlation between sucrose accumulation and SPS activity. A possible reason for this discrepancy is that sucrose is the major soluble sugar in tomato (Dali et al., 1992) and watermelon (Liu et al., 2013; Zhu et al., 2017) but the 'Jiefangzhong' loquat mainly showed the accumulation of fructose (Li et al., 2015a).

The enzyme known as sucrose synthase (SS) is also capable of catalyzing the reversible process of the production of sucrose. In peaches and pears, the SS activity has a positive correlation with the amount of sucrose present, but in strawberries and papaya, the correlation is negative (Moriguchi et al., 1992; Lo Bianco et al., 2000; Zhou and Paull, 2001; Basson et al., 2010). It has been hypothesised that when there is a high quantity of glucose and fructose, the SS may be able to be down-regulated in order to lower the enzyme activity (Stein and Granot, 2019). In this study, the *EjSS1-4* showed negative correlation with sucrose content. The *EjSS3,5* showed positive correlation with glucose and fructose. Similar to sucrose, *EjSS2,4* showed negative

correlation with glucose and fructose. These results indicated that *EjSS3* or *EjSS5* might were the candidate genes related to fructose and glucose synthesis, while *EjSS2,4* for sucrose degradation at fruit ripening stage.

The glucose and fructose content, activities of their metabolism related enzymes and expressions *EjHK* and *EjFK* genes increased in loquats with the application of B. All *EjHK* and *EjFK* genes exhibited significantly positive correlation with fructose and glucose contents as well as SPS, HK and FK activity of loquat fruits. However, the expression level of *EjFK3* showed negative correlation with glucose and fructose contents, suggesting that *EjFK3* may play a crucial role in regulating the accumulation of glucose through post-transcriptional level (Jiang et al., 2019).

## Organic acids

Aliphatic carboxylic acids, sugar-derived organic acids, and phenolic acids are the three categories that may be used to classify fruit organic acids (Ren et al., 2017). The majority of the organic acids found in loquat fruits are aliphatic carboxylic acids. Some examples of these types of acids are fumaric acid, ascorbic acid, and malic acid (Kumar et al., 2017; Batista-Silva et al., 2018; Sáenz-Galindo et al., 2018). In the present study, the optimized UPLC-MS method was used to detect fumaric acid, ascorbic acid, malic acid, *cis*-aconitic acid and acetic acid from the fruit pulp of loquat under the influence of foliar applied B. Among them, the content of malic acid accounted for about 70%-80% of the total acid. These results are in line with the previous findings about organic acid profile of loquat (2009; Chen et al., 2007; Yang et al., 2021). The composition and content of organic acids in loquat fruits have genetic variation (Famiani et al., 2015), and the differences are also manifested between different varieties (Chen et al., 2009). In present study, the cultivar "Jiefangzhong" was used as plant material which is already reported as high-acid cultivar (Chen et al., 2007; 2009; Ali et al., 2021a; Yang et al., 2021).

Fruits with intermediate acidity tend to be more palatable, but increasing acid content can often lower the quality of the fruit (Zhang et al., 2021). Organic acids build throughout fruit development and are utilised as respiratory substrates as the fruit ripens (Raza et al., 2022). The balance of organic acid production, membrane transit, and breakdown or use determines the ultimate organic acid content in ripened fruits (Sadka et al., 2000; Cercós et al., 2006; Sharma et al., 2022). In this process, malic acid metabolism-related enzymes including phospho*enol*pyruvate carboxylase (PEPC), NADP – dependent malic enzyme (NADP-ME), and NAD-malate dehydrogenase (NAD-MDH) may potentially play a role in fruit malic acid biosynthesis and degradation (Chen et al., 2009; Wu and Chen, 2016). The first step in the production of malic acid begins in the cytosol with phospho*enol*pyruvate (PEP), which is then actively transported into the mitochondria and transformed to oxaloacetate (OAA) by phospho*enol*pyruvate carboxylase (PEPC) (Tayal et al., 2022). Then, NAD-malate dehydrogenase (NAD-MDH) catalyses the condensation of OAA to produce malic acid. The cytosolic enzyme NADP - dependent malic enzyme (NADP-ME) catalyses the conversion of pyruvate to malic acid (Chen et al., 2009; Ma et al., 2019). According to these metabolic routes, malic acid is mostly synthesised by the catalytic activities of PEPC, NADP-ME and NAD-MDH (Wu and Chen, 2016; Zhou et al., 2019) (Figure 10B).

Because of the relevance and high quantity of malic acid in fruits, great progress has been made in determining the metabolism of malic acid in fruits. NAD-MDH activity is inversely linked to NADP-ME activity (Chen et al., 2009), indicating that NAD-MDH and NADP-ME may both play essential roles in malate production and degradation, respectively. Yang et al. (Yang et al., 2011) also cloned the genes encoding *EjPEPC*, *EjNADP-ME*, and *EjcyNAD-MDH*, and they discovered that the transcript level of *EjNADP-ME* in the high-acid cultivar was considerably greater than that in the low-acid cultivar, but *EjNADP-ME* and *EjmNAD-MDH* expression patterns were comparable in both cultivars, however *EjPEPC* and *EjcyNAD-MAD* expression patterns were different, suggesting that the expression of these genes may be crucial in controlling malic acid production in loquat fruit.

Due to coenzyme specificity, subcellular localization, and biochemical function, NAD-malic enzyme (NAD-ME) contributes 70-80% to malic acid accumulation (Rao and Dixon, 2016). In a recent study, it has been proved that *NAD-cytMDH* is a key gene that regulates the acidity of peach fruits (Etienne et al., 2002). The overexpression of *MdNAD-ME* genes significantly increased the content of malic acid in apple callus (Drincovich et al., 2001). It has been reported earlier that NADP-ME catalyzes the carboxylation of pyruvate and fixes $CO_2$ to produce malic acid in grapes (Sweetman et al., 2009). NADP-ME plays a major role in the degradation of malic acid in the cytoplasm, such as the content of organic acids in apple were negatively correlated with NADP-ME activity (Yao et al., 2009). The change in the activity of NAD-ME is consistent with the biosynthesis of malic acid, the increase in fruit respiration, and the gradual decrease of malic acid during fruit ripening (Khan et al., 2018). During storage of climacteric fruits e.g., apple, pear, banana, etc. the respiration increases, accompanied by accelerated degradation of malic acid (Farrar et al., 2000; Ruan, 2014). In the current study, the fruit malic acid content was significantly and positively correlated with *EjSS1*, *EjPEPC3*, *EjNAD-MDH1*, *EjNAD-MDH5*, *EjNAD-MDH8* and *EjNAD-MDH13*, while significantly ($p \leq 0.05$) negatively correlated with *EjSPS1-3*, *EjSS5*, *EjHK1,3*, *EjFK1,2,4, EjNAD-ME1,2*, and *NAD-MDH11*.

## Conclusions

The results of the current study suggest that fructose and malic acid are the predominant sugar and acid in fruit pulp of loquat, respectively. Among B treatments, 0.2% borax was the promising treatment to enhance soluble sugars and reduce malic acid concentration in fruit pulp of loquat. Boron treatments remarkably improved the soluble sugars content by regulating the activities of SPS, SS, HK and FK enzymes, and altering the expressions of related genes. The combined activity of many enzymes, including PEPC, NADP-ME, and NAD-MDH, was responsible for controlling the dynamics of the malic acid concentrations evaluated in the present investigation. Correlation analysis suggested that NAD-MDH played a vital role in the decrease of malic acid. These findings not only elucidated previously unknown aspects of the metabolism of soluble sugars and organic acids, but they also provide a significant resource for prospective studies on the application of molecular breeding techniques to loquat fruit.

## Data availability statement

The original contributions presented in the study are included in the article/Supplementary Material. Further inquiries can be directed to the corresponding authors.

## Author contributions

Conceptualization, MA, YH, and FC; Data curation, MA and RA; Funding acquisition, YH; Methodology, MA, AY, and FC; Supervision, YH and FC; Writing – original draft, MA; Writing – review & editing, RA, RR, SEj, SA, SEr, YH, and FC. All authors contributed to the article and approved the submitted version.

## Funding

This research was funded by Ministerial and Provincial Joint Innovation Centre for Safety Production of Cross-Strait Crops, Fujian Agriculture and Forestry University, Fuzhou 350002, China.

## Conflict of interest

The authors declare that the research was conducted in the absence of any commercial or financial relationships that could be construed as a potential conflict of interest.

## Publisher's note

All claims expressed in this article are solely those of the authors and do not necessarily represent those of their affiliated organizations, or those of the publisher, the editors and the reviewers. Any product that may be evaluated in this article, or claim that may be made by its manufacturer, is not guaranteed or endorsed by the publisher.

## Supplementary material

The Supplementary Material for this article can be found online at: https://www.frontiersin.org/articles/10.3389/fpls.2022.1039360/full#supplementary-material

## References

Abdullah, M., Cao, Y., Cheng, X., Meng, D., Chen, Y., Shakoor, A., et al. (2018). The sucrose synthase gene family in chinese pear (*Pyrus bretschneideri* rehd.): structure, expression, and evolution. *Molecules* 23, 1144. doi: 10.3390/molecules23051144

Ali, M. M., Alam, S. M., Anwar, R., Ali, S., Shi, M., Liang, D., et al. (2021a). Genome-wide identification, characterization and expression profiling of aluminum-activated malate transporters in *Eriobotrya japonica* lindl. *Horticulturae* 7, 441. doi: 10.3390/horticulturae7110441

Ali, M. M., Anwar, R., Shafique, M. W., Yousef, A. F., and Chen, F. (2021b). Exogenous application of mg, zn and b influences phyto-nutritional composition of leaves and fruits of loquat (*Eriobotrya japonica* lindl.). *Agronomy* 11, 224. doi: 10.3390/agronomy11020224

Ali, M., Ezz, T., Abd El-Megeed, N., and Flefil, M. (2019). Effect of foliar application with some micronutrients on 'Florida prince' cultivar peach tree. *J. Adv. Agric. Res.* 24, 410–425. doi: 10.21608/jalexu.2019.163473

Ali, M. M., Li, B., Zhi, C., Yousef, A. F., and Chen, F. (2021c). Foliar-supplied molybdenum improves phyto-nutritional composition of leaves and fruits of loquat (*Eriobotrya japonica* lindl.). *Agronomy* 11, 892. doi: 10.3390/agronomy11050892

Ali, M. M., Rizwan, H. M., Yousef, A. F., Zhi, C., and Chen, F. (2021d). Analysis of toxic elements in leaves and fruits of loquat by inductively coupled plasma-mass spectrometry (ICP-MS). *Acta Sci. Pol. Hortorum Cultus* 20, 33–42. doi: 10.24326/asphc.2021.5.4

Anees, M., Tahir, F. M., Shahzad, J., Mahmood, N., and Genetics, M. (2011). Effect of foliar application of micronutrients on the quality of mango (*Mangifera indica* l .) cv . dusehri fruit. *Mycopath* 9, 25–28.

Babu, K. D., and Yadav, D. S. (2005). Foliar spray of micronutrients for yield and quality improvement in khasi mandarin (*Citrus reticulata* blanco.). *Indian J. Hortic.* 62, 280–281.

Badenes, M. L., Canyamas, T., Romero, C., Soriano, J. M., Martínez, J., and Llácer, G. (2003). Genetic diversity in european collection of loquat (*Eriobotrya japonica* lindl.). *Acta Hortic.* 620, 169–174. doi: 10.17660/ActaHortic.2003.620.17

Basson, C. E., Groenewald, J.-H., Kossmann, J., Cronjé, C., and Bauer, R. (2010). Sugar and acid-related quality attributes and enzyme activities in strawberry fruits: Invertase is the main sucrose hydrolysing enzyme. *Food Chem.* 121, 1156–1162. doi: 10.1016/j.foodchem.2010.01.064

Batista-Silva, W., Nascimento, V. L., Medeiros, D. B., Nunes-Nesi, A., Ribeiro, D. M., Zsögön, A., et al. (2018). Modifications in organic acid profiles during fruit development and ripening: correlation or causation? *Front. Plant Sci.* 9. doi: 10.3389/fpls.2018.01689

Bermejo, A., and Cano, A. (2012). Analysis of nutritional constituents in twenty citrus cultivars from the mediterranean area at different stages of ripening. *Food Nutr. Sci.* 03, 639–650. doi: 10.4236/fns.2012.35088

Borsani, J., Budde, C. O., Porrini, L., Lauxmann, M. A., Lombardo, V. A., Murray, R., et al. (2009). Carbon metabolism of peach fruit after harvest: changes in enzymes involved in organic acid and sugar level modifications. *J. Exp. Bot.* 60, 1823–1837. doi: 10.1093/jxb/erp055

Broadley, M., Brown, P., Cakmak, I., Rengel, Z., and Zhao, F. (2012). "Function of nutrients," in *Marschner's mineral nutrition of higher plants* (Amsterdam, Netherlands:Elsevier), 191–248. doi: 10.1016/B978-0-12-384905-2.00007-8

Brown, P. H., Bellaloui, N., Wimmer, M. A., Bassil, E. S., Ruiz, J., Hu, H., et al. (2002). Boron in plant biology. *Plant Biol.* 4, 205–223. doi: 10.1055/s-2002-25740

Cercós, M., Soler, G., Iglesias, D. J., Gadea, J., Forment, J., and Talón, M. (2006). Global analysis of gene expression during development and ripening of citrus fruit flesh. a proposed mechanism for citric acid utilization. *Plant Mol. Biol.* 62, 513–527. doi: 10.1007/s11103-006-9037-7

Chen, F. X., Lin, Q. L., Liu, X. H., She, W. Q., Chen, L. S., and Wu, D. Y. (2007). Effects of magnetic field and fertilizations on organic acids in loquat fruit. *Acta Hortic.* 750, 355–360. doi: 10.17660/ActaHortic.2007.750.56

Chen, F., Liu, X., and Chen, L. (2009). Developmental changes in pulp organic acid concentration and activities of acid-metabolising enzymes during the fruit development of two loquat (*Eriobotrya japonica* lindl.) cultivars differing in fruit acidity. *Food Chem.* 114, 657–664. doi: 10.1016/j.foodchem.2008.10.003

Chen, Y., Zhang, Q., Hu, W., Zhang, X., Wang, L., Hua, X., et al. (2017). Evolution and expression of the fructokinase gene family in saccharum. *BMC Genomics* 18, 197. doi: 10.1186/s12864-017-3535-7

Dali, N., Michaud, D., and Yelle, S. (1992). Evidence for the involvement of sucrose phosphate synthase in the pathway of sugar accumulation in sucrose-accumulating tomato fruits. *Plant Physiol.* 99, 434–438. doi: 10.1104/pp.99.2.434

Damari-Weissler, H., Rachamilevitch, S., Aloni, R., German, M. A., Cohen, S., Zwieniecki, M. A., et al. (2009). *LeFRK2* is required for phloem and xylem differentiation and the transport of both sugar and water. *Planta* 230, 795–805. doi: 10.1007/s00425-009-0985-4

Davarpanah, S., Tehranifar, A., Davarynejad, G., Abadía, J., and Khorasani, R. (2016). Effects of foliar applications of zinc and boron nano-fertilizers on pomegranate (*Punica granatum* cv. ardestani) fruit yield and quality. *Sci. Hortic. (Amsterdam)* 210, 57–64. doi: 10.1016/j.scienta.2016.07.003

de Oliveira, R. H., Dias Milanez, C. R., Moraes-Dallaqua, M. A., and Rosolem, C. A. (2006). Boron deficiency inhibits petiole and peduncle cell development and reduces growth of cotton. *J. Plant Nutr.* 29, 2035–2048. doi: 10.1080/01904160600932617

De Rossi, S., Di Marco, G., Bruno, L., Gismondi, A., and Canini, A. (2021). Investigating the drought and salinity effect on the redox components of *Sulla coronaria* (L.) medik. *Antioxidants* 10, 1048. doi: 10.3390/antiox10071048

Drincovich, M. F., Casati, P., and Andreo, C. S. (2001). NADP-malic enzyme from plants: a ubiquitous enzyme involved in different metabolic pathways. *FEBS Lett.* 490, 1–6. doi: 10.1016/S0014-5793(00)02331-0

El-Sheikh, M. H., Khafgy, S. A. A., and Zaied, S. S. (2007). Effect of foliar application with some micronutrients on leaf mineral content, yield and fruit quality of Florida prince desert red peach trees. *J. Agric. Biol. Sci.* 3, 309–315.

Engels, C., Kirkby, E., and White, P. (2012). "Mineral nutrition, yield and source–sink relationships," in *Marschner's mineral nutrition of higher plants* (Amsterdam, Netherlands:Elsevier), 85–133. doi: 10.1016/B978-0-12-384905-2.00005-4

Etienne, C., Moing, A., Dirlewanger, E., Raymond, P., Monet, R., and Rothan, C. (2002). Isolation and characterization of six peach cDNAs encoding key proteins in organic acid metabolism and solute accumulation: involvement in regulating peach fruit acidity. *Physiol. Plant* 114, 259–270. doi: 10.1034/j.1399-3054.2002.1140212.x

Famiani, F., Battistelli, A., Moscatello, S., Cruz-Castillo, J. G., and Walker, R. P. (2015). The organic acids that are accumulated in the flesh of fruits: occurrence, metabolism and factors affecting their contents – a review. *Rev. Chapingo Ser. Hortic.* XXI, 97–128. doi: 10.5154/r.rchsh.2015.01.004

Farrar, J., Pollock, C., and Gallagher, J. (2000). Sucrose and the integration of metabolism in vascular plants. *Plant Sci.* 154, 1–11. doi: 10.1016/S0168-9452(99)00260-5

Fedorova, E. N., Varlamova, D. O., Kivero, A. D., Guk, K. D., and Ptitsyn, L. R. (2020). Ultra-performance liquid chromatography (UPLC) for the determination of organic acids – the intermediates of branched-chain amino acid biosynthesis in *Escherichia coli* strains. *J. Liq. Chromatogr. Relat. Technol.* 43, 844–851. doi: 10.1080/10826076.2020.1832894

Gan, X., Jing, Y., Shahid, M. Q., He, Y., Baloch, F. S., Lin, S., et al. (2020). Identification, phylogenetic analysis, and expression patterns of the SAUR gene family in loquat (*Eriobotrya japonica*). *Turkish J. Agric. For.* 44, 15–23. doi: 10.3906/tar-1810-98

German, M. A., Dai, N., Matsevitz, T., Hanael, R., Petreikov, M., Bernstein, N., et al. (2003). Suppression of fructokinase encoded by LeFRK2 in tomato stem inhibits growth and causes wilting of young leaves. *Plant J.* 34, 837–846. doi: 10.1046/j.1365-313X.2003.01765.x

Ghosh, S., Singh, U. K., Meli, V. S., Kumar, V., Kumar, A., Irfan, M., et al. (2013). Induction of senescence and identification of differentially expressed genes in tomato in response to monoterpene. *PloS One* 8, e76029. doi: 10.1371/journal.pone.0076029

Goldbach, H. E., Yu, Q., Wingender, R., Schulz, M., Wimmer, M., Findeklee, P., et al. (2001). Rapid response reactions of roots to boron deprivation. *J. Plant Nutr. Soil Sci.* 164, 173–181. doi: 10.1002/1522-2624(200104)164:2<173::AID-JPLN173>3.0.CO;2-F

Hortwitz, W. (1960). Official and tentative methods of analysis. *Assoc. Off. Anal. Chem. Washington U.S.A.*

Irfan, M., Ghosh, S., Kumar, V., Chakraborty, N., Chakraborty, S., and Datta, A. (2014). Insights into transcriptional regulation of -D-N-acetylhexosaminidase, an n-glycan-processing enzyme involved in ripening-associated fruit softening. *J. Exp. Bot.* 65, 5835–5848. doi: 10.1093/jxb/eru324

Irfan, M., Ghosh, S., Meli, V. S., Kumar, A., Kumar, V., Chakraborty, N., et al. (2016). Fruit ripening regulation of α-mannosidase expression by the MADS box transcription factor RIPENING INHIBITOR and ethylene. *Front. Plant Sci.* 7. doi: 10.3389/fpls.2016.00010

Irfan, M., Kumar, P., Ahmad, I., and Datta, A. (2021). Unraveling the role of tomato bcl-2-associated athanogene (BAG) proteins during abiotic stress response and fruit ripening. *Sci. Rep.* 11, 21734. doi: 10.1038/s41598-021-01185-7

Irfan, M., Kumar, P., Kumar, V., and Datta, A. (2022). Fruit ripening specific expression of β-D-N-acetylhexosaminidase (β-hex) gene in tomato is transcriptionally regulated by ethylene response factor SlERF.E4. *Plant Sci.* 323, 111380. doi: 10.1016/j.plantsci.2022.111380

Jiang, C.-C., Fang, Z.-Z., Zhou, D.-R., Pan, S.-L., and Ye, X.-F. (2019). Changes in secondary metabolites, organic acids and soluble sugars during the development of plum fruit cv. 'Furongli' (*Prunus salicina* lindl). *J. Sci. Food Agric.* 99, 1010–1019. doi: 10.1002/jsfa.9265

Kakita, H., Kamishima, H., Komiya, K., and Kato, Y. (2002). Simultaneous analysis of monosaccharides and oligosaccharides by high-performance liquid chromatography with postcolumn fluorescence derivatization. *J. Chromatogr. A* 961, 77–82. doi: 10.1016/S0021-9673(02)00655-6

Karadeniz, T., Şenyurt, M., and Bak, T. (2012). Loquat as a source of nectar and pollen in the winter for beekeeping. *Sci. Pap. - Ser. B Hortic.* 56, 319–322. doi: 10.13140/RG.2.1.1796.6567

Khan, A. S., Singh, Z., and Ali, S. (2018). "Postharvest biology and technology of plum," in *Postharvest biology and technology of temperate fruits* (Cham: Springer International Publishing), 101–145. doi: 10.1007/978-3-319-76843-4_5

Kumar, V., Irfan, M., and Datta, A. (2019). Manipulation of oxalate metabolism in plants for improving food quality and productivity. *Phytochemistry* 158, 103–109. doi: 10.1016/j.phytochem.2018.10.029

Kumar, V., Irfan, M., Ghosh, S., Chakraborty, N., Chakraborty, S., and Datta, A. (2016). Fruit ripening mutants reveal cell metabolism and redox state during ripening. *Protoplasma* 253, 581–594. doi: 10.1007/s00709-015-0836-z

Kumari, C., Sharma, M., Kumar, V., Sharma, R., Kumar, V., Sharma, P., et al. (2022). Genome editing technology for genetic amelioration of fruits and vegetables for alleviating post-harvest loss. *Bioengineering* 9, 176. doi: 10.3390/bioengineering9040176

Kumar, V., Sharma, A., Bhardwaj, R., and Thukral, A. K. (2017). Analysis of organic acids of tricarboxylic acid cycle in plants using GC-MS, and system modeling. *J. Anal. Sci. Technol.* 8, 20. doi: 10.1186/s40543-017-0129-6

Langenkämper, G., Fung, R. W. M., Newcomb, R. D., Atkinson, R. G., Gardner, R. C., and MacRae, E. A. (2002). Sucrose phosphate synthase genes in plants belong to three different families. *J. Mol. Evol.* 54, 322–332. doi: 10.1007/s00239-001-0047-4

LaRue, R. G. (2020) *Loquat fact sheet. fruit nut res. inf. center, univ. calif.* Available at: http://fruitsandnuts.ucdavis.edu/dsadditions/Loquat_Fact_Sheet/ (Accessed January 30, 2020).

Li, M., Feng, F., and Cheng, L. (2012). Expression patterns of genes involved in sugar metabolism and accumulation during apple fruit development. *PloS One* 7, e33055. doi: 10.1371/journal.pone.0033055

Li, S., Liu, X., Xie, X., Sun, C., Grierson, D., Yin, X., et al. (2015b). *CrMYB73* , a PH -like gene, contributes to citric acid accumulation in citrus fruit. *Sci. Hortic. (Amsterdam)* 197, 212–217. doi: 10.1016/j.scienta.2015.09.037

Liu, J., Guo, S., He, H., Zhang, H., Gong, G., Ren, Y., et al. (2013). Dynamic characteristics of sugar accumulation and related enzyme activities in sweet and non-sweet watermelon fruits. *Acta Physiol. Plant* 35, 3213–3222. doi: 10.1007/s11738-013-1356-0

Liu, S., Liu, Y., Liu, N., Zhang, Y., Zhang, Q., Xu, M., et al. (2016). Sugar and organic acid components in fruits of plum cultivar resources of genus prunus. *Sci. Agric. Sin.* 49, 3188–3198. doi: 10.3864/j.issn.0578-1752.2016.16.012

Livak, K. J., and Schmittgen, T. D. (2001). Analysis of relative gene expression data using real-time quantitative pcr and the $2^{-\Delta\Delta CT}$ method. *Methods* 25, 402–408. doi: 10.1006/meth.2001.1262

Li, P., Wu, W., Chen, F., Liu, X., Lin, Y., and Chen, J. (2015a). *Prunus salicina* 'Crown', a yellow-fruited chinese plum. *HortScience* 50, 1822–1824. doi: 10.21273/HORTSCI.50.12.1822

Lo Bianco, R., Rieger, M., and Sung, S.-J. S. (2000). Effect of drought on sorbitol and sucrose metabolism in sinks and sources of peach. *Physiol. Plant* 108, 71–78. doi: 10.1034/j.1399-3054.2000.108001071.x

Maity, A., Gaikwad, N., Babu, K. D., Sarkar, A., and Patil, P. (2021). Impact of zinc and boron foliar application on fruit yield, nutritional quality and oil content of three pomegranate (*Punica granatum* l.) cultivars. *J. Plant Nutr.* 44, 1841–1852. doi: 10.1080/01904167.2021.1884711

Ma, B., Liao, L., Fang, T., Peng, Q., Ogutu, C., Zhou, H., et al. (2019). A *Ma10* gene encoding p-type ATPase is involved in fruit organic acid accumulation in apple. *Plant Biotechnol. J.* 17, 674–686. doi: 10.1111/pbi.13007

Marschner, H. (1995). *Mineral nutrition of higher plants. 2nd edition* (Gt. Britain: Acad).

Moriguchi, T., Abe, K., Sanada, T., and Yamaki, S. (1992). Levels and role of sucrose synthase, sucrose-phosphate synthase, and acid invertase in sucrose accumulation in fruit of asian pear. *J. Am. Soc Hortic. Sci.* 117, 274–278. doi: 10.21273/JASHS.117.2.274

Munhoz, C. F., Santos, A. A., Arenhart, R. A., Santini, L., Monteiro-Vitorello, C. B., and Vieira, M. L. C. (2015). Analysis of plant gene expression during passion fruit- *Xanthomonas axonopodis* interaction implicates lipoxygenase 2 in host defence. *Ann. Appl. Biol.* 167, 135–155. doi: 10.1111/aab.12215

Nour, V., Trandafir, I., and Ionica, M. E. (2010). Organic acid analysis in different citrus juices under reversed phase conditions. *Not. Bot. Horti. Agrobot. Cluj-Napoca* 38, 44–48. doi: 10.15835/nbha3814569

Pan, T., Ali, M. M., Gong, J., She, W., Pan, D., Guo, Z., et al. (2021). Fruit physiology and sugar-acid profile of 24 pomelo (*Citrus grandis* (L.) osbeck) cultivars grown in subtropical region of china. *Agronomy* 11, 2393. doi: 10.3390/agronomy11122393

Pancera, S. M., Gliemann, H., Schimmel, T., and Petri, D. F. S. (2006). Adsorption behavior and activity of hexokinase. *J. Colloid Interface Sci.* 302, 417–423. doi: 10.1016/j.jcis.2006.06.066

Papagianni, M., and Avramidis, N. (2011). *Lactococcus lactis* as a cell factory: A twofold increase in phosphofructokinase activity results in a proportional increase in specific rates of glucose uptake and lactate formation. *Enzyme Microb. Technol.* 49, 197–202. doi: 10.1016/j.enzmictec.2011.05.002

Rao, X., and Dixon, R. A. (2016). The differences between NAD-ME and NADP-ME subtypes of $C_4$ photosynthesis: more than decarboxylating enzymes. *Front. Plant Sci.* 7. doi: 10.3389/fpls.2016.01525

Raza, A., Salehi, H., Rahman, M. A., Zahid, Z., Madadkar, H. M., Najafi-Kakavand, S., et al. (2022). Plant hormones and neurotransmitter interactions mediate antioxidant defenses under induced oxidative stress in plants. *Front. Plant Sci.* 13. doi: 10.3389/fpls.2022.961872

Ren, J.-N., Tai, Y.-N., Dong, M., Shao, J.-H., Yang, S.-Z., Pan, S.-Y., et al. (2015). Characterisation of free and bound volatile compounds from six different varieties of citrus fruits. *Food Chem.* 185, 25–32. doi: 10.1016/j.foodchem.2015.03.142

Ren, M., Wang, X., Tian, C., Li, X., Zhang, B., Song, X., et al. (2017). Characterization of organic acids and phenolic compounds of cereal vinegars and fruit vinegars in China. *J. Food Process. Preserv.* 41, e12937. doi: 10.1111/jfpp.12937

Renz, A., and Stitt, M. (1993). Substrate specificity and product inhibition of different forms of fructokinases and hexokinases in developing potato tubers. *Planta* 190, 166–175. doi: 10.1007/BF00196608

Ribani, M., Bottoli, C. B. G., Collins, C. H., Jardim, I. C. S. F., and Melo, L. F. C. (2004). Validation for chromatographic and electrophoretic methods. *Quim. Nova* 27, 771–780. doi: 10.1590/S0100-40422004000500017

Ruan, Y.-L. (2014). Sucrose metabolism: gateway to diverse carbon use and sugar signaling. *Annu. Rev. Plant Biol.* 65, 33–67. doi: 10.1146/annurev-arplant-050213-040251

Ruffner, H. P., Possner, D., Brem, S., and Rast, D. M. (1984). The physiological role of malic enzyme in grape ripening. *Planta* 160, 444–448. doi: 10.1007/BF00429761

Sadka, A., Dahan, E., Cohen, L., and Marsh, K. B. (2000). Aconitase activity and expression during the development of lemon fruit. *Physiol. Plant* 108, 255–262. doi: 10.1034/j.1399-3054.2000.108003255.x

Sáenz-Galindo, A., López-López, L. I., Cruz-Duran, F. N., de la, Castañeda-Facio, A. O., Rámirez-Mendoza, L. A., Córdova-Cisneros, K. C., et al. (2018). "Applications of carboxylic acids in organic synthesis, nanotechnology and polymers," in *Carboxylic acid - key role in life sciences* (London, United Kingdom:InTech). doi: 10.5772/intechopen.74654

Schrader, S., and Sauter, J. J. (2002). Seasonal changes of sucrose-phosphate synthase and sucrose synthase activities in poplar wood (*Populus* × *canadensis* moench ' robusta ') and their possible role in carbohydrate metabolism. *J. Plant Physiol.* 159, 833–843. doi: 10.1078/0176-1617-00730

Sharma, S., Shree, B., Aditika,, Sharma, A., Irfan, M., and Kumar, P. (2022). Nanoparticle-based toxicity in perishable vegetable crops: Molecular insights, impact on human health and mitigation strategies for sustainable cultivation. *Environ. Res.* 212, 113168. doi: 10.1016/j.envres.2022.113168

Sheng, O., Song, S. W., Chen, Y. J., Peng, S. A., and Deng, X. X. (2009). Effects of exogenous b supply on growth, b accumulation and distribution of two navel orange cultivars. *Trees* 23, 59. doi: 10.1007/s00468-008-0254-3

Spampinato, C. P., Colombo, S. L., and Andreo, C. S. (1994). Interaction of analogues of substrate with NADP-malic enzyme from maize leaves. *Photosynth. Res.* 39, 67–73. doi: 10.1007/BF00027144

Stein, O., and Granot, D. (2019). An overview of sucrose synthases in plants. *Front. Plant Sci.* 10. doi: 10.3389/fpls.2019.00095

Subedi, A., Shrestha, A. K., Tripathi, K. M., and Shrestha, B. (2019). Effect of foliar spray of boron and zinc on fruit quality of papaya (*Carica papaya* l.) cv. red lady in chitwan, Nepal. *Int. J. Hortic* 9, 10–14. doi: 10.5376/ijh.2019.09.0002

Sweetman, C., Deluc, L. G., Cramer, G. R., Ford, C. M., and Soole, K. L. (2009). Regulation of malate metabolism in grape berry and other developing fruits. *Phytochemistry* 70, 1329–1344. doi: 10.1016/j.phytochem.2009.08.006

Tayal, R., Kumar, V., and Irfan, M. (2022). Harnessing the power of hydrogen sulphide (H 2 s) for improving fruit quality traits. *Plant Biol.* 24, 594–601. doi: 10.1111/plb.13372

Tian, S., Qin, G., and Li, B. (2011). "Loquat," in *Postharvest biology and technology of tropical and subtropical fruits* (Sawston, Cambridge:Woodhead Publishing), vol. 444. doi: 10.1016/B978-1-84569-735-8.50017-6

Toker, R., Gölükcü, M., Tokgöz, H., and Tepe, S. (2013). Organic acids and sugar compositions of some loquat cultivars (*Eriobotrya japonica* l.) grown in Turkey. *Tarım Bilim. Derg.* 19, 121–128. doi: 10.1501/Tarimbil_0000001236

Wang, Z., Wei, P., Wu, M., Xu, Y., Li, F., Luo, Z., et al. (2015). Analysis of the sucrose synthase gene family in tobacco: structure, phylogeny, and expression patterns. *Planta* 242, 153–166. doi: 10.1007/s00425-015-2297-1

Wei, Y., Xu, F., and Shao, X. (2017). Changes in soluble sugar metabolism in loquat fruit during different cold storage. *J. Food Sci. Technol.* 54, 1043–1051. doi: 10.1007/s13197-017-2536-5

Wiesler, F. (2012). "Nutrition and quality," in *Marschner's mineral nutrition of higher plants* (Amsterdam, NetherlandsElsevier), 271–282. doi: 10.1016/B978-0-12-384905-2.00009-1

Wu, W., and Chen, F. (2016). Malate transportation and accumulation in fruit cell. *Endocytobiosis Cell Res.* 27, 107–112.

Xu, L., Xu, H., Cao, Y., Yang, P., Feng, Y., Tang, Y., et al. (2017). Validation of reference genes for quantitative real-time pcr during bicolor tepal development in asiatic hybrid lilies (*Lilium* spp.). *Front. Plant Sci.* 8. doi: 10.3389/fpls.2017.00669

Xu, X., Yang, Y., Liu, C., Sun, Y., Zhang, T., Hou, M., et al. (2019). The evolutionary history of the sucrose synthase gene family in higher plants. *BMC Plant Biol.* 19, 566. doi: 10.1186/s12870-019-2181-4

Yang, L. T., Xie, C. Y., Jiang, H. X., and Chen, L. S. (2011). Expression of six malate-related genes in pulp during the fruit development of two loquat (*Eriobotrya japonica*) cultivars differing in fruit acidity. *Afr. J. Biotechnol.* 10, 2414–2422. doi: 10.4314/ajb.v10i13

Yang, J., Zhang, J., Niu, X.-Q., Zheng, X.-L., Chen, X., Zheng, G.-H., et al. (2021). Comparative transcriptome analysis reveals key genes potentially related to organic acid and sugar accumulation in loquat. *PloS One* 16, e0238873. doi: 10.1371/journal.pone.0238873

Yao, Y.-X., Li, M., Liu, Z., You, C.-X., Wang, D.-M., Zhai, H., et al. (2009). Molecular cloning of three malic acid related genes *MdPEPC*, *MdVHA-a*, *MdcyME* and their expression analysis in apple fruits. *Sci. Hortic. (Amsterdam)* 122, 404–408. doi: 10.1016/j.scienta.2009.05.033

Yao, Y.-X., Li, M., Zhai, H., You, C.-X., and Hao, Y.-J. (2011). Isolation and characterization of an apple cytosolic malate dehydrogenase gene reveal its function in malate synthesis. *J. Plant Physiol.* 168, 474–480. doi: 10.1016/j.jplph.2010.08.008

Yu, X., Ali, M. M., Li, B., Fang, T., and Chen, F. (2021). Transcriptome data-based identification of candidate genes involved in metabolism and accumulation of soluble sugars during fruit development in 'Huangguan' plum. *J. Food Biochem.* 45, e13878. doi: 10.1111/jfbc.13878

Zaman, Q. U., and Schumann, A. W. (2006). Nutrient management zones for citrus based on variation in soil properties and tree performance. *Precis. Agric.* 7, 45–63. doi: 10.1007/s11119-005-6789-z

Zhang, Y., Hu, C.-X., Tan, Q.-L., Zheng, C.-S., Gui, H.-P., Zeng, W.-N., et al. (2014). Plant nutrition status, yield and quality of satsuma mandarin (*Citrus unshiu* marc.) under soil application of fe-EDDHA and combination with zinc and manganese in calcareous soil. *Sci. Hortic. (Amsterdam)* 174, 46–53. doi: 10.1016/j.scienta.2014.05.005

Zhang, Y. H., Wang, Z. M., Huang, Q., and Shu, W. (2008). Phospho*enol*pyruvate carboxylase activity in ear organs is related to protein concentration in grains of winter wheat. *J. Cereal Sci.* 47, 386–391. doi: 10.1016/j.jcs.2007.04.011

Zhang, X., Wei, X., Ali, M. M., Rizwan, H. M., Li, B., Li, H., et al. (2021). Changes in the content of organic acids and expression analysis of citric acid accumulation-related genes during fruit development of yellow (*Passiflora edulis* f. flavicarpa) and purple (*Passiflora edulis* f. edulis) passion fruits. *Int. J. Mol. Sci.* 22, 5765. doi: 10.3390/ijms22115765

Zhao, D., and Oosterhuis, D. M. (2002). Cotton carbon exchange, nonstructural carbohydrates, and boron distribution in tissues during development of boron deficiency. *F. Crop Res.* 78, 75–87. doi: 10.1016/S0378-4290(02)00095-3

Zheng, S., Johnson, A. J., Li, Y., Chu, C., and Hulcr, J. (2019). *Cryphalus eriobotryae* sp. nov. (Coleoptera: Curculionidae: Scolytinae), a new insect pest of loquat *Eriobotrya japonica* in China. *Insects* 10, 180. doi: 10.3390/insects10060180

Zhi, C., Ali, M. M., Zhang, J., Shi, M., Ma, S., and Chen, F. (2021). Effect of paper and aluminum bagging on fruit quality of loquat (*Eriobotrya japonica* lindl.). *Plants* 10, 2704. doi: 10.3390/plants10122704

Zhou, D., Chen, S., Xu, R., Tu, S., and Tu, K. (2019). Interactions among chilling tolerance, sucrose degradation and organic acid metabolism in UV-c-irradiated peach fruit during postharvest cold storage. *Acta Physiol. Plant* 41, 79. doi: 10.1007/s11738-019-2871-4

Zhou, L., and Paull, R. E. (2001). Sucrose metabolism during papaya (*Carica papaya*) fruit growth and ripening. *J. Am. Soc Hortic. Sci.* 126, 351–357. doi: 10.21273/JASHS.126.3.351

Zhu, Q., Gao, P., Liu, S., Zhu, Z., Amanullah, S., Davis, A. R., et al. (2017). Comparative transcriptome analysis of two contrasting watermelon genotypes during fruit development and ripening. *BMC Genomics* 18, 3. doi: 10.1186/s12864-016-3442-3

frontiers | Frontiers in Plant Science

TYPE Original Research
PUBLISHED 03 November 2022
DOI 10.3389/fpls.2022.1021297



OPEN ACCESS

EDITED BY
Mohammad Irfan,
Cornell University, United States

REVIEWED BY
Rajeev Ranjan,
Purdue University, United States
Shiv Tiwari, Intrexon, United States

*CORRESPONDENCE
Vijay Gahlaut
zone4vijay@gmail.com
Vandana Jaiswal
vandana@ihbt.res.in

†These authors have contributed equally to this work and share first authorship

SPECIALTY SECTION
This article was submitted to Plant Breeding, a section of the journal Frontiers in Plant Science

RECEIVED 17 August 2022
ACCEPTED 20 October 2022
PUBLISHED 03 November 2022

CITATION
Gangwar H, Kumari P, Gahlaut V, Kumar S and Jaiswal V (2022) Identification and comprehensive analysis of MIPSs in Rosaceae and their expression under abiotic stresses in rose (*Rosa chinensis*). *Front. Plant Sci.* 13:1021297. doi: 10.3389/fpls.2022.1021297



# Identification and comprehensive analysis of MIPSs in Rosaceae and their expression under abiotic stresses in rose (*Rosa chinensis*)

Himanshi Gangwar[1,2†], Priya Kumari[1,2†], Vijay Gahlaut[1,2*], Sanjay Kumar[1,2] and Vandana Jaiswal[1,2*]

[1]Biotechnology Division, CSIR-Institute of Himalayan Bioresource Technology, Palampur, Himachal Pradesh, India, [2]Academy of Scientific and Innovative Research (AcSIR), Ghaziabad, India

The Myo-Inositol-1-phosphate synthase (MIPS) gene family is involved in the myo-inositol synthesis and plays a significant role in signal transduction, membrane biogenesis, oligosaccharides synthesis, auxin storage and transport, programmed cell death and abiotic stress tolerance in plants. This study comprehensively identified the MIPS genes in Rosaceae plant species, and 51 MIPS genes were identified from 26 Rosaceae species. The phylogenetic analysis divided the MIPSs into two clades (clade I; subfamily *Amygdaloideae* specific, and clade II; subfamily *Rosoideae* specific). MIPS genes of all 26 Rosaceae species consist of similar gene structure, motif and domain composition, which shows their conserved nature. The cis-regulatory elements (CREs) analysis revealed that most *Rosaceae* MIPS genes play a role in growth, development, and stress responses. Furthermore, the qRT-PCR analysis also revealed the involvement of *RcMIPS* gene in plant development and response to abiotic stresses, including drought and heat. The results of the present study contribute to the understanding of the biological function of Rosaceae MIPS genes, and that could be used in further functional validations.

KEYWORDS

**myo-inositol 1-phosphate synthase, phylogenetic analysis, gene structure, *cis*-elements, drought stress**

## Introduction

The Myo-inositol phosphate synthase (MIPS) is a key enzyme in the myo-inositol biosynthesis pathway, that produces myo-inositol (Loewus and Loewus, 1980). Myo-inositol is an important component that regulates plant growth and development processes (Martin, 1998), membrane biogenesis (Roth, 2004), oligosaccharides

synthesis (Karner et al., 2004), auxin storage and transport (Abreu and Aragao, 2007), programmed cell death (Meng et al., 2009), phytic acid biosynthesis (Ali et al., 2013), etc.

MIPS enzymes have been ubiquitously found in a wide range of organisms, including higher plants and animals, parasites, fungi, green algae, bacteria, and archaea, and it is thought to be a primordial protein/gene (Majumder et al., 1997). Recent reports have also specified its functional diversity and shared evolutionary clues from archaea to higher plants and animals (Majumder et al., 2003). A genome-wide investigation of MIPS copies in plant kingdom was carried out to unveil the mystery of sequence conservation and divergence (Hazra et al., 2019). MIPS evolved from a single common algal ancestor to seed plants, and functional diversification is perhaps controlled by genomic variations. The differences in the number and properties of MIPS genes result from tandem, block, whole genome duplication and subsequent divergence. Different MIPS gene variants acquired distinct functions during duplication and speciation events (Hazra et al., 2019).

Additionally, MIPSs are also involved in abiotic stress regulation in plants (Taji et al., 2006; Kaur et al., 2013; Tan et al., 2013; Sharma et al., 2020; Alok et al., 2022). For instance, under NaCl treatment, salt-resistant rice varieties (*Oryza sativa* L.) show increased activity of the chloroplast version of MIPS either at the seedling stage or on fully grown plants (Raychaudhuri and Majumder, 1996). The expression of wheat *TaMIPS2* was induced in various developmental seed stages during heat stress treatment. Unfertilized ovaries also showed greater *TaMIPS2* transcript levels, with considerable quantities remaining during the recovery phase, indicating that MIPS is important for heat stress recovery and flower development (Khurana et al., 2012). The expression of the *MfMIPS1* gene was induced by salt and drought stresses in *Medicago falcata*. The overexpressed *MfMIPS1* tobacco lines have increased levels of Myo-inositol, leading to enhanced tolerance to multiple abiotic stress, i.e., cold, salt and drought stress (Tan et al., 2013). The *IbMIPS1* overexpressed lines of sweet potato also exhibited increased salt and drought tolerance (Zhai et al., 2016). Recently, it was shown that *MdMIPS1* overexpressing apple lines showed enhanced drought stress tolerance (Hu et al., 2022). The above studies suggested that the *MIPS* genes were involved in the regulation of various abiotic stresses in plants.

The MIPS genes have been investigated thoroughly in several plant species, including the model plant Arabidopsis (Johnson and Sussex, 1995), maize (Larson and Raboy, 1999), sesame (Chun et al., 2003), rice (Feng and Yoshida, 2004), soybean (Kumari et al., 2012), wild rice; *Porteresia coarctata* (Basak et al., 2018), cotton (Ma et al., 2019), and oat (Qin et al., 2021). Compared with other species, studies on the characterization of MIPS genes and their function in growth and abiotic stress regulation in the *Rosaceae* family are limited. Therefore, in this study, we comprehensively analysed the distribution of MIPS genes in 26 different species of the *Rosaceae* family. We also characterized the MIPS gene with respect to its exon-intron structure, motif analysis, conserved domain, phylogenetic relationship, cis-regulatory elements, and gene ontology. Furthermore, the expression pattern of the rose *MIPS* gene was also performed in different tissues and response to the drought and heat stresses using qRT-PCR analysis. Altogether, this comprehensive information on MIPS genes of *Rosaceae* could be used for further functional validation and also provide insight into their functional role during abiotic stresses in roses.

# Materials and methods

## Sequence retrieval and identification of MIPSs in Rosaceae family

The genome sequences of 26 Rosaceae species available at the Genome Database for Rosaceae (GDR) (https://www.rosaceae.org; Jung et al., 2019) were utilized for the annotation and identification of the MIPS genes (more details were provided in Table S1). The three Arabidopsis MIPS protein sequences (IDs: AT2G22240, AT4G39800 and AT5G10170) were retrieved from the TAIR database (https://www.arabidopsis.org/) used as a query in the BLASTp program (e-value < $1\times 10^{-5}$) to obtain MIPSs of the *Rosaceae*. Following that, all MIPS proteins were further verified for the presence of MIPS signature domains (NAD_5 Binding; PF07994 and Inos-1-P Synth; PF01658) using the Pfam database (http://pfam.xfam.org; El-Gebali et al., 2019). The molecular characteristics (aa length, molecular weight and isoelectric point) were predicted using the online tool ExPASy (http://web.expasy.org/; Artimo et al., 2012).

## Multiple sequence alignments and phylogenetic analysis of MIPSs

Using the MUSCLE package available in MEGA X software (Stecher et al., 2020), all 51 MIPS protein sequences representing 26 *Rosaceae* species were aligned. The phylogenetic tree was created using the maximum-likelihood (ML) method with Poisson model, pair-wise deletion and 1000 bootstraps in MEGA X software. The web programme iTOL (Letunic and Bork, 2007) has been used to visualize the phylogenetic tree.

## Gene structure and motif analysis of MIPSs

The exon-intron structure of the MIPS gene was determined using the online server GSDS 2.0 (Gene Structure and Display server 2.0; http://gsds.cbi.pku.edu.cn/Gsds_abou.php). The conserved motif was predicted by using the Motif Elicitation

(MEME) program with the parameter set to find 20 motifs (http://meme-suit.org; Bailey et al., 2015) and visualize the structure using the TBtool software (Chen et al., 2020).

## *Cis*-regulatory elements analysis

To analyze the *cis* regulatory elements (CREs) of MIPSs, the upstream sequences (2,000 bp) of the start codon were fetched from the GDR database. The CREs were identified in MIPS genes using the PlantCARE online server (Lescot et al., 2002).

## Nuclear localization signals, subcellular localization and GO analysis

The NLS in MIPS were predicted using the web tool cNLS Mapper (Kosugi et al., 2009). Using the WoLF PSOPT II online resource (https://www.genscript.com/wolf-psort.html?src=leftbar), the subcellular localization of Rosaceae MIPSs was predicted. The rose MIPS gene ID were subjected to the ShinyGO v0.75 database (Ge et al., 2020) to obtain gene ontology (GO) annotation.

## Plant material and stress treatment

In this study, the rose genotype (*Rosa chinensis*) was used. The plants were grown in plastic pots containing soil, peat, and sand mixed in a ratio of 1:2:1 and under greenhouse conditions (photoperiod=14 h light/10 h dark and temperature=22 ± 2°C) for the expression analysis of the *RcMIPS* gene. For tissue-specific expression analysis, the following tissues, stem, leaf, bud and flower tissues were harvested at the flowering stage. To impose the heat stress (HS), plants were kept at 42°C for 24 h. For drought stress (DS) treatment, we irrigated the plants with 20% PEG 6000. Leaf samples were harvested at the following different times: 0h, 6h, 12h and 24h for both HS and DS. During the experiment, the control tissues were collected from the unstressed plants. In addition, we collected apple (*Malus domestica*) stem and leaf tissues for *MdMIPS* tissue-specific expression analyses. All of the tissues were collected in three biological replications and kept at -80°C till further use.

## RNA isolation and quantitative real-time PCR

The PureLinkTMRNA Mini Kit (Invitrogen) was used to isolate total RNA according to the manufacturer's instructions. Then total RNA was converted to cDNA using Thermo Scientific's Verso cDNA Synthesis Kit. In the QuantStudio 3 applied biosystems Real-Time PCR System, quantitative RT-PCR (qRT-PCR) was performed using SYBR green master mix (Applied Biosystems, Foster City, USA). ApE–A plasmid Editor (https://jorgensen.biology.utah.edu/wayned/ape/) was used to generate primers for the specified *RcMIPS*; Forward primer–AGGAGGAACACTTTGATTGGTGG and Reverse primer–GGTTTGTGGAGCTGAAAGGTTC. As an internal control, the housekeeping gene *RcActin* (RchiOBHm_Chr1g0322051) was employed. For expression of *MdMIPS*, Forward primer–ACAACTACGAGACCACCGAG and Reverse primer–GTGAGGGTTGAGCCATTGTT, as well as an internal control *nad5*, was used (Menzel et al., 2002). Each sample received three biological replicates and three technical replicates for qRT-PCR. The 2−ΔΔCt technique was used to determine the relative expression level of *RcMIPS* gene (Livak and Schmittgen, 2001).

# Results

## Distribution of MIPS genes in Rosaceae family

The genome-wide search through BLASTp searches and verification of the 26 Rosaceae species reference genomes identified a total of 51 MIPS genes (Table 1). These 26 species belong to two Rosaceae subfamilies (*Amygdaloideae* and *Rosoideae*). The genes were then named based on the reported genes in Arabidopsis and their chromosome location from top to bottom. The length of the *Rosaceae MIPS* gene ranged from 1042 (*MbMIPS3*) to 4079 bp (*FnMIPS*), and the average length was 2810 bp. The protein length ranged from 197aa (*MbMIPS2*) to 585 aa (*PpyMIPS2*), and the average length was 492 aa. The predicted molecular weight of Rosaceae MIPS protein varied from 22.0 kDa (*MdMIPS2*) to 64.6 kDa (*PpyMIPS2*), and the average molecular weight was 54.2 kDa. As shown in Table 1, there are variations in the number of MIPS genes among 26 *Rosaceae* species, it ranges from one (14 species see Table 1) to six (*Pyrus bretschneideri*). However, most of *Rosaceae* species (14 out of 26) were found to have single copy of MIPS gene and some have multiple copies like *Gillenia trifoliata* (2), *Malus domestica* (3), *Malus sieversii* (4), *Prunus domestica* (5), and *Pyrus bretschneideri* (6). To find out the reason behind the expansion of *Rosaceae* MIPS genes, we looked at gene duplication events in different *Rosaceae* genomes. A total of 43 pairs of duplications were found in the 26 *Rosaceae* species (for details see Table S2). We also calculated Ka/Ks value for duplicated gene pairs, the Ka/Ks values for all gene pairs were less than 1, with an average of 0.185 (Table S2). These results

TABLE 1 Detailed information of *MIPS* genes from 26 Rosaceae plant species.

| Subfamily/Plant species | Gene name | Gene ID | Chromosome; location* | Gene length (bp) | E | Protein | | |
|---|---|---|---|---|---|---|---|---|
| | | | | | | L | pI | MW(KDa) |
| **Amygdaloideae** | | | | | | | | |
| *Gillenia trifoliata* | *GtMIPS1* | Gtrc1702g28691.t1 | contig_1702_RaGOO; 37185 | 1625 | 8 | 200 | 8.15 | 22.21 |
| | *GtMIPS2* | Gtr09g3310.t1 | 9; 4198065 | 2422 | 8 | 510 | 5.70 | 56.13 |
| *Malus baccata* | *MbMIPS1* | MABA000009 | scaffold1; 236392 | 3061 | 8 | 510 | 5.81 | 56.17 |
| | *MbMIPS2* | MABA026953 | scaffold531; 444372 | 3968 | 5 | 197 | 5.05 | 22.00 |
| | *MbMIPS3* | MABA045782 | scaffold7500; 1 | 1042 | 3 | 228 | 6.06 | 24.64 |
| *Malus domestica* | *MdMIPS1* | Mdg_01B002770 | 1B; 9309046 | 2499 | 8 | 511 | 5.51 | 56.17 |
| | *MdMIPS2* | Mdg_01A002870 | 1A; 10195884 | 2683 | 8 | 511 | 5.51 | 56.17 |
| | *MdMIPS3* | Mdg_15A031080 | 15A; 36243538 | 2463 | 8 | 511 | 5.51 | 56.17 |
| *Malus sieversii* | *MsiMIPS1* | Msi_01B002550 | 1B; 9466735 | 2500 | 8 | 511 | 5.51 | 56.17 |
| | *MsiMIPS2* | Msi_01A002550 | 1A; 10121248 | 2498 | 8 | 511 | 5.51 | 56.17 |
| | *MsiMIPS3* | Msi_15A029500 | 15A; 36274631 | 2463 | 8 | 511 | 5.70 | 56.16 |
| | *MsiMIPS4* | Msi_15B030020 | 15B; 37382931 | 2463 | 8 | 511 | 5.81 | 56.17 |
| *Malus sylvestris* | *MsyMIPS1* | Msy_01A002440 | 1A; 9097312 | 2491 | 8 | 511 | 5.51 | 56.17 |
| | *MsyMIPS2* | Msy_01B002610 | 1B; 9839865 | 2493 | 8 | 511 | 5.51 | 56.20 |
| | *MsyMIPS3* | Msy_15A028140 | 15A; 34739104 | 2466 | 8 | 511 | 5.70 | 56.20 |
| *Prunus armeniaca* | *PaMIPS* | PARG01757m01 | LG1; 13998443 | 3238 | 8 | 510 | 5.37 | 56.38 |
| *Prunus avium* | *PavMIPS* | CpS0039G320m0 | 6; 15056760 | 3519 | 8 | 511 | 5.53 | 56.32 |
| *Pyrus bretschneideri* | *PbMIPS1* | rna28649-v1.1-pbr | NA; 453960 | 2970 | 8 | 510 | 5.45 | 56.17 |
| | *PbMIPS2* | rna33244-v1.1-pbr | 1; 13180500 | 3671 | 8 | 510 | 5.51 | 56.17 |
| | *PbMIPS3* | rna43611-v1.1-pbr | NA; 100556 | 2920 | 8 | 510 | 5.81 | 56.15 |
| | *PbMIPS4* | rna43612-v1.1-pbr | NA; 248286 | 2975 | 8 | 510 | 5.81 | 56.18 |
| | *PbMIPS5* | rna48894-v1.1-pbr | NA; 116663 | 2892 | 8 | 510 | 5.51 | 56.21 |
| | *PbMIPS6* | rna52790-v1.1-pbr | NA; 16022 | 1647 | 1 | 547 | 6.45 | 60.72 |
| *Pyrus communis* | *PcMIPS1* | pycom01g05310 | 1; 4948196 | 2506 | 8 | 511 | 5.61 | 56.25 |
| | *PcMIPS2* | pycom15g29820 | 15; 26879374 | 1925 | 6 | 401 | 5.31 | 44.00 |
| *Prunus domestica* | *PdMIPS1* | Pd.00g802200.m01-v1.0 | scaffold17206; 51476 | 2901 | 8 | 510 | 5.61 | 56.36 |
| | *PdMIPS2* | Pd.00g872390.m01-v1.0 | scaffold5369; 2100778 | 2892 | 8 | 510 | 5.71 | 56.41 |
| | *PdMIPS3* | Pd.00g936150.m01-v1.0 | scaffold4694; 333516 | 2901 | 8 | 510 | 5.61 | 56.36 |
| | *PdMIPS4* | Pd.00g945110.m01-v1.0 | scaffold6401; 146743 | 2134 | 6 | 455 | 5.21 | 50.44 |
| | *PdMIPS5* | Pd.00g1179490.m01-v1.0 | scaffold2249; 1935754 | 2903 | 8 | 510 | 5.61 | 56.36 |
| *Prunus dulcis* | *PduMIPS* | Prudul26A029919 | 6; 17553058 | 3386 | 8 | 511 | 5.38 | 56.43 |
| *Prunus mandshurica* | *PmaMIPS* | Pruma.6G300700.t1.p1_1 | 6; 17234362 | 2892 | 8 | 511 | 5.31 | 56.33 |
| *Prunus mira* | *PmMIPS* | Pmi06g1995 | 6; 19591497 | 3252 | 8 | 511 | 5.37 | 56.39 |
| *Prunus persica* | *PpMIPS* | Prupe.6G180500.1 | 6; 18691855 | 3659 | 8 | 511 | 5.38 | 56.39 |
| *Pyrus pyrifolia* | *PpyMIPS1* | Ppy01g0259.1 | 1; 6678562 | 2506 | 8 | 510 | 5.51 | 56.18 |
| | *PpyMIPS2* | Ppy15g2730.1 | 15; 26879374 | 2728 | 9 | 585 | 7.70 | 64.61 |
| *Prunus sibirica* | *PsiMIPS* | Prusib.6G327400.t1.p1_1 | 6; 19203084 | 3405 | 9 | 515 | 5.31 | 56.82 |
| *Prunus sanyueli* | *PsMIPS* | PsSY0029765.1 | LG04; 26042866 | 3288 | 8 | 511 | 5.61 | 56.36 |
| *Pyrus ussuriensis x communis* | *PuMIPS1* | Pdr1g002830.1 | 1; 7456171 | 2918 | 8 | 511 | 5.51 | 56.21 |
| | *PuMIPS2* | Pdr15g005650.1 | 15; 10111698 | 2950 | 8 | 511 | 5.70 | 56.18 |
| **Rosoideae** | | | | | | | | |
| *Fragaria ananassa* | *FaMIPS1* | FxaC_1g25440 | 1; 12191169 | 3327 | 8 | 511 | 5.38 | 56.48 |
| | *FaMIPS2* | FxaC_2g28890 | 2; 14519335 | 3138 | 8 | 511 | 5.38 | 56.53 |
| | *FaMIPS3* | FxaC_3g25020 | 3; 13883855 | 3145 | 8 | 511 | 5.38 | 56.47 |
| *Fragaria nilgerrensis* | *FnMIPS* | evm.model.chr1.2310 | 1; 22143807 | 4079 | 8 | 511 | 5.38 | 56.47 |
| *Fragaria viridis* | *FviMIPS* | evm.model.ctg108.72 | 1; 13382776 | 2701 | 8 | 511 | 5.31 | 56.45 |

*(Continued)*

TABLE 1 Continued

| Subfamily/Plant species | Gene name | Gene ID | Chromosome; location* | Gene length (bp) | E | Protein | | |
|---|---|---|---|---|---|---|---|---|
| | | | | | | L | pI | MW(KDa) |
| *Fragaria vesca* | *FvMIPS1* | Fv2339_1g21380 | 1; 13374562 | 2909 | 8 | 510 | 5.38 | 56.47 |
| | *FvMIPS2* | FvH4_1g21450 | 1; 13385153 | 3252 | 8 | 511 | 5.38 | 56.47 |
| *Rubus chingii* | *RchMIPS* | LG01.1699 | LG01; 14815667 | 2588 | 8 | 511 | 5.45 | 56.40 |
| *Rosa chinensis* | *RcMIPS* | RC2G0276300 | 2; 27109903 | 2715 | 8 | 510 | 5.31 | 56.51 |
| *Rubus occidentalis* | *RoMIPS* | Ro01_G10705 | 1; 11491881 | 2737 | 8 | 510 | 5.45 | 56.40 |
| *Rosa rugosa* | *RrMIPS* | evm.model.Chr6.2780 | 6; 25125675 | 2626 | 3 | 510 | 5.31 | 56.47 |

*start position; E, Exons; L, length (aa); NA, not available.

suggested that the *MIPS* genes in *Rosaceae* species are continuously evolving *via* purifying selection.

## Phylogenetic analysis of Rosaceae MIPSs

To gain insights into the evolutionary relationship of the MIPSs in 26 *Rosaceae* species, a phylogenetic tree was made using ML-based multiple sequence alignments of 51 full-length protein sequences. The phylogenetic analysis divided the MIPSs into two clades (clade I and clade II) (Figure 1). Clade I had 40 MIPSs belonging to 18 species of *Rosaceae* subfamily *Amygdaloideae* and clade II had 11 MIPSs belonging to 8 species of *Rosaceae* subfamily *Rosoideae* (Figure 1).

## Gene structure, motif and domain composition of MIPSs

The analysis of the exon-intron structures of the 51 MIPS genes in 26 *Rosaceae* species showed that the lengths of the MIPS genes were mainly distributed within the range of 1.5–4.0 kb. The number of exons ranges from one (*PbMIPS6*) to nine (*PsiMIPS* and *PpyMIPS2*). A total number of eight exons are most abundant and found in 43 *MIPS* genes (84%) (Figure 2). Motif distribution analysis predicted 20 different conserved motifs in 51 Rosaceae MIPS genes. The motif's amino acid length was varied from 6 to 50. The 13 motifs (motifs 1 to 13) were present in all Rosaceae MIPS genes (except *GtMIPS1, MbMIPs2, MbMIPS3, PbMIPS6* and *PpyMIPS2*), and the

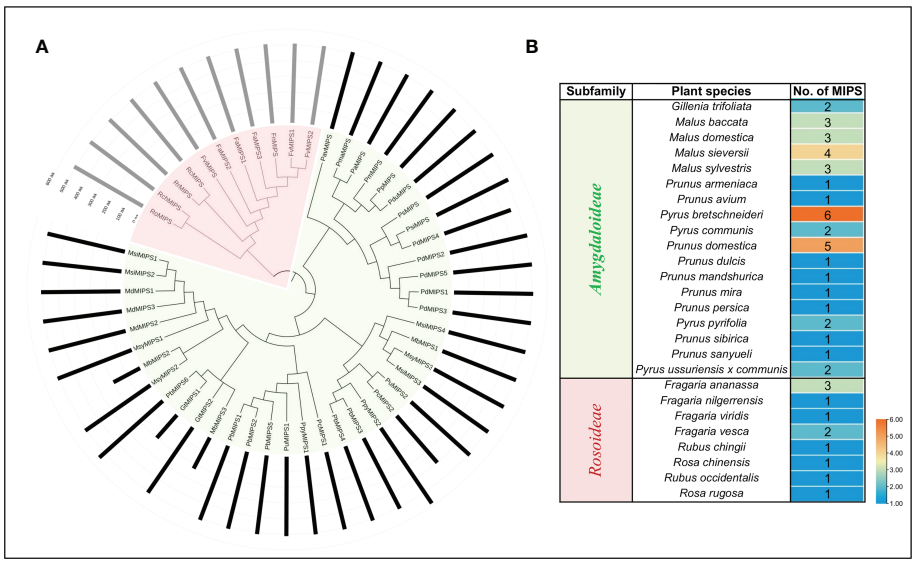


FIGURE 1
**(A)** Phylogenetic relationship among MIPSs belonging to the 26 Rosaceae plant species. **(B)** Table showing the number of MIPS genes present in each clade/sub-family.

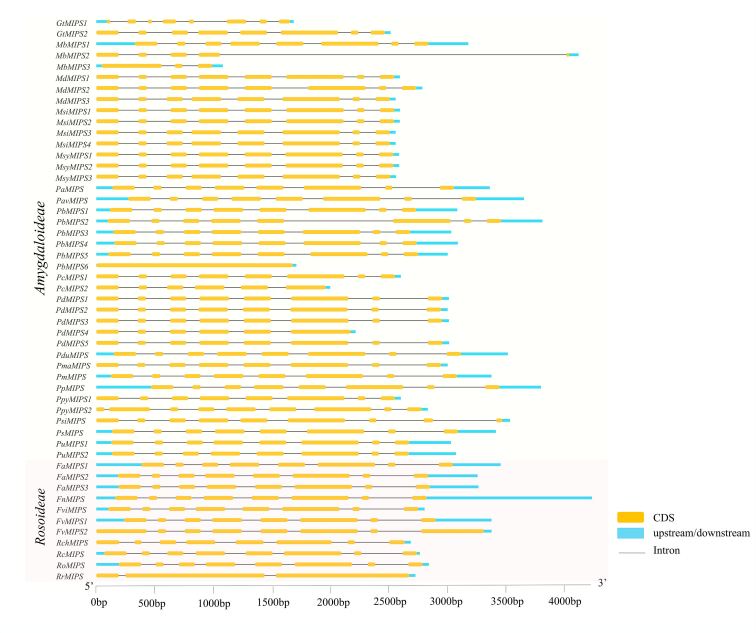


FIGURE 2
Exon–intron structures of Rosaceae MIPS genes. Exons are shown as yellow boxes, introns were denoted by thin dark grey lines and upstream/downstream regions are shown as sky-blue boxes. The lengths of exons and introns can be determined using the scale bar on the bottom.

organization pattern of these 13 motifs in the MIPS protein sequence was similar in all 26 Rosaceae plant species (Figure 3). These data suggest that MIPS is a highly conserved *Rosaceae* species. The conservation of MIPS genes was further confirmed as all Rosaceae plant species MIPS protein possessed NAD binding domain (NAD_5_Binding; PF07994) and myo-inositol-1-phosphate synthase (Inos-1-P_synth; PF01658) domain (Figure 4A). Additionally, the stretches of conserved


FIGURE 3
Motifs organization of Rosaceae MIPS proteins. Colour boxes represent the position of different motifs and box sizes show the length of motifs. Amino acid sequences for 20 different motifs (motif 1 to 20) are also provided on the right side.

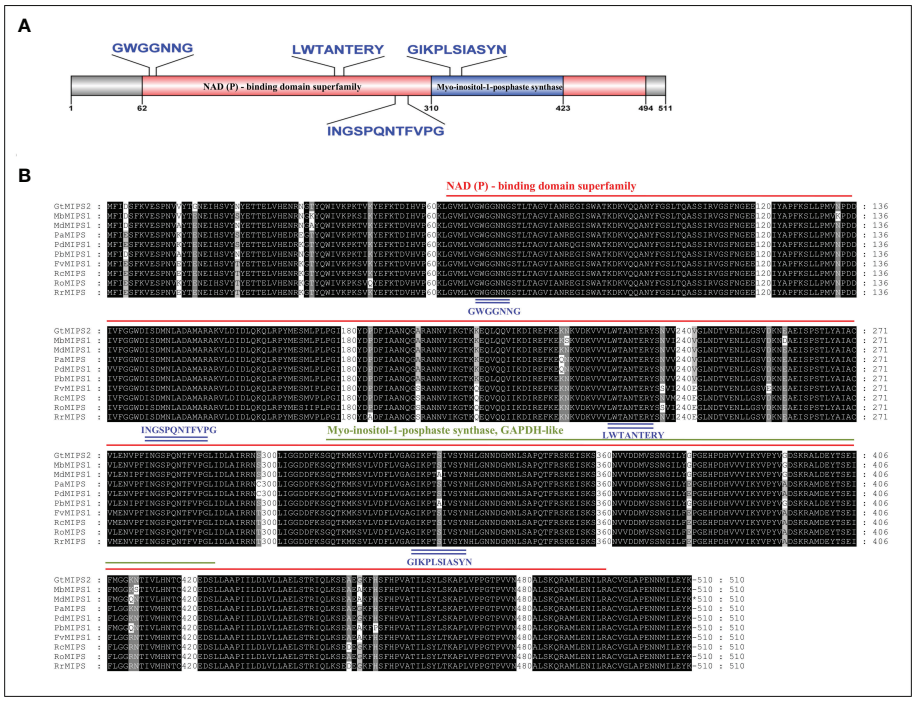


FIGURE 4
**(A)** Schematic representation of the conserved domain of Rosaceae MIPS protein. Two different conserved domains i.e., NAD binding domain (NAD_5_Binding) and myo-inositol-1-phosphate synthase (Inos-1-P_synth) are shown in different coloured boxes. **(B)** Multiple sequence alignment of ten representative Rosaceae MIPS proteins. Conserved domains are indicated with red and green underlines, the four stretches of conserved amino acid residues within domains are indicated by blue underlines.

amino acid residues such as (1) GWGGNNG, (2) LWTANTERY, (3) INGSPQNTFVPG, and (3) GIKPLSIASYN were also present in Rosaceae plant species (Figure 4B).

## Prediction of NLS and subcellular localization of MIPSs

The NLS prediction results showed that all the Rosaceae MIPSs had bipartite NLSs. The 51 *Rosaceae* MIPSs sequences have 41 NLSs sites (Supplementary Table S3). The PpyMIPS2 protein sequence also contains two monopartite sites in addition to bipartite NLSs. The results of subcellular localization prediction showed that all 51 Rosaceae MIPSs were localized in the cytoplasm (Supplementary Table S3).

## *Cis*–regulatory elements analysis of MIPSs

To understand more about the possible role of *MIPS* genes in regulating growth and development and abiotic stress responses in Rosaceae species, we search for possible CREs in the two kb promoter regions of Rosaceae MIPSs genes. In total, 2243 representing 64 types of CREs were present in 51 Rosaceae MIPS genes (Figure 5). The preponderance of the cis-acting elements found were hormone response factors. The majority of the identified CREs were abiotic stress response elements (992; 44.22%), followed by plant growth-related elements (728; 32.45%), light-responsive elements (288; 12.83%), and hormone response factors (235; 10.47%).

Among the CREs of the stress response, drought-responsive CREs (ARE, DRE, MYB, MYC, MBS, F-box and ABRE) were predominantly present in the *Rosaceae* MIPS gene as compared to other stress-responsive elements. These findings suggest that *Rosaceae* MIPSs are involved in response to abiotic stresses, particularly drought. The 10 CREs involved in the growth and development of plants were identified in *Rosaceae* MIPS genes. These include AAGAA-motif, A-Box, TATA-box, AT-rich element, CAT-box, CTAG -motif, circadian, GCN4 motif, $O_2$ site and HD-Zip1. The TATA-box and O2site CREs seemed to be the most prevalent and were detected in almost all MIPS genes. We also notice that three AT-rich element, CAT-box and CTAG -motif CREs found only in the *Amygdaloideae* subfamily of Rosaceae and absent in the *Rosoideae* subfamily. The 20 different types of light-responsive CREs were also predicted in Rosaceae MIPS genes. Among them, four CREs (Box 4, GATA-motif, GT1-motif and TCT-motif) seemed to be the most

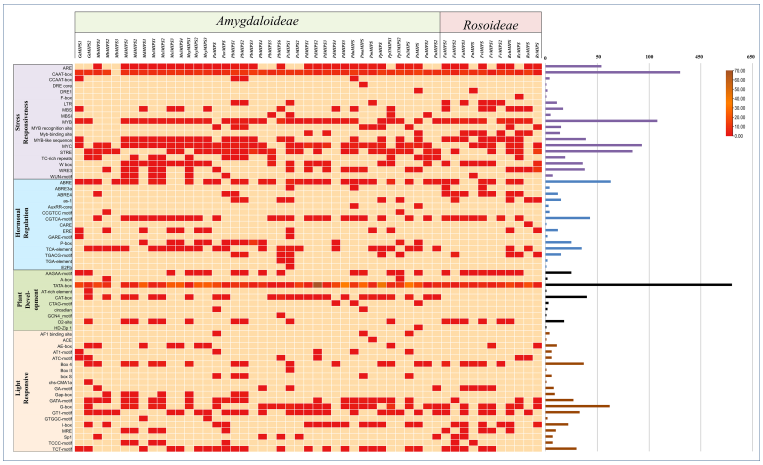


FIGURE 5
Showing the number of *cis*-regulatory elements (CREs) belonging to the following four categories (stress-responsive, hormonal regulation, plant development and light-responsive) per Rosaceae MIPS gene as a heatmap. Bar plots on the right represent the number of CREs for each MIPS gene.

prevalent and appeared in almost all MIPS genes. Plant hormones-related CREs include the abscisic acid-responsive elements (ABRE), methyl jasmonate responsive elements (CGTCA-motif, TGACG-motif), salicylic acid-responsive elements (TCA-element), gibberellins responsive elements (P-box, GARE-motif), ethylene-responsive elements (ERE), and auxin-responsive elements (AuxRR-core, TGA-element). Altogether, these results indicate that MIPS genes may be involved in a variety of abiotic stress responses as well as plant growth regulation.

## GO annotation of MIPS gene

To gain more insight into the function of the Rosaceae *MIPS* genes, we also performed a GO enrichment analysis for the *RcMIPS* gene. The results of GO enrichment analysis revealed that the *RcMIPS* gene was involved in the Inositol (phytic acid) biosynthesis, intramolecular lyase activity, Inositol (phytic acid) metabolic process and Polyol biosynthesis process (Figure 6). This GO annotation suggested that the *MIPS* genes might play an important role in phytic acid biosynthesis.

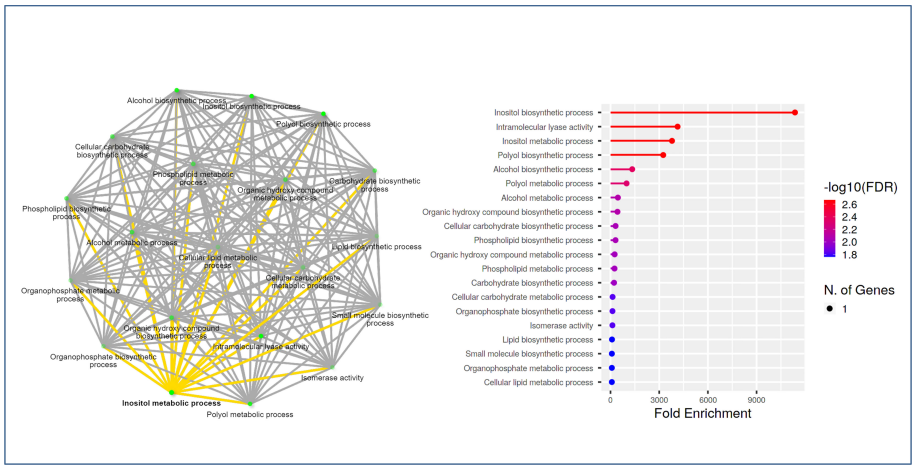


FIGURE 6
GO analysis using ShinyGo identified enriched biological processes of *RcMIPS* gene. The green dots represent the nodes for each GO biological process, while the lines (yellow and grey) represent the interaction between the nodes (minimum of 20% genes common between two connected) GO processes.

## Expression profile of MIPS gene

To investigate the putative biological role of Rosaceae MIPS genes, we performed expression analysis in *Malus domestica* (subfamily, *Amygdaloideae*) and *Rosa chinensis* (subfamily, *Rosoideae*). In *Malus domestica*, the MIPS gene was expressed in the leaf and stem. The expression level of the MIPS gene in both tissues was almost similar; only a slightly higher expression (although non-significant) was observed in the leaf as compared to stem tissue (Figure 7A). In case of rose, a significant difference in the relative expression of *RcMIPS* gene was observed in different plant tissue (Figure 7A). Among the four tissues, least expression was observed in the stem, however, the flower bud showed maximum expression of *RcMIPS* (62.66 fold higher than the stem). In the leaf and flower tissues, *RcMIPS* expressed 54.39 fold and 12.58 fold higher than the stem, respectively.

The significant difference of MIPS expression was observed in the case of rose; thus, further experiments were focused only in the rose. We performed drought stress treatment for six to 24 h on *R. chinensis* plants using 20% PEG-6000, and then we checked the expression of *RcMIPS* gene using qRT-PCR analysis. Expression analysis identified that under drought stress, *RcMIPS* gene was significantly upregulated (12.82-fold) as compared to control at only 24 h and before that its expression under drought stress was at par with control (Figure 7B). In the same tissues, we also calculated Fv/Fm to determine the physiological stress. As expected, at 0 h, no significant difference was observed in Fv/Fm values of control and drought stress tissue. Physiological stress was induced at 6 h and enhanced till 12 h, however, at 24 h physiological stress disappeared under drought stress. At 24 h, *RcMIPS* got upregulated and provided tolerance to plants to cope with stress conditions, and this might be one of the reasons that at 24 h no physiological stress was observed and Fv/Fm values of control tissue and drought stress tissue were almost same (Figure 7B). These results indicate that MIPS is possibly involved in drought stress tolerance in rose and a similar phenomenon might be operational in entire Rosaceae plant species.

We also explored the expression dynamics of *RcMIPS* under heat stress. For this purpose, plants were exposed to 42°C and leaf samples were collected at 0 h (control) and three-time points under heat stress i.e., 6 h, 12 h and 24 h. Under heat stress conditions, *RcMIPS* got significantly downregulated (Figure 7C). Further, physiological stress was also prominent in plants as Fv/Fm values significantly dropped under heat stress (Figure 7C).

# Discussion

The MIPS is a key enzyme in the myo-inositol biosynthesis pathway and has been involved in multiple biological roles in plants i.e., signal transduction, membrane biogenesis, oligosaccharides synthesis, auxin storage and transport, programmed cell death, phytic acid biosynthesis (Martin, 1998; Roth, 2004; Karner et al., 2004; Abreu and Aragao, 2007; Meng et al., 2009; Ali et al., 2013; Hazra et al., 2019). MIPS genes have been reported in various organisms including, bacteria, fungi, animals, and plants (Abid et al., 2009). However, no systematic identification and characterization of *MIPS* genes in the *Rosaceae* family have been reported. Here, by utilizing the reference genome sequence data of 26 *Rosaceae* species, we have identified 51 *MIPS* genes in Rosaceae (Table 1). The gene

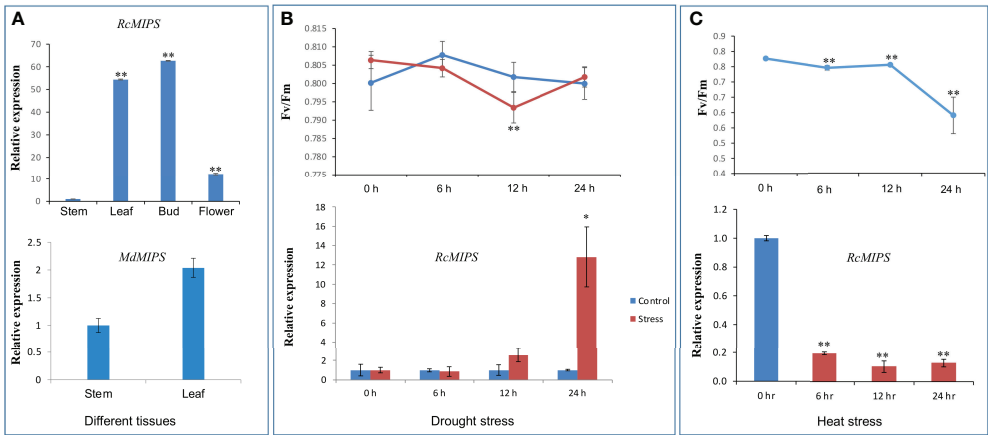


FIGURE 7
Relative expression level of MIPS in different plant tissue, during drought and heat stress, and effect of drought and heat stresses on quantum yield efficiency (Fv/Fm). **(A)** Relative expression level of *RcMIPS* and *MdMIPS* in different plant tissue. **(B)** Relative expression level of *RcMIPS* in leaf tissue at different times (0 h, 6 h, 12 h, and 24 h) treated with 20% PEG and effect of drought stress on quantum yield efficiency (Fv/Fm). **(C)** Relative expression level of *RcMIPS* in leaf tissue at different times (0 h, 6 h, 12 h, and 24 h) under heat stress at 42°C and effect of heat stress on quantum yield efficiency (Fv/Fm). * and ** represent the significant difference at $p$ <0.05 and $p$ <0.01, respectively using Student's $t$ test.

structures, phylogenetic relationships, conserved domain and motifs, CREs, GO annotation and expression profiling during drought and heat stresses for *RcMIPS* were also analyzed.

The number of MIPS genes among 26 Rosaceae species ranges from one to six and more than 50% of Rosaceae species had a single copy of MIPS genes. In earlier studies conducted in plants, it was observed that algal members, bryophyte (Marchantia), Gymnosperm (Ginkgo), Amborella, and important dicots (*Vitis vinifera*, *Eucalyptus grandis*, and *Daucus carota*) had only one copy of MIPS gene (Hegeman et al., 2001; Abid et al., 2009; Hazra et al., 2019). More than one copy of MIPS (two to four) was also reported in several plant species including rice (two MIPS copies) (Khurana et al., 2012), Arabidopsis (three MIPS copies) (Mitsuhashi et al., 2008), cotton and soybean (four MIPS copies) (Chappell et al., 2006; Ma et al., 2019). These results suggested that MIPSs are highly conserved and expanded and diversified in some higher plants including some *Rosaceae* species (*Gillenia trifoliata*, *Malus* spp., *Pyrus* spp., *Prunus* spp., *Fragaria* spp.) *via* genome duplication and polyploidization events.

The phylogenetic analysis showed that 51 MIPSs belonging to 26 *Rosaceae* species were grouped into two distinct clades (*Amygdaloideae* and *Rosoideae* subfamily specific) (Figure 1). Interestingly, the MIPSs of 26 *Rosaceae* species were randomly dispersed in every clade, demonstrating that *Rosaceae* MIPSs were conserved and existed prior to *Rosaceae* plant species divergence. Further, most of the *Rosaceae* MIPS genes had similar exon-intron, motif and domain configurations (Figures 2 & 3). Earlier research has found that several key catalytic domains are highly conserved in MIPS amino acid sequence throughout evolutionary lines, indicating that they are catalytically active (Majumder et al., 2003; Hazra et al., 2019). The four highly conserved amino acid stretches i.e., GWGGNG, LWTANTERY, INGSPQNTFVPG and GIKPLSIASYN present in all 26 Rosaceae plant species (Figure 4) are also highly conserved in other plant species (Majumder et al., 2003; Hazra et al., 2019).

Most of the *Rosaceae* MIPS have NLS domains (Table S3), which are essential for these proteins' precise targeting of the nucleus. The sub-cellular localization analysis predicts that *Rosaceae* MIPS were positioned in the cytoplasm (Table S3). As reported in earlier studies on different plant species MIPS is usually located in the cytoplasm but is also found in the nucleus, plasma membrane and endomembrane (Mitsuhashi et al., 2008; Donahue et al., 2010; Ray et al., 2010; Khurana et al., 2012; Ma et al., 2019). These results suggested that MIPS may be involved in signal transduction, membrane trafficking and regulation of gene expression.

We also predict 64 types CREs in the promoter of *Rosaceae* MIPS genes and these were associated with abiotic stress-response, plant development, light-responsive and hormonal regulation (Figure 5). In the promoter regions of MIPS genes in various plants, analogous CREs have been found (Khurana et al., 2012; Hazra et al., 2019; Ma et al., 2019). We also observed that drought-responsive CREs (ARE, DRE, MYB, MYC, MBS, F-box and ABRE) were predominantly present in the Rosaceae MIPS gene as compared to other stress-responsive elements. These findings suggest Rosaceae MIPS genes might play role in the growth and development, and stress response regulations in plants.

The MIPSs have been shown to be involved in the regulation of plant growth and development (Hazra et al., 2019). The significant difference (up to 62.66 fold) of *RcMIPS* in different plant parts like stem, leaf, bud, and flower suggested the important role of this gene in the growth and development of rose plants also (Figure 7A). MIPSs are also reported to play important role in abiotic stress tolerance including drought (Wei et al., 2010; Khurana et al., 2012; Kiranmai et al., 2018) and heat (Khurana et al., 2012). For instance, in groundnut, the *MIPS* gene was considered one of the drought-responsive genes and upregulated in transgenic lines which were more tolerant against drought as compared to wild type (Kiranmai et al., 2018). Similarly, in the case of other plant species like *Jatropha curcas* (Wang et al., 2011), *Ricinus communis* (Wei et al., 2010) *Ipomea batata* (Zhai et al., 2016) etc. *MIPS* genes were upregulated under drought stress. In the case of rice, splice variants of the *MIPS* gene (*OsMIPS1*) were also upregulated under drought stress (Khurana et al., 2012). Overexpression of chickpea *CaMIPS2* gene in Arabidopsis transgenic plants shows improved tolerance to drought stress (Kaur et al., 2013). Ectopic expression of *Medicago falcate* MIPS (*MfMIPS1*) gene in tobacco enhanced resistance to drought stress (Tan et al., 2013). During the present study, significant enhancement in expression of *MIPS* gene was observed under drought stress in the case of rose and suggested the positive role of the *MIPS* gene in providing tolerance against drought case of rose (Figure 7B). Additionally, we also identified drought-responsive elements CREs (i.e., ABRE, DRE, MYB and MYC) in the promoter sequence of *MIPS* genes which further suggested the involvement of MIPS in providing tolerance to plants under limited water conditions. Perhaps a similar kind of function may also be expected in the entire Rosaceae family. Further, biochemical studies also found an increase in myo-inositol levels under drought stress in the case of *Vigna umbellata* (Wanek and Richter, 1997) and *Cicer arietinum* (Boominathan et al., 2004). Altogether, MIPS genes were found to be a positive regulator which got upregulated under drought stress and increase the synthesis of Myo-inositol and ultimately provide tolerance to plants under drought stress.

Under heat stress, the expression of MIPS was reported to be different in different tissues. In the case of wheat, *TaMIPS* got upregulated in root and shoot tissues, however, downregulated in

flower tissues under heat stress (Khurana et al., 2012). During the present study, *RcMIPS* got downregulated under heat stress and consequently, physiological stress (in form of Fv/Fm) was also observed (Figure 7C). These results may be explained by the fact that the genotype used in the present study was *R. chinensis*, and *R. chinensis* is a heat-susceptible species (Qi et al., 2021). Further, in *R. chinensis*, RNA seq study also suggested that genes involved in carbohydrate biosynthesis and cell wall biosynthesis genes were downregulated and resulted into physiological stress in *R. chinensis* (Li et al., 2019). All these observations suggested that allele of the *RcMIPS* gene in *R. chinensis* might be a susceptible allele for heat stress which got downregulated under heat stress and resulted in physiological stress in plants. However, the situation might be reversible with heat tolerant rose accession where MIPS genes (with tolerant allele) perhaps provide tolerance to plants under heat stress.

In conclusion, we identified 51 MIPS genes in 26 *Rosaceae* species of plants which were grouped into two clades. Gene structure analysis suggested one to nine exons in MIPS and the total gene length of MIPS were found up to 4079 bp. In promoter sequence, the presence of different elements including abiotic stress-responsive elements suggested the important role of MIPSs in different plant developmental processes as well as abiotic stresses. Expression analysis of *RcMIPS* empathized the potential role of MIPS in plant development, drought and heat stress tolerance. Altogether, the present study provides compressive preliminary information on *MIPS* genes which can be a good foundation for functional characterization of this important gene family.

## Data availability statement

The datasets presented in this study can be found in online repositories. The names of the repository/repositories and accession number(s) can be found in the article/Supplementary Material.

## Author contributions

HG and PK: Performed experiments, analysed data and wrote the first draft. VG and VJ: Conceptualization, supervision, writing and editing. SK: Overall supervision and funding acquisition. All authors contributed to the article and approved the submitted version.

## Funding

This work was supported by the CSIR, India under Grant MLP201; the Department of Science and Technology (DST) for the INSPIRE faculty award; and Science and Engineering Research Board (SERB) for the Early Career Research Award.

## Acknowledgments

This is a short text to acknowledge the contributions of specific colleagues, institutions, or agencies that aided the efforts of the authors. This study was supported by the Council of Scientific and Industrial Research (CSIR) for providing funds (MLP-201), VJ also thanks to the Science and Engineering Research Board (SERB) for the Early Career Research Award. VJ and VG thank the Department of Science and Technology (DST) for the INSPIRE faculty award. HG and PK thank CSIR for Junior Research Fellowship. This manuscript represents CSIR-IHBT communication number 5181.

## Conflict of interest

The authors declare that the research was conducted in the absence of any commercial or financial relationships that could be construed as a potential conflict of interest.

## Publisher's note

All claims expressed in this article are solely those of the authors and do not necessarily represent those of their affiliated organizations, or those of the publisher, the editors and the reviewers. Any product that may be evaluated in this article, or claim that may be made by its manufacturer, is not guaranteed or endorsed by the publisher.

## Supplementary material

The Supplementary Material for this article can be found online at: https://www.frontiersin.org/articles/10.3389/fpls.2022.1021297/full#supplementary-material

## References

Abid, G., Silue, S., Muhovski, Y., Jacquemin, J. M., Toussaint, A., and Baudoin, J. P. (2009). Role of myo-inositol phosphate synthase and sucrose synthase genes in plant seed development. *Gene* 439, 1–10. doi: 10.1016/j.gene.2009.03.007

Abreu, E. F. M., and Aragao, F. J. L. (2007). Isolation and characterization of a myo-inositol-1-phosphate synthase gene from yellow passion fruit (*Passifloraedulis f. flavicarpa*) expressed during seed development and environmental stress. *Ann. Bot.* 99, 285–292. doi: 10.1093/aob/mcl256

Ali, N., Paul, S., Gayen, D., Sarkar, S. N., Datta, K., and Datta, S. K. (2013). Development of low phytate rice by RNAi mediated seed-specific silencing of inositol 1, 3, 4, 5, 6-pentakisphosphate 2-kinase gene (*IPK1*). *PLos One* 8, e68161. doi: 10.1371/journal.pone.0068161

Alok, A., Singh, S., Kumar, P., and Bhati, K. K. (2022). Potential of engineering the myo-inositol oxidation pathway to increase stress resilience in plants. *Mol. Biol. Rep.* 49, 8025–8035. doi: 10.1007/s11033-022-07333-0

Artimo, P., Jonnalagedda, M., Arnold, K., Baratin, D., Csardi, G., De Castro, E., et al. (2012). ExPASy: SIB bioinformatics resource portal. *Nucleic Acids Res.* 40, 597–603. doi: 10.1093/nar/gks400

Bailey, T. L., Johnson, J., Grant, C. E., and Noble, W. S. (2015). The MEME suite. *Nucleic Acids Res.* 43, 39–49. doi: 10.1093/nar/gkv416

Basak, P., Sangma, S., Mukherjee, A., Agarwal, T., Sengupta, S., Ray, S., et al. (2018). Functional characterization of two myo-inositol-1-phosphate synthase (MIPS) gene promoters from the halophytic wild rice (*Porteresia coarctata*). *Planta* 248, 1121–1141. doi: 10.1007/s00425-018-2957-z

Boominathan, P., Shukla, R., Kumar, A., Manna, D., Negi, D., Verma, P. K., et al. (2004). Long term transcript accumulation during the development of dehydration adaptation in *Cicer arietinum*. *Plant Physiol.* 135, 1608–1620. doi: 10.1104/pp.104.043141

Chappell, A. S., Scaboo, A. M., Wu, X., Nguyen, H., Pantalone, V. R., and Bilyeu, K. D. (2006). Characterization of the MIPS gene family in *Glycine max*. *Plant Breed.* 125, 493–500. doi: 10.1111/j.1439-0523.2006.01264.x

Chen, C., Chen, H., Zhang, Y., Thomas, H. R., Frank, M. H., He, Y., et al. (2020). TBtools: an integrative toolkit developed for interactive analyses of big biological data. *Mol. Plant* 13, 1194–1202. doi: 10.1016/j.molp.2020.06.009

Chun, J. A., Jin, U. H., Lee, J. W., Yi, Y. B., Hyung, N. I., Kang, M. H., et al. (2003). Isolation and characterization of a myo-inositol 1-phosphate synthase cDNA from developing sesame (*Sesamum indicum* l.) seeds: functional and differential expression, and salt-induced transcription during germination. *Planta* 216, 874–880. doi: 10.1007/s00425-002-0940-0

Donahue, J. L., Alford, S. R., Torabinejad, J., Kerwin, R. E., Nourbakhsh, A., Ray, W. K., et al. (2010). The arabidopsis thaliana myo-inositol 1-phosphate synthase1 gene is required for myo-inositol synthesis and suppression of cell death. *Plant Cell* 22, 888–903. doi: 10.1105/tpc.109.071779

El-Gebali, S., Mistry, J., Bateman, A., Eddy, S. R., Luciani, A., Potter, S. C., et al. (2019). The pfam protein families database in 2019. *Nucleic Acids Res.* 47, 427–432. doi: 10.1093/nar/gky995

Feng, X., and Yoshida, K. T. (2004). Molecular approaches for producing low-phytic-acid grains in rice. *Plant Biotechnol. J.* 21, 183–189. doi: 10.5511/plantbiotechnology.21.183

Ge, S. X., Jung, D., and Yao, R. (2020). ShinyGO: a graphical gene-set enrichment tool for animals and plants. *Bioinformatics* 36, 2628–2629. doi: 10.1093/bioinformatics/btz931

Hazra, A., Dasgupta, N., Sengupta, C., and Das, S. (2019). MIPS: Functional dynamics in evolutionary pathways of plant kingdom. *Genomics* 111, 1929–1945. doi: 10.1016/j.ygeno.2019.01.004

Hegeman, C. E., Good, L. L., and Grabau, E. A. (2001). Expression of d-myo-inositol-3-phosphate synthase in soybean. implications for phytic acid biosynthesis. *Plant Physiol.* 125, 1941–1948. doi: 10.1104/pp.125.4.1941

Hu, L. Y., Hong, Y. U. E., Zhang, J. Y., Yang-tian-su, L. I., Gong, X. Q., Kun, Z. H. O. U., et al. (2022). Overexpression of MdMIPS1 enhances drought tolerance and water-use efficiency in apple. *J. Integr. Agric.* 21, 1968–1981. doi: 10.1016/S2095-3119(21)63822-4

Johnson, M. D., and Sussex, I. M. (1995). 1 l-myo-inositol 1-phosphate synthase from *Arabidopsis thaliana*. *Plant Physiol.* 107, 613–619. doi: 10.1104/pp.107.2.613

Jung, S., Lee, T., and Cheng, C. H. (2019). 15 years of GDR: New data and functionality in the genome database for rosaceae. *Nucleic Acids Res.* 47, 1137–1145. doi: 10.1093/nar/gky1000

Karner, U., Peterbauer, T., Raboy, V., Jones, D. A., Hedley, C. L., and Richter, A. (2004). *myo*-inositol and sucrose concentrations affect the accumulation of raffinose family oligosaccharides in seeds. *J. Exp. Bot.* 55, 1981–1987. doi: 10.1093/jxb/erh216

Kaur, H., Verma, P., Petla, B. P., Rao, V., Saxena, S. C., and Majee, M. (2013). Ectopic expression of the ABA-inducible dehydration-responsive chickpea l-myo-inositol 1-phosphate synthase 2 (*CaMIPS2*) in arabidopsis enhances tolerance to salinity and dehydration stress. *Planta* 237, 321–335. doi: 10.1007/s00425-012-1781-0

Khurana, N., Chauhan, H., and Khurana, P. (2012). Expression analysis of a heat-inducible, myo-inositol-1-phosphate synthase (MIPS) gene from wheat and the alternatively spliced variants of rice and *Arabidopsis*. *Plant Cell Rep.* 31, 237–251. doi: 10.1007/s00299-011-1160-5

Kiranmai, K., Rao, G. L., Pandurangaiah, M., Kumar, A. M., Reddy, V. A., Lokesh, U., et al. (2018). A novel WRKY transcription factor, *MuWRKY3* (*Macrotyloma uniflorum* lam. verdc.) enhances drought stress tolerance in transgenic groundnut (*Arachis hypogaea* l.) plants. *Front. Plant Sci.* 9. doi: 10.3389/fpls.2018.00346

Kosugi, S., Hasebe, M., Tomita, M., and Yanagawa, H. (2009). Systematic identification of cell cycle-dependent yeast nucleocytoplasmic shuttling proteins by prediction of composite motifs. *Proc. Natl. Acad. Sci.* 106, 10171–10176. doi: 10.1073/pnas.090060410

Kumari, S., Jolly, M., Krishnan, V., Dahuja, A., and Sachdev, A. (2012). Spatial and temporal expression analysis of d-myo-inositol 3-phosphate synthase (MIPS) gene family in *Glycine max*. *Afr. J. Biotechnol.* 11, 16443–16454. doi: 10.5897/AJB12.2811

Larson, S. R., and Raboy, V. (1999). Linkage mapping of maize and barley myo-inositol 1-phosphate synthase DNA sequences: correspondence with a low phytic acid mutation. *Theor. Appl. Genet.* 99, 27–36. doi: 10.1007/s001220051205

Lescot, M., Patrice, D., Thijs, G., Marchal, K., Moreau, Y., de Peer, Y. V., et al. (2002). PlantCARE, a database of plant cis-acting regulatory elements and a portal to tools for in silico analysis of promoter sequences. *Nucleic Acids Res.* 30, 325–327. doi: 10.1093/nar/30.1.325

Letunic, I., and Bork, P. (2007). Interactive tree of life (iTOL): an online tool for phylogenetic tree display and annotation. *Bioinformatics* 23, 127–128. doi: 10.1093/bioinformatics/btl529

Livak, K. J., and Schmittgen, T. D. (2001). Analysis of relative gene expression data using real-time quantitative PCR and the 2(-delta delta C(T)) method. *Methods* 25, 402–408. doi: 10.1006/meth.2001.1262

Li, Z. Q., Xing, W., Luo, P., Zhang, F. J., Jin, X. L., and Zhang, M. H. (2019). Comparative transcriptome analysis of *Rosa chinensis* 'Slater's crimson china' provides insights into the crucial factors and signaling pathways in heat stress response. *Plant Physiol. Biochem.* 142, 312–331. doi: 10.1016/j.plaphy.2019.07.002

Loewus, F. A., and Loewus, M. W. (1980). "Myo-inositol: biosynthesis and metabolism," in *The biochemistry of plants: Carbohydrate structure and function*. Ed. J. Preiss (New York: Academic Press), 43–76.

Majumder, A. L., Chatterjee, A., Dastidar, K. G., and Majee, M. (2003). Diversification and evolution of l-myo-inositol 1-phosphate synthase. *FEBS Lett.* 553, 3–10. doi: 10.1016/S0014-5793(03)00974-8

Majumder, A., Johnson, M. D., and Henry, S. A. (1997). 1L-myo-inositol-1-phosphate synthase. *Biochim. Biophys. Acta* 1348, 245–256. doi: 10.1016/S0005-2760(97)00122-7

Martin, T. F. J. (1998). Phosphoinositide lipids as signaling molecules: common themes for signal transduction, cytoskeletal regulation, and membrane trafficking. *Annu. Rev. Cell Dev. Biol.* 14, 231–264. doi: 10.1146/annurev.cellbio.14.1.231

Ma, R., Song, W., Wang, F., Cao, A., Xie, S., Chen, X., et al. (2019). A cotton (*Gossypium hirsutum*) myo-inositol-1-phosphate synthase (*GhMIPS1D*) gene promotes root cell elongation in arabidopsis. *Int. J. Mol. Sci.* 20, 1224. doi: 10.3390/ijms20051224

Meng, P. H., Raynaud, C., Tcherkez, G., Blanchet, S., Massoud, K., Domenichini, S., et al. (2009). Crosstalks between myo-inositol metabolism, programmed cell death and basal immunity in arabidopsis. *PLos One* 4, e7364. doi: 10.1371/journal.pone.0007364

Menzel, W., Jelkmann, W., and Maiss, E. (2002). Detection of four apple viruses by multiplex RT-PCR assays with coamplification of plant mRNA as internal control. *J. Virol. Methods* 99, 81–92. doi: 10.1016/S0166-0934(01)00381-0

Mitsuhashi, N., Kondo, M., Nakaune, S., Ohnishi, M., Hayashi, M., Nishimura, I. H., et al. (2008). Localization of myo-inositol-1-phosphate synthase to the endosperm in developing seeds of arabidopsis. *J. Exp. Bot.* 59, 3069–3076. doi: 10.1093/jxb/ern161

Qin, D., Toyonaga, D., and Saneoka, H. (2021). Characterization of myo-inositol-1-phosphate synthase (MIPS) gene expression and phytic acid accumulation in oat (*Avena sativa*) during seed development. *Cereal Res. Commun* 50, 379–384. doi: 10.1007/s42976-021-00186-6

Qi, W., Zhang, C., Wang, W., Cao, Z., Li, S., Li, H., et al. (2021). Comparative transcriptome analysis of different heat stress responses between self-root grafting line and heterogeneous grafting line in rose. *Hortic. Plant J.* 7, 243–255. doi: 10.1016/j.hpj.2021.03.004

Raychaudhuri, A., and Majumder, A. L. (1996). Salinity-induced enhancement of l-myo-inositol 1-phosphate synthase in rice (*Oryza sativa* l.). *Plant Cell Environ.* 19, 1437–1442. doi: 10.1111/j.1365-3040.1996.tb00023.x

Ray, S., Patra, B., Das-Chatterjee, A., Ganguli, A., and Majumder, A. (2010). Identification and organization of chloroplastic and cytosolic l-myo-inositol 1-phosphate synthase coding gene (s) in *Oryza sativa*: comparison with the wild halophytic rice, *Porteresia coarctata*. *Planta* 231, 1211–1227. doi: 10.1007/s00425-010-1127-8

Roth, M. G. (2004). Phosphoinositides in constitutive membrane traffic. *Physiol. Rev.* 84, 699–730. doi: 10.1152/physrev.00033.2003

Sharma, N., Chaudhary, C., and Khurana, P. (2020). Wheat myo-inositol phosphate synthase influences plant growth and stress responses *via* ethylene mediated signaling. *Sci. Rep.* 10, 1–14. doi: 10.1038/s41598-020-67627-w

Stecher, G., Tamura, K., and Kumar, S. (2020). Molecular evolutionary genetics analysis (MEGA) for macOS. *Mol. Biol. Evo.* 37, 1237–1239. doi: 10.1093/molbev/msz312

Taji, T., Takahashi, S., and Shinozaki, K. (2006). Inositols and their metabolites in abiotic and biotic stress responses. *Subcell. Biochem.* 39, 239–264. doi: 10.1007/0-387-27600-9_10

Tan, J., Wang, C., Xiang, B., Han, R., and Guo, Z. (2013). Hydrogen peroxide and nitric oxide mediated cold-and dehydration-induced myo-inositol phosphate synthase that confers multiple resistances to abiotic stresses. *Plant Cell Environ.* 36, 288–299. doi: 10.1111/j.1365-3040.2012.02573.x

Wanek, W., and Richter, A. (1997). Biosynthesis and accumulation of d-ononitol in *Vigna umbellata* in response to drought stress. *Physiol. Plant* 101, 416–424. doi: 10.1111/j.1399-3054.1997.tb01016.x

Wang, Y., Huang, J., Gou, C. B., Dai, X., Chen, F., and Wei, W. (2011). Cloning and characterization of a differentially expressed cDNA encoding myo-inositol-1-phosphate synthase involved in response to abiotic stress in *Jatropha curcas*. *Plant Cell Tissue Organ Cult.* 106, 269–277. doi: 10.1007/s11240-011-9917-7

Wei, W., Dai, X., Wang, Y., Gou, C. B., and Chen, F. (2010). Cloning and expression analysis of 1 l-myo-inositol-1-phosphate synthase gene from *Ricinus communis* l. *Z. Naturforsch. C.* 65, 501–507. doi: 10.1515/znc-2010-7-814

Zhai, H., Wang, F., Si, Z., Huo, J., Xing, L., An, Y., et al. (2016). A myo-inositol-1-phosphate synthase gene, *IbMIPS1*, enhances salt and drought tolerance and stem nematode resistance in transgenic sweet potato. *Plant Biotechnol. J.* 14, 592–602. doi: 10.1111/pbi.12402

frontiers | Frontiers in Plant Science

TYPE Original Research
PUBLISHED 14 December 2022
DOI 10.3389/fpls.2022.1060492



OPEN ACCESS

EDITED BY
Weibiao Liao,
Gansu Agricultural University, China

REVIEWED BY
Ravish Choudhary,
Indian Agricultural Research Institute (ICAR), India
Jiban Shrestha,
Nepal Agricultural Research Council, Nepal

*CORRESPONDENCE
Mohan Lal
drmohanlal80@gmail.com

SPECIALTY SECTION
This article was submitted to Plant Breeding, a section of the journal Frontiers in Plant Science

RECEIVED 03 October 2022
ACCEPTED 28 November 2022
PUBLISHED 14 December 2022

CITATION
Lal M, Munda S, Gogoi A, Begum T, Baruah J, Chanda SK and Lekhak H (2022) Use of stability statistics in the selection of *Clausena heptaphylla* (Roxb.) Wight & Arn for novel anethole rich strain (Jor Lab CH-2). *Front. Plant Sci.* 13:1060492. doi: 10.3389/fpls.2022.1060492



# Use of stability statistics in the selection of *Clausena heptaphylla* (Roxb.) Wight & Arn for novel anethole rich strain (Jor Lab CH-2)

Mohan Lal*, Sunita Munda, Anindita Gogoi, Twahira Begum, Joyashree Baruah, Sanjoy K. Chanda and Himangshu Lekhak

Agrotechnology and Rural Development (ARD) Division, CSIR-North East Institute of Science and Technology (NEIST), Jorhat, Assam, India

**Introduction:** Anethole is an industrially important compound which is extensively used in pharmaceuticals, cosmetics, perfumery, food and confectioneries. Anethole is primarily obtained from fennel, anise, and star anise which is highly expensive. Therefore, a study was performed to identify a cost-effective and natural anethole rich strain of *Clausena heptaphylla* through selection and confirmed through multilocation trial.

**Methods:** The study was conducted using 23 accessions collected from North eastern region of India from 2014-2018 (initial evaluation trial) and 2018-2022 (multilocation trial). The initial trial was conducted in the experimental farm of CSIR-NEIST, Jorhat, Assam using Complete Randomized Block Design with three replications. Five agronomical traits (plant height, leaf length, leaf width, number of stem branching, herbage yield per plant per cutting) along with essential oil yield and anethole content were evaluated which led to the identification of anethole rich strain of *C. heptaphylla*. This identified strain was further evaluated along with the two check genotypes for stability based on three yield parameters *viz.* herbage yield, essential oil yield and anethole content at four multi-locations (Imphal, Jorhat, Runne and Madang) for four years using the same experimental design.

**Results and discussion:** The identified superior line (Jor Lab CH-2) showed consistent performance for the studied yield parameters across all the environments maintaining its superiority. The identified strain exhibited average herbage yield of 1.2 Kg/plant/cutting and essential oil yield of 1.22%. The GC-MS analysis of the essential oil depicted trans anethole as the major constituent (93.25%) followed by estragole (4.85%) while benzene, 1,2-dimethoxy-4-(1-propenyl Isoeugenol methyl ether and *cis*-anethole were the trace components. This is the first novel report of anethole rich variant of *C. heptaphylla* which has undergone multilocational trial over the years. Jor Lab CH-2 strain will open a new scope for the industries to isolate anethole from a different source in a cost-effective approach.

KEYWORDS

**selection breeding, GC/MS, multilocation trial, superior strain, stability**

## Introduction

Herbal drugs, natural health products and secondary metabolites of medicinal plants are increasing enormously as people are realizing globally the valuable sources of medicinal plants and thereby focusing extensively more on conservation and sustainable use of medicinal plants. There is enumerable availability of medicinally important plant species worldwide where several species of the genus *Clausena* are used as traditional medicine for human ailment (Pandey et al., 2012). The genus *Clausena* includes more than 30 species namely *C.anisata*, *C. excavata*, *C. harmandiana*, *C. indica*, *C. heptaphylla* which are allocated all over tropical and subtropical areas (Guo et al., 2018). Among all, *Clausena heptaphylla* belonging to Rutaceae family is one of the important medicinal and aromatic shrubs. It is commonly known as panbahar which is distributed widely in South and South east Asia (Majumder and Rahman, 2016). *Clausena* species are basically self-pollinated plant and is bisexual in nature having chromosome number 2n = 4x = 36 (Mehra and Khosla, 1973). Morphologically, *C. heptaphylla* is a shrub or tree which measure up-to 2-4 m long, leaves are compound, alternate and spiral which emits most agreeable fragrance with petiole slightly marginate, terminal paniculate cymes in inflorescence with flower about 5 mm long, greenish yellow and glabrous. A detailed investigation revealed that *C. heptaphylla* posseses carbazole alkaloids like heptazolicine extracted from roots (Bhattacharyya et al., 1984), clausenalene extracted from bark stem (Bhattacharyya et al., 1993), clausnapin (Bhattacharyya et al., 1984), clausenal (Chakraborty et al., 1995), coumarins like lunamarin A and lunamarin B (Sohrab et al., 1999), clausmarin A (Sohrab et al., 2001), lunamarin C (Sohrab et al., 2002) extracted from leaves.

Ethnobotanical survey revealed that *Clausena heptaphylla* are beneficial for the cure of paralysis, ulcerated nose, headache and muscular pain. They are also putative to be used as diurectic, astringent, insecticide, tonic, vermifuge (Yusuf et al., 1994; Fakruddin et al., 2012) and have antiseptic properties (Begum et al., 2011). It is chewed with leaves of Piper beetle 2-3 times daily to cure digestive problem (Mannaf et al., 2013). The leaf part is also used in fever, remove nicotine addiction and foul odor from mouth (Hossan et al., 2009). The bark of the plant is used for curing cattle wounds and sprains (Sohrab et al., 2001). The plant essential oil and flower extracts are used for skin inflammation and ophthalmia (Agarwal, 1986; Lal et al., 2022). A recent report suggested that the aqueous extracts of *C. heptaphylla* leaves were used for relieving cigarette craving and anti-obesity (Jerajasin et al., 2014). Various experiments have been performed where it was found that this plant possess various antimicrobial, antifungal, antioxidant, antidiabetic properties (Sohrab et al., 2001; Fakruddin et al., 2012; Lal et al., 2022).

In comparison with costly synthetic drugs which have adverse effects, the inclination towards extraction of essential oil for preparation of green medicine which is safe and dependable is increasing tremendously (Pandey et al., 2021). Many scientific reports suggested that essential oil has therapeutic proficiency in curing various diseases (Lal et al., 2021; Dutta et al., 2021). The previous report on composition of essential oil mentioned that *Clausena heptaphylla* possesses a predominant component known as anethole (Lockwood, 1984; Nath et al., 1996; Lal et al., 2022). Anethole act as a flavoring agent and is widely used in food industry, cosmetics, perfumery and pharmaceuticals industries (Lal et al., 2022). It has multiple propitious effects in human health such as anti-inflammatory, antidiabetic, immunomodulatory, anticarcinogenic, antithrombotic consequence (Aprotosoaie et al., 2016; Lal et al., 2022). Till now very few studies are found where a detailed survey has been done on anethole rich essential oil composition of *Clausena heptaphylla*. Recent report on the biological activity of *C. heptaphylla* essential oil revealed skin whitening effect, anti-diabetic, anti-inflammatory, antimicrobial, antihelminthic, antinociceptive, gastroprotective, sedative properties representatives which is non-toxic in nature (Marinov and Kuzmanova, 2015; Munda et al., 2019; Lal et al., 2022). Therefore, to meet the demand of the industries and owing to the wide application of biological friendliness of this species, a study was conducted to identify high anethole rich strain of *Clausena heptaphylla* which will be stable across different locations over the years. The ability of a genotype to maintain the consistency of the character at high or low yield in various environments or during various years is known as stability (Munda et al., 2020). Genotype stability performance is a prerequisite for identification of superior variety and must be carried out in many conditions since genotypes are greatly influenced by the environment, locations, and years (Gupta et al., 2015). Several stability models are developed to study the consistency of the genotypes out of which AMMI, GGE biplot and MTSI models are used in the study for proper validation of the results. Earlier no studies were performed to validate the superiority and consistency of anethole rich strain of *C. heptaphylla*, therefore, this can be considered as the first report for varietal development of anethole rich Jor Lab CH-2. The development of a plant variety with good and consistent performance under many environmental conditions is quite difficult for plant breeder. Therefore, the identification of this beneficial line can be contemplated as a novel and resourceful report as it will help in conservation of this species for future prospect help in betterment of farmers as well as pharmaceuticals industries thereby making the strain a good candidate for further drug development program. Further, Jor Lab CH-2 will open a new scope for the industries to isolate anethole from a different source in a cost-effective approach.

## Materials and methods

### Initial evaluation trial

The matured seeds of *Clausena heptaphylla* were collected in a total of 23 accessions from various parts of North East India in the year 2014 and planted in augmented design for an initial field

evaluation trial in March 2014. The list and source of the collected germplasm are provided in the Table S1. The field trial was conducted in the experimental farm of CSIR-NEIST, Jorhat, Assam, India having GPS location of 26° 44' 15.6948" N latitude, 94° 9' 25.4628" E longitude and elevation 94 m above MSL. The texture of the soil was sandy loam with pH of 5.2. The climatic conditions of the experimental site were recorded with minimum temperature of 8.1°C, maximum temperature of 37.8°C; minimum relative humidity (%) of 64.3, maximum relative humidity (%) of 100; average annual rainfall of 2480 mm respectively during the evaluation period. The field trial's plot was 3 x 2 m in size, with a 45 x 45 cm gap between each plant and line, respectively. The leaf specimens of the genotypes were used to prepare the herbarium voucher which was deposited at departmental herbarium of the institute. The data of an initial field evaluation trial for morphological, essential oil yield and its constituents were tracked and recorded in the year 2016, 2017 and 2018. The maturity of the species can be attained after two years; therefore, the leaves were harvested for three years after every four months. A high essential oil and high herbage yielding accession (RRLCH-2) was found after the review of the selection trial's data which was later named as Jor Lab CH-2.

## Multilocation trials

The seeds of the selected line along with two check genotypes was further planted in four separate locations of Northeast India namely, Imphal (Manipur), Jorhat (Assam), Runne (Arunachal Pradesh) and Madang (Assam) for four years during 2018-2022. The agro-climatic conditions of the selected multilocations for the study are represented in Table S2. The trial was conducted in Randomized Complete Block Design (RCBD) with three replications. All the morphological as well as essential oil and its components were documented for two years (2021 and 2022) after maturity which were further analysed statistically to check its productivity, essential oil content and quality. A total of eight environments (coded: E1, E2, E3, E4, E5, E6, E7, and E8) were studied comprising of four locations for two-year evaluation.

## Data observation and collection

A total of five agronomical traits like plant height (cm), leaf length (cm), leaf width (cm), number of stem branching, herbage yield per plant per cutting (Kg) were tracked for the evaluation. The chemical profiling of the essential oil extracted from all the accessions were documented as per the standard protocol (Lal et al., 2022). For data collection, ten healthy and mature plants were randomly chosen from each genotype of each replication, eliminating the border plants. The average values were considered to be the final values.

## Isolation of essential oil and chemical profiling

The Clevenger apparatus (3000 mL) was used to isolate the essential oil from the leaves of *Clausena heptaphylla* (300 gm) for four hours at a temperature of 99°C. The standardized procedure was formulated by Clevenger (1928) which was modified by Lal et al., (2022). The essential oil was subjected to anhydrous sodium sulphate for absorption of moisture content present followed by preservation in the glass vial. The essential oil percentage (v/w) of the isolated essential oils was estimated using the following formula given by Munda et al., (2020):

$$\text{Essential oil (FWB)} = \frac{volume\ of\ essential\ oil\ isolated\ (mL)}{weight\ of\ fresh\ leaves\ used\ (g)} \times 100$$

## Qualitative analysis of essential oil

The qualitative analysis was performed in the Sophisticated Analytical Instrument Facility of the institute (CSIR-NEIST, Jorhat) during all the studied years for the initial (2016, 2017 and 2018) as well as multilocation (2021 and 2022) evaluation. Thermo Scientific TRACE 1110 gas chromatograph instrument was used to assess the chemical profiling of *C.heptaphylla* leaf essential oil integrated with TG-WAXMS column and FID (Flame Ionization Detector). The column dimension was 60 m × 0.25 µm. The initial temperature of the oven was at 40°C for 2 minutes which was progressively escalated to 250°C at a rate of 5°C/min. The concluding temperature was maintained at 30°C/min for 30 min at 300°C. The carrier gas used was Helium gas at 1mL/min flow rate. The prepared sample was diluted at a ratio of 1:100 (v/v) in acetone with a split ratio of 1:20 for 1min. Similarly, Agilent technologies gas chromatograph mass spectroscopy instrument fused with HP-5MS silica capillary column and mass selective detector (MSD5975 C) was utilized for GC/MS. The dimension of HP-5MS column was 30 m × 0.25 mm i.d with film thickness of 0.25 µm. The range for the GC/MS scan was set at 45-650 amu. The conditions used for GC/MS were in accordance with the GC parameters used for GC analysis. The mass spectral data from NIST/Willey library was deployed to compare the detected peaks of the sample followed by confirmation with Kovat's index on HP-5MS. The standards (Fluka and Sigma Aldrich, Germany) were run for authentication of the isolated compounds. The conditions for the GC used in the study were as per standardized by Lal et al., (2022).

## Statistical analysis

Analysis of variance (ANOVA) for both pooled and individual data were estimated for the multi-location trial for two years. The F-test was used for the significant analysis of ANOVA. The stability models like AMMI (Additive multiplicative mean interaction

model), GGE (genotype+ genotype × environment) biplot and (MTSI) Multi trait stability index was measured through stability analysis by Olivoto et al., (2019) developed R-package "metan". The consistent and better performing genotypes were identified by using these multivariate analyses.

The G x E interaction of AMMI model is given by:

$Y_{ij}$ =μ+$g_i$+$e_j$ +dij

where $Y_{ij}$ is the yield of the genotype; μ is the grand mean; $g_i$ is the deviation of the mean of genotype i from μ; $e_j$ is the deviation of the environment j from μ

The GGE biplot was studied using the following equation:

$$\widehat{Y_{ij}} - \mu = G_i + E_j + GE_{ij}$$

where $\hat{Y}_{ij}$ =average phenotype for genotype i in environment j; $\mu$ = overall constant; $G_i$ = random influence of genotype i; $E_j$ = fixed effect of environment j; and $GE_{ij}$ =random effect of the genotype i versus environment j interaction

Similarly, the formula for MTSI is as follows:

$$\text{MTSI} = \left[\sum_{j=1}^{f}\left(F_{ij} - F_j\right)^2\right]^{0.5}$$

Where $F_j$= ideotype's $j^{th}$ score; $F_{ij}$ = $i^{th}$ genotype's $j^{th}$ score

## Results and discussion

All the five morphological data for *Clausena heptaphylla*, its essential oil and anethole content were recorded and evaluated after two years of plantation in the year 2016, 2017 and 2018. The range of different morphological and chemical characteristics of the collected germplasm of *C. heptaphylla* were depicted in Table 1. The outcome of the selection trial was the identification of superior genotype rich in anethole content which was later named as Jor Lab CH-2. The average quantitative and qualitative data of the anethole rich genotype Jor Lab CH-2 of *C. heptaphylla* are indicated in Table 2. The herbage yield per plant per cutting was found to be 1.2 Kg while the essential oil yield and anethole content were recorded to be 1.22% and 92.59% respectively. The leaf essential oil yield of *C. heptaphylla* of North eastern region was found to be 0.81% with methyl chavicol as the major (57.5%) component followed by anethole content of 40.3% (Nath and Bordoloi, 1992). Later, Nath et al., in 1996 reported leaf essential oil yield of 1.40% in flowering stage and 1.20% in fruiting stage. Similarly, Munda et al., (2019) also reported essential oil yield of 1.28% from the *C. heptaphylla* leaves which was in accordance to the present study. The essential oil isolated from the leaves of *C. heptaphylla* in the current study was observed to be similar with the earlier study.

The stability of the selected line was further analysed through multilocation trial conducted at four different places of North East India planted for four years to confirm its consistency across different environments. The two check genotypes i.e., CV-1 and CV-2 which are the local genotypes of Assam and Manipur respectively were considered for comparison due to the absence of registered *C. heptaphylla* varieties till date. The most essential requirement for validation of genotype consistency and variety development is the trial conducted in multi-locations or multi-years (Lal et al., 2017; Munda et al., 2020). There are different parameters to check the stability of the genotypes out of which AMMI (Additive multiplicative mean interaction model), GGE (genotype+ genotype × environment) biplot and MTSI (Multi trait stability index) was used to confirm the stability of the selected superior lines and the check genotypes. The multilocation data of the selected strain Jor Lab CH-2 and check genotypes CV-1 and CV-2 for the year 2021 and 2022 are depicted in the Tables S3, S4.

Analysis of variance (ANOVA) was computed using the genotypes and multi-environment trial data which indicated that all the seven traits were statistically significant in the studied environments (E1, E2, E3, E4, E5, E6, E7, and E8). The genotypes were found to be statistically significant for all the studied traits. The genotype × environment (G × E) interaction was observed for the traits leaf width, herbage yield, essential oil and anethole content (Table 3). Since, G × E interaction was observed in the economic traits, therefore, stability analysis was performed for the three traits (HY, EO and AN). The variation

TABLE 1 Range for morphological and chemical data of *C.heptaphylla* germplasm in initial evaluation and multilocation trial.

| S. No. | Characters | Range | |
|---|---|---|---|
| | | Initial evaluation trial | Multilocation trial |
| 1. | Plant height (cm) | 108-260 | 120 - 234 |
| 2. | Leaf length (cm) | 4.6-15 | 4.3 - 8.6 |
| 3. | Leaf width (cm) | 2.7-5.6 | 1.8 - 2.85 |
| 4. | No. of stem branching | 1-7 | 2 - 6 |
| 5. | Herbage yield/plant/cutting (kg) | 0.6-1.2 | 0.41 - 1.12 |
| 6. | Essential oil (%) | 0.8-1.22 | 0.43 - 1.25 |
| 7. | Anethole (%) | 52-92.59 | 40.84 – 93.25 |

TABLE 2 Average quantitative and qualitative data of the anethole rich genotype Jor Lab CH-2 of *C. heptaphylla* during the initial trial.

| S. No. | Characters | Quantitative data |
|---|---|---|
| 1. | Plant height (cm) | 234 ± 2.48 |
| 2. | Leaf length (cm) | 9.3 ± 1.06 |
| 3. | Leaf width (cm) | 3.2 ± 0.68 |
| 4. | No. of stem branching | 7 ± 0.92 |
| 5. | Herbage yield/plant/cutting (Kg) | 1.2 ± 0.23 |
| 6. | Essential oil (%) | 1.22 ± 0.08 |
| 7. | Anethole (%) | 92.59 ± 0.12 |

observed in the three genotypes for the yield traits are represented as boxplots for herbage yield/plant/cutting (Kg), essential oil yield and anethole content (Figure 1). Boxplots are the representative of the concerned traits on the basis of variation, mean and range. The herbage yield (HY) varied from 0.41 (CV1 in E4) to 1.12 (Jor Lab CH-2 in E6) Kg per plant irrespective of different genotypes and multi-environments. Similarly, essential oil ranged from 0.43 (CV1 in E3) to 1.25% (Jor Lab CH-2 in E1) with CV of 44.25% and anethole content varied from 40.84 (CV1 in E7) to 93.25% (Jor Lab CH-2 in E1) with CV of 32.11%. The CV (coefficient of variation) was highest for essential oil yield (44.25%) followed by the number of stem branching per plant (41.03%) and herbage yield per plant (35.99%). The least variation was observed for leaf width (12.89%) with a range of 1.8–2.85 cm. The genotype variability in different environments was indicated for the studied traits. The AMMI ANOVA for herbage yield per plant depicted 97.85% of the total sum of squares (SS) was due to genotype, 0.78 and 0.47% due to environment and interaction between genotype-environment (GEI) respectively. Similarly, 98.64, 0.24, and 0.39% of the SS for essential oil yield was due to genotype, environment and GEI respectively. The anethole content revealed highest SS% due to genotype (98.88), lowest for environment (0.30) and GEI (0.49) (Table 3). The high value of SS% for genotype depicted strong influence of genotypes on the yield parameters while very low environmental influence can be predicted. High value for sum of squares is an indication of strong influence of the source as well as specifies its diverse nature (Alam et al., 2015; Singh et al., 2019). The interaction of genotype with the environment was partitioned into two principal components for all the studied traits. Therefore, the effects of environment as well as genotypes were illustrated simultaneously in biplots of AMMI1 (additive main effects vs IPCA1) and AMMI2 (IPCA1 vs IPCA2). The consistency and high yield of the selected superior line (Jor Lab CH-2) was clearly revealed in the AMMI biplots compared with the check genotypes (Figures 2–4). The key to successful breeding program for development of superior varieties is high yield together with the consistent performance of the genotype in different environments (Lal et al., 2020; Munda et al., 2021). The GGE biplot was also generated since it enables evaluation of environments due to discriminativeness and representativeness of genotype plus genotype-environment interaction which makes it superior to the AMMI biplot analysis (Figure 5) (Yan et al., 2007). Similarly, MTSI analysis clearly demonstrated that Jor Lab CH-2 is the most stable and high yielding genotypes based on all the yield and quality traits (Figure 6). MTSI is a unique technique for selecting stable preferred genotypes in crop breeding programmes based on multiple traits (Benakanahalli et al., 2021). All these parametric analysis supports the notion that the selected strain performed well in all the multi-locations over the years making it a novel anethole rich strain of *C. heptaphylla*. The suitable environment for the herbage yield, essential oil yield and anethole content were also determined in GGE biplot. The environment E7 followed by E6 showed best suitability for herbage yield while for essential oil yield (E2 followed by E6) and anethole content, environment E3 followed

TABLE 3 AMMI Analysis of variance for the seven traits in *C. heptaphylla* in MLT.

| Source | | Plant Height | | Leaf Length | | Leaf Width | | Number of Stem Branching | | Herbage Yield | | Essential Oil % | | Anethole content | |
|---|---|---|---|---|---|---|---|---|---|---|---|---|---|---|---|
| | DF | MS | SS% | MS | SS% | MS | SS% | MS | SS% | MS | SS% | MS | SS% | MS | SS% |
| ENV | 7 | 87.6 | 613.2 | 0.109 | 0.760 | 0.032 | 0.221 | 0.159 | 1.111 | 0.005 | 0.033 | 0.003 | 0.019 | 12.57 | 88.0 |
| REP (ENV) | 16 | 31.4 | 502.7 | 0.329 | 5.274 | 0.048 | 0.773 | 0.917 | 14.667 | 0.002 | 0.038 | 0.003 | 0.055 | 5.83 | 93.3 |
| GEN | 2 | 64653.3 | 129306.7 | 67.334 | 134.668 | 1.578 | 3.156 | 43.931 | 87.861 | 2.072 | 4.145 | 3.709 | 7.419 | 14298.39 | 28596. |
| GEN × ENV | 14 | 17.5 | 245.5 | 0.107 | 1.496 | 0.051 | 0.707 | 0.248 | 3.472 | 0.001 | 0.020 | 0.002 | 0.029 | 10.21 | 142.9 |
| PC1 | 8 | 24.2 | 193.3 | 0.153 | 1.225 | 0.067 | 0.534 | 0.363 | 2.905 | 0.002 | 0.017 | 0.002 | 0.018 | 11.28 | 90.2 |
| PC2 | 6 | 8.7 | 52.2 | 0.045 | 0.271 | 0.029 | 0.173 | 0.095 | 0.567 | 0.001 | 0.003 | 0.002 | 0.011 | 8.78 | 52.7 |
| Residuals | 32 | 36.6 | 1171.1 | 0.274 | 8.753 | 0.044 | 1.394 | 0.667 | 21.333 | 0.004 | 0.113 | 0.002 | 0.073 | 7.60 | 243.2 |
| Total | 85 | 1553.9 | 132084.6 | 1.794 | 152.447 | 0.082 | 6.959 | 1.522 | 131.917 | 0.051 | 4.369 | 0.089 | 7.623 | 344. 79 | 29307.1 |
| CV | | 25.95 | | 23.35 | | 12.89 | | 41.03 | | 35.99 | | 44.25 | | 32.11 | |

ENV, environment; REP, replication; GEN, genotype; PC, Principal components; DF, degree of freedom; MS, mean sum of squares; CV, coefficient of variation.

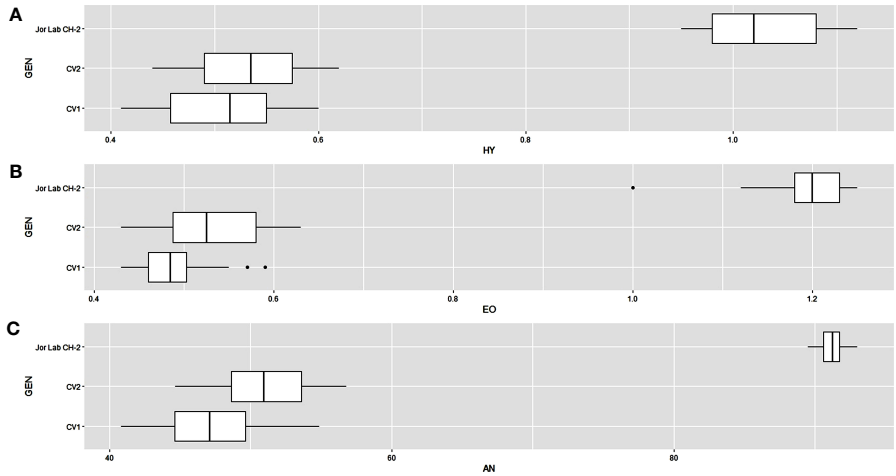


FIGURE 1
Box plots depicting the variation in **(A)** Herbage yield plant$^{-1}$ (HY), **(B)** Essential oil yield (EO) and **(C)** Anethole content (AN) for individual genotypes over the environments. The dashed line shows the overall mean.

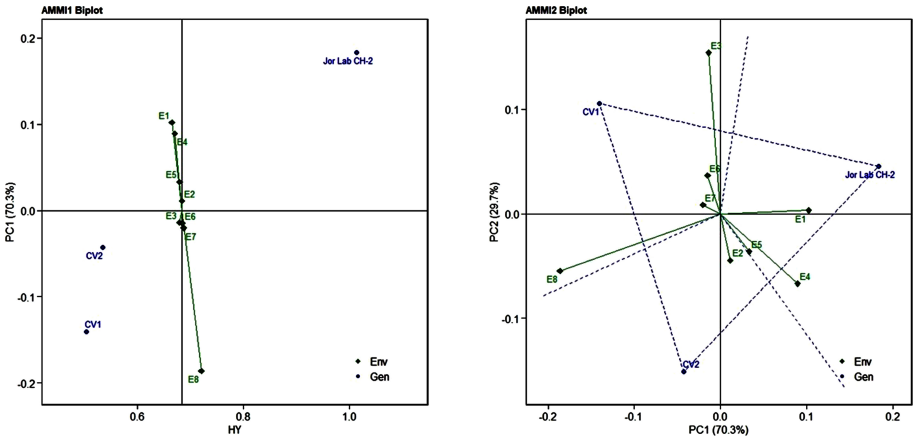


FIGURE 2
AMMI 1 and 2 model biplot for herbage yield/plant (Kg) of Jor Lab CH-2 compared with the check genotypes (CV1 and CV2) evaluated in eight environments.

by E2 were the most favorable environments. The location Imphal and Madang located in Manipur and Assam respectively could be considered as the suitable location for Jor Lab CH-2.

The chemical profiling of the essential oil analysis for Jor Lab CH-2 led to the identification of four compounds accounting for 98.54% of the total essential oil (Figure 7). The compound trans-Anethole was the principal constituent with area percentage of 93.25% which was followed by estragole (4.85%). The trace components were cis-Anethole (0.27%) and Benzene, 1,2-dimethoxy-4-(1-propenyl Isoeugenol methyl ether (0.17%) (Table 4). Trans anethole is an ethanol soluble volatile compound characterized by grassy and sweet aroma. It is an isomer of E-anethole and is widely used in pharmaceutical, cosmetic, food and fragrance industries (Akcan et al., 2018). Anethole is dominantly present in the essential oil of *Illicium verum* (72-92%) and also in *Foeniculum vulgare* and *Pimpinella anisum* seed (Sharafan et al., 2022). In contrast, the present study demonstrated that the superior strain of *Clausena heptaphylla* essential oil exhibited an average of 92.59% trans anethole which

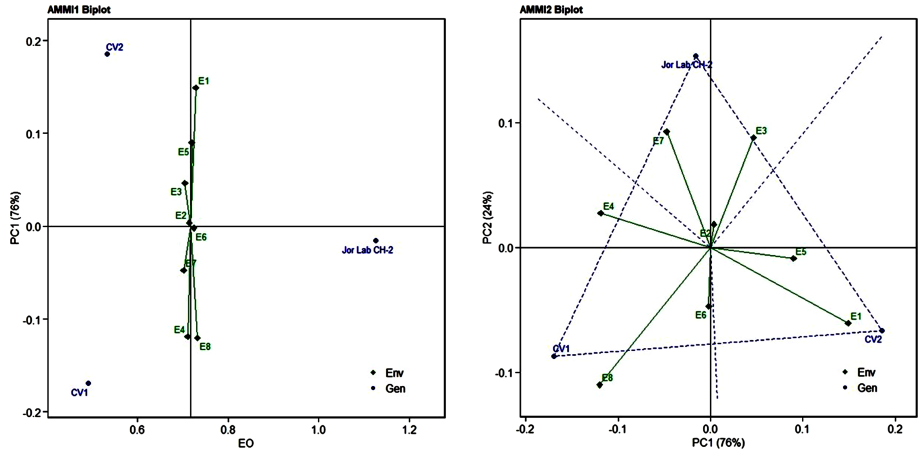


FIGURE 3
AMMI 1 and 2 model biplot for essential oil yield (%) of Jor Lab CH-2 compared with the check genotypes (CV1 and CV2) evaluated in eight environments.

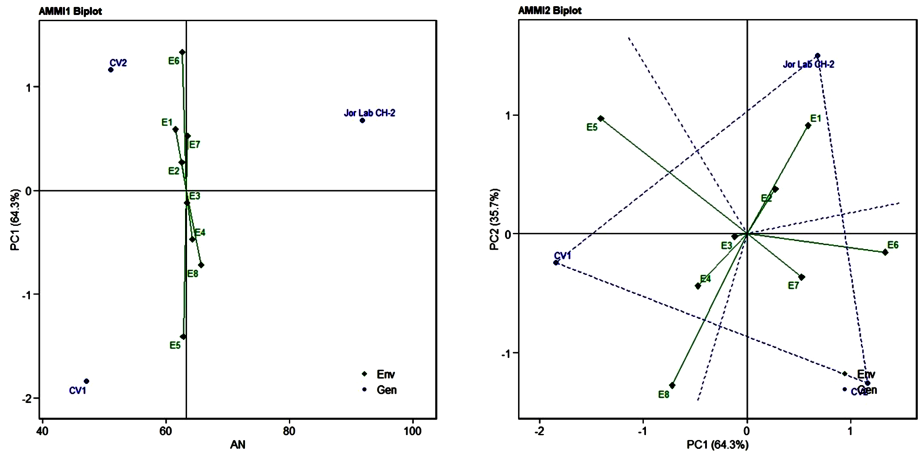


FIGURE 4
AMMI 1 and 2 model biplot for anethole content (%) of Jor Lab CH-2 compared with the check genotypes (CV1 and CV2) evaluated in eight environments.

is higher than the *Illicium verum* essential oil. The essential oil of *I. verum*, *F. vulgare* and *P. anisum* seeds are very expensive which could be substituted with the easily available *C. heptaphylla* proving to be a cost-effective alternative source. The essential oil of the identified strain Jor Lab CH-2 can be a good source of anethole for industrial applications due to its various biological activities as pharmaceutical applications. A recent study reported the efficiency of anethole rich Jor Lab CH-2 as skin whitening agent, anti-diabetic and anti-inflammatory representatives which is non-toxic in nature (Lal et al., 2022). Similarly, other pharmacological applications include antimicrobial, anti-helminthic, antinociceptive, gastroprotective, sedative properties (Marinov and Kuzmanova, 2015; Munda et al., 2019). Additionally, it also serves as a masking agent to cover up unpleasant odors in various products like mouthwash, toothpaste, soaps etc. It is also used in food industry as flavoring agent and additives in chewing gums, candies, baked foods etc. Therefore, the anethole rich strain of *C. heptaphylla* will be highly beneficial to the essential oil, food, perfumery and pharmaceutical industries. Earlier studies from North Eastern region of India performed on *C. heptaphylla* essential oil revealed only 40.3% E-anethole in leaf essential oil and 12.7% in fruit essential oil which

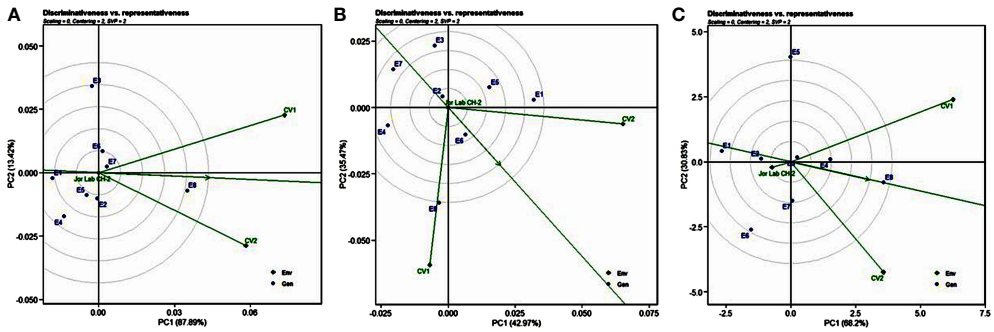


FIGURE 5
interaction effect of Jor Lab CH-2, CV1 and CV2 over two years across four multilocations for **(A)** Herbage yield plant$^{-1}$ **(B)** Essential oil yield **(C)** Anethole content. The biplots were created based on Scaling = 0, Centering = 0,SVP = 2.

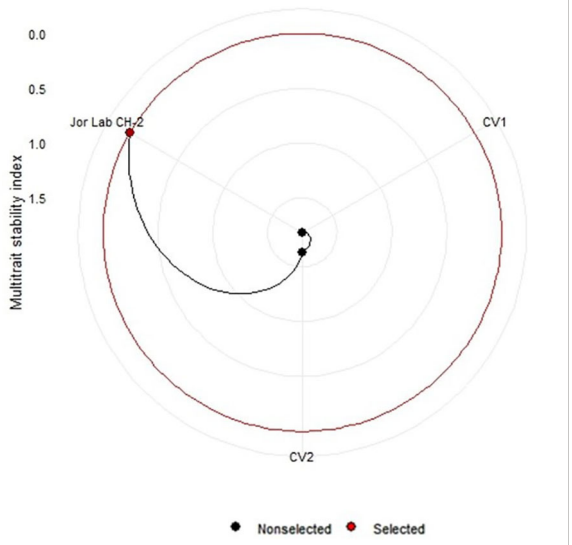


FIGURE 6
Multi trait stability index (MTSI) of Jor Lab CH-2 and check genotypes based on three yield parameters (Herbage yield plant$^{-1}$, Essential oil yield and Anethole content).

is much lower to the present strain (Nath and Bordoloi, 1992). Later, Nath et al., (1996) reported the presence of E-anethole as the major component in *C. heptaphylla* essential oil with 98.2% in leaf essential oil at both fruiting and flowering stage while 61.67% anethole was revealed in fruit essential oil. Some investigation also reported that other species of *Clausena* like *C. anisate*, *C. austroindica* and *C. harmandiana* possesses anethole (80.00–97.44%) as major component in leaf essential oil (Addae-Mensah et al., 1996; Johnson et al., 2022). Another report mentioned that *C. indica* essential oil was rich in myristicin (35.3%) content (Diep et al., 2009) while *C. pentaphylla* yielded 0.80% essential oil having methyl eugenol (38.1%) as the principal volatile constituent (Pandey et al., 2012). The variation in the chemical constituents of the essential oil may serve as the chemotaxonomic value for intraspecific differentiation of *Clausena* species. A recent report was published by the same team on the biological activities of Jor Lab CH-2 which indicated the presence of anethole (88.59%) as the principal component (Lal et al., 2022). However, the stability analysis was not performed to observe its consistency across different locations over the years which is an essential criterion for varietal development. The strain clearly represented its stability based on herbage yield, essential oil yield and anethole content across four different multi-locations of NE India.

## Conclusions

*Clausena heptaphylla* is a plant of industrial importance because the essential oil of this plant consists of anethole which is used in pharmaceutical, perfumery and food industries. Currently, the industries rely on *Illicium verum*, *Foeniculum vulgare* and *Pimpinella anisum* seeds to produce anethole but the essential oil of these species are very expensive. Therefore, the essential oil of these species can be substituted with Jor Lab CH-2 which is anethole rich strain and cost effective. This high anethole rich strain of *C. heptaphylla* was identified through evaluation trial for four years followed by multilocation trial in four different locations for four years with a total of eight-year study. The agronomical and the biochemical data clearly indicated that Jor Lab CH-2 was superior than the other studied genotypes with plant height of 234 cm, leaf length (9.3 cm), leaf width (3.2 cm), number of stem branching (7), herbage yield of 1.2 Kg per plant, essential oil% (1.22%) and

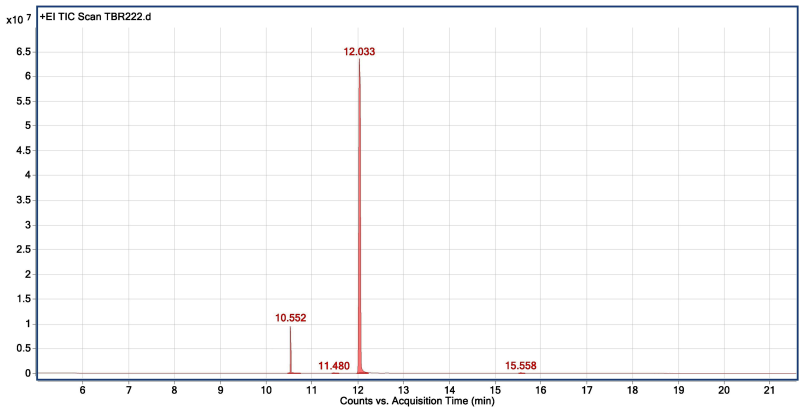


FIGURE 7
Chromatogram for GC-MS analysis of anethole rich variety Jor Lab CH-2 of *Clausena heptaphylla*.

TABLE 4 GC-MS analysis of anethole rich variety of *C. heptaphylla* (Jor Lab CH-2) leaf essential oil planted at Madang location.

| Compound | Retention Time | Retention Indices$^{exp}$ | Retention Indices$^{lit}$ | Area% |
|---|---|---|---|---|
| Estragole | 10.55 | 1196 | 1198 | 4.85 |
| cis-Anethole | 11.48 | 1254 | 1256 | 0.27 |
| trans-Anethole | 12.03 | 1284 | 1285 | 93.25 |
| Benzene, 1,2-dimethoxy-4-(1-propenyl Isoeugenolmethyl ether | 15.55 | 1492 | 1492 | 0.17 |
| Total identified | | | | 98.54 |
| Total identified | | | | 1.46 |
| Total | | | | 100.00 |

exp, experimental; lit, literature.

anethole% (92.59%). Stability along with the superiority is an important step in varietal development programme; therefore, stability parameters like AMMI, GGE and MTSI were used to confirm the results of the identified strain along with the check genotypes indicating the stable performance of Jor Lab CH-2 in terms of economic yield. This is the first report on the identification of anethole rich novel strain of *C. heptaphylla* which was followed by stability analysis, the results were found to be consistent and satisfactory. This new strain will expand the possibilities for the commercial production of anethole and offer the pharmaceutical, perfumery and food industries new cheap sources of raw materials.

## Data availability statement

The original contributions presented in the study are included in the article/Supplementary Material, further inquiries can be directed to the corresponding author.

## Author contributions

ML: Conceptualization, methodology, supervision, resources, review and editing. SM: Investigation, methodology, formal and software analysis, writing - original draft. AG: Writing, formatting and editing. TB: GC-MS analysis of essential oil. JB: Data curation. SC: Formal analysis. HL: Data curation. All authors contributed to the article and approved the submitted version.

## Funding

The authors are grateful to CSIR-Aroma Mission (Phase-II) for funding in the form of project HCP007.

## Acknowledgments

We appreciate the Director, CSIR-North East Institute of Science and Technology, Jorhat, Assam, for providing the field and laboratory infrastructure necessary to carry out the study.

## Conflict of interest

The authors declare that the research was conducted in the absence of any commercial or financial relationships that could be construed as a potential conflict of interest.

## Publisher's note

All claims expressed in this article are solely those of the authors and do not necessarily represent those of their affiliated organizations, or those of the publisher, the editors and the reviewers. Any product that may be evaluated in this article, or claim that may be made by its manufacturer, is not guaranteed or endorsed by the publisher.

## Supplementary material

The Supplementary Material for this article can be found online at: https://www.frontiersin.org/articles/10.3389/fpls.2022.1060492/full#supplementary-material

## References


Addae-Mensah, I., Asomaning, W. A., Oteng-Yeboah, A., Garneau, F. X., Gagnon, H., Jean, F. I., et al. (1996). (E)-anethole as a major essential oil constituent of *Clausena anisata*. *J. Essent. Oil Res.* 8 (5), 513–516. doi: 10.1080/10412905.1996.9700678

Agarwal, V. S. (1986). *Economic plants of India* (Calcutta: Khailash Prakashan).

Akcan, R., Lale, A., and Tumer, A. R. (2018). Trans-anethole: A key compound in bogma raki. *Acta Med.* 49, 26–31.

Alam, M. A., Sarker, Z. I., Farhad, M., Hakim, M. A., Barma, N. C. D., Hossain, M. I., et al. (2015). Yield stability of newly released wheat varieties in multi-environments of Bangladesh. *Int. J. Plant Soil Sci.* 6, 150–161. doi: 10.9734/IJPSS/2015/14824

Aprotosoaie, A. C., Costache, I. I., and Miron, A. (2016). Anethole and its role in chronic diseases. *Adv. Exp. Med. Biol.* 929, 247–267. doi: 10.1007/978-3-319-41342-6_11

Begum, R., Kaisar, M. A., Rahman, M. S., Chowdhury, A. M. S., Rahman, M. M., Hasan, C. M., et al. (2011). Clausenolide-1-methyl ether from *Clausena heptaphylla* W & A. *Bol. Latinoam. Caribe. Plant Med. Aromat.* 10 (2), 136–138.

Benakanahalli, N. K., Sridhara, S., Ramesh, N., Olivoto, T., Sreekantappa, G., Tamam, N., et al. (2021). A framework for identification of stable genotypes based on MTSI and MGDII indexes: An example in guar (*Cymopsis tetragonoloba* l.). *Agron.* 11 (6), 1221. doi: 10.3390/agronomy11061221

Bhattacharyya, P., Biswas, G. K., Barua, A. K., Saha, C., Roy, I. B., and Chowdhury, B. K. (1993). Clausenalene, a carbazole alkaloid from *Clausena heptaphylla*. *Phytochem* 33, 248. doi: 10.1016/0031-9422(93)85437-V

Bhattacharyya, P., Chakraborty, A., and Chowdhury, B.K. (1984). Heptazolicine, a carbazole alkaloid from *Clausena heptaphylla*. *Phytochem* 23 (10), 2409–2410. doi: 10.1016/S0031-9422(00)80575-0

Chakraborty, A., Saha, C., Podder, G., Chowdhury, B. K., and Bhattacharyya, P. (1995). Carbazole alkaloid with antimicrobial activity from *Clausena heptaphylla*. *Phytochem.* 38 (3), 787–789. doi: 10.1016/0031-9422(94)00666-H

Clevenger, J. F. (1928). Apparatus for the determination of volatile oil. *JAPhA* 17 (4), 345–349. doi: 10.1002/jps.3080170407

Diep, P. T. M., Pawlowska, A. M., Cioni, P. L., Minh, C. V., Huong, L. M., and Braca, A. (2009). Chemical composition and antimicrobial activity of *Clausena indica* (Dalz) oliv. (Rutaceae) essential oil from Vietnam. *Nat. Prod. Commun.* 4 (6), 869–872. doi: 10.1177/1934578X090040062

Dutta, P., Sarma, N., Saikia, S., Gogoi, R., Begum, T., and Lal, M. (2021). Pharmacological activity of *Trachyspermum ammi* l. seeds essential oil grown from northeast India. *J. Essent. Oil Bear. Plants* 24 (6), 1373–1388. doi: 10.1080/0972060X.2022.2028681

Fakruddin, M., Mannan, K. S. B., Mazumdar, R. M., and Afroz, H. (2012). Antibacterial, antifungal and antioxidant activities of the ethanol extract of the stem bark of *Clausena heptaphylla*. *BMC Complement Altern. Med.* 12 (1), 1–9. doi: 10.1186/1472-6882-12-232

Guo, S. S., Wang, Y., Chen, Z. Y., Zhang, Z., Cao, J. Q., Pang, X., et al. (2018). Essential oils from *Clausena species* in China: Santalene sesquiterpenes resource and toxicity against *Liposcelis bostrychophila*. *J. Chem.* 2018, 7813675. doi: 10.1155/2018/7813675

Gupta, P., Dhawan, S. S., and Lal, R. K. (2015). Adaptability and stability based differentiation and selection in aromatic grasses (*Cymbopogon* species) germplasm. *Ind. Crops Prod* 78, 1–8. doi: 10.1016/j.indcrop.2015.10.018

Hossan, M. S., Hanif, A., Khan, M., Bari, S., Jahan, R., and Rahmatullah, M. (2009). Ethnobotanical survey of the tripura tribe of bangladesh. am. -Eurasian. *J. Sustain. Agric.* 3 (2), 253–261.

Jerajasin, T., Pradermwong, K. P., and Watthanachaiyingcharoen, R. (2014). "Antioxidant activities and cytotoxic effects of aqueous extracts from *Clausena heptaphylla* Wright and arn. leaves and *Vernonia cinerea* less," in *Agricultural Sciences: Leading Thailand to World Class Standards. Proceedings of the 52nd Kasetsart University Annual Conference*, 4-7 February 2014. Vol 4. Kasetsart University, Thailand: Science, Natural Resources and Environment, 1–8.

Johnson, A. J., Venukumar, V., Varghese, T. S., Viswanathan, G., Leeladevi, P. S., Remadevi, R. K. S., et al. (2022). Insecticidal properties of clausena austroindica leaf essential oil and its major constituent, trans-anethole, against *Sitophilus oryzae* and *Tribolium castaneum*. *Ind. Crops Prod* 182, 114854. doi: 10.1016/j.indcrop.2022.114854

Lal, M., Begum, T., Gogoi, R., Sarma, N., Munda, S., Pandey, S. K., et al. (2022). Anethole rich *Clausena heptaphylla* (Roxb.) Wight &Arn., essential oil pharmacology and genotoxic efficiencies. *Sci. Rep.* 12 (1), 1–13. doi: 10.1038/s41598-022-13511-8

Lal, M., Munda, S., Begum, T., and Pandey, S. K. (2021). Identification of a stable rhizome essential oil-rich variety (Jor Lab SM-2) of *Homalomena aromatica* schott., through biometrical method. *J. Essent. Oil Bear. Plants* 24 (5), 1026–1041. doi: 10.1080/0972060X.2021.1995510

Lal, M., Munda, S., Dutta, S., Baruah, J., and Pandey, S. K. (2017). Identification of the newhigh oil and rhizome yielding variety of *Kaempferia galanga* (Jor Lab K-1): A highly important in digenous medicinal plants of north East India. *J. Essent. Oil-Bear. Plants* 20 (5), 1275–1282. doi: 10.1080/0972060X.2017.1400405

Lal, M., Munda, S., Dutta, S., and Pandey, S. K. (2020). Identification of a novel germplasm (Jor Lab l-9) of lemon grass (*Cymbopogon khasianus*) rich in methyl eugenol. *Crop Breed. App. Biotechnol.* 20 (3), e320720315. doi: 10.1590/1984-70332020v20n3c49

Lockwood, G. B. (1984). The essential oil from leaves of *Clausena heptaphylla*. *Fitoterapia* 55, 123–124.

Majumder, S., and Rahman, M. M. (2016). Effect of different plant growth regulators on *in vitro* propagation of *Clausena heptaphylla* (Roxb.)–an aromatic and medicinal Shrub.J. *Pharmacogn. Phytochem.* 5 (3), 58–63.

Mannaf, M. A., Islam, M. A., Akter, S., Akter, R., Nasrin, T., Zarin, I., et al. (2013). A randomized survey of differences in medicinal plant selection as well as diseases treated among folk medicinal practitioners and between folk and tribal medicinal practitioners in bangladesh. am. -Eurasian. *J. Sustain. Agric.* 7 (3), 196–209.

Marinov, V., and Valcheva-Kuzmanova, S. (2015). Review on the pharmacological activities of anethole. *Script. Sci. Pharmaceut.* 2 (2), 14–19. doi: 10.14748/ssp.v2i2.1141

Mehra, P. N., and Khosla, P. K. (1973). Cytological studies of Himalayan rutaceae. *Silvae Genetica* 22 (5-6), 182–188.

Munda, S., Dutta, S., and Lal, M. (2021). Variability estimation and genetic divergence in *Cymbopogon winterianus* for development of superior genotype. *Agron. J.* 113 (2), 993–1007. doi: 10.1002/agj2.20505

Munda, S., Dutta, S., Pandey, S. K., Sarma, N., and Lal, M. (2019). Antimicrobial activity of essential oils of medicinal and aromatic plants of the north-east India: A biodiversity hot spot. *J. Essent. Oil Bear. Plants* 22 (1), 105–119. doi: 10.1080/0972060X.2019.1601032

Munda, S., Sarma, N., and Lal, M. (2020). GxE interaction of 72 accessions with three year evaluation of cymbopogon winterianus jowitt. using regression coefficient and additive main effects and multiplicative interaction model (AMMI). *Ind. Crop Prod.* 146, 112169. doi: 10.1016/j.indcrop.2020.112169

Nath, S. C., and Bordoloi, D. N. (1992). Major components of the leaf and fruit oil of *Clausena heptaphylla* W&A growing in northeast India. *J. Essent. Oil Res.* 4,6, 655–656. doi: 10.1080/10412905.1992.9698154

Nath, S. C., Hazarika, A. K., and Sarma, K. K. (1996). Chemical composition of the leaf and fruit oil of *Clausena heptaphylla* W&A from northeast India. *J. Essent. Oil Res.* 8 (2), 197–198. doi: 10.1080/10412905.1996.9700593

Olivoto, T., Lucio, A. D. C., da Silva, J. A. G., Sari, B. G., and Diel, M. I. (2019). Mean performance and stability in multi-environment trials II: selection based on multiple traits. *J. Agron.* 111 (6), 2961–2969. doi: 10.2134/agronj2019.03.0221

Pandey, S. K., Bhandari, S., Sarma, N., Begum, T., Munda, S., Baruah, J., et al. (2021). Essential oil compositions, pharmacological importance and agro technological practices of patchouli (*Pogostemon cablin* benth.): A review. *J. Essent. Oil Bear. Plants* 24 (6), 1212–1226. doi: 10.1080/0972060X.2021.1995511

Pandey, A. K., Singh, P., Mohan, M., and Tripathi, N. N. (2012). New report on the chemical composition of the essential oil from leaves of clausena pentaphylla from India. *Chem. Nat. Compd.* 48 (5), 896–897. doi: 10.1007/s10600-012-0416-9

Sharafan, M., Jafernik, K., Ekiert, H., Kubica, P., Kocjan, R., Blicharska, E., et al. (2022). *Illicium verum* (Star anise) and *Trans*-anethole as valuable raw materials for medicinal and cosmetic applications. *Molecules* 27, 650. doi: 10.3390/molecules27030650

Singh, C., Gupta, A., Gupta, V., Kumar, P., Sendhil, R., Tyagi, B. S., et al. (2019). Genotype x environment interaction analysis of multi-environment wheat trials in India using AMMI and GGE biplot models. *Crop Breed. Appl. Biotechnol.* 19, 309–318. doi: 10.1590/1984-70332019v19n3a43

Sohrab, M. H., Mazid, M. A., Rahman, E., Hasan, C., and Rashid, M. A. (2001). Antibacterial activity of clausena heptaphylla. *Fitoterapia* 72 (5), 547–549. doi: 10.1016/S0367-326X(00)00320-8

Sohrab, M. H., Hasan, C. M., and Rashid, M. A. (1999). Lunamarins A and B: two novel terpenoid coumarins from *Clausena heptaphylla*. *Nat. Prod. Lett.* 14 (1), 47–53. doi: 10.1080/10575639908045434

Sohrab, M. H., Hasan, C. M., and Rashid, M. A. (2002). Lunamarin C a novel terpenoid coumarin from *Clausena heptaphylla*. *Pharmazie* 57 (8), 573–574.

Yan, W., Kang, M. S., Ma, B., Woods, S., and Cornelius, P. (2007). GGE biplot vs. AMMI analysis of genotype-by-environment data. *Crop Sci.* 47, 643–655. doi: 10.2135/cropsci2006.06.0374

Yusuf, M., Chowdhury, J. U., Wahab, M. A., and Begum, J. (1994). *Medicinal plants of Bangladesh* (Chittagong, Bangladesh: BCSIR Laboratories).

frontiers | Frontiers in Plant Science

TYPE Original Research
PUBLISHED 10 January 2023
DOI 10.3389/fpls.2022.1089445



OPEN ACCESS

EDITED BY
Weibiao Liao,
Gansu Agricultural University, China

REVIEWED BY
Twahira Begum,
North East Institute of Science and Technology (CSIR), India
Fantao Zhang,
Jiangxi Normal University, China

*CORRESPONDENCE
Qingwen Yang
yangqingwen@caas.cn

SPECIALTY SECTION
This article was submitted to Plant Breeding, a section of the journal Frontiers in Plant Science

RECEIVED 04 November 2022
ACCEPTED 19 December 2022
PUBLISHED 10 January 2023

CITATION
Han ZY, Li F, Qiao WH, Zheng XM, Cheng YL, Zhang LF, Huang JF, Wang YY, Lou DJ, Xing M, Fan WY, Nie YM, Guo WL, Wang SZ, Liu ZR and Yang QW (2023) Global whole-genome comparison and analysis to classify subpopulations and identify resistance genes in weedy rice relevant for improving crops. *Front. Plant Sci.* 13:1089445. doi: 10.3389/fpls.2022.1089445



# Global whole-genome comparison and analysis to classify subpopulations and identify resistance genes in weedy rice relevant for improving crops

Zhenyun Han[1], Fei Li[1], Weihua Qiao[1,2], Xiaoming Zheng[1,2,3], Yunlian Cheng[1], Lifang Zhang[1], Jingfen Huang[1], Yanyan Wang[1], Danjing Lou[1], Meng Xing[1], Weiya Fan[1], Yamin Nie[1], Wenlong Guo[1], Shizhuang Wang[1], Ziran Liu[1] and Qingwen Yang[1,2]*

[1]National Key Facility for Crop Gene Resources and Genetic Improvement, Institute of Crop Sciences, Chinese Academy of Agricultural Sciences, Beijing, China, [2]National Nanfan Research Institute (Sanya), Chinese Academy of Agricultural Sciences, Sanya, China, [3]International Rice Research Institute, Metro Manila, Philippines

Common weedy rice plants are important genetic resources for modern breeding programs because they are the closest relatives to rice cultivars and their genomes contain elite genes. Determining the utility and copy numbers of *WRKY* and nucleotide-binding site (*NBS*) resistance-related genes may help to clarify their variation patterns and lead to crop improvements. In this study, the weedy rice line LM8 was examined at the whole-genome level. To identify the *Oryza sativa japonica* subpopulation that LM8 belongs to, the single nucleotide polymorphisms (SNPs) of 180 cultivated and 23 weedy rice varieties were used to construct a phylogenetic tree and a principal component analysis and STRUCTURE analysis were performed. The results indicated that LM8 with admixture components from *japonica* (GJ) and *indica* (XI) belonged to GJ-admixture (GJ-adm), with more than 60% of its genetic background derived from XI-2 (22.98%), GJ-tropical (22.86%), and GJ-subtropical (17.76%). Less than 9% of its genetic background was introgressed from weedy rice. Our results also suggested LM8 may have originated in a subtropical or tropical geographic region. Moreover, the comparisons with Nipponbare (NIP) and Shuhui498 (R498) revealed many specific structure variations (SVs) in the LM8 genome and fewer SVs between LM8 and NIP than between LM8 and R498. Next, 96 *WRKY* and 464 *NBS* genes were identified and mapped on LM8 chromosomes to eliminate redundancies. Three *WRKY* genes (*ORUFILM02g002693*, *ORUFILM05g002725*, and *ORUFILM05g001757*) in group III and one RNL [including the resistance to powdery mildew 8 (RPW8) domain, NBS, and leucine rich repeats (LRRs)] type *NBS* gene (*ORUFILM12g000772*) were detected in LM8. Among the *NBS* genes, the

RPW8 domain was detected only in *ORUFILM12g000772*. This gene may improve plant resistance to pathogens as previously reported. Its classification and potential utility imply LM8 should be considered as a germplasm resource relevant for rice breeding programs.

KEYWORDS

weedy rice, population classification, structural variation, WRKY, NBS

## 1 Introduction

The genus *Oryza* comprises plants with an evolutionary history spanning 15 million years, during which they underwent both natural selection and artificial selection. Weedy rice (*Oryza sativa* f. *spontanea*), which is a conspecific relative of cultivated rice that commonly grows in close proximity to cultivated rice, has certain wild rice characteristics that combine to form diverse features (Li et al., 2017; Wu et al., 2021). Previous research indicated that hybridizations between crops and weeds are relatively uncommon, and alleles for excellent agronomic traits in compatible rice plants may be introgressed into weed populations (Lu et al., 2016; Merotto et al., 2016). According to a recent analysis of genome sequencing data, Chinese weedy rice lines independently de-domesticated from locally cultivated rice varieties and were modified by balancing selection during the de-domestication process (Qiu et al., 2017). Meanwhile, Li et al. (2017) detected two strains of weedy rice in the USA that originated from Asian *indica* and *aus* rice plants *via* de-domestication events. On the basis of population genomic analyses, weedy rice at high latitudes and weedy rice at middle latitudes were grouped with *japonica* and *indica* accessions, respectively (Sun et al., 2019). To date, the commonly used rice reference genomes are from Nipponbare (NIP; Kawahara et al., 2013), 93-11 (International Rice Genome Sequencing Project, 2005), Shuhui498 (R498; Du et al., 2017), as well as Zhenshan 97 and Minghui 63 (Zhang J W et al., 2016). To accelerate the identification of beneficial alleles in weedy rice potentially useful for enhancing cultivated rice, the genomes of WR04-6 (Sun et al., 2019) and LM8 (Li et al., 2021), which are two weedy rice lines, have been assembled.

Unlike animals, which can move toward the most appropriate areas within their habitats and avoid diverse stresses, plants are sessile and continuously exposed to various abiotic and biotic stresses. Accordingly, identifying genetic variations in resistant germplasms and clarifying complex pathways regulating resistance are critical for the breeding of resistant crop species. The immunity network and mechanisms underlying the adaptation of plants to adverse environmental stimuli remain to be thoroughly characterized, although WRKY and NBS genes resistance genes are confirmed contributors. Specifically, WRKY-encoding proteins, also as one of transcription factors (TFs), are involved in regulating plant responses to multiple stresses, including pathogen or bacterial infections, drought, cold, freezing, and wounding (Li et al., 2020). They usually contain a DNA-binding region comprising the highly conserved WRKYGQK sequence (i.e., WRKY domain) at the N-terminus as well as a zinc finger structure ($CX_{4-5}CX_{22-23}HXH$) (Eulgem et al., 2000). Both the W-box region with the consensus sequence (C/T)TGAC(T/C) and the sugar-responsive element comprising TAAAGATTACTAATAGGAA in the downstream target gene promoters are specifically recognized by WRKY TFs, resulting in activated transcription (Sun et al., 2003). The WRKY TFs in group I contain two WRKY domains, whereas the group II and III members have one WRKY domain. The WRKY TFs in groups II and III may be distinguished by their $C_2H_2$ and $C_2HC$ zinc fingers, respectively (Chen et al., 2017). The WRKY domain has been detected in two Arabidopsis TIR-NBS-LRR (TNL) proteins (Narusaka et al., 2009).

In fact, the TIR-NBS-LRR proteins, which are also called TNL proteins, consist of a nucleotide-binding (NB) domain and C-terminal leucine rich repeats (LRRs) along with a Toll/interleukin-1 receptor/resistance (TIR) domain in the N-terminal region (Collier and Moffett, 2009). The presence of a coiled-coil (CC) domain instead of a TIR domain in the NBS-LRR N-terminal region results in a CC-NBS-LRR (CNL) protein (Collier and Moffett, 2009). Apart from TNL and CNL genes, RPW8-NBS-LRR (RNL) represent a special N-terminal domain known as RPW8 (resistance to powdery mildew 8) domain containing NBS-LRR region (Zhang Y M et al., 2016). The NB and LRR domains are separated by an ARC (Apaf-1, R protein, and CED-4) domain (Collier and Moffett, 2009). The functional central nucleotide-binding pocket includes the NB and ARC domains (Collier and Moffett, 2009). During the co-evolution with pathogenic microorganisms, plants evolved a series of resistance (*R*) and avirulence genes that protect against infections. Similar to other crops, rice has evolved two defense strategies, namely pathogen-associated molecular pattern (PAMP)-triggered immunity (PTI) and effector-triggered immunity (ETI) (Dodds and Rathjen, 2010). Of the

known *R* genes, *NBS* genes are the most prevalent and they encode proteins with important roles in the ETI system (Meyers et al., 2003). The WRKY TFs and NBS proteins in *Oryza* species have been identified and analyzed, including those in cultivated rice and wild rice; however, those in weedy rice species have not been studied (Ross et al., 2007; Xu et al., 2016; Rawal et al., 2018).

The LM8 weedy rice line was named because its pericarp is green until maturity. There is increasing interest in this weedy rice line among breeders because of its green pericarp and small grains, which may be preferred by consumers. In this study, LM8 was used for a whole-genome analysis after a high-quality genome was assembled. The subpopulation classification of LM8 was completed using cultivated *japonica* and *indica* strains. Moreover, a comparative analysis was performed using NIP and R498 reference genomes. In addition, the weedy rice *WRKY* and *NBS* gene family members were identified and collated for a comprehensive genome-wide analysis and comparison with diverse species. Phylogenetic relationships and the conserved motifs among families were investigated to provide useful insights into the conserved regulator. On the basis of our study findings, LM8 may be used to clarify the rice de-domestication process, while also serving as a resource for plant biotechnologists and breeders interested in enhancing rice traits through genetic modifications.

# 2 Materials and methods

## 2.1 Plant materials and data selection

The 203 *Oryza* species used for the subgroup classification of LM8 included 180 cultivated varieties and 23 weedy rice varieties. The *O. sativa* groups *japonica* and *indica* were designated as GJ and XI, respectively. Using the 3K database (Wang et al., 2018; https://registry.opendata.aws/3kricegenome/), 20 cultivated varieties were randomly selected from the GJ-adm (admixture components within *japonica* and *indica*), GJ-trp (Southeast Asian tropical), GJ-sbtrp (Southeast Asian subtropical), GJ-tmp (primarily East Asian temperate), XI-1A (East Asia), XI-1B (modern varieties of diverse origins), XI-2 (South Asia), XI-3 (Southeast Asia), and XI-adm groups. The NIP and R498 genomes were selected as the representative *japonica* and *indica* reference genomes for the whole-genome comparison with LM8.

## 2.2 Detection and annotation of SNPs

The SNP databases for the 180 cultivated varieties are available online (SNP-Seek; http://snp-seek.irri.org). Information for 10 straw hull (SH) and 10 black hull awned (BHA) US weedy rice lines and 3 Chinese weedy rice lines was downloaded from the National Center for Biotechnology Information (NCBI) database (SRR4334499). The NIP, R498, and Arabidopsis genome data at the chromosome level were obtained from online databases (www.rice.uga.edu/, www.mbkbase.org/R498/, and www.ncbi.nlm.nih.gov/data-hub/genome/GCF_000001735.4/, respectively). Details regarding the LM8 genome are available in the NCBI BioProject database (accession number PRJNA754271).

Variant SNPs and insertions/deletions (InDels) were detected using the GATK (4.2.2.0) software, which was followed by (1) identification of active regions; (2) assembly of plausible haplotypes; (3) estimation of the per read likelihoods using the PairHMM algorithm; and (4) determination of the sample genotype. First, the GATK-HaplotypeCaller tool (versions 4.2.2.0) was used to analyze the bam files to obtain the sample GVCFs, after GATK-GenotypeGVCFs were used to genotype the variants with CombineGVCFs. Second, raw variants generated from the calling steps were filtered to identify the high-quality variants using the following parameters of GATK VariantFiltration: QD <2.0, MQ <40.0, FS >60.0, MQRankSum <−12.5, ReadPosRankSum <−8.0, and SOR >4.0. After combining the 3K-SNP data, the 5.12 Mb raw variants were filtered again (mis <10% and maf >5%) to generate the 4.03 Mb variant files (Table S1).

## 2.3 Population structure and phylogenetic analyses

On the basis of the whole-genome SNPs among the 201 *Oryza* species included in this study, a neighbor-joining phylogenetic tree was constructed using the Treebest (versions 1.9.2) software, with 1,000 bootstrap replicates. As previously described (Lee et al., 2014), a typical method to construct trees has been: 1) calculating p-distance from all SNP data between two samples, 2) making the p-distance matrix for all samples, 3) constructing and drawing the phylogenetic tree image. The principal component analysis (PCA) of the SNPs was completed using the GCTA software to cluster the principal components into different subsets according to the differences in the individual genome SNPs. The population structure was analyzed using the ADMIXTURE software. Low cross-entropy values reflected high-quality runs. Independent runs were performed for each simulated *K* value (from 2 to 10). The *K* value for which the cross-entropy curve reflected a sensible model was chosen (i.e., based on the likelihood value).

## 2.4 Genome comparison and analysis

Two comparisons were completed (LM8 *versus* NIP and LM8 *versus* R498) using the MUMmer (4.0.0rc1) software with the following parameters: nucmer -l 50 -c 100 -mum; delta-filter -i 90 -l 100 -1. According to the results of the collinearity

analysis, presence-absence variations (PAVs) and structural variations (SVs) were identified using the SVUM and SYRI programs, respectively. In the final sequence variation files, variant sequences longer than 50 kb were retained, whereas variant sequences in the gap region were eliminated during the original variation test. Each SV was calculated for 1 Mb windows to generate the final Circos results.

### 2.5 *WRKY* and *NB-LRR* gene family analysis

To identify the *WRKY* and *NB-LRR* genes, the WRKY and TIR, CC, NBS, or LRR amino acid motifs were searched. The *WRKY* and *NLR* sequences in the LM8, NIP, and Arabidopsis genomes were obtained from database (accession number PRJNA754271 in the NCBI BioProject, www.rice.uga.edu, and www.ncbi.nlm.nih.gov/data-hub/genome/GCF_000001735.4/, respectively). The Molecular Evolutionary Genetics Analysis (MEGA; v11) program was used to construct a maximum-likelihood gene family phylogenetic tree, with 1,000 bootstrap replicates. Next, the *WRKY* and *NB-LRR* genes were mapped to 12 chromosomes using MapChart (2.3).

## 3 Results

### 3.1 Subpopulation classification of LM8 in *Oryza* plants

In 2021, Li et al. published the LM8 high-quality genome sequence and revealed LM8 is a *japonica*-type weedy rice line. To further classify LM8 within the *japonica* group, its SNPs as well as those in other weedy rice lines and accessions from the 3K database selected on the basis of the 3K classifications were downloaded to construct a neighbor-joining phylogenetic tree. The *indica* group (XI) served as the control. The phylogenetic tree constructed according to pairwise Nei's genetic distances showed that the 10 subpopulations could be clustered into two groups (*japonica* and *indica*) (Figure 1A). Additionally, LM8 was located in the 'adm' branch (Figure 1A), implying that it was admixed (i.e., between *japonica* and *indica*). Moreover, LM8 was also classified in the *japonica* group. To verify the classification of LM8 in GJ-adm, a PCA was performed using the genome-wide SNPs in domesticated and weedy rice varieties (Figures 1B, C, and S1). The first three principal components (PCs), which explained 36.68% of the variance (Table S2), corresponded to genetic evolutionary factors as follows: PC1 separated the *japonica* (GJ-adm, GJ-trp, GJ-sbtrp, and GJ-tmp) and *indica* (XI-1A, XI-1B, XI-2, XI-3, XI-adm, SH, and BHA) subgroups (Figures 1B, C), whereas PC2 and PC3 distinguished between the weedy rice lines. Consistent with this finding, the weedy rice lines SH and BHA formed two clusters. The centralized subpopulation classification suggested the population clustering according to 3K was accurate. In terms of LM8, PC1 revealed the obvious differences between LM8 and the cultivated (*japonica* and *indica* groups) or weedy rice varieties (Figure 1B).

Next, the STRUCTURE program and an increasing subpopulation ($K$) value (2 to 10) were used to assign individuals to population structures and to explain the PC1-based clustering of LM8. The final population subgroups were determined according to (1) the likelihood value of these models and (2) the previously reported classification of accessions on the basis of the 3K database. When $K$ was set to 2, the likelihood value was highest (0.570) and most of the rice accessions were clearly divided into the *indica* and *japonica* groups (Figure S3). Additionally, 50.43% and 49.57% suggested the "misplaced" LM8 was derived from a *japonica* and *indica* mixture (Table S3). Of the nine runs for $K = 9$, the run with the lowest likelihood value (0.462) was optimal for grouping samples and was selected for assigning the posterior membership coefficients to each accession (Figure S3). These rice accessions were grouped into the following 11 subpopulations: SH, BHA, GJ-adm, GJ-trp, GJ-sbtrp, GJ-tmp, XI-1A, XI-1B, XI-2, XI-3, and XI-adm (Figure 1D). In addition, the *indica*/*japonica* admixture of LM8 was easily identified and was in accordance with the phylogenetic relationships, with 22.98% from XI-2, 22.86% from GJ-trp, 17.76% from GJ- sbtrp, 9.86% from GJ-tmp, 8.63% from XI-3, 8.44% from BHA, 6.59% from XI-1A, 2.36% from XI-1B, and 0.52% from SH (Table S3). Nearly 10% of the genome contained genetic remnants of weedy rice, but in terms of geographical locations, LM8 tended to be similar to the tropical or subtropical accessions. These results suggested that the LM8 admixed genetic background was derived mostly from *indica*/*japonica* hybridizations rather than from weedy rice lines. Furthermore, LM8 is a *japonica*-type weedy rice line.

### 3.2 Whole-genome comparisons with NIP and R498

Considering a considerable proportion of its admixture components was from XI and GJ, LM8 may be a novel rice resource with a complementary gene pool. To further explore genome-wide diversity, the PAVs and SVs in the genomes of NIP (a typical *japonica* variety), R498 (a typical *indica* variety), and LM8 were detected and examined. Next, the deletion (DELs), insertion (INSs), inversion (INVs), translocations (TRANS) and duplication (DUPs) were identified between LM8 and NIP (as reference) and between LM8 and R498 (as reference; Figure 2). No matter comparing to NIP or R498, DELs and INSs were distributed relatively evenly across 12 chromosomes in the LM8 genome (Figures 2A, B). In contrast, INVs, TRANS and DUPs were unevenly distributed across 12 chromosomes in LM8, with many of them detected on chromosomes 2, 5, 6, 7, 8, 10, 11, and 12 (Figures 2A, B).

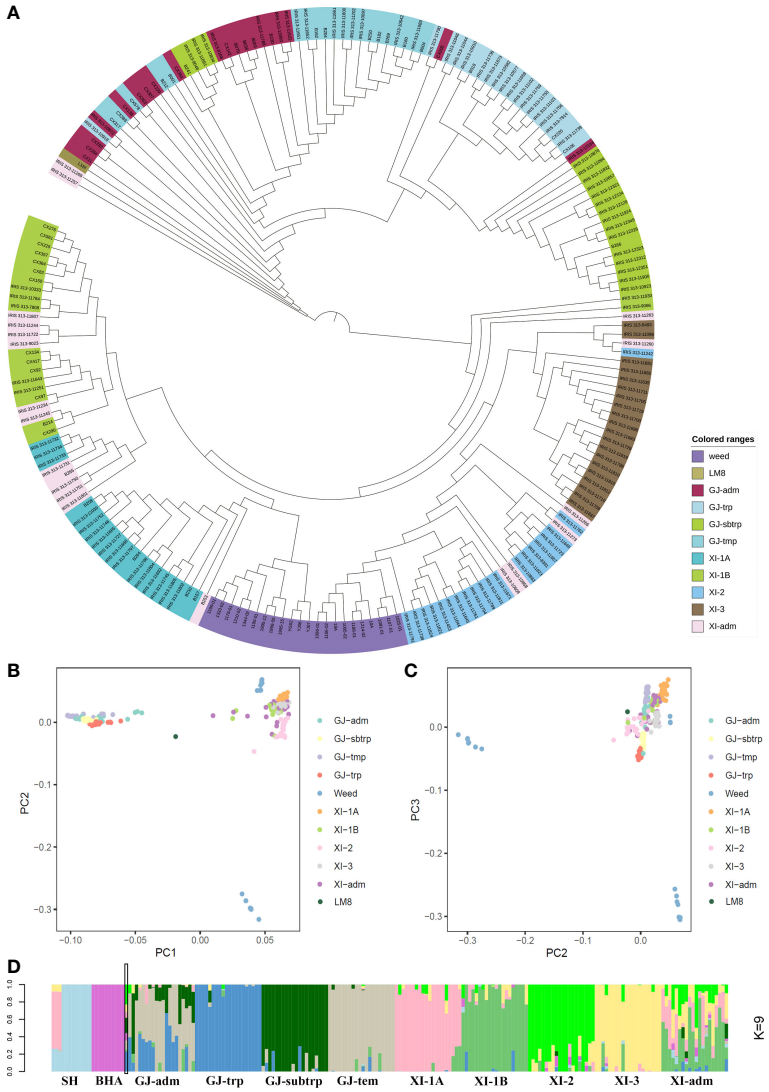


FIGURE 1
Subpopulation classification of LM8. LM8 was classified and its population structure was determined *via* an analysis of genome-wide SNPs in 203 cultivated and weedy rice lines. **(A)** Maximum-likelihood phylogenetic tree. **(B–C)** Principal component analysis. **(D)** Genetic proportions calculated using STRUCTURE ADMIXTURE ($K$ = 9). GJ and XI represent the *O. sativa* groups *japonica* and *indica*, respectively. As described by Wang et al. (2018), GJ-adm and XI-adm represent admixture components within *japonica* and *indica*. Additionally, GJ-trp, GJ-sbtrp, GJ-tmp, XI-1A, XI-1B, XI-2, and XI-3 represent Southeast Asian tropical, Southeast Asian subtropical, primarily East Asian temperate, East Asia, modern varieties of diverse origins, South Asia, and Southeast Asia, respectively.

Comparisons to NIP, the higher variation density of INVs were detected in the position of Chromosome 3 (20000001-21000000), Chromosome 5 (16000001-17000000), Chromosome 6 (12000001-19000000), Chromosome 8 (6000001-8000000 and 12000001-13000000), Chromosome 11 (18000001-19000000) and Chromosome 12 (14000001-15000000; Figure 2A, Table S4). Besides, there was a sharp peak in the 5000001-6000000 region of chromosome 8 and 78 variation density of TRANSs (Figure 2A, Table S4). Also, the obvious variation density peak of DUPs were detected in the position of Chromosome 3 (20000001-21000000), Chromosome 5 (15000001-16000000), Chromosome 6 (12000001-20000000), Chromosome 7 (11000001-14000000), Chromosome 8 (5000001-15000000), Chromosome 11 (9000001-10000000), Chromosome 12 (14000001-18000000; Figure 2A, Table S4). Differently, the maximum value of TRANSs located the 12000001-13000000 position on Chromosome 12 in the comparison of LM8 and R498 group (Figure 2B, Table S5). And comparisons to R498, the distinct peak value of INVs and DUPs were detected in the 14000001-16000000, 9000001-

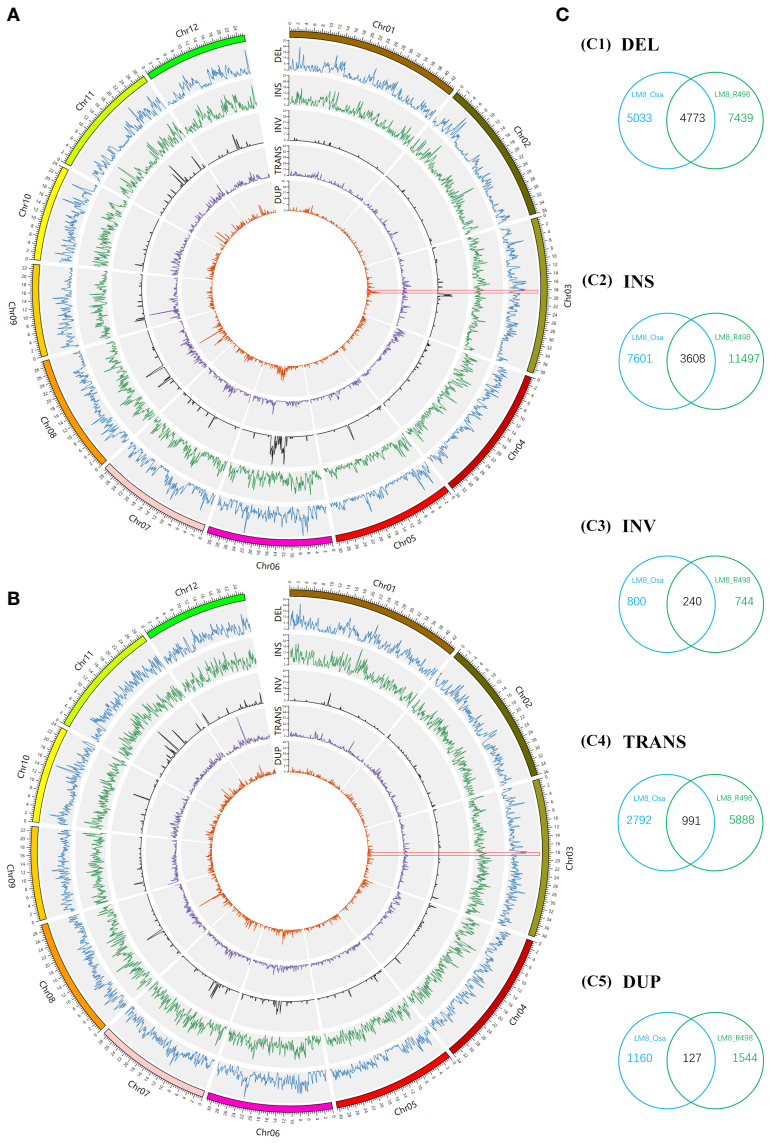


FIGURE 2
Whole-genome comparisons between LM8 and NIP and between LM8 and R498. **(A)** Circular diagram of the variation distribution and density on 12 chromosomes in LM8 revealed by the LM8 *vs* NIP comparison. **(B)** Circular diagram of the variation distribution and density on 12 chromosomes in LM8 revealed by the LM8 *vs* R498 comparison. **(C)** Venn diagram analysis of the number of variations. DEL, deletion; INS, insertion; INV inversion; TRANS, translocation; DUP, duplication.

12000000, 12000001-14000000, 14000001-15000000, 11000001-15000000 region of chromosome 6, 7, 8, 10, 11, respectively (Figure 2B, Table S5). According to the result of the above description, there were significant correlation between INVs and DUPs of distribution in both LM8 *versus* NIP and LM8 *versus* R498 comparisons.

As expected, there were fewer SVs between LM8 and NIP than between LM8 and R498. The LM8 *vs* NIP comparison revealed 27,125 SVs, of which 9,806 were DELs, 11,209 were INSs, 1,040 were INVs, 3,783 were TRANSs, and 1,287 were DUPs in LM8 (Figures 2A, C). Among the 36,760 SVs detected by the LM8 *vs* R498 comparison, 12,121 were DELs, 15,105 were INSs, 984 were INVs, 6,879 were TRANSs, and 1,671 were DUPs in LM8 (Figures 2B, C). We defined the SVs exclusive to NIP or R498 as specific SVs, whereas the SVs in both NIP and R498 were designated as common SVs. Of the 63,885 SVs revealed by the two comparisons, 9,739 were common SVs (15.24%), including 4,773 DELs, 3,608 INSs, 240 INVs, 991 TRANSs, and 127 DUPs in LM8. In contrast, 27.21% (17,386/63,885) and 42.29% (27,021/63,885) of the SVs were specific to the LM8 *vs* NIP and LM8 *vs* R498 comparisons, respectively.

## 3.3 WRKY transcription factor families

The WRKY TFs have core functions affecting plant hormone crosstalk and processes influencing plant growth and development (e.g., stress responses). It is unclear whether the abundant SVs in LM8 affect *WRKY* gene responses to various biotic and abiotic stresses under natural conditions. To identify *WRKY* genes and determine their chromosomal distribution, 96 *WRKY* genes in the LM8 and NIP genomes and 73 *WRKY* genes in the Arabidopsis genome were analyzed (Figure S4). Details regarding these genes, such as their gene IDs and WRKY domains and positions, are listed in Table S6. In LM8, *WRKY* genes were detected on 12 chromosomes, some of which were included in four clusters comprising at least four genes (Figure 3A). These clusters were distinct from those in Arabidopsis (Figure S5), with cluster 1 on chromosome 1 (35,398,161-35,468,751), cluster 2 on chromosome 5 (28,617,903-28,933,603), cluster 3 on chromosome 11 (756,297-803,420), and cluster 4 on chromosome 12 (854,961-904,182; Table S6 and Figure 3A). Interestingly, 15 of the 18 *WRKY* genes in the four clusters belonged to group III. More specifically, the comparison with Arabidopsis indicated 13 of these 15 genes were clustered in subgroup IIIb (Figure 3B). These 13 *WRKY* genes were identified as follows: *ORUFILM01g003806*, *ORUFILM01g003807*, *ORUFILM01g003809*, *ORUFILM01g003811*, *ORUFILM11g002299*, *ORUFILM11g002300*, *ORUFILM11g002301*, *ORUFILM11g002302*, *ORUFILM11g002303*, *ORUFILM12g001262*, *ORUFILM12g001263*, *ORUFILM12g001266*, and *ORUFILM12g001268*.

The maximum-likelihood phylogenetic tree constructed using the *WRKY* gene sequences in LM8, NIP, and Arabidopsis and MEGA (v11) (Figure 3B) divided the genes into subgroups Ia, Ib, IIa, IIb, IIc, IId, IIIa, IIIb, and IV, which was in accordance with previously reported classifications (Ross et al., 2007). The group IV WRKYs lack a complete zinc-finger motif (Eulgem et al., 2000). An earlier study indicated japonica contains relatively few group IV WRKY TFs (Ross et al., 2007). In another study, Xie et al. (2005) proposed that group IV genes may be incorrectly annotated because of genome sequencing errors or they might be pseudogenes that lack biological functions. Thus, the three main groups of WRKY family genes (i.e., I, II, and III) are indicated by three red circles in Figure 3B. The phylogenetic analysis suggested group I diverged into two clades (subgroups Ia and Ib), whereas group II diverged into four clades, with subgroups IIa and IIb clustered in one clade and subgroups IIc and IId in another (Figure 3B). Group III was the largest, with subgroup IIIa and IIIb in two clades (Figure 3B). One of the subgroup IIIb members in LM8 was related to a gene in NIP (Figure 3B). In the phylogenetic tree, the following three genes were clustered with Arabidopsis genes and not NIP genes: *ORUFILM02g002693* (chromosome 2: 26,334,166-26,346,714), *ORUFILM05g002725* (chromosome 5: 1,733,309-1,734,147), and *ORUFILM05g001757* (chromosome 5: 15,083,202-15,087,922) (Figure 3B). Moreover, they were specifically detected in the LM8 genome and not in the NIP genome (Figure 3A). According to the constructed tree, *ORUFILM02g002693* is most closely related to *AT2G44745*, whereas *ORUFILM05g002725* and *ORUFILM05g001757* are most closely related to *AT2G23320* and *AT2G40740*, respectively (Figure 3B).

## 3.4 *NBS* gene families

To clarify the pathogen resistance associated with sequence variants that may be applicable for breeding, the NBS-encoding genes in LM8, NIP, and Arabidopsis were downloaded and analyzed. The NIP genome had the most *NBS* genes (496), followed by the genomes of LM8 (464) and Arabidopsis (165) (Table S7 and Figure S6). The *NBS* genes in Arabidopsis were detected on 5 chromosomes, while the *NBS* genes in LM8 and

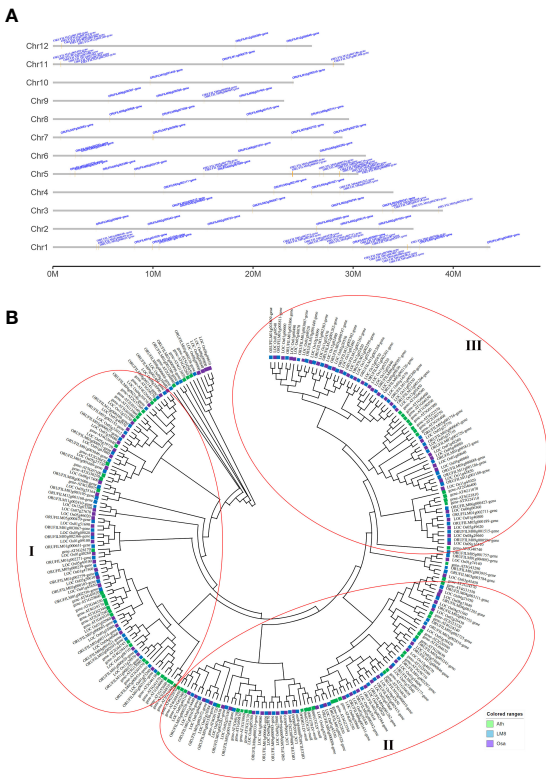


FIGURE 3
*WRKY* gene family analysis. **(A)** Distribution of *WRKY* genes across 12 chromosomes in the LM8 genome. **(B)** Phylogenetic tree containing *WRKY* genes from Arabidopsis, Nipponbare, and LM8. Ath, *Arabidopsis thaliana*; Osa, *Oryza sativa*. Nipponbare was selected as a typical cultivated rice variety, whereas Ath and Osa served as controls. The conserved WRKY structural domains were used to classify the *WRKY* genes, which are indicated by three red circles.

NIP were on 12 chromosomes. In Arabidopsis, the *NBS* genes were mainly designated as CNL and TNL types (Mondragón-Palomino et al., 2002), according to Xiang et al. (2017), which followed by CN, NBS, NL, RN, RNL, and TN types (Figure 4). With the exception of one RNL-encoding gene (*ORUFILM12g000772*) in LM8, the *NBS* genes in the LM8 and NIP genomes were mainly CN, CNL, NBS, NL, and TN types (Figure 4). These results are consistent with the findings of an earlier study, in which CN- and CNL-encoding genes were identified in *Oryza* species (i.e., non-TNLs) (Zhou et al., 2004). In the LM8 and NIP genomes, there were three TN-encoding genes that lacked the LRR domain (Figure 4). Compared with the NIP genome, the LM8 genome had fewer CN-encoding genes, but more CNL-encoding genes (Figure 4). To elucidate the evolutionary relationships among the predicted *NBS* genes, a phylogenetic tree were constructed based on the fact the diversity of the protein domain was generally consistent with that of the NBS region (Figure 5). The tree revealed a lack of specific clustering, with the *NBS* genes divided into almost 200 groups. One of the clades included most of the CN-encoding genes in LM8 and NIP and the TNL-encoding genes in Arabidopsis, implying they may share a common origin and may be functionally similar. Furthermore, the phylogenetic tree indicated the *NBS* genes in Arabidopsis and rice (LM8 and NIP) formed distinct clusters, unlike the *WRKY* genes (Figures 3, 5).

## 4 Discussion

*Oryza sativa* has been divided into two major groups (*indica* and *japonica*). Advances in biotechnology-based research have clarified the differences among these two groups and other varietal types at the isozyme, DNA, and genome levels. The diverse 3K-RG accessions of Asian rice cultivars were classified into the XI-1A, XI-1B, XI-2, XI-3, XI-adm, GJ-adm, GJ-trp, GJ-sbtrp, and GJ-tmp subpopulations following a neighbor-joining method-based phylogenetic analysis of genomic SNPs. The results of the current study are consistent with previously reported findings regarding *japonica* rice (Wang et al., 2018), while also demonstrating that LM8 is closely related to GJ-adm subpopulations and may have originated in tropical or subtropical regions. Moreover, consistent with a previous report (Li et al., 2017), the weedy rice lines SH and BHA were included in the indica group and they were closely related to the XI-1A and XI-2 subpopulations, respectively (Figure 1A). These results directly supported the findings of earlier research on rice evolution and further indirectly confirmed the accuracy of our result that LM8 belongs to GJ-adm. Accordingly, LM8 may be a source of heat resistance genes that can be exploited by breeders. As expected, the LM8 genetic background was mostly derived from cultivated rice varieties and was generally not altered by selective breeding, thereby avoiding problems associated with distant hybridizations. In terms of the genome SVs, 27.21% and 42.29% of the specific SVs were revealed by the LM8 *vs* NIP and LM8 *vs* R498 comparisons, respectively. This may explain the detection of LM8 between *japonica* and *indica* during the PCA (PC1-3). Additionally, there were more specific SVs than common SVs, reflecting the clear difference between the evolution of LM8 and the evolution of NIP and R498. Besides, considering of yield-related traits in rice, the small grain is another representative characterize to LM8. As a results, the quantitative trait loci for grain length were localized to

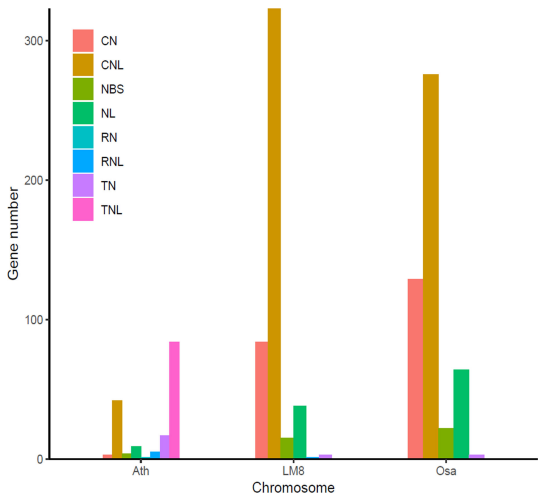


FIGURE 4
Number of different types of *NBS* genes in the LM8 genome. Ath, *Arabidopsis thaliana*; Osa, *Oryza sativa*. Nipponbare was selected as a typical cultivated rice variety, whereas Ath and Osa served as controls.

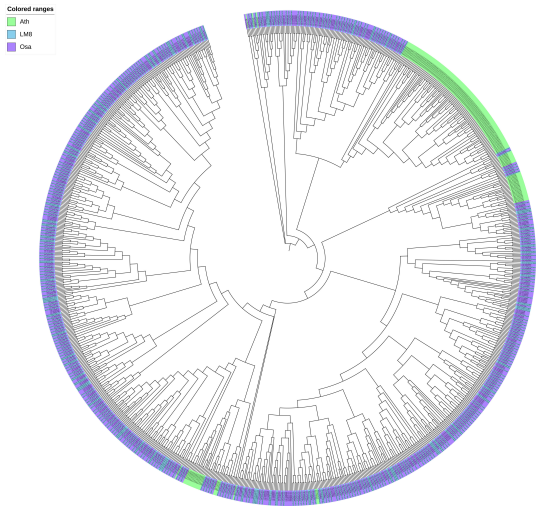


FIGURE 5
Phylogenetic analysis of *WRKY* genes in Arabidopsis, Nipponbare, and LM8. Ath, *Arabidopsis thaliana*; Osa, *Oryza sativa*. Nipponbare was selected as a typical cultivated rice variety, whereas Ath and Osa served as controls.

chromosome 3 (Li et al., 2021) in LM8. The detected sequence variations on chromosome 3 (18,000,001-19,000,000, Table S4, S5) suggested that the SVs of DELs or INSs may be associated with the production of short grains (Figures 2A, B). However, the almost identical positions of the INVs and DUPs will need to be further analyzed to uncover additional evolutionary relationships and functions.

Similar to other weedy rice lines, LM8 grows in rice fields. It has also survived because of stochastic introduction. Thus, the genetic resistance of LM8 and other weedy rice lines to biotic and abiotic stresses developed under complex environmental conditions (Guan et al., 2019; Jia and Gealy, 2018). Many plant *R* genes have been studied. For example, there are hundreds of representative *NBS* genes that confer resistance to a wide range of plant pathogens, including bacteria (Zhao et al., 2005), fungi (Li et al., 2018), nematodes (Esmenjaud et al., 1996), and viruses (Seo et al., 2006), as well as insects (Quisenberry and Clement, 2002). In addition, *NBS* genes belong to the most important class of resistance-related gene families and they encode proteins that recognize pathogen-secreted factors, thereby activating downstream signaling pathways leading to defense responses. To activate defense activities following the perception of pathogen signals, TFs (e.g., WRKYs) bind to plant-specific cis-regulatory elements and activate gene expression. Furthermore, diverse plant processes may be responsive to various WRKY TF family members during exposures to a variety of stresses (Viana et al., 2018). Hence, genome-wide analyses of *NBS* and *WRKY* genes may expand our understanding of the effects of the proteins encoded by these genes on stress resistance, but future investigations will need to further clarify the functions of these proteins under natural conditions and/or the complex network of associated responses.

Many WRKY TF-encoding genes have been identified in the genomes of *Oryza* relatives. For example, Ross et al. (2007) mapped non-redundant *WRKY* genes to individual chromosomes, which resulted in the identification of 102 and 98 *WRKY* genes in *indica* and *japonica*, respectively. A total of 89 *WRKY* genes in NIP (*japonica*) and 97 *WRKY* genes in the *Oryza nivara* genome have been identified and mapped to the corresponding chromosomes. Wu et al. (2005) detected 102 putative *WRKY* genes in the rice genome and compared them with Arabidopsis genes. Future research on *WRKY* genes may further elucidate their genetic diversity and contributions to stress resistance. In this study, 96 *WRKY* genes were identified in the weedy rice line LM8 and then clustered into nine groups. The distribution of the *WRKY* genes on 12 chromosomes resulted from a long de-domestication process and the evolution of *Oryza* species. Our findings suggest that the group III rice *WRKY* gene family expanded more quickly than the other gene families. This phenomenon likely contributed to the adaptive responses of rice to complex environmental conditions. By using an online resource (https://www.arabidopsis.org/), three genes in LM8 (*ORUFILM02g002693*, *ORUFILM05g002725*, and *ORUFILM05g001757*) were predicted to affect the flowering stage, embryo cotyledonary stage, and vascular leaf senescence stage.

The *NBS* genes encode proteins responsible for plant immune responses to pathogens. Most of these genes in rice were identified in earlier genome-wide re-sequencing analyses. In 2004, Zhou et al. identified 535 NB domain-encoding sequences in the NIP genome, but genes encoding TIR-NB-LRR proteins were not reported. The *NB-LRR* genes in the genomes of *O. rufipogon* Griff. wild rice lines Huaye 1 and Huaye 2 reportedly differ from the corresponding genes in two reference genomes. More than 108 of these genes were revealed by different comparisons (Huaye 1 *vs* 93-11, Huaye 2 *vs* 93-11, Huaye 1 *vs* NIP, and Huaye 2 *vs* NIP). Furthermore, these *NB-LRR* genes were mainly localized to chromosomes 2 and 11. In an earlier investigation, 2,688 *NB-LRR* genes served as queries for a BLAST search; these genes were anchored to 12 chromosomes in three rice cultivars and eight wild rice accessions (Rawal et al., 2018). In the present study, we determined that LM8 contains one RNL-encoding gene (*ORUFILM12g000772*). This gene includes sequences for the CC, NB-ARC, and LRR domains. The ORUFILM12g000772 protein sequence was downloaded and aligned with LOC_Os12g39620, At5g66900, At5g66910, and AtRWP8.1 (Figure S7). The analysis of the five alternatively spliced sequences of LOC_Os12g39620 (Figure S7A) suggested amino acids 1-251 may correspond to the Arabidopsis RPW8 domain (Figure S7B, C). As previously reported for Arabidopsis, the *RPW8* loci, including *RPW8.1* and *RPW8.2*, mediate the resistance to the oomycete and fungal pathogens responsible for downy mildew and powdery mildew, respectively (Xiao et al., 2001). Li et al. (2018) confirmed that the ectopic expression of *RPW8.1* leads to increased resistance to the blast fungus *Pyricularia oryzae* and the bacterial pathogen *Xanthomonas oryzae* pv. *oryzae*. The *ORUFILM12g000772* gene described herein will need to be functionally characterized to assess whether LM8 may be useful for breeding novel rice varieties with enhanced resistance to various diseases.

Although the weedy rice line LM8 is one of many Oryza resources, its diverse genetic background and GJ-adm subpopulation closely related to rice cultivars should be considered by rice breeders. The results of our whole-genome analysis of LM8 and the comparison with the NIP and R498 genomes revealed specific SVs, indicative of genes that may be useful for distinguishing between rice accessions. Perhaps not surprisingly, four unique resistance genes were identified, among which the RNL-encoding gene may confer broad resistance to multiple pathogens. Hence, global whole-genome comparisons and analyses may facilitate the classification of subpopulations and the identification of elite genes that may be exploited by rice breeding programs.

## Data availability statement

The datasets presented in this study can be found in online repositories. The names of the repository/repositories and accession number(s) can be found in the article/Supplementary Material.

## Author contributions

ZYH performed the research, analyzed the sequencing data, and wrote the first draft of the manuscript. QWY designed the study and edited the manuscript. WHQ and XMZ supervised the project and provided experimental advice. FL, YLC and LFZ prepared the supplementary materials. JFH, YYW, DJL, MX, WYF, YMN, WLG, SZW and ZRL retrieved and reviewed the relevant literature and downloaded publicly available data. All authors contributed to and approved the final manuscript.

## Acknowledgments

The study was supported by the National Key R&D Program of China (2021YFD1200102-004), the Scientific and Technological Innovation Project (2060302), the National Natural Science Foundation of China (31970237), the 2020 Research Program of Sanya Yazhou Bay Science and Technology City (SKJC-2020-02-001), and the China Postdoctoral Science Foundation (2021M693466). We thank Liwen Bianji (Edanz) (www.liwenbianji.cn) for editing the English text of a draft of this manuscript.

## Conflict of interest

The authors declare that the research was conducted in the absence of any commercial or financial relationships that could be construed as a potential conflict of interest.

## Publisher's note

All claims expressed in this article are solely those of the authors and do not necessarily represent those of their affiliated organizations, or those of the publisher, the editors and the reviewers. Any product that may be evaluated in this article, or claim that may be made by its manufacturer, is not guaranteed or endorsed by the publisher.

## Supplementary material

The Supplementary Material for this article can be found online at: https://www.frontiersin.org/articles/10.3389/fpls.2022.1089445/full#supplementary-material

## References

Chen, F., Hu, Y., Vannozzi, A., Wu, K. C., Cai, H. Y., Qin, Y., et al. (2017). The WRKY transcription factor family in model plants and crops. *Crit. Rev. Plant Sci.* 36(5-6), 311–335. doi: 10.1080/07352689.2018.1441103

Collier, S. M., and Moffett, P. (2009). NB-LRRs work a "bait and switch" on pathogens. *Trends Plant Sci.* 14 (10), 521–529. doi: 10.1016/j.tplants.2009.08.001

Dodds, P. N., and Rathjen, J. P. (2010). Plant immunity: Towards an integrated view of plant-pathogen interactions. *Nat. Rev. Genet.* 11, 539–548. doi: 10.1038/nrg2812

Du, H. L., Yu, Y., Ma, Y. F., Gao, Q., Cao, Y. H., Chen, Z., et al. (2017). Sequencing and *de novo* assembly of a near complete indica rice genome. *Nat. Commun.* 8, 15324. doi: 10.1038/ncomms15324

Esmenjaud, D., Minot, J. C., Voisin, R., Bonnet, A., and Salesses, G. (1996). Inheritance of resistance to the root-knot nematode *Meloidogyne arenaria* in myrobalan plum. *Theor. Appl. Genet.* 92, 873–879. doi: 10.1007/BF00221900

Eulgem, T., Rushton, P. J., Robatzek, S., and Somssich, I. E. (2000). The WRKY superfamily of plant transcription factors. *Trends Plant Sci.* 5, 199–206. doi: 10.1016/S1360-1385(00)01600-9

Guan, S., Xu, Q., Ma, D., Zhang, W., Xu, Z., Zhao, M., et al. (2019). Transcriptomics profiling in response to cold stress in cultivated rice and weedy rice. *Gene*. 685, 96–105. doi: 10.1016/j.gene.2018.10.066

International Rice Genome Sequencing Project (2005). The map-based sequence of the rice genome. *Nature* 436, 793–800. doi: 10.1038/nature03895

Jia, Y. L., and Gealy, D. (2018). Weedy red rice has novel sources of resistance to biotic stress. *Crop J.* 6(5), 443–450. doi: 10.1016/j.cj.2018.07.001

Kawahara, Y., de Bastide, M., Hamilton, J. P., Kanamori, H., McCombie, W. R., Ouyang, S., et al. (2013). Improvement of the oryza sativa nipponbare reference genome using next generation sequence and optical map data. *Rice* 6, 4. doi: 10.1186/1939-8433-6-4

Lee, T. H., Guo, H., Wang, X. Y., Kim, C. S., and Paterson, A. H. (2014). SNPhylo: A pipeline to construct a phylogenetic tree from huge SNP data. *BMC Genomics* 15, 162. doi: 10.1186/1471-2164-15-162

Li, F., Han, Z. Y., Qiao, W. H., Wang, J. R., Song, Y., Cui, Y. X., et al. (2021). High-quality genomes and high-density genetic map facilitate the identification of genes from a weedy rice. *Front. Plant Sci.* 12. doi: 10.3389/fpls.2021.775051

Li, L. F., Li, Y. L., Jia, Y. L., Caicedo, A. L., and Olsen, K. M. (2017). Signatures of adaptation in the weedy rice genome. *Nat. Genet.* 49, 811–814. doi: 10.3390/plants9111515

Li, W. X., Pang, S. Y., Lu, Z. G., and Jin, B. (2020). Function and mechanism of WRKY transcription factors in abiotic stress responses of plants. *Plants* 9, 1515. doi: 10.3390/plants9111515

Li, Y., Zhang, Y., Wang, Q. X., Wang, T. T., Cao, X. L., Zhao, Z. X., et al. (2018). *RESISTANCE TO POWDERY MILDEW8.1* boosts pattern-triggered immunity against multiple pathogens in arabidopsis and rice. *Plant Biotechnol. J.* 16, 428–441. doi: 10.1111/pbi.12782

Lu, B. R., Yang, X., and Ellstrand, N. C. (2016). Fitness correlates of crop transgene flow into weedy populations: A case study of weedy rice in China and other examples. *Evol. Appl.* 9, 857–870. doi: 10.1111/eva.12377

Merotto, A., Ives, C. G. R. G., Anderson, L. N., Augusto, K., Catarine, M., Valmir, G. M., et al. (2016). Evolutionary and social consequences of introgression of nontransgenic herbicide resistance from rice to weedy rice in Brazil. *Evol. Appl.* 9, 837–846. doi: 10.1111/eva.12387

Meyers, B. C., Kozik, A., Griego, A., Kuang, H., and Michelmore, R. W. (2003). Genome-wide analysis of NBS-LRR encoding genes in arabidopsis. *Plant Cell* 15, 809–834. doi: 10.1105/tpc.009308

Mondragón-Palomino, M., Meyers, B. C., Michelmore, R. W., and Gaut, B. S. (2002). Patterns of positive selection in the complete NBS-LRR gene family of *Arabidopsis thaliana*. *Genome Res.* 12 (9), 1305–1315. doi: 10.1101/gr.159402

Narusaka, M., Shirasu, K., Noutoshi, Y., Kubo, Y., Shiraishi, T., Iwabuchi, M., et al. (2009). *RRS1* and *RPS4* provide a dual *Resistance*-gene system against fungal and bacterial pathogens. *Plant J.* 60, 218–226. doi: 10.1111/j.1365-313X.200

Qiu, J., Zhou, Y. J., Mao, L. F., Ye, C. Y., Wang, W. D., Zhang, J. P., et al. (2017). Genomic variation associated with local adaptation of weedy rice during de-domestication. *Nat. Commun.* 8, 15323. doi: 10.1038/ncomms15323

Quisenberry, S. S., and Clement, S. L. (2002). Conservation and use of global plant genetic resources for insect resistance. *Aust. J. Agric. Res.* 53, 865–872. doi: 10.1071/AR02017

Rawal, H. C., Mithra, S. V. A., Arora, K., Kumar, V., Goel, N., Mishra, D. C., et al. (2018). Genome-wide analysis in wild and cultivated *Oryza* species reveals abundance of NBS genes in progenitors of cultivated rice. *Plant Mol. Biol. Rep.* 36, 373–386. doi: 10.1007/s11105-018-1086-y

Ross, C. A., Liu, Y., and Shen, Q. X. (2007). The WRKY gene family in rice (*Oryza sativa*). *J. Integr. Plant Biol.* 49 (6), 827–842. doi: 10.1111/j.1744-7909.2007.00504.x

Seo, Y. S., Rojas, M. R., Lee, J. Y., Lee, S. W., Jeon, J. S., Ronald, P., et al. (2006). A viral resistance gene from common bean functions across plant families and is up-regulated in a non-virus- specific manner. *Proc. Natl. Acad. Sci. U.S.A.* 103, 11856–11861. doi: 10.1073/pnas.0604815103

Sun, J., Ma, D. R., Tang, L., Zhao, M. H., Zhang, G. C., Wang, W. J., et al. (2019). Population genomic analysis and *de novo* assembly reveal the origin of weedy rice as an evolutionary game. *Mol. Plant* 12, 632–647. doi: 10.1016/j.molp.2019.01.019

Sun, C., Palmqvist, S., Olsson, H., Borén, M., Ahlandsberg, S., and Jansson, C. (2003). A novel WRKY transcription factor, SUSIBA2, articipates in sugar signaling in barley by binding to the sugar-responsive elements of the *Iso1* promoter. *Plant Cell* 15, 2076–2092. doi: 10.1105/tpc.014597

Viana, V. E., Busanello, C., Maia, L. C., Pegoraro, C., and de Oliveira, A. C. (2018). Activation of rice WRKY transcription factors: An army of stress fighting soldiers? *Curr. Opin. Plant Biol.* 45, 1–8. doi: 10.1016/j.pbi.2018.07.007

Wang, W. S., Mauleon, R., Hu, Z. Q., Chebotarov, D., Tai, S. S., Wu, Z. C., et al. (2018). Genomic variation in 3,010 diverse accessions of Asian cultivated rice. *Nature* 557, 43–49. doi: 10.1038/s41586-018-0063-9

Wu, D. Y., Lao, S. ,. T., and Fan, L. J. (2021). De-domestication: An extension of crop evolution. *Trends Plant Sci.* 26, 560–574. doi: 10.1016/j.tplants.2021.02.003

Wu, K. L., Guo, Z. J., Wang, H. H., and Li, J. (2005). The WRKY family of transcription factors in rice and Arabidopsis and their origins. *DNA Res.* 12, 9–26. doi: 10.1093/dnares/12.1.9

Xiang, L. X., Liu, J. G., Wu, C. F., Deng, Y. S., Cai, C. W., Zhang, X., et al. (2017). Genome-wide comparative analysis of NBS encoding genes in four *Gossypium* species. *BMC Genomics* 18, 292. doi: 10.1186/s12864-017-3682-x

Xiao, S., Ellwood, S., Calis, O., Patrick, E., Li, T., Coleman, M., et al. (2001). Broad-spectrum mildew resistance in arabidopsis thaliana mediated by RPW8. *Science* 291, 118–120. doi: 10.1126/science.291.5501.118

Xie, Z., Zhang, Z. L., Zou, X. L., Huang, J., Ruas, P., Thompson, D., et al. (2005). Annotations and functional analyses of the rice *WRKY* gene superfamily reveal positive and negative regulators of abscisic acid signaling in aleurone cells. *Plant Physiol.* 137, 176–189. doi: 10.1104/pp.104.054312

Xu, H. J., Watanabe, K. A., Zhang, L. Y., and Shen, Q. X. J. (2016). WRKY transcription factor genes in wild rice *Oryza nivara*. *DNA Res.* 23 (4), 311–323. doi: 10.1093/dnares/dsw025

Zhang, J. W., Chen, L. L., Sun, S., Kudrna, D., Copetti, D., Li, W. M., et al. (2016). Data descriptor: Building two indica rice reference genomes with PacBio long-read and illumina paired-end sequencing data. *Sci. Data* 3, 160076. doi: 10.1038/sdata.2016.76

Zhang, Y. M., Shao, Z. Q., Wang, Q., Hang, Y. Y., Xue, J. Y., Wang, B., et al. (2016). Uncovering the dynamic evolution of nucleotide-binding site-leucine-rich repeat (NBS-LRR) genes in brassicaceae. *J. Integr. Plant Biol.* 58, 165–177. doi: 10.1111/jipb.12365

Zhao, B., Lin, X., Poland, J., Trick, H., Leach, J., and Hulbert, S. (2005). A maize resistance gene functions against bacterial streak disease in rice. *Proc. Natl. Acad. Sci.* 102 (43), 15383–15388. doi: 10.1073/pnas.0503023102

Zhou, T., Wang, Y., Chen, J. Q., Araki, H., Jing, Z., Jiang, K., et al. (2004). Genome-wide identification of NBS genes in japonica rice reveals significant expansion of divergent non-TIR NBS-LRR genes. *Mol. Gen. Genomics* 271, 402–415. doi: 10.1007/s00438-004-0990-z

frontiers | Frontiers in Plant Science

TYPE Review
PUBLISHED 19 January 2023
DOI 10.3389/fpls.2022.1048217



OPEN ACCESS

EDITED BY
Mohammed Wasim Siddiqui,
Bihar Agricultural University, India

REVIEWED BY
Md Shamim,
Bihar Agricultural University, India
Abid Khan,
University of Haripur, Pakistan

*CORRESPONDENCE
Shabir Hussain Wani
shabirhwani@skuastkashmir.ac.in

SPECIALTY SECTION
This article was submitted to Plant Breeding, a section of the journal Frontiers in Plant Science

RECEIVED 19 September 2022
ACCEPTED 09 November 2022
PUBLISHED 19 January 2023

CITATION
Manzoor I, Samantara K, Bhat MS, Farooq I, Bhat KM, Mir MA and Wani SH (2023) Advances in genomics for diversity studies and trait improvement in temperate fruit and nut crops under changing climatic scenarios. *Front. Plant Sci.* 13:1048217. doi: 10.3389/fpls.2022.1048217



# Advances in genomics for diversity studies and trait improvement in temperate fruit and nut crops under changing climatic scenarios

Ikra Manzoor[1], Kajal Samantara[2], Momin Showkat Bhat[3], Iqra Farooq[4], Khalid Mushtaq Bhat[1], Mohammad Amin Mir[5] and Shabir Hussain Wani[6*]

[1]Division of Fruit Science, Faculty of Horticulture, Sher-e-Kashmir University of Agricultural Sciences and Technology of Kashmir, Srinagar, India, [2]Department of Genetics and Plant Breeding, Institute of Agricultural Sciences, Siksha 'O' Anusandhan (Deemed to be University), Bhubaneswar, Odisha, India, [3]Division of Floriculture and Landscape Architecture, Faculty of Horticulture, Sher-e-Kashmir University of Agricultural Sciences and Technology of Kashmir, Srinagar, India, [4]Field Station Bonera, Pulwama, Council of Industrial and Scientific Research (CSIR) Indian Institute of Integrative Medicine, J&K, Jammu, India, [5]Ambri Apple Research Centre, Sher-e-Kashmir University of Agricultural Sciences and Technology of Kashmir, Shopian, India, [6]Mountain Research Centre for Field Crops, Sher-e-Kashmir University of Agricultural Sciences and Technology of Kashmir, Jammu and Kashmir, Anantnag, India

Genetic improvement of temperate fruit and nut crops through conventional breeding methods is not sufficient alone due to its extreme time-consuming, cost-intensive, and hard-to-handle approach. Again, few other constraints that are associated with these species, *viz*., their long juvenile period, high heterozygosity, sterility, presence of sexual incompatibility, polyploidy, etc., make their selection and improvement process more complicated. Therefore, to promote precise and accurate selection of plants based on their genotypes, supplement of advanced biotechnological tools, *viz*., molecular marker approaches along with traditional breeding methods, is highly required in these species. Different markers, especially the molecular ones, enable direct selection of genomic regions governing the trait of interest such as high quality, yield, and resistance to abiotic and biotic stresses instead of the trait itself, thus saving the overall time and space and helping screen fruit quality and other related desired traits at early stages. The availability of molecular markers like SNP (single-nucleotide polymorphism), DArT (Diversity Arrays Technology) markers, and dense molecular genetic maps in crop plants, including fruit and nut crops, led to a revelation of facts from genetic markers, thus assisting in precise line selection. This review highlighted several aspects of the molecular

marker approach that opens up tremendous possibilities to reveal valuable information about genetic diversity and phylogeny to boost the efficacy of selection in temperate fruit crops through genome sequencing and thus cultivar improvement with respect to adaptability and biotic and abiotic stress resistance in temperate fruit and nut species.

KEYWORDS

gene mapping, genome sequencing, gene tagging, metabolomics, micro-satellites, molecular markers, QTL, transcriptomics

## Introduction

Traditional methods of genetic improvement of temperate fruit and nut crops that are generally propagated asexually face a dozen of problems which include a long juvenile phase, absence of seed, higher degree of intra- and interspecific incompatibility, frequent heterozygosity, sterile seeds, and particularly presence of certain specific traits in wild species only (Mehlenbacher, 1995). Natural processes and older tools for generating novel varieties or cultivars of plant species are being used in conventional/classical breeding techniques which are time-consuming, are labor-intensive, and often have less efficiency (Jain and Kharkwal, 2004). The term "molecular markers" refers to naturally occurring polymorphisms in nucleic acids (Thottappilly et al., 2000). A particular segment of the DNA (deoxyribonucleic acid) which represents variations at the genome levels comprises a molecular marker (Dhutmal et al., 2018). At the DNA level, polymorphisms are revealed by molecular markers and might be applied in many genetic studies. A gene or DNA sequence that has a well-known location on a chromosome and is linked to a specific gene or trait is called a genetic marker. It can be characterized as a variance that may result from a mutation or other noticeable modification in the genetic locus (Al-Samarai and Al-Kazaz, 2015). The development of high-throughput molecular markers and genetic maps facilitated the location of genes governing the agronomically important traits and may possibly help in boosting the breeding through MAS (marker-assisted selection). As compared with traditional breeding approaches, MAS is capable of surpassing the obscurity of phenotypic selection including significant efficiency of selection (Wani et al., 2022). A primary gene or several other genes governing an individual trait that is distributed in multiple chromosomal regions are known as quantitative trait loci (QTLs) (Igarashi et al., 2015). Molecular markers can be found at the position of a particular gene in prominent locations of the genome mapping (Raza et al., 2015). Molecular markers which are actually the nucleotide sequences are generally differentiated on the basis of polymorphism or variability present between these nucleotide sequences of different living beings (Nadeem et al., 2018). With the help of genetic marker patterns of heredity, variations in the genome, evolutionary analysis, and marker-assisted breeding can be done for the improvement of different crop species (Hayward et al., 2015).

The role of molecular markers for the characterization and improvement of various genotypic and phenotypic traits in temperate fruit and nut crops such as assessment of genetic diversity in almond, red skin color in apple, sharka disease resistance in apricot, and genome sequencing in almond has been extensively studied in the last few years (Lozano et al., 2014; Halasz et al., 2019; Mori et al., 2019; Alioto et al., 2020). Therefore, to overcome such difficulties, the implementation of radical and sophisticated tools of molecular breeding along with classical breeding would be an efficient and reliable alternative. The molecular marker approach is a viable option which selects desirable individuals in a breeding program based on the use of DNA markers rather than, or in addition, to their trait values. This review provides facts regarding several applications of molecular marker and omics approaches in temperate fruit and nut crop breeding in terms of their genetic improvement and cultivar development.

## Genetic diversity assessment

Recent advances in molecular markers propose great possibilities to assess the genetic diversity in a vast range of germplasms (Nawaz et al., 2013; Nawaz et al., 2016; Wang et al., 2017). Genetic diversity estimation is very useful to study the plant evolution and in turn the comparative genomics of plants, for understanding the composition and construction of various populations (Liu et al., 2015; Nawaz et al., 2017). In recent years, a lot of research has been done for the assessment of genetic diversity in temperate fruit and nut crops *via* the molecular marker approaches (Table 1). Thurow et al. (2016) reported that a population genetic assessment of Brazilian peach breeding germplasm was determined using SSR (simple sequence repeat) markers, selected by their high polymorphism levels. This

TABLE 1 DNA markers for genetic diversity assessment in temperate fruit and nut crops.

| Fruit/nut crop | Molecular marker types | References |
|---|---|---|
| Peach (*Prunus persica* L. Batsch.) | SSR | Thurow et al. (2016) |
| Strawberry (*Fragaria* × *ananassa* Duch.) | SSR | Lim et al. (2016) |
| Sandy pear (*Pyrus pyrifolia* Nakai.) | SSR | Jan (2016) |
| Hazelnut (*Corylus avellana*) | AFLP (amplified fragment length polymorphism) and SSR | Öztürk et al. (2017) |
| Kiwifruit (*Actinidia* spp.) | SNP (single-nucleotide polymorphism) | Oh et al. (2019) |
| Grapes (*Vitis vinifera* L.) | SSR | Riaz et al. (2018) |
| Plum (*Prunus* spp.) | ISSR (inter-simple sequence repeats) | Wu et al. (2018) |
| Sweet cherry (*Prunus avium* L.) | SSR | Patzak et al. (2019) |
| Almond (*Prunus dulcis* (Mill.) D.A Webb.) | SSR | Halasz et al. (2019) |
| Apple (*Malus* ×*domestica* Borkh.) | SSR | Syed (2019) |
| Pecan nut (*Carya* spp.) | SSR | Zhang et al. (2020) |
| European chestnut (*Castanea sativa* Mill.) | RAPD (random amplified polymorphic DNA) | Nunziata et al. (2020) |
| Walnut (*Juglans regia* L.) | ISSR | Houmanat et al. (2020) |
| Apricot (*Prunus* spp.) | SNP | Li et al. (2020) |
| Peach (*Prunus persica* L. Batsch.) | SNP | Mas-Gomez et al. (2021) |

study was conducted in 204 desirable peach genotypes and is the first acumen of available peach genetic variability. Later studies laid the evidence of the population structure of peach to be exploited facilitating the genome-wide similarity and relationship studies. Lim et al. (2016) conducted a study using 5SSR markers that are highly polymorphic in nature, to report the genetic diversity among 160 strawberry accessions. They discovered 60 distinct alleles, with allele frequencies ranging from 0.006 to 1 and similarity ratings ranging from 0.034 to 0.963 (average: 0.507). There was frequent clubbing of accessions within a pedigree, and further study revealed a total of 30 unique accessions classified along with the existing accessions, allowing fruit breeders to develop strategies in order to assess genetic diversity present in the new cultivars.

A similar study was conducted for estimating divergence in 30 sandy pear (*Pyrus pyrifolia* Nakai.) selections with 26 SSR markers. On the basis of SSR dendrogram data provided by Jan (2016), the selections were divided into two groups with four subgroups and one independent selection. The similarity coefficients ranged between 0.12 and 0.69, depicting a wide diversity due to the nature of genotypes and interspecific hybridization. A total of 48 cultivars and 54 wild accessions of Slovenian hazelnut (*Corylus avellana*) were evaluated for the genetic variability and subsequently the population structure using AFLP and SSR markers. These studies demonstrated higher levels of genetic diversity, with mean dissimilarity values of 0.50 and 0.60 for cultivars and wild accessions, respectively. There were 49 SSR markers and 11 AFLP primer combinations that produced 532 and 504 polymorphic fragments, respectively, showing high levels of genetic diversity. Additionally, these accessions were categorized for seven kernels and 10 nut attributes, with some wild accessions exhibiting breeding potential. In all, 49 SSRs were prominently linked with nut and kernel traits. Later studies by Öztürk et al. (2017) demonstrated the first application of association mapping in hazelnut and revealed that molecular markers are linked to significant qualitative features.

Genotyping by sequencing was adopted to determine the genetic diversity in *Actinidia* species, including the native *A. arguta* of Korea. As stated by Oh et al., later investigations cleared the path for kiwifruit breeding programs to generate cultivars employing *A. arguta* that are disease and cold stress tolerant and may be utilized as a base material for further breeding improvements (2018). A genetic diversity analysis of 1, 378 wild and cultivated grapevine accessions (*Vitis vinifera* L.) around Central Asia and the Mediterranean Basin was conducted employing 20 nuclear SSR markers in order to understand the possible events of domestication, gene flow, and adaptive introgression (Riaz et al., 2018). Using 14 ISSR primers, Wu et al. (2018) examined the genetic diversity and structure of 33 plum (*Prunus* spp.) cultivars grown in Southern China. They observed a total of 146 bands, 130 of which were found to be polymorphic. This indicates that there is frequent genetic exchange across closed subpopulations and existence of genetic diversity within the population.

By using molecular SSR markers and 110 amplified polymorphic markers for hierarchical cluster analysis of genetic variability, Patzak et al. (2019) assessed the genetic

diversity within sweet cherry accessions of Czech genetic resources. The resulting dendrogram was in line with the ancestry and geobotanical traits of individual accessions, which were divided into five clusters. In order to assess genetic diversity metrics, characterize genetic differentiation, and investigate the mechanisms underlying the maintenance of population structure and genetic diversity in almond, 15 SSR loci were genotyped on 86 accessions of diverse ancestries (Halasz et al., 2019). Genetic divergence studies were examined in 17 clonal rootstocks (M9, MM106, MM111) of apple (*Malus ×domestica* Borkh.) using eight SSR markers, revealing that rootstocks were highly diverse as the SSR dendrogram data grouped rootstocks into two clusters with two-way similarity coefficients ranging from 0.00 to 0.32 (Syed, 2019).

The distribution of simple sequence repeat (SSR) motifs in two draft pecan genomes was examined in a study by Zhang et al. (2020). In pecan, PCR (polymerase chain reaction) amplification validated 66 SSR loci. In this work, it was discovered that 22 new development markers can be used to advance genetic research in the genus *Carya*. According to Nunziata et al. (2020), a group of cultivars were initially defined to assess the extent of genetic variation using random amplified polymorphic DNA (RAPD) markers for the purpose of varietal identification in European chestnut (*Castanea sativa* Mill.). Also, high-resolution melting (HRM) was employed for SNP mining inside 64 expressed sequence tags (EST) that involved all linkage groups and was validated by target resequencing. Genetic diversity estimation among 33 local Moroccan walnut (*Juglans regia* L.) trees which were compared with eight Bulgarian varieties belonging to an ex situ collection was studied employing ISSR markers, grown in two contrasted agroecosystems. In this study by using 13 primers, 120 ISSR markers (reproducible) were generated, demonstrating the high rate of polymorphism among genotypes with 7 to 13 bands and an average of nine bands per primer. According to these investigations, the overall polymorphism level (average) was 75.2%, with an average polymorphic informativeness content of 0.32 and a range of 0.212 to 0.370 (Houmanat et al., 2020). From these studies, it was concluded that ISSR markers were found to be more systematic in measuring the genetic diversity of walnut genotypes among two major areas in Morocco in comparison with foreign varieties as reported by Houmanat et al. (2020).

By using restriction site-associated DNA sequencing (RAD-seq) to sequence 168 apricot (*Prunus* spp.) accessions distributed in five ecological groups, Li et al. (2020) examined the genetic diversity and genetic relationships of these accessions. This study included 74 accessions of cultivated apricots (*Prunus armeniaca* L.) and 94 accessions of wild apricots (*Prunus armeniaca* L. and *Prunus sibirica* L.). This study provided authentic and relevant genomic resources to significantly promote apricot improvement and its effective utilization. Genome-wide diversity in peach germplasm in Spain has been explored by a new high-density (HD) Illumina peach SNP chip (9 + 9K). In this study, 9, 796 SNPs were used to genotype 90 peach accessions. There were 15 separate groups with genetically similar members found with the aid of identity-by-descent (IBD) estimate analysis. This study elucidated exchange of valuable germplasm among various regions of Spain for efficient management of the National Peach Germplasm Collection for preservation of genetic resources and benefit of impending genome-wide association studies (GWAS) of economically important fruit-related traits in peach as reported by Mas-Gomez et al. (2021). Although different DNA markers have been successfully used in estimation of genetic diversity as well as categorization of genetic material (Tiwari et al., 2013; Naeem et al., 2015; Wang et al., 2015), nowadays marker platforms particularly diversity array technology (DArT), as reported by Sanchez-Sevilla et al. (2015) for diversity analysis in octoploid cultivated strawberry (*Fragaria × ananassa*), are most commonly used for more efficient and reliable estimation.

## Gene tagging

When a gene is at close proximity to a known genetic marker, it is termed as "tagged." Since the genetic markers operate as "signs" or "flags" rather than as the target genes themselves, they represent the genetic variation between certain organisms or species. Gene "tags" are genetic markers that are present physically next to genes (i.e., closely related to them). Due to their proximity to or "linking" to the genes governing the trait, these markers do not affect the phenotyping of the trait of interest by themselves (Collard et al., 2005). Molecular markers are being extensively used for breeding of modern temperate fruit crops for the selection of desired phenotypic traits. There are several previous studies demonstrating the applications of molecular markers for gene tagging in temperate fruit and nut crops (Table 2). Chaney et al. (2015) studied various traits in pecan (*Carya illinoinensis*). Genomic areas containing EST sequences, conserved gene sequences from various plant species, and simple sequence repetitions were amplified using PCR. This study offers a foundation for characterizing germplasm and locating molecular markers connected to features of practical significance.

As reported by Hale et al. (2018), in two different species of kiwifruit, *viz*., *Actinidia arguta* and *Actinidia kolomikta*, sex-linked polymorphism was investigated *via* the genotyping-by-sequencing (GBS) method and from where independent populations were validated from both the species which were then converted into PCR markers (gel-based) for marker-assisted breeding programs. In this study, a 157-bp GBS amplicon marker for *Actinidia arguta* was created, and it displayed absolute sex linkage throughout the entire series of the kiwifruit germplasm. In a similar way, a 161-bp marker for *Actinidia kolomikta* was

TABLE 2 Traits of economic importance tagged with molecular markers in temperate fruit and nut crops.

| Trait/gene | Fruit/nut crop | Markers/analysis | References |
|---|---|---|---|
| Nut characteristics, disease resistance and maturity | Pecan (*Carya illinoinensis* (Wangenh.) K.Koch) | CTAB method (cetyltrimethylammonium bromide) | Chaney et al. (2015) |
| Sex-linked polymorphism | Kiwifruit spp.(*Actinidia arguta*) and (*Actinidia kolomikta*) | GBS (genotyping-by-sequencing) analyses/SNP | Hale et al. (2018) |
| Apple flesh firmness (ACO and ACS) | Apple (*Malus* × *domestica* Borkh) | Md-ACS1 and Md-ACO1 | Rasool (2018) |
| Sugar accumulation in apple | Apple (*Malus* × *domestica* Borkh.) | SSR and CAPS (cleaved amplified polymorphic sequence) | Zhen et al. (2018) |
| Almond blooming time | Almond (*Prunus dulcis* (Mill.) D.A Webb.) | RAPD and SSR | Rasouli et al. (2018) |
| Brachytic dwarfism (*Dw*) | Peach (*Prunus persica* L. Batsch.) | SNP | Cantin et al. (2018) |
| Self-incompatibility in Sweet cherry (*S*-locus) | Sweet cherry (*Prunus avium* L.) | PCR analyses | Patzak et al. (2019) |
| Fruit quality traits | Apricot (*Prunus armeniaca* L.) | qPCR (quantitative polymerase chain reaction) analyses | Garcia-Gomez et al. (2019) |
| Dwarfism (*PcDw* locus) | Pear (*Pyrus communis* L.) | qRT-PCR (quantitative reverse transcription polymerase chain reaction) analyses | Xiao et al. (2019) |
| Phenology, yield, and pellicle color | Persian walnut (*Juglans regia* L.) | Axiom$^{TM}$ 700K SNP array and GWAS (genome-wide association study) | Marrano et al. (2019) |
| Epistatic suppression of repeat fruiting | Strawberry (*Fragaria* × *ananassa* Duch.) | SSR | Lewers et al. (2019) |
| Cultivar improvement | Hazelnut (*Corylus avellana*) | SSR | Frary et al. (2019) |
| Phenology, fruit quality, and post-harvest quantitative parameters | Japanese plum (*Prunus salicina* Lindl.) | GLM (generalized linear model)/MQM (multiple-QTL mapping) analyses | Salazar et al. (2020) |
| Stem photosynthetic capability (SPC) | Wild almond (*Prunus arabica* (Olivier) Meikle) | SNPs | Brukental et al. (2021) |

created with specific male allele primers pertaining to a 3-bp indel in a 270-bp GBS fragment, which displayed absolute sex linkage. The sex screening estimations of seedling populations with higher throughput now frequently use both of the markers, which were validated in separate populations.

Marker analysis has been done for fruit firmness by screening of 40 genotypes of *Malus* × *domestica* Borkh. (apple) maintained at the Division of Fruit Science SKUAST-Kashmir. In this study, the Md-ACO1 and Md-ACS1 markers were adopted and it was found that there are two allelic forms of Md-ACO1 and Md-ACS1, which are amplified in the forms Md-ACO1-1, Md-ACO1-2, and Md-ACS1-1 and each having three allelic combinations as ACS1-1/1 and ACS1-1/2, ACS1-2/2 and ACO1-1/1, and ACO1-1/2 and ACO1-/2/2, out of which ACS1-2/2 and ACO1-1/1 confirm high firmness with low ethylene production. Out of the 40 genotypes, for Md-ACS1, three were found to be homozygous ACS1-2/2 which include Gala Redlum, Gala Mast, and Fuji Zhen Aztec and were found to be highly firm. For Md-ACO1, three genotypes were found to be homozygous ACO1-1/1, including Red Velox, Shalimar Apple-1, and Oregon Spur which were found to be firm (Rasool, 2018). MdSWEET genes governing the sugar accumulation with high expression in *Malus* × *domestica* Borkh. were identified by Zhen et al. (2018), through development of gene-tagged SSR and CAPS (cleaved amplified polymorphism sequence) markers which revealed considerable phenotypic variation, thereby serving as an efficient tool in apple-breeding programs for genetic improvement of fruit sweetness.

To determine the time of flowering in *Prunus dulcis* Mill. D.A Webb. (almond), 140 RAPD primers, 87 nuclear SSR markers, and five chloroplast SSR markers were used. The results of this study directly indicated that the trait is quantitatively inherited. This study is also applicable to other *Prunus* species as mentioned by Rasouli et al. (2018). Cantin et al. (2018) detected one new allele for the gene *Dw* determining brachytic dwarfism in *Prunus persica* (peach). The gibberellin-insensitive dwarf 1 (G1D1) gene underwent a single-nucleotide polymorphism (SNP) mutation that was described in this study. In peach breeding programs, this study was used as a marker-assisted selection tool and undertaken to verify this marker in the $F_2$ population of the cultivar "Nectavantop." Using PCR molecular techniques, Patzak et al. (2020) evaluated the S-

incompatibility locus in 153 accessions of sweet *Prunus avium* L. (cherry), identifying 13 distinct S-alleles in 29 S-locus combinations for 24 distinct incompatibility groups. The most prevalent S-alleles in this investigation were S1 (60 cultivars), S2 (34 cultivars), S3 (88 cultivars), S4 (54 cultivars), and S6 (28 cultivars).

In a study by Garcia-Gomez et al. (2019), *Prunus armeniaca* L. (apricot) was examined for eight important fruit quality traits, *viz*., fruit diameter, fruit weight, stone weight, blush color, skin ground color, firmness, acidity content, and soluble solid content. QTLs associated with these traits were identified, and the biological validity of these QTLs was assessed using qPCR gene expression analysis. Xiao et al. (2019) studied candidate genes governing dwarfism in pear revealed by comparative transcriptome analysis. This study offered a systemic perspective on the intricate regulatory networks governing the dwarf and standard phenotypes of the pear. The genetic regulation of Persian walnut (*Juglans regia* L.) phenology, yield, and pellicle color was uncovered by Marrano et al. (2019). In this study, the most recent Axiom™ *J. regia* 700K SNP array was used to create genetic profiles using phenotypic data. Furthermore, these research findings made a turning point in Persian walnut breeding as it moved from traditional to genome-assisted breeding.

By creating advanced markers (SSR) for the repeat fruiting region, Lewers et al. (2019) reported evidence of epistatic suppression of repeat fruiting in cultivated strawberries. This trait in strawberry is under the control of a dominant allele at a single locus, which has been formerly mapped by numerous research groups. It was found that repeat fruiting is suppressed by two more genes, among which one is dominant and the other one is recessive. The European hazelnut (*Corylus avellana*) was studied by Frary et al. (2019) by combining phenotypic data of kernel and nut with the corresponding genotypic data resulting from 406 SSR marker alleles with association mapping of quantitative trait loci for the respective traits. This analysis resulted in the identification of loci for cultivar improvement and revealed the effect of domestication and subsequent selection on kernel and nut traits. In this study, 78 loci were found, with the largest percentages for the parameters of the kernel (26%) and nut (24%) followed by other attributes like shell thickness (16%), quality (19%), and yield-related (15%) attributes. The loci regulating fruit quality, phenology, and post-harvest quantitative characteristics in *Prunus salicina* Lindl. (Japanese plum) were investigated, as found by Salazar et al. (2020). By using two genome association QTL analysis methodologies, general linear model (GLM)-based single marker–trait association and multiple QTL model analysis, 23 phenotypic traits were assessed over three harvest seasons to find the best linear unbiased predictors (MQM). According to these investigations, the most important QTLs in LG (linkage groups) were 4 and 2, which were related to the fruit weight and fruit developmental periods, respectively. In contrast, it was noted that small QTLs for fruit firmness evolution were validated in LG 4 and 5 using destructive and non-destructive approaches. In the existing and next breeding efforts for *Prunus salicina*, this study will offer useful information for MAS. *Prunus arabica* (Olivier) Meikle is a wild species of almond where there is assimilation of $CO_2$ at greater levels by its green stem in the winter period on comparison with *Prunus dulcis* cv. Um el Fahem (U.E.F.) improving rates of carbohydrates in the dormant period. While unrevealing the inheritance pattern along with the mechanism for stem photosynthetic capability (SPC) in *Prunus arabica*, an F1 segregating population has been developed through crossing between *Prunus arabica* and *Prunus dulcis* cv. Um el Fahem (U.E.F.). The whole genome of both the parent plants has been sequenced, and with identification of 4, 887 informative SNPs for genotype assessment. There was the generation of a genetic map (robust) for *Prunus dulcis* cv. Um el Fahem (U.E.F.) and *Prunus arabica* involving (971 and 571 markers, respectively). Through mapping *via* QTLs (quantitative trait loci) and an association study (AS) with the phenotype for SPC, it was found that there were major QTLs [log of odd (LOD) = 20.8] upon chromosome number 7 and another minor (significant) upon chromosome number 1 (LOD = 3.9). This study investigated the physiology of the SPC trait in almond nut crop to breed varieties acquainted to winter temperature (Brukental et al., 2021). These studies indicate that the evolving gene-tagged markers are quite efficient to explore the functionality of genes and can be directly employed in temperate fruit and nut breeding programs in case of any association with horticultural traits of interest.

## Gene mapping

Another important subject of molecular marker utility is the preparation of molecular maps that help in identifying genomic regions controlling the horticultural important traits in temperate fruit crops. On the basis of markers of phenotypic nature, traditional linkage mapping allocates a specific location of genes for a desired chromosome. Based on cytogeny, there can be localization of genes for a specific band of chromosomes like association of the improved phenotype through deleting a desired band of chromosomes. Vast areas of a chromosome require the molecular marker approach for mapping in case of a specific type of special restriction endonucleases which check the specific sites as per intervals that are non-frequent. Into those fragments, subdivisions can be made and mapping can be done *via* endonucleases of traditional origin. Also, the contig type of maps locates desired genes with a specified fragment for precise gene mapping. The large-scale mapping of genes is shown in Figure 1. The principle behind gene mapping is the chromosomal recombination during meiosis, which results in the segregation of genes (Nadeem et al., 2018). Till date, QTL mapping and genome-wide association studies have successfully

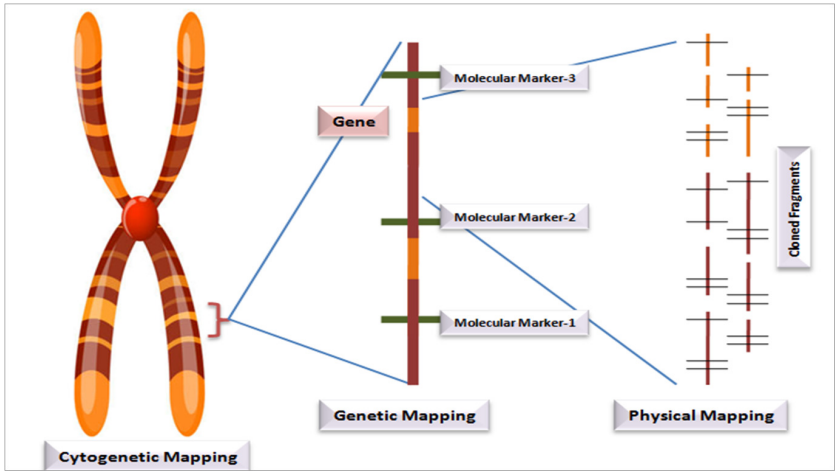


FIGURE 1
Large-scale gene mapping.

been implemented for mining several desirable alleles in a diverse range of crops and fruits species (Samantara et al., 2021). An overview of the QTL mapping is depicted in Figure 2. A vast range of linkage maps has been constructed in various temperate fruit crops employing the molecular marker approach (Table 3). Wang et al. (2015) created a mapping population from 'Wanhongzhu' and 'Lapins' and, moreover, constructed a linkage map in commercial sweet cherry along with QTL analysis for trunk diameter. This study used the SLAF sequencing technique (specific locus-amplified fragment) that included an SNP (single-nucleotide polymorphism) platform that produced 701 genotypic assays, together with 16 SSRs and the S (incompatibility) gene to prepare a map that covered 849.0 cM of distance involving eight LGs with a mean distance of 1.18 cM and had few gaps longer than 5 cM (centimorgan). This map demonstrated that four loci, corresponding to three distinct LGs (linkage groups), are responsible for controlling trunk diameter. This high-density map favors better-resolution identification of QTLs for horticultural important traits and speeds up improvement of sweet cherries. A genetic linkage map of *Castanea crenata* Sieb. Et Zucc. (Japanese chestnut) was prepared by Nishio et al. (2018) using two breeding populations, *viz*., 'Kunimi' and '709-034 (Kx709) and 'Porotan' and 'Tsukuba-43' (Px43). In this study, maps of four parents along with two integrated ones were constructed employing 443 SSRs and 554 SNPs. Out of which, Kx709 was the most saturated map involving 12 LGs, covering 668 and 1 cM, with an inter-distance of 0.8 cM. By using anchor SSRs, all the six maps were aligned to a Chinese chestnut consensus map. Eight agronomic traits were evaluated to identify molecular markers associated with them and at least one QTL was detected for each of the traits. With the help of this map, it was revealed that these mapping populations and their parents are essential material for Japanese chestnut breeding programs with these QTLs to be used for MAS to improve breeding programs. In the Japanese plum (*Prunus salicina* L.), Carrasco et al. (2018) created a linkage map that was intensely saturated utilizing GBS for SNP calling, the mapping population (*Angelenox aurora*), and the identification of 49, 826 SNPs while using the V2.1 peach genome as a reference. After rigorous filtering, 137 (*Angelenox aurora*) offspring revealed about 1, 441 SNPs of high quality that were mapped in eight linkage groups. An inter-distance of 0.96 cM was created utilizing 732 SNPs spanning 617 cM to create a consensus map. This map revealed a greater degree of collinearity and synteny between the genomes of peach and Japanese plum.

Aradhya et al. (2018) built a fine-scale genetic linkage map with 2, 220 SNPs in 16 linkage groups with a mapping population, spanning 1, 141.1 cM, deciphering genomic regions governing economic traits *viz*., yield, lateral fruitfulness, harvest date, nut weight shell thickness, and kernel fill in walnut (*Juglans regia*). At LG 1, two to three pleiotropic QTLs were in charge of controlling the thickness of the shell, nut weight, and kernel fullness. QTLs showed a negligible impact on such trait expressions, as seen by their tiny positive cumulative effects for shell thickness, harvest date, and nut weight and minor negative cumulative impacts for kernel fill. Using the Gulcan-2 × Lauranne mapping population, an SSR-based linkage map for almonds was created. The consensus map has 168 markers spread across eight LGs. According to this study, there were 13 mapped markers (LG 6) and 31 markers (LG 2), and the length of the LGs ranged between 47.8 cm (LG 6) and 84.6 cm (LG 1), with a mean distance of 3.1 cm. This study came to the conclusion that

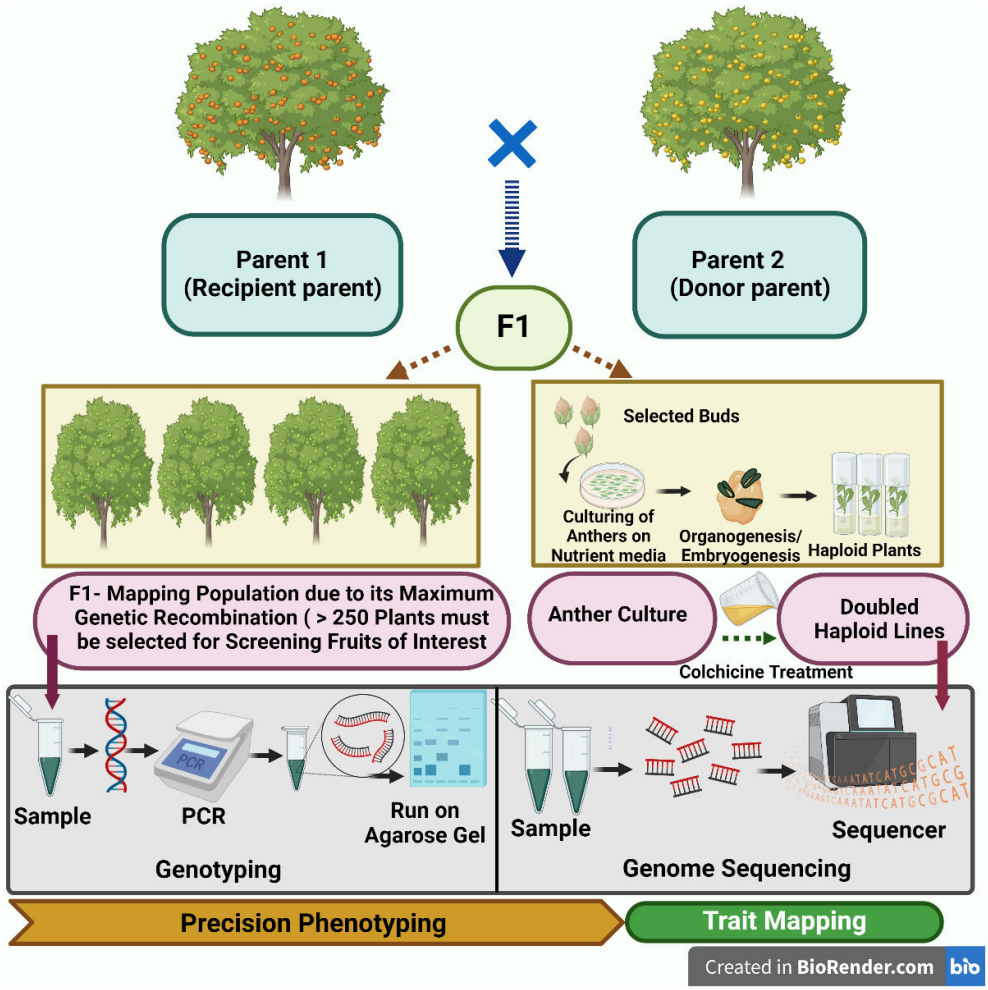


FIGURE 2
An outline of mapping of genes/QTL in fruit crops.

this map served as a foundation for the development of markers associated with critical almond features after the completion of the phenotypic data, as reported by Paizila et al. (2019).

Using the ddRAD (double digest restriction-associated DNA) sequencing approach, Hossain et al. (2019) was able to identify 13, 181 SNPs for the development of a high-density linkage map and QTL mapping for runner production in *Fragaria* × *ananassa* (octaploid strawberry). Mendelian segregation was detected in 3, 051 SNPs in F1, among which 1, 268 were linked to 46 linkage groups covering 2, 581.57 cM with a 2.22-cM intergenic distance. In addition, seven QTLs were found for runner production, the LOD values of which ranged between 3.5 and 7.24 and phenotypic variances of 22–38%. From this research, it was concluded that both vegetative and reproductive behaviors of strawberry could be determined and can serve as a tool for breeding targets regarding flowering and runner production. Zhang et al. (2019) crossed two Chinese cultivars, "Chuanzhihong" and "Luotuohuang, " along with a recently built reduced representation library, to create a high-density linkage map and QTL analysis for pistil abortion in *Prunus armeniaca* L. (apricot). A total of 12, 451 polymorphic markers were created for this map using resequencing data; the final map was composed of eight linkage groups with 1991 markers encompassing 886.25 cM, with a mean distance of 0.46 cM. This is the most detailed genetic map of the apricot currently available. This map was used in this study to identify the QTL responsible for apricot pistil abortion by analyzing the central regions of LG 5 (51.005–59.4 cM) and LG 6 (72.884–76.562 cM), which contained nine SLAF markers that were strongly associated with pistil abortion. It was determined by this analysis to be a very valuable connection map. This study deciphered that it is a quite valuable linkage map for identifying

TABLE 3 Development of molecular maps in temperate fruit and nut crops.

| Fruit/nut crop | Parents/population used | Marker type and number | Total map length (cM) and linkage groups (LG) | References |
|---|---|---|---|---|
| Sweet cherry (*Prunus avium* L.) | 'Wanhongzhu' and 'Lapins' | SNPs and 16 SSRs | 849.0 cM<br>8 LG | Wang et al. (2015) |
| Japanese chestnut (*Castanea crenata* Sieb. Et Zucc.) | 'Kunimi' and '709-034 (Kx709) 'Porotan' and 'Tsukuba-43'(Px43) | 554 SNPs and 443 SSRs | 668.1 cM<br>12 LG | Nishio et al. (2018) |
| Japanese plum (*Prunus salicina* Lindl.) | Angelenox aurora | 732 SNPs | 617 cM<br>8 LG | Carrasco et al. (2018) |
| Walnut (*Juglans regia* L.) | Chandler × Idaho | 2, 220 SNPs | 1, 141.1 cM<br>16 LG | Aradhya et al. (2018) |
| Almond (*Prunus dulcis* (Mill.) D.A Webb.) | Gulcan-2 × Lauranne | 168 SSR | 47.8–84.6 cM<br>8 LG | Paizila et al. (2019) |
| Strawberry (*Fragaria* × *ananassa.*) | Maehyang × Albino | 13, 181 SNPs | 2581.57 cM<br>46 LG | Hossain et al. (2019) |
| Apricot (*Prunus armeniaca* L.) | 'Chuanzhihong' and 'Luotuohuang' | 1, 991 polymorphic markers | 886.25 cM<br>8 LG | Zhang et al. (2019) |
| Korean pears (Pyrus hybrid) | 'Whangkeumbae' and 'Minibae' | 321 SNPs and 30 SSRs | 1, 511.1 cM<br>17 LG | Han et al. (2019) |
| Apple (*Malus* ×*domestica* Borkh.) | ' Fuji' × 'Red 3' | 7, 630 SNPs | 2, 270.21 cM<br>17 LG | Yang et al. (2020) |
| Grapes (*Vitis vinifera* L.) | Muscut Hamburg × Crimson Seedless $F_1$ population | 26, 039 SNPs | 1463.38 cM<br>19 LG | Jiang et al. (2020) |
| Sweet cherry (*Prunus avium* L.) | 'Vic' × 'Cristobalina' $F_1$ population | 910 SNPs (Vic)<br>789 SNPs (Cristobalina) | 636.7 cM (Vic)<br>666.0 cM (Cristobalina) | Calle et al. (2021) |

QTLs related to different agronomic traits in apricot and the well-organized markers are useful for molecular breeding of apricot.

Han et al. (2019) created an integrated linkage map of Korean pears (*Pyrus hybrid*) as per the pseudo-chromosomes of the reference genome of the Chinese pear known as "Dangshansuli" (*Pyrus bretschneideri*), using GBS-based SNPs and SSRs with consensus maps for "Whangkeumbae" and "Minibae" that contains 321 SNP and 30 SSR markers with 1511.1 cm with an average genetic distance of 4.3 cm. This consensus map was compared to other apple and pear maps using 30 SSR markers in total. According to the results of this investigation, SSRs coming from pear and apple maps exhibit strong synteny. With the help of pseudo-chromosomes and SNPs, 17 linkage groups of this genus' physical length were revealed, and genome-based regions that were discovered by QTL analysis were annotated. The genotyping by sequencing-based SNPs integrated with SSRs provide a description of the genome structure of the Korean pear resources serving as a reference map. A high-density linkage map was constructed in apple (*Malus* × *domestica* Borkh.) employing the 'Fuji' × 'Red 3' population with homozygous alleles R1R1 and R6R6, respectively, by Yang et al. (2020). The linkage map contains 7, 630 SNPs that distinguish between "Fuji" and "Red 3, " of which 3, 903 and 3, 925 were mapped into the linkage groups of the parents, respectively, the male and the female. The number of "Fuji" SNP markers for the female parent linkage group ranged from 108 to 366, with a mean of 231. The distance between all linkage groups ranged between 70.17 and 168.23 cM, with a mean value of 109.14 cM. Each linkage group's SNP count ranged from 58 to 434 for the male father "Red 3, " with an average of 230. Each linkage group's distance ranged between 72.11 and 227.10 cM, with a mean distance of 140.26 cM. With 17 linkage groups and a mean density of 0.30 cM per marker, the consensus map covered 2, 270.21 cM. With 0.19 cM per marker, LG10 exhibited the lowest heterozygosity, whereas LG17 displayed a high level of heterozygosity at 0.73 cM per marker, according to this map. The SNP density of other 15 LGs ranged between 0.21 and 0.48 cM.

In order to discover loci determining the firmness of the berry in grapes, a high-density genetic map with 19 linkage groups, 1, 662 bin markers including 26, 039 SNPs, spanning a total distance of 1, 463.38 cM, and an inter-marker distance of 0.88 cM was generated (*Vitis vinifera* L.). Four potential genes related to abscisic acid (ABA), endoglucanase, and transcription factors were linked in this study to berry hardness. Using qRT-PCR research, it was discovered that Muscat Hamburg had higher levels of the endoglucanase 3 gene and abscisic-aldehyde oxidase-like gene expression at the veraison stage

than Crimson Seedless, which was consistent with the parent berry firmness. The above two genes were found to be the candidate genes determining berry firmness in grapes as reported by Jiang et al. (2020). In the sweet cherry (*Prunus avium* L.) 'Vic' × 'Cristobalina' $F_1$ population, QTL mapping of phenolic substances and that of cherry fruit color was done by Calle et al. (2021) using 6 + 9K SNPs, 910 SNPs (Vic), and 789 SNPs (Cristobalina) array genetic map with a map distance of 636.7 cM (Vic) and 666.0 cM (Cristobalina). These studies reflect that the genetic linkage maps play a vital role to explore the genetic control of important traits and serve as a DNA-based diagnostic tool in future for marker-aided breeding techniques.

## Abiotic and biotic stress tolerance

Molecular markers have made it possible to impart abiotic and biotic stress tolerance in temperate fruit and nut crops by tapping resistant genes from their wild relatives and incorporating them into commercial cultivated varieties, thereby reducing the yield losses due to various stresses (Table 4). Zhu et al. (2015) built a high-density genetic map of anthracnose resistance in walnut according to specific AFLP markers (total 153, 820), out of which 2, 577 markers were employed to build genetic linkage maps (448 for male, 2, 395 into 16 LGs for female map, and 2, 577 for integrated map). By considering the range of all LGs, the marker coverage for the integrated map was 2, 457.82 cM, with an average interval of 0.95 cM. In addition, 5, 043 SNP loci correspond to two SNP loci per SLAF marker. In this study, for identifying anthracnose resistance, QTLs were detected ranging from 165.51 to 176.33 cM on LG 14. The phenotypic variation in this study varied from 16.2 to 19.9% with LOD scores (logarithm of odds) (3.22 to 4.04). This study is a base for aiding molecular marker-assisted breeding for identification of walnut resistance gene. A study was described by Montanari et al. (2016) who detected a QTL on LG 2 using a previously conducted genetic map published in 2013 with SSR and SNP markers for the segregating population of PEAR3x 'Moonglow'. This QTL corresponds with the QTL for fire blight disease resistance earlier found in 'Harrow Sweet' (Le

TABLE 4 DNA markers for abiotic and biotic stress tolerance in temperate fruit and nut crops.

| Trait/resistance | Fruit crop/parents | Markers/genes/technique | References |
|---|---|---|---|
| Anthracnose | Walnut (*Juglans regia* L.) | SLAF (specific locus-amplified fragment)/ SNPs | Zhu et al. (2015) |
| Fire blight | PEAR3 (PremP003, *P.* × *bretschneideri* × *P. communis*) × 'Moonglow'(*P. communis*) | QTL | Montanari et al. (2016) |
| X-Disease | Chokecherry (*Prunus virginiana*) | QTL | Lenz and Dai (2017) |
| Ink disease | *Castanea sativa* × *Castanea crenata* | Microsatellite/SNPs | Santos et al. (2017) |
| Powdery mildew | Strawberry (*Fragaria* × *ananassa.*) | QTL | Cockerton et al. (2018) |
| Apple scab | Apple (*Malus* × *domestica* Borkh.) | AL07 and AM19 (SSR) | Rasool (2018) |
| Brown rot | Almond 'Texas' × Peach 'Earlygold' population | QTL | Baro-Montel et al. (2019) |
| Downy mildew | Grapes (*Vitis vinifera* L.) | SSR/RT-qPCR (quantitative reverse transcription polymerase chain reaction) | Zhao et al. (2019) |
| Sharka disease | Apricot (*Prunus armeniaca* L.) | SNP | Mori et al. (2019) |
| Wilt | Kiwifruit (*Actinidia* spp.) | SSR | Oliveira et al. (2020) |
| Powdery mildew | Peach (*Prunus persica* L. Batsch.) | Vr3/*Prupe2G111700*/*Prupe2G112800* | Marimon et al. (2020) |
| Black spot | Japanese pear (*Pyrus pyrifolia* (Burm.) Nak.) | SSR | Terakami et al. (2021) |
| Abiotic stress | Apple (*Malus* × *domestica* Borkh.) | qRT-PCR/MdDREB2A transcription factor | Lian et al. (2021) |
| Codling moth *Cydia pomonella* (Linnaeus) (Lepidoptera: Tortricidae) | Sweet cherry *(Prunus avium* (L.)) | PCR/(COI) gene | Yokomi et al., 2021) |

Roux et al., 2012), additionally giving an insight that these two favorable alleles were not identical by descent. In this study, few little effect QTLs were identified from susceptible parent PEAR3. This study proposed that the SNP and SSR markers were linked to the higher effect QTL on LG2 candidates for MAB for resistance of pear fire blight disease. Lenz and Dai (2017) mapped X-disease phytoplasma resistance in *Prunus virginiana*, employing chokecherry consensus map "Cho" containing 16 LGs covering 2, 172 cM with average marker density of 3.97 cM. Also, three QTLs were associated with this trait, accounting for about 45.9% of phenotypic variation. This study deciphered a framework for genomics, molecular genetics, and further breeding aspects for X-disease resistance in Chokecherry and other *Prunus* species. Ink disease resistance in European chestnut was imparted by Santos et al. (2017) through an approach involving construction of a genetic linkage map from *Castanea sativa* × *Castanea crenata* for detection of QTL for this trait. In this study, chestnut populations were genotyped with 452 SNPs and microsatellites derived from available chestnut transcriptomes. Non-parametric approaches and composite interval mapping identified two QTLs in two LGs, E and K. The presence of QTL in LG E is in accordance with a previous study by Santos et al. (2015) in American × Chinese chestnut populations, depicting the presence of a defense system throughout the species. From the above research, it was concluded that genomic resources of *Castanea* genus act as a tool for future breeding aspects.

For regulating abiotic stresses, viz., drought, salinity, and stresses due to ABA, in apple (*Malus* ×*domestica* Borkh.), the MdDREB2A transcription factor from the AP2/ERF family has been isolated from cultivar 'Royal Gala'. By using quantitative reverse transcription polymerase chain reaction (qRT-PCR), it was found that the length of the open reading frame is 1, 197 bp encoding a 398-long amino acid chain protein with a molecular weight of 43.8 kD (Lian et al., 2021).

The fruit export can be easily facilitated with implementation of advanced molecular techniques to improvise the pest diagnostics in a faster way *via* polymerase chain reaction (PCR) and latest techniques of sequencing. The larvae of codling moth *Cydia pomonella* (Linnaeus) (Lepidoptera: Tortricidae) were found in a pack house of cherry *Prunus avium* (L.) being differentiated *via* PCR compared to various other internal fruit moth larvae, *viz*., the oriental fruit moth, *Grapholita molesta* (Busck) (Lepidoptera: Tortricidae); lesser appleworm, *G. prunivora* (Walsh) (Lepidoptera: Tortricidae); cherry fruitworm, *G. packardi* (Zeller) (Lepidoptera: Tortricidae); and filbertworm, *Cydia latiferreana* (Walsingham) (Lepidoptera: Tortricidae). Also, there is conformity of identifying pests *via* amplicon sequencing (301 bp) part of the (COI) gene obtained *via* PCR in the DNA of suspected moth through comparison with other (COI) gene sequences from the rest of the internal fruit borers in fruits of the pome group. This study was conducted for meeting phytosanitary aspects to export fruits globally (Yokomi et al., 2021).

Resistance against powdery mildew was identified by Cockerton et al. (2018) using genotypes from two phenotyped bi-parental mapping populations, "Emily" × "Fenella" and "Redgauntlet" × "Hapil, " to present quantitative trait loci in *Fragaria* × *ananassa* (strawberry). Multiple QTLs were found in this study, and six of them demonstrated a level of persistent resistance across different phenotyping events. It was examined whether found QTL showed close linkage to associated genes for resistance in the larger germplasm after the identified QTL was subjected to screening across an evaluation set. This study showed that quantitative resistance develops across the strawberry germplasm *via* several predominantly additive sources. An investigation was carried out to document and characterize the apple germplasm comprising 40 apple cultivars in which molecular characterization was performed for scab resistance using *AL07* (codominant primer) and *AM19* (dominant primer), and the results obtained with primers confirmed the presence and absence of the *Vf* gene. It was also found that *AL07* (codominant primer) are helpful to discriminate homozygous from heterozygous plants for the *Vf* gene as analyzed by Rasool (2018). As reported by Baro-Montel et al. (2019), resistance to brown rot disease caused by *Monilinia* spp. in stone fruits as explored in an interspecific almond 'Texas' × peach 'Earlygold' population (named T1E) was identified. This study revealed that 'Texas' is a resistant source for brown rot disease and many quantitative trait loci were detected in various linkage groups, but two proximal QTLs were identified in G4, accounting for 11.3–16.2% of phenotypic variation. Hence, a MAS-based strategy is needed to incorporate this trait into the susceptible parent peach with other desirable traits for sustainable crop production.

The variations in the rates of downy mildew resistance of various Chinese wild grapevine were identified by Zhao et al. in 2019. In this study, *in vitro* leaf disc testing was used to assess the level of downy mildew resistance, and RT-qPCR (quantitative reverse transcription polymerase chain reaction) was used to determine the expression pattern of various important genes following *Plasmopara viticola* inoculation. Using 30 pairs of SSR markers, 120 grapevine germplasm resources were chosen, showing a disease index range of 0.00 to 78.70. The RGA9 marker was a standard marker that, among other markers, expressed the highest phenotypic variation of 80.83% that may be used in the generation of disease resistance, providing the basis for widespread as well as rapid discovery of downy mildew disease resistance in many organisms. Mori et al. (2019) reported that resistance to sharka disease in apricot was identified by comparing phase-constructed susceptible and resistant haplophytes of 'Lito' and Chromosome 1 along with assessment of candidate genes. A pseudo-test cross-mating design with 231 individuals was followed to discover the fact that the 'Lito' genotype had heterozygosity for the resistance that

has been used to map a significant QTL on LG 1. Additionally, this analysis included 19 SNP markers that covered 236 kb of chromosome 1 in total. A BAC (bacterial artificial chromosome) library for the 'Lito' cultivar was created, and markers for the area were used to screen it. Positive BAC clones were then sequenced. The whole genome of the given cultivar was sequenced for refinement for a high coverage using PacBio technology, deciphering a detailed analysis of the genes in the QTL region. This cultivar drastically distinguished structural variants between two haplophytic regions and also predicted specific allelic expression leading to mining of the PPVres locus. Therefore, a valuable prediction method has been developed to study the substitute transcription and regulatory mechanisms underpinning PPV resistance.

Oliveira et al. (2020) conducted a study for resistance to *Ceratocystis* wilt in kiwifruit cultivars, employing 46 isolates with 14 SSR markers for genotyping. Among 14 markers, 13 were polymorphic and 26 genotypes were identified. On susceptible cultivar, 14 prominent genotypes were tested for identification of aggressive ones, eventually by inoculating an equal mixture of five of the most aggressive ones for evaluating seven resistant types, *viz*., Red Arguta, Green Arguta, Chieftain, Allison, Hayward, Monty, and Tomuri, which could be used as rootstocks for future programs. The powdery mildew-resistant (Vr3) gene in peaches was mapped to a genome area of 270 kb containing 27 identified genes to get molecular markers strongly connected to this gene. The results of this study's analysis revealed that there was a difference in the expression of a gene known as Disease Resistance Protein RGA2 (Prupe2G111700) or Eceriferum 1 protein resulting in biosynthesis of epicuticular wax (Prupe2G112800) between resistant and susceptible individuals. Only Prupe2G111700 contains a variant that has an adverse impact on the protein encoded, which showed overexpression in both homozygous and heterozygous individuals. With the help of this study, molecular markers tightly linking and flanking the *Vr3* gene could be identified and validated as reported by Marimon et al. (2020). Terakami et al. (2021) developed the SSR marker set, *viz*., Mdo.chr11.27 and Mdo.chr11.34, for efficient selection for black spot disease resistance in pear breeding by performing inoculation tests and genotyping with 207 pear cultivars. In addition to this, with the molecular marker approach, pyramiding multiple resistant genes into the host plant with accelerated breeding programs provide durable and broad-spectrum resistance for further research in temperate fruit and nut breeding programs.

## Genome sequencing

The ultimate goal of genomics is sequencing of the whole genome and understanding of the function of each gene. For both functional genomics and breeding programs in fruit crops, the publication of a dozen genomes represents a milestone. This review provides some insights regarding various genome sequencing projects in temperate fruit and nut crops employing the molecular marker approach (Table 5). Along with high-throughput sequencing technology, rapid advances have revolutionized the manner and scale of genomics in temperate fruit and nut crops. Employing shotgun sequencing of a nearly homozygous genotype (cv.PN40024) which was originally derived from Pinot Noir by a French-Italian public consortium, the first 8X version of the *Vitis vinifera* genome sequence was obtained and was the first sequenced fruit crop (Jaillon et al., 2007). The presence of the grape genome sequence with a haploid chromosome number of 19, containing 490 Mb with 30, 000 protein-coding genes, is causing a rapid increase in *Vitis* genetic research by providing tools for genetic improvement to grow well with stresses like diseases and pests

TABLE 5 Status of sequencing projects in temperate fruit and nut crops.

| Species | Common name | Genome size (Mb) | References |
|---|---|---|---|
| *Vitis vinifera* | Grapes | 490 | Martinez-Zapater et al. (2010) |
| *Malus* × *domestica* Borkh. | Apple | 742 | Velasco et al. (2010) |
| *Prunus persica* L. Batsch. | Peach | 230 | Arus et al. (2012) |
| *Fragaria* × *ananassa* | Strawberry | 813.4 | Hirakawa et al. (2014) |
| *Pyrus communis* L. 'Bartlett' | European pear | 577.3 | Chagné et al. (2014) |
| *Juglans regia* L. | Walnut | 667 | Martinez-Garcia et al. (2016) |
| *Prunus dulcis* cv. Texas | Almond | 238 | Alioto et al., 2020 |
| *Prunus armeniaca* L. | Apricot | 221.9 | Jiang et al. (2019) |
| *Actinidia chinensis* | Kiwifruit | 653 | Wu et al. (2019) |
| *Prunus fruticosa* Pall. | Ground cherry | 366 | Wohner et al. (2021) |

while maintaining specific fruit composition and a new research framework, which was confirmed by Martinez-Zapater et al. (2010).

A significant scientific milestone was reached for *Malus* × *domestica* Borkh. variety Golden Delicious in 2010 with the publishing of the first drought whole-genome sequence (WGS), which had a genome size of 742 Mb (Velasco et al., 2010). As the first reference for sequencing data, precise mapping, gene discovery, variation finding, and tool creation, this WGS, v1.0, proved useful. The reference genome for apples is now GDDH13v1.1, a fresh, high-quality whole-genome sequence for apple that was published in 2017. These whole-genome sequences of apple have a significant effect on understanding the biological functioning of apple, its trait physiology, and subsequently its inheritance, which find practical applications for enhancing this high-value crop, as stated by Peace et al. (2019), with immense potential for crop improvement. The genome sequencing of *Prunus persica* L. Batsch (peach) has just lately been made accessible to the scientists and researchers. With its short juvenile period (2–4 years) and self-mating design, the peach's short (230 Mbp), simple, diploid distribution on eight pairs of chromosomes provide a great way to build a robust sequence of its entire genome, which improves the way for the rapid development of genomics in peaches (Arus et al., 2012). Guo et al. (2020) gave an integrated structural map of the peach genome with 202, 274 SVs (structural variations) which influence 2, 268 genes. Using genome-wide association studies, 26 horticultural traits with the help of those SVs detected various candidate variants, *viz*., 9-bp insertion in *Prupe.4G186800* (encoding NAC transcription factor) for early bearing and 487-bp deletion with the *PpMYB10.1* promoter for flesh color around the stone. In addition, 1.67 MB inversion relates to fruit shape and a gene adjacent to inversion breakpoint, *PpOFP1*, relates to flat shape type.

*Fragaria vesca* (woodland strawberry; 2n = 2x = 14), a herbaceous perennial with a genomic size of 240 MB, is highly specific to genetic transformation and shares a large sequence identity with *Fragaria* × *ananassa* (the cultivated strawberry). Through gene prediction modeling which is supported by transcriptome mapping, almost 34, 809 genes have been identified. These genes are valuable to critical horticultural traits like nutritional values, flavor, and flowering time. The strawberry sequence is diploid, whereas other rosids' massive genomic duplications are absent (Shulaev et al., 2011). The assembly and annotation of the *Fragaria* ×*ananassa* (octoploid strawberry) genome have been completed in cultivar "Camarosa, " with an average genome size of 813.4 Mb (Hirakawa et al., 2014). A high-quality reference genome is required for the octaploid strawberry in order to properly utilize it as a model system for investigating allopolyploidy and to provide a platform for discovering physiologically and horticulturally significant genes and using genome enabled breeding techniques (Collard and Mackill, 2008).

Using second-generation sequencing technology, Chagné et al. (2014) presented a dwarf assembly of the *Pyrus communis* (European pear) 'Bartlett' genome from single-end, 2- and 7-kb insert paired end reads using Newbler (v 2.7). This assembly included 142, 083 scaffolds longer than 499 bases, with a maximum scaffold length of 1.2 Mb, spanning 577.3 Mb, and its re-sequencing of the samples "Old Home" and "Louise Bonne de Jersey" allowed the detection of 8, 29, 823 potential SNPs. About 2, 279 genetically mapped SNPs anchor 171 Mb of the assembled genome. This study revealed that the draft assembly 'Bartlett' v 1.0 is an incredible tool for detecting important horticultural traits in Pyrus enabling marker-assisted and genomic selection for speeding pear breeding progress. To discover target genes and additional unknown genes, in Persian walnut (*Juglans regia* L.), the genome sequence was obtained from cultivar 'Chandler'. Using two methods, viz., SOAPdenovo2 and MaSuRCA, a genome of the size 667 Mbp was congregated having an N50 scaffold size of 464, 955 bp (according to the genome size of 606 Mbp), 37% GC content, and 221, 640 contigs. The walnut genome sequence provides information to boost the breeding and favor the complex traits in genetic dissection as reported by Martinez-Garcia et al. (2016). In a recent study by Marrano et al. (2020), Chandler v2.0 (the new chromosome level assembly of the reference genome for walnut) was obtained employing combination of Oxford Nanopore long-read sequencing with Hi-C (chromosome conformation capture) technology. In comparison with the former reference genome, the new assembly possesses a 84.4-fold increase in N50 size and assemblage of 16 chromosomal pseudomolecules, accounting for 95% of the total length. With this Chandler v2.0, walnut biology can be better explored for future breeding aspects.

Alioto et al. (2020) attempted the genome sequencing of Texas, a highly heterozygous cultivar of almond (*Prunus dulcis*). From about 238-Mb estimated size of the almond genome, genome assembly of 227.6 Mb was obtained, from which 91% is clamped to eight pseudomolecules leading to its haploid chromosome constituent, elucidating about 27, 969 coding genes (protein) and 6, 747 non-coding transcripts. According to a phylogenomic analysis of 16 genomes of other nearby and far-off species, the almond and peach diverged roughly 5.88 million years before. With 20 nucleotide substitutions per kilobase, these two genomes exhibit remarkable sequence conservation and strong collinearity. Transposable elements (TE) have evolved into a variety of presence/absence variants between peach and almond, depicting a recent history of the movement of TE looks markedly between them, suggesting that TE share an important role in the history and diversification of peach and almond. This study revealed that TE have evolved into a variety of presence/absence variants between almond and peach. A high-quality reference genome has been elucidated by Jiang et al. (2019), using long-read single-molecule sequencing with 40.46 Gb, corresponding with a genetic map for

chromosome scaffolding. The assembled genome covers 221.9 Mb, with a contig NG50 size of 1.02 Mb. In over eight chromosomes, scaffolds spanning 92.88% of the assembled genome were anchored. This study concluded that this highly contiguous reference genome of *Prunus armeniaca* will elucidate Rosaceae family evolution for future breeding endeavors by identifying agronomic traits of interest for further improvement. Based on PacBio long reads and Hi-C data, Wu et al. (2019) built a revised chromosome-level reference genome of *A. chinensis* (v3.0), which is 653 Mb long and contains 0.76% heterozygosity. At least 43% of the sequences in this genome repeat, and the most prevalent long terminal repeats, which make up 23.38% of the unique genome, have also been found.

Wohner et al. (2021) drafted chromosome-level genome assembly of tetraploid ground cherry (*Prunus fruticosa* Pall.) with 366 Mb comprising eight chromosomes to pave a way for breeding, molecular, and evolutionary studies in *Prunus*. With this research, it was suggested that molecular assessment of diverse genetic traits can be done for further breeding and evolutionary studies. In addition to this, advances are required to upgrade the basic nucleotide sequences in the genome of different temperate fruit crops as summarized by Peace et al. (2019), in apple with a view to improve the reference WGS (whole-genome sequencing) genome ensuring its accuracy and completeness so as to mark all the suspicious regions identified while comparing the WGS with high-quality genetic linkage maps. Also, advances in genome sequencing are required by devising a gene atlas of different temperate fruit and nut crops to describe the functions and relationships of different genes to explore the role of various putative protein-coding genes which are unknown.

## Omics approach in temperate fruits and nuts

Over the recent decades, the advent of several omics approaches has proven to be highly beneficial against different biotic and abiotic stress responses by developing novel crop species through modification of the genetic and molecular pathways *via* alteration of DNAs, transcripts, proteins, metabolites, and mineral nutrient levels (Muthamilarasan et al., 2019). The analysis of transcriptome, metabolome, and proteome profiles promotes insights on several functional roles of different genes. It also assists in identification and quantification of transcripts, non-coding RNAs, and pathways that are concerned with fruit traits such as sugar metabolism, their developmental and ripening process, shelf life, quality characteristics, and resistance mechanism under adverse physiological and environmental stresses (Zheng et al., 2021). Overall, the integrated omics approaches, *viz*., genomics, transcriptomics, metabolomics, and proteomics, could elucidate precise genomic information and may offer further opportunities for their genetic alteration *via* gene engineering tools like CRISPR (clustered regularly interspaced short palindromic repeats) and RNAi (RNA interference), in terms of better fruit quality and production through accelerating the long breeding generations (Mathiazhagan et al., 2021). Currently, GAB (genomics-assisted breeding) has tremendous utilization in terms of addressing better quality, yield, and several biotic and abiotic stress (drought and salt) resistances (in a wide range of crop species; Ganie et al., 2021; Wani et al., 2022). Also, several applications of omics platforms have been implemented in the way of different fruit improvements. For instance, a comparative transcriptomics study between unripe and ripe berries of grapevine demonstrated several ripening-linked secondary metabolisms, viz., anthocyanins (Wu et al., 2014), proanthocyanidins (Carrier et al., 2013), and volatile compounds (Cramer et al., 2014). A transcriptome analysis of Chinese pear showed high variation of gene expressions during the developmental phase of tissues and fruits (Xie et al., 2013). In strawberry, a multiomics approach revealed the association of different genes regulating volatile organic compounds behind the flavor characteristics of its berries (Fan et al., 2022). A comparative transcriptome analysis among several apple verities exhibited 34 genes regulating the anthocyanin contents which are associated with preferred appearance of apples (El-Sharkawy et al., 2015). Zaini et al. (2020) conducted a deep comparative proteomics study in kernel pellicle tissues of two elite walnut cultivars and detected proteins that are concerned with secondary metabolism governing the pigmentation leading to nut qualities. In avocado, an integrated proteomics and metabolomics study indicated the induction of ripening homogeneity through heat treatment that boosts the sugar soluble accumulation, *viz*., sucrose and galactose and other stress-related enzymes (Gavicho Uarrota et al., 2019). Similarly, another study has been carried out by combining transcriptomics with network analysis to determine the control mechanisms concerned with acid accumulation and citrate in sweet orange varieties that contributes to their fruit quality and tastes (Huang et al., 2016). These omics approaches have also played crucial roles in deciphering different gene regulations behind abiotic and biotic stress responses. For example, a metabolomics analysis in peach determined the association of different metabolites, *viz*., mannitol, galactinol, and raffinose, particularly higher raffinose accumulation under freezing stress conditions (Brizzolara et al., 2018). In case of biotic stress, a comparative proteomics study in resistant and susceptible apple leaves affected with *Alternaria alternate* disease demonstrated a major involvement of 43 differentially expressed proteins behind both pathogenesis and defense mechanism (Zhang et al., 2015). Another study through a quantitative proteomics analysis revealed up- and downregulation of several differential accumulated proteins that are associated behind gray mold disease of kiwifruits (Liu et al., 2018).

## Conclusions and future prospects

The temperate fruit and nut crops being perennial in nature undergoes several difficulties in terms of their genetic improvement through classical methods of breeding, which involves long-term deliberate crossing of closely and distantly related individuals to develop desired cultivars and varieties. Therefore, the advance molecular breeding approach since the last three decades have been widely adapted and assisted in revolutionizing the fruit crop improvements. The current advances in gene sequencing technologies have facilitated deep insights on genes regulating desirable fruit qualities, their ripening, and aroma development mechanisms, including biotic and abiotic stress responses. However, a systemic method in using sequence information on the complex pathways of fruit crop development is still less frequently utilized. Hence, an integrated systems biology approach through implementation of the multiomics approach which can generate functionally validated genomic knowledge is required for fruit improvement programs. The genome-wide association study and genomic selection approaches can assist in association of multiple traits and eliminate the requirement for developing mapping population, thus shortening the duration and space necessary for fruit orchard maintenance. Next, the cutting-edge technologies, *viz*., CRISPR-mediated genome editing, can be a beneficial asset in the way of transgene-free precise genetic modification that facilitate no genetic footprints and no off-targets in developing novel and resistant qualitative fruit and nut varieties. Hence, for improvement in commercial temperate fruit and nut crops, the integration of various biotechnological tools, *viz*., high-throughput molecular markers along with the CRISPR gene editing systems can accelerate the pace of precision breeding programs in future, opening greater avenues for research and sustainability to farmers and consumers.

## Author contributions

All authors listed have made a substantial, direct, and intellectual contribution to the work, and approved it for publication.

## Conflict of interest

The authors declare that the research was conducted in the absence of any commercial or financial relationships that could be construed as a potential conflict of interest.

## Publisher's note



## References

Alioto, T., Alexiou, K. G., Bardil, A., Barteri, F., Castanera, R., Cruz, F., et al. (2020). Transposons played a major role in the diversification between the closely related almond and peach genomes:results from the almond genome sequence. *Plant J.* 101 (2), 455–472. doi: 10.1111/tpj.14538

Al-Samarai, F. R., and Al-Kazaz, A. A. (2015). Molecular markers:an introduction and applications. *Eur. J. Mol. Biotechnol.* 9 (3), 118–130. doi: 10.13187/ejmb.2015.9.118

Aradhya, M. K., Velasco, D., Wang, J., Ramasamy, R., You, F. M., Lesli, C., et al. (2018). A fine-scale genetic linkage map reveals genomic regions associated with economic traits in walnut (*Juglans regia*). *Plant Breed.* 138, 635–646. doi: 10.1111/pbr.12703

Arus, P., Verde, I., Sosinski, B., Zhebentyayeva, T., and Abbott, A. G. (2012). The peach genome. *Tree Genet. &Genomes* 8 (3), 531–547. doi: 10.1007/s11295-012-0493-8

Baro-Montel, N., Eduardo, I., Usall, J., Casals, C., Arus, P., Teixido, N., et al. (2019). Exploring sources of resistance to brown rot in an interspecific almond x peach population. *J. Sci. Food Agric.* 99 (8), 4105–4113. doi: 10.1002/jsfa.9640

Brizzolara, S., Hertog, M., Tosetti, R., and Nicolai B.and Tonutti, P. (2018). Metabolic responses to low temperature of three peach fruit cultivars differently sensitive to cold storage. *Front. Plant Sci.* 9, 706. doi: 10.3389/fpls.2018.00706

Brukental, H., Doron-Faigenboim, A., Bar-Yaakov, I., Harel-Beja, R., Attia, Z., Azoulay-Shemer, T., et al. (2021). Revealing the genetic components responsible for the unique photosynthetic stem capability of the wild almond *Prunus arabica* (Olivier) meikle. *Front. Plant Sci.* 12, 779–970. doi: 10.3389/fpls.2021.779970

Calle, A., Serradilla, M. J., and Wunsch, A. (2021). QTL mapping of phenolic compounds and fruit colour in sweet cherry using a 6 + 9K SNP array genetic map. *Scientia Hortic.* 280, 109900. doi: 10.1016/j.scienta.2021.109900

Cantin, C. M., Arus, P., and Eduardo, I. (2018). Identification of a new allele of the dw gene causing brachytic dwarfing in peach. *BMC Res. Notes* 11, 386. doi: 10.1186/s13104-018-3490-7

Carrasco, B., Gonzalez, M., Gebauer, M., Garcia-Gonza lez, R., Maldonado, J., and Silva, H. (2018). Construction of a highly saturated linkage map inJapanese plum (*Prunus salicina* l.) using GBS for SNP marker calling. *PloS One* 13 (12), 1–14. doi: 10.1371/journal.pone.0208032

Carrier, G., Huang, Y. F., Le Cunff, L., Fournier-Level, A., Vialet, S., Souquet, J. M., et al. (2013). Selection of candidate genes for grape proanthocyanidin pathway by an integrative approach. *Plant Physiol. Biochem.* 72, 87–95. doi: 10.1016/j.plaphy.2013.04.014

Chagné, D., Crowhurst, R. N., Pindo, M., Thrimawithana, A., Deng, C., Ireland, H., et al. (2014). The draft genome sequence of European pear (*Pyrus communis* L.'Bartlett'). *PloS One* 9 (4), e92644. doi: 10.1371/journal.pone.0092644

Chaney, W., Yuanhong, H., Rohla, C., Monteros, M. J., and Grauke, L. J. (2015). Developing molecular marker resources for pecan. *Acta Horticul.* 1070, 127–132. doi: 10.17660/ActaHortic.2015.1070.13

Cockerton, H. M., Vickerstaff, R. J., Karlstrom, A., Wilson, F., Sobczyk, M., He, J. Q., et al. (2018). Identification of powdery mildew resistance QTL in strawberry (*Fragaria* × *ananassa*). *Theor. Appl. Genet.* 131, 1995–2007. doi: 10.1007/s00122-018-3128-0

Collard, B. C. Y., Jahufer, M. Z. Z., Brouwer, J. B., and Pang, E. C. K. (2005). An introduction to markers, quantitative trait loci (QTL) mapping and marker-assisted selection for crop improvement: The basic concepts. *Euphytica* 142, 169–196. doi: 10.1007/s10681-005-1681-5

Collard, B. C. Y., and Mackill, D. J. (2008). Marker-assisted selection:an approach for precision plant breeding development twenty-first century. *PhilosophicalTransactionsof RoyalSociety Of London* 363, 557–572. doi: 10.1098/rstb.2007.2170

Cramer, G. R., Ghan, R., Schlauch, K. A., Tillett, R. L., Heymann, H., Ferrarini, A., et al. (2014). Transcriptomic analysis of the late stages of grapevine (*Vitis vinifera* cv. Cabernet sauvignon) berry ripening reveals significant induction of ethylene signaling and flavor pathways in the skin. *BMC Plant Biol.* 14, 370. doi: 10.1186/s12870-014-0370-8

Dhutmal, R. R., Mundhe, A. G., and More, A. W. (2018). Molecular marker techniques: A review. *Int. J. Curr. Microbiol. Appl. Sci.* 6, 816–825.

El-Sharkawy, I., Liang, D., and Xu, K. (2015). Transcriptome analysis of an apple (*Malus* × *domestica*) yellow fruit somatic mutation identifies a gene network module highly associated with anthocyanin and epigenetic regulation. *JournalOf Exp. Bot.* 66, 7359–7376. doi: 10.1093/jxb/erv433

Fan, Z., Tieman, D. M., Knapp, S. J., Zerbe, P., Famula, R., Barbey, C. R., et al. (2022). A multiomics frameworkreveals strawberry flavor genes and their regulatory elements. *New Phytol.* 236 (3), 1089–1107. doi: 10.1111/nph.18416

Frary, A., Ozturk, S. C., Balik, H. I., Balik, S. K., Kizilci, G., Doganlar, S., et al. (2019). Analysis of European hazelnut (*Corylus avellana*)reveals loci for cultivar improvement and the effects of domestication and selection on nut and kernel traits. *Mol. Genet. Genomics* 294, 519–527. doi: 10.1007/s00438-018-1527-1

Ganie, S. A., Wani, S. H., Henry, R., and Hensel, G. (2021). Improving rice salt tolerance by precision breeding in a new era. *Curr. Opin. Plant Biol.* 60, 101996. doi: 10.1016/j.pbi.2020.101996

Garcia-Gomez, B. E., Salazar, J. A., Dondini, L., Martinez-Gomez, P., and Ruiz, D. (2019). Identification of QTLs linked to fruit quality traits in apricot (*Prunus armeniaca* l.) and biological validation through gene expression analysis using qPCR. *Mol. Breed.* 39, 28. doi: 10.1007/s11032-018-0926-7

Gavicho Uarrota, V., Fuentealba, C., Hernández, I., Defilippi-Bruzzone, B., Meneses, C., Campos- Vargas, R., et al. (2019). Integration of proteomics and metabolomics data of early and middle season hass avocados under heat treatment. *Food Chem.* 289, 512–521. doi: 10.1016/j.foodchem.2019.03.090

Guo, J., Cao, K., Deng, C., Li, Y., Zhu, G., Fang, W., et al. (2020). An integrated peach genome structural variation map uncovers genes associated with fruit traits. *Genome Biol.* 21, 258. doi: 10.1186/s13059-020-02169-y

Halasz, J., Kodad, O., Galiba, G. M., Skola, I., Ercisli, S., Ledbetter, C. A., et al. (2019). Genetic diversity is preserved among strongly differentiated and geographically diverse almond germplasm:an assessment by simple sequence repeat markers. *Tree Genet. &Genomes* 15, 12. doi: 10.1007/s11295-019-1319-8

Hale, I., Melo, A. T. O., and Gustafson, H. (2018). Sex-linked molecular markers for two cold-hardy kiwifruit species, *Actinidia arguta* and a.kolomikta. *Eur. J. Hortic. Sci.* 83 (4), 236–246. doi: 10.17660/eJHS.2018/83.4.4

Han, H., Oh, Y., Kim, K., Oh, S., Cho, S., Kim, Y., et al. (2019). Integrated genetic linkage maps for Korean pears (*Pyrus* hybrid) using GBS-based SNPs and SSRs. *Horticul. Environment Biotechnol.* 60, 779–786. doi: 10.1007/s13580-019-00171-3

Hayward, A. C., Tollenaere, R., Morgan, J. D., and Batley, J. (2015). Molecular marker applications in plants. *Methods Mol. Biol.* 1245, 13–27. doi: 10.1007/978-1-4939-1966-6_2

Hirakawa, H., Shirasawa, K., Kosugi, S., Tashiro, K., Nakayama, S., Yamada, M., et al. (2014). Dissection of the octoploid strawberry genome by deep sequencing of the genomes of fragaria species. *DNA Res.* 21, 169–181. doi: 10.1093/dnares/dst049

Hossain, M. R., Natarajan, S., Kim, H. T., Jesse, D. M. I., Lee, C. G., Park, J. I., et al. (2019). High density linkage map construction and QTL mapping for runner production in allo-octoploid strawberry fragaria x *ananassa* based on dd RAD-seq derived SNPs. *Sci. Rep.* 9, 3275. doi: 10.1038/s41598-019-39808-9

Houmanat, K., Abdellah, K., Hssaini, L., Razouk, R., Hanine, H., Jaafary, S., et al. (2020). Molecular diversity in walnut(*Juglans regia* l.)among two major areas in Morocco in contrast with foreign varieties. *Int. J. Fruit Sci.* 21 (1), 180–192. doi: 10.1080/15538362.2020.1862734

Huang, D., Zhao, Y., Cao, M., Qiao, L., and Zheng, Z. (2016). Integrated systems biology analysis of transcriptomes reveals candidate genes for acidity control in developing fruits of sweet orange (*Citrus sinensis* l. osbeck). *Front. Plant Sci.* 7, 486. doi: 10.3389/fpls.2016.00486

Igarashi, M., Hatsuyama, Y., Harada, T., and Fukasawa-Akada, T. (2015). Biotechnology and apple breeding in Japan. *Breed. Sci.* 66, 18–33. doi: 10.1270/jsbbs.66.18

Jaillon, O., Aury, J. M., Noel, B., Policriti, A., Clepet, C., Casagrande, A., et al. (2007). The grapevine genome sequence suggests ancestral hexaploidization in major angiosperm phyla. *Nature* 449 (7161), 463–467. doi: 10.1038/nature06148

H. K. Jain and M. C. Kharkwal (Eds.) (2004). *Plant breeding mendelian to molecular approaches* (New Delhi, India: Narosa publishing House), 810.

Jan, A. (2016). Morpho-genetic diversity studies in sandy pear (Pyrus pyrifolia.Nakai) (Shalimar Campus Srinagar: Faculty of Horticulture SKUAST-Kashmir), 98.

Jiang, J., Fan, X., Zhang, Y., Tang, X., Li, X., Liu, C., et al. (2020). Construction of a high-density genetic map and mapping of firmness in grapes (*Vitis vinifera* l.) based on whole genome resequencing. *Int. J. Mol. Sci.* 21 (3), 797. doi: 10.1038/s41438-019-0215-6

Jiang, F., Zhang, J., Wang, S., Yang, L., Luo, Y., Gao, S., et al. (2019). The apricot (*Prunus armeniaca* l.) genome elucidates rosaceae evolution and beta-carotenoid synthesis. *Horticul. Res.* 6, 128. doi: 10.3390/ijms21030797

Lenz, R. R., and Dai, W. (2017). Mapping X-disease phytoplasma resistance in *Prunus virginiana*. *Front. Plant Sci.* 8, 2057. doi: 10.3389/fpls.2017.02057

Le Roux, P. M. F., Christen, D., Duffy, B., Tartarini, S., Dondini, L., Yamamoto, T., et al. (2012). Redefinition of the map position and validation of a major quantitative trait locus for fire blight resistance of the pear cultivar " harrow sweet" (*Pyrus communis* l.). *Plant Breed.* 131, 656–664. doi: 10.1111/j.1439-0523.2012.02000.x

Lewers, K. S., Castro, P., Hancock, J. F., Weebadde, C. K., Die, J. V., and Rowland, L. J. (2019). Evidence of epistatic suppression of repeat fruiting in cultivated strawberry. *BMC Plant Biol.* 19, 386. doi: 10.1186/s12870-019-1984-7

Li, W., Liu, L., Wang, Y., Zhang, Q., Fan, G., Zhang, S., et al. (2020). Genetic diversity, population structure, and relationships of apricot (Prunus) based on restriction site-associated DNA sequencing. *Horticult. Res.* 7. doi: 10.1038/s41438-020-0284-6

Lian, X., Zhao, X., Zhao, Q., Wang, G., Li, Y., and Hao, Y. (2021). MdDREB2A in apple is involved in the regulation of multiple abiotic stress responses. *Hortic. Plant J.* 7 (3), 197–208. doi: 10.1016/j.hpj.2021.03.006

Lim, S., Lee, J., Lee, H. J., Park, K. H., Kim, D. S., Min, S. R., et al. (2016). The genetic diversity among strawberry breeding resources based on SSRs. *Scientia Agricola* 74 (3), 226–234. doi: 10.1590/1678-992X-2016-0046

Liu, W., Shahid, M. Q., Bai, L., Lu, Z., Chen, Y., Jiang, L., et al. (2015). Evaluation of genetic diversity and development of a core collection of wild rice(*Oryza rufipogon* griff.)populations in China. *PloS One* 10 (12), e0145990. doi: 10.1371/journal.pone.0145990

Liu, J., Sui, Y., Chen, H., Liu, Y., and Liu, Y. (2018). Proteomic analysis of kiwifruit in response to the postharvest pathogen, *Botrytis cinerea*. *Front. Plant Sci.* 9, 158. doi: 10.3389/fpls.2018.00158

Lozano, L., Iglesias, I., Micheletti, D., Troggio, M., Kumar, S., Volz, R. K., et al. (2014). Feasibility of genome-wide association analysis using a small single nucleotide polymorphism panel in an apple breeding population segregating for fruit skin color. *J. Am. Soc. Hortic. Sci.* 139 (6), 619–526. doi: 10.21273/JASHS.139.6.619

Marrano, A., Britton, M., Zaini, P. A., Zimin, A. V., Workman, R. E., Puiu, D., et al. (2020). High-quality chromosome-scale assembly of the walnut (Juglans regia l.) reference genome. *Gigascience* 9 (5), giaa050. doi: 10.1093/gigascience/giaa050

Marimon, N., Luque, J., Arus, P., and Eduardo, I. (2020). Fine mapping and identification of candidate genes for the peach powdery mildew resistance gene *Vr3*. *Horticul. Res.* 7, 175. doi: 10.1038/s41438-020-00396-9

Marrano, A., Sideli, G. M., Leslie, C. A., Cheng, H., and Neale, D. B. (2019). Deciphering of the genetic control of phenology, yield, and pellicle color in Persian walnut (*Juglans regia* l.). *Front. Plant Sci.* 10, 1140. doi: 10.3389/fpls.2019.01140

Martinez-Garcia, P. J., Crepeau, M. W., Puiu, D., Gonzalez-Ibeas, D., Whalen, J., Stevens, K. A., et al. (2016). The walnut(*Juglans regia*) genome sequence reveals diversity in genes coding for the biosynthesis of non-structural polyphenols. *Plant J.* 87 (5), 507–532. doi: 10.1111/tpj.13207

Martinez-Zapater, J. M., Carmona, M. J., DiazRiquelme, J., Fernandez, L., and Lijavetzky, D. (2010). Grapevinegenetics after the genome sequence: Challenges and limitations. *Aust. J. Grape Wine Res.* 16, 33–46. doi: 10.1111/j.1755-0238.2009.00073.x

Mas-Gomez, J., Cantin, C. M., Moreno, M. A., Prudencio, A. S., GomezAbajo, M., Bianco, L., et al. (2021). Exploring genome-wide diversity in the national Peach (*Prunus persica*) germplasm collection at CITA (Zaragoza, Spain). *Agronomy* 11, 481. doi: 10.3390/agronomy11030481

Mathiazhagan, M., Chidambara, B., Hunashikatti, L. R., and Ravishankar, K. V. (2021). Genomic approaches for improvement of tropical fruits: fruit quality, shelf life and nutrient content. *Genes* 12 (12), 1881. doi: 10.3390/genes12121881

Mehlenbacher, S. A. (1995). Classical and molecular approaches to breeding fruit and nutcrops for diseases resistance. *Hortic. Sci.* 30, 466–477.

Montanari, S., Perchepied, L., Renault, D., Frijters, L., Velasco, R., Horner, M., et al. (2016). A QTL detected in an interspecific pear population confers stable fire blight resistance across different environments and genetic backgrounds. *Mol. Breed.* 36, 47. doi: 10.1007/s11032-016-0473-z

Mori, G. D., Falchi, R., Testolin, R., Bassi, D., Savazzini, F., Dondini, L., et al. (2019). Resistance to sharka in apricot:Comparison of phase-reconstructed resistant and susceptible haplotypes of 'Lito'chromosome 1 and analysis of candidate genes. *Front. Plant Sci.* 10, 1576. doi: 10.3389/fpls.2019.01576

Muthamilarasan, M., Singh, N. K., and Prasad, M. (2019). Multi-omics approaches for strategic improvement of stress tolerance in underutilized crop species: a climate change perspective. *Advanced Genet.* 103, 1–38. doi: 10.1016/bs.adgen.2019.01.001

Nadeem, M. A., Nawaz, M. A., Shahid, M. Q., Dogan, Y., Comertpay, G., Yildiz, M., et al. (2018). DNA Molecular markers in plant breeding:current status and recent advancements in genomic selection and genome editing. *Biotechnol. Biotechnol. Equip.* 32 (2), 261–285. doi: 10.1080/13102818.2017.1400401

Naeem, M., Ghouri, F., Shahid, M. Q., Iqbal, M., Baloch, F. S., Chen, L., et al. (2015). Genetic diversity in mutated and non-mutated rice varieties. *Genet. Mol. Res.* 14 (4), 17109–17123. doi: 10.4238/2015.December.16.11

Nawaz, M. A., Baloch, F. S., Rehman, H. M., Le, B., Akther, F., Yang, S. H., et al. (2016). Development of a competent and trouble free DNA protocol for downstream genetic analysis in glycine species. *Turkish J. Agriculture-Food Sci. Technol.* 4 (8), 700–705. doi: 10.24925/turjaf.v4i8.700-705.788

Nawaz, M. A., Rehman, H. M., Baloch, F. S., Ijaz, B., Ali, M. A., Khan, I. A., et al. (2017). Genome and transcriptome-wide analysis of cellulose synthase gene superfamily in soyabean. *J. Plant Physiol.* 215, 163–175. doi: 10.1016/j.jplph.2017.04.009

Nawaz, M. A., Sadia, B., Awan, F. S., Zia, M. A., and Khan, I. A. (2013). Genetic diversity in hyper glucose oxidase producing *Aspergillus niger* UAF mutants by using molecular markers. *Int. J. Agric. Biotechnol.* 15 (2), 362–366.

Nawaz, M. A., Yang, S. H., Rehman, H. M., Baloch, F. S., Lee, J. D., Park, J. H., et al. (2017). Genetic diversity and population structure of Korean wild soyabean (*Glycine soja* sieb. and zucc.) inferred from microsatellite markers. *Biochem. Systematics Ecol.* 71, 87–96. doi: 10.1016/j.bse.2017.02.002

Nishio, S., Terakami, S., Matsumoto, T., Yamamoto, T., Takada, N., Kato, H., et al. (2018). Identification of QTLs for agronomic traits in Japanese chestnut (*Castanea crenata* sieb.et zucc.) breeding. *Horticul. J.* 87 (1), 43–54. doi: 10.2503/hortj.OKD-093

Nunziata, A., Ruggieri, V., Petriccione, M., and Masi, L. D. (2020). Single nucleotide polymorphisms as practical molecular tools to support European chestnut agrobiodiversity management. *Int. J. Mol. Sci.* 21, 4805. doi: 10.3390/ijms21134805

Oh, S., Lee, M., Kim, K., Han, H., Won, K., Kwack, Y., et al. (2019). Genetic diversity of kiwifruit(*Actinidia* spp.), including Korean native *A.arguta*, using single nucleotide polymorphisms derived from genotyping-by-sequencing. *Horticul. Biotechnol. Biotechnol.* 60 (1), 105–114. doi: 10.1007/s13580-018-0106-z

Oliveira, L. S. S., Pimenta, L. V. A., Guimaraes, L. M. S., deSouza, P. V. D., Bhering, L. L., and Alfenas, A. C. (2020). Resistance of kiwifruit cultivars to *Ceratocystis* wilt:an approach considering the genetic diversity and variation in aggressiveness of the pathogen. *Plant Pathol.* 70 (2), 349–357. doi: 10.1111/ppa.13305

Öztürk, S. C., Balık, H. İ., Balık, S. K., Kızılcı, G., Duyar, Ö., Doğanlar, S., et al. (2017). Molecular genetic diversity and association mapping of nut and kernel traits in Slovenian hazelnut (*Corylus avellana*) germplasm. *Tree Genet. Genomics* 13 (5), 1–10.

Paizila, A., Kafkas, S., Ziya-Motalebipour, E., Acar, I., and Turemis, N. (2019). Construction of an almond genetic linkage map using F1 population 'Gulcan -2'x 'Lauranne' by SSR markers. *Acta Horticul.* 1242, 543–548. doi: 10.17660/ActaHortic.2019.1242.79

Patzak, J., Henychová, A., Paprštein, F., and Sedlák, J. (2019). Evaluation of genetic variability within sweet cherry (Prunus avium L.) genetic resources by molecular SSR markers. *Acta Sci. Pol. Hortorum Cultus* 18, 157–165. doi: 10.24326/asphc.2019.3.15

Patzak, J., Henychova, A., Paprstein, F., and Sedlak, J. (2020). Evaluation of s-incompatibility locus, genetic diversity and structure of sweet cherry (*Prunus avium* l.) genetic resources by molecular methods and phenotypic characteristics. *J. Hortic. Sci. Biotechnol.* 95 (1), 84–92. doi: 10.1080/14620316.2019.1647798

Peace, C. P., Bianco, L., Troggio, M., vandeWeg, E., Howard, N. P., Cornille, A., et al. (2019). Apple whole genome sequences: recent advances and new prospects. *Horticul. Res.* 6, 59. doi: 10.1038/s41438-019-0141-7

Rasool, A. (2018). Morpho-molecular characterization of apple (Malusxdomestica.Borkh) germplasm (Shalimar Campus Srinagar: Faculty of Horticulture SKUAST-Kashmir), 121.

Rasouli, M., Fatahi, R., Zamani, Z., Imani, A., and Martinez-Gomez, P. (2018). Identification of DNA markers linked to blooming time in almond. *J. Nuts* 92 (2), 105–122. doi: 10.22034/JON.2018.543679

Raza, S., Farooqi, S., and Mubeen, H. (2015). Role of molecular markers and their significance. *Am. J. Pharm. Health Res.* 3 (12), 23–30.

Riaz, S., Lorenzis, G. D., Velasco, D., Koehmstedt, A., Maghradze, D., Bobokashvili, Z., et al. (2018). Genetic diversity analysis of cultivated and wild grapevine (*Vitis vinifera* l.) accessions around the Mediterranean basin and central Asia. *BMC Plant Biol.* 18, 137.

Salazar, J. A., Pacheco, I., Zapata, P., Shinya, P., Ruiz, D., Martinez-Gomez, P., et al. (2020). Identification of loci controlling phenology, fruit quality and post-harvest quantitative parameters in Japanese plum(*Prunus saliciana* lindl.). *Postharvest Biol. Technol.* 169, 111292. doi: 10.1016/j.postharvbio.2020.111292

Samantara, K., Reyes, V. P., Agrawal, N., Mohapatra, S. R., and Jena, K. K. (2021). Advances and trends on the utilization of multi-parent advanced generation intercross (MAGIC) for crop improvement. *Euphytica* 217 (10), 1–22.

Sanchez-Sevilla, J. F., Horvath, A., Botella, M. A., Gaston, A., Folta, K., Kilian, A., et al. (2015). Diversity arrays technology (DarT) marker platforms for diversity analysis and linkage mapping in a complex crop, the octoploid strawberry (*Fragaria* x *ananassa*). *PloS One* 10 (12), e0144960. doi: 10.1371/journal.pone.0144960

Santos, C., Nelson, C. D., Zhebentyayeva, T., Machado, H., Gomes-Laranjo, J., and Costa, R. L. (2017). First interspecific genetic linkage map for *Castanea sativa* x *Castanea crenata* revealed QTLs for resistance to *Phytophthora cinnamomi*. *PloS One* 12 (9), e0184381. doi: 10.1371/journal.pone.0184381

Santos, C., Zhebentyayeva, T., Serrazina, S., Nelson, C. D., and Costa, R. (2015). Development and characterization of EST-SSR markers for mapping reaction to phytophthora cinnamomi in castanea spp. *Scientia Hortic.* 194, 181–187. doi: 10.1016/j.scienta.2015.07.043

Shulaev, V., Sargent, D. J., Crowhurst, R. N., Mockler, T. C., Folkerts, O., Delcher, A. L., et al. (2011). The genome of woodland strawberry (*Fragaria vesca*). *Nat. Genet.* 43, 109–116. doi: 10.1038/ng.740

Syed, S. (2019). Identification of selected apple clonal rootstocks through molecular and morphological approaches (Shalimar Campus Srinagar: Faculty of Horticulture SKUAST-Kashmir).

Terakami, S., Adachi, Y., Takeuchi, Y., Takada, N., Nishio, S., Saito, T., et al. (2021). Development of an SSR marker set for efficient selection for resistance to black spot disease in pear breeding. *Breed. Sci.* 71 (2), 240–252. doi: 10.1270/jsbbs.20136

Thottappilly, G., Magonouna, H. D., and Omitogun, O. G. (2000). The use of DNA markers for rapid improvement of crops in Africa. *Afr. Crop Sci. J.* 8, 99–108. doi: 10.4314/acsj.v8i1.27720

Thurow, L. B., Raseira, M. D. C. B., Bonow, S., Arge, L. W. P., and Castro, C. M. (2016). Population genetic analysis of Brazilian peach breeding germplasm. *Rev. Bras. Fruiticul.* 39 (5), 166. doi: 10.1590/0100-29452017166

Tiwari, J. K., Singh, B. P., Gopal, J., Poonam, P., and Patil, V. U. (2013). Molecular characterization of the Indian andigena potato core collection using microsatellite markers. *Afr. J. Biotechnol.* 12 (10), 1025–1033.

Velasco, R., Zharkikh, A., Affourtit, J., Gardiner, S. E., Skolnick, M., Egholm, M., et al. (2010). The genome of the domesticated apple (*Malusxdomestica* borkh.). *Nat. Genet.* 42 (10), 833–839. doi: 10.1038/ng.654

Wang, Y., Ghouri, F., Shahid, M. Q., Naeem, M., and Baloch, F. S. (2017). The genetic diversity and population structure of wild soyabean evaluated by chloroplast and nuclear gene sequences. *Biochem. Systematics Ecol.* 71, 170–178. doi: 10.1016/j.bse.2017.02.008

Wang, Y., Shahid, M. Q., Ghouri, F., Wang, Y., and Huang, H. (2015). Evaluation of the geographical pattern of genetic diversity of glycine soja and *Glycine max* based on four single copy nuclear gene loci:for conservation of soyabean germplasm. *Biochem. Systematics Ecol.* 62, 229–235. doi: 10.1016/j.bse.2015.09.006

Wang, J., Zhang, K., Zhang, X., Yan, G., Zhou, Y., Feng, L., et al. (2015). Construction of commercial sweet cherry linkage maps and QTL analysis for trunk diameter. *PloS One* 10 (10), e0141261. doi: 10.1371/journal.pone.0141261

Wani, S. H., Choudhary, M., Barmukh, R., Bagaria, P. K., Samantara, K., Razzaq, A., et al. (2022). Molecular mechanisms, genetic mapping, and genome editing for insect pest resistance in field crops. *Theor. Appl. Genet.*, 1–21. doi: 10.1007/s00122-022-04060-9

Wani, S. H., Samantara, K., Razzaq, A., Kakani, G., and Kumar, P. (2022). Back to the wild: mining maize (*Zea mays* l.) disease resistance using advanced breeding tools. *Mol. Biol. Rep.* 22, 1–17.

Wohner, T. W., Emeriewen, O. F., Wittenberg, A. H. J., Schneiders, H., Vrijenhoek, I., Halasz, J., et al. (2021). The draft chromosome-level genome assembly of tetraploid ground cherry (*Prunus fruticosa* pall.) from long reads. *Genomics* 113, 4173–4183. doi: 10.1016/j.ygeno.2021.11.002

Wu, B. H., Cao, Y. G., Guan, L., Xin, H. P., Li, J. H., and Li, S. H. (2014). Genome-wide transcriptional profiles of the berry skin of two red grape cultivars (*Vitis vinifera*) in whichanthocyanin synthesis is sunlight-dependent or -independent. *PloS One* 9, e105959. doi: 10.1371/journal.pone.0105959

Wu, W., Chen, F., Yeh, K., and Chen, J. (2018). ISSR analysis of genetic diversity and structure of plum varieties cultivated in southern china. *Biology* 8, 2.

Wu, H., Ma, T., Kang, M., Ai, F., Zhang, J., Dong, G., et al. (2019). A high –quality *Actinidia chinensis* (kiwifruit) genome. *Horticul. Res.* 6, 117. doi: 10.1038/s41438-019-0202-y

Xiao, Y., Wang, C., Tian, Y., Yang, S., Shen, J., Liu, Q., et al. (2019). Candidates responsible for dwarf pear phenotype as revealed by comparative transcriptome analysis. *Mol. Breed.* 39, 1. doi: 10.1007/s11032-018-0907-x

Xie, M., Huang, Y., Zhang, Y., Wang, X., Yang, H., Yu, O., et al. (2013). Transcriptome profiling of fruit development and maturation in Chinese white pear (*Pyrus bretschneideri* rehd). *BMC Genomics* 14, 823. doi: 10.1186/1471-2164-14-823

Yang, C., Sha, G., Wei, T., Ma, B., Li, C., Li, P., et al. (2020). Linkage map and QTL mapping of red flesh locus in apple using a R1R1 x R6R6 population. *Hortic. Plant J.* 7 (5), 393–400. doi: 10.1016/j.hpj.2020.12.008

Yokomi, R., Delgado, J. K., Unruh, T. R., Barcenas, N. M., Garczynski, S. F., Walse, S., et al. (2021). Molecular advances in larval fruit moth identification to facilitate fruit export from Western united states under systems approaches. *Ann. Entomol. Soc. America* 115 (1), 105–112. doi: 10.1093/aesa/saab040

Zaini, P. A., Feinberg, N. G., Grilo, F. S., Saxe, H. J., Salemi, M. R., Phinney, B. S., et al. (2020). Comparative proteomic analysis of walnut (*Juglans regia* l.) pellicle tissues reveals the regulation of nut quality attributes. *Life* 10 (12), 314. doi: 10.1139/cjps- 2018-0177

Zhang, J., Sun, H., Yang, L., Jiang, F., Zhang, M., and Wang, Y. (2019). Construction of a high-density linkage map and QTL analysis for pistil abortion in apricot (*Prunus armeniaca* l.). *Can. J. Plant Sci.* 99, 599–610. doi: 10.1139/cjps-2018-0177

Zhang, C.-x., Tian, Y., and Cong, Ph (2015). Proteome analysis of pathogenresponsive proteins from apple leaves induced by the alternaria blotch *Alternaria alternata*. *PloS One* 10, e0122233.

Zhang, C., Yao, X., Ren, H., Chang, J., Wu, J., Shao, W., et al. (2020). Characterization and development of genomic SSRs in Pecan (*Carya illinoinensis*). *Forests* 11, 61. doi: 10.3390/f11010061

Zhao, H., Ju, Y., Jiang, J., Min, Z., Fang, Y., and Liu, C. (2019). Downy mildew resistance identification and SSR molecular marker screening of different grape germplasm resources. *Scientia Hortic.* 252, 212–221. doi: 10.1016/j.scienta.2019.03.025

Zhen, Q., Fang, T., Peng, Q., Liao, L., Zhao, L., Owiti, A., et al. (2018). Developing gene-tagged molecular markers for evaluation of genetic association of apple SWEET genes with fruit sugar accumulation. *Horticul. Res.* 5, 14. doi: 10.1038/s41438-018-0024-3

Zheng, S., Hao, Y., Fan, S., Cai, J., Chen, W., Li, X., et al. (2021). Metabolomic and transcriptomic profiling provide novel insights into fruit ripening and ripening disorder caused by 1-MCP treatments in papaya. *Int. JournalOf Mol. Sci.* 22, 916. doi: 10.3390/ijms22020916

Zhu, Y., Yin, Y., Yang, K., Li, J., Sang, Y., Huang, L., et al. (2015). Construction of high-density genetic map using specific length amplified fragment markers and identification of a quantitative trait locus for resistance in walnut (*Juglans regia* l.). *BMC Genomics* 16 (1), 1–13. doi: 10.1186/s12864-015-1822-8

frontiers | Frontiers in Plant Science

TYPE Original Research
PUBLISHED 09 March 2023
DOI 10.3389/fpls.2023.1126606



OPEN ACCESS

EDITED BY
Weibiao Liao,
Gansu Agricultural University, China

REVIEWED BY
Sajid Ali,
Bahauddin Zakariya University, Pakistan
Cengiz Kaya,
Harran University, Türkiye

*CORRESPONDENCE
Jian Yu
yjian0515@163.com

SPECIALTY SECTION
This article was submitted to Plant Breeding, a section of the journal Frontiers in Plant Science

RECEIVED 18 December 2022
ACCEPTED 22 February 2023
PUBLISHED 09 March 2023

CITATION
Niu L, Tang Y, Zhu B, Huang Z, Wang D, Chen Q and Yu J (2023) Nitric oxide promotes adventitious root formation in cucumber under cadmium stress through improving antioxidant system, regulating glycolysis pathway and polyamine homeostasis.
*Front. Plant Sci.* 14:1126606.
doi: 10.3389/fpls.2023.1126606



# Nitric oxide promotes adventitious root formation in cucumber under cadmium stress through improving antioxidant system, regulating glycolysis pathway and polyamine homeostasis

Lijuan Niu, Yunlai Tang, Bo Zhu, Zhenfu Huang, Dan Wang, Qiyang Chen and Jian Yu*

School of Life Science and Engineering, Southwest University of Science and Technology, Mianyang, Sichuan, China

Cadmium (Cd) as a potentially toxic heavy metal that not only pollutes the environment but also interferes with plant growth. Nitric oxide (NO) regulates plant growth and development as well as abiotic stress response. However, the mechanism underpinning NO-induced adventitious root development under Cd stress remains unclear. In this study, cucumber (*Cucumis sativus* 'Xinchun No. 4') was used as the experimental material to investigate the effect of NO on the development of adventitious roots in cucumber under Cd stress. Our results revealed that, as compared to Cd stress, 10 μM SNP (a NO donor) could considerably increase the number and length of adventitious roots by 127.9% and 289.3%, respectively. Simultaneously, exogenous SNP significantly increased the level of endogenous NO in cucumber explants under Cd stress. Our results revealed that supplementation of Cd with SNP significantly increased endogenous NO content by 65.6% compared with Cd treatment at 48 h. Furthermore, our study indicated that SNP treatment could improve the antioxidant capacity of cucumber explants under Cd stress by up-regulating the gene expression level of antioxidant enzymes, as well as reducing the levels of malondialdehyde (MDA), hydrogen peroxide ($H_2O_2$) and superoxide anion ($O_2^{\cdot-}$) to alleviate oxidative damage and membrane lipid peroxidation. Application of NO resulted in a decrease of the $O_2^{\cdot-}$, MDA, and $H_2O_2$ level by 39.6%, 31.4% and 60.8% as compared to Cd-alone treatment, respectively. Besides that, SNP treatment significantly increased the expression level of related genes involved in glycolysis processes and polyamine homeostasis. However, application of NO scavenger 2-(4-carboxy -2-phenyl)-4, 4, 5, 5-tetramethy limidazoline -1-oxyl -3-oxide (cPTIO) and the inhibitor tungstate significantly reversed the positive role of NO in promoting the adventitious root formation under Cd stress. These results suggest that exogenous NO can increase the level of endogenous NO, improve antioxidation ability, promote

glycolysis pathway and polyamine homeostasis to enhance the occurrence of adventitious roots in cucumber under Cd stress. In summary, NO can effectively alleviate the damage of Cd stress and significantly promote the development of adventitious root of cucumber under Cd stress.

KEYWORDS

nitric oxide, cadmium, rooting response, antioxidants, glycolysis, polyamine pathway

# 1 Introduction

Cadmium (Cd), a widely spread heavy metal, is easily absorbed by plant roots, thus enters the food chain, and eventually poses a substantial threat to human health (Falco et al., 2005; Ahmad et al., 2016a; Ahmad et al., 2016b). It has been discovered that Cd, as a non-essential element for plant growth and development, disturbs nutrient and water uptake/transport (Rivelli et al., 2014; Hafsi et al., 2022). Moreover, Cd induces a number of stress responses in plants including ion balance changes (Kucerova et al., 2020; Hafsi et al., 2022), change in antioxidant enzymes activities (Guo et al., 2019), photosynthesis inhibition (Rizwan et al., 2018), and changes in the expression of related genes and proteins (Muhammad et al., 2019; Manara et al., 2020). Plant response to abiotic stress is usually accompanied by an increase in the level of reactive oxygen species (ROS) (Polle and Schützendübel, 2003; Kohli et al., 2019; Mansoor et al., 2022), and the increase in ROS content caused the destruction of cell structure and function (Panyuta et al., 2016; Kohli et al., 2019; Mansoor et al., 2022). Previous research have demonstrated that Cd stress could trigger the ROS generation, such as hydrogen peroxide ($H_2O_2$) and superoxide radical ($O_2^{\cdot-}$) accumulation in plants (Qi et al., 2021; Li et al., 2022). Some studies have also shown that excessive accumulation of ROS under Cd stress can trigger protein post-translational modification (Gzyl et al., 2015), enzyme inactivation and denaturation, DNA and RNA damage, resulting in cell damage and cell death (Singh et al., 2016). These series of reactions may aggravate the degree of lipid peroxidation (Heyno et al., 2008), disrupts metabolic activities and eventually affect plant growth and development (Yu et al., 2015; Anwar et al., 2021; El Rasafi et al., 2022). It has been demonstrated that plants have a series of antioxidant defense system to mitigate the oxidative damage caused by ROS (Gill and Tuteja, 2010). Antioxidant enzymes such as ascorbate peroxidase (APX), superoxide dismutase (SOD), catalase (CAT) or glutathione reductase (GR) have been demonstrated to regulate accumulation of ROS and protect plants from oxidative damage under Cd stress (Irfan et al., 2014; Guo et al., 2019). Therefore, the possibility of oxidative signal or oxidative damage depends on the balance between antioxidant enzyme activity and ROS level (Møller et al., 2007).

Nitric oxide (NO) has been implicated as an essential signaling molecule in plants. Numerous studies have discovered that NO plays an essential role in the regulation of plant growth and development including seed germination (Ren et al., 2020), root growth and development (Pagnussat et al., 2002; Sun et al., 2019; Liu et al., 2022a), pollen tube germination (Prado et al., 2004) and fruit senescence (Zuccarelli et al., 2021). The increasing evidence indicates that, NO function in plant stress response. As a multi-functional regulator, NO signaling is involved in a range of abiotic stress responses to mitigate oxidative damage caused by abiotic stress (Parankusam et al., 2017; Gao et al., 2022; Xia et al., 2022). For example, exogenous NO could stabilize the cell membranes in hulless barley under drought stress (Gan et al., 2015). Moreover, application of NO could upregulate the gene expression of antioxidative enzymes to enhance the antioxidant capacity under Cd stress (Chen et al., 2010).Thus, the protective roles of NO in alleviating oxidative injury have focused on regulating antioxidant systems, reducing the generation of ROS, mediating related gene expression, and maintaining protein stability, eventually enhancing plant stress tolerance (Terrón-Camero et al., 2019; Wei et al., 2020).

Cucumber is a member of the Cucurbitaceae family (Hashem et al., 2018). As one of the most popular vegetables, cucumber is shallow-rooted crop and is used to be an bioindicator species to assess toxicity of soils polluted by Cd (An et al., 2004). As mentioned above, NO plays an essential role in regulating plant growth and development. Moreover, it has been shown that NO is involved in the response to Cd stress. However, the mechanism underpinning NO-induced adventitious root development in cucumber under Cd stress remains unclear. The aim of this study was to investigate the role of NO in promoting the development of adventitious root in cucumber under Cd stress. Therefore, we conduct this experiment to test the effect of NO on root development, oxidative defence, glycolysis and polyamine metabolism in cucumber under Cd stress. The objective of this study was to provide evidence to elucidate the potential mechanism of NO signaling in responses to Cd stress in plants.

# 2 Materials and methods

## 2.1 Plant materials

*Cucumis sativus* L. ('Xinchun No. 4') was used in this experiment. The sterilized cucumber seeds were pre-soaked in distilled water for 5 hours. The seeds were germinated on filter paper in petri dishes and then incubated in a climate box at 25°C

with a 14 h photoperiod (200 $\mu mols^{-1}m^{-2}$). The experiment was repeated three times, with 10 seedlings per replicate.

## 2.2 Explant treatments

**Experiment 1**: Sodium nitroprusside (SNP, purity≥98.5%, Solarbio, China) as a NO donor. Cucumber explants were placed in petri dishes containing distilled water or different concentrations of SNP (0, 1, 10, 100, 500 μM) under Cd stress for 5 days. The concentrations of NO was selected based on the results of our previous studies (Niu et al., 2017; Niu et al., 2019). These media were changed every day in order to keep the solution fresh.

**Experiment 2:** 200 μM 2-(4-carboxy-2-phenyl)-4, 4, 5, 5-tetramethylimidazoline -1-oxyl-3-oxide (c-PTIO, purity≥98%, Sigma, USA) as NO scavenger, 200 μM tungstate (Solarbio, China) as a NO inhibitor. The concentrations of $CdCl_2$, NO scavenger or inhibitor were based on the results of a preliminary experiment.

## 2.3 Endogenous NO content

The NO content was determined using the Greiss reagent method with minor modifications (Xuan et al., 2012). Cucumber explants were ground and mixed with 4 mL of 50 mM ice cold acetic acid buffer (containing 4% zinc diacetate). The mixture was centrifuged at 10000 *g* for 15 min at 4°C, and the supernatant was collected. Then, 0.1 g of charcoal was added. After vortex and filtration, the filtrate was mixed with 1mL Greiss reagent at room temperature for 30 min. Finally, the absorbance was assayed at 540 nm.

## 2.4 Malondialdehyde, superoxide anion ($O_2$) and hydrogen peroxide ($H_2O_2$) content

For measuring MDA, 0.2 g of samples were ground in ice bath and extracted with 5 mL trichloroacetic acid (TCA). The homogenate was transferred to a centrifuge tube and centrifuged at 4°C at 12000 *g* for 15 min. The supernatant was added to 0.5% TBA solution. The mixture is heated in a boiling water bath for 30 min and then centrifuged for 10 min. The absorbance of the supernatant was measured at 450 nm, 532 nm and 600 nm (Liu et al., 2022b). For estimating $O_2^{\cdot-}$ generation, the samples were homogenized with potassium phosphate buffer (pH 7.8) and centrifuged for 10 min. The supernatant was added to hydroxylamine hydrochloride and reacted at 25°C for 20 min. Finally, the absorbance was measured at 530 nm (Gong et al., 2014). Superoxide accumulation was also examined by nitroblue tetrazolium (NBT) staining, as described previously (Wang et al., 2019). $H_2O_2$ content in cucumber explants was determined as described by the method with minor modification (Liao et al., 2011). 0.5 g of cucumber explants were ground in liquid nitrogen and then homogenized in 3 mL ice-cold aceton. After centrifugation at 10000 *g* for 10 min at 4°C, the reaction mixture composed of 0.5 mL of the supernatant, 0.5 mL of trichloromethane ($CHCl_3$), 1.5 mL carbon tetrachloride ($CCl_4$) and 2.5 mL of distilled water. The mixture was then centrifuged at 1000 *g* for 1 min and the supernatant fractions were collected for $H_2O_2$ determination. In addition, $H_2O_2$ was detected with the DAB method with some modifications. Briefly, leaves were placed in the diaminobenzidine (DAB) staining solution. After then, the treated leaves were placed in 95% ethanol for 10 min. The reaction of DAB with $H_2O_2$ could produce the deep brown polymerization product (Yang et al., 2013).

## 2.5 Quantitive real-time PCR assays

In order to investigate the effect of NO on antioxidant system, glycolysis and polyamine pathway during adventitious rooting under Cd stress. The relative expression of genes encoding for antioxidant enzymes, glycolysis pathway and polyamine biosynthetic enzymes were measured. Cucumber explants were ground into powder with liquid nitrogen. Total RNA was extracted using the DP419 kit (TianGen, Beijing, China). Quantitative real-time PCR reactions were performed using SYBR Green SuperReal PreMix Plus kit (TianGen, Beijing, China) according to the cycling parameters: 95°C for 15 min; 95°C for 10 s and 60°C for 32 s, 40 cycles. qRT-PCR amplification primers are shown in Table 1. The relative expression of the gene was calculated by the $2^{-\Delta\Delta CT}$ method.

## 2.6 Statistical analysis

Three independent replicates were set for each experiment. Means were separated by Duncan test at 0.05 probability level. Analysis of variance (ANOVA) was done. SPSS V. 13.0 was used for statistical analysis.

# 3 Results

## 3.1 Effect of exogenous NO on adventitious root formation under Cd stress

To understand the effect of exogenous NO on the development of adventitious root under Cd stress, we performed a dose-response experiment with NO. As shown in Figure 1, compared to CK treatment, $CdCl_2$ treatment significantly reduced root number and root length by 66.3% and 81.7%, respectively. Moreover, the development of adventitious roots altered considerably with increasing concentrations of NO donor, SNP (1, 10, 100, 500 μM). As shown in Figure 1, the root number and root length of 10 μM NO treatment was significantly increased by 127.9% and 289.3%, respectively, as compared to $CdCl_2$ treatments. However, a high concentration of NO (500 μM) obviously decreased the number and length of adventitious roots under Cd stress (Figures 1A, B). Therefore, exogenous NO displayed a concentration-dependent influence on adventitious rooting under Cd stress, and these results

10.3389/fpls.2023.1126606

TABLE 1 Sequences of primers used for this study.

| Gene | Forward Primer | Reverse Primer |
|---|---|---|
| Actin | 5'-TTGAATCCCAAGGCGAATAG-3' | 5'-TGCGACCACTGGCATAAAG-3' |
| *CsPOD* | 5'-TTGTGATGGGTCGGTGCTAC-3' | 5'-TGTCCTGATGCCAAGGTGAC-3' |
| *CsCAT* | 5'- CATGGACGGTTCAGGTGTCA-3' | 5'- CCACTCAGGGTAGTTGCCAG-3' |
| *CsAPX* | 5'-CTGCTACTGTTTTTGGAACCGCCG-3' | 5'- GCGGAGGAGAGGAAACGAGTAGTT-3' |
| *CsSOD* | 5'-CACCCAAGAAGGAGACGGTC-3' | 5'- CAGCAGGGTTGAAATGTGGC-3' |
| *CsGR* | 5'-GATATGAGAGCCGTGGTTGC-3' | 5'-AGTCGCAAACAACACAGCAT-3' |
| *CsPFK* | 5'-TTGGTTGATAATTGGCATAAG-3' | 5'-GCATCCACTATCTTCTTCA-3' |
| *CsPK* | 5'-TGCTGTCATCACCTATTG-3' | 5'-ACAAGAGTCGGTTTACAC-3' |
| *CsFK* | 5'-CCTGGATGAAGAATACTATGA-3' | 5'-CGGCGTGTAATGATAATG-3' |
| *CsHK* | 5'-TGTTGTGGTGAAGTTCTT-3' | 5'-CCTCCATTTCCCTCTATTC-3' |
| *CsADC* | 5'-GGATCCCAGATCCCTTCTAC-3' | 5'-GTCAATACCCAGACCACCTC-3' |
| *CsODC* | 5'-CGTCGTTGGCGTGTCATTT-3' | 5'- CAAGTCGGACTGCCGTTTC-3' |
| *CsPAO* | 5'-TCTCCTTCTCGTTCCTCCGT-3' | 5'-CCACCGACTCCAACAATCCA-3' |

indicated that 10 μM NO significantly ameliorated the adverse effect of Cd stress on the development of adventitious roots.

## 3.2 Effect of cPTIO or tungstate on adventitious root formation under Cd stress

To further investigate the key role of NO in affecting adventitious root formation in cucumber under Cd stress, NO scavengers or inhibitor was utilized in this experiment. As shown in Figure 2, NO treatment obviously induced the adventitious rooting under Cd stress. However, application of cPTIO or tungstate significantly inhibited the NO-promoted adventitious rooting under Cd stress. The number of adventitious roots which treated with NO scavenger or inhibitor decreased by 73% and 67.6%, respectively, when compared to $CdCl_2$ + NO treatment (Figure 2A). Meanwhile, the adventitious root length of explants treated with cPTIO or tungstate reduced by 68.9% and 44.3%, respectively, as compared to that of NO treatment (Figure 2B). These results implied that NO might be responsible for promoting the formation of adventitious root under Cd stress.

## 3.3 Changes in the endogenous NO level during NO-induced adventitious root formation under Cd stress

In order to further validate the influence of NO on adventitious root production under Cd stress, endogenous NO level was detected during NO-induced adventitious rooting under Cd stress condition (Figure 3). The concentration of endogenous NO in $CdCl_2$ treatment gradually decreased during the process of adventitious root development (Figure 3). However, the level of endogenous NO which treated with $CdCl_2$+NO was considerably higher than those in Cd group, reaching a maximum at 48 h. As shown in Figure 3, at 48 h, exogenous NO treatment significantly enhanced endogenous NO level by 65.6% as compared to $CdCl_2$. However, cPTIO and tungstate treatments obviously decreased endogenous NO level during adventitious root development, which was 65.3% and 55.5% lower than that of NO treatment, respectively (Figure 3).

## 3.4 Effect of NO on reactive oxygen species during adventitious root development in cucumber under Cd stress

The levels of MDA, $H_2O_2$ and $O_2^{\cdot-}$ in cucumber explants under Cd stress were measured in our experiment (Figure 4). As shown in Figure 4A, $CdCl_2$ treatment significantly increased MDA content in cucumber explants which compared to that of control. However, exogenous NO significantly decreased MDA level under Cd stress. As compared to Cd stress, the MDA content which treated with NO treatment significantly decreased by 31.4% (Figure 4A). However, cPTIO or tungstate treatment significantly elevated the content of MDA compared to $CdCl_2$ + NO treatment. Also, $CdCl_2$ treatment significantly increased the content of $O_2^{\cdot-}$ in cucumber explants. Exogenous NO could reverse the increase in $O_2^{\cdot-}$ level which caused by Cd stress (Figures 4B, D). As shown in Figure 4B, application of NO obviously decreased the $O_2^{\cdot-}$ level by 39.6% when compared to $CdCl_2$ treatment. However, the content of $O_2^{\cdot-}$ in cucumber explants which treated with cPTIO or tungstate was significantly higher than that of $CdCl_2$ + NO treatment. Furthermore, the effect of NO treatment on $H_2O_2$ level followed the same pattern as the effect on $O_2^{\cdot-}$ level (Figures 4C, E). These results indicated that NO could obviously alleviate membrane lipid peroxidation and inhibit the accumulation of ROS, thus reducing

10.3389/fpls.2023.1126606

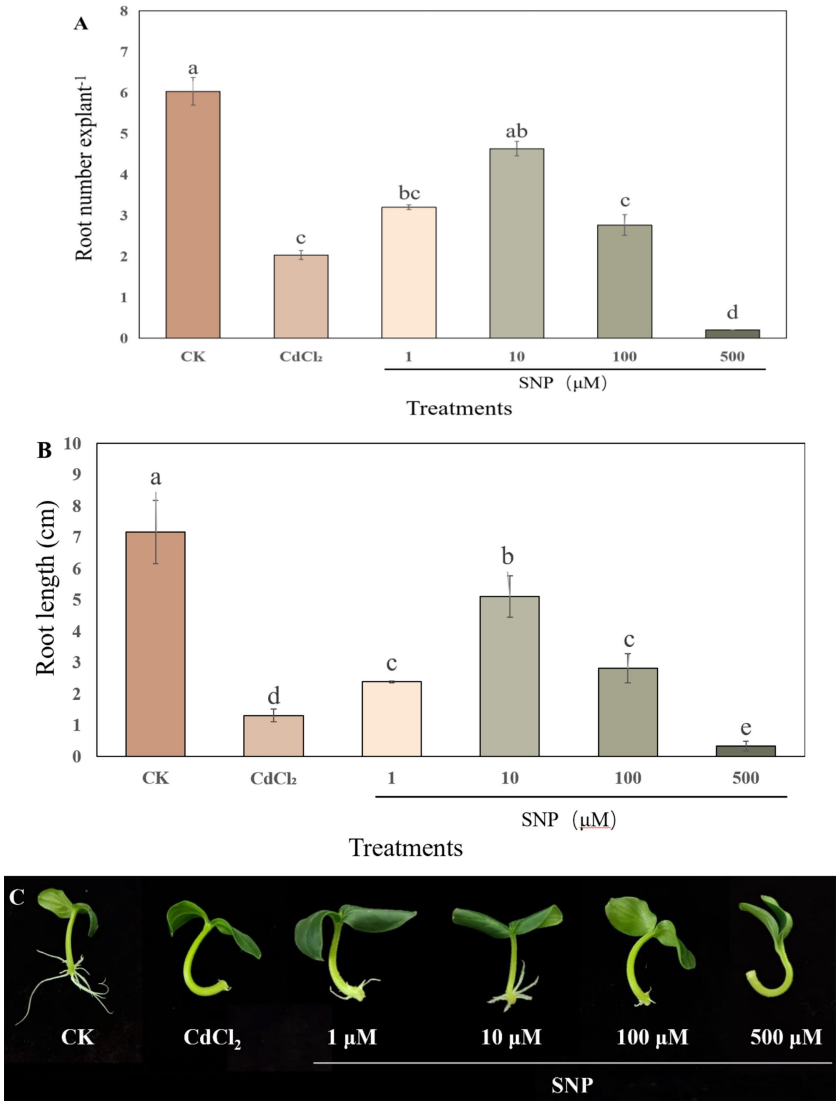


FIGURE 1
Effect of NO on adventitious root formation under Cd stress. The primary roots were removed from 5-day-old seedlings. Explants were then incubated for 5 days with distilled water (CK) or 1 μM $CdCl_2$, 1 μM $CdCl_2$ +1 μM SNP, 1 μM $CdCl_2$ + 10 μM SNP, 1 μM $CdCl_2$ + 100 μM SNP, 1 μM $CdCl_2$ + 500 μM SNP. Ten explants were used per replicate. The numbers **(A)** and root length **(B)** of adventitious roots were expressed as mean ± SE (n = 3). Photographs **(C)** were taken after five days of the treatments indicated. Bars with different letters are significantly different at $P < 0.05$ according to Duncan's multiple range test.

oxidative damage and promoting the formation of adventitious root in cucumber under Cd stress.

## 3.5 Effect of NO on the expression level of antioxidant enzymes under Cd stress

We further explored the effect of NO on the antioxidant system during adventitious root development under Cd stress. As shown in Figure 5, $CdCl_2$ treatment has a significant effect on the expression level of antioxidant enzymes during the process of adventitious root formation. Compared to CK treatment, Cd treatment significantly decreased the expression level of ascorbate peroxidase (*APX*), Cu, Zn-superoxide dismutase (*Cu, Zn-SOD*), glutathione reductase (*GR*) and peroxidase (*POD*) (Figure 5). However, the expression of these genes in NO treatment was significantly higher than that of Cd stress alone (Figure 5). As shown in Figure 5A, exogenous NO significantly increased *APX* relative expression by 90.8% compared with Cd treatment alone. Meanwhile, *Zn/Cu-SOD*, *CAT*, *GR* and *POD* relative expression of $CdCl_2$ + NO treatment was significantly higher 63.3%, 31.0%, 43.0% and 40.9% than those of Cd treatment, respectively (Figure 5). Nevertheless, NO scavengers or inhibitor obviously down-regulated the transcriptional levels of the antioxidant enzymes compared to those of NO treatment under Cd stress (Figure 5). Thus, these results might give an exploration of the positive role of NO in hindering ROS production by regulating the transcriptional levels of antioxidant enzymes.

10.3389/fpls.2023.1126606

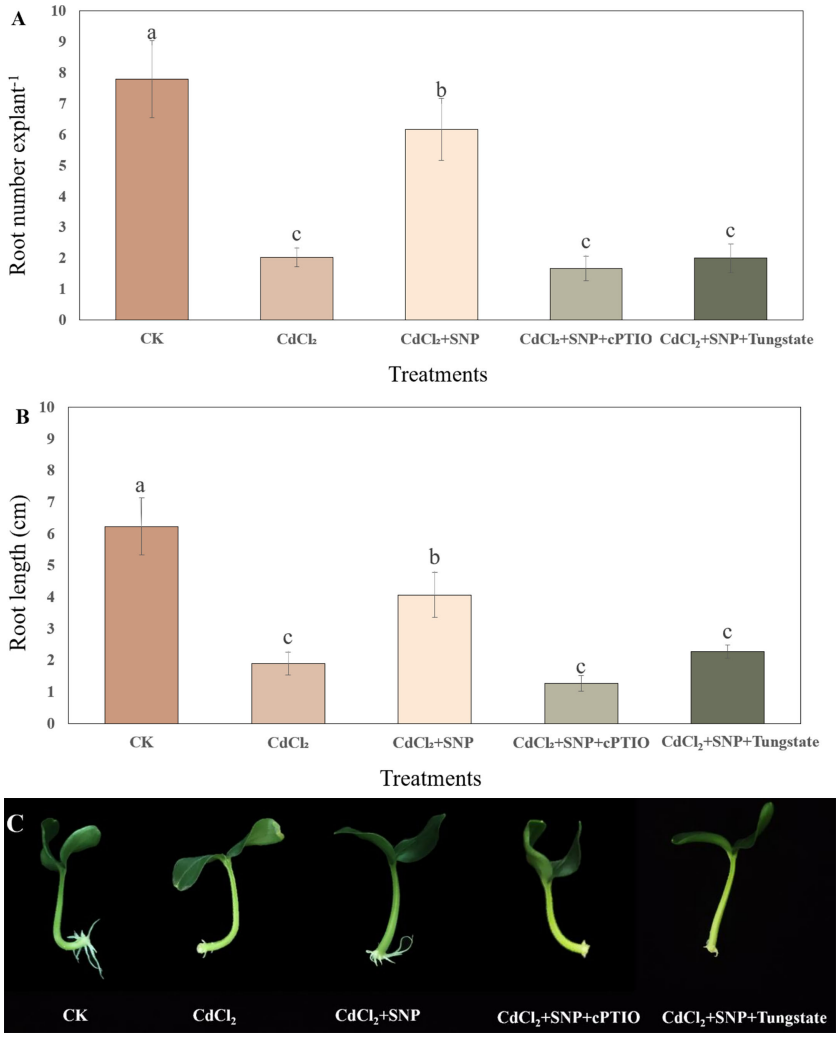


FIGURE 2
Effect of cPTIO or tungstate on adventitious root formation under Cd stress. The primary roots were removed from 5-day-old seedlings. Explants were then incubated for 5 days with distilled water (CK) or 1 μM $CdCl_2$, 1 μM $CdCl_2$ +10 μM SNP, 1 μM $CdCl_2$ + 10 μM SNP + 200 μM cPTIO, 1 μM $CdCl_2$ + 10 μM SNP + 200 μM tungstate. Ten explants were used per replicate. The numbers **(A)** and root length **(B)** of adventitious roots were expressed as mean ± SE (n = 3). Photographs **(C)** were taken after five days of the treatments indicated. Bars with different letters are significantly different at $P < 0.05$ according to Duncan's multiple range test.

## 3.6 Effect of NO on the expression level of glycolysis-related genes under Cd stress

We evaluated the effect of NO on glycolysis pathway during the development of adventitious root in cucumber under Cd stress. As shown in Figure 6, compared with CK treatment, $CdCl_2$ treatment significantly down-regulated the gene expression levels of *FK, PK* and HK. However, compared to those of Cd treatment, exogenous NO significantly enhanced the expression level of glycolysis-related genes. As shown in Figures 6A, B, exogenous NO resulted in a 83.8% increase in *PFK* relative expression and a 87.1% increase in *FK* relative expression compared with Cd treatment alone, respectively. Moreover, Cd treatment decreased *PK* relative expression by 12.4% and caused a 52.7% decrease in *HK* relative expression compared with NO + Cd treatment, respectively (Figures 6C, D). On the contrary, NO scavengers or inhibitor obviously reversed the positive effect of NO on regulating the mRNA transcription level of these genes (Figure 6). Therefore, NO promoted adventitious rooting under Cd stress through regulating glycolysis-related gene expression.

## 3.7 Effect of NO on the expression level of polyamine enzymes under Cd stress

Cd stress significantly decreased the expression level of arginine decarboxylase (ADC) and ornithine decarboxylase (ODC) in our experiment (Figures 7A, B). As shown in Figure 7, compared to $CdCl_2$ treatment, the expression level of *ADC* and *ODC* in $CdCl_2$ + NO treatment were significantly higher than those of $CdCl_2$ treatment alone. Moreover, $CdCl_2$ + NO treatment resulted in a 32.2% decrease in *PAO* relative expression compared with Cd treatment. However, NO scavenger or inhibitor treatment could

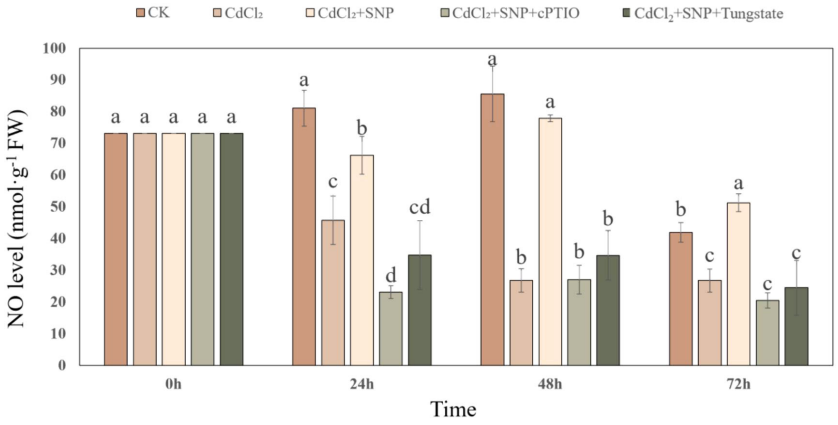


FIGURE 3
Changes in the endogenous NO level during NO-induced adventitious root formation under Cd stress. The primary roots were removed from 5-day-old seedlings. Explants were then incubated for 72 h with distilled water (CK) or 1 μM $CdCl_2$, 1 μM $CdCl_2$ +10 μM SNP, 1 μM $CdCl_2$ + 10 μM SNP + 200 μM cPTIO, 1 μM $CdCl_2$ + 10 μM SNP + 200 μM tungstate. Bars with different letters are significantly different at $P < 0.05$ according to Duncan's multiple range test.

reverse the effect of NO on the expression level of polyamine enzymes (Figure 7). These results imply that application of NO could regulate polyamine homeostasis during adventitious root development in response to Cd stress.

## 4 Discussion

Cadmium stress as an environmental factor has a significant impact on the growth and development of plants. It has been confirmed that Cd stress is an important limiting factor for plant growth and development, which inhibits the growth of plants to a certain extent (Azevedo et al., 2012; El Rasafi et al., 2022). As an important signal molecule in plants, NO is involved in a variety of abiotic stress response in plants. In this experiment, we demonstrated that NO could promote the development of adventitious roots of cucumber under Cd stress. In our study, the root number and root length of adventitious roots under Cd stress condition were significantly lower than those of the control (Figure 1). These results showed that Cd stress could significantly inhibit the process of adventitious root in cucumber explants. Previous studies found that Cd stress inhibited the adventitious root formation in plants (Li et al., 2019; Gong et al., 2022). However, suitable concentration of NO treatment significantly promoted adventitious root formation under Cd stress (Figure 1). Previous studies have shown that NO can resist abiotic stress through protecting cell membrane stability, up-regulating antioxidant enzyme activity and inducing resistance-related gene expression (Fan et al., 2015; Kaya et al., 2015). For example, it has been reported that NO could alleviate Cd toxicity through maintaining the growth regulation and nutritional status in cauliflower (Ma et al., 2022). Also, Zhao et al (2022) found that NO enhanced Cd resistance of *Pleurotus eryngii* through overcoming oxidative damage and regulating short-chain dehydrogenase/reductase famliy. Our results implied that suitable concentration of NO might alleviate the negative effect of Cd stress on the adventitious rooting of cucumber. Moreover, several studies indicated that NO could regulate the growth and development of plant roots, including root elongation, lateral root growth and adventitious root formation (Díaz et al., 2021; Wang et al., 2021; Liu Y.Y. et al., 2022). In our experiment, low concentration of NO significantly alleviated the inhibitory effect of Cd stress on the formation of adventitious root, while high concentration of NO obviously inhibited the occurrence of adventitious root under Cd stress (Figure 1). These results showed that NO had a concentration-dependent effect on adventitious root formation under Cd stress. In addition, NO scavengers or inhibitor dramatically reduced the root number and root length of cucumber explants (Figure 2), implying that NO plays a vital role in the development of adventitious roots under Cd stress.

Several reports suggested that the endogenous NO accumulation has been implicated as being responsible for the development of adventitious root in plants (Kang et al., 2018; Altamura et al., 2023). Compared to CK treatment, Cd stress significantly decreased endogenous NO levels during adventitious root development (Figure 3), implying that Cd stress might lead to a significant reduction of adventitious root formation through inhibiting endogenous NO production. However, exogenous NO significantly increased the endogenous NO production during adventitious root formation under Cd stress (Figure 3). Our results are in agreement with previous data on the implication of NO generation during root growth and development under stress conditions. For example, Zhang et al. (2022) suggested that endogenous NO was required for melatonin to stimulate the lateral roots growth of cucumber seedlings under nitrate stress. Moreover, Li et al., (2019) reported that NO significantly elevated endogenous NO level during the adventitious root formation in mung bean hypocotyl under cadmium and osmotic stresses. These observations support the view that NO could promote the formation of adventitious root through enhancing the endogenous NO production under Cd stress.

10.3389/fpls.2023.1126606

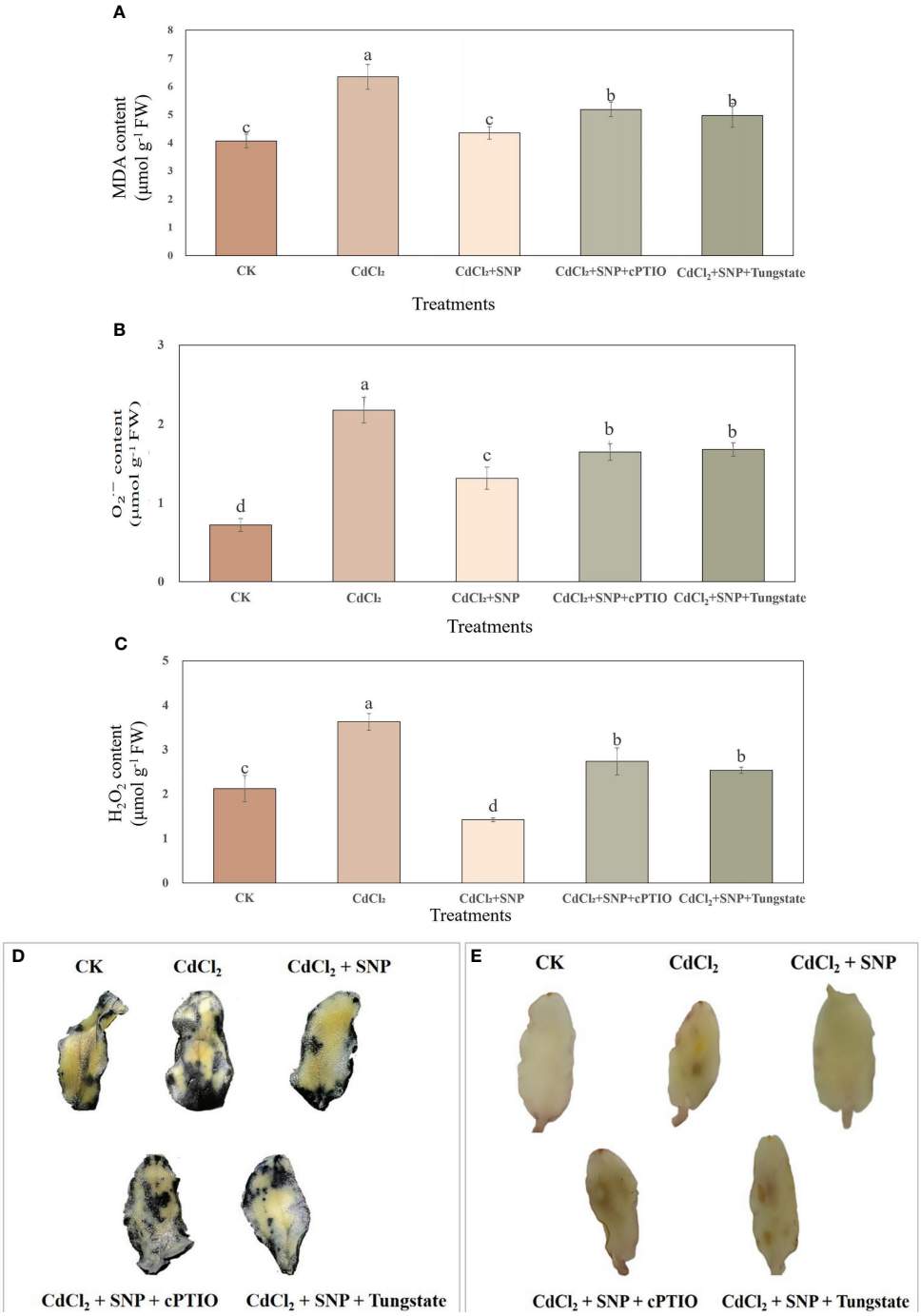


FIGURE 4
Effect of NO on MDA content (**A**), $O_2^{\cdot-}$ content **(B)** and $H_2O_2$ content **(C)** during adventitious root development in cucumber under Cd stress. Explants were incubated for 48 h with distilled water (CK) or 1 μM $CdCl_2$, 1 μM $CdCl_2$ +10 μM SNP, 1 μM $CdCl_2$ + 10 μM SNP + 200 μM cPTIO, 1 μM $CdCl_2$ + 10 μM SNP + 200 μM tungstate. Photograph showing NBT **(D)** and DAB **(E)** staining after 48 h of treatments. Bars with different letters are significantly different at $P < 0.05$ according to Duncan's multiple range test.

Excessive ROS results in membrane lipid peroxidation and cell oxidation, causing serious damage to plants (Huang et al., 2019). Meanwhile, MDA level is considered to be an indicator of lipid peroxidation during response to various environmental stresses (Gaweł et al., 2004). Previous study has suggested that Cd treatment caused oxidative stress (He et al., 2014) by increasing the contents of $H_2O_2$ and MDA of rice seedlings. Moreover, under Cd stress, $H_2O_2$ and MDA in wheat plants significantly increased (Kaya et al., 2019). Similarly, in our study, the results showed that $CdCl_2$ treatment significantly increased the ROS level and MDA content of cucumber explants during adventitious root formation (Figure 4), resulting in oxidative damage (Jaleel et al., 2007), eventually inhibiting adventitious root formation. However, exogenous NO significantly decreased the levels of MDA, $H_2O_2$

10.3389/fpls.2023.1126606

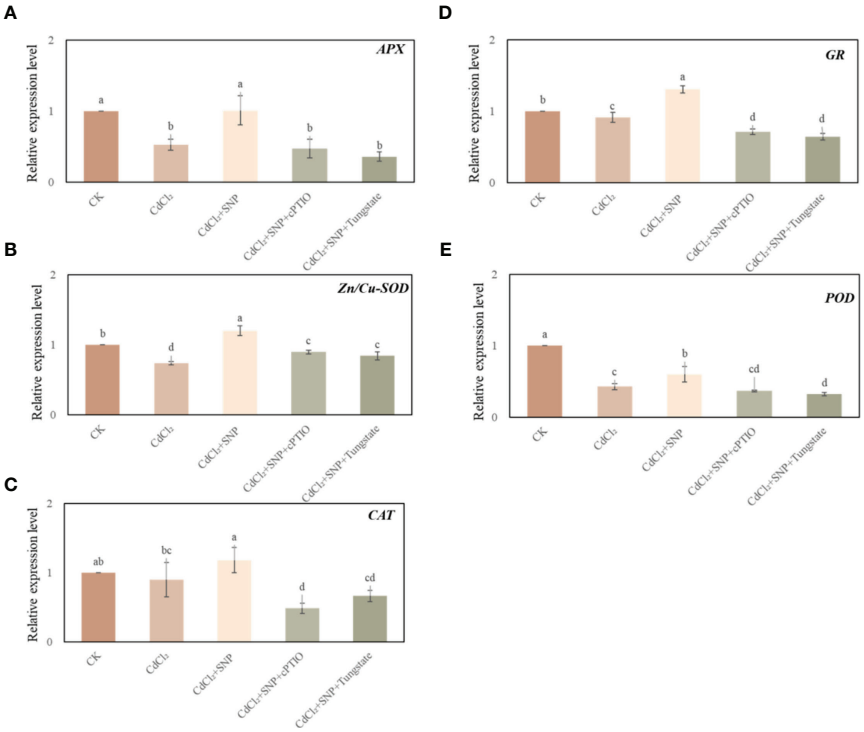


FIGURE 5
Effect of NO on the expression level of *APX* (**A**), *Zn/Cu-SOD* (**B**), *CAT* (**C**), GR (**D**) and *POD* (**E**) in cucumber explants under Cd stress at 48 (h) Explants were incubated for 2 days with distilled water (CK) or 1 μM $CdCl_2$, 1 μM $CdCl_2$ +10 μM SNP, 1 μM $CdCl_2$ + 10 μM SNP + 200 μM cPTIO, 1 μM $CdCl_2$ + 10 μM SNP + 200 μM Tungstate. The values (means ± SE) are the average of three independent experiments. Bars with different letters are significantly different at $P < 0.05$ according to Duncan's multiple range test.

and $O_2^{\cdot-}$ in cucumber explants to further alleviate the oxidative damage and membrane lipid peroxidation of cucumber explants under Cd stress (Laspina et al., 2005; Jaleel et al., 2007). Previous studies have shown that NO plays a key role in alleviating oxidative stress under Cd stress (Panda et al., 2011; Kaya et al., 2020). For instance, exogenously applied NO significantly reduced oxidative stress and proline content of wheat seedlings under Cd stress (Kaya et al., 2020). Similar to our results, application of NO resulted in an

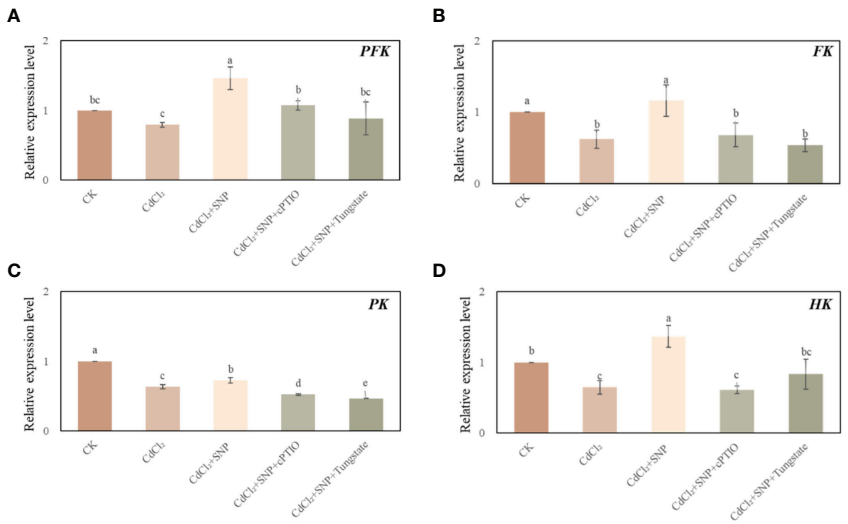


FIGURE 6
Effect of NO on the expression level of *PFK* (**A**), *FK* (**B**), *PK* (**C**) and *HK* (**D**) in cucumber explants under Cd stress at 48 (h) Explants were incubated for 2 days with distilled water (CK) or 1 μM $CdCl_2$, 1 μM $CdCl_2$ +10 μM SNP, 1 μM $CdCl_2$ + 10 μM SNP + 200 μM cPTIO, 1 μM $CdCl_2$ + 10 μM SNP + 200 μM Tungstate. The values (means ± SE) are the average of three independent experiments. Bars with different letters are significantly different at $P < 0.05$ according to Duncan's multiple range test.

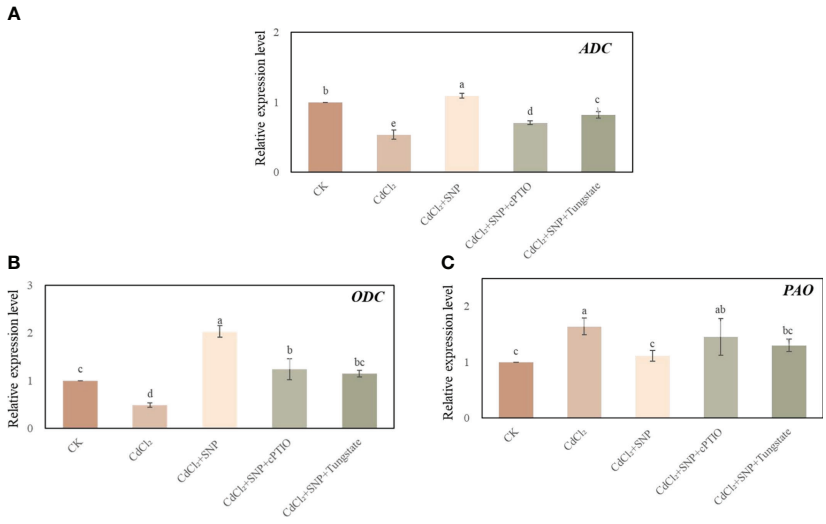


FIGURE 7
Effect of NO on the expression level of *ADC* (**A**), *ODC* **(B)** and *PAO* (**C**) in cucumber explants under Cd stress at 48 (h) Explants were incubated for 2 days with distilled water (CK) or 1 μM $CdCl_2$, 1 μM $CdCl_2$ +10 μM SNP, 1 μM $CdCl_2$ + 10 μM SNP + 200 μM cPTIO, 1 μM $CdCl_2$ + 10 μM SNP + 200 μM Tungstate. The values (means ± SE) are the average of three independent experiments. Bars with different letters are significantly different at $P < 0.05$ according to Duncan's multiple range test.

obviously decrease of $O_2^{\cdot-}$, $H_2O_2$ and MDA content to decrease the Cd stress of cauliflower (Ma et al., 2022). These results suggested that NO is involved in ameliorating oxidative impairment under Cd stress. However, the treatment of NO scavengers or inhibitor significantly reversed the positive effect of NO on alleviating the oxidative damage during adventitious root formation under Cd stress (Figure 4). These results indicated that NO could significantly reduce the degree of membrane lipid peroxidation and alleviate oxidative stress under Cd stress, thus promoting the occurrence of adventitious roots under Cd stress.

Overproduction of ROS caused oxidative damage, plants need to counteract the toxicity of ROS through a highly efficient antioxidative defense system (Dumanović et al., 2021). At present, plants have effective antioxidant defense mechanisms to alleviate the effects of oxidative stress in plants. Xu et al. (Xu et al., 2008) found that transgenic *Arabidopsis* plants structurally overexpressed peroxisome gene *HvAPX1*, which reduced ROS accumulation and significantly improved the tolerance of *Arabidopsis* plants to Cd stress. In addition, Cd stress mediates the transcriptional expression of *APX*, *GR*, *Cu/ZnSOD* and other related antioxidant enzyme genes in ryegrass, which effectively alleviates the oxidative damage (Luo et al., 2011). Our results showed that Cd stress significantly affected the expression level of antioxidant enzyme genes (Figure 5). Moreover, compared to Cd treatment, exogenous NO significantly up-regulated the gene expression levels of these antioxidant enzymes, indicating that NO could alleviate oxidative damage of cucumber explants through enhancing the antioxidant system as well as eliminating excess ROS and MDA (Mostofa et al., 2019; Terrón-Camero et al., 2019). It has been investigated that NO significantly increased the activities of antioxidant enzymes of wheat under Cd stress (Kaya et al., 2019). Moreover, NO have the ability to enhance the antioxidant activities in bamboo plants under Cd stress (Emamverdian et al., 2021). Our present investigation suggested that NO could obviously enhance the plant defense system during adventitious rooting in the response to Cd stress.

The glycolysis process is the basis for controlling carbohydrate metabolism, which also considered to be one of the key pathways for plant respiration (Plaxton, 1996; Sun et al., 2021). In addition, glycolysis has been demonstrated to be involved in the plant response to abiotic stress (Zhang et al., 2011a; Dong et al., 2020; Sun et al., 2021). For example, it has been reported that the increase of PFK and PK activity could enhance the tolerance to salt stress (Zhong et al., 2016). Moreover, the enhancement of the expression level of *PFK*, *PK* and *PEPC* of cucumber leaves allows to convert more carbohydrates and maintain the normal physiological metabolism of cucumber (Zhong et al., 2016). Previous study found that Cd stress caused changes in carbohydrate metabolism, glycolysis and pentose phosphate pathway-related enzymes in pea (Devi et al., 2007). Moreover, Shahid et al (2019) found that Cd treatment significantly inhibited the activities of FK, HK, PFK and PK in potato plants. In our study, we found that Cd stress significantly down-regulated the gene expression levels of key glycolysis enzymes during adventitious root formation (Figure 6), indicating that Cd stress may lead to the inhibition of glycolysis pathway and further affect respiratory pathway during the adventitious rooting. However, under Cd stress, NO treatment could significantly up-regulate the gene expression levels of *PFK*, *PK*, *FK* and *HK* (Figure 6). In agreement with the present study, NO could obviously elevate the activities of FK to improve the chilling tolerance of banana fruit (Wang et al., 2015). Similarly, Pandey et al (2019) found that NO treatment may up-regulated the expressional level of *HK1-like*, *phosphofructokinase 6-like* and *PK* which involved in glycolysis pathway during seed germination of chickpea. Furthermore, previous study suggested exogenous nitric oxide improved NaCl tolerance by enhancing glycolysis metabolism in barley seedlings (Ma et al., 2021). These results implied that NO

plays an essential role in regulating glycolysis metabolism in plant. In the present study, NO may trigger glycolysis metabolic pathway through increasing the gene expression levels of key glycolysis enzymes to produce more energy and activate intermediate metabolism during the process of adventitious root formation under Cd stress, in order to enhance resistance to Cd stress (Shu et al., 2011).

Previous studies found that polyamines (PAs) play an essential role in plant growth and development, as well as response to biotic and abiotic stress (Wimalasekera et al., 2011; Rakesh et al., 2021). In plants, it has been reported that PAs could be produced by ornithine decarboxylase (ODC) or arginine decarboxylase (ADC) pathway, respectively (Groppa and Benavides, 2008). Meanwhile, polyamine oxidase (PAO) plays a major role in mediating PAs degradation in plant (Goyal and Asthir, 2010). In our study, the gene expression of *ADC* and *ODC* was significantly down-regulated in $CdCl_2$ treatment, as compared to CK (Figures 7A, B). However, exogenous NO obviously enhanced the gene expression of *ADC* and *ODC* which compared with Cd stress, resulting in the accumulation of endogenous polyamine. In addition, removing endogenous NO further implied that NO is involved in PAs accumulation through increasing the expression of *ADC* and *ODC* (Figures 7A, B) under Cd stress. Previous studies indicated that PAs metabolism plays a vital role in abiotic stress responses (Gupta et al., 2013). Also, it has been reported that NO could obviously regulate the transcriptional level of polyamine metabolism genes of *Medicago truncatula* (Filippou et al., 2013). Moreover, exogenous NO resulted in cold tolerance by regulating the expression level of *ADC* and *ODC* of tea root (Wang et al., 2020). Furthermore, application of NO could significantly increase the expression of PA biosynthetic enzyme and lower the activity of PAO activity under salt stress (Tailor et al., 2019). In our study, Cd stress remarkably enhanced the expression of *PAO* while a significant decline in *PAO* expression was observed in NO treatment (Figure 7C) which may help maintaining PAs levels. These results suggested that NO might enhance abiotic stress tolerance through regulating PAs metabolim. Thus, during adventitious root development under Cd stress, exogenous NO might positively modulate PAs homeostasis through regulating polyamines - related genes expression for adapting to Cd stress condition.

## Conclusion

Exogenous application of NO alleviated Cd damage and promoted the adventitious rooting in cucumber explants under Cd stress. Through further studies, our results suggested that NO could reduce oxidative damage and depress lipid peroxidation through improving the antioxidant capacity of cucumber during adventitious root formation in response to Cd stress. Additionally, NO alleviated the damage of Cd stress on the process of adventitious rooting through regulating glycolysis processes and polyamine homeostasis. Therefore, our study may provide new insights into the positive role of NO in promoting adventitious root development under Cd stress. Taken together, our study provided evidence that NO promoted the adventitious root development under Cd stress in cucumber explants through enhancing antioxidant capability, promoting glycolysis pathway and maintaining polyamine homeostasis. However, the regulatory mechanism underlying NO-induced adventitious root development under Cd stress is complex. Further research should focus on the molecular mechanism of NO-regulated rooting response under Cd stress.

## Data availability statement

The original contributions presented in the study are included in the article/Supplementary Material. Further inquiries can be directed to the corresponding author.

## Author contributions

JY designed the experiments. LN and JY performed the experiments. LN, DW and QC performed data analysis. LN wrote the manuscript. YT, BZ and ZH edited the manuscript. All authors contributed to the article and approved the submitted version.

## Funding

This work was supported by Doctoral Scientific Fund Project of Southwest University of Science and Technology (20zx7135) and Doctoral Scientific Fund Project of Southwest University of Science and Technology (20zx7132).

## Conflict of interest

The authors declare that the research was conducted in the absence of any commercial or financial relationships that could be construed as a potential conflict of interest. The handling editor WL declared a past co-authorship with the author LN.

## Publisher's note

# References


Ahmad, P., Abd Allah, E. F., Hashem, A., Sarwat, M., and Gucel, S. (2016a). Exogenous application of selenium mitigates cadmium toxicity in *Brassica juncea* l. (Czern & cross) by up-regulating antioxidative system and secondary metabolites. *J. Plant Growth Regul.* 35, 936–950. doi: 10.1007/s00344-016-9592-3

Ahmad, P., Abdel Latef, A. A., Abd Allah, E. F., Hashem, A., Sarwat, M., Anjum, N. A., et al. (2016b). Calcium and potassium supplementation enhanced growth, osmolyte secondary metabolite production, and enzymatic antioxidant machinery in cadmium-exposed chickpea (*Cicer arietinum* l.). *Front. Plant Sci.* 7. doi: 10.3389/fpls.2016.00513

Altamura, M. M., Piacentini, D., Rovere, F. D., Fattorini, L., Falasca, G., and Betti, C. (2023). New paradigms in brassinosteroids, strigolactones, sphingolipids, and nitric oxide interaction in the control of lateral and adventitious root formation. *Plants* 12, 413. doi: 10.3390/plants12020413

An, Y. J., Kim, Y. M., Kwon, T. I., and Jeong, S. W. (2004). Combined effect of copper, cadmium, and lead upon cucumis sativus growth and bioaccumulation. *Sci. Total Environ.* 326, 85–93. doi: 10.1016/j.scitotenv.2004.01.002

Anwar, S., Shafiq, F., Nisa, Z. U., Usman, U., Ashraf, M. Y., and Ali, N. (2021). Effect of cadmium stress on seed germination, plant growth and hydrolyzing enzymes activities in mungbean seedlings. *J. Seed Sci.* 43, e202143042. doi: 10.1590/2317-1545v43256006

Azevedo, R. A., Gratão, P. L., Monteiro, C. C., and Carvalho, R. F. (2012). What is new in the research on cadmium-induced stress in plants? *Food Energy Secur.* 1, 133–140. doi: 10.1002/fes3.10

Chen, F., Wang, F., Sun, H. Y., Cai, Y., Mao, W. H., Zhang, G. P., et al. (2010). Genotype-dependent effect of exogenous nitric oxide on cd-induced changes in antioxidative metabolism, ultrastructure, and photosynthetic performance in barley seedlings (*Hordeum vulgare*). *J. Plant Growth Regul.* 29, 394–408. doi: 10.1007/s00344-010-9151-2

Devi, R., Munjral, N., Gupta, A. K., and Kaur, N. (2007). Cadmium induced changes in carbohydrate status and enzymes of carbohydrate metabolism, glycolysis and pentose phosphate pathway in pea. *Environ. Exp. Bot.* 61, 167–174. doi: 10.1016/j.envexpbot.2007.05.006

Díaz, A. S., da Cunha Cruz, Y., Duarte, V. P., de Castro, E. M., Magalhães, P. C., and Pereira, F. J. (2021). The role of reactive oxygen species and nitric oxide in the formation of root cortical aerenchyma under cadmium contamination. *Physiol. Plantarum* 173, 2323–2333. doi: 10.1111/ppl.13582

Dong, W. K., Ma, X., Jiang, H. Y., Zhao, C. X., and Ma, H. L. (2020). Physiological and transcriptome analysis of poa pratensis var. anceps cv. qinghai in response to cold stress. *BMC Plant Biol.* 20, 1–18. doi: 10.1186/s12870-020-02559-1

Dumanović, J., Nepovimova, E., Natić, M., Kuča, K., and Jaćević, V. (2021). The significance of reactive oxygen species and antioxidant defense system in plants: A concise overview. *Front. Plant Sci.* 11. doi: 10.3389/fpls.2020.552969

El Rasafi, T., Oukarroum, A., Haddioui, A., Song, H., Kwon, E. E., Bolan, N., et al. (2022). Cadmium stress in plants: A critical review of the effects, mechanisms, and tolerance strategies. *Crit. Rev. Env. Sci. Tec.* 52, 675–726. doi: 10.1080/10643389.2020.1835435

Emamverdian, A., Ding, Y. L., Barker, J., Mokhberdoran, F., Ramakrishnan, M., Liu, G. H., et al. (2021). Nitric oxide ameliorates plant metal toxicity by increasing antioxidant capacity and reducing Pb and cd translocation. *Antioxidants* 10, 1981. doi: 10.3390/antiox10121981

Falco, G., Bocio, A., Llobet, J. M., and Domingo, J. L. (2005). Health risks of dietary intake of environmental pollutants by elite sportsmen and sportswomen. *Food Chem. Toxicol.* 43, 1713–1721. doi: 10.1016/j.fct.2005.05.014

Fan, J. B., Chen, K., Amombo, E., Hu, Z. R., Chen, L., and Fu, J. M. (2015). Physiological and molecular mechanism of nitric oxide (NO) involved in *bermudagrass* response to cold stress. *PloS One* 10, e0132991. doi: 10.1371/journal.pone.0132991

Filippou, P., Antoniou, C., and Fotopoulos, V. (2013). The nitric oxide donor sodium nitroprusside regulates polyamine and proline metabolism in leaves of *Medicago truncatula* plants. *Free Radical Bio. Med.* 56, 172–183. doi: 10.1016/j.freeradbiomed.2012.09.037

Gan, L. P., Wu, X. L., and Zhong, Y. (2015). Exogenously applied nitric oxide enhances the drought tolerance in hulless barley. *Plant Prod. Sci.* 18, 52–56. doi: 10.1626/pps.18.52

Gao, Z. Q., Zhang, J. Y., Zhang, J., Zhang, W. X., Zheng, L. L., Borjigin, T., et al. (2022). Nitric oxide alleviates salt-induced stress damage by regulating the ascorbate-glutathione cycle and $Na^+/K^+$ homeostasis in *Nitraria tangutorum* bobr. *Plant Physiol. Bioch.* 173, 46–58. doi: 10.1016/j.plaphy.2022.01.017

Gaweł, S., Wardas, M., Niedworok, E., and Wardas, P. (2004). Malondialdehyde (MDA) as a lipid peroxidation marker. *Wiadomosci Lekarskie* 57, 453–455.

Gill, S. S., and Tuteja, N. (2010). Reactive oxygen species and antioxidant machinery in abiotic stress tolerance in crop plants. *Plant Physiol. Bioch.* 48 (12), 909–930. doi: 10.1016/j.plaphy.2014.08.004

Gong, B., Miao, L., Kong, W. J., Bai, J. G., Wang, X. F., Wei, M., et al. (2014). Nitric oxide, as a downstream signal, plays vital role in auxin induced cucumber tolerance to sodic alkaline stress. *Plant Physiol. Bioch.* 83, 258–266. doi: 10.1016/j.plaphy.2014.08.004

Gong, W. T., Niu, L. J., Wang, C. L., Wei, L. J., Pan, Y., and Liao, W. B. (2022). Hydrogen peroxide is involved in salicylic acid-induced adventitious rooting in cucumber under cadmium stress. *J. Plant Biol.* 65, 43–52. doi: 10.1007/s12374-021-09332-3

Goyal, M., and Asthir, B. (2010). Polyamine catabolism influences antioxidative defense mechanism in shoots and roots of five wheat genotypes under high temperature stress. *Plant Growth Regul.* 60, 13–25. doi: 10.1007/s10725-009-9414-8

Groppa, M. D., and Benavides, M. P. (2008). Polyamines and abiotic stress: recent advances. *Amino Acids* 34, 35–45. doi: 10.1007/s00726-007-0501-8

Guo, J. J., Qin, S. Y., Rengel, Z., Gao, W., Nie, Z. J., Liu, H. G., et al. (2019). Cadmium stress increases antioxidant enzyme activities and decreases endogenous hormone concentrations more in cd-tolerant than cd-sensitive wheat varieties. *Ecotox. Environ. safe.* 172, 380–387. doi: 10.1016/j.ecoenv.2019.01.069

Gupta, K., Dey, A., and Gupta, B. (2013). Plant polyamines in abiotic stress responses. *Acta Physiol. Plant* 35, 2015–2036. doi: 10.1007/s11738-013-1239-4

Gzyl, J., Chmielowska-Bąk, J., Przymusiński, R., and Gwóźdź, E. A. (2015). Cadmium affects microtubule organization and post-translational modifications of tubulin in seedlings of soybean (*Glycine max* l.). *Front. Plant Sci.* 6. doi: 10.3389/fpls.2015.00937

Hafsi, C., Collado-Arenal, A. M., Wang, H., Sanz-Fernández, M., Sahrawy, M., Shabala, S., et al. (2022). The role of NADPH oxidases in regulating leaf gas exchange and ion homeostasis in arabidopsis plants under cadmium stress. *J. Hazard. Mater.* 429, 128217. doi: 10.1016/j.jhazmat.2022.128217

Hashem, A., Alqarawi, A. A., Radhakrishnan, R., Al-Arjani, A. B. F., Aldehaish, H. A., Egamberdieva, D., et al. (2018). Arbuscular mycorrhizal fungi regulate the oxidative system, hormones and ionic equilibrium to trigger salt stress tolerance in *Cucumis sativus* l. *Saudi J. Biol. Sci.* 25, 1102–1114. doi: 10.1016/j.sjbs.2018.03.009

He, J. Y., Ren, Y. F., Chen, X. L., Chen, H., et al. (2014). Protective roles of nitric oxide on seed germination and seedling growth of rice (Oryza sativa L.) under cadmium stress. *Ecotox. Environ. Safe.* 108, 114–119. doi: 10.1016/j.ecoenv.2014.05.021

Heyno, E., Klose, C., and Krieger-Liszkay, A. (2008). Origin of cadmium-induced reactive oxygen species production: mitochondrial electron transfer versus plasma membrane NADPH oxidase. *New Phytol.* 179, 687–699. doi: 10.1111/j.1469-8137.2008.02512.x

Huang, H. L., Ullah, F., Zhou, D. X., Yi, M., and Zhao, Y. (2019). Mechanisms of ROS regulation of plant development and stress responses. *Front. Plant Sci.* 10. doi: 10.3389/fpls.2019.00800

Irfan, M., Ahmad, A., and Hayat, S. (2014). Effect of cadmium on the growth and antioxidant enzymes in two varieties of brassica juncea. *Saudi J. Biol. Sci.* 21, 125–131. doi: 10.1016/j.sjbs.2013.08.001

Jaleel, C. A., Manivannan, P., Sankar, B., Kishorekumar, A., Gopi, R., Somasundaram, R., et al. (2007). Water deficit stress mitigation by calcium chloride in catharanthus roseus: Effects on oxidative stress, proline metabolism and indole alkaloid accumulation. *Colloids Surfaces B: Biointerfaces* 60, 110–116. doi: 10.1016/j.colsurfb.2007.06.006

Kang, W., Wang, L. Y., Li, R., Zhang, C. C., Wu, L. Y., Li, H. L., et al. (2018). Endogenous nitric oxide and hydrogen peroxide detection in indole-3-butyric acid-induced adventitious root formation in *Camellia sinensis*. *J. Integr. Agric.* 17, 2273–2280. doi: 10.1016/S2095-3119(18)62059-3

Kaya, C., Ashraf, M., Alyemeni, M. N., and Ahmad, P. (2020). Responses of nitric oxide and hydrogen sulfide in regulating oxidative defence system in wheat plants grown under cadmium stress. *Physiol. Plantarum* 168, 345–360. doi: 10.1111/ppl.13012

Kaya, C., Ashraf, M., Sönmez, O., Tuna, A. L., and Aydemir, S. (2015). Exogenously applied nitric oxide confers tolerance to salinity-induced oxidativestress in two maize (*Zea mays* l.) cultivars differing in salinity tolerance. *Turk. J. Agric. For.* 39, 909–919. doi: 10.3906/tar-1411-26

Kaya, C., Okant, M., Ugurlar, F., Alyemeni, M. N., Ashraf, M., and Ahmad, P. (2019). Melatonin-mediated nitric oxide improves tolerance to cadmium toxicity by reducing oxidative stress in wheat plants. *Chemosphere* 225, 627–638. doi: 10.1016/j.chemosphere.2019.03.026

Kohli, S. K., Khanna, K., Bhardwaj, R., Abd Allah, E. F., Ahmad, P. , and Corpas, F. J. (2019). Assessment of subcellular ROS and NO metabolism in higher plants: multifunctional signaling molecules. *Antioxidants* 8, 641. doi: 10.3390/antiox8120641

Kucerova, D., Labancova, E., Vivodova, Z., and Kollarova, K. (2020). The modulation of ion homeostasis by silicon in cadmium treated poplar callus cells. *Environ. Sci. pollut. R.* 27, 2857–2867. doi: 10.1007/s11356-019-07054-1

Laspina, N. V., Groppa, M. D., Tomaro, M. L., and Benavides, M. P. (2005). Nitric oxide protects sunflower leaves against cd-induced oxidative stress. *Plant Sci.* 169, 323–330. doi: 10.1016/j.plantsci.2005.02.007

Li, B. B., Fu, Y. S., Li, X. X., Yin, H. N., and Xi, Z. M. (2022). Brassinosteroids alleviate cadmium phytotoxicity by minimizing oxidative stress in grape seedlings: Toward regulating the ascorbate-glutathione cycle. *Sci. Hortic.* 299, 111002. doi: 10.1016/j.scienta.2022.111002

Li, S. W., Li, Y., Leng, Y., Zeng, X. Y., and Ma, Y. H. (2019). Nitric oxide donor improves adventitious rooting in mung bean hypocotyl cuttings exposed to cadmium and osmotic stresses. *Environ. Exp. Bot.* 164, 114–123. doi: 10.1016/j.envexpbot.2019.05.004

Liao, W. B., Huang, G. B., Yu, J. H., Zhang, M. L., and Shi, X. L. (2011). Nitric oxide and hydrogen peroxide are involved in indole-3-butyric acid-induced adventitious root development in marigold. *J. Hortic. Sci. Biotech.* 86, 159–165. doi: 10.1080/14620316.2011.11512742

Liu, H. W., Wang, C. L., Li, C. X., Zhao, Z. X., Wei, L. J., Liu, Z. Y., et al. (2022a). Nitric oxide is involved in hydrogen sulfide-induced adventitious rooting in tomato (*Solanum lycopersicum*). *Funct. Plant Biol.* 49, 245–258. doi: 10.1071/FP21288

Liu, Y. Y., Wei, L. J., Feng, L., Zhang, M. L., Hu, D. L., Tie, J. Z., et al. (2022b). Hydrogen sulfide promotes adventitious root development in cucumber under salt stress by enhancing antioxidant ability. *Plants* 11, 935. doi: 10.3390/plants11070935

Luo, H. J., Li, H. Y., Zhang, X. Z., and Fu, J. M. (2011). Antioxidant responses and gene expression in perennial ryegrass (*Lolium perenne* l.) under cadmium stress. *Ecotoxicology* 20, 770–778. doi: 10.1007/s10646-011-0628-y

Møller, I. M., Jensen, P. E., and Hansson, A. (2007). Oxidative modifications to cellular components in plants. *Annu. Rev. Plant Biol.* 58, 459–481. doi: 10.1146/annurev.arplant.58.032806.103946

Ma, J., Saleem, M. H., Alsafran, M., Jabri, H. A., Mehwish,, Rizwan, M., et al. (2022). Response of cauliflower (*Brassica oleracea* l.) to nitric oxide application under cadmium stress. *Ecotox. Environ. Safe.* 243, 113969. doi: 10.1016/j.ecoenv.2022.113969

Ma, Y., Yao, Y., Wang, Q. E., Gu, Z. X., Wang, P., Han, Y. B., et al. (2021). Mechanism of nitric oxide enhancing NaCl tolerance of barley seedlings based on physiol-biochemical analysis and LC-MS metabolomics. *Environ. Exp. Bot.* 189, 104533. doi: 10.1016/j.envexpbot.2021.104533

Manara, A., Fasani, E., Molesini, B., DalCorso, G., Pennisi, F., Pandolfini, T., et al. (2020). The tomato metallocarboxypeptidase inhibitor I, which interacts with a heavy metal-associated isoprenylated protein, is implicated in plant response to cadmium. *Molecules* 25, 700. doi: 10.3390/molecules25030700

Mansoor, S., Wani, O. A., Lone, J. K., Manhas, S., Kour, N., Alam, P., et al. (2022). Reactive oxygen species in plants: from source to sink. *Antioxidants* 11, 225. doi: 10.3390/antiox11020225

Mostofa, M. G., Rahman, M. M., Ansary, M. M. U., Fujita, M., and Tran, L. S. P. (2019). Interactive effects of salicylic acid and nitric oxide in enhancing rice tolerance to cadmium stress. *Int. J. Mol. Sci.* 20, 5798. doi: 10.3390/ijms20225798

Muhammad, T., Zhang, J., Ma, Y., Li, Y., Zhang, F., Zhang, Y., et al. (2019). Overexpression of a mitogen-activated protein kinase *SlMAPK3* positively regulates tomato tolerance to cadmium and drought stress. *Molecules* 24, 556. doi: 10.3390/molecules24030556

Niu, L. J., Yu, J. H., Liao, W. B., Xie, J. M., Yu, J., Lv, J., et al. (2019). Proteomic investigation of s-nitrosylated proteins during NO-induced adventitious rooting of cucumber. *Int. J. Mol. Sci.* 20, 5363. doi: 10.3390/ijms20215363

Niu, L. J., Yu, J. H., Liao, W. B., Yu, J. H., Zhang, M. L., and Dawuda, M. M. (2017). Calcium and calmodulin are involved in nitric oxide-induced adventitious rooting of cucumber under simulated osmotic stress. *Front. Plant Sci.* 8. doi: 10.3389/fpls.2017.01684

Pagnussat, G. C., Simontacchi, M., Puntarulo, S., and Lamattina, L. (2002). Nitric oxide is required for root organogenesis. *Plant Physiol.* 129, 954–956. doi: 10.1104/pp.004036

Panda, P., Nath, S., Chanu, T. T., Sharma, G. D., and Panda, S. K. (2011). Cadmium stress-induced oxidative stress and role of nitric oxide in rice (*Oryza sativa* l.). *Acta Physiol. Plant* 33, 1737–1747. doi: 10.1007/s11738-011-0710-3

Pandey, S., Kumari, A., Shree, M., Kumar, V., Singh, P., Bharadwaj, C., et al. (2019). Nitric oxide accelerates germination *via* the regulation of respiration in chickpea. *J. Exp. Bot.* 70, 4539–4555. doi: 10.1093/jxb/erz185

Panyuta, O., Belava, V., Fomaidi, S., Kalinichenko, O., Volkogon, M., and Taran, N. (2016). The effect of pre-sowing seed treatment with metal nanoparticles on the formation of the defensive reaction of wheat seedlings infected with the eyespot causal agent. *Nanoscale Res. Lett.* 11, 1–5. doi: 10.1186/s11671-016-1305-0

Parankusam, S., Adimulam, S. S., Bhatnagar-Mathur, P., and Sharma, K. K. (2017). Nitric oxide (NO) in plant heat stress tolerance: current knowledge and perspectives. *Front. Plant Sci.* 8. doi: 10.3389/fpls.2017.01582

Plaxton, W. C. (1996). The organization and regulation of plant glycolysis. *Annu. Rev. Plant Biol.* 47, 185–214. doi: 10.1146/annurev.arplant.47.1.185

Polle, A., and Schützendübel, A. (2003). "Heavy metal signalling in plants: linking cellular and organismic responses," in *Plant responses to abiotic stress*. Eds. H. Hirt and K. Shinozaki (Berlin, Heidelberg: Springer Press), 187–215. doi: 10.1007/978-3-540-39402-0_8

Prado, A. M., Porterfield, D. M., and Feijó, J. A. (2004). Nitric oxide is involved in growth regulation and re-orientation of pollen tubes. *Development* 131, 2707–2714. doi: 10.1242/dev.01153

Qi, W. Y., Li, Q., Chen, H., Liu, J., Xing, S. F., Xu, M., et al. (2021). Selenium nanoparticles ameliorate *Brassica napus* l. cadmium toxicity by inhibiting the respiratory burst and scavenging reactive oxygen species. *J. Hazard. Mater.* 417, 125900. doi: 10.1016/j.jhazmat.2021.125900

Rakesh, B., Sudheer, W. N., and Nagella, P. (2021). Role of polyamines in plant tissue culture: An overview. *Plant Cell Tiss. Org.* 145, 487–506. doi: 10.1007/s11240-021-02029-y

Ren, Y. F., Wang, W., He, J. Y., Zhang, L. Y., Wei, Y. J., and Yang, M. (2020). Nitric oxide alleviates salt stress in seed germination and early seedling growth of pakchoi (*Brassica chinensis* l.) by enhancing physiological and biochemical parameters. *Ecotox. Environ. Safe.* 187, 109785. doi: 10.1016/j.ecoenv.2019.109785

Rivelli, A. R., Puschenreiter, M., and De Maria, S. (2014). Assessment of cadmium uptake and nutrient content in sunflower plants grown under cd stress. *Plant Soil Environ.* 60, 80–86. doi: 10.17221/520/2013-pse

Rizwan, M., Ali, S., Abbas, T., Adrees, M., Zia-ur-Rehman, M., Ibrahim, M., et al. (2018). Residual effects of biochar on growth, photosynthesis and cadmium uptake in rice (*Oryza sativa* l.) under cd stress with different water conditions.J. *Environ.Manage.* 206, 676–683. doi: 10.1016/j.jenvman.2017.10.035

Shahid, M. A., Balal, R. M., Khan, N., Zotarelli, L., Liu, G. D., Sarkhosh, A., et al. (2019). Selenium impedes cadmium and arsenic toxicity in potato by modulating carbohydrate and nitrogen metabolism. *Ecotox. Environ. Safe.* 180, 588–599. doi: 10.1016/j.ecoenv.2019.05.037

Shu, L. B., Lou, Q. J., Ma, C. F., Ding, W., Zhou, J., Wu, J. H., et al. (2011). Genetic, proteomic and metabolic analysis of the regulation of energy storage in rice seedlings in response to drought. *Proteomics* 11, 4122–4138. doi: 10.1002/pmic.201000485

Singh, S., Singh, A., Bashri, G., and Prasad, S. M. (2016). Impact of cd stress on cellular functioning and its amelioration by phytohormones: an overview on regulatory network. *Plant Growth Regul.* 80, 253–263. doi: 10.1007/s10725-016-0170-2

Sun, H. W., Feng, F., Liu, J., and Zhao, Q. Z. (2019). Nitric oxide affects rice root growth by regulating auxin transport under nitrate supply. *Front. Plant Sci.* 9. doi: 10.3389/fpls.2019.01123

Sun, L. Y., Song, F. B., Zhu, X. C., Liu, S. Q., Liu, F. L., Wang, Y. J., et al. (2021). Nano-ZnO alleviates drought stress *via* modulating the plant water use and carbohydrate metabolism in maize. *Arch. Agron. Soil Sci.* 67, 245–259. doi: 10.1080/03650340.2020.1723003

Tailor, A., Tandon, R., and Bhatla, S. C. (2019). Nitric oxide modulates polyamine homeostasis in sunflower seedling cotyledons under salt stress. *Plant Signal. Behav.* 14, 1667730. doi: 10.1080/15592324.2019.1667730

Terrón-Camero, L. C., Pelaez-Vico, M. A., Del-Val, C., Sandalio, L. M., and Romero-Puertas, M. C. (2019). Role of nitric oxide in plant responses to heavy metal stress: exogenous application versus endogenous production. *J. Exp. Bot.* 70, 4477–4488. doi: 10.1093/jxb/erz184

Wang, B., Bian, B. T., Wang, C. L., Li, C. X., Fang, H., Zhang, J., et al. (2019). Hydrogen gas promotes the adventitious rooting in cucumber under cadmium stress. *Plas One* 14, e0212639. doi: 10.1371/journal.pone.0212639

Wang, Y. H., Xiong, F., Nong, S. H., Liao, J. R., Xing, A. Q., Shen, Q., et al. (2020). Effects of nitric oxide on the GABA, polyamines, and proline in tea (*Camellia sinensis*) roots under cold stress. *Sci. Rep.* 10, 12240. doi: 10.1038/s41598-020-69253-y

Wang, Y. S., Luo, Z. S., Khan, Z. U., Mao, L. C., and Ying, T. J. (2015). Effect of nitric oxide on energy metabolism in postharvest banana fruit in response to chilling stress. *Postharvest Biol. Tec.* 108, 21–27. doi: 10.1016/j.postharvbio.2015.05.007

Wang, Y. Q., Lv, P. X., Kong, L. S., Shen, W. B., and He, Q. J. (2021). Nanomaterial-mediated sustainable hydrogen supply induces lateral root formation *via* nitrate reductase-dependent nitric oxide. *Chem. Eng. J.* 405, 126905. doi: 10.1016/j.cej.2020.126905

Wei, L. J., Zhang, J., Wang, C. L., and Liao, W. B. (2020). Recent progress in the knowledge on the alleviating effect of nitric oxide on heavy metal stress in plants. *Plant Physiol. Bioch.* 147, 161–171. doi: 10.1016/j.plaphy.2019.12.021

Wimalasekera, R., Tebartz, F., and Scherer, G. F. E. (2011). Polyamines, polyamine oxidases and nitric oxide in development, abiotic and biotic stresses. *Plant Sci.* 181, 593–603. doi: 10.1016/j.plantsci.2011.04.002

Xia, H., Liu, X. L., Wang, Y. M., Lin, Z. Y., Deng, H. H., Wang, J., et al. (2022). 24-Epibrassinolide and nitric oxide combined to improve the drought tolerance in kiwifruit seedlings by proline pathway and nitrogen metabolism. *Sci. Hortic* 297, 110929. doi: 10.1016/j.scienta.2022.110929

Xu, P. L., Guo, Y. K., Bai, J. G., Shang, L., and Wang, X. J. (2008). Effects of long-term chilling on ultrastructure and antioxidant activity in leaves of two cucumber cultivars under low light. *Physiol. Plantarum* 132, 467–478. doi: 10.1111/j.1399-3054.2007.01036.x

Xuan, W., Xu, S., Li, M. Y., Han, B., Zhang, B., Zhang, J., et al. (2012). Nitric oxide is involved in hemin-induced cucumber adventitious rooting process. *J. Plant Physiol.* 169, 1032–1039. doi: 10.1016/j.jplph.2012.02.021

Yang, W., Zhu, C. H., Ma, X. L., Li, G. J., Gan, L. J., Ng, D., et al. (2013). Hydrogen peroxide is a second messenger in the salicylic acid-triggered adventitious rooting process in mung bean seedlings. *PloS One* 8, e84580. doi: 10.1371/journal.pone.0084580

Yu, C. L., Sun, C. D., Shen, C. J., Wang, S. K., Liu, F., Liu, Y., et al. (2015). The auxin transporter, OsAUX 1, is involved in primary root and root hair elongation and in Cd stress responses in rice (Oryza sativa L.). *Plant J* 83, 818–830. doi: 10.1111/tpj.12929

Zhang, J. T., Zhang, Y., Du, Y. Y., Chen, S. Y., and Tang, H. R. (2011a). Dynamic metabonomic responses of tobacco (*Nicotiana tabacum*) plants to salt stress. *J. Proteome Res.* 10, 1904–1914. doi: 10.1021/pr101140n

Zhang, Y. T., Liu, A. L., Hao, Y. W., Su, W., Sun, G. W., Song, S. W., et al. (2022). Nitric oxide is essential for melatonin to enhance nitrate tolerance of cucumber seedlings. *Molecules* 27, 5806. doi: 10.3390/molecules27185806

Zhao, C. S., Bao, Z. J., Feng, H. Y., Chen, L. C., and Li, Q. (2022). Nitric oxide enhances resistance of pleurotus eryngii to cadmium stress by alleviating oxidative damage and regulating of short-chain dehydrogenase/reductase family. *Environ. Sci. pollut. R.* 29, 53036–53049. doi: 10.1007/s11356-022-19613-0

Zhong, M., Yuan, Y. H., Shu, S., Sun, J., Guo, S. R., Yuan, R. N., et al. (2016). Effects of exogenous putrescine on glycolysis and Krebs cycle metabolism in cucumber leaves subjected to salt stress. *Plant Growth Regul.* 79, 319–330. doi: 10.1007/s10725-015-0136-9

Zuccarelli, R., Rodríguez-Ruiz, M., Lopes-Oliveira, P. J., Pascoal, G. B., Andrade, S. C. S., Furlan, C. M., et al. (2021). Multifaceted roles of nitric oxide in tomato fruit ripening: NO-induced metabolic rewiring and consequences for fruit quality traits. *J. Exp. Bot.* 72, 941–958. doi: 10.1093/jxb/eraa526

frontiers | Frontiers in Plant Science

TYPE Original Research
PUBLISHED 11 May 2023
DOI 10.3389/fpls.2023.1143778



OPEN ACCESS

EDITED BY
Weibiao Liao,
Gansu Agricultural University, China

REVIEWED BY
Abdurrahim Yılmaz,
Abant Izzet Baysal University, Türkiye
Ananya Kuanar,
Siksha O Anusandhan University, India

*CORRESPONDENCE
Mohan Lal
mohan@neist.res.in

RECEIVED 13 January 2023
ACCEPTED 16 March 2023
PUBLISHED 11 May 2023

CITATION
Begum T, Munda S, Gupta T, Gogoi R, Choubey VK, Chanda SK, Lekhak H, Sastry GN and Lal M (2023) Stability estimation through multivariate approach among solasodine-rich lines of *Solanum khasianum* (C.B. Clarke): an important industrial plant.
*Front. Plant Sci.* 14:1143778.
doi: 10.3389/fpls.2023.1143778



# Stability estimation through multivariate approach among solasodine-rich lines of *Solanum khasianum* (C.B. Clarke): an important industrial plant

Twahira Begum[1], Sunita Munda[1], Tanmita Gupta[1], Roktim Gogoi[1], Vikash Kumar Choubey[1], Sanjoy K. Chanda[1], Himangshu Lekhak[1], G. N. Sastry[2] and Mohan Lal[1]*

[1]Agrotechnology and Rural Development Division, Council of Scientific and Industrial Research (CSIR)-North East Institute of Science and Technology, Jorhat, Assam, India, [2]Advanced Computation and Data Sciences Division, Council of Scientific and Industrial Research (CSIR)-North East Institute of Science and Technology, Jorhat, Assam, India

*Solanum khasianum* is a medicinally important plant that is a source of steroidal alkaloids 'solasodine.' It has various industrial applications, including oral contraceptives and other pharmaceutical uses. The present study was based on 186 germplasm of *S. khasianum*, which were analyzed for the stability of economically important traits like solasodine content and fruit yield. The collected germplasm was planted during *Kharif* 2018, 2019, and 2020 in RCBD with three replications at the experimental farm of CSIR-NEIST, Jorhat, Assam, India. A multivariate approach for stability analysis was applied to identify stable germplasm of *S. khasianum* for economically important traits. The germplasm was analyzed for additive main effects and multiplicative interaction (AMMI), GGE biplot, multi-trait stability index, and Shukla's variance which were evaluated for three environments. The AMMI ANOVA revealed significant GE interaction for all the studied traits. The stable and high-yielding germplasm was identified from the AMMI biplot, GGE biplot, Shukla's variance value, and MTSI plot analysis. Lines no. 90, 85, 70, 107, and 62 were identified as highly stable fruit yielders while, lines no. 1, 146, and 68 were identified as stable high solasodine lines. However, considering both traits, i.e., high fruit yield and solasodine content, MTSI analysis was performed which showed that lines 1, 85, 70,155, 71, 114, 65, 86, 62, 116, 32, and 182 could be used in a breeding program. Thus, this identified germplasm can be considered for further varietal development and could be used in a breeding program. The findings of the present study would be beneficial for the *S. khasianum* breeding program.

KEYWORDS

**anova, AMMI, GGE biplot, MTSI, Shukla's variance, solasodine, *Solanum khasianum***

# 1 Introduction

The Solanaceae family with worldwide distribution comprises 90 genera, containing more than 3000 species. The Solanaceae family's largest genus is Solanum with more than 2000 species (Kaunda and Zhang, 2019). *Solanum khasianum* (C.B. Clarke), also called *Solanum aculeatissimum* Jacq., is a member of the Solanaceae family and is cultivated in China, Bhutan, and the Indian states of Assam, Arunachal Pradesh, Meghalaya, Sikkim, Manipur, Orissa, Nilgiri Hill, and West Bengal (Gogoi et al., 2021). Alkaloids, flavonoids, phenols, and numerous other phytoconstituents found in *S. khasianum* are recognized to have the ability to reduce inflammation, blood sugar levels, and oxidative stress (Gupta, 2019). The potential glycoalkaloids reported to be present in *S. khasianum* include solasodine, solamargine, solanine, and solasonine (Srivastava et al., 2016; Kaunda and Zhang, 2019). Among the Solanum plants screened for solasodine production, *S. khasianum* was found to possess the maximum solasodine content (Weissenberg, 2001; Begum et al., 2022; Lal et al., 2022a). It is widely known for its range of therapeutic applications. Solasodine was found to possess many pharmacological properties like anti-inflammatory, antioxidant, antinociceptive, antimicrobial, cytotoxic, anti-obesity, antiandrogenic, and hepatoprotective properties (Srivastava et al., 2016; Kumar et al., 2019; Gogoi et al., 2021). Moreover, previous reports suggested that the berries possess anti-diabetic, anti-inflammatory, anti-cholinesterase, anticancer, and antibacterial properties (Rosangkima and Jagetia, 2015; Gogoi et al., 2021; Pavani and Shasthree, 2021). As an ethnomedicine, the plant has been used for treating diseases like whooping cough, bronchitis, smallpox, trachoma, snake bites, rheumatism, and tooth and skin infections (Schmelzer and Gurib, 2008; Chirumamilla et al., 2021; Lal et al., 2022a).

*Solanum khasianum* is a sturdy, branched shrub with a height of approximately 0.75 to 1.5 m. The stem and leaves bear spines on both its surfaces with the shape of ovate to lobate. It possesses hermaphrodite flowers and abundant berries and turns yellowish upon maturity (Begum et al., 2022; Lal et al., 2022a). The cultivation area of *S. khasianum* is more than 4000 ha in India across the states of Assam, Meghalaya, Tripura, Manipur, Maharashtra, and Karnataka (Gogoi et al., 2021). *S. khasianum* is a storehouse of solasodine, the steroidal alkaloid which has high industrial and medicinal significance (Sanwal et al., 2016; Gogoi et al., 2021). It is the starting base for synthesizing steroid hormones, such as cortisone and oral contraceptives (Begum et al., 2022). Solasodine is a key intermediate and substrate in steroidal drugs and sex hormone production (Sanwal et al., 2016; Lal et al., 2022a). It is used in steroidal hormone production for commercial use in oral pills or injections (Sinani and Eltayeb, 2017; Lal et al., 2022a). It, thus, plays a crucial role in human birth control purposes. The valuable part of the plant is the berries which contain the source of solasodine that can be extracted from ripened berries. The maximum content of solasodine is produced when the berries have ripened and turned yellow in color. The seeds are mucilage in nature, small in size, and are the primary source of propagation (Begum et al., 2022). Increased consumption of this medicine and reckless harvesting of the plant from the wild as a raw material source has led to the depletion of genetic diversity and habitat loss (Canter et al., 2005; Julsing et al., 2007). Due to its rapid growth and low initial culture cost, it is one of the best sources of affordable raw materials for industrially significant solasodine extraction. Therefore, it would be very advantageous to identify and include plant breeding for this neglected plant species.

As for the definition of stability, a genotype that can consistently produce consistent performance regardless of any change in its environmental conditions can be termed a stable genotype. In plant breeding, the stability of yield traits is a significant aspect. However, with ever-changing fluctuations in environmental conditions, the determination of yield factor is challenging. The phenotypic expression of a genotype is a controlled result of both genotypic constitutions of the genotype and the environment. Hence, the genotype may show inconsistent performance under varying environmental conditions. A stable genotype with superior yield in varying environments is considered the mostly desired genotype. This compels the necessary study of the genotype × environment to identify stable genotypes with desirable traits.

A stable genotype is one which produces a stable yield in an environment (Annicchiarico, 2002; Munda et al., 2020). The performance of a genotype in multi-environments is difficult to study when the genotype-environment interaction is stronger (Alwala et al., 2010). The selection of a stable genotype is difficult due to the interaction between genotype × environments (Gupta et al., 2015). The genotypic response to an environment is multivariate; hence, the determination of stability using parametric and nonparametric statistical analysis which is univariate would not be very effective. There are many multivariate models available for the analysis of stability. Among the various multivariate model, additive main effects and multiplicative interaction (AMMI) method and 'GGE biplot' are widely used (Lal et al., 2022b). The AMMI model is an amalgamation of the analysis of variance and the principal component analysis. It efficiently illustrates the adaptive responses of genotypes to the environment by providing details on the main and interaction effects along with a biplot. The main effects of G × E are assessed using variance analysis (main additive effects) while the G × E interaction is estimated using the principal analysis components (multiplicative interactions). The GGE biplot was developed to represent graphically the G × E interaction and genotype main effects. Shukla's variance analysis is effective to partition the total G × E interaction for the estimation of the variance attribution for each of the genotypes in an unbiased manner. For the simultaneous estimation of stability and identification of genotypes with multiple superior traits, the MTSI is useful for exploiting wide adaptability. The plant breeding program is aimed at the identification of superior yielding lines due to varying genotypes' performance and varying environments. Thus, the results obtained are either for the identification of genotypes with high-yielding traits or different environment-adapted genotypes. However, with the multivariate approach for stability analysis across multilocation, both the issues of varying genotypic and environmental interactions can be addressed. The present stability analysis was verified by AMMI, GGE, MTSI, and Shukla's variance methods. High fruit-yielding germplasm with

high solasodine content, which shows a consistent performance across different locations of NE India, is the major selection criteria for the identification of elite lines.

So far, none of the stability studies in *S. khasianum* are available in the public domain. Hence the present study was conducted for the first time to assess the performance of large numbers of germplasm of *S. khasianum* with high solasodine content.

# 2 Materials and methods

## 2.1 Materials and methods

Initially, 273 germplasm of *S. khasianum* were collected from different regions of NE India. Among them, 186 high solasodine content-rich (>0.8%) lines were identified and used in the present study (Begum et al., 2022). The identified 186 germplasm were planted for three years in *Kharif* in 2018, 2019, and 2020 at the experimental farm of CSIR-North East Institute of Science and Technology (NEIST), Jorhat, Assam, India, and were evaluated for three years. The plant specimens were identified by the plant breeder of CSIR-NEIST, Jorhat, India, and the prepared herbarium was deposited in the departmental record with identification ID: RRLJ-SK-1 to RRLJ-SK-186.

## 2.2 Morphological characters recorded

The morphological data were recorded for the three years of study. The data included plant spread (cm), plant height (cm), leaf width (cm), leaf length (cm), fruit diameter (cm), number of fruits/plants, fresh fruit weight per plant (kg), and days to maturity. Along with the morphological characters, the solasodine content (%) was also recorded for each year (Table S1). All the data were recorded for ten randomly selected healthy plants for each germplasm.

## 2.3 Solasodine extraction and quantification

The dried ripe berries of *S. khasianum* were used for the estimation of solasodine. Solasodine extraction and quantification were done as per the method suggested by Begum et al. (2022).

## 2.4 Statistical analysis

R software was used for performing all the statistical analyses. The mean-multi-environment trial analysis package in R software was used in the study (Olivoto et al., 2019). The analysis of variance (ANOVA), AMMI, multi-trait stability index (MTSI), GGE, and Shukla's variance were used to analyze the three-year data of *Solanum khasianum* for economic traits like solasodine content and fresh fruit weight per plant.

# 3 Results

The evaluation of germplasm is pivotal to elite germplasm; therefore, the identified or selected germplasm needs to be further assessed for its stability and consistent performance in varied environments. The present study focuses on the identification of stable germplasm of *S. khasianum* for economically important traits. The pooled data for three years were analyzed with ANOVA and various stability analyses (AMMI, GGE, MTSI, and Shukla's variance). The coefficient of variation is a significant parameter for the comparison between traits based on phenotypic variation. Concerning the coefficient of variation, a higher variation was found in the fresh fruit weight per plant followed by plant height while a moderate coefficient of variation was observed for solasodine content and days to maturity (Table 1).

The AMMI analysis of variance (ANOVA) revealed that the environmental effect was significant for all the traits while the genotypic effect was significant for plant height, fruit diameter, fresh fruit weight per plant, solasodine content, and days to maturity. Significant G × E interaction was observed for all the studied traits indicating divergent performances across the different environments. Thus, a precise selection of germplasm with elite traits is essential for a breeding program. The interaction effect was analyzed from the principal component analysis (IPCA) of AMMI ANOVA from which G × E interaction sum of squares percentage value of 48.660 and 16.955 was recorded for fresh fruit weight per plant and solasodine content, respectively (Table 2). A more precise analysis for the selection of germplasm with elite traits from the genotype-environment interaction was identified through the AMMI biplot. The genotype-environment interaction for yield is an important analysis in which the less interacting genotypes are closer to the center of the AMMI biplot and considered more stable than their counterpart for that region. In contrast, the far-centered genotypes have individual stability with each environment which indicates the high-performing germplasm for each environment. The AMMI was performed for the economically important traits *i.e.*, solasodine content and fresh fruit weight per plant for which AMMI biplots were constructed. From the AMMI results, it was found that lines no. 1, 146, 68, 178, 52, 107, and 44 were among the high yielders and were stable for solasodine content (Figure 1). Lines no. 90, 85, 70, 107, and 62 were considered stable and high yielders for fresh fruit weight per plant (Figure 2). The individual competence of the genotypes in the studied environments was evaluated using the AMMI2 model in which the first two principal components (Factor 1 and Factor 2) were used to generate the plot. In the AMMI2 biplot for solasodine content, line no. 116 was considered a high yielder in environment one, line no. 51 and 32 in environment two, and line no. 105 in environment three, respectively (Figure 3).

Similarly, for the fresh fruit weight per plant, line no. 128 and 7 were considered stable in environment one, lines no. 29 and 35 in environment two, and line no. 30 in environment three, respectively

10.3389/fpls.2023.1143778

TABLE 1 The analysis of variance on the three-year data of *Solanum khasianum* germplasm that was used in the study.

| Source | DF | PH | | PS | | LL | | LW | | NOF | | FD | | FWP | | SOL | | DOM | |
|---|---|---|---|---|---|---|---|---|---|---|---|---|---|---|---|---|---|---|---|
| | | SS% | MS | SS% | MS | SS% | MS | SS% | MS | SS% | MS | SS% | MS | SS% | MS | SS% | MS | SS% | MS |
| ENV | 2 | 376989.419 | 188494.710 | 8049.256 | 4024.628 | 19.915 | 9.957 | 0.932 | 0.466 | 2172.553 | 1086.277 | 27.026 | 13.513 | 0.021 | 0.011 | 0.007 | 0.004 | 2588.649 | 1294.324 |
| REP (ENV) | 6 | 4285.538 | 714.256 | 1788.864 | 298.144 | 0.339 | 0.057 | 0.477 | 0.080 | 2842.380 | 473.730 | 12.929 | 2.155 | 0.026 | 0.004 | 0.085 | 0.014 | 624.781 | 104.130 |
| GEN | 185 | 416682.056 | 2252.335 | 1693809.673 | 9155.728 | 793.179 | 4.287 | 1642.942 | 8.881 | 1235319.272 | 6677.401 | 393.950 | 2.129 | 1.739 | 0.009 | 10.606 | 0.057 | 132502.973 | 716.232 |
| GEN × ENV | 370 | 569760.358 | 1539.893 | 171910.078 | 464.622 | 374.612 | 1.012 | 136.330 | 0.368 | 13090.780 | 35.380 | 68.407 | 0.185 | 1.668 | 0.005 | 2.167 | 0.006 | 61248.018 | 165.535 |
| Residuals | 1110 | 985714.462 | 888.031 | 117275.136 | 105.653 | 171.167 | 0.154 | 311.590 | 0.281 | 112908.953 | 101.720 | 127.211 | 0.115 | 4.892 | 0.004 | 8.601 | 0.008 | 144715.885 | 130.375 |
| Total | 2043 | 376989.419 | 188494.710 | 8049.256 | 4024.628 | 19.915 | 9.957 | 0.932 | 0.466 | 2172.553 | 1086.277 | 27.026 | 13.513 | 0.021 | 0.011 | 0.007 | 0.004 | 2588.649 | 1294.324 |
| CV (%) | | 34.014 | | 10.659 | | 5.746 | | 8.542 | | 16.457 | | 5.046 | | 38.526 | | 9.470 | | 6.361 | |

ENV, environment; REP, replication; GEN, genotype; DF, degree of freedom; MS, mean sum of squares; PH,plant height; PS= plant spread; LL, leaf length; LW, leaf width; NOF, number of fruit/plant; FD, fruit diameter; FWP, fresh fruit weight/plant; SOL, solasodine content; DOM= days to maturity; CV, coefficient of variation.

(Figure 4). The above-identified genotypes showed the best performance in the studied environments and were found to be highly competent.

The genotype in a studied environment that possesses the highest mean performance and absolute stability can be considered the ideal genotype. Such a genotype possessing a superior trait with zero-G × E interaction is ideal. It should be described as the one possessing the most excellent vector length from genotype markers to the origin of the biplot. In the GGE biplot, lines no. 149, 61, and 32 were the most unstable lines. Their vector lengths were longer compared to the other genotypes. Whereas lines no.1, 169, and 146 had high solasodine content and were found to be stable genotypes since their vector lengths were short (Figures 5, 6). While considering the trait of the fresh fruit weight per plant from the GGE biplot, genotypes 29, 30, and 35 had higher weights of fresh fruit/plant than average but were unstable as they exhibited longer vector lengths. Lines no. 90, 85, and 114 had high fresh fruit weight per plant and exhibited short vector lengths which characterize a stable genotype (Figures 7, 8). The discriminating ability is directly proportional to the vector length. Environments E2 and E3 had longer vectors than E1 for the trait fresh fruit weight per plant (Figure 8). While, for the trait solasodine content, E1 and E2 had longer vectors than E3 (Figure 6). Thus, E2 and E3 were the best environments to exhibit germplasm differentiation for fresh fruit yield per plant while environment E1 and E2 were the most discriminating environment for solasodine content.

Shukla's variance was studied for genotype performance across the environments according to how the germplasm with minimum values is intended to be more stable. On the basis of our present results, lines no. 153, 135, 149, 163, 166, and 123 were considered stable for fresh fruit weight per plant while lines no. 149, 3, 4, 2, 16, 181, 5, and 28 were considered stable for solasodine content (Table 3). The MTSI study revealed that the mean of the selected germplasm (Xs) was higher than the mean of the original (Xo) for fresh fruit weight per plant and solasodine content. The selection gain (SG) was positive for both traits with SG% of 7.022 and 7.610 for the traits of fresh fruit weight per plant and solasodine content, respectively. The selection differential (SD) was favorable for both traits and heritability of 0.520 and 0.873 for fresh fruit weight per plant and solasodine content, respectively (Table 4). As per the MTSI analysis, lines no. 90, 1, 85, 70, 155, 63, 115, 107, 71, 103, 114, 65, 86, 124, 101, 62, 34, 110, 137, 171, 174, 116, 12, 32, 22, 182, 147, and 33 were considered as stable germplasm (Figure 9). Based on the multivariate and univariate approaches used in the study, it can be concluded that lines 90, 85, 107, and 62 were the elite lines with a high yield and stable nature. The study of stability is an important aspect in the identification of stable genotypes with elite traits. The elite germplasm in the study refers to the stable germplasm with a high fruit yield and solasodine content. The study of *S. khasianum* is significant for commercially cultivating the industrially important solasodine-rich plant.

## 4 Discussion

The assessment of the different landraces worldwide is crucial for identifying and preserving genetically rich

TABLE 2 The AMMI Analysis of variance on the three-year data of *Solanum khasianum* germplasm that was used in the study.

| A | | | | | | | | | | | | | | | |
|---|---|---|---|---|---|---|---|---|---|---|---|---|---|---|---|
| Source | DF | PH | | | PS | | | LL | | | LW | | | NOF | | |
| | | SS | MS | % | SS | MS | % | SS | MS | % | SS | MS | % | SS | MS | % |
| ENV | 2 | 376989.4 | 188494.7 | 27.650*** | 8049.256 | 4024.628 | 0.430*** | 19.915 | 9.957 | 1.677*** | 0.932 | 0.466 | 0.052*** | 2172.553 | 1086.277 | 0.174* |
| REP (ENV) | 6 | 4285.538 | 714.2563 | 0.314* | 1788.864 | 298.144 | 0.095*** | 0.339 | 0.057 | 0.029* | 0.477 | 0.080 | 0.027* | 2842.380 | 473.730 | 0.227*** |
| GEN | 185 | 416682.1 | 2252.335 | 30.561*** | 1693809.673 | 9155.728 | 90.396 | 793.179 | 4.287 | 66.782 | 1642.942 | 8.881 | 92.290 | 1235319.272 | 6677.401 | 98.780 |
| GEN × ENV | 370 | 569760.4 | 1539.893 | 41.789*** | 171910.078 | 464.622 | 9.175*** | 374.612 | 1.012 | 31.541*** | 136.330 | 0.368 | 7.658*** | 13090.780 | 35.380 | 1.047* |
| PC1 | 186 | 462109.9 | 2484.462 | 33.893 | 169330.977 | 910.382 | 9.037 | 370.031 | 1.989 | 31.155 | 133.316 | 0.717 | 7.489 | 9711.842 | 52.214 | 0.777* |
| PC2 | 184 | 107650.4 | 585.0567 | 7.896* | 2579.101 | 14.017 | 0.138* | 4.581 | 0.025 | 0.386 | 3.014 | 0.016 | 0.169 | 3378.938 | 18.364 | 0.270* |
| Residuals | 1110 | 985714.5 | 888.031 | 72.297 | 117275.136 | 105.653 | 6.259 | 171.167 | 0.154 | 14.412 | 311.590 | 0.281 | 17.503 | 112908.953 | 101.720 | 9.029 |
| Total | 2043 | 2923192 | 1430.833 | 27.650 | 2164743.084 | 1059.590 | 0.430 | 1733.825 | 0.849 | 1.677 | 2228.601 | 1.091 | 0.052 | 1379424.719 | 675.196 | 0.174 |

| B | | | | | | | | | | | | |
|---|---|---|---|---|---|---|---|---|---|---|---|---|
| Source | DF | FD | | | FWP | | | SOL | | | DOM | | |
| | | SS | MS | % | SS | MS | % | SS | MS | % | SS | MS | % |
| ENV | 2 | 27.026 | 13.513 | 5.522** | 0.021 | 0.011 | 0.615** | 0.0071 | 0.0035 | 0.055* | 2588.649 | 1294.324 | 1.318*** |
| REP (ENV) | 6 | 12.929 | 2.155 | 2.642*** | 0.026 | 0.004 | 0.762** | 0.0846 | 0.0141 | 0.662** | 624.781 | 104.130 | 0.318* |
| GEN | 185 | 393.950 | 2.129 | 80.499*** | 1.739 | 0.009 | 50.725*** | 10.6063 | 0.0573 | 82.989*** | 132502.973 | 716.232 | 67.487*** |
| GEN × ENV | 370 | 68.407 | 0.185 | 13.978*** | 1.668 | 0.005 | 48.660** | 2.1670 | 0.0059 | 16.955* | 61248.018 | 165.535 | 31.195*** |
| PC1 | 186 | 59.108 | 0.318 | 12.078 | 1.300 | 0.007 | 37.907 | 1.1767 | 0.0063 | 9.207* | 34686.809 | 186.488 | 17.667*** |
| PC2 | 184 | 9.299 | 0.051 | 1.900 | 0.369 | 0.002 | 10.753 | 0.9903 | 0.0054 | 7.748* | 26561.209 | 144.354 | 13.528** |
| Residuals | 1110 | 127.211 | 0.115 | 25.994 | 4.892 | 0.004 | 142.686 | 8.6013 | 0.0077 | 67.301 | 144715.885 | 130.375 | 73.707 |
| Total | 2043 | 697.930 | 0.342 | 5.522 | 10.016 | 0.005 | 0.615 | 1110 | 8.601 | 0.055 | 402928.324 | 197.224 | 1.318 |

ENV, environment; REP, replication; GEN, genotype; PC, Principal component; DF, degree of freedom; MS, mean sum of squares; FD, Fruit diameter; FWP, fresh fruit weight/plant; SOL, Solasodine content; DOM, Days to maturity; CV, coefficient of variation, %, explained %; ***, significant at $p < 0.005$; **, significant at $p < 0.01$; *, significant at $p < 0.05$.





10.3389/fpls.2023.1143778

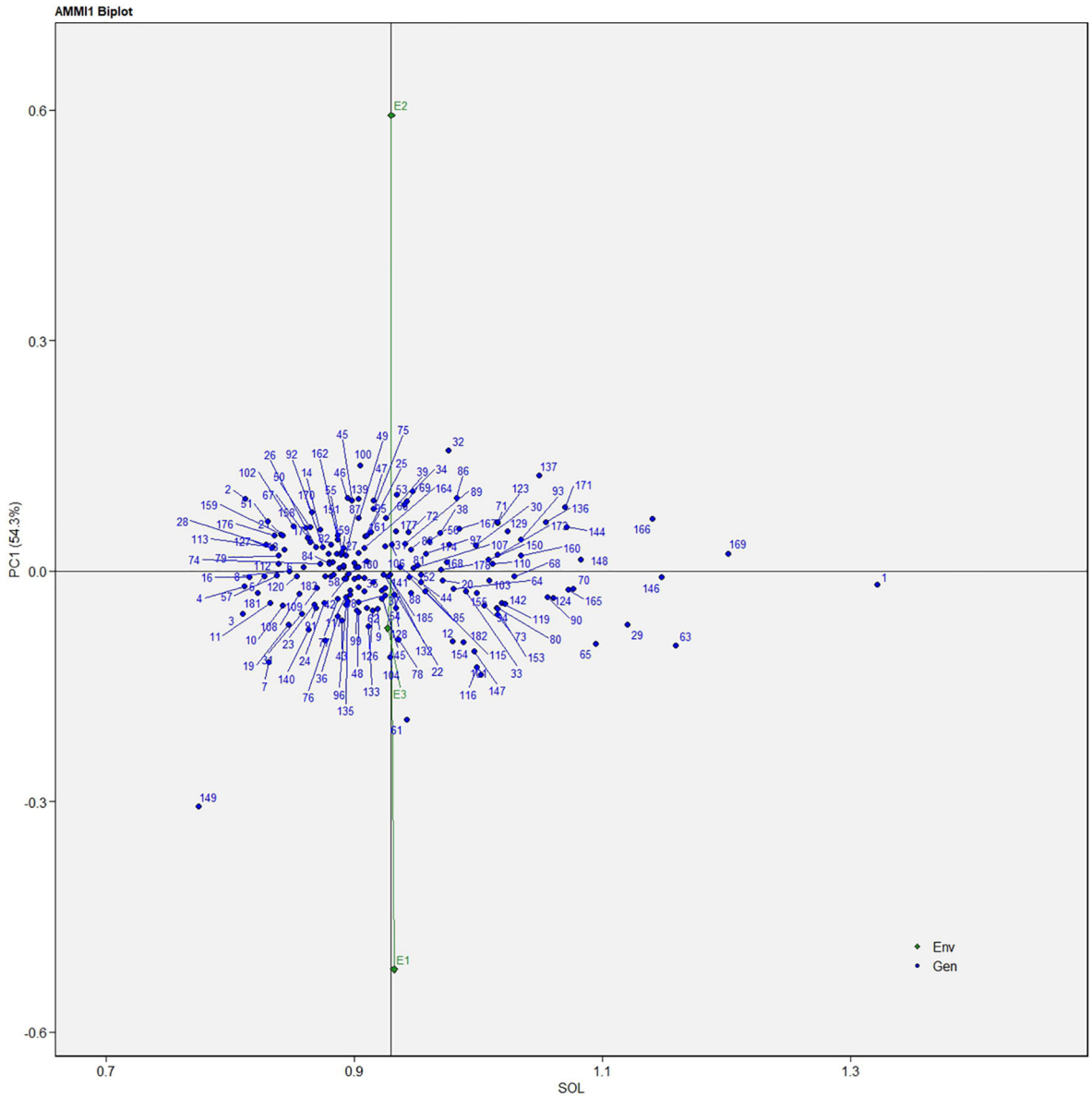


FIGURE 1
AMMI biplot model 1 for solasodine content in 186 germplasm of *S. khasianum*.

resources. The various landraces of different crops have been the storehouse for significant desirable traits. These are widely used in various breeding programs, which can be exploited to increase genetic variability. Hashemi et al. (2018) stated that different crop genotypes exhibit variable responses under different environmental conditions; hence, to reduce the influence of the environment on the genotypes, the compatibility and stability of the genotype need to be studied for multiple years at the multilocation. The most preferable genotype from the breeding point of view is the one exhibiting stability along with a significantly positive main effect, or in other terms, which has broad adaptability (Lal et al., 2022c; Munda et al., 2023). So far, no stability analysis has been studied to date for *S. khasianum*; hence, the results were considered with previous reports of the Solanaceae family.

A study on *Solanum melongena* from Iran was performed by Khankahdani et al. (2022) on fifteen germplasm for stability analysis by using the AMMI model. The AMMI biplot revealed that genotype 7 (AM5) followed by genotypes 12 (Y7), 5 (AM7), and 13 (SA15) were identified and ranked for their stability against yield factor since they revealed the lowest genotype × environment interaction. The least stable genotypes were the ones that exhibited the highest level of genotype × environment interaction, and the most unstable identified genotypes were genotypes 1 (Y), 8 (AM4), and 19 (GHE12), respectively. Similar results were obtained in our study on the basis of which germplasm with commercially important traits and stability were identified for future breeding programs.

A similar study by Bagheri et al. (2016) reported the AMMI stability assay where 22 germplasm of the long eggplant were

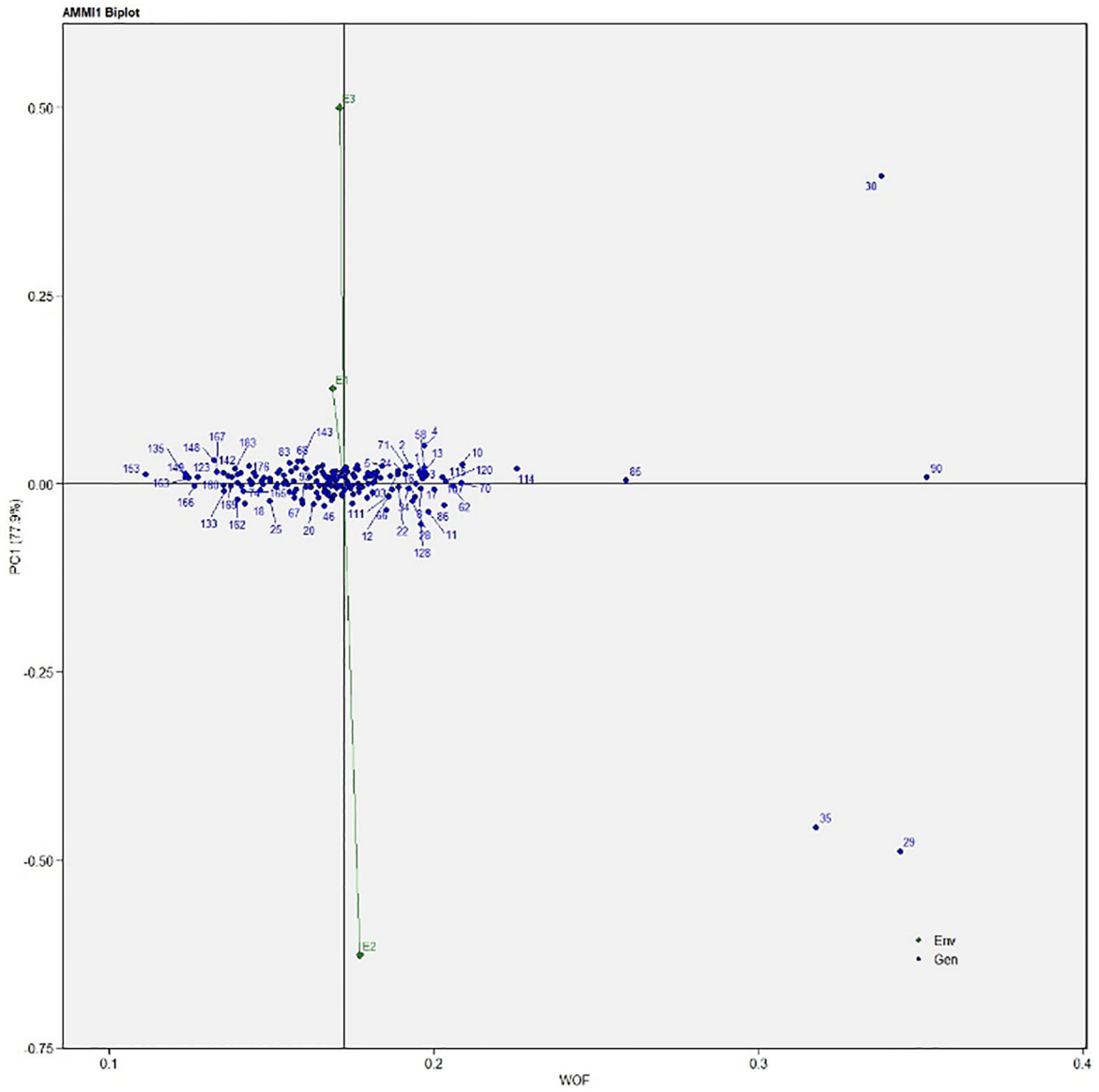


FIGURE 2
AMMI biplot model 1 for the weight of fruit in 186 germplasm of *S. khasianum*.

studied for three years. A report on the stability analysis in tobacco by the AMMI model has been previously reported by Sadeghi and Samizadeh (2011). The AMMI model was also used to study stability in general along with individual stability in different studied environments for production yield in numerous other crops like cotton (Damavandi-Kamali et al., 2011), barley (Koocheki et al., 2012), bread wheat (Bigonah, 2012), Soybean (Soltan Mohamadi et al., 2017), and durum wheat (Sadeghzadeh et al., 2018). Scavo et al. (2023) assessed six genotypes of *Solanum tuberosum* L. for AMMI and GGE. The study revealed the Salad Blue genotype as the most suitable genotype for total phenolic content, dry matter, FRAP, and vitamin C throughout eight studied environments due to its above-average mean values and stability. Another study by Das et al. (2021) was conducted on 21 potato cultivars in the eastern sub-Himalayan plains of West Bengal, India, to assess their suitability, stability, and yield factors. The study revealed 'Kufri Pukhraj' and 'Kufri Chipsona-3' as higher yielder cultivars along with 'Kufri Surya' as the heat-resistant cultivar. However, two cultivars, namely, 'Kufri Khyati'and 'HPS II/67' were identified as stable for eastern Himalayan conditions. A study on stability analysis for nine genotypes of Elite Irish Potato (*Solanum tuberosum* L.) was conducted in western Ethiopia. The study revealed CIP384321.30 as the stable genotype for the region on the basis of the mean tuber yield, regression slope identified, and GGE biplot (Fufa and Fufa, 2021). Similar conclusions were drawn from our present study in which stable germplasm was identified across the studied environments along with individual stable germplasm for each environment with the which-won-where pattern approach.

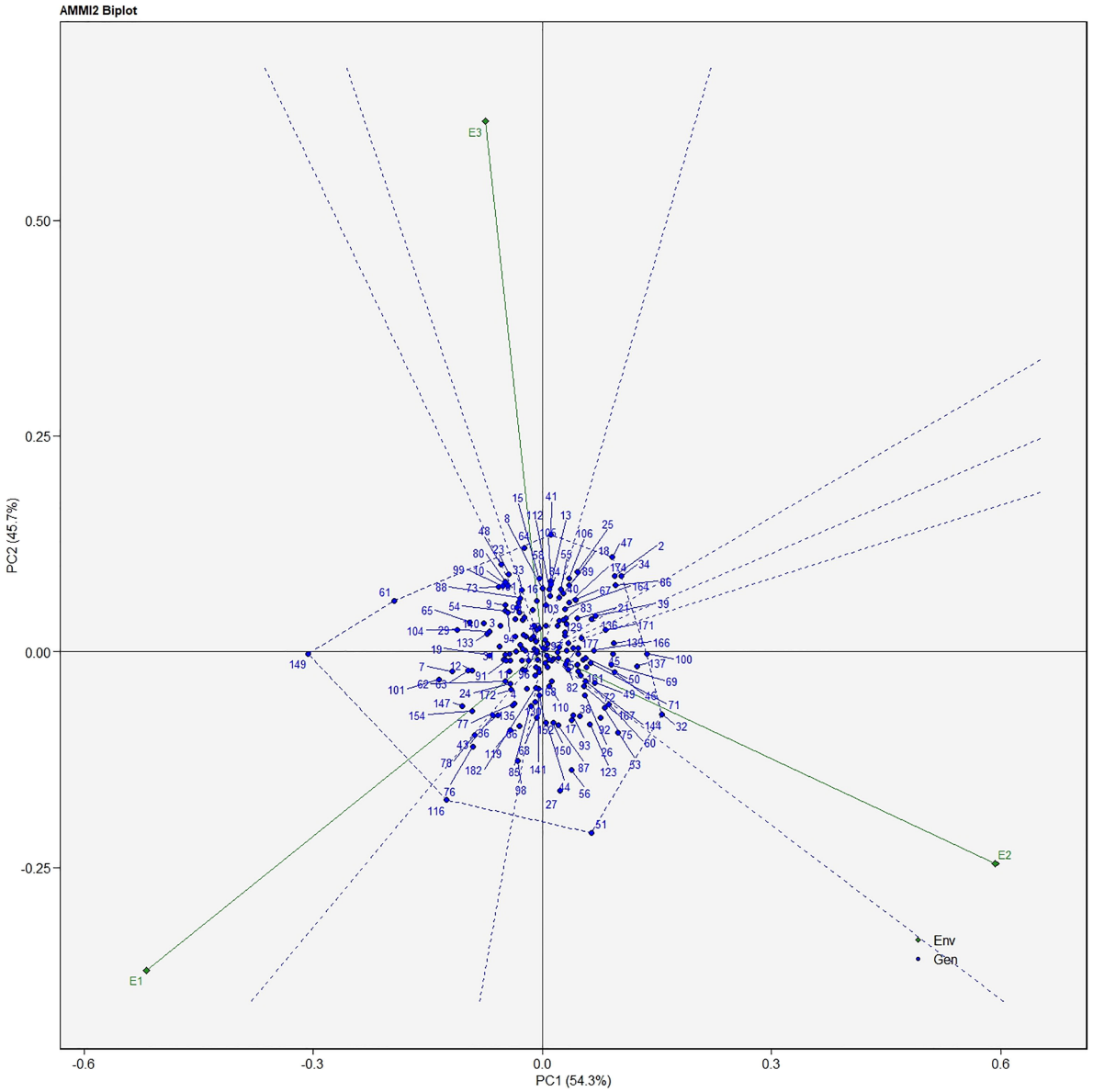


FIGURE 3
AMMI biplot model 2 for solasodine content in 186 germplasm of *S. khasianum*.

A study on the African tomato landraces was reported by Tembe et al. (2018) in which the morphological traits were assessed. The study revealed that significant variations among the studied samples can be useful as a potential source of genetic diversity for the crop improvement of tomatoes. Similar previous findings on other vegetable crops have also been reported by different workers in tomato (Manzano et al., 2015; Sousaraei et al., 2021), lettuce (Missio et al., 2018), and eggplant fields (Taher et al., 2017; Gramazio et al., 2019), identifying superior genetic resources. Tonk et al. (2011) studied the GGE biplot analysis in maize, revealing that the G16 hybrid was found to have high suitability to the tested environments for grain yield. A study was conducted on 10 genotypes of potatoes in different environments for AMMI by Almohammedi et al. (2019). The percentage of variation of 98.44%, 0.24%, and 1.31% was recorded for genotypes, environments, and GEI, respectively, which revealed that genotypes contributed more towards variation than the other parameters. As per the definition by Bernardo (2002), when the progeny of a genotype shows consistent results for the traits of interest, the genotype is regarded as possessing a good breeding value. Based on our study, lines no.1, 90, 146, 68, 85, 107, 70, and 62 were identified as superior stable germplasm. Germplasm no. 90, 85, 70, 107, and 62 were identified as high yielding and stable for fresh fruit weight per plant. While germplasm no. 1, 146, and 68 were identified for high solasodine stable lines. Thus, this identified germplasm can be considered for further large-scale cultivation on a commercial level or can be used in breeding programs.

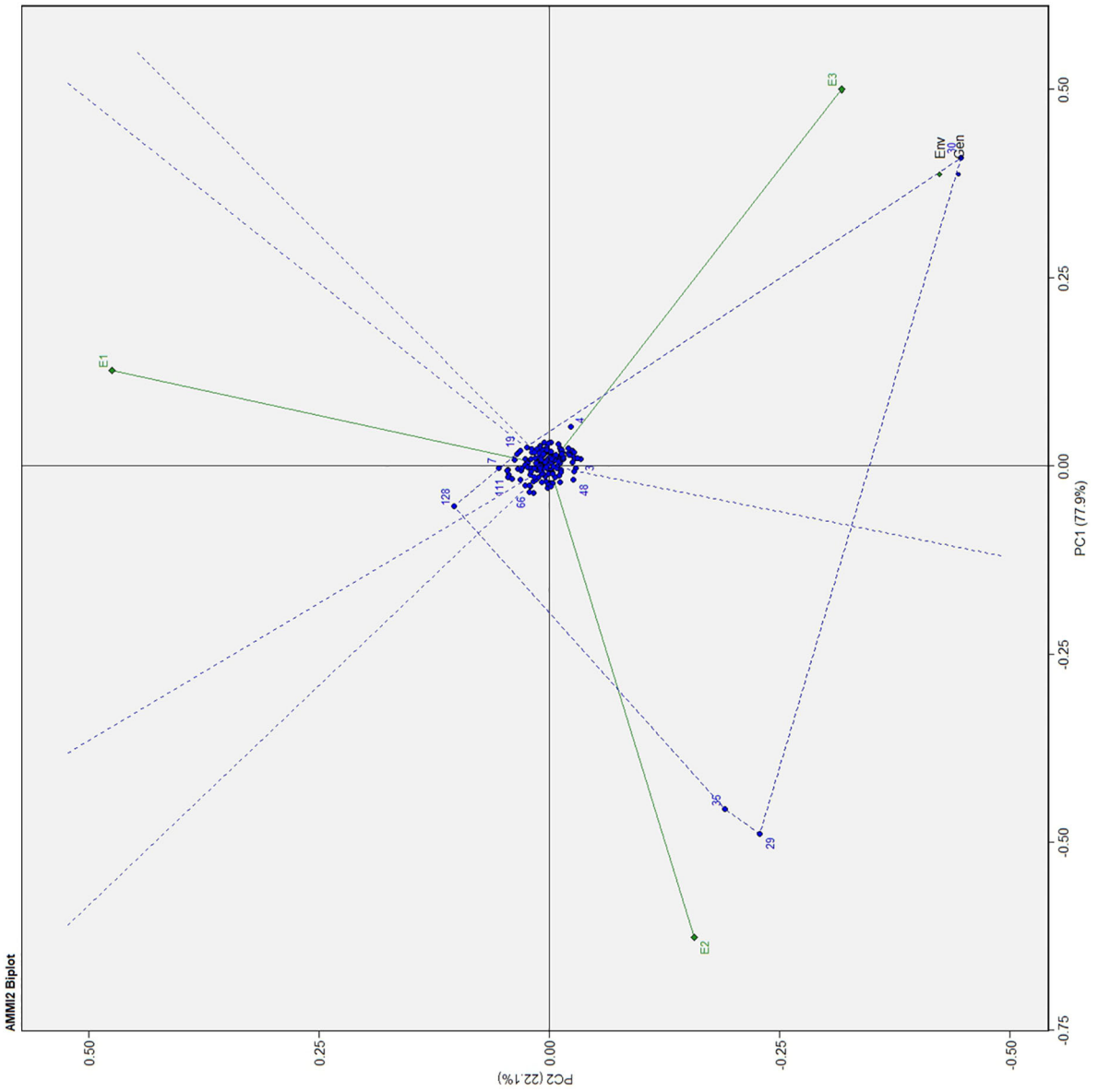


FIGURE 4
AMMI biplot model 2 for the weight of fruit in 186 germplasm of *S. khasianum*.

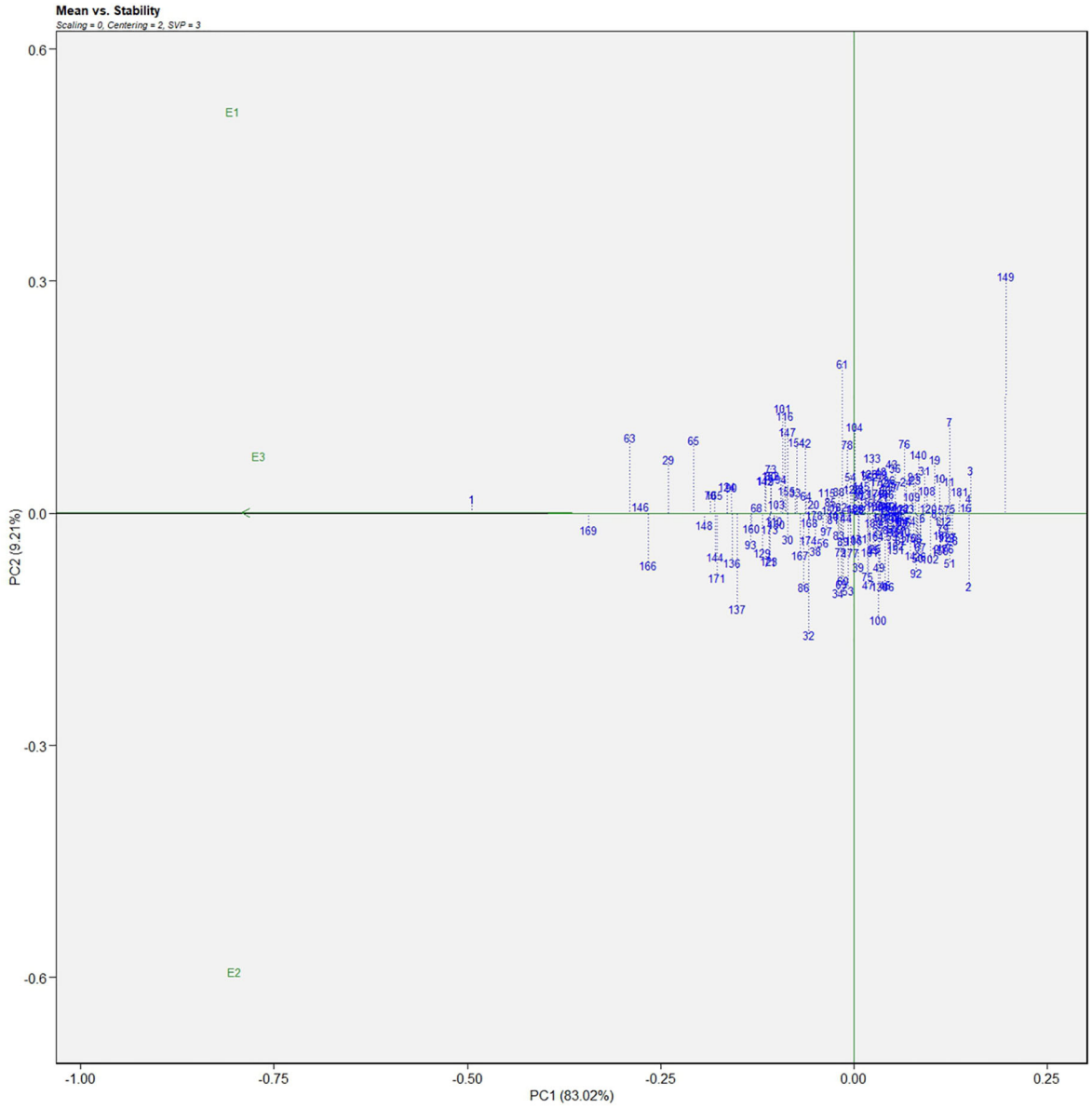


FIGURE 5
Average environment coordination views of the GGE-biplot based on environment-focused scaling for the mean performance and stability 186 germplasm of *S. khasianum* for solasodine content.



10.3389/fpls.2023.1143778

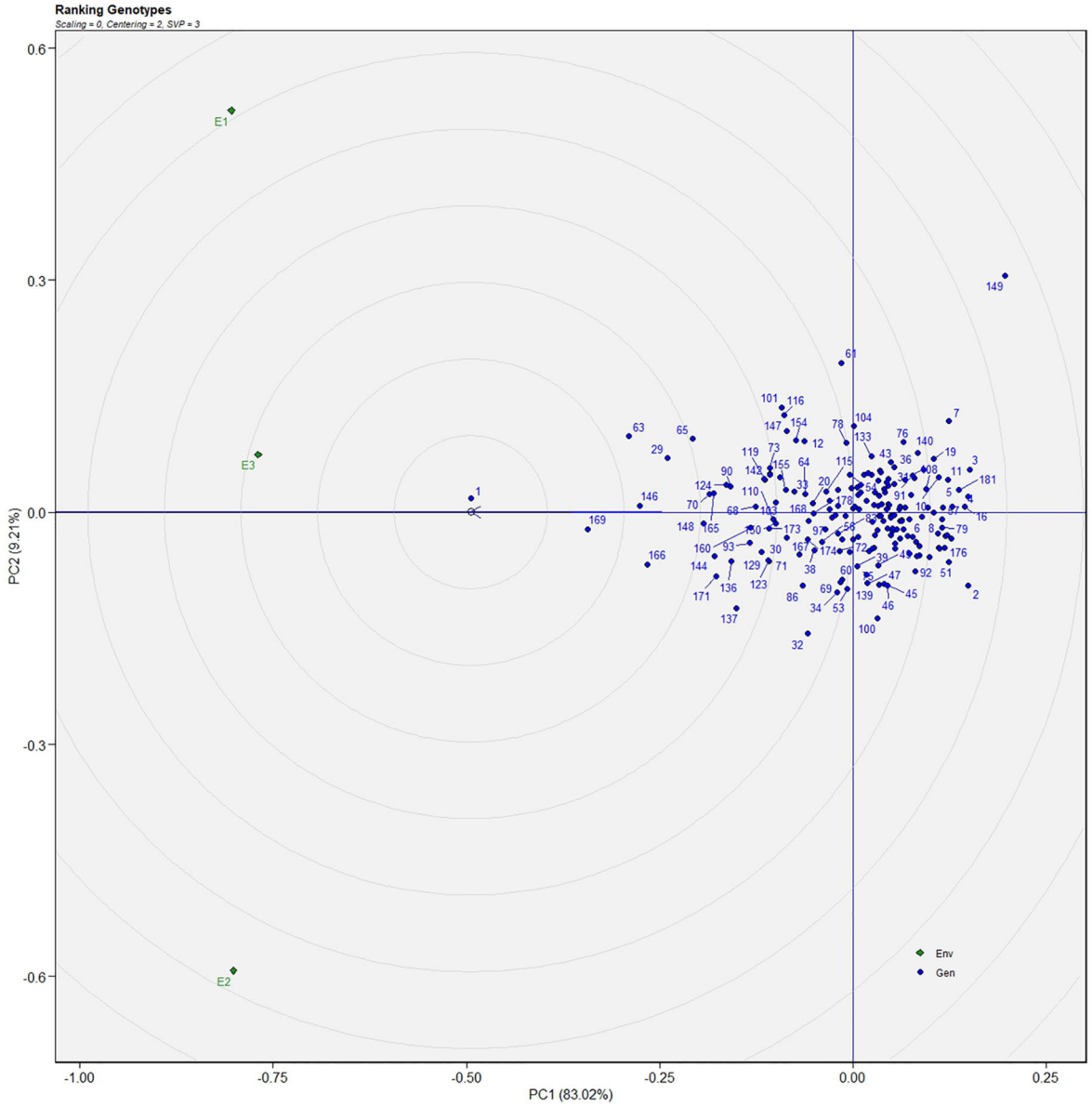


FIGURE 6
GGE-biplot based on genotype and environment-focused scaling for the comparison of genotype and environments for solasodine content.





10.3389/fpls.2023.1143778

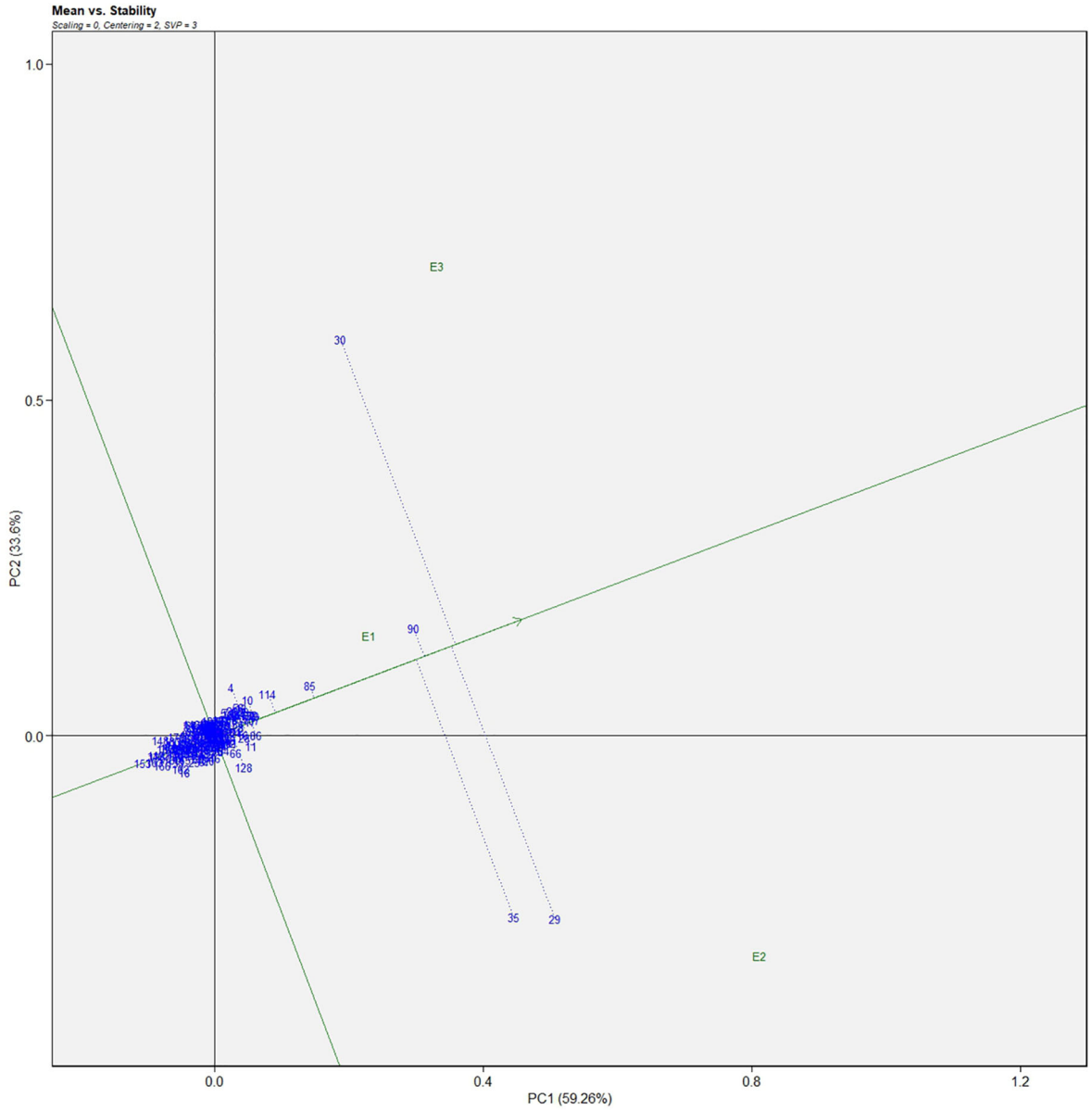


FIGURE 7
Average environment coordination views of the GGE-biplot based on environment-focused scaling for the mean performance and stability 186 germplasm of *S. khasianum* for the weight of fruit.





10.3389/fpls.2023.1143778

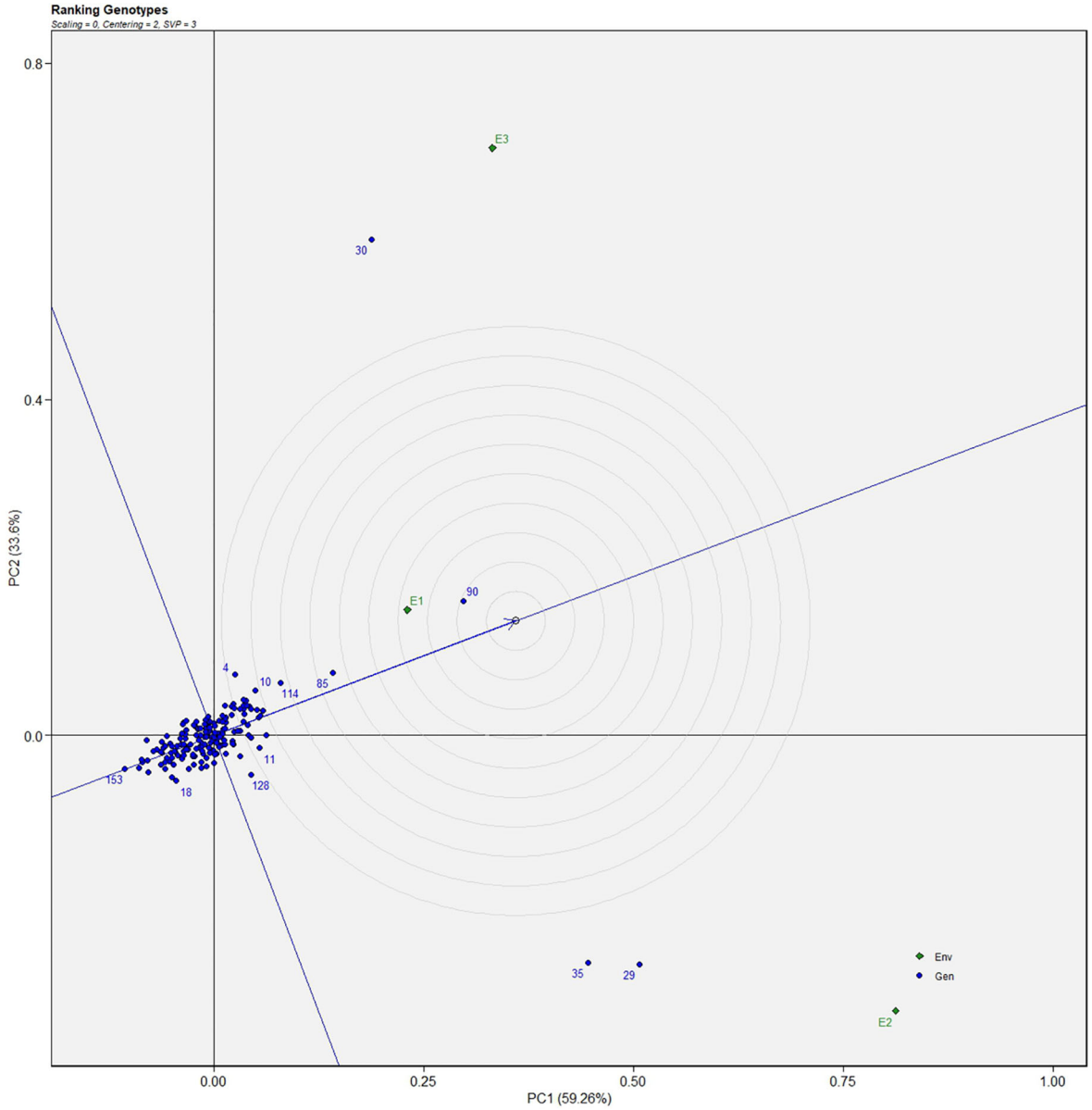


FIGURE 8
GGE-biplot based on genotype and environment-focused scaling for the comparison of genotype and environments for the weight of fruit.



10.3389/fpls.2023.1143778

10.3389/fpls.2023.1143778

TABLE 3 Shukla's variance on the three-year data for solasodine content and weight of fruit for *Solanum khasianum* germplasm that was used in the study.

| Shukla's variance for solasodine content | | | | | | Shukla's variance for fresh fruit weight per plant | | | | | |
|---|---|---|---|---|---|---|---|---|---|---|---|
| GEN | Y | GEN | Y | GEN | Y | GEN | Y | GEN | Y | GEN | Y |
| 1 | 1.321 | 63 | 1.158 | 125 | 0.894 | 1 | 0.197 | 63 | 0.169 | 125 | 0.172 |
| 2 | 0.812 | 64 | 0.98 | 126 | 0.914 | 2 | 0.192 | 64 | 0.174 | 126 | 0.169 |
| 3 | 0.81 | 65 | 1.094 | 127 | 0.833 | 3 | 0.196 | 65 | 0.173 | 127 | 0.176 |
| 4 | 0.811 | 66 | 0.896 | 128 | 0.932 | 4 | 0.197 | 66 | 0.185 | 128 | 0.195 |
| 5 | 0.827 | 67 | 0.862 | 129 | 1.023 | 5 | 0.184 | 67 | 0.159 | 129 | 0.153 |
| 6 | 0.858 | 68 | 1.028 | 130 | 0.907 | 6 | 0.196 | 68 | 0.158 | 130 | 0.149 |
| 7 | 0.831 | 69 | 0.942 | 131 | 0.924 | 7 | 0.177 | 69 | 0.155 | 131 | 0.179 |
| 8 | 0.847 | 70 | 1.076 | 132 | 0.927 | 8 | 0.195 | 70 | 0.208 | 132 | 0.167 |
| 9 | 0.918 | 71 | 1.015 | 133 | 0.911 | 9 | 0.179 | 71 | 0.191 | 133 | 0.135 |
| 10 | 0.842 | 72 | 0.943 | 134 | 0.895 | 10 | 0.208 | 72 | 0.166 | 134 | 0.171 |
| 11 | 0.832 | 73 | 1.015 | 135 | 0.894 | 11 | 0.198 | 73 | 0.161 | 135 | 0.123 |
| 12 | 0.978 | 74 | 0.872 | 136 | 1.054 | 12 | 0.186 | 74 | 0.140 | 136 | 0.144 |
| 13 | 0.882 | 75 | 0.915 | 137 | 1.048 | 13 | 0.197 | 75 | 0.167 | 137 | 0.169 |
| 14 | 0.872 | 76 | 0.876 | 138 | 0.891 | 14 | 0.154 | 76 | 0.160 | 138 | 0.136 |
| 15 | 0.883 | 77 | 0.886 | 139 | 0.903 | 15 | 0.181 | 77 | 0.164 | 139 | 0.161 |
| 16 | 0.815 | 78 | 0.935 | 140 | 0.863 | 16 | 0.194 | 78 | 0.166 | 140 | 0.146 |
| 17 | 0.864 | 79 | 0.838 | 141 | 0.928 | 17 | 0.200 | 79 | 0.171 | 141 | 0.169 |
| 18 | 0.843 | 80 | 1.015 | 142 | 1.021 | 18 | 0.141 | 80 | 0.155 | 142 | 0.135 |
| 19 | 0.846 | 81 | 0.951 | 143 | 0.903 | 19 | 0.182 | 81 | 0.153 | 143 | 0.159 |
| 20 | 0.971 | 82 | 0.881 | 144 | 1.071 | 20 | 0.162 | 82 | 0.195 | 144 | 0.139 |
| 21 | 0.842 | 83 | 0.945 | 145 | 0.922 | 21 | 0.151 | 83 | 0.155 | 145 | 0.168 |
| 22 | 0.923 | 84 | 0.88 | 146 | 1.147 | 22 | 0.189 | 84 | 0.194 | 146 | 0.140 |
| 23 | 0.867 | 85 | 0.953 | 147 | 0.996 | 23 | 0.174 | 85 | 0.259 | 147 | 0.171 |
| 24 | 0.875 | 86 | 0.982 | 148 | 1.082 | 24 | 0.191 | 86 | 0.203 | 148 | 0.132 |
| 25 | 0.908 | 87 | 0.893 | 149 | 0.774 | 25 | 0.149 | 87 | 0.171 | 149 | 0.123 |
| 26 | 0.861 | 88 | 0.945 | 150 | 1.007 | 26 | 0.162 | 88 | 0.166 | 150 | 0.155 |
| 27 | 0.903 | 89 | 0.941 | 151 | 0.886 | 27 | 0.173 | 89 | 0.157 | 151 | 0.151 |
| 28 | 0.828 | 90 | 1.055 | 152 | 0.953 | 28 | 0.193 | 90 | 0.351 | 152 | 0.177 |
| 29 | 1.12 | 91 | 0.868 | 153 | 1.014 | 29 | 0.343 | 91 | 0.157 | 153 | 0.111 |
| 30 | 0.997 | 92 | 0.865 | 154 | 0.987 | 30 | 0.337 | 92 | 0.163 | 154 | 0.171 |
| 31 | 0.857 | 93 | 1.034 | 155 | 0.998 | 31 | 0.172 | 93 | 0.159 | 155 | 0.196 |
| 32 | 0.975 | 94 | 1.004 | 156 | 0.9 | 32 | 0.176 | 94 | 0.163 | 156 | 0.147 |
| 33 | 0.99 | 95 | 0.91 | 157 | 0.885 | 33 | 0.169 | 95 | 0.180 | 157 | 0.139 |
| 34 | 0.946 | 96 | 0.893 | 158 | 0.868 | 34 | 0.192 | 96 | 0.165 | 158 | 0.143 |
| 35 | 0.915 | 97 | 0.957 | 159 | 0.841 | 35 | 0.317 | 97 | 0.166 | 159 | 0.151 |
| 36 | 0.886 | 98 | 0.924 | 160 | 1.034 | 36 | 0.154 | 98 | 0.168 | 160 | 0.135 |
| 37 | 0.924 | 99 | 0.902 | 161 | 0.913 | 37 | 0.181 | 99 | 0.172 | 161 | 0.143 |
| 38 | 0.968 | 100 | 0.904 | 162 | 0.886 | 38 | 0.175 | 100 | 0.181 | 162 | 0.139 |

*(Continued)*

TABLE 3 Continued

| Shukla's variance for solasodine content | | | | | | Shukla's variance for fresh fruit weight per plant | | | | | |
|---|---|---|---|---|---|---|---|---|---|---|---|
| GEN | Y | GEN | Y | GEN | Y | GEN | Y | GEN | Y | GEN | Y |
| 39 | 0.925 | 101 | 1.002 | 163 | 0.922 | 39 | 0.164 | 101 | 0.187 | 163 | 0.124 |
| 40 | 0.878 | 102 | 0.851 | 164 | 0.907 | 40 | 0.175 | 102 | 0.179 | 164 | 0.177 |
| 41 | 0.9 | 103 | 1.008 | 165 | 1.072 | 41 | 0.171 | 103 | 0.188 | 165 | 0.141 |
| 42 | 0.893 | 104 | 0.928 | 166 | 1.14 | 42 | 0.156 | 104 | 0.167 | 166 | 0.126 |
| 43 | 0.89 | 105 | 0.88 | 167 | 0.984 | 43 | 0.169 | 105 | 0.176 | 167 | 0.133 |
| 44 | 0.936 | 106 | 0.93 | 168 | 0.974 | 44 | 0.169 | 106 | 0.178 | 168 | 0.146 |
| 45 | 0.897 | 107 | 0.947 | 169 | 1.201 | 45 | 0.167 | 107 | 0.205 | 169 | 0.137 |
| 46 | 0.894 | 108 | 0.855 | 170 | 0.874 | 46 | 0.166 | 108 | 0.164 | 170 | 0.169 |
| 47 | 0.915 | 109 | 0.87 | 171 | 1.07 | 47 | 0.170 | 109 | 0.197 | 171 | 0.166 |
| 48 | 0.903 | 110 | 1.011 | 172 | 0.903 | 48 | 0.179 | 110 | 0.173 | 172 | 0.171 |
| 49 | 0.903 | 111 | 0.901 | 173 | 1.015 | 49 | 0.183 | 111 | 0.186 | 173 | 0.168 |
| 50 | 0.864 | 112 | 0.838 | 174 | 0.976 | 50 | 0.147 | 112 | 0.168 | 174 | 0.179 |
| 51 | 0.83 | 113 | 0.834 | 175 | 0.888 | 51 | 0.163 | 113 | 0.137 | 175 | 0.145 |
| 52 | 0.887 | 114 | 0.892 | 176 | 0.835 | 52 | 0.172 | 114 | 0.225 | 176 | 0.143 |
| 53 | 0.934 | 115 | 0.956 | 177 | 0.933 | 53 | 0.166 | 115 | 0.202 | 177 | 0.165 |
| 54 | 0.933 | 116 | 0.998 | 178 | 0.97 | 54 | 0.169 | 116 | 0.175 | 178 | 0.152 |
| 55 | 0.89 | 117 | 0.893 | 179 | 0.907 | 55 | 0.181 | 117 | 0.172 | 179 | 0.143 |
| 56 | 0.96 | 118 | 0.891 | 180 | 0.91 | 56 | 0.175 | 118 | 0.182 | 180 | 0.178 |
| 57 | 0.837 | 119 | 1.018 | 181 | 0.822 | 57 | 0.177 | 119 | 0.157 | 181 | 0.171 |
| 58 | 0.903 | 120 | 0.853 | 182 | 0.944 | 58 | 0.197 | 120 | 0.203 | 182 | 0.188 |
| 59 | 0.891 | 121 | 0.903 | 183 | 0.876 | 59 | 0.157 | 121 | 0.160 | 183 | 0.138 |
| 60 | 0.94 | 122 | 0.881 | 184 | 0.887 | 60 | 0.172 | 122 | 0.156 | 184 | 0.149 |
| 61 | 0.942 | 123 | 1.015 | 185 | 0.927 | 61 | 0.168 | 123 | 0.127 | 185 | 0.167 |
| 62 | 0.91 | 124 | 1.06 | 186 | 0.896 | 62 | 0.203 | 124 | 0.174 | 186 | 0.186 |

GEN, genotype; Y, variance response.

## 5 Conclusions

The natural source of solasodine from *S. khasianum* is an important medicinal plant species. The identification of high fruit-yielding and solasodine-rich germplasm is significant for the commercial success of the industrially important solasodine. The multivariate stability analysis is a novel approach that provides an easy way to select high-performance and stable lines in *S. khasianum* that performs better under varied environmental conditions. On the basis of the present study, lines no. 90, 85, 70, 107, and 62 were identified as stable and high-yielding fruit yields per plant. Further, lines no. 1, 146, and 68 were identified as stable and high-solasodine lines. MTSI analysis revealed lines 1, 85, 70, 155, 71, 114, 65, 86, 62, 116, 32, and 182 as stable for both high yielders, high fruit yields, and high solasodine lines. The large-scale cultivation of this germplasm can prove to be a cheap natural source of steroidal alkaloid solasodine. Moreover, the AMMI, GGE, MTSI, and

TABLE 4 Estimates of selection differential, selection gain, and heritability based on MTSI for 186 *S. khasianum* germplasm across three environments.

| VAR | Factor | Xo | Xs | SD | SD % | $h^2$ | SG | SG % |
|---|---|---|---|---|---|---|---|---|
| FWP | FA 1 | 0.172324 | 0.195579 | 0.023256 | 13.49529 | 0.520354 | 0.012101 | 7.022332 |
| SOL | FA 1 | 0.929534 | 1.010556 | 0.081022 | 8.716357 | 0.873092 | 0.070739 | 7.610179 |

Xo, Overall mean of genotypes; Xs, Mean of the selected genotypes; SD, Selection differential; SG, Selection gain or impact; $h^2$, heritability; FWP, fresh fruit weight/plant; SOL, Solasodine content.

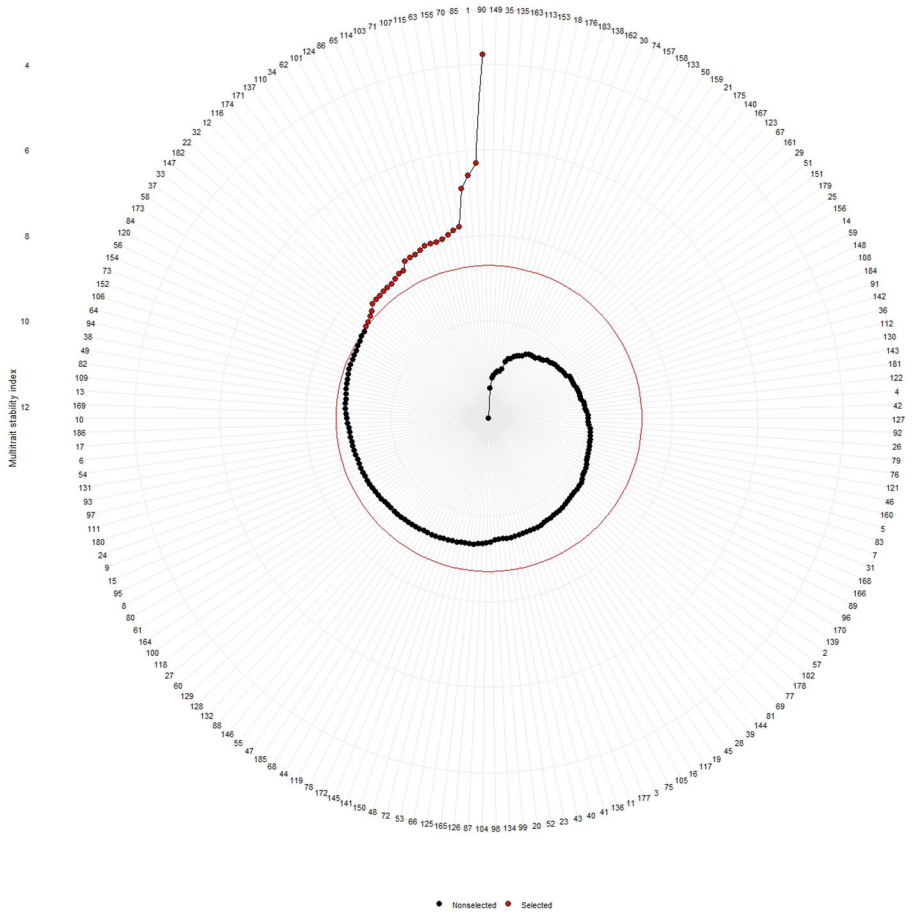


FIGURE 9
Multi trait stability index (MTSI) of 186 germplasm of *S. khasianum* based on the traits of solasodine content and weight of fruit.

Shukla's variance models were found to be effective plant breeding models for the evaluation of stability which would maximize the utilization of resources thereby making a significant contribution to the sustainability of breeding programs. The identified genotypes of the study can be utilized for commercial cultivation and can be useful in future breeding programs.

## Data availability statement

The original contributions presented in the study are included in the article/Supplementary Material. Further inquiries can be directed to the corresponding author.

## Author contributions

TB: wrote the original draft, methodology, and edited the manuscript; SM: software analysis; TG: wrote the original draft; RG: editing; VKC: data curation; SC: formal analysis and visualization; HL: data curation and formal analysis; GNS: editing and supervision; ML: conceptualization, methodology, editing, validation, and supervision. All authors contributed to the article and approved the submitted version.

## Funding

The present work was supported by NMPB, New Delhi, Ministry of Ayush, govt. of India in the form of project no. R&D/AS-01/2018-19.

## Acknowledgments

The authors are thankful to the Director, CSIR-NEIST, Jorhat, for providing the laboratory and field facility of the institute.

## Conflict of interest

The authors declare that the research was conducted in the absence of any commercial or financial relationships that could be construed as a potential conflict of interest.

## Publisher's note

All claims expressed in this article are solely those of the authors and do not necessarily represent those of their affiliated organizations, or those of the publisher, the editors and the reviewers. Any product that may be evaluated in this article, or claim that may be made by its manufacturer, is not guaranteed or endorsed by the publisher.

## Supplementary material

The Supplementary Material for this article can be found online at: https://www.frontiersin.org/articles/10.3389/fpls.2023.1143778/full#supplementary-material

## References


Almohammedi, O. H. M., Al-Abdaly, M. M., and Mahmod, S. A. (2019). Study of genotype and environmental interaction on yield analysis of tuber of potato (*Solanum tuberosum* l.) using AMMI in Iraq. *Plant Arch.* 19 (1), 978–982.

Alwala, S., Kwolek, T., McPherson, M., Pellow, J., and Meyer, D. (2010). A comprehensive comparison between Eberhart and Russell joint regression and GGE biplot analyses to identify stable and high yielding maize hybrids. *Field Crops Res.* 119, 225–230. doi: 10.1016/j.fcr.2010.07.010

Annicchiarico, P. (2002). *Genotype × environmental interactions; challenges and opportunities for plant breeding and cultivar recommendations. FAO plant production and protection Paper.174* (Rome: FAO).

Bagheri, M., Keshavarz, S., and Kakhki, A. (2016). Evaluation of selected lines from eggplant (*Solanum melongena* l.) landraces. *J. Seed Plant Breed.* 32-1 (2), 165–180. doi: 10.22092/SPIJ.2017.111295

Begum, T., Munda, S., Pandey, S. K., and Lal, M. (2022). Estimation of selection criteria through multi-year assessment of variability parameters, association studies and genetic diversity of *Solanum khasianum* CB Clarke. *Sci. Hortic.* 297, 110923. doi: 10.1016/j.scienta.2022.110923

Bernardo, R. (2002). Reinventing quantitative genetics for plant breeding: something old, something new, something borrowed, something BLUE. *Heredity* 125, 375–385. doi: 10.1038/s41437-020-0312-1

Bigonah, H. H. (2012). Yield stability of promising lines of winter and facultative wheat in different climate of Iran. *Afr. J. Agric. Res.* 7 (15), 2304–2311. doi: 10.5897/AJAR11.931

Canter, P. H., Thomas, H., and Ernst, E. (2005). Bringing medicinal plants into cultivation: opportunities and challenges for biotechnology. *Trend Biotechnol.* 23, 180–185. doi: 10.1016/j.tibtech.2005.02.002

Chirumamilla, P., Gopu, C., Jogam, P., and Taduri, S. (2021). Highly efficient rapid micropropagation and assessment of genetic fidelity of regenerants by ISSR and SCoT markers of *Solanum khasianum* Clarke. *Plant Cell Tissue Organ Cult.* 144 (2), 397–407. doi: 10.1007/s11240-020-01964-6

Damavandi-Kamali, S., Babaeian, J. N., and Aalishah, A. (2011). Evaluation of stability and compatibility of the yield of cotton varieties based on one-variable parametric and non-parametric methods and AMMI model. *Iranian J. Crop Sci.* 42 (2), 397–407.

Das, S., Mitra, B., Luthra, S. K., Saha, A., Hassan, M. M., and Hossain, A. (2021). Study on morphological, physiological characteristics and yields of twenty-one potato (*Solanum tuberosum* l.) cultivars grown in Eastern Sub-Himalayan plains of India. *Agron* 11, 335. doi: 10.3390/agronomy11020335

Fufa, T. W., and Fufa, A. N. (2021). Yield stability analysis of elite Irish potato (*Solanum tuberosum* l.) varieties in Western Ethiopia. *In. J. Biochem. Biophy Mol. Biol.* 6 (1), 6–10. doi: 10.11648/j.ijbbmb.20210601.13

Gogoi, R., Sarma, N., Pandey, S. K., and Lal, M. (2021). Phytochemical constituents and pharmacological potential of *Solanum khasianum* C.B. clarke., extracts: special emphasis on its skin whitening, anti-diabetic, acetylcholinesterase, genotoxic activities. *Trends Phytochem. Res.* 5 (2), 47–61. doi: 10.30495/TPR.2021.1917249.1190

Gramazio, P., Chatziefstratiou, E., Petropoulos, C., Chioti, V., Mylona, P., Kapotis, G., et al. (2019). Multi-level characterization of eggplant accessions from Greek islands and the mainland contributes to the enhancement and conservation of this germplasm and reveals a large diversity and signatures of differentiation between both origins. *Agronomy* 9 (887), 1–20. doi: 10.3390/agronomy9120887

Gupta, S. (2019). *In-vitro* anti-inflammatory activity of s. xanthocarpum and *A. ofcinarum* herb by human red blood cell membrane stabilization method. *J. Drug Deliv.Ther.* 9 (3), 9663–9666. doi: 10.22270/jddt.v9i3-s2948

Gupta, P., Dhawan, S. S., and Lal, R. K. (2015). Adaptability and stability based differentiation and selection in aromatic grasses (*Cymbopogon* species) germplasm. *Ind. Crop Prod.* 78, 1–8. doi: 10.1016/j.indcrop.2015.10.018

Hashemi, A., Nematzadeh, G. A., Oladi, M., Afkhami, G. A., and Gholizadeh, G. A. (2018). Study of rapeseed (*Brassica napus*) promising genotypes adaptation in different regions of mazandaran. *J. Crop Breed.* 10 (28), 119–124. doi: 10.29252/jcb.10.28.119

Julsing, M. K., Quax, W. J., and Kysar, O. (2007). The engineering of medicinal plants prospects and limitation of medicinal biotechnology. *Med. Plant Biotechnol.* 3, 6. doi: 10.1002/9783527619771.ch1

Kaunda, J. S., and Zhang, Y. J. (2019). The genus solanum: an ethnopharmacological, phytochemical and biological properties review. *Nat. Products Bioprospect* 9, 77–137. doi: 10.1007/s13659-019-0201-6

Khankahdani, H. H., Bagheri, M., and Khoshkam, S. (2022). Stability and compatibility of some Iranian eggplant (*Solanum melongena* l.) lines using AMMI method. *Int. J. Hortic. Sci. Technol.* 9 (1), 52–39. doi: 10.22059/ijhst.2020.301667.364

Koocheki, A. R., Sorkhi, B., and Eslamzadeh, H. M. R. (2012). Study on stability of elite barley (*Hordeum vulgar* l.) genotypes for cold regions of Iran using AMMI method. *Cereal Res.* 2 (4), 249–261. doi: 20.1001.1.22520163.1391.2.4.1.7

Kumar, R., Khan, M. I., and Prasad, M. (2019). Solasodine: A perspective on their roles in health and disease. *Res. J. Pharm. Technol.* 12 (5), 2571–2576. doi: 10.5958/0974-360X.2019.00432.3

Lal, M., Munda, S., Begum, T., Gupta, T., Paw, M., Chanda, S. K., et al. (2022b). Identification and registration for high-yielding strain through ST and MLT of *Curcuma caesia* Roxb.(Jor Lab KH-2): A high-value medicinal plant. *Genes* 13 (10), 1807. doi: 10.3390/genes13101807

Lal, M., Munda, S., Bhandari, S., Saikia, S., Begum, T., and Pandey, S. K. (2022a). Molecular genetic diversity analysis using SSR marker amongst high solasodine content lines of *Solanum khasianum* C.B. Clarke, an industrially important plant. *Ind. Crops Prod.* 184, 115073. doi: 10.1016/j.indcrop.2022.115073

Lal, M., Munda, S., Gogoi, A., Begum, T., Baruah, J., Chanda, S. K., et al. (2022c). Use of stability statistics in the selection of *Clausena heptaphylla* (Roxb.) Wight & arn for novel anethole rich strain (Jor Lab CH-2). *Front. Plant Sci.* 13, 1060492. doi: 10.3389/fpls.2022.1060492

Manzano, S., Navarro, P., Martínez, C., Megías, Z. M., Rebolloso, M. M., and Jamilena, M. (2015). Evaluation of fruit quality in tomato landraces under organic greenhouse conditions. *Acta Hortic* 1099, 645–652. doi: 10.3389/fpls.2018.10491

Missio, J. C., Rivera, A., Figàs, M. R., Casanova, C., Camí, B., Soler, S., et al. (2018). A comparison of landraces vs. modern varieties of lettuce in organic farming during the winter in the Mediterranean area: an approach considering the viewpoints of breeders, consumers, and farmers. *Front. Plant Sci.* 9 (1491), 1–15.

Munda, S., Paw, M., Saikia, S., Begum, T., Baruah, J., and Lal, M. (2023). Stability and selection of trait specific genotypes of *Curcuma caesia* roxb. using AMMI, BLUP, GGE, WAAS and MTSI model over three years evaluation. *JARMAP* 32, 100446. doi: 10.1016/j.jarmap.2022.100446

Munda, S., Sarma, N., and Lal, M. (2020). GxE interaction of 72 accessions with three year evaluation of *Cymbopogon winterianus* jowitt. using regression coefficient and additive main effects and multiplicative interaction model (AMMI). *Ind. Crop Prod.* 146, 112169. doi: 10.1016/j.indcrop.2020.112169

Olivoto, T., L'ucio, A. D. C., da silva, J. A. G., Marchioro, V. S., de Souza, V. Q., and Jost, E. (2019). Mean performance and stability in multi-environment trials I: combining features of AMMI and BLUP techniques. *Agron. J* 111, 2949–2960. doi: 10.2134/agronj2019.03.0220

Pavani, C., and Shasthree, T. (2021). Biological activity of green synthesized silver nanoparticles and different plant extracts of *Solanum khasianum* Clarke. *Int. Res. J. Adv. Sci. Hub.* 3, 12–17. doi: 10.47392/irjash.2021.103

Rosangkima, G., and Jagetia, G. C. (2015). *In-vitro* anticancer screening of medicinal plants of mizoram state, India, against dalton's lymphoma, MCF-7 and HELA cells. *Int. J. Recent Sci. Res.* 6, 5648–5653.

Sadeghi, S. M., and Samizadeh, H. (2011). Evaluation of yield stability of Virginia tobacco hybrids using stability parameters and pattern analysis *via* AMMI model. *Electronic J. Crop Prod.* 4 (2), 103–119. https://www.sid.ir/paper/134936/en.

Sadeghzadeh, B., Mohammadi, R., Ahmadi, H., Abedi, G., Ahmadi, M. M., Mohammadfam, M., et al. (2018). GGE biplot and AMMI application in the study of adaptability and grain yield stability of durum wheat lines under dryland conditions. *Env. Stresses Crop Sci.* 11 (2), 241–260. doi: 10.22077/escs.2018.381.1075

Sanwal, C. S., Kumar, R., Anwar, R., Kakade, V., Kerketta, S., and Bhardwaj, S. D. (2016). Growth and yield of *Solanum khasianum* in *Pinus roxburghii* forest based silvi-medicinal system in mid hills of Indian himalaya. *Ecosyst* 3, 19. doi: 10.1186/S40663-016-0078-3

Scavo, A., Mauromicale, G., and Ierna, A. (2023). Genotype × environment interactions of potato tuber quality characteristics by AMMI and GGE biplot analysis. *Scientia Hortic.* 310, 111750. doi: 10.1016/j.scienta.2022.111750

Schmelzer, G. H., and Gurib, F. A. (2008). "Medicinal plants 1," in *Plant resources of tropical Africa, Netherlands*, vol. 11. (Netherlands: PROTA Foundation), 518–520.

Sinani, S. S. S., and Eltayeb, E. A. (2017). The steroidal glycoalkaloids solamargine and solasonine in solanum plants. *S. Afr. J. Bot.* 112, 253–269. doi: 10.1016/j.sajb.2017.06.002

Soltan Mohamadi, S., Peyghambri, S. A., and Babaei, H. R. (2017). Study the adaptability and yield sustainability of soybean genotypes in four regions of Iran. *Iranian. J. Crop Sci.* 48 (2), 389–397. doi: 10.22059/IJFCS.2017.63482

Sousaraei, N., Mashayekhi, K., Mousavizadeh, S. J., Akbarpour, V., Medina, J., and Aliniaeifard, S. (2021). Screening of tomato landraces for drought tolerance based on growth and chlorophyll fluorescence analyses. *Hortic. Env. Biotech.* 62, 521–535. doi: 10.1007/s13580-020-00328-5

Srivastava, M., Sharma, S., and Misra, P. (2016). Elicitation based enhancement of secondary metabolites in *Rauwolfia serpentina* and *Solanum khasianum* hairy root cultures. *Pharmacogn. Mag* Suppl. 3, S315–S320. doi: 10.4103/0973-1296.185726

Taher, D., Solberg, S., Prohens, J., Chou, Y., Rakha, M., and Wu, T. (2017). World vegetable center eggplant collection: origin, composition, seed dissemination and utilization in breeding. *Front. Plant Sci.* 8 (1484), 1–12. doi: 10.3389/fpls.2017.01484

Tembe, K. O., Chemining'wa, G., Ambuko, J., and Owino, W. (2018). Evaluation of African tomato landraces (*Solanum lycopersicum*) based on morphological and horticultural traits. *Agricu. Nat. Resources* 52, 536–542. doi: 10.1016/j.anres.2018.11.014

Tonk, F. A., Ilker, E., and Tosun, M. (2011). Evaluation of genotype X environment interactions in maize hybrids using GGE biplot analysis. *Crop Breed. App. Biotech.* 11, 1–9. doi: 10.1590/S1984-70332011000100001

Weissenberg, M. (2001). Isolation of solasodine and other steroidal alkaloids and sapogenins by direct hydrolysis-extraction of solanum plants or glycosides there from. *Phytochem* 58 (3), 501–508. doi: 10.1016/S0031-9422(01)00185-6

frontiers | Frontiers in Plant Science

TYPE Original Research
PUBLISHED 03 July 2023
DOI 10.3389/fpls.2023.1149669



OPEN ACCESS

EDITED BY
Weibiao Liao,
Gansu Agricultural University, China

REVIEWED BY
Dinesh Joshi,
ICAR-Vivekananda Institute of Hill Agriculture, India
Amin Ebrahimi,
Shahrood University of Technology, Iran

*CORRESPONDENCE
Suping Gao
gao_suping@sicau.edu.cn

RECEIVED 22 January 2023
ACCEPTED 06 June 2023
PUBLISHED 03 July 2023

CITATION
Li Y, Cheng X, Lai J, Zhou Y, Lei T, Yang L, Li J, Yu X and Gao S (2023) ISSR molecular markers and anatomical structures can assist in rapid and directional screening of cold-tolerant seedling mutants of medicinal and ornamental plant in *Plumbago indica* L.
*Front. Plant Sci.* 14:1149669.
doi: 10.3389/fpls.2023.1149669



# ISSR molecular markers and anatomical structures can assist in rapid and directional screening of cold-tolerant seedling mutants of medicinal and ornamental plant in *Plumbago indica* L.

Yirui Li, Xu Cheng, Junlin Lai, Yunzhu Zhou, Ting Lei, Lijuan Yang, Jiani Li, Xiaofang Yu and Suping Gao*

College of Landscape Architecture, Sichuan Agricultural University, Chengdu, China

*Plumbago indica* L. is a perennial herb with ornamental and anticancer medicinal functions widely distributed in the tropics. It is affected by temperature and cannot bloom normally in colder subtropical regions, which seriously affects its ornamental value. To create low-temperature resistance mutants and enrich new germplasm resources, this study used tissue culture and chemical reagent (0.5 mmol/L $NaN_3$) and low-temperature stress (0°C, full darkness for 48h) induction to target and screen for cold-resistance mutants. The results showed that the ISSR band polymorphism ratio of the 24 suspected mutant materials was 87.5%. The DNA profiles of the 9 mutants initially identified were altered. The content of plumbagin in the stems and leaves of the mutants was examined, and it was found that the accumulation in the leaves of the mutant SA24 could be as high as 3.84 times that of the control, which was 0.5991%. There were significant differences in the anatomical structures of roots, stems and leaves. The mutants mostly exhibited reduced root diameter (only 0.17-0.69 times that of CK), increased stem diameter (up to 2.19 times that of CK), enlarged mesophyll cells, increased thickness (up to 1.83 times that of CK) and high specificity, which are thought to be important for the different cold resistance obtained by the mutants. In the cold resistance experiment, four cold-tolerant mutants were successfully screened according to their morphological characteristics and physiological indexes, and the mutagenesis efficiency could be as high as 2.22% and did not affect the accumulation of plumbagin in their stems and leaves, even higher than CK. The responses of the screened mutants SA15, SA19, SA23 and SA24 to low temperature showed slower leaf wilting, higher light energy conversion efficiency, less accumulation of MDA content, increased enzymatic activities of antioxidant enzymes (SOD, CAT, POD) and more accumulation of soluble sugars and proline content. These characteristics are consistent with the response of cold-resistance plants to low temperatures. The cold- resistance mutants cultivated in soil were observed of agronomic and ornamental traits for one year, mainly manifested as delayed flowering and

delayed entry into the senescence stage. This study provides a more rapid and accurate technique for identifying and screening cold-tolerant mutants, and lays the foundation for future experiments on the creation of new cold-resistant varieties.

KEYWORDS

**combined tissue culture and chemical mutagenesis techniques, ISSR analysis, anatomical structure, targeted screening for cold-resistant mutants, cold resistance evaluation**

## 1 Introduction

Cold is one of the major environmental stresses that limit plant growth and development, affects geographic distribution, and significantly reduces plant biomass. The increasing frequency and severity of extreme weather and climate events are one of the most pressing threats facing humanity today (Robinson, 2021; Liu et al., 2022). Extreme environmental changes have led to serious threats to the survival and growth of ornamentals introduced and cultivated from higher heat locations (Zheng et al., 2022). These plants are usually subjected to cold stress at temperatures below 10°C, or even higher (Zhuang et al., 2021).Cold damage leads to complex changes in plant morphology, physiology and biochemistry, which trigger complex cellular tissue dysfunction in plants (Knight and Knight, 2012), such as epidermal tissue damage or even necrosis in plant organs (Chen et al., 2020b). Plants establish cold acclimation in order to overcome the stress caused by exposure to freezing-injurious environments through complex biological system regulation that induces changes affecting biomass such as lignin in nutrient organs such as rhizomes (Podgorbunskikh et al., 2020), as well as changes in photosynthesis, enzyme activity, carbon metabolism, and protein metabolism *in vivo* (Theocharis et al., 2012).

*Plumbago indica* L. is a tropical evergreen perennial plant of the genus Plumbago in the family Plumbaginaceae. In China, it is native to areas such as Yunnan (Hekou), Guangdong and Hainan provinces, where heat accumulation is high. Its corolla is purplish red or crimson and flowers from November to April (in some places it blooms all year round). Its root secondary metabolite, plumbagin, is also utilized as an anticancer (Li et al., 2014; Vasav et al., 2020) and antibacterial (Venkateswarulu et al., 2018) drug ingredient. This is introduced to the subtropical region (Chengdu region, for example), and the temperature starts to drop in November every year. Although the flower buds can be differentiated normally and some branches can form flakes, the low temperature at the time of flowering has a serious impact on the complete unfolding of the petals, resulting in a serious shortening of the flowering period and a major loss of ornamental value (Figure 1). Therefore, improving

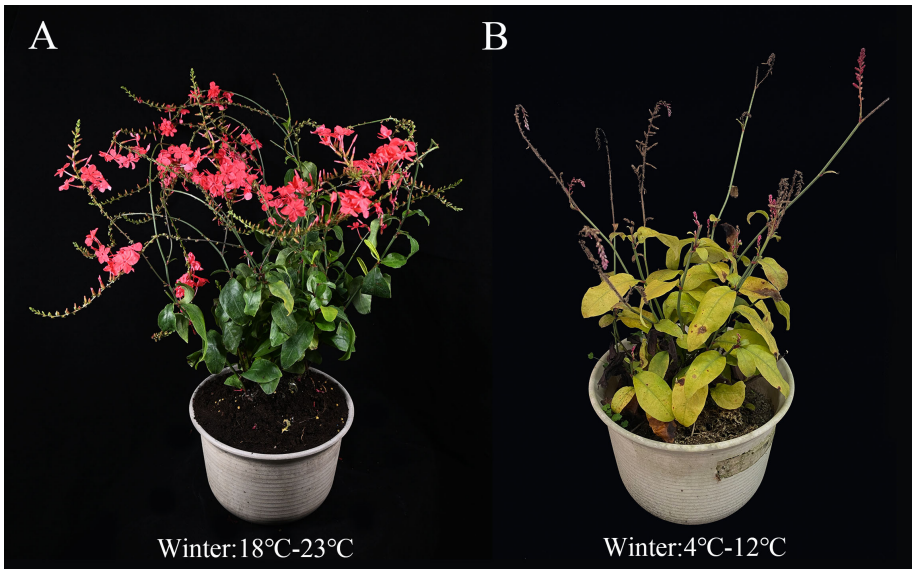


FIGURE 1
Comparison diagram of growth status of *Plumbago indica* L. wild planted in Hainan province and Sichuan province from December to February (winter average temperature). **(A)**, cultivated in Hainan province; **(B)**, cultivated in Sichuan province.

its cold tolerance is an important goal for breeding. Since *Plumbago indica* L. is a heterostylous plant and has not been seen to bear fruit in nature, it is difficult to improve its cold hardiness by cross breeding. Integrated tissue culture and chemical mutagenesis for mutant induction provides a new breeding technique for creating new cold-tolerant mutant materials that can shorten breeding cycles and accelerate breeding programs (Shi et al., 2022) and has been successfully applied to several plants, including rice (Chen et al., 2013), *Cerastigma willmottianum* Stapf (Shi et al., 2022), olive (Sheikh and Moradnejad, 2014).

Traditional plant breeding utilizes natural mutation that can randomly produce a number of variant traits, and since the discovery of mutagens, various mutagenesis methods have been widely used in plant molecular breeding to identify new traits conferred to plants (Shelake et al., 2019). The use of DNA technology, mutation breeding to create new varieties in response to abiotic stresses has become a popular research theme (Janni et al., 2020). Among them, the effect of chemical mutagens can be detected by morphological characteristics, genetic mapping and changes in chromosome number (Chaudhary et al., 2019). Traditionally morphological character changes can be used to screen for mutants. However, this method is both time-consuming and unreliable due to environmental and multiple factors. In addition, mutations in many plant genes may not result in readily identifiable phenotypes. Molecular markers have been used for genetic identification and improvement of many crop species. Recently, molecular breeding and traditional breeding techniques have been used to obtain new varieties (Gentile and La Malfa, 2019). Therefore, direct selection based on DNA markers circumvents these limitations, thereby increasing efficiency and reducing the cost and time of selection.

Molecular marker technologies have different approaches based on different principles, but all contribute to the successful identification of variation loci in the whole genome (Polat et al., 2015). Among them, ISSR has been widely used to assess plant genetic diversity, genetic stability, and the identification and screening of mutant plants (Wu et al., 2020). The advantage of this technique is that the designed microsatellite sequences are randomly distributed in the plant, deletions/duplications at binding sites can be used with ISSR primers, and multiple motifs can be detected simultaneously with high reliability and reproducibility (Li et al., 2018a), making it particularly suitable for the analysis of many mutants with limited genetic variation. This technique has been used previously in the screening of mutants in several ornamental plants, such as tulips (Li et al., 2022c), chrysanthemums (Wu et al., 2020), and has also worked well. Therefore, the present study uses ISSR-PCR markers combined with anatomical structural features of nutrient organs to identify mutant ideas, which is a combination of microscopic and macroscopic identification tools, and provides a practical technical solution for the identification of new mutant materials created by tissue culture and chemical mutagenesis ($NaN_3$) in *Plumbago indica* L. Meanwhile, artificial low temperature stress experiments using plant tissue culture ex vivo platform provide a new pathway for rapid screening of cold-tolerant mutant strains for early targeted breeding.

## 2 Materials and methods

### 2.1 Plant materials

The experimental materials were cultivated species in Sanya, Hainan Province. After being introduced and cultivated from Chengdu, Sichuan Province, sterile seedlings were cultivated for mutation breeding (Figure 2). These were 26 plants 90 d tissue culture seedlings of the same genotype, which contained 24 suspected mutant plants and 2 wild control plants. The 24 suspected mutants were sourced from: A single-factor experiment was conducted to mutagenize the terminal buds of sterile seedlings of *Plumbago indica* L. using $NaN_3$ as mutagen. And it was set at 0

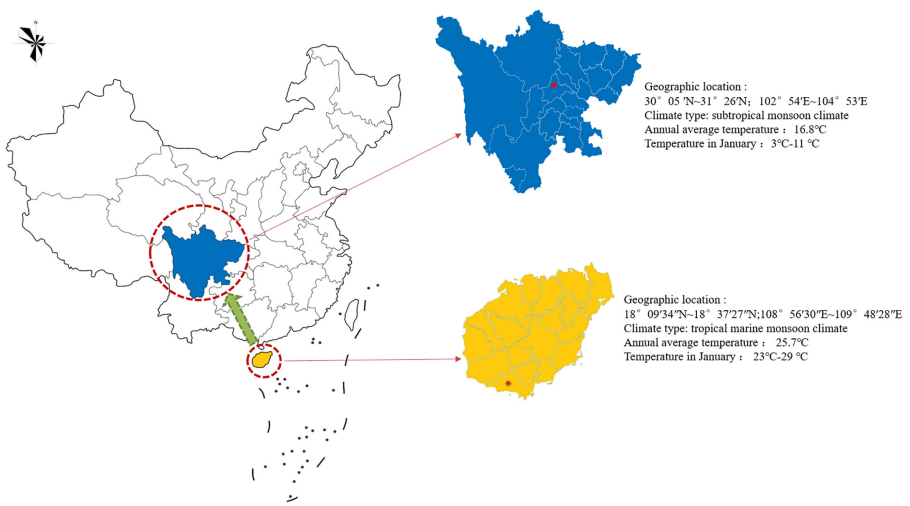


FIGURE 2
Geographical tagging of the research area in China. The red circle indicates the introduction or cultivation site of *Plumbago indica* L. in China, and the green arrow indicates the introduction and cultivation direction in China.

mmol/L, 0.1 mmol/L, and 0.2 mmol/L, 0.3 mmol/L, 0.4 mmol/L, 0.5 mmol/L, 0.6 mmol/L, 0.7 mmol/L, 0.8 mmol/L, 0.9 mmol/L; 0h, 0.5h, 1h, 2h, 4h, 8h; pH=3.0, $NaN_3$ concentration was referenced Sen (2016) and Szurman-Zubrzycka et al. (2018); single-factor experiments were used to mutate the terminal buds of *Plumbago indica* L. sterile seedlings (30 as a group, biological replicated 3 times), and the survival rate was counted after 20 d. The $LD_{50}$ was used as the best mutagenic formulation of $NaN_3$. Based on the pretreatment results, 180 sterile terminal buds ($VM_0$) from the same mother plant (60 in one group, biological replicates three times) were finally treated with *in vitro* chemical mutagenesis using the best $NaN_3$ mutagenesis formulation (0.5 mmol/L, 1 h, pH=3.0). The terminal buds of $VM_1$ were inoculated and succeeded as $VM_2$. And so on, successive successions were cultured for 5 generations to $VM_5$. Rooted plants were counted under environmental conditions of 25 ± 1°C, 12 h/d photoperiod, and 1500-2000 lx light intensity. After 30d acclimatization, the seedlings were transplanted to pots and cultivated for 90d, and plant morphological variation was observed and evaluated in the field. Plants with morphological variation rate greater than 25% were used as suspected mutant plants for this experiment, and a total of 24 suspected mutant plants were obtained. Two controls were wild-type plants without $NaN_3$ treatment, one treated with sterile water set as CK and one treated with phosphate buffer solution set as PBS.

## 2.2 ISSR molecular markers and analysis

The CTAB method was used to extract the total DNA from the young leaves of CK, PBS and 24 suspected mutant plants, respectively, and the extracted DNA was stored in a refrigerator at -20°C for backup. Synthesis of 100 universal primers (Sangon Biotech, Shanghai) published by UBC (University of British Columbia) for mutant plant screening. The optimized 25 μL ISSR-PCR amplification system (Li et al., 2022c) was 12.5 μL 2xPCR Master Mix, 1 μL template DNA, 1 μL primer, and 10.5 μL ddH2O. The PCR reaction system was pre-denatured at 95°C for 3 min, denatured at 95°C for 15 s, annealed at 61°C for 15 s, extended at 72°C for 1 min, 32 cycles, and then extended at 72°C for 5 min to complete the amplification and terminate the program at 12°C. The obtained products were used for gel electrophoresis experiments. The gel was evaluated on a 1.5% agarose gel with 10 μL TS-GelRed Ver.2 Nuclear Staining Dyes and 8 μL product, and the plate was run in 1× TAE buffer at 150 V for 20 min. After completing electrophoresis, pictures were taken and analyzed on a gel imaging system.

## 2.3 Plumbagin content of medicinal ingredients in stems and leaves by HPLC

9 plants from each of the CK and nine mutant strains (three plants per group in three biological replicates) were transplanted for 60 d, and fresh samples of stems and leaves were collected separately and stored in liquid nitrogen for freezing. The cryopreservation samples were dried at 65°C for 24h, followed by adjusting the temperature to 45°C and drying to constant weight, and then ground into powder for later using. Precisely weigh 0.10 g of sample powder, extract with 1 mL of methanol (HPLC, purity ≥ 99.9%) at ordinary temperature for 30 min by ultrasonication, collect the extract and filter using 0.22 μm microporous filter (Li et al., 2022c), and store the filtered extract at 4°C away from light. The analysis of plumbagin was performed by LabSolitions-PAD system. Experimental reference Nayak et al. (2015) experimental method, and the method was optimized the sample injection volumes were all 20 μL, and the separation was performed on a Shim-pack GIS C18 (4.6×250 mm, 5 μm) column at a flow rate of 1mL/min and a column temperature of 35°C. The mobile phase A was methanol and liquid B was 0.1% $H_3PO_4$ (vacuum filtered through a 0.45 μm filter membrane before use). The gradient elution steps were: 40% A, 60% B, 0 min; 75% A, 25% B, 21 min; 90% A, 10% B, 23 min; 90% A, 19% B, 30 min; 40% A, 60% B, 40 min. Plumbagin was detected at 254 nm. A linear regression equation $y$=8.20712×$10^7$x+151720.60002 ($R_2$ = 0.98543) was constructed for the quantitative analysis using plumbagin standard (CAS: 481-42-5, Solarbio, purity≥98%).

## 2.4 Analysis of cellular anatomy

At 9:00 a.m., 26 (including 2 controls) plants of 120d seedlings after acclimatization cultivation were taken for cytological observation of roots (main root maturation zone about 1 cm long), stems (about 1 cm long) and leaves (1 cm wide and 2 cm long). Samples were taken and fixed individually in microcentrifuge tubes containing FAA fixative. The slices were prepared by paraffin sectioning method, observed, measured and micrographically photographed with an Olympus BX53 fluorescent microscope (Li et al., 2022a), and the thickness of leaf spongy tissue (μm), fenestrated tissue thickness (μm), leaf thickness (μm), main vein thickness (μm), root diameter (μm), stem diameter (μm), and stem epidermal cell thickness (μm) were measured and counted.

## 2.5 Cold-tolerant mutant screening and identification

### 2.5.1 Low temperature stress treatment

The materials were identified mutant plants, seedlings aged 120d, and un-mutagenized wild-type plants of the same age were used as controls, and three pots of uniform growth each were selected for the cold stress experiment. Pre-treatment first: the mutant and control plants were pre-cultured in a light incubator (light intensity 3000 lx, light time 14h, day/night temperature 25/20°C, relative humidity 65%) for 3 d. Then the temperature was gradually lowered by 5°C for every 5 h interval (Zheng et al., 2022), and after 24h, the temperature was reduced to 0°C, at which point the low-temperature stress treatment was carried out: the design was 0°C with full dark period treatment. Ambient temperature of 25°C and a photoperiod of 12/12h were used as controls. After 48h of incubation, the plants were placed at room temperature for 24h to recover for morphological observation, and the leaves of mutant

and control plants were taken simultaneously by punching method, snap frozen in liquid nitrogen and stored in -80°C refrigerator for physiological index determination.

### 2.5.2 Preliminary identification of cold hardiness of mutant appearance and morphological index after low temperature treatment

During the low-temperature stress treatment, the morphological characteristics of *Plumbago indica* L. mutants and wild-type plants were observed, including leaf shape, leaf color, degree of leaf chlorosis, and curling or not. After the low-temperature treatment, the morphological injury indexes were observed after 24h of recovery at room temperature, and the preliminary identification of cold tolerance was carried out.

### 2.5.3 Identification of physiological and biochemical indicators of cold resistance in mutants after low temperature treatment

Seven time periods, 0, 3, 8, 16, 24, 36, and 48 h, were selected during the low temperature stress treatment for the determination of chlorophyll fluorescence kinetic parameters (Li et al., 2022b). The fluorescence parameters such as Fo, Fm, Fm/Fo, Fv/Fm were measured by Handy PEA plant efficiency meter after 30 min of dark acclimation by taking the vigorously growing leaves without pests and diseases in the upper middle part of the plant, avoiding the leaf veins as much as possible and making the leaves be evenly clamped in the leaf clips when measuring. In addition, the leaves of the mutant and control plants were taken after 48 h of low temperature treatment and 24 h of recovery, and the two materials at room temperature were used as controls (Peng et al., 2018). The MDA content was determined using the thiobarbituric acid (TBA) method (Janero, 1990; Chen et al., 2020a) SOD, CAT and POD activities, and soluble sugar content and proline (Pro) content were determined using kits (Li et al., 2022b).

### 2.5.4 Observation on field morphological indicators of cold resistant mutants

The consistent growth of *Plumbago indica* L. control and four mutant strains were selected for morphological observation. Three pots of each strain were selected and each pot was a biological replicate. Measurement method reference Shen et al. (2020).

Plant height: The vertical distance (cm) from the collar to the top of the plant was measured under natural conditions (no support with flower racks) (estimation: 0.01 cm).

Crown diameter: Based on the vertical projection as a theory, the length of longest axis and its horizontal and vertical axis are recorded and the average value (estimation: 0.01cm) was taken.

Number of inflorescences and inflorescence length: The number of inflorescences per pot was recorded, while the distance from the bottom of a single inflorescence to the base of the top flower was randomly measured in each pot and recorded as inflorescence length (estimation: 0.01cm).

Flower length: The vertical distance from the base of the sepals of three fully open flowers to the top of a single flower was measured randomly per pot (mm).

Flower diameter: The maximum diameter of the flower (mm) was measured for three fully open flowers randomly per pot.

### 2.5.5 Data processing

CTR = fence tissue thickness/leaf thickness × 100%

SR=sponge tissue thickness/leaf thickness×100%

MDA concentration: $C(\mu mol/L) = 6.45(A_{532}-A_{600})-0.56A_{450}$

MDA content ratio in fresh weight: MDA = C (μmol/L) × volume of extraction solution (L)/fresh weight of leaf tissue (g)

CAT (U/g fresh weight) = 764.5 × ΔA/leaf tissue fresh weight (g)

In the formula: ΔA: the difference between the OD value before and after the reaction.

POD (U/g fresh weight) = 9800 × ΔA/leaf tissue fresh weight (g)

In the formula: ΔA: the difference between the OD values before and after the reaction.

Soluble sugar content (%) = (C × V/a × n) (W×1000)

In the formula: C: standard equation for the amount of sugar (μg); a: volume of aspirated sample liquid (mL); V: volume of extraction solution (mL); n: dilution times; W: weight of tissue (g).

Proline (μg/g FW or DW) = C × V/a × W

In the formula: C: standard equation for pro volume (μg); V: volume of extraction solution (mL); a: volume of aspirated sample liquid (mL); W: weight of tissue (g)

Data from this study were correlated using SPSS 26.0 software and analyzed for significance ($P$ <0.05), with Excel 2013 for data statistics and Origin9 for graphs. All data were subjected to three biological replicates, and the analysis is expressed as $s \pm \bar{x}$ (standard deviation).

The band loci were generated according to ISSR-PCR amplification, and the band polymorphisms were counted. In the same loci, the presence of the strip loci was recorded as "1" and the absence was recorded as "0" to construct a binary data matrix, while the genetic similarity coefficient of Dice was calculated using the biological software NTSYS-pc2.10, and the unweighted group average method (UPGMA) was used to cluster the ISSR-PCR amplified bands for genetic similarity analysis and used construct a dendrogram by the Mega.

## 3 Results

### 3.1 ISSR primer screening and polymorphism analysis

PCR amplification of wild-type DNA was performed with 100 UBC (University of British Columbia) ISSR universal primers, and the amplification products were detected by agarose gel electrophoresis. 9 primers, UBC807, UBC811, UBC818, UBC826, UBC844, UBC866, UBC874, UBC888, and UBC891, showed the best amplification results (Table 1), and it was finally determined that these 9 ISSR primers were used for PCR amplification of the suspected mutant of *Plumbago indica* L. $ddH_2O$ control under the same conditions to exclude false positive results. The amplification products range from 500bp to 2000bp (Figures 3, 4).

10.3389/fpls.2023.1149669

TABLE 1 ISSR primer screening results and primer sequences.

| Primers | Primer sequences |
|---|---|
| UBC807 | AGA GAG AGA GAG AGA GT |
| UBC811 | GAG AGA GAG AGA GAG AC |
| UBC818 | CAC ACA CAC ACA CAC AG |
| UBC826 | ACA CAC ACA CAC ACA CC |
| UBC844 | CTC TCT CTC TCT CTC TRC |
| UBC866 | CTC CTC CTC CTC CTC CTC |
| UBC874 | CCC TCC CTC CCT CCC T |
| UBC888 | BDB CAC ACA CAC ACA CA |
| UBC891 | HVH TGT GTG TGT GTG T |

The screened nine ISSR universal primers (Table 1) were used to PCR amplify the DNA of 24 *Plumbago indica* L. suspected mutant materials, and a total of 32 bands were amplified, of which 28 were polymorphic bands with a polymorphism ratio of 87.5%, indicating that the test materials were rich in variation. Each primer could amplify 2-5 bands, with an average of 3.6 bands and an average of 3.1 polymorphic bands, among which UBC888 amplified the most bands and polymorphic bands, both of which were 5, as detailed in Table 2.

The results of partial ISSR amplification of 26 (including 2 controls) materials with 9 primers are shown in Figure 3, and some of the 24 strains showed band increases and deletions. For example, under UBC818 amplification, material SA15 has one more band between 1000-2000 bp compared with the wild type, material SA16, SA17, SA21 and SA23 have one missing band between 500-750 bp, and material SA18 and SA24 have completely missing bands; under UBC866 amplification, material SA24 has one more band between 500-750 bp compared with the wild type. Under UBC866 amplification, material SA24 is missing one band between 500-750 bp compared with wild type, and SA13, SA21, and SA23 are completely missing. These examples indicate that these numbered materials are likely to be mutants.

## 3.2 Genetic similarity and clustering analysis

Based on the 28 polymorphic sites amplified by the 9 primers, the genetic similarity coefficients of the 24 suspected mutations and the 2 wild type materials were calculated and were shown in the Supplementary Material. Based on the ISSR genetic similarity

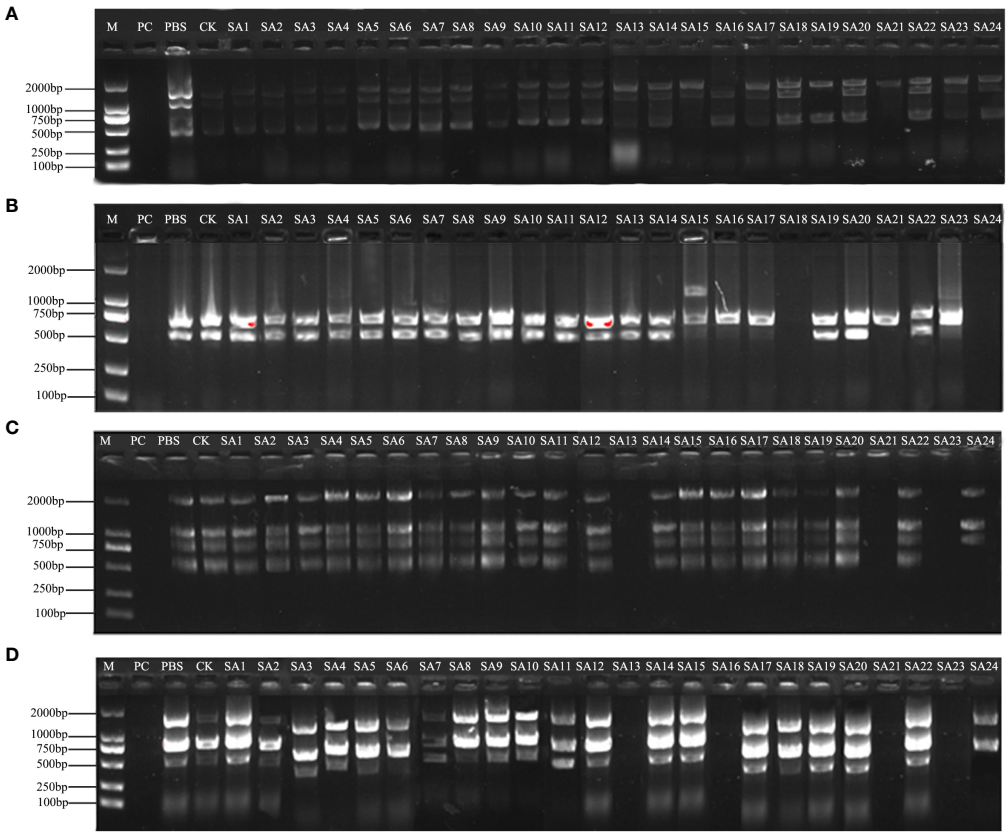


FIGURE 3
Amplification profile of ISSR partial primers. PC is the positive control, PBS is the control with phosphate buffer as the solution, and CK is the wild-type control. **(A–D)** are the amplification profiles of primers UBC807, UBC818, UBC866, UBC874, respectively.

10.3389/fpls.2023.1149669

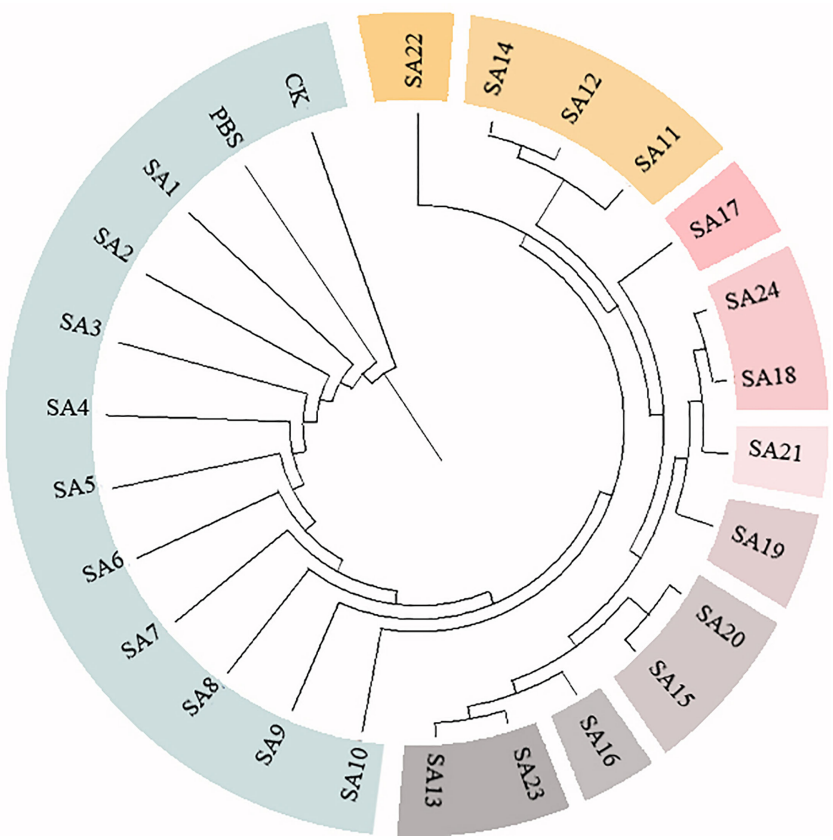


FIGURE 4
Cluster analysis of 24 suspected mutants of *Plumbago indica* L. and wild materials. 24 putative mutants (SA1 to SA24) derived from simple intersequence repeats (ISSR), 2 controls (CK, PBS); horizontal coordinates are genetic distances.

coefficients, the cluster analysis of the 26 test materials constructed using UPGMA by the Mega unweighted arithmetic mean method was shown in Figure 4, which could be classified into 10 classes, among which SA1-SA10 had close genetic coefficients to CK and PBS and were the most closely related, followed by SA22, and SA11, SA12, and SA14. The remaining 9 materials had low genetic similarity coefficients and were more distantly related to CK.

In conclusion, after further molecular marker identification and cluster analysis of the 24 suspected mutants initially identified by morphology, 9 materials SA13, SA15, SA16, SA18, SA19, SA20, SA21, SA23, and SA24 could be tentatively judged as mutant strains of *Plumbago indica* L.

TABLE 2 Amplification polymorphism analysis of 24 suspected mutant strain materials by 9 primers of ISSR.

| Primers | Number of amplified bands | Number of polymorphic bands | Polymorphism ratio (%) |
|---|---|---|---|
| UBC807 | 3 | 3 | 100.0 |
| UBC811 | 4 | 2 | 50.0 |
| UBC818 | 3 | 3 | 100.0 |
| UBC826 | 4 | 4 | 100.0 |
| UBC844 | 2 | 1 | 50.0 |
| UBC866 | 4 | 4 | 100.0 |
| UBC874 | 3 | 3 | 100.0 |
| UBC888 | 5 | 5 | 100.0 |
| UBC891 | 4 | 3 | 75.0 |
| Total | 32 | 28 | 87.5 |

## 3.3 Analysis of plumbagin content in stem and leaves of mutants

The contents of the medicinal component plumbagin in control and nine mutant strains were detected, as shown in Figures 5A, B. As with the standard solution, both stem and leaf extracts of control plants and mutant strains had signal peaks at about 25 min, indicating that the mutant stems and leaves contained plumbagin. The content of plumbagin in the leaves was calculated (Figure 5C), and it was found that except for SA13, SA16 and SA18, which were significantly lower than CK, the content of all plants was not significantly different compared with CK, indicating that mutagenesis affected the accumulation of plumbagin in the leaves of SA13, SA16 and SA18. In the stems, only SA24 had significantly higher plumbagin content than CK, 0.5991%, which was 3.84 times higher than the control, while SA16 was significantly lower than the

10.3389/fpls.2023.1149669

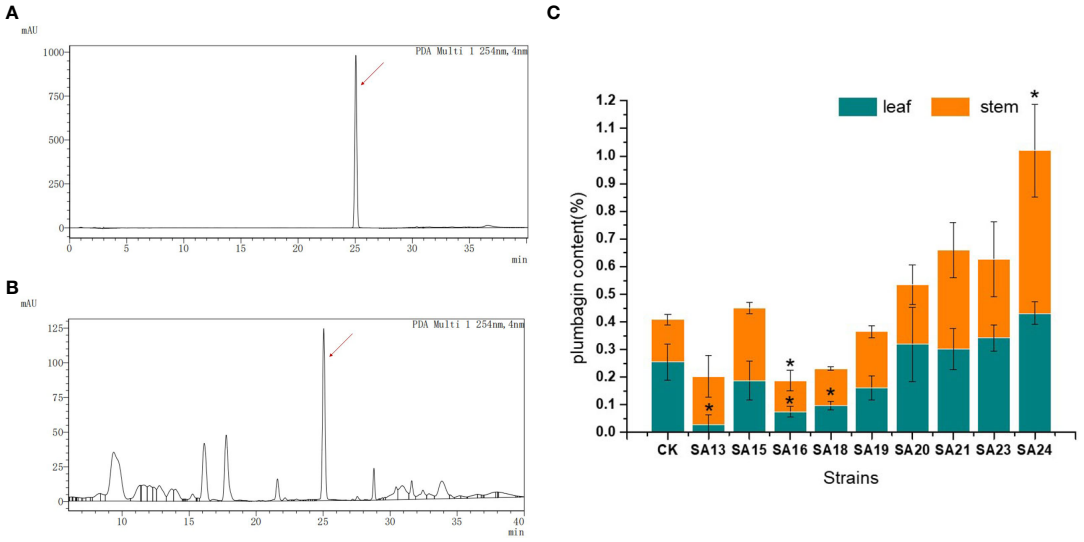


FIGURE 5
Plumbagin content of 9 mutants in stems and leaves. Note: **(A)** the peak plot of plumbagin standard product; **(B)** the peak plot of the plant sample (CK as an example); **(C)** The comparison chart of plumbagin content between plant samples; "*" means with significant differences between different mutants and the control group ( at P<0.05).

control group. For the above-ground parts, the total plumbagin content was highest in SA24, followed by SA21. Therefore, SA15, SA19, SA20, SA21, SA23 and SA24 can be continuously observed as better mutants, provided that their medicinal value is not affected.

## 3.4 Characterization of the anatomical features of the nutrient organs of nine mutants of *Plumbago indica* L.

### 3.4.1 Anatomical features of the root

The wild strain's roots of the nine mutants identified by ISSR molecular markers were separated, and their anatomical characteristics are displayed (Figure 6; Table 3). The xylem, vascular cambium, and phloem cells in the root cross-section of CK are all tightly packed and clearly bound. Compared with CK, mutants SA13, SA16, SA18, SA19, and SA24 (Figures 6B, D–F, J) had tightly arranged xylem cells and reduced the number of cambium cell layers in the vascular bundle, and SA13 root cross-sections were irregularly elliptical. SA15 and SA23 root cross-sectional areas were significantly reduced (Figures 6C, I; Table 3), and SA23 phloem cells were large and had a reduced number of cell layers. SA21 (Figure 6H) has a small xylem area, small and dense cells, and is closely surrounded by vascular cambium; the cells of the phloem are large, and this part accounts for the majority of the root cross-sectional area.

Root cross-sections of CK, SA13, SA15, SA16, SA18, SA19, SA20, SA21, SA23, SA24(a-j); Root diameter(RD); In Figure 3A, 1 is the xylem of the root, 2 is the cambium, and 3 is the phloem.

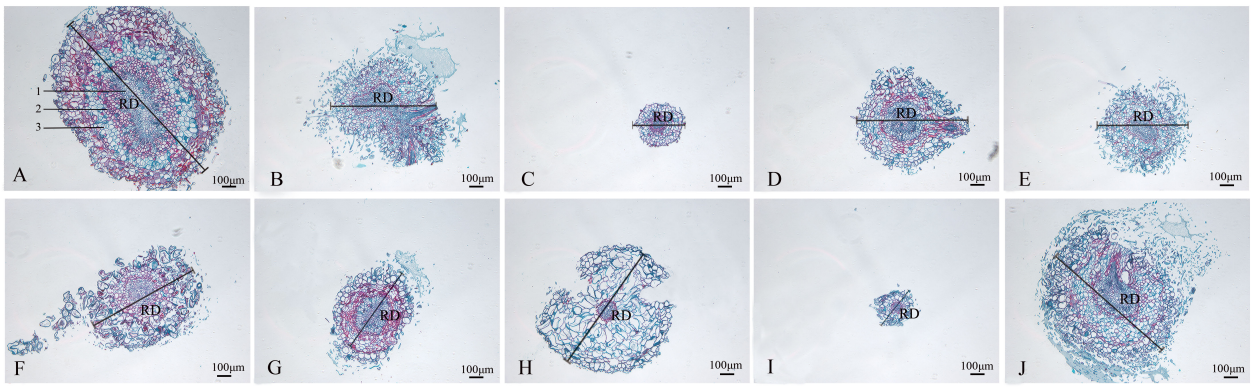


FIGURE 6
Comparison of the anatomical and structural characteristics of the roots of nine *Plumbago indica* L. mutants with the wild type: *Root cross-sections of CK, SA13, SA15, SA16, SA18, SA19, SA20, SA21, SA23, SA24 **(A–J)**; Root diameter (RD); In **(A)**, 1 is the xylem of the root, 2 is the cambium, and 3 is the phloem..

TABLE 3 Root diameter of nine mutants and wild-type material of *Plumbago indica* L.

| Strain | Root diameter(μm) |
|---|---|
| CK | 1337.86 ± 18.76[a] |
| SA13 | 811.66 ± 20.99[d] |
| SA15 | 317.08 ± 8.92[h] |
| SA16 | 656.14 ± 21.04[e] |
| SA18 | 507.31 ± 7.73[f] |
| SA19 | 435.41 ± 21.68[g] |
| SA20 | 506.28 ± 13.32[f] |
| SA21 | 926.53 ± 14.98[c] |
| SA23 | 228.89 ± 9.64[i] |
| SA24 | 961.40 ± 12.09[b] |

The same letters are non-significantly different for different mutants and controls (at P<0.05).

### 3.4.2 Anatomical features of the stem

The stem anatomical features of the nine mutant and wild-type materials are displayed (Figure 7; Table 4). Stem diameter and stem epidermal cell thickness showed significant differences ($P$<0.05) from CK, manifested as an increase (7 plants) or decrease (2 plants) in stem diameter; among them, SA13, SA16, SA20, and SA24 (Figures 7B, D, G, J) showed significant differences ($P$<0.05) from wild type in stem epidermal cell thickness, and SA24 was the most significant in both stem diameter and stem epidermal cell thickness, with 1.19-fold and 1.15-fold increase respectively. The cross-sectional shape did not change significantly in the other eight mutant materials compared with CK, except for SA16 (Figure 7). On the cell arrangement characteristics, the xylem, cambium, and phloem of SA15 showed no ring arrangement, and the collenchyma on one side was obviously thickened, and the epidermal cells formed in the middle divided the transverse section of the stem into two parts (Figure 7C). SA16 has a "lunar" shaped stem cross-section, with xylem, cambium, and phloem scattered in the middle expansion area and abnormal distribution of cellular tissue structure (Figure 7D). The collenchyma on one side of SA18 was thickened and irregularly distributed on the thickened side in addition to the circularly arranged xylem, cambium, and phloem. The rest of the mutant strains showed no significant abnormalities compared with the CK, and only differences in the degree of compactness of collenchyma and cortical cell arrangement were observed (Figure 7E).

### 3.4.3 Anatomical features of the leaf

The structures of mesophyll and leaf main vein cross-sections of nine mutant and wild-type leaves are shown (Figure 8; Table 5). The mutant plants exhibited changes in leaf thickness and main vein cross-sectional size; the results of statistical analysis of the relevant parameters are shown in Table 5.

In terms of leaf thickness, only SA13, SA19 and SA23 were not significantly different from the wild type, while the rest were significantly thicker than the wild type; leaf main vein thickness was significantly greater than the wild type except for SA16. The largest of them was SA15, reaching 980.333 μm, which was 1.48 times more than the wild type. As can be seen, most of the mutant strains exhibited plump leaves with prominent veins.

The microstructure also showed some differences. The lower epidermis was thicker than the upper epidermis in general, and the thickness of the upper epidermis cells ranged from 16.1063-21.8013 μm, which was not significantly different from CK. The thickness of the lower epidermal cells ranged from 18.59-28.91 μm, with only SA16, SA18 and SA19 mutant strains being thicker than the wild type that showed significant differences. Compared with the CK spongy tissue thickness, seven of the nine materials showed thickening, SA20 thickness was the largest, and the cells were more loosely arranged at 81.0693 μm, which was a 0.97-fold increase; the palisade tissue thickness was no difference among the seven materials.

Analysis of cell tense ratio (CTR) and spongy ratio (SR) of the nine mutant materials and the wild type showed that only SA16 and CK had no significant difference in CTR and SR. In terms of CTR,

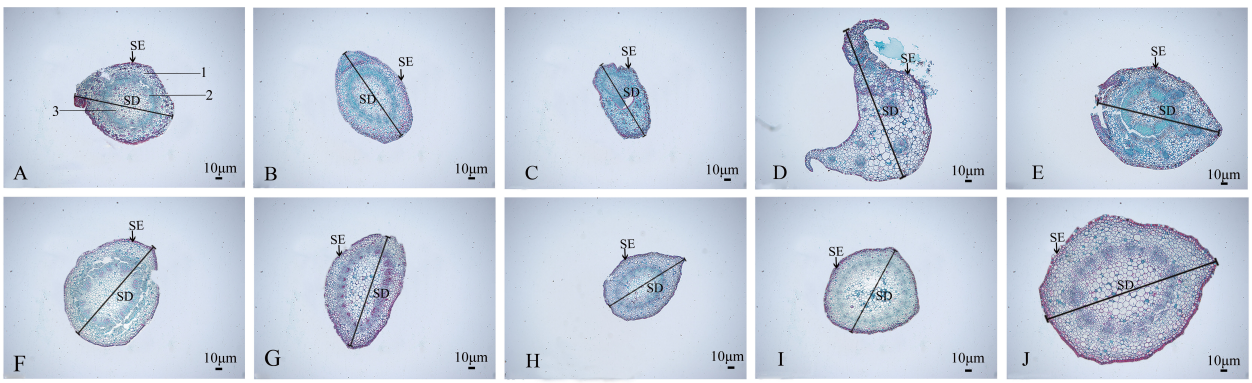


FIGURE 7
Comparison of the anatomical and structural characteristics of the stem of nine *Plumbago indica* L. mutants with the wild type: Stem cross-sections of CK, SA13, SA15, SA16, SA18, SA19, SA20, SA21, SA23, SA24 **(A–J)**; Stem epidermal cells(SE); Stem diameter(SD); **(A)** 1 is the xylem of the stem, 2 is the cambium, and 3 is the phloem.

10.3389/fpls.2023.1149669

TABLE 4 Parameters related to the stem anatomical features of nine putatively mutants and wild type of *Plumbago indica* L.

| Strain | Stem diameter (μm) | Stem epidermal cell thickness (μm) |
|---|---|---|
| CK | 239.38 ± 1.81$^{g}$ | 3.33 ± 0.41$^{e}$ |
| SA13 | 333.54 ± 4.31$^{c}$ | 4.91 ± 0.48$^{bc}$ |
| SA15 | 217.56 ± 6.86$^{h}$ | 3.43 ± 0.15$^{de}$ |
| SA16 | 221.31 ± 2.99$^{h}$ | 5.34 ± 1.11$^{b}$ |
| SA18 | 321.50 ± 9.06$^{d}$ | 3.81 ± 0.59$^{de}$ |
| SA19 | 328.86 ± 2.11$^{cd}$ | 3.63 ± 0.59$^{de}$ |
| SA20 | 350.14 ± 6.52$^{b}$ | 4.21 ± 0.50$^{cd}$ |
| SA21 | 258.68 ± 7.38$^{f}$ | 3.25 ± 0.40$^{e}$ |
| SA23 | 279.66 ± 6.16$^{e}$ | 3.64 ± 0.36$^{de}$ |
| SA24 | 525.28 ± 8.41$^{a}$ | 7.18 ± 0.78$^{a}$ |

The same letters are non-significantly different for different mutants and controls (at P<0.05).

SA23 had the largest value of 27.93%, followed by SA13, SA19, SA16, and SA24 in descending order, all of which were not significantly different from the wild type. In terms of SR, it was found that SA24 had the largest value, followed by SA21, SA19, SA23, and SA18 in descending order, all of which were larger and significantly different than CK.

In summary, the nine mutant materials differed significantly from the wild type in the anatomical features of the leaf.

Combining the anatomical features of the mutant material in the root, stem, and leaf nutrient organs (Figures 8, 9), it can be seen that, compared with the wild type, the thickness of the root of the mutant strain is smaller than that of the wild strain, and there are significant differences; the stem diameter is generally thicker, with SA24 being the most prominent in terms of stem diameter and stem epidermal cell thickness. The leaves mostly changed morphologically, as shown by an increase in leaf thickness, and the microstructure showed the same trend. In summary, the nine mutant materials differed significantly from the wild-type plants in the three nutritional organs of roots, stems, and leaves, both in macroscopic and microscopic anatomical features, and this result confirmed the reliability of the ISSR molecular marker identification results. The nine *Plumbago indica* L. materials, SA13, SA15, SA16, SA18, SA19, SA20, SA21, SA23 and SA24, were further identified as mutants.

## 3.5 Changes in the morphological characteristics of *Plumbago indica* L. mutants under low-temperature stress

The morphological changes of the mutants and wild type after low-temperature stress are shown (Figure 10). Compared with CK, all nine mutant and wild-type plants were damaged to different degrees, showing leaf crinkling and wilting, yellowing of leaves, and stem collapse, with SA13 and SA18 being more severely damaged than the wild type. After 24 h of rewarming, the mutants SA15, SA19, SA23 and SA24 were found to have only slightly crinkled leaves and slightly yellowed leaves, and the damage was weaker than that of wild-type plants. We tentatively judged that these four mutants could be the focus of observation.

## 3.6 Changes in the physiological and biochemical characteristics of *Plumbago indica* L. mutants under low-temperature stress

### 3.6.1 Chlorophyll fluorescence kinetic parameters of the mutant

It shows the changes of Fv/Fm in the leaves of nine mutant materials and wild-type plants under low-temperature stress (Figure 11), and it can be seen that after 48 h of low-temperature treatment, there was an overall decreasing trend, from 0.75-0.81 before treatment to between 0.48-0.66. Except for SA20 which Fv/Fm value decreased by 50.42%, which was greater than CK (0.40,

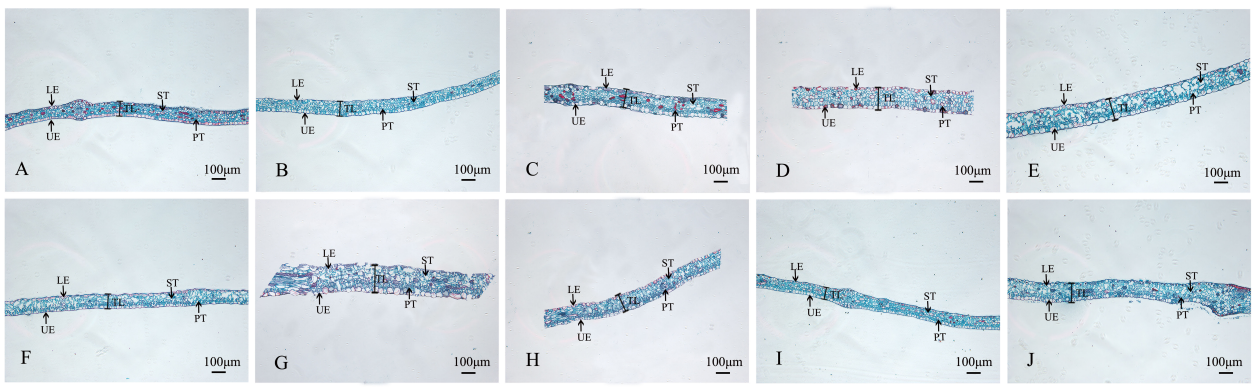


FIGURE 8
Comparison of the mesophyll cross-sections of nine *Plumbago indica* L. mutants with the wild type Mesophyll cross-sections of CK, SA13, SA15, SA16, SA18, SA19, SA20, SA21, SA23, SA24 **(A–J)**; Upper Epidermal(UR); Lower Epidermal (LE); Leaf Thickness(LT); Spongy Tissue(ST); Palisade Tissue(PT).

TABLE 5 Parameters related to the leaf anatomical features of nine mutants and wild type of *Plumbago indica* L.

| Strain | Leaf thickness (μm) | Main vein thickness (μm) | Upper epidermal cell thickness (μm) | Lower epidermal cell thickness (μm) | Spongy tissue thickness (μm) | Palisade tissue thickness (μm) | CTR (%) | SR (%) |
|---|---|---|---|---|---|---|---|---|
| CK | 101.44 ± 1.13$^{f}$ | 394.62 ± 13.14$^{h}$ | 18.26 ± 1.15$^{ab}$ | 21.88 ± 14$^{cde}$ | 41.13 ± 3.36$^{f}$ | 25.01 ± 2.43$^{cd}$ | 24.65 ± 2.27$^{ab}$ | 40.56 ± 3.44$^{d}$ |
| SA13 | 102.25 ± 0.56$^{f}$ | 544.50 ± 11.47$^{e}$ | 17.39 ± 1.17$^{ab}$ | 20.83 ± 1.36$^{de}$ | 40.30 ± 4.91$^{f}$ | 27.72 ± 3.21$^{c}$ | 27.11 ± 3.15$^{a}$ | 39.42 ± 4.86$^{d}$ |
| SA15 | 145.26 ± 13.37$^{d}$ | 980.33 ± 23.04$^{a}$ | 18.71 ± 0.53$^{ab}$ | 26.98 ± 2.73$^{ab}$ | 61.01 ± 3.82$^{d}$ | 28.38 ± 4.17$^{c}$ | 19.64 ± 3.21$^{c}$ | 42.19 ± 3.94$^{cd}$ |
| SA16 | 156.72 ± 5.31$^{c}$ | 380.50 ± 0.85$^{h}$ | 19.73 ± 0.55$^{ab}$ | 28.91 ± 1.71$^{a}$ | 68.90 ± 3.21$^{c}$ | 38.29 ± 6.29$^{a}$ | 24.24 ± 4.62$^{ab}$ | 43.99 ± 2.17$^{cd}$ |
| SA18 | 169.82 ± 9.63$^{b}$ | 729.35 ± 13.68$^{c}$ | 21.80 ± 2.92$^{a}$ | 28.75 ± 3.15$^{a}$ | 77.66 ± 6.21$^{ab}$ | 33.82 ± 5.14$^{b}$ | 19.85 ± 2.58$^{c}$ | 45.83 ± 4.36$^{c}$ |
| SA19 | 103.95 ± 3.95$^{f}$ | 448.97 ± 7.22$^{g}$ | 19.55 ± 0.99$^{ab}$ | 26.23 ± 1.74$^{ab}$ | 54.17 ± 5.25$^{e}$ | 27.62 ± 1.94$^{c}$ | 26.62 ± 2.42$^{a}$ | 52.16 ± 2.57$^{b}$ |
| SA20 | 185.63 ± 5.02$^{a}$ | 950.37 ± 15.42$^{b}$ | 20.08 ± 2.07$^{ab}$ | 23.13 ± 1.90$^{bcd}$ | 81.07 ± 4.68$^{a}$ | 23.97 ± 2.10$^{cd}$ | 12.93 ± 1.14$^{d}$ | 43.68 ± 2.37$^{cd}$ |
| SA21 | 135.09 ± 2.98$^{de}$ | 491.13 ± 4.46$^{f}$ | 18.01 ± 2.39$^{ab}$ | 25.31 ± 3.08$^{abc}$ | 74.92 ± 3.69$^{b}$ | 21.62 ± 3.30$^{d}$ | 16.01 ± 2.49$^{d}$ | 55.46 ± 3.02$^{ab}$ |
| SA23 | 98.46 ± 6.66$^{f}$ | 561.88 ± 3.99$^{e}$ | 16.11 ± 0.93$^{b}$ | 18.59 ± 2.27$^{e}$ | 41.57 ± 2.66$^{f}$ | 24.53 ± 0.96$^{cd}$ | 27.93 ± 4.67$^{a}$ | 47.13 ± 3.75$^{c}$ |
| SA24 | 127.60 ± 1.36$^{e}$ | 667.99 ± 13.81$^{d}$ | 21.61 ± 2.67$^{a}$ | 20.98 ± 1.21$^{de}$ | 73.48 ± 5.19$^{bc}$ | 27.53 ± 5.77$^{c}$ | 21.62 ± 0.56$^{bc}$ | 57.70 ± 4.03$^{a}$ |

The same letters are non-significantly different for different mutants and controls (at P<0.05).

46.41%), the other eight mutant materials decreased by less than CK, between 18.90% and 42.34% indicated that the mutant plant as a whole had a stronger ability to cope with short-term low-temperature stress than CK, among which SA23 decreased the least compared with CK, 18.90%, and the damage of photosynthesis was the least. This was followed by SA24 (20.49%), SA15 (22.16%) and SA19 (24.29%). It can be seen that the mutant materials generally have better cold tolerance than the wild type, among which SA15, SA19, SA23 and SA24 have higher light energy conversion efficiency and better ability to cope with low-temperature stress.

### 3.6.2 Malondialdehyde content of *Plumbago indica* L. mutants under low-temperature stress

The changes in MDA content are shown (Figure 12). Before the treatment without low-temperature stress, the MDA content of both the treatment group and CK was low. After 48 h of low-temperature stress treatment, the MDA content in the leaves of all materials increased rapidly, the relative MDA content and the rise in CK were 42.82 mmol/L and 112.21%, respectively. The mutant materials increased between 50.00% and 114.00%, except for SA16, the rest eight mutant materials increased less than the wild strain and showed better resistance than the wild type, among which, SA24 MDA relative content increased the least, 17.99%, indicating the lowest degree of cell membrane injury and the strongest resistance to low-temperature stress, followed by SA15, SA19, and SA23, with relative MDA content increased by 26.80 mmol/mL, 18.06 mmol/mL, and 26.07 mmol/mL, respectively.

### 3.6.3 SOD, CAT, and POD activities of *Plumbago indica* L. mutants under low-temperature stress

The changes of SOD, CAT, and POD activities after low temperature stress in the nine mutant materials and the control are shown in Figure 13. Before low temperature stress treatment, all mutant strains except SA13 had significantly higher SOD activity than CK ($P$<0.05) (Figure 13A); only SA19 had significantly higher CAT activity than CK(Figure 13B); only SA15 had significantly higher POD activity than CK (Figure 13C). After 48 h of low temperature stress treatment, SOD activity in the leaves of all materials increased rapidly, and all mutant strains were higher than that of CK, among which the highest SOD activity was SA24, with 679.04 U/g, was 1.09 times higher than that of CK after stress, followed by SA15 (493.25 U/g, 0.62 times), SA23 (493.23 U/g, 0.58 times), and SA19 (458.74 U/g, 0.53 times); CAT activity showed that SA15, SA23, and SA24 were significantly higher than that of the control ($P$<0.05), with 429.71 U/g, 278.985 U/g and 593.316, respectively. while the CAT enzyme activities of SA16 and SA18 were significantly lower than those of the control ($P$<0.05); in the performance of POD activities, all four mutant strains of SA19-SA24 were significantly higher than that of CK ($P$<0.05), and SA19 was the highest at 30627.76 U/g, followed by SA24 at 30052.09 U/g.

### 3.6.4 The soluble sugar content of *Plumbago indica* L. mutants under low-temperature stress

None of the mutant materials had high soluble sugar content before low-temperature stress, but all were significantly higher than

10.3389/fpls.2023.1149669

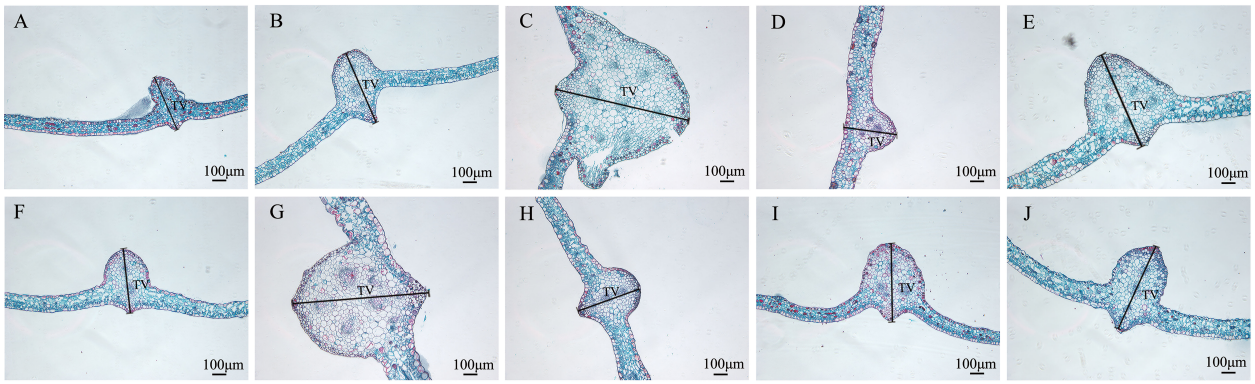


FIGURE 9
Comparison of the main leaf vein cross-sections of nine *Plumbago indica* L. mutants with the wild type. * Main leaf vein cross-sections of CK, SA13, SA15, SA16, SA18, SA19, SA20, SA21, SA23, SA24**(A–J)**; Thickness of main vein(TV).

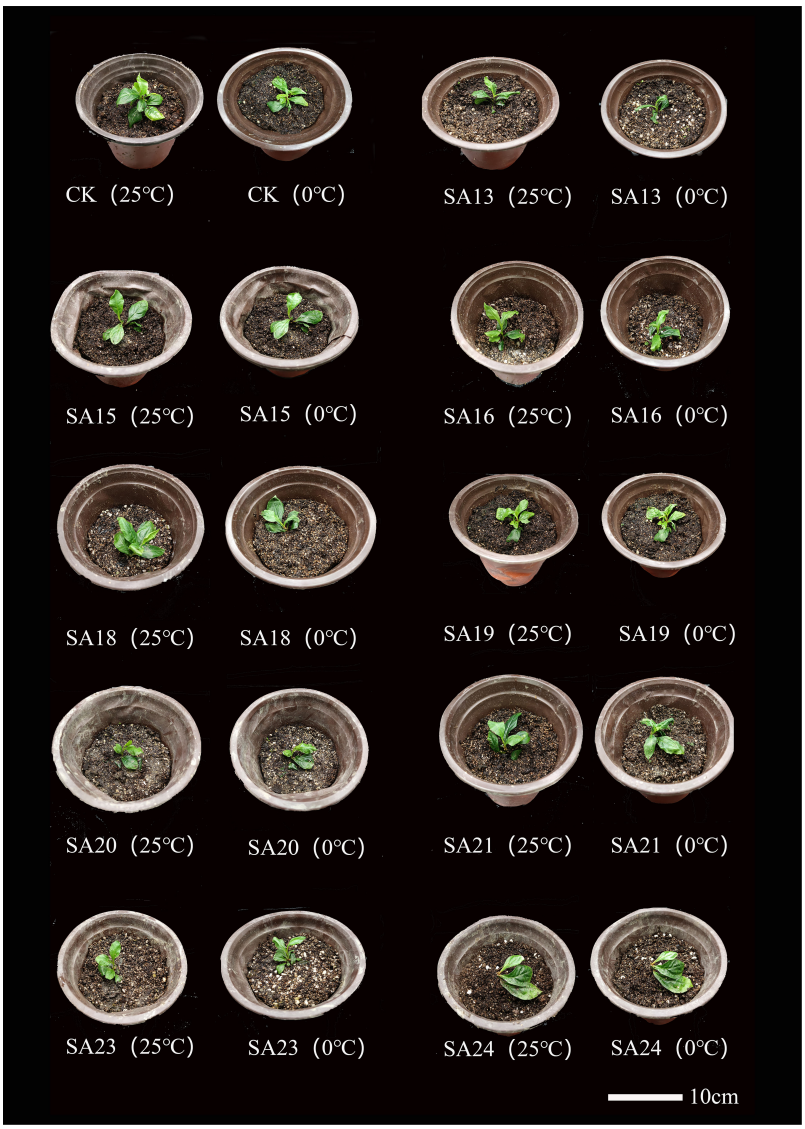


FIGURE 10
Comparison of the morphology of mutant material and wild type of *Plumbago indica* L. under low-temperature stress.

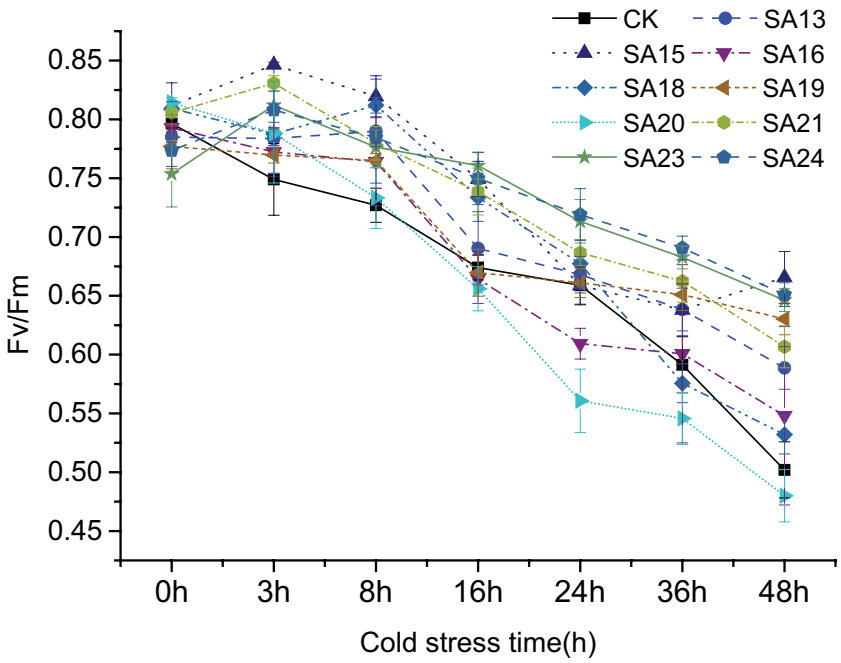


FIGURE 11
Variation of Fv/Fm in leaves of *Plumbago indica* L. mutants and wild material under low-temperature stress.

CK ($P$<0.05), ranging from 5.33-8.14 μg/g. After 48 h of low-temperature stress, the contents of both mutants and CK increased significantly ($P$<0.05), and the contents of mutant materials rose to between 8.85-21.9 μg/g, with SA24 showing the highest increment of 14.39 μg/g, a 1.92-fold increase compared to CK, followed by SA15 (10.42 μg/g, 1.30-fold), SA23 (8.21 μg/g, 1.25-fold), and SA21 (5.51 μg/g, 0.68-fold), indicating that they were stronger than CK in mobilizing osmoregulatory substances to resist low-temperature stress, which laterally reflected that their cold tolerance was also stronger than CK (Figure 14).

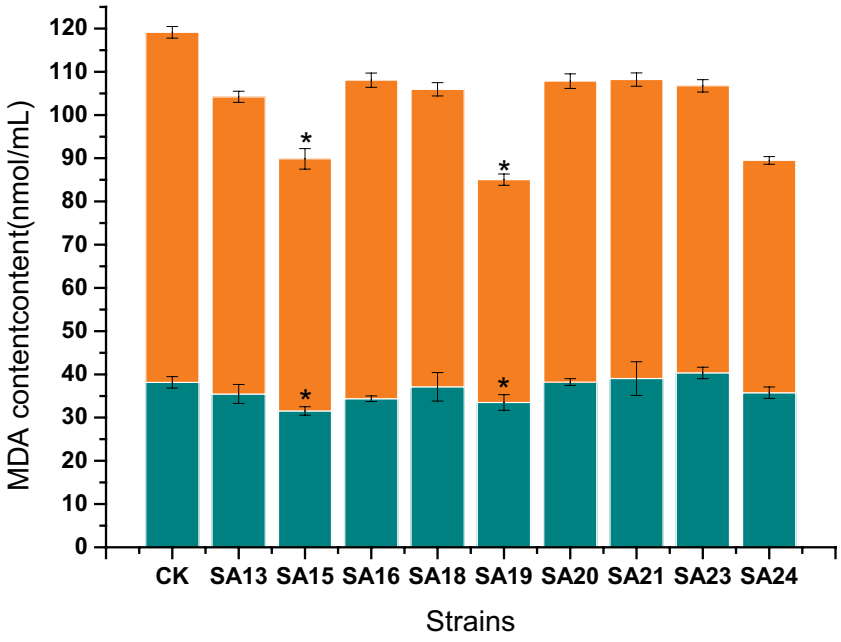


FIGURE 12
Effect of low-temperature stress on the MDA content of mutant material of *Plumbago indica* L.. *"*"* means with significant differences between different mutants and the control group (at $P$<0.05). The green part is the MDA content of each strain before treatment, the total column length is the MDA content of each strain after treatment, and the orange part is the relative MDA content.

10.3389/fpls.2023.1149669

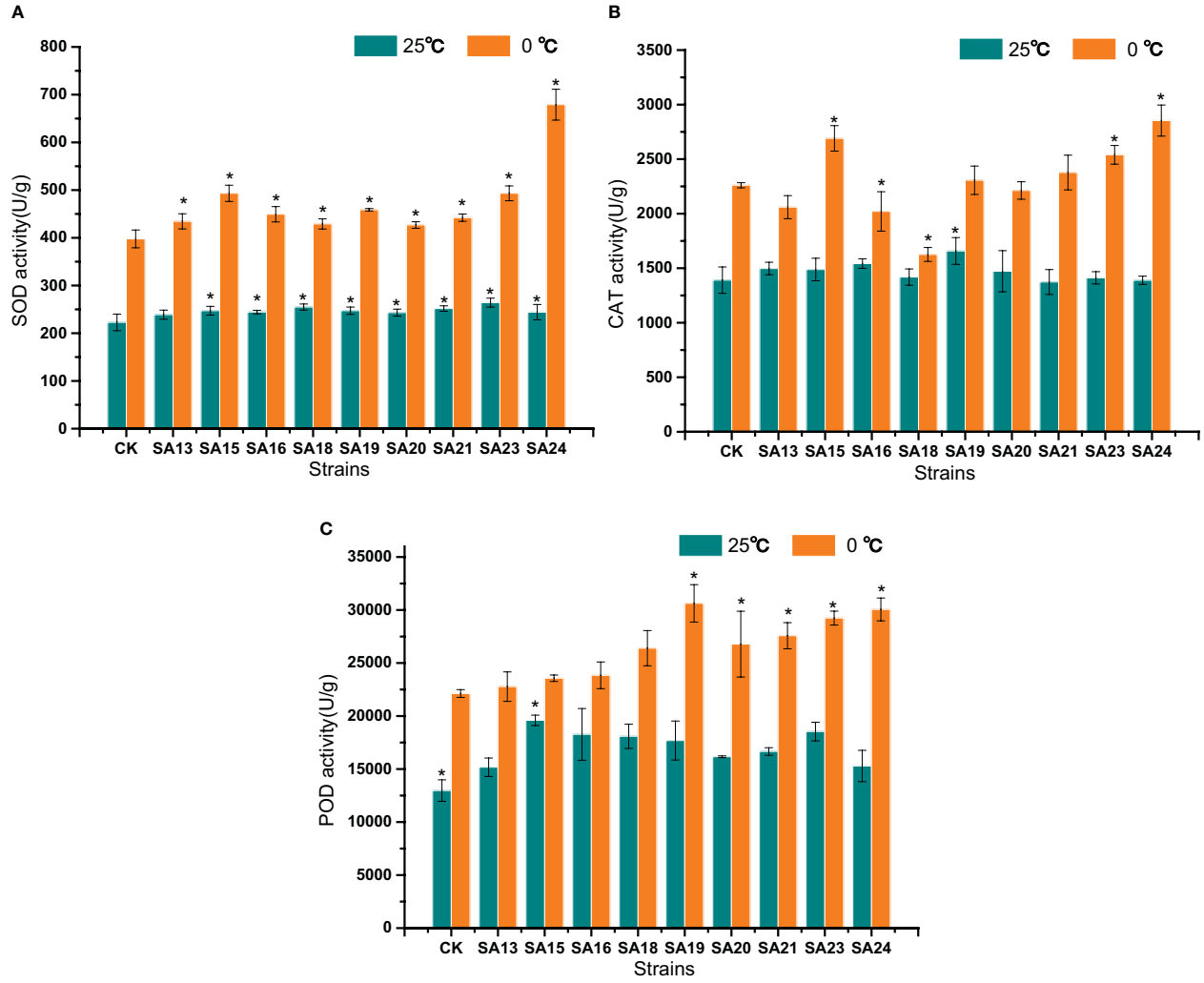


FIGURE 13
Effects of low-temperature stress on SOD **(A)**, CAT **(B)**, and POD **(C)** activities of mutant material of *Plumbago indica* L.. "*" means with significant differences between different mutants and the control group (at $P<0.05$).

### 3.6.5 Proline content of *Plumbago indica* L. mutants under low-temperature stress

After low-temperature stress treatment, the Pro content in CK increased from 2.64 mg/g to 5.08 mg/g, and compared with CK, the Pro content of all eight mutant materials increased significantly, except for SA13, SA16, and SA20, the increase was significantly greater ($P<0.05$). SA24 had the highest Pro content of 11.77 mg/g, a2.74-fold increase compared to CK, followed one is SA23 (9.36 mg/g, 2.70-fold), SA15 (7.63 mg/g, 1.75-fold), and SA19 (7.11 mg/g, 1.67-fold). It reflected that these four mutants had a higher ability to withstand cold stress than CK from the side (Figure 15).

In conclusion, by analyzing the changes in chlorophyll fluorescence parameters, MDA, soluble sugar, and proline contents between the mutant and wild plant CK before and after the onset of low-temperature stress, it was evident that the two types of materials differed to different degrees in their cold tolerance. Compared with CK, some mutant materials showed weaker cold tolerance and some showed stronger cold tolerance. Taken together, the four mutant materials SA15, SA19, SA23, and SA24 showed higher light energy conversion efficiency, less accumulation of MDA content, have the capable of actively mobilizing the activity of antioxidant enzymes. and they also have more accumulation of soluble sugar and proline content in response to low-temperature stress, and did not affect or even exceed the accumulation of plumbagin in stems and leaves in control. They showed some cold tolerance at the level of physiological and biochemical characteristics, which was more consistent with the morphological observation of low-temperature injury performance. Therefore, these four mutants can be used as backup materials for the screening of cold-tolerant *Plumbago indica* L. varieties for subsequent field observations.

### 3.6.6 Observation on morphological indicators in the field of cold-resistant mutants

Agronomic ornamental traits were observed in the end of November of the next year (temperature 12°C-18°C) for the cold-tolerant mutants grown in soil culture for one year. As shown in Table 6 and Figure 16, the plant height of SA19 and SA24 was significantly lower than that of CK ($P<0.05$), which showed a dwarf

10.3389/fpls.2023.1149669

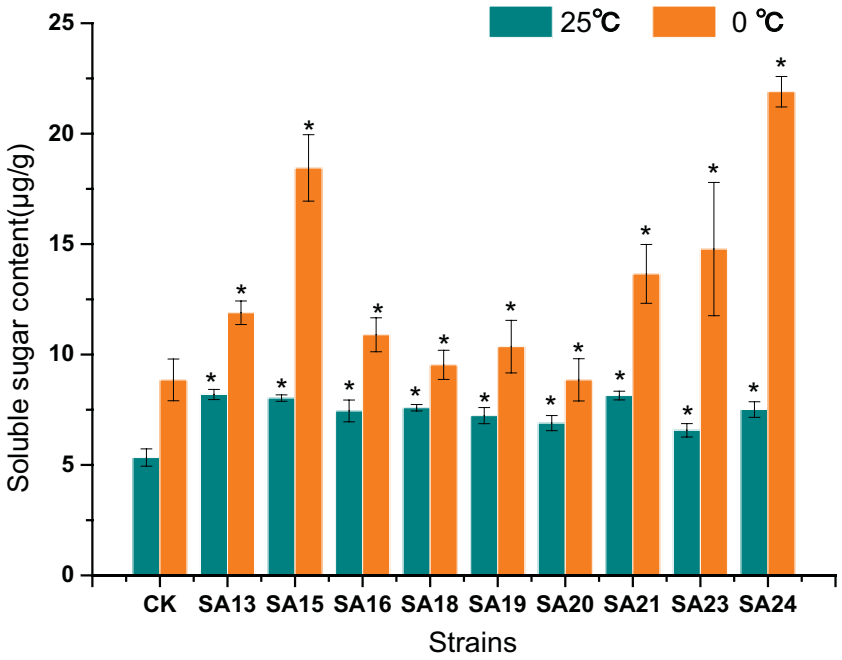


FIGURE 14
Effect of low-temperature stress on the soluble sugar content of mutant material of *Plumbago indica* L.. "*" means with significant differences between different mutants and the control group (at $P<0.05$).

and compact plant size; the crown diameter of SA19, SA23 and SA24 was significantly smaller than that of CK ($P<0.05$), and only SA15 retained the original crown diameter but the inflorescence length was significantly lower than that of control and more compact compared with control; SA19 and SA24 mainly showed lagging inflorescence growth. In Figure 16, the leaves of control gradually yellowed and wilted, and the flowers started to wither gradually; the leaves of the cold-tolerant mutant became green to dark green, and SA15 and SA23 were in full flowering stage, while SA19 and SA24 were under reproductive growth. Therefore, the cold-resistant mutant mainly

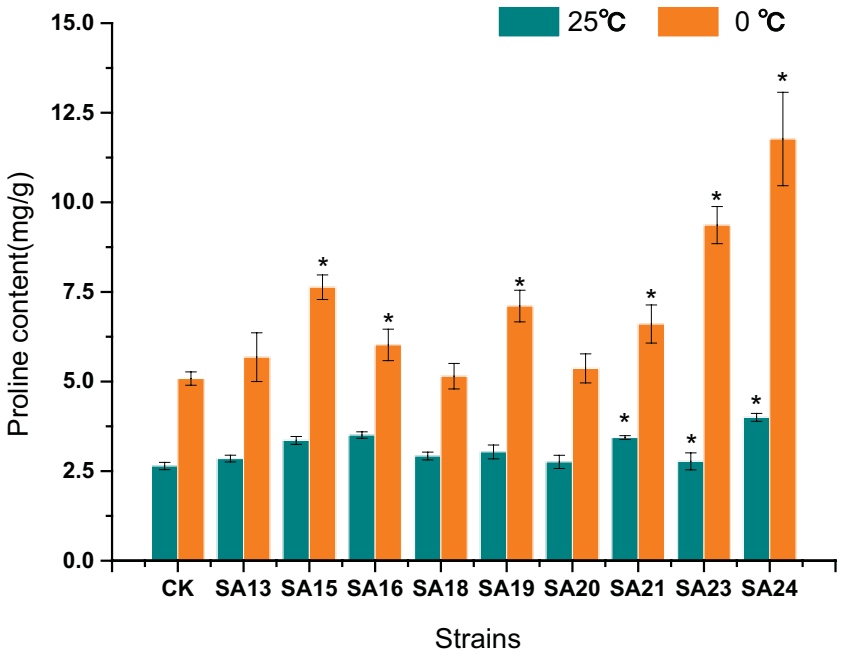


FIGURE 15
Effect of low-temperature stress on the proline content of mutant material of *Plumbago indica* L.. "*" means with significant differences between different mutants and the control group (at $P<0.05$).

TABLE 6 Statistics of morphological indicators of cold-tolerant mutants at the end of November.

| Strain | Plant height (cm) | Crown diameter (cm) | Inflorescence number | Inflorescence length (cm) | Flower diameter (mm) | Flower length (mm) |
|---|---|---|---|---|---|---|
| CK | 48.60 ± 1.55$^{a}$ | 50.80 ± 2.23$^{a}$ | 10.33 ± 2.52$^{a}$ | 21.47 ± 5.86$^{a}$ | 20.45 ± 1.02$^{a}$ | 22.35 ± 3.33$^{a}$ |
| SA15 | 45.73 ± 1.31$^{ab}$ | 51.80 ± 2.93$^{a}$ | 13.67 ± 2.52$^{a}$ | 14.59 ± 3.12$^{b}$ | 19.98 ± 1.79$^{a}$ | 24.20 ± 3.49$^{a}$ |
| SA19 | 33.83 ± 3.07$^{c}$ | 19.80 ± 1.87$^{d}$ | 3.67 ± 1.53$^{b}$ | – | – | – |
| SA23 | 43.47 ± 1.30$^{b}$ | 43.63 ± 1.40$^{b}$ | 11.33 ± 1.53$^{a}$ | 23.21 ± 3.99$^{a}$ | 21.25 ± 3.49$^{a}$ | 23.80 ± 4.36$^{a}$ |
| SA24 | 35.90 ± 1.95$^{c}$ | 28.13 ± 1.81$^{c}$ | 1.00 ± 1.00$^{b}$ | – | – | – |

"-" means with the data is not available, and the same letters are non-significantly different for different mutants and controls. (at $P<0.05$).

showed the characteristics of delayed flowering and delayed senescence, and had a longer ornamental period.

# 4 Discussion

## 4.1 $NaN_3$ mutagenesis is an effective method to obtain mutants of *Plumbago indica* L.

The genotoxicity of $NaN_3$ has been extensively studied, and its produced metabolite β-azidoalanine fraction [$N^3$-$CH^2$-$CH(NH^2)$-COOH] plays a mutagenic role, inducing chromosomal mutations at a lower rate than other chemical mutagens (Gomez et al., 2019). Thus $NaN_3$ is characterized by random regions causing a high frequency of mutations and a low frequency of chromosomal abnormalities (Turkoglu et al., 2022). In this study, plants treated with $NaN_3$ and low-temperature stress in the field mainly showed dwarf plants, slightly curled leaves and slightly yellowed leaves, consistent with the mutagenic characteristics of $NaN_3$. The concentration of mutagen affects tissue survival and mutagenic capacity, and using the optimal concentration of mutagen is necessary to achieve successful mutagenesis by balancing reasonable survival rates and finding the desired mutant sample (Wannajindaporn et al., 2016). The $LD_{50}$ concentration that results in 50% mortality is usually considered to be the better equilibrium point. The material for this experiment was derived from the optimal protocol 0.5 mmol/L, treated for 1h, at which time LD50 = 53.33%, closest to 50% mortality, and mutagenesis efficiency of 5% by morphological and anatomical features, mutants confirmed by the combination of ISSR molecular markers, corroborates the feasibility of the previous conclusions on the equilibrium point. Therefore, $NaN_3$ was further demonstrated to be a better mutagen for mutant induction in plants (e.g. *Plumbago indica* L.) due to its low damage to genes and high mutagenic efficiency.

## 4.2 ISSR molecular markers can be an effective method for screening mutant strains of *Plumbago indica* L. at the seedling stage

ISSR amplification techniques are sensitive enough to distinguish closely related individuals and assess the genetic diversity of germplasm and an effective means of assessing mutants (Velu et al., 2008). ISSR and genetic distance analysis allow better determination of variations originating from the same genotype (Ziarovska et al., 2013). In this study, the disappearance of normal bands and the appearance of new bands due to the effect of $NaN_3$ mutagen were found under the characterization of ISSR technique using $NaN_3$ *in vitro* mutagenesis of *Plumbago indica* L. New bands

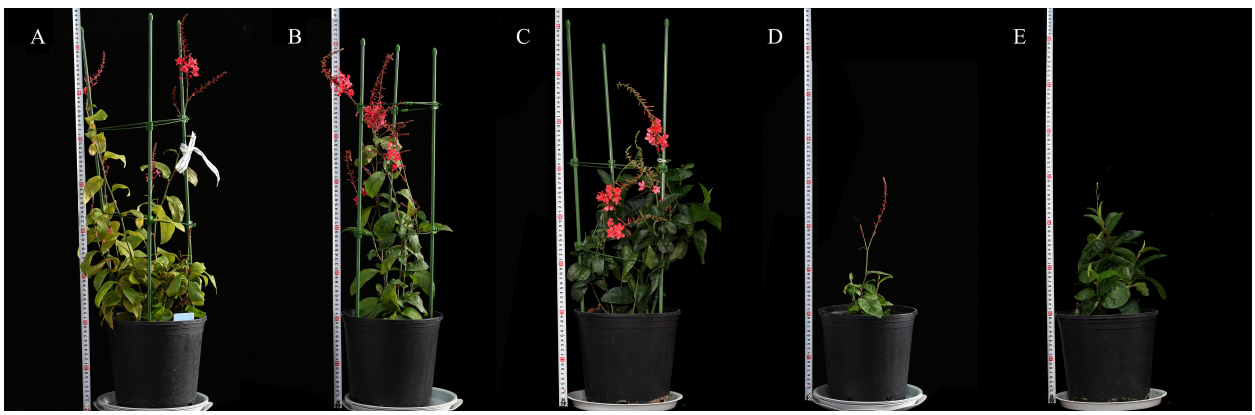


FIGURE 16
Comparison of the growth of the four *Plumbago indica* L. mutant materials at the end of November 2022 (12°C-18°C) **(A–E)** in the figure are CK, SA23, SA15, SA19, and SA24, in that order.

may be associated with mutations, while loss of bands may be associated with DNA damage, DNA methylation and chromosomal damage (Turkoglu et al., 2022). In the dendrogram and genetic data analysis, it was demonstrated that the mutant strains SA19, SA16, SA15, SA20, SA18, SA24, SA21, SA13, and SA23 had sequentially increased genetic distances compared to the parent and that the mutual strains showed different physiological, biochemical, and anatomical characteristics, which also indicated the uniqueness of each mutant strain (Ziarovska et al., 2013). ISSR marker clustering analysis is associated with differences in phenotypic traits (Wu et al., 2020), and this identification technique can help distinguish between morphologically distinct plants; it can also provide a solution for early seedling targeted breeding to screen for mutants, as the undirected nature of mutagenesis leads breeders to overlook invisible resistance indicators. Sulu et al. (2020) also used this approach to demonstrate induced mutations and genetic differentiation of citrus and lemon mutant genotypes as an effective tool for determining plant genotypes. In this study, the initial screening of mutants by clever use of ISSR molecular markers was more advantageous than morphological markers, and the mutant strains initially identified by this method were corroborated by subsequent anatomical evidence, indicating the reliability of ISSR molecular marker identification. In addition, using this marker technology, that solves the hidden variation of non-appearance changes that are difficult to screen by *in vitro* mutagenesis, and can quickly locate the plant body at the seedling stage, which facilitates later narrowing down the observation and testing population and targeted screening of target plants. Therefore, we believe that ISSR molecular markers can be used as a reliable method to screen $NaN_3$ *in vitro* mutagenesis of *Plumbago indica* L. mutants at the seedling stage.

## 4.3 Accumulation of plumbagin content in *Plumbago indica* L. mutants

Previous studies have pointed out that a biologically active secondary metabolite, plumbagin, isolated from Plumbaginaceae plant, clearly showed anticancer potential both *in vitro* and *in vivo* (Liu et al., 2017b). Medicinal plants have a special function to produce a large number of bioactive substances in response to biotic or abiotic stresses, which are not only involved in plant growth, development or reproduction, but also enhance plant resistance (Singh et al., 2020). In our study, the accumulation of plumbagin content in the stems and leaves of *Plumbago indica* L. mutants were almost unaffected or even higher than that of CK, which could be that mutagenesis was an abiotic stress for *Plumbago indica* L., and responded to this stress. *Plumbago indica* L.retained or even enhanced this property, which was consistent with the results of previous studies. In addition, it had also been suggested that enhanced antioxidant enzyme activity, expression of resistance genes, and production of defense signaling molecules could stimulate the production and accumulation of secondary metabolites (Katoch et al., 2022), and in this study we screened cold-resistant mutants, and the original accumulation of plumbagin in the cold- resistant *Plumbago indica* L. mutants was greater than or equal to that of the control, suggesting that this the cold-resistant mutant, in addition to better mobilization of antioxidant enzyme activity, may also derive from its higher plumbagin content, which has better cold tolerance.

## 4.4 Relationship between anatomical and structural properties and cold resistance of *Plumbago indica* L. mutants

Mutagenesis causes morphological changes in plants (Li et al., 2021), and there are still limitations to the study of cellularity dissections. In ISSR polymorphism studies, it was found that $NaN_3$ mutagenesis leads to a random point mutation of Hologene in *Plumbago indica* L. resulting in the deletion or increase of the DNA gene fragment may result in the acquisition of mutants with specific functions (Mago et al., 2017). Janosevic et al. (2011) also found leaf development in *Arabidopsis* mutants that the mesophyll cell became loose and the cellular layers were irregularly arranged, among other phenomena. In this study, the microstructure of the nine mutant plants screened also changed in varying degrees, with the more cold-tolerant mutants changing root, stem, and leaf microanatomy in response to cold stress. Sun et al. (2017) found in the anatomical feature of sugarcane roots after cold stress that the root cells gradually expanded, the cell walls started to break down and the structure started to be disordered. In cold-tolerant strains of *Plumbago indica* L., the cell of the root became larger and the thickness of xylem, phloem and cambium changed, which is consistent with the result that mutant strains have different cold resistance. Meanwhile, in a study on cold domestication of *rhododendron*, it was demonstrated that the ability of plants to acquire resistance to cold was correlated with lignin content (Liu et al., 2022). Unfortunately, although changes in the xylem in roots, stems, and leaves were found in this study, the lignin content and the size of the area occupied by the xylem were not examined, and relevant studies will be conducted in the next step.

Plant size reduction due to low temperature is a common phenomenon in temperate species and the phenomenon is considered to be an adaptive value of the plant to the cold environment (Lorenzo et al., 2019). At the same time, mutagenesis can cause dwarf due to damage to cells (Li et al., 2022c). The cold-resistant mutant strain screened in this case was also found to have dwarfed plants, which will be an important shape for future field performance to follow. Based on plant variation, cold environmental conditions lead to longer leaf epidermal cell margins, increased leaf thickness, and smaller leaves (Lorenzo et al., 2019). In turn, the increase in leaf thickness was correlated with the increase in the size of the mesophyll cell (Wang et al., 2008) or the number of mesophyll cell layers (Dumlao et al., 2012). We found a significant increase in leaf thickness of SA15 and SA24, which is consistent with the results of previous studies, so it is inferred that the level of cold resistance is positively correlated with leaf thickness. However, no significant changes were observed in SA19 and SA23, which were finally screened in this study, also indicating that plants acquire cold resistance as a complex process of multiple changes, and a single index cannot accurately determine their cold tolerance.

At the same time, cold stress tends to alter intracellular osmotic substances, resulting in leaf palisade tissue cellular structure that can be loosened by water loss, and SA19 in the study had the same cytological manifestation (Xu et al., 2022). In general, an increase in leaf thickness usually corresponds to an increase in palisade thickness, which is accompanied by an increase in leaf light driving capacity (Coble and Cavaleri, 2017). Thicker palisade tissues contain more chloroplasts to maximize light absorption, and there is growing evidence that f palisade tissues and spongy tissues are the main limiting factors for optimal photosynthesis, as evidenced by an increase in CTR with decreasing temperature and a gradual decrease in SR (He et al., 2018). In our study, we found an increase in CTR except for SA20, SA23, and SA24, indicating that the plant's protective strategy when encountering cold damage tends to increase leaf photosynthetic capacity, which is another reason why cold-tolerant strains of *Plumbago indica* L. are resistant to cold. SA23 and SA24 were not increased, which may be related to the specificity of the mutant. In addition, SR values were found in the study and increased in different mutant strains, this reason is most likely due to the specificity exhibited by *Plumbago indica* L. being an herbaceous plant with high water use efficiency (He et al., 2018).

## 4.5 Physiological and ornamental traits assessment of cold tolerance in cold-tolerant mutants of *Plumbago indica* L.

When exposed to cold stress, plants naturally create a defense system. This process involves a number of physiological and biochemical changes, such as maintaining altered photosynthesis, maintaining ROS homeostasis, and altering the structure of the soluble sugar plasma membrane (Zhu, 2016; Zheng et al., 2022). Photosynthesis is an important physiological process in plants that is highly sensitive to changes in temperature, and Fv/Fm is an important parameter indicating plant exposure to cold stress (Yamori et al., 2014). In the present study, cold stress significantly reduced Fv/Fm, and these results are consistent with previous reports that cold stress reduces Fv/Fm. Second, cold stress may promote oxidative stress by inducing excessive production of ROS, while greatly reducing photosynthetic activity(Li et al., 2018b), when MDA levels and hydrogen peroxide levels are significantly elevated and cold damage occurs in the plant body, which is consistent with the results of the present study. Our study also found that the cold-tolerant mutant strains SA15, SA19, SA23, and SA24 had reduced relative MDA content, and increased SOD, CAT and POD activities, and were therefore more cold-tolerant, which also indicated that plants would mobilize different levels of antioxidant enzyme activity in the face of abiotic stress to respond to or alleviate injury (Li et al., 2022b; Duan et al., 2023). In addition, peroxidase plays a key role in cell elongation and cell wall thickening (Lorenzo et al., 2019), and the thickening of leaves and the thickening of epidermal cells found in this study all show the functional significance of mutants with stronger production of peroxidase to eliminate peroxide damage.

Sugar can also act as an inducer of signals to affect photosynthesis in response to low temperatures in winter (Liu et al., 2017a). The accumulation of sugars by plants in response to cold injury is also an important factor affecting cell structure, especially the cell wall and the mesophyll cell (Bilska-Kos et al., 2018). Sugars accumulate strongly in response to cold stress, polysaccharide was catabolized into soluble sugars and different types of sugars were accumulated to regulate osmotic potential depending on the severity and nature of the stress (Zheng et al., 2016). Proline, which has been widely reported to play an important role in cold stress or cold domestication for protection from cold injury, is considered another tolerance mechanism for abiotic stresses (Shin et al., 2018). The results of this study showed that the significant accumulation of soluble sugars and proline in the cold-tolerant strains SA15, SA19, SA23, and SA24 reflects one of the mechanisms to obtain higher tolerance from the physiological level. Therefore, combining anatomical features and physiological and biochemical indices, is a proven method to comprehensive screen for cold-tolerant mutants of *Plumbago indica* L.

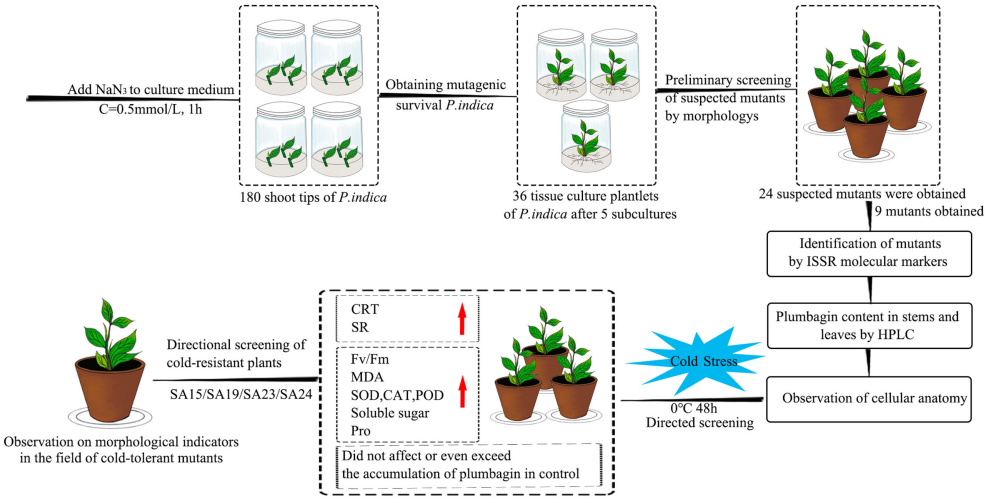


FIGURE 17
Flowchart for targeted screening of cold-tolerant mutants and evaluation of cold-tolerance in *Plumbago indica* L.

In the field, the cold-tolerant mutants SA19 and SA24 were found to have reduced plant height, delayed flowering and short inflorescences, which are consistent with the studies of Li et al. (2022c) and Li et al. (2021). The phenomenon may be related to plant cell damage or DNA mutation due to mutagenesis, resulting in damage during plant growth and development, but such damage does not necessarily affect the ornamental traits of the plant (Amirikhah et al., 2019). In this study, the *Plumbago indica* L. cold-resistant mutant showed overall delayed flowering and delayed senescence, and was able to maintain good ornamental traits, making it a better mutant for both cold tolerance and medicinal ornamental properties.

## 5 Conclusion

In this study, four cold-tolerant mutants were targeted and screened by a combination of ISSR molecular markers, morphological anatomy, and artificial low-temperature stress experiments using $NaN_3$ mutagenesis treatment of *Plumbago indica* L., and their cold-tolerance characteristics were reported for the first time, and the technical procedure is shown (Figure 17). The mutagenic effect of $NaN_3$ on the genetic variation occurring in the same genotype of *Plumbago indica* L.was remarkable, with 87.5% molecular marker polymorphism and 5.00% mutagenic efficiency of mutants. The four cold-tolerant mutants showed consistency in morphological and physiological and biochemical characteristics and initially showed the ability to adapt to short-term stress at low temperature of 0°C for 48h using ISSR markers combined with plumbagin content and morphological anatomical structures identification has a high accuracy in identifying *Plumbago indica* L. mutants.

## Data availability statement

The original contributions presented in the study are included in the article/Supplementary Material. Further inquiries can be directed to the corresponding author.

## Author contributions

XC and YL performed the experiments, and analyzed experimental data. JL and YZ participated in some data analysis. TL, LY, JNL and XY contributed by collecting some experimental materials. XC and SG designed the experiments. YL drafted the manuscript and supervised the project. SG supervised the project. The authors take responsibility for all aspects of the reliability and freedom from bias of the data presented and their interpretation. All authors have read and approved the final manuscript.

## Funding

This work was supported by the Natural Science Foundation of Sichuan Province (2022NSFSC0099) and the Sichuan Province Science and Technology Support Program (2021YFYZ0006).

## Acknowledgments

We acknowledge the support provided by our labs at Sichuan Agricultural University.

## Conflict of interest

The authors declare that the research was conducted in the absence of any commercial or financial relationships that could be construed as a potential conflict of interest.

## Publisher's note



## Supplementary material

The Supplementary Material for this article can be found online at: https://www.frontiersin.org/articles/10.3389/fpls.2023.1149669/full#supplementary-material

## References

Amirikhah, R., Etemadi, N., Sabzalian, M. R., Nikbakht, A., and Eskandari, A. (2019). Physiological consequences of gamma ray irradiation in tall fescue with elimination potential of epichloë fungal endophyte. *Ecotoxicol. Environ. Saf.* 182, 109412. doi: 10.1016/j.ecoenv.2019.109412

Bilska-Kos, A., Panek, P., Szulc-Głaz, A., Ochodzki, P., Cisło, A., and Zebrowski, J. (2018). Chilling-induced physiological, anatomical and biochemical responses in the leaves of miscanthus × giganteus and maize (*Zea mays* l.). *J. Plant Physiol.* 228, 178–188. doi: 10.1016/j.jplph.2018.05.012

Chaudhary, J., Alisha, A., Bhatt, V., Chandanshive, S., Kumar, N., Mir, Z., et al. (2019). Mutation breeding in tomato: advances, applicability and challenges. *Plants-Basel* 8, (5). doi: 10.3390/plants8050128

Chen, Y. L., Liang, H. L., Ma, X. L., Lou, S. L., Xie, Y. Y., Liu, Z. L., et al. (2013). An efficient rice mutagenesis system based on suspension-cultured cells. *J. Integr. Plant Biol.* 55 (2), 122–130. doi: 10.1111/jipb.12000

Chen, L., Long, C., Wang, D., and Yang, J. (2020a). Phytoremediation of cadmium (Cd) and uranium (U) contaminated soils by *Brassica juncea* l. enhanced with exogenous application of plant growth regulators. *Chemosphere* 242, 125112. doi: 10.1016/j.chemosphere.2019.125112

Chen, L., Pan, Y., Li, H., Jia, X., Guo, Y., Luo, J., et al. (2020b). Methyl jasmonate alleviates chilling injury and keeps intact pericarp structure of pomegranate during low temperature storage. *Food Sci. Technol. Int.* 27 (1), 22–31. doi: 10.1177/1082013220921597

Coble, A. P., and Cavaleri, M. A. (2017). Vertical leaf mass per area gradient of mature sugar maple reflects both height-driven increases in vascular tissue and light-driven increases in palisade layer thickness. *Tree Physiol.* 37 (10), 1337–1351. doi: 10.1093/treephys/tpx016

Duan, Y., Lei, T., Li, W., Jiang, M., Zhao, Z., Yu, X., et al. (2023). Enhanced na(+) and cl(-) sequestration and secretion selectivity contribute to high salt tolerance in the tetraploid recretohalophyte *Plumbago auriculat*a lam. *Planta* 257 (3), 52. doi: 10.1007/s00425-023-04082-7

Dumlao, M. R., Darehshouri, A., Cohu, C. M., Muller, O., Mathias, J., Adams, W. W., et al. (2012). Low temperature acclimation of photosynthetic capacity and leaf morphology in the context of phloem loading type. *Photosynthesis Res.* 113 (1-3), 181–189. doi: 10.1007/s11120-012-9762-5

Gentile, A., and La Malfa, S. (2019). "New breeding techniques for sustainable agriculture," in *Innovations in sustainable agriculture*. Eds. M. Farooq and M. Pisante (Cham: Springer International Publishing), 411–437. doi: 10.1007/978-3-030-23169-9_13

Gomez, D., Hernandez, L., Martinez, J., Escalante, D., Zevallos, B. E., Yabor, L., et al. (2019). Sodium azide mutagenesis within temporary immersion bioreactors modifies sugarcane *in vitro* micropropagation rates and aldehyde, chlorophyll, carotenoid, and phenolic profiles. *Acta Physiol. Plantarum* 41, (7). doi: 10.1007/s11738-019-2911-0

He, N. P., Liu, C. C., Tian, M., Li, M. L., Yang, H., Yu, G. R., et al. (2018). Variation in leaf anatomical traits from tropical to cold-temperate forests and linkage to ecosystem functions. *Funct. Ecol.* 32 (1), 10–19. doi: 10.1111/1365-2435.12934

Janero, D. R. (1990). Malondialdehyde and thiobarbituric acid-reactivity as diagnostic indices of lipid peroxidation and peroxidative tissue injury. *Free Radical Biol. Med.* 9 (6), 515–540. doi: 10.1016/0891-5849(90)90131-2

Janni, M., Gulli, M., Maestri, E., Marmiroli, M., Valliyodan, B., Nguyen, H. T., et al. (2020). Molecular and genetic bases of heat stress responses in crop plants and breeding for increased resilience and productivity. *J. Exp. Bot.* 71 (13), 3780–3802. doi: 10.1093/jxb/eraa034

Janosevic, D., Uzelac, B., Stojicic, D., Tubic, L., and Budimir, S. (2011). Early stages of leaf development in has mutant of *Arabidopsis thaliana*. *Biol. Plantarum* 55 (4), 641–646. doi: 10.1007/s10535-011-0162-z

Katoch, K., Gupta, S., Gupta, A. P., Goyal, P., Devi, R., Dey, A., et al. (2022). Biotic elicitation for enhanced production of plumbagin in regenerated shoot cultures of *Plumbago zeylanica* using response surface methodology. *Plant Cell Tissue Organ Culture (PCTOC)* 151 (3), 605–615. doi: 10.1007/s11240-022-02375-5

Knight, M. R., and Knight, H. (2012). Low-temperature perception leading to gene expression and cold tolerance in higher plants. *New Phytol.* 195 (4), 737–751. doi: 10.1111/j.1469-8137.2012.04239.x

Li, Y., Chen, L., Zhan, X., Liu, L., Feng, F., Guo, Z., et al. (2022c). Biological effects of gamma-ray radiation on tulip (*Tulipa gesneriana* l.). *PeerJ* 10, e12792. doi: 10.7717/peerj.12792

Li, W., Gao, S., Lei, T., Jiang, L., Duan, Y., Zhao, Z., et al. (2022b). Transcriptome analysis revealed a cold stress-responsive transcription factor, PaDREB1A, in *Plumbago auriculata* that can confer cold tolerance in transgenic *Arabidopsis thaliana*. *Front. Plant Sci.* 13. doi: 10.3389/fpls.2022.760460

Li, X., Gao, F., Wu, Z., Wang, X., and Zhu, B. (2018a). Genetic diversity analysis of lantern pepper germplasm resources for sauce use by ISSR. *Mol. Plant Breed.* 16 (15), 1711–1716.

Li, Y. C., He, S. M., He, Z. X., Li, M. H., Yang, Y. X., Pang, J. X., et al. (2014). Plumbagin induces apoptotic and autophagic cell death through inhibition of the PI3K/Akt/mTOR pathway in human non-small cell lung cancer cells. *Cancer Lett.* 344 (2), 239–259. doi: 10.1016/j.canlet.2013.11.001

Li, Y. R., Liu, L., Wang, D., Chen, L., and Chen, H. (2021). Biological effects of electron beam to target turning X-ray (EBTTX) on two freesia (Freesia hybrida) cultivars. *PeerJ* 9, e10742. doi: 10.7717/peerj.10742

Li, X., Wei, J. P., Scott, E. R., Liu, J. W., Guo, S., Li, Y., et al. (2018b). Exogenous melatonin alleviates cold stress by promoting antioxidant defense and redox homeostasis in *Camellia sinensis* l. *Molecules* 23, (1). doi: 10.3390/molecules23010165

Li, S., Yang, N., and Chen, L. (2022a). Paraffin section observation of flower bud differentiation of *Chimonanthus praecox* in kunming and comparison of the differentiation processes in different regions, China. *Hortic. Plant J.* 8 (2), 221–229. doi: 10.1016/j.hpj.2021.11.001

Liu, Y. L., Cai, Y. E., He, C. W., Chen, M. W., and Li, H. (2017b). Anticancer properties and pharmaceutical applications of plumbagin: a review. *Am. J. Of Chin. Med.* 45 (3), 423–441. doi: 10.1142/S0192415X17500264

Liu, B., Zhao, F. M., Cao, Y., Wang, X. Y., Li, Z., Shentu, Y., et al. (2022). Photoprotection contributes to freezing tolerance as revealed by RNA-seq profiling of rhododendron leaves during cold acclimation and deacclimation over time. *Hortic. Res.* 9, uhab025. doi: 10.1093/hr/uhab025

Liu, B., Zhou, H., Cao, S., Xia, Y. P., and Arora, R. (2017a). Comparative physiology of natural deacclimation in ten azalea cultivars. *Hortscience* 52 (10), 1451–1457. doi: 10.21273/hortsci12197-17

Lorenzo, M., Pinedo, M. L., Equiza, M. A., Fernandez, P. V., Ciancia, M., Ganem, D. G., et al. (2019). Changes in apoplastic peroxidase activity and cell wall composition are associated with cold-induced morpho-anatomical plasticity of wheat leaves. *Plant Biol.* 21, 84–94. doi: 10.1111/plb.12709

Mago, R., Till, B., Periyannan, S., Yu, G., Wulff, B. B. H., and Lagudah, E. (2017). Generation of loss-of-Function mutants for wheat rust disease resistance gene cloning. *Methods Mol. Biol. (Clifton NJ)* 1659, 199–205. doi: 10.1007/978-1-4939-7249-4_17

Nayak, P., Sharma, M., Behera, S. N., Thirunavoukkarasu, M., and Chand, P. K. (2015). High-performance liquid chromatographic quantification of plumbagin from transformed rhizoclones of *Plumbago zeylanica* l.: inter-clonal variation in biomass growth and plumbagin production. *Appl. Biochem. Biotechnol.* 175 (3), 1745–1770. doi: 10.1007/s12010-014-1392-2

Peng, D., Zhou, B., Jiang, Y., Tan, X., Yuan, D., and Zhang, L. (2018). Enhancing freezing tolerance of brassica napus l. by overexpression of a stearoyl-acyl carrier protein desaturase gene (SAD) from *Sapium sebiferum* (L.) roxb. *Plant Sci.* 272, 32–41. doi: 10.1016/j.plantsci.2018.03.028

Podgorbunskikh, E. M., Bychkov, A. L., Ryabchikova, E. I., and Lomovsky, O. I. (2020). The effect of thermomechanical pretreatment on the structure and properties of lignin-rich plant biomass. *Molecules* 25, (4). doi: 10.3390/molecules25040995

Polat, I., Turgutoglu, E., and Kurt, S. (2015). Determination of genomic diversity within mutant lemon (*citrus limon* l.) and mandarin (citrus reticulata) using molecular markers. *Pakistan J. Bot.* 47 (3), 1095–1102.

Robinson, W. A. (2021). Climate change and extreme weather: a review focusing on the continental united states. *J. Air Waste Manage. Assoc.* 71 (10), 1186–1209. doi: 10.1080/10962247.2021.1942319

Sen, A. (2016). Retrotransposon insertion variations in doubled haploid bread wheat mutants. *Plant Growth Regul.* 81 (2), 325–333. doi: 10.1007/s10725-016-0209-4

Sheikh, A. A. D., and Moradnejad, M. (2014). Mutagenesis in olive (*Olea europaea* l.) calli caused by sodium azide and detection of mutants using ISSR and RAPD markers. *J. Hortic. Sci. Biotechnol.* 89 (2), 153–158. doi: 10.1080/14620316.2014.11513062

Shelake, R. M., Pramanik, D., and Kim, J. Y. (2019). Evolution of plant mutagenesis tools: a shifting paradigm from random to targeted genome editing. *Plant Biotechnol. Rep.* 13 (5), 423–445. doi: 10.1007/s11816-019-00562-z

Shen, P., Gao, S., Chen, X., Lei, T., Li, W., Huang, Y., et al. (2020). Genetic analysis of main flower characteristics in the F1 generation derived from intraspecific hybridization between *Plumbago auriculata* and *Plumbago auriculata* f. alba. *Scientia Hortic.* 274, 109652. doi: 10.1016/j.scienta.2020.109652

Shi, L. S., Gao, S. P., Lei, T., Duan, Y. F., Yang, L. J., Li, J. N., et al. (2022). An integrated strategy for polyploidization of *Cerastigma willmottianum* stapf based on tissue culture and chemical mutagenesis and the carbon dioxide fixation ability of tetraploids. *Plant Cell Tissue Organ Culture* 149 (3), 783–783. doi: 10.1007/s11240-022-02302-8

Shin, H., Min, K., and Arora, R. (2018). Exogenous salicylic acid improves freezing tolerance of spinach (Spinacia oleracea l.) leaves. *Cryobiology* 81, 192–200. doi: 10.1016/j.cryobiol.2017.10.006

Singh, T., Sharma, U., and Agrawal, V. (2020). Isolation and optimization of plumbagin production in root callus of plumbago zeylanica l. augmented with chitosan and yeast extract. *Ind. Crops Products* 151, 112446. doi: 10.1016/j.indcrop.2020.112446

Sulu, G., Kacar, Y. A., Polat, I., Kitapci, A., Turgutoglu, E., Simsek, O., et al. (2020). Identification of genetic diversity among mutant lemon and mandarin varieties using different molecular markers. *Turkish J. Agric. Forestry* 44 (5), 465–478. doi: 10.3906/tar-1909-67

Sun, B., Liu, G. L., Phan, T. T., Yang, L. T., Li, Y. R., and Xing, Y. X. (2017). Effects of cold stress on root growth and physiological metabolisms in seedlings of different sugarcane varieties. *Sugar Tech* 19 (2), 165–175. doi: 10.1007/s12355-016-0452-z

Szurman-Zubrzycka, M. E., Zbieszczyk, J., Marzec, M., Jelonek, J., Chmielewska, B., Kurowska, M. M., et al. (2018). HorTILLUS-a rich and renewable source of induced mutations for Forward/Reverse genetics and pre-breeding programs in barley (*Hordeum vulgare* l.). *Front. Plant Sci.* 9. doi: 10.3389/fpls.2018.00216

Theocharis, A., Clement, C., and Barka, E. A. (2012). Physiological and molecular changes in plants grown at low temperatures. *Planta* 235 (6), 1091–1105. doi: 10.1007/s00425-012-1641-y

Turkoglu, A., Tosun, M., and Haliloglu, K. (2022). Mutagenic effects of sodium azide on *in vitro* mutagenesis, polymorphism and genomic instability in wheat (Triticum aestivum l.). *Mol. Biol. Rep.* 49 (11), 10165-10174. doi: 10.1007/s11033-022-07896-y

Vasav, A. P., Pable, A. A., and Barvkar, V. T. (2020). Differential transcriptome and metabolome analysis of *Plumbago zeylanica* l. reveal putative genes involved in plumbagin biosynthesis. *Fitoterapia* 147, 104761. doi: 10.1016/j.fitote.2020.104761

Velu, D., Ponnuvel, K. M., Muthulakshmi, M., Sinha, R. K., and Qadri, S. M. H. (2008). Analysis of genetic relationship in mutant silkworm strains of bombyx mori using inter simple sequence repeat (ISSR) markers. *J. Genet. Genomics* 35 (5), 291–297. doi: 10.1016/s1673-8527(08)60042-9

Venkateswarulu, N., Shameer, S., Bramhachari, P. V., Basha, S. K. T., Nagaraju, C., and Vijaya, T. (2018). Isolation and characterization of plumbagin (5- hydroxyl- 2-methylnaptalene-1,4-dione) producing endophytic fungi cladosporium delicatulum from endemic medicinal plants: isolation and characterization of plumbagin producing endophytic fungi from endemic medicinal plants. *Biotechnol. Rep. (Amsterdam Netherlands)* 20, e00282. doi: 10.1016/j.btre.2018.e00282

Wang, X., Arora, R., Horner, H. T., and Krebs, S. L. (2008). Structural adaptations in overwintering leaves of thermonastic and nonthermonastic *Rhododendron species*. *J. Am. Soc. Hortic. Sci.* 133 (6), 768–776. doi: 10.21273/jashs.133.6.768

Wannajindaporn, A., Kativat, C., and Tantasawat, P. A. (2016). Mutation induction of *Dendrobium* 'Earsakul' using sodium azide. *Hortscience* 51 (11), 1363–1370. doi: 10.21273/hortsci10860-16

Wu, J.-H., Zhang, J., Lan, F., Fan, W.-F., and Li, W. (2020). Morphological, cytological, and molecular variations induced by gamma rays in ground-grown chrysanthemum 'Pinkling'. *Can. J. Plant Sci.* 100 (1), 68–77. doi: 10.1139/cjps-2019-0064

Xu, H., Huang, C., Jiang, X., Zhu, J., Gao, X., and Yu, C. (2022). Impact of cold stress on leaf structure, photosynthesis, and metabolites in *Camellia weiningensis* and c. *oleifera Seedlings. Hortic.* 8 (6), 494. doi: 10.3390/horticulturae8060494

Yamori, W., Hikosaka, K., and Way, D. A. (2014). Temperature response of photosynthesis in c-3, c-4, and CAM plants: temperature acclimation and temperature adaptation. *Photosynthesis Res.* 119 (1-2), 101–117. doi: 10.1007/s11120-013-9874-6

Zheng, C., Wang, Y., Ding, Z. T., and Zhao, L. (2016). Global transcriptional analysis reveals the complex relationship between tea quality, leaf senescence and the responses to cold-drought combined stress in *Camellia sinensis*. *Front. Plant Sci.* 7. doi: 10.3389/fpls.2016.01858

Zheng, L., Wu, W., Gao, Y., Wu, Y., Xu, Y., Zhang, G., et al. (2022). Integrated transcriptome, small RNA and degradome analysis provide insights into the transcriptional regulatory networks underlying cold acclimation in jojoba. *Scientia Hortic.* 299, 111050. doi: 10.1016/j.scienta.2022.111050

Zhu, J.-K. (2016). Abiotic stress signaling and responses in plants. *Cell* 167 (2), 313–324. doi: 10.1016/j.cell.2016.08.029

Zhuang, Q., Chen, S., Jua, Z., and Yao, Y. (2021). Joint transcriptomic and metabolomic analysis reveals the mechanism of low-temperature tolerance in hosta ventricosa. *PloS One* 16 (11), e0259455. doi: 10.1371/journal.pone.0259455

Ziarovska, J., Razna, K., and Labajova, M. (2013). Using of inter microsatellite polymorphism to evaluate gamma-irradiated amaranth mutants. *Emirates J. Food Agric.* 25 (9), 673–681. doi: 10.9755/ejfa.v25i9.15879

frontiers | Frontiers in Plant Science

TYPE Original Research
PUBLISHED 11 July 2023
DOI 10.3389/fpls.2023.1164467



OPEN ACCESS

EDITED BY
Weibiao Liao,
Gansu Agricultural University, China

REVIEWED BY
Weihua Qiao,
Chinese Academy of Agricultural Sciences, China
Ze Wu,
Nanjing Agricultural University, China

*CORRESPONDENCE
Zhimin Wang
minzniwang_555@163.com
Shibing Tian
2508436730@qq.com

†These authors have contributed equally to this work

RECEIVED 12 February 2023
ACCEPTED 16 June 2023
PUBLISHED 11 July 2023

CITATION
Hu R, Wang J, Yang H, Wei D, Tang Q, Yang Y, Tian S and Wang Z (2023) Comparative transcriptome analysis reveals the involvement of an MYB transcriptional activator, *SmMYB108*, in anther dehiscence in eggplant.
*Front. Plant Sci.* 14:1164467.
doi: 10.3389/fpls.2023.1164467



# Comparative transcriptome analysis reveals the involvement of an MYB transcriptional activator, *SmMYB108*, in anther dehiscence in eggplant

Ruolin Hu[1,2†], Jiali Wang[1,2†], Huiqing Yang[1,2], Dayong Wei[1,2], Qinglin Tang[1,2], Yang Yang[3], Shibing Tian[3*] and Zhimin Wang[1,2*]

[1]College of Horticulture and Landscape Architecture, Southwest University, Chongqing, China, [2]Chongqing Key Laboratory of Olericulture, Chongqing, China, [3]The Institute of Vegetables and Flowers, Chongqing Academy of Agricultural Sciences, Chongqing, China

Male sterility is a highly attractive agronomic trait as it effectively prevents self-fertilization and facilitates the production of high-quality hybrid seeds in plants. Timely release of mature pollen following anther dehiscence is essential for stamen development in flowering plants. Although several theories have been proposed regarding this, the specific mechanism of anther development in eggplant remains elusive. In this study, we selected an R2R3-MYB transcription factor gene, *SmMYB108*, that encodes a protein localized primarily in the nucleus by comparing the transcriptomics of different floral bud developmental stages of the eggplant fertile line, F142. Quantitative reverse transcription polymerase chain reaction revealed that *SmMYB108* was preferentially expressed in flowers, and its expression increased significantly on the day of flowering. Overexpression of *SmMYB108* in tobacco caused anther dehiscence. In addition, we found that *SmMYB108* primarily functions as a transcriptional activator *via* C-terminal activation (amino acid 262–317). Yeast one-hybrid and dual-luciferase reporter assays revealed that genes (*SmMYB21*, *SmARF6*, and *SmARF8*) related to anther development targeted the *SmMYB108* promoter. Overall, our results provide insights into the molecular mechanisms involved in the regulation of anther development by *SmMYB108*.

KEYWORDS

**eggplant, MYB transcription factor, anther dehiscence, regulation of gene expression, RNA-seq**

## Highlights

- Excavating the differentially expressed gene *SmMYB108* of eggplant fertile line F142 in anther different developmental stages.
- Elucidating that *SmMYB108* functioned as a transcriptional activator to regulate anther development.
- Finding some genes related to anther development directly targeted *SmMYB108* promoter.
- The research results are of great significance to understand the molecular mechanism of *SmMYB108* regulating anther development.

## Introduction

Eggplant (*Solanum melongena*), an important vegetable crop, cultivated in tropical, subtropical, and temperate regions, exhibits heterosis and is mainly produced by hybrids. The use of a strict pollination control system is a prerequisite to avoid self-fertilization in plants (Kempe and Gils, 2011). Male sterility is generally used to produce hybrid seeds that can effectively avoid self-fertilization and solve the difficulties of traditional seed production. Molecular mechanisms of male infertility have been reported in previous studies (Ma et al., 2015; Singh et al., 2015). RNA-sequencing (RNA-seq) technology helps in understanding the gene expression patterns and inferring the candidate genes related to male infertility. Many studies have conducted RNA-seq analyses of the male sterile floral organs of tomatoes (Jeong et al., 2014), cotton (Wei et al., 2013), peppers (Liu et al., 2013), *Brassica napus* (Yan et al., 2013), and watermelons (Rhee et al., 2015).

Stamen is the male reproductive organ of flowering plants, which consists of an anther, a space for pollen development, and a filament that provides the anther with structural support and nutrients. Development of anther, an important component of stamens, is mainly divided into two stages. In the first stage, the initial stamen primordium forms a complete pollen sac wall after tissue specialization and meiosis, which is followed by the formation of the outer epidermis, endothecium, middle layer, and tapetum from the outside to the inside. Tetrad structure of the microspores is located at the center of the anther chamber. In the second stage, the anther continues to expand, filament elongates, microspores develop into pollen grains from the tetrad structure, pollens sac cracks and releases pollens, and pollination and fertilization are completed, after which, the anther tissue gradually ages and degenerates (Goldberg et al., 1993; Wilson et al., 2011).

An anther dehisces in a timely manner to release mature pollen for complete pollination and fertilization. Transcription factors (TFs) containing the MYB domain in plants are known as MYB TFs. MYB domain consists of one to four amino acid (aa) sequences and forms a helix-turn-helix motif (Dubos et al., 2010). On the basis of the number of adjacent repeats, MYB proteins are divided into four categories: 1R-MYB (MYB-related), 2R-MYB (R2R3-MYB), 3R-MYB (R1R2R3-MYB), and 4R-MYB (Katiyar et al., 2012). Among them, R2R3-MYB TFs are one of the most abundant gene families in plants (Stracke et al., 2001) that are involved in plant cell development and morphogenesis, biological and non-biological stress responses, hormone signal transduction, and secondary metabolism regulation (Wang et al., 2016; Kocábek et al., 2018; Guan et al., 2019).

Secondary thickening of the inner wall of the anther chamber is essential for anther dehiscence (Zhao and Dong, 2015). *AtMYB26* is vital for secondary thickening, directly inducing the expression of *AtNST1* and *AtNST2* in the anthers. Both *myb26* and *nst1 nst2* mutants failed to exhibit anther dehiscence (Yang et al., 2017). Previous studies have reported that *AtMYB103*, *AtMYB83*, and *AtMYB46* are direct targets of *AtNST1* and *AtNST2*, regulating secondary wall biosynthesis to affect anther dehiscence and pollen development. Another study reported that *AtMYB83* acts redundantly with *AtMYB46* as a key molecular in the regulating of secondary wall biosynthesis (Zhong et al., 2008; McCarthy et al., 2009; Zhong et al., 2007). Li et al. (2019) revealed that *RUS*4 affects the synthesis of the secondary wall of the inner wall of the drug chamber by indirectly activating the expression of the TFs, *AtMYB103* and *AtMYB85* (Li et al., 2019). Because of the defects in filament elongation, anther dehiscence, and pollen viability, *myb21 myb24* double-mutant plants are male sterile. R2R3-MYB TFs, *MYB21 a*nd *MYB24*, are essential for filament elongation, anther dehiscence, and pollen maturation, jasmonic acid (JA) regulation of male fertility in *Arabidopsis thaliana* (Song et al., 2011). Overexpression of *GhMYB24* in Arabidopsis severely decreases the fertility by inhibiting filament elongation and anther dehiscence and decreasing the pollen viability. *atmyb21 atmyb24* double-mutant plants have been reported to be severely male sterile, and the expression of *GhMYB24* in the *atmyb21 atmyb24* double-mutant has been reported to partially rescued the sterile phenotype (Li et al., 2013). Several studies have investigated the role of the TF, *MYB108*, in anther development. *AtMYB108* and *AtMYB24* have been reported to coordinate the JA pathway during anther dehiscence (Mandaokar and Browse, 2009). Sun et al. reported that a JA-induced R2R3-MYB TF, *CaMYB108*, is involved in the regulation of capsaicinoids, cap biosynthesis, and stamen development. Silencing of *CaMYB108* has been reported to delay anther dehiscence and decrease the pollen viability (Sun et al., 2019). *arf17* mutant anther is indehiscent, and the auxin response factor, *ARF17*, can directly bind to the *AtMYB108* promoter and induce its expression in *arf17* mutant to rescue its anther dehiscence phenotype (Xu et al., 2019).

Molecular mechanism by which TF *MYB108* regulates the development of anthers remains poorly understood. In this study, we identified differentially expressed gene (DEG), *SmMYB108*, in eggplant, whose expression was highest on the day of flowering (FD). We verified that this TF was involved in stamen development. In addition, we found that proteins related to anther development (SmMYB21, SmARF6, and SmARF8) directly bound to the promoter of *SmMYB108*. Our findings indicate that *SmMYB108* plays a central role in anther development.

## Results

### Identification of DEGs

We determined the mRNA (messenger Ribonucleic Acid) expression levels in the floral buds of the eggplant fertile line, F142, at different developmental stages. The FPKM (fragments per kilobase

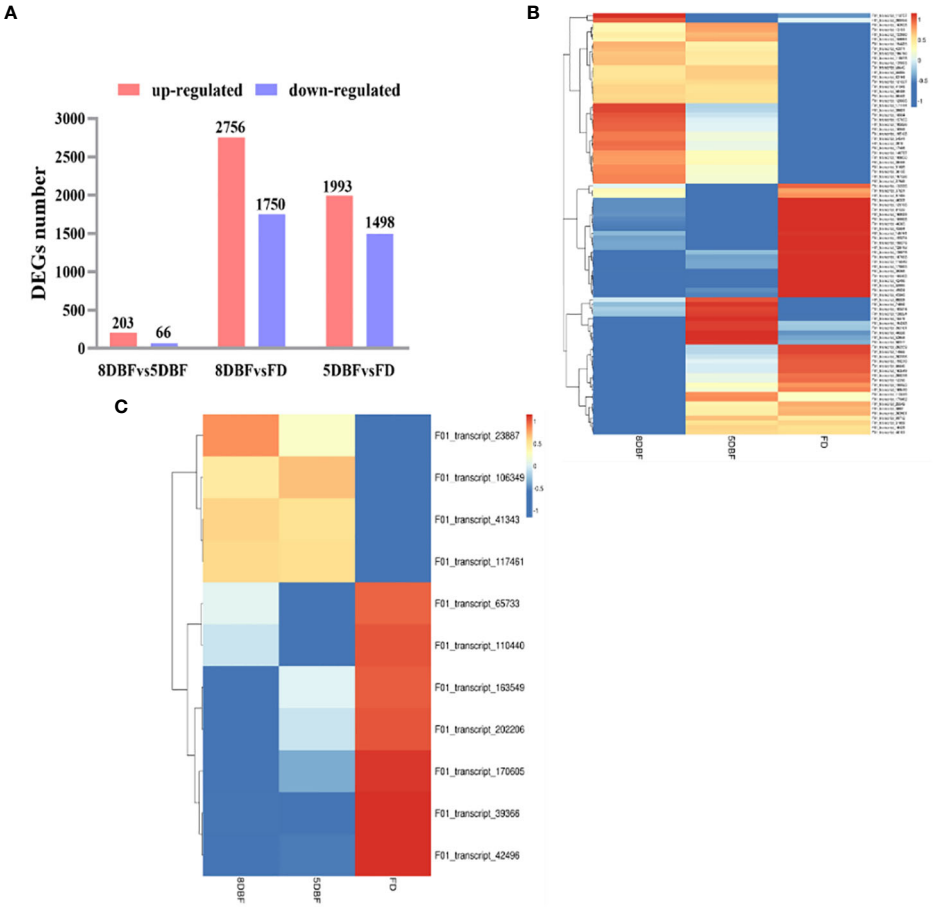


FIGURE 1
Analysis of DEGs between the eggplant fertile line F142 in different stages of flower buds. **(A)** The total number of upregulated and downregulated DEGs. **(B)** Heat map of differentially expressed transcription factors. **(C)** Heat map analysis of 11 common differentially expressed genes.

of exon per million mapped fragments) method was used to identify the DEGs. In total, 5,549 DEGs were identified *via* pairwise comparisons. Comparison of 8 days before flowering (DBF) and 5 DBF revealed the lowest number, 269 DEGs, of which 203 were upregulated and 66 were downregulated. The maximum number of DEGs was between 8 DBF and the day of flowering (FD), including 2,756 upregulated and 1,750 downregulated genes (Figure 1A). Notably, 2,552 common DEGs (1,739 upregulated and 816 downregulated) were shared between the 8 DBF and FD and between 5 DBF and FD groups (Supplementary Figures S1A–C).

TFs play an important role in anther development. Eighty-nine TFs were identified among all DEGs, which could be classified into 29 families. The important families were bHLH (basic helix-loop-helix) (19.10%), MYB(v-myb avian myeloblastosis viral oncogene homolog)-related (13.48%), AP2 (APETALA2) (11.24%), NAC (NAM、ATAF1/2、CUC1/2) (1.12%), WRKY (7.87%), TCP ((TEOSINTE BRANCHED1/CYCLOIDEA/PROLIFERATING CELL FACTORS) (7.87%), and the MADS (2.25%) families (Supplementary Figure S2A). On the basis of the similarity in gene expression, hierarchical clustering was performed using the 89 differentially expressed TFs in samples (Figure 1B; Supplementary Table 2). Hierarchical clustering of the gene expression profiles in the three stages revealed different expression patterns in these samples, providing an overall understanding of the changes in gene expression. Forty-two MYB TFs were identified among 89 TFs, of which 31 were upregulated and 11 were downregulated. Moreover, 11 common MYB TFs between 8 DBF and FD and between 5 DBF and FD were identified, and the expression pattern was visualized using a heat map (Supplementary Figure S2B; Supplementary Table 3). Interestingly, we found that the expression levels of gene F01_transcript_42496 (referred as *SmMYB108* in this study) were significantly higher in FD than that in 8 and 5 DBF (Figure 1C). These results suggest the involvement of an extremely intricate transcriptional network in anther development.

## *SmMYB108* is highly expressed during the flowering period

To verify the RNA-seq data, quantitative reverse transcription polymerase chain reaction (qRT-PCR) was conducted on nine randomly selected genes, and the results confirmed the accuracy of transcriptome analysis (Supplementary Figure S3). We found that *SmMYB108* was predominantly expressed in the flowers, followed by roots, but its transcript levels were low in the stems, leaves, anthers, petals, and sepals through qRT-PCR (Figure 2A).

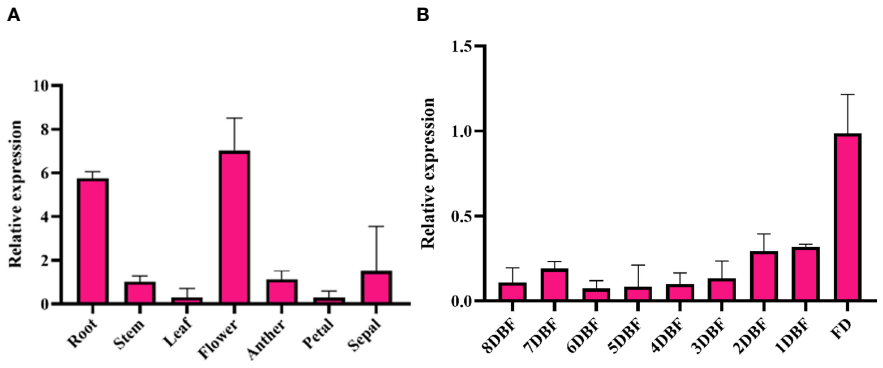


FIGURE 2
Expression analysis of *SmMYB108*. **(A)** Expression of *SmMYB108* in different tissues. **(B)** Expression of *SmMYB108* in different developmental stages of flower buds.

Moreover, we quantitatively analyzed the expression levels of *SmMYB108* at different developmental stages. Within the floral buds, *SmMYB108* transcript level was stable from 8 to 3 DBF, increased slightly 2 DBF, and reached the maximum level at flowering (Figure 2B). Taken together, our results indicate *SmMYB108* as a candidate regulator of anther development. Moreover, *SmMYB108* may have roles other than anther development regulation in plants.

To visualize the detailed expression patterns of *SmMYB108*, its promoter was cloned approximately 2-kb 5′ upstream of the sequence included in *gSmMYB108* in this study. We generated *prSmMYB108:GUS Arabidopsis* transgenic lines expressing GUS (B-glucuronidase) fused with the promoter sequence of *SmMYB108* to detect *SmMYB108* expression patterns. Consistent with the gene expression pattern, blue staining was high in the roots, flowers, and leaves of mature plants (Figures 3B–I) and mainly observed in the mature anthers in flowers (Figures 3E, J). GUS staining was observed in all organs in approximately 2-week-old seedlings (Figures 3A, F). These findings highlight the potential role of *SmMYB108* in anther development.

## *SmMYB108* encodes a nucleus-localized R2R3 MYB TF

Full-length coding sequence (CDS) of *SmMYB108* was isolated from the eggplant fertile line F142, and its open reading frame was 954 bp, encoding a protein of 317 amino acids, located on chromosome 5 (Figure 4A). Aa sequence analysis revealed that *SmMYB108* contains two motif DNA-binding domains (BDs) (R2-R3 MYB type) next to the N-terminus (Figure 4B). We retrieved *SmMYB108* homologs from *Solanum lycopersicum*, *S. tuberosum*, *Nicotiana attenuata*, *Capsicum annuum*, and *A. thaliana*. A phylogenetic tree was constructed to identify the orthologs of these genes. We found that the nearest MYB TFs from *StMYB108* (*S. tuberosum*), *CaMYB108* (*C. annuum*), *SlMYB78* (*S. lycopersicum*), and *NaMYB108* (*N. attenuata*), shared sequence identity > 90% (Figure 4C). *AtMYB108*, which showed only 60% aa sequence identity, was the MYB TF most closely related to *A. thaliana*. Interestingly, both *CaMYB108* and *AtMYB108* were induced by JA to participate in anther development (Mandaokar and Browse, 2009; Sun et al., 2019), suggesting that *SmMYB108* may also play a role in stamen development.

TFs regulate transcription depending on their localization in the nucleus. To determine the subcellular localization of *SmMYB108*, the CDS of *SmMYB108* was fused in frame with the green fluorescence protein (GFP) to generate a *35Spro::GFP-SmMYB108* fusion protein (Figure 4D). *35Spro::GFP-SmMYB108* was transiently expressed in the nucleus of *N. benthamiana* leaf epidermal cells. GFP-SmMYB108 was observed exclusively in the nucleus, whereas free GFP (35S::GFP) was observed in both the cytoplasm and nucleus of epidermal cells (Figure 4E), suggesting that *SmMYB108* is localized in the nucleus.

## Overexpression of *SmMYB108* promotes stamen development

To further study the function of *SmMYB108*, we constructed an overexpression vector used for the *Agrobacterium*-mediated transformation of tobacco. We successfully developed 14 transgenic tobacco plants overexpressing *SmMYB108*. In $T_0$ plants, *SmMYB108-OE-2*, *SmMYB108-OE-3*, and *SmMYB108-OE-5* were selected for further analysis (Figure 5A). Floral organ morphology and pollen vitality were not significantly different between the wild-type and *SmMYB108-OE* lines as they exhibited normal anther dehiscence and released viable pollen (Figure 5B). However, the anthers of transgenic tobacco were completely dehiscent and covered by pollen, whereas those of wild-type tobacco were partially dehiscent and covered by a small amount of pollen. These results revealed that the degree of anther dehiscence in transgenic tobacco was greater than that in wild-type tabacco. Moreover, flower buds immediately at the top of tobacco developed earlier than those in transgenic tobacco and wild-type plants. Taken together, these results suggest that *SmMYB108* overexpression promotes the early dehiscence of anthers (Figure 5C).

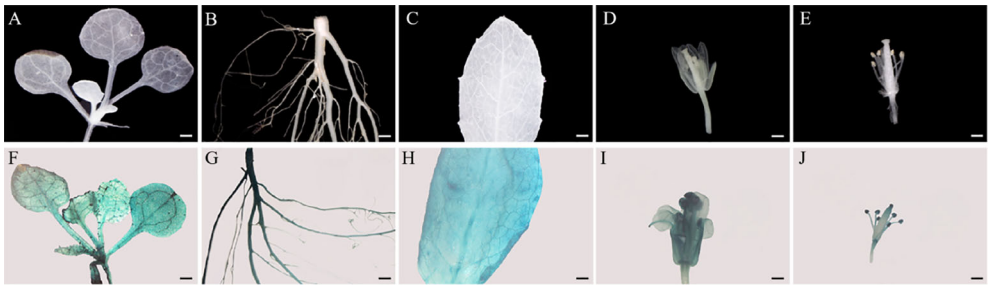


FIGURE 3
Tissue-specific expression analysis of *SmMYB108* in *prSmMYB108:GUS* transgenic plants. **(A–E)** Seedling, root, leaf, mature flower, and anther (from left to right) were from wild type. **(F–J)** Gus-stained seedling, root, leaf, mature flower, and anther (from left to right) were from *prSmMYB108:GUS* transgenic plants. Bar, 500 μm.

## *SmMYB108* functions as a transcriptional activator

*SmMYB108* contains an N-terminal R2R3 repeat domain, responsible for DNA binding, and a C-terminal domain. Transcriptional activation domain of the R2-R3 type MYB TF, which encodes the aa, was located at the C-terminus, as previously reported (Song et al., 2011). We performed a transactivation activity assay in yeast to test the transcriptional activation activity of *SmMYB108*. On the basis of the presence of conserved domains, full-length and a series of truncations were fused in-frame with the GAL4 DNA-binding domain (BD) in the pGBKT7 (BD) vector, and the constructs were transformed into the yeast two-hybrid (Y2H) gold yeast strain. Yeast carrying BDSmMYB108 grew and turned blue on SD/−Trp selective medium along with X-α-gal, indicating that TF *SmMYB108* acts as a transcriptional activator (Figure 6). To determine the specific domain influencing the activation activity of *SmMYB108*, the constructed truncated SmMYB108 was transformed into the Y2H gold yeast strain (Figure 6). The results showed reduced transcriptional activation of SmMYB108 (275–317 aa) and SmMYB108 (262–274 aa), indicating destruction of the self-activating domain. Therefore, the C-terminus (262–317 aa) was essential for the activation activity of *SmMYB108* (Figure 6).

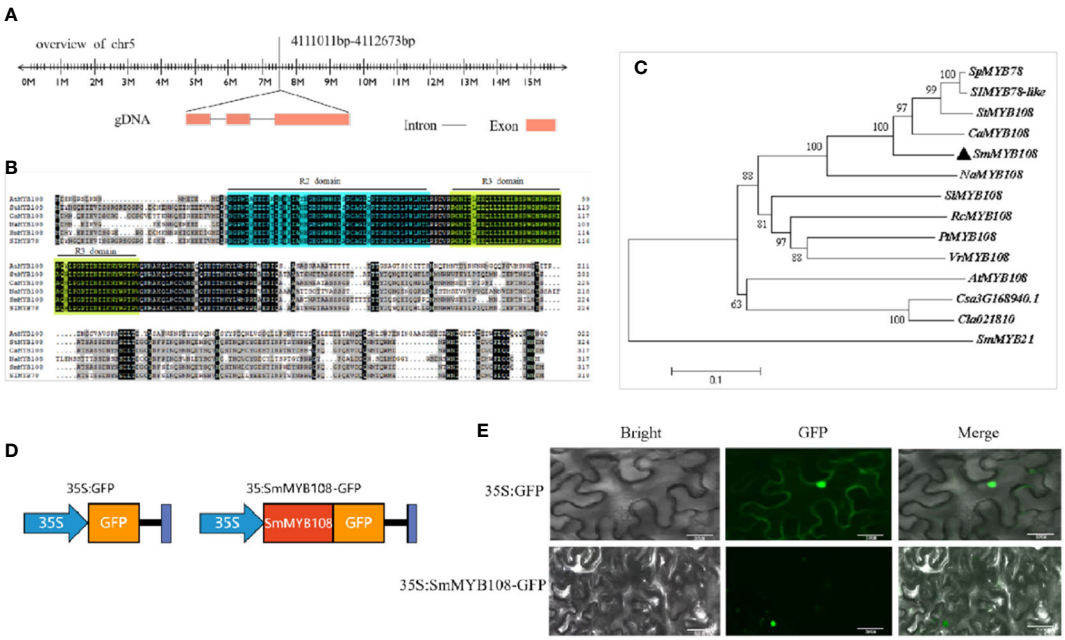


FIGURE 4
Phylogenetic and subcellular analyses of SmMYB108. **(A)** The genomic sequence of *SmMYB108* that is mapped to eggplant genome. **(B)** Sequence analysis of *SmMYB108*. To compare the MYB sequences among different plant species, *SmMYB108* was used as a bait gene and searched in National Center for Biotechnology Information (NCBI) database for highly similar sequences MYB TFs in other species. **(C)** A phylogenetic tree showing aa sequence similarities among *SmMYB108* and closely related MYB TFs in other species. **(D, E)** Subcellular localization of 35S:SmMYB108-GFP fusion protein in Tobacco epidermal cells. 35S::GFP served as a control. Bar, 50 μm.

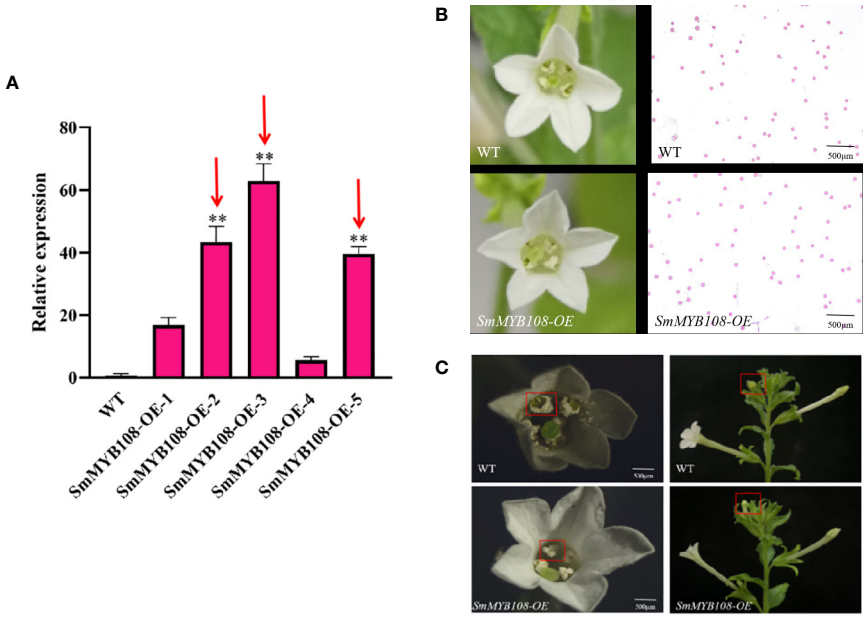


FIGURE 5
Morphological characterization of *SmMYB108-OE* plants floral organ. **(A)** RT-qPCR analysis of SmMYB108 transcripts present in wild-type (WT) and *SmMYB108-OE* lines. Error bars, 6 SEM (n = 3). Three lines were selected for further research (red arrows). **(B)** Morphological features of flowers in the same period in wild type and *SmMYB108-OE* lines. **(C)** The degree of antherin the same period in wild type and SmMYB108-OE lines.

## Anther development-related genes directly target *SmMYB108*

*AtMYB21*, *AtMYB26*, *AtARF6*, and *AtARF8* participated in anther development in *A. thaliana*, as previously reported (Song et al., 2011; Yang et al., 2017; Nagpal et al., 2005). To determine the direct target genes of *SmMYB108*, we selected *SmMYB21*, *SmMYB26*, *SmARF6*, and *SmARF8* as candidate target genes for screening *via* Y1H assay. *SmMYB108* promoters were ligated into the pAbAi vector to construct bait vectors (pAbAi-ProSmMYB108). *SmMYB21*, *SmMYB26*, *SmARF6*, and *SmARF8* were ligated into the pGADT7 vector to construct a prey vector. Subsequently, bait and prey vectors

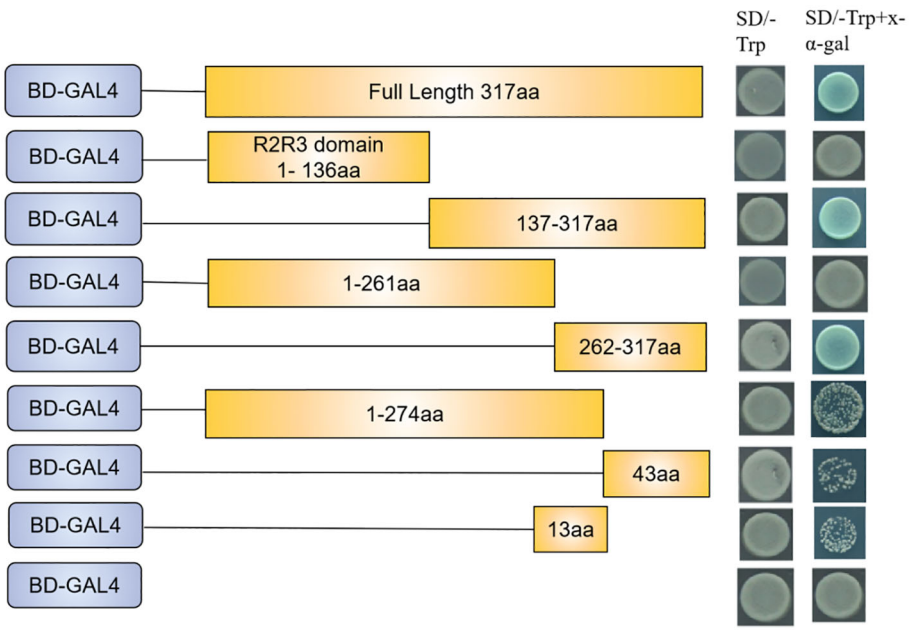


FIGURE 6
*SmMYB108* is a transcription activator. Activation analysis of *SmMYB108* in yeast. Full-length and truncated SmMYB108 was used for activation analysis. The number shown on the right indicates the protein region used for activation analysis. Auxotroph plates of SD/−Trp(left) and SD/−Trp−x-α-gal(right) showing transcriptional activation of protein.

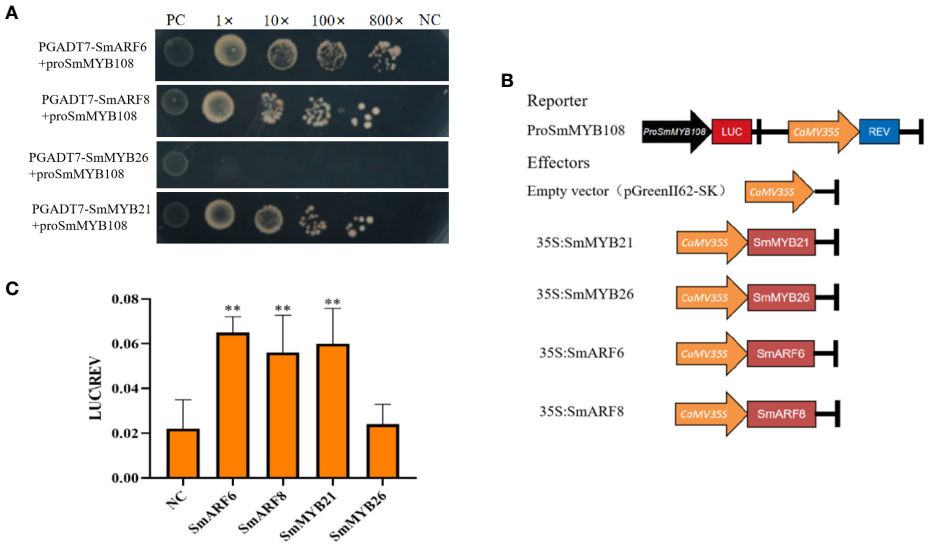


FIGURE 7
Anther development-related genes targets the promoters of *SmMYB108*. **(A)** Y1H analysis of SmMYB21, SmARF6, and SmARF8 associated with the promoters of SmMYB108. **(B)** ProSmMYB108, empty vector (pGreenII62-SK), 35S:SmMYB21, 35S:SmMYB26, 35S:SmARF6, and 35S:SmARF8 were infected into *N. benthamiana* cells. **(C)** Dual-luciferase reporter assay of SmMYB21, SmARF6, and SmARF8 activated the transcription of SmMYB108 promoters. Values are the mean ± SD of six replicates. One-way ANOVA was used to identify significant differences (**p < 0.01).

were transformed into the Y1H gold yeast strain. As shown in Figure 7A, the negative control (pGADT7 + ProSmMYB108) and transformant (pGADT7-SmMYB26 + ProSmMYB108) did not grow well on the medium containing aureobasidin A (AbA; 600 ng $ml^{-1}$). However, the positive control (p53 + Prop53) and transformants (pGADT7-SmMYB21 + ProSmMYB108, pGADT7-SmARF6 + ProSmMYB108, and pGADT7-SmARF8 + ProSmMYB108) grew well on the medium containing AbA. These findings indicate that *SmMYB21*, *SmARF6*, and *SmARF8* are associated with the *SmMYB108* promoters *in vitro*.

Next, we used a dual-luciferase (LUC) reporter assay to confirm whether *SmMYB108* promoter transcription could be activated by *SmMYB21*, *SmMYB26*, *SmARF6*, and *SmARF8 in vivo*. *SmMYB108* promoter fragment was fused to a firefly LUC reporter sequence and co-transformed into tobacco leaves either with 35S:SmMYB21, 35S:SmMYB26, 35S:SmARF6, and 35S:SmARF8 effector constructs or with an empty vector before determining the relative LUC activity using the LUC/Renilla (REN) ratio (Figure 7B). We found that *SmMYB21*, *SmARF6*, and *SmARF8* activated the transcription of *SmMYB108* promoter in a gene-dependent manner. *SmMYB108* promoter transcription was strongly activated by *SmMYB21*, *SmARF6*, and *SmARF8* in *N. benthamiana* leaves. However, no difference was observed between *SmMYB108* promoter-driven and empty vector LUC activity (Figure 7C). Taken together, these results indicate that *SmMYB21*, *SmARF6*, and *SmARF8* are the transcriptional activators of *SmMYB108*.

## Discussion

RNA-seq is used to determine the gene expression patterns and analyze DEGs responsible for genetic variation. Transcriptome analysis is often used to identify the DEGs involved in male sterility in various species (Jeong et al., 2014; Wang et al., 2021; Yuan et al., 2021). In this study, we conducted RNA-seq to determine the gene expression changes at different developmental stages (8 DBF, 5 DBF, and FD) in eggplant floral buds. Overall, 5,549 genes were identified *via* pairwise comparisons (Figure 1A). The anther is not only an important part of the stamens but also the place of pollen development. Normal dehiscence of anthers and timely release of pollen are essential for the completion of pollination and fertilization in plants (Goldberg et al., 1993; Wilson et al., 2011). Various TFs, including MYB TFs, play an important role in anther development (Veenstra and Wolffe, 2001). We identified 11 common MYB TFs in 8 DBF vs. FD and 5 DBF vs. FD groups. The expression of *SmMYB108* (F01_transcript_42496) was significantly increase on the FD (Figure 1C). Nine genes among all DEGs were randomly selected, and their expression levels were of consistent in both platforms (Supplementary Figure S3). qRT-PCR analysis revealed that the expression of *SmMYB108* was highest on the FD (Figure 2). *pSmMYB108:GUS Arabidopsis* transgenic lines also exhibited consistent gene expression patterns (Figure 3).

N-terminal of MYB TFs has a conserved MYB domain, which is divided into four types: 4R-MYB, 2R-MYB (R2R3-MYB), 3R-MYB (R1R2R3-MYB), and 1R-MYB (MYB-related) (Katiyar et al., 2012). We identified a novel MYB TF, *SmMYB108*, in the nucleus that had a length of 317 aa. It encoded a R2R3-MYB protein in the N-terminus and was involved in anther development. (Figure 4E). Sequence analysis of *SmMYB108* and its orthologs revealed that *CaMYB108*, *StMYB108*, *SlMYB78*, and *NaMYB108* shared a fairly high sequence identity with *SmMYB108* (>90% aa sequence identity), whereas *AtMYB108*, which is most closely related to *SmMYB108*, shared only 60% sequence identify. JA-inducible

*AtMYB108* has been reported to mediate stamen and pollen maturation as well as response to pathogens. Silencing the JA-inducible *CaMYB108* resulted in delayed anther dehiscence, decreased pollen viability, and promoted the synthesis of capsaicin. In our study, phenotypic analysis of transgenic tobacco revealed that the overexpression of *SmMYB108* promoted anther dehiscence (Figure 5C). Our results indicated an intriguingly convergent evolution of *MYB108* gene function among different plant species (Mandaokar and Browse, 2009; Sun et al., 2019); however, *MYB108* gene function is known to differ among different plant species. Zhang et al. (2019) reported that *RhMYB108* participates in the interaction between ethylene and JA signals and is strongly expressed in rose petals. Silencing *RhMYB108* promoted the expression of senescence associated genes, delaying the petal senescence (Zhang et al., 2019). Both *PsnMYB108* and *MdMYB108L* mediate plant stress resistance and can improve plant salt tolerance under abiotic stress (Wang et al., 2019; Zhao et al., 2020). However, the specific roles of *SmMYB108* in different species require further investigation.

In addition to the conserved R2R3 DNA-BD, the C-terminus performs several vital functions (Dubos et al., 2010). Transcriptional activation domain of *CaMYB31* is at the C-terminus (213–234 aa) (Zhu et al., 2019). *CaMYB48* has a motif that is rich in amino acids at the C-terminus (168–191 aa) that functions as a transcriptional activation domain (Sun et al., 2020). In this study, transcriptional activation analysis of yeast showed that C-terminus (262–317 aa) was crucial for the activation activity of *SmMYB108* (Figure 6). Multiple transcriptional binding sites were identified in the *myb108* promoter sequence. Y1H and dual-LUC reporter assays revealed that *SmMYB21*, *SmARF6*, and *SmARF8*, but not *SmMYB26*, could activate the *SmMYB108* promoter (Figure 7). *AtARF6* and *AtARF8* promote anther dehiscence in floral buds (Nagpal et al., 2005). JA and auxin are important hormones in plant development and stress response, which are also involved in the regulation of anther dehiscence. *AtARF6* and *AtARF8* regulate anther dehiscence by activating *DAD1*, a key gene in JA biosynthesis, to mediate JA synthesis (Tabata et al., 2010). Moreover, *AtMYB21* mediates the JA pathway during anther dehiscence (Song et al., 2011). Whether *SmMYB108* also regulates anther development *via* the hormone pathway needs to be investigated further in future studies.

# Conclusion

In summary, we found that the promoter of *SmMYB108* directly combines with the targets genes related to anther development—*SmMYB21*, *SmARF6*, and *SmARF8*, but not *SmMYB26*. We also found that *SmMYB108* functions as a transcriptional activator to regulate anther development. Our findings provide mechanistic insights into the evolution of male sterility in plants and can aid in future investigation of the transcriptional regulatory networks involved in anther development in eggplant.

# Materials and methods

## Plant materials

F142, a fertile eggplant (*Solanum melongena*) line, was provided by the Institute of Vegetables and Flowers, Chongqing Academy of Agricultural Sciences (Chongqing, China). All plants were cultivated in a controlled chamber (16/8-h light/night photoperiod and 28/22° C light/night temperature with 60%~65% relative humidity). Floral buds were collected respectively at 8 DBF, 5 DBF, and the FD for transcriptome sequencing. Various tissues (roots, stems, leaves, anthers, sepal, petals, and flower buds at different periods) were collected for qRT-PCR. Every sample was set three biological replicates. *N. benthamiana* is kept and supplied by our laboratory. Wild-type *Arabidopsis thaliana* is provided by our laboratory.

## RNA-seq analysis

The transcriptome data of the fertile line F142 were retrieved from the previous studies (Wang et al., 2021; Yuan et al., 2021). These data included transcription data of genes from different developmental stages of floral buds. Raw reads were first filtered to obtain clean reads, which were aligned to the eggplant HQ-1315 genome using Hisat2 (version 2.1.0). Only reads with a perfect match or one mismatch were further analyzed and annotated based on the reference genome. Each gene expression level was calculated as FPKM. Differential expression analysis (three biological replicates at different developmental stages) was performed using the DESeq. Genes with an adjusted P-value <0.01, as found by DESeq, were considered as differentially expressed (Anders and Huber, 2010).

## Quantitative reverse transcription polymerase chain reaction analysis

For the extraction of total RNA from the samples, the RNAprep Pure Plant Kit polysaccharide and polyphenol total RNA extraction kit (Tianmo, China) were used. cDNA was synthesized from RNA (1 μg per sample) using the Prime Script RT Kit (Takara, China) according to the manufacturer's instructions. Using real-time qRT-PCR validated the RNA-seq data and performed the expression of gene in different tissues. qRT-PCR primers were designed using Primer Premier 5.0 (Supplementary Table 1). The reactions of qRT-PCR were performed with the SYBR Green qPCR Mix (Takara, Japan) on the Bio-Rad CFX96 Touch Real Time PCR detection System (Bio-Rad Laboratories). In addition, reactions were performed three biological replicates and three technical replicates. The GAPDH (Glyceraldehyde -3-phosphate dehydrogenase) gene was used as the reference to quantify transcript levels. The $2^{-\triangle\triangle CT}$ approach was applied to

calculate the relative expression levels of target genes (Livak and Schmittgen, 2001; Vandesompele et al., 2002).

## Histochemical analysis of GUS expression

A section (2 kb) of the *SmMYB108* promoter was cloned into the pGreen vector harboring the GUS reporter to construct *pSmMYB108:GUS*. Tissues for GUS staining were first infiltrated with staining solution [50 mM sodium phosphate buffer (pH 7.0), 0.5 mM potassium ferrocyanide, 0.5 mM potassium ferricyanide, and X-Gluc (0.5 mg $ml^{-1}$)] in a vacuum chamber and, subsequently, incubated with the same solution at 37°C for 4 h.

## Sequence alignment and phylogenetic tree construction

To understand the location of the TFs on chromosome, the protein sequence of *SmMYB108* was obtained from eggplant reference genome HQ-1315. Other MYB TF sequences that showed the higher sequence identity with *SmMYB108* was retrieved from the public database National Center for Biotechnology Information (NCBI; https://www.ncbi.nlm.nih.gov/) and Sol Genomics Network (http://solgenomics.net/) and used for phylogenetic tree construction. The MYB TF sequences were aligned by CLUSTALW with the default parameters, and the phylogenetic tree was constructed by MEGA 7.0 using the neighbor-joining method with 1,000 bootstrap replications.

## Subcellular localization

The full-length *SmMYB108* cDNA was cloned from fertile line F142, which was inserted into the pCAMBIA1300 vector without the stop codon and fused with GFP-generating SmMYB108-GFP fusion proteins under the control of the CaMV35S promoter. The SmMYB108-GFP fusion proteins were introduced into Agrobacterium tumefaciens strain GV3101, which was infiltrated into tobacco leaves epidermal cells along with empty plasmids. After 48 h of inoculation, the GFP signal was visualized by confocal fluorescence microscopy (Carl Zeiss, Germany). The primers used in this study were listed in Supplementary Table 1.

## Transcriptional activation analysis

The ability of SmMYB108 to activate transcription was verified by a yeast transcriptional activation assay according to the manufacturer's instructions of the Matchmaker Gold yeast two-hybrid system (Takara, China). Full-length or deleted *SmMYB108* was fused in frame with the GAL4 DNA-BD in pGBKT7 vector. The pGBKT7 empty vector that only expressed GAL4 BD was used as a negative control. Recombinant plasmids and empty vector were transformed into yeast strain Y2H Gold. Yeast cells were incubated on SD/-Trp medium at 30°C for 3 days. The positive clones were diluted in 0.9% NaCl solution, and 10 μl of each dilution was inoculated on SD/-Trp +X-α-gal medium at 30°C for 3–5 days; the clones were stained with x-α-Gal (Takara, China). The primers used in this study were listed in Supplementary Table 1.

## Y1H assay

The ORF (Open reading frame) of four genes (*SmMYB21*, *SmMYB26*, *SmARF6*, and *SmARF8*) were inserted into *Sma*I and *Xho*I of the pGADT7 vector to generate prey. The promoter fragments of *SmMYB108* were ligated into *Sac*I and *Sma*I of the pAbAi vector as bait. The Y1H experiment was carried out using the Matchmaker Gold yeast one-hybrid system (Takara, China) according to the manufacturer's protocol. The primers used in this study were listed in Supplementary Table 1.

## Dual-LUC assay

The *SmMYB108* promoter (2,000 bp) was amplified by PCR from eggplant fertile line F142 and inserted into the *Sac*I and *BamH*I of pGreenII-0800-LUC vector to serve as the reporters. The full-length CDS of four genes (*SmMYB21*, *SmMYB26*, *SmARF6*, and *SmARF8*) was cloned into the *Sac*I and *BamH*I of pGreenII62-SK vector under the CaMV35S promoter to serve as an effector. The recombinant plasmids were transformed to the Agrobacterium tumefaciens strain GV3101 (pSoup-p19). The GV3101 harboring the *SmMYB108* reporter and the corresponding effectors were injected into 30-day-old tobacco (*Nicotiana tabacum*) leaves. After incubation for 48–72 h, the firefly LUC and REN LUC activities were measured with the Dual Luciferase Reporter Gene Assay Kit (Yisheng, Shanghai) according to the manufacturer's introduction. The Varioskan$^{TM}$LUX (Thermo Fisher Scientific, USA) was used to carry out the assay. Activity was expressed as the ratio of firefly LUC activity to REN LUC activity. The primers for all constructs in this study were listed in Supplementary Table 1.

## Construction of a pCAMBIA-2301G-SmMYB108 vector and tobacco transformation

*SmMYB108* was generated through PCR amplification by using specific primers containing *BamH*I and *Sac*I sites. The fragments were inserted into the pCAMBIA-2301G vector (Lü et al., 2017) to form the construct pCAMBIA-2301G-SmMYB108. Agrobacterium-mediated transformation of *N. benthamiana* was then performed, as previously described (Zhao et al., 2012). The sterile tobacco leaves of 15–20 days were cut into 1-$cm^2$ size into resuspension for 10 min at 25°C dark culture for 2 days and transferred to screening medium for differentiation to induce indefinite shoots; differentiated shoots were transferred to culture medium for rooting screening.

## Data availability statement

The datasets presented in this study can be found in online repositories. The names of the repository/repositories and accession number(s) can be found below: NCBI accession PRJNA941250.

## Author contributions

ZW, RH, and JW designed the research; RH and JW performed the molecular biology experiments; HY, DW, QT, YY and ST carried out the bioinformatics analysis; RH and JW analyzed the data and wrote the paper manuscript. All authors contributed to the article and approved the submitted version.

## Funding

This work was supported by grants from the earmarked fund for CARS (Grant No. CARS-23-A08), Sichuan Chongqing cooperation project (cstc2021jscx-cylhX0002).

## Conflict of interest

The authors declare that the research was conducted in the absence of any commercial or financial relationships that could be construed as a potential conflict of interest.

## Publisher's note



## Supplementary material

The Supplementary Material for this article can be found online at: https://www.frontiersin.org/articles/10.3389/fpls.2023.1164467/full#supplementary-material

## References

Anders, S., and Huber, W. (2010). Differential expression analysis for sequence count data. *Genome Biol.* 11, R106. doi: 10.1186/gb-2010-11-10-r106

Dubos, C., Stracke, R., Grotewold, E., Weisshaar, B., Martin, C., and Lepiniec, L. (2010). MYB transcription factors in *Arabidopsis*. *Trends Plant Sci.* 15, 573–581. doi: 10.1016/j.tplants.2010.06.005

Goldberg, R. B., Beals, T. P., and Sanders, P. M. (1993). Anther development: basic principles and practical applications. *Plant Cell* 5, 1217–1229. doi: 10.1105/tpc.5.10.1217

Guan, S. Y., Jiao, P., Jiang, Z. Z., Qi, Z., Xia, H. F., Qu, J., et al. (2019). Research progress of MYB transcription factors in plant abiotic stress. *J. Jilin Agric. Univ* 41, 253–260. doi: 10.13327/j.jjlau.2019.5023

Jeong, H. J., Kang, J. H., Zhao, M., Kwon, J. K., Choi, H. S., Bae, J. H., et al. (2014). Tomato Male sterile 1035 is essential for pollen development and meiosis in anthers. *J. Exp. Bot.* 65 (22), 6693–6709. doi: 10.1093/jxb/eru389

Katiyar, A., Smita, S., Lenka, S. K., Rajwanshi, R., Chinnusamy, V., and Bansal, K. C. (2012). Genome-wide classification and expression analysis of MYB transcription factor families in rice and arabidopsis. *BMC Genomics* 13, 544. doi: 10.1186/1471-2164-13-544

Kempe, K., and Gils, M. (2011). Pollination control technologies for hybrid breeding. *Mol. Breed.* 27, 417–437. doi: 10.1007/s11032-011-9555-0

Kocábek, T., Mishra, A. K., Matoušek, J., Patzak, J., Lomnická, A., Khare, M., et al. (2018). The R2R3 transcription factor HlMYB8 and its role in flavonoid biosynthesis in hop (*Humulus lupulus* l.). *Plant Sci.* 269, 32–46. doi: 10.1016/j.plantsci.2018.01.004

Li, Y., Jiang, J., Du, M. L., Li, L., Wang, X. L., and Li, X. B. (2013). A cotton gene encoding MYB-like transcription factor is specifically expressed in pollen and is involved in regulation of late anther/pollen development. *Plant Cell Physiol.* 54, 893–906. doi: 10.1093/pcp/pct038

Li, W. C., Zhang, Y., and Zhao, S. Q. (2019). Silencing of arabidopsis RUS4 impairs anther endothecium secondary cell wall thickening. *Chin. J. Cell Biol.* 41, 619–626. doi: 10.11844/cjcb.2019.04.0009

Liu, C., Ma, N., Wang, P. Y., Fu, N., and Shen, H. L. (2013). Transcriptome sequencing and DeNovo analysis of a cytoplasmic male sterile line and its near-isogenic restorer line in chili pepper (*Capsicum annuum* l.). *PloS One* 8, e65209. doi: 10.1371/journal.pone.0065209

Livak, K. J., and Schmittgen, T. D. (2001). Analysis of relative gene expression data using real-time quantitative PCR and the 2(-delta delta C(T)) method. *Methods* 25, 402–408. doi: 10.1006/meth.2001.1262

Lü, J., Sui, X., Ma, S., Li, X., Liu, H., and Zhang, Z. (2017). Suppression of cucumber stachyose synthase gene (*CsSTS*) inhibits phloem loading and reduces low temperature stress tolerance. *Plant Mol. Biol.* 95, 1–1. doi: 10.1007/s11103-017-0621-9

Ma, Y., Kang, J., Wu, J., Zhu, Y., and Wang, X. (2015). Identification of tapetum-specific genes by comparing global gene expression of four different male sterile lines in *Brassica oleracea*. *Plant Mol. Biol.* 87, 541–554. doi: 10.1007/s11103-015-0287-0

Mandaokar, A., and Browse, J. (2009). MYB108 acts together with MYB24 to regulate jasmonate-mediated stamen maturation in arabidopsis. *Plant Physiol.* 149, 851–862. doi: 10.1104/pp.108.132597

McCarthy, R. L., Zhong, R., and Ye, Z. H. (2009). MYB83 is a direct target of SND1 and acts redundantly with MYB46 in the regulation of secondary cell wall biosynthesis in arabidopsis. *Plant Cell Physiol.* 50, 1950–1964. doi: 10.1093/pcp/pcp139

Nagpal, P., Ellis, C. M., Weber, H., Ploense, S. E., Barkawi, L. S., Guilfoyle, T. J., et al. (2005). Auxin response factors ARF6 and ARF8 promote jasmonic acid production and flower maturation. *Development*. 132, 4107–18. doi: 10.1242/dev.01955

Rhee, S. J., Seo, M., Jang, Y. J., Cho, S., and Lee, G. P. (2015). Transcriptome profiling of differentially expressed genes in floral buds and flowers of male sterile and fertile lines in watermelon. *BMC Genomics* 16, 914. doi: 10.1186/s12864-015-2186-9

Singh, S. P., Srivastava, R., and Kumar, J. (2015). Male Sterility systems in wheat and opportunities for hybrid wheat development. *Acta Physiol. Plant* 37, 1713. doi: 10.1007/s11738-014-1713-7

Song, S., Qi, T., Huang, H., Ren, Q., Wu, D., Chang, C., et al. (2011). The jasmonate-ZIM domain proteins interact with the R2R3-MYB transcription factors MYB21 and MYB24 to affect jasmonate-regulated stamen development in *Arabidopsis*. *Plant Cell* 23, 1000–1013. doi: 10.1105/tpc.111.083089

Stracke, R., Werber, M., and Weisshaar, B. (2001). The R2R3-MYB gene family in *Arabidopsis thaliana*. *Curr. Opin. Plant Biol.* 4, 447–456. doi: 10.1016/S1369-5266(00)00199-0

Sun, B., Zhou, X., Chen, C., Chen, C., Chen, K., Chen, M., et al. (2020). Coexpression network analysis reveals an MYB transcriptional activator involved in capsaicinoid biosynthesis in hot peppers. *Hortic. Res.* 7, 162. doi: 10.1038/s41438-020-00381-2

Sun, B., Zu, Z., Chen, C., Chen, G., Cao, B., Chen, C., et al. (2019). Jasmonate-inducible R2R3-MYB transcription factor regulates capsaicinoid biosynthesis and stamen development in capsicum. *J. Agric. Food Chem.* 67, 10891–10903. doi: 10.1021/acs.jafc.9b04978

Tabata, R., Ikezaki, M., Fujibe, T., Aida, M., Tian, C. E., Ueno, Y., et al. (2010). Arabidopsis auxin response factor6 and 8 regulate jasmonic acid biosynthesis and floral organ development *via* repression of class 1 KNOX genes. *Plant Cell Physiol.* 51, 164–175. doi: 10.1093/pcp/pcp176

Vandesompele, J., De Preter, K., Pattyn, F., Poppe, B., Van Roy, N., De Paepe, A., et al. (2002). Accurate normalization of real-time quantitative RT-PCR data by geometric averaging of multiple internal control genes. *Genome Biol.* 3, RESEARCH0034. doi: 10.1186/gb-2002-3-7-research0034

Veenstra, G. J., and Wolffe, A. P. (2001). Gene-selective developmental roles of general transcription factors. *Trends Biochem. Sci.* 26, 665–671. doi: 10.1016/S0968-0004(01)01970-3

Wang, H. Q., Guo, X. R., Yang, X. B., Su, J., and Cao, X. Y. (2016). Screening of the proteins interacting with SmPAP1 of R2R3-MYB transcription factor from *Salvia miltiorrhiza bunge* by yeast two-hybrid system. *Genom Appl. Biol.* 35, 2819–2826. doi: 10.13417/j.gab.035.002819

Wang, Y., Mao, Z., Jiang, H., Zhang, Z., and Chen, X. (2019). A feedback loop involving MdMYB108L and MdHY5 controls apple cold tolerance. *Biochem. Biophys. Res. Commun.* 512, 381–386. doi: 10.1016/j.bbrc.2019.03.101

Wang, Z., Yuan, C., Zhang, S. W., Tian, S. B., Tang, Q. L., Wei, D. Y., et al. (2021). Screening and interaction analysis identify genes related to anther dehiscence in *Solanum melongena* l. *Front. Plant Sci.* 12, 648193. doi: 10.3389/fpls.2021.648193

Wei, M. M., Song, M. Z., Fan, S. L., and Yu, S. X. (2013). Transcriptomic analysis of differentially expressed genes during anther development in genetic male sterile and wild type cotton by digital gene-expression profiling. *BMC Genomics* 14, 97. doi: 10.1186/1471-2164-14-97

Wilson, Z. A., Song, J., Taylor, B., and Yang, C. (2011). The final split: the regulation of anther dehiscence. *J. Exp. Bot.* 62, 1633–1649. doi: 10.1093/jxb/err014

Xu, X. F., Wang, B., Feng, Y. F., Xue, J. S., Qian, X. X., Liu, S. Q., et al. (2019). AUXIN RESPONSE FACTOR17 directly regulates MYB108 for anther dehiscence. *Plant Physiol.* 181, 645–655. doi: 10.1104/pp.19.00576

Yan, X. H., Dong, C. H., Yu, J. Y., Liu, W. H., Jiang, C. H., Liu, J., et al. (2013). Transcriptome profileanalysis of young floral buds of fertile and sterile plants from the self-pollinated offspring of the hybrid between novel restorer line NR1 and nsa CMS line in brassica napus. *BMC Genomics* 14, 26. doi: 10.1186/1471-2164-14-26

Yang, C., Song, J., Ferguson, A. C., Klisch, D., Simpson, K., Mo, R., et al. (2017). Transcription factor MYB26 is key to spatial specificity in anther secondary thickening formation. *Plant Physiol.* 175, 333–350. doi: 10.1104/pp.17.00719

Yuan, C., Zhang, S. W., Hu, R. L., Wei, D. Y., Tang, Q. L., Wang, Y. Q., et al. (2021). Comparative transcriptome analysis provides insight into the molecular mechanisms of anther dehiscence in eggplant (*Solanum melongena* l.). *Genomics* 113, 497–506. doi: 10.1016/j.ygeno.2020.12.032

Zhang, S., Zhao, Q., Zeng, D., Xu, J., Zhou, H., Wang, F., et al. (2019). RhMYB108, an R2R3-MYB transcription factor, is involved in ethylene- and JA-induced petal senescence in rose plants. *Hortic. Res.* 6, 131. doi: 10.1038/s41438-019-0221-8

Zhao, K., Cheng, Z., Guo, Q., Yao, W., Liu, H., Zhou, B., et al. (2020). Characterization of the poplar R2R3-MYB gene family and over-expression of PsnMYB108 confers salt tolerance in transgenic tobacco. *Front. Plant Sci.* 11. doi: 10.3389/fpls.2020.571881

Zhao, S. Q., and Dong, J. J. (2015). Genetic regulation of anther and pollen development in *Arabidopsis thaliana*. *J. Shanxi Univ: Nat. Sci. Ed* 38, 177–184. doi: 10.13451/j.cnki.shanxi.univ(nat.sci.).2015.01.030

Zhao, Q., Wang, G., and Ji J and Jin, C. (2012). Construction of plant expression vector with constitutive activation DREB2A and its genetic transformation to tobacco. *China Biotech.* 32, 42–48. doi: 10.1007/s11783-011-0280-z

Zhong, R., Lee, C., Zhou, J., McCarthy, R. L., and Ye, Z. H. (2008). A battery of transcription factors involved in the regulation of secondary cell wall biosynthesis in arabidopsis. *Plant Cell* 20, 2763–2782. doi: 10.1105/tpc.108.061325

Zhong, R., Richardson, E. A., and Ye, Z. H. (2007). The MYB46 transcription factor is a direct target of SND1 and regulates secondary wall biosynthesis in arabidopsis. *Plant Cell* 19, 2776–2792. doi: 10.1105/tpc.107.053678

Zhu, Z., Sun, B., Cai, W., Zhou, X., Mao, Y., Chen, C., et al. (2019). Natural variations in the MYB transcription factor MYB31 determine the evolution of extremely pungent peppers. *New Phytol.* 223, 922–938. doi: 10.1111/nph.15853

frontiers | Frontiers in Plant Science

TYPE Original Research
PUBLISHED 01 September 2023
DOI 10.3389/fpls.2023.1168947



OPEN ACCESS

EDITED BY
Weibiao Liao,
Gansu Agricultural University, China

REVIEWED BY
João Ricardo Bachega Feijó Rosa,
Federal University of Viçosa, Brazil
Bishun Deo Prasad,
Dr. Rajendra Prasad Central Agricultural University, India

*CORRESPONDENCE
Nusrat Perveen
nusrat.8oct@gmail.com
M. Sankaran
kmsankaran@gmail.com

RECEIVED 18 February 2023
ACCEPTED 11 August 2023
PUBLISHED 01 September 2023

CITATION
Perveen N, Dinesh MR, Sankaran M, Shivashankara KS, Ravishankar KV, Venugopal R and Mir H (2023) Volatile profiling as a potential biochemical marker for validation of gamma irradiation derived putative mutants in polyembryonic genotypes of mango (*Mangifera indica* L.). *Front. Plant Sci.* 14:1168947. doi: 10.3389/fpls.2023.1168947



# Volatile profiling as a potential biochemical marker for validation of gamma irradiation derived putative mutants in polyembryonic genotypes of mango (*Mangifera indica* L.)

Nusrat Perveen[1]*, M. R. Dinesh[1], M. Sankaran[1]*, K. S. Shivashankara[2], K. V. Ravishankar[2], R. Venugopal[3] and Hidayatullah Mir[4]

[1]Division of Fruit Crops, Indian Council of Agricultural Research (ICAR)-Indian Institute of Horticultural Research, Bengaluru, India, [2]Division of Basic Sciences, Indian Council of Agricultural Research (ICAR)-Indian Institute of Horticultural Research, Bengaluru, India, [3]Division of Social Sciences and Training, Indian Council of Agricultural Research (ICAR)-Indian Institute of Horticultural Research, Bengaluru, India, [4]Department of Horticulture (Fruit and Fruit Technology), Bihar Agricultural University, Bhagalpur, India

**Introduction:** Putative mutants were generated through gamma irradiation in the polyembryonic mango genotype Nekkare. The putative mutant progenies along with control seedlings and mother plants were evaluated by comparing the compositions and relative proportions of their major volatile compounds.

**Methods:** Volatile profiling was done using headspace-solid phase micro-extraction (HS SPME) method coupled with gas chromatography–mass spectrometry (GC-MS MS). Furthermore, characterisation of putative mutants and control seedlings was carried out using simple sequence repeat (SSR) markers to ascertain the genetic diversity present in the samples under study.

**Results:** Monoterpenes were the most abundant volatile compound in all the studied samples (ranging from 34.76% to 91.41%) out of which l-Phellandrene and cis-Ocimene formed the major fraction in mother plants (20.45%–21.86% and 16.17%–21.27%, respectively) and control seedlings (23.32%–24.95% and 18.95%–20.81%, respectively), while beta-Phellandrene was dominant in the selected putative mutant samples (2.34%–29.53%). Among sesquiterpenes, trans-Caryophyllene was detected only in the putative mutant samples (0.10%–30.18%). Grouping together of mother plants and control seedlings was seen in the cluster analysis, while the putative mutants grouped apart from them suggesting genetic diversity. Genetic distance between the mother plants and control seedlings ranged from 0.97 to 2.73, while between putative mutants, control seedlings, and mother plants, it ranged from 6.54 to 9.82. SSR-based characterisation of putative mutant seedlings showed that mutation caused variability in the treated population. This was evident from the high allelic richness ranging from 4 to 12 with a mean of 7 and a higher mean Shannon's Information Index (1.50) of the putative mutant population.

**Discussion:** The study demonstrates that volatile profiling and molecular characterisation using SSR markers could be used as a tool to detect variation in a mutated population. In addition, volatile profiling can be used to validate putative mutants in polyembryonic mango genotypes where the seedlings of nucellar origin are similar to mother plants.

KEYWORDS

mango, polyembryony, mutation, nucellar seedlings, SSR markers, volatile profiling

# 1 Introduction

Polyembryony is a trait in certain mango genotypes where multiple apomictic embryos develop from the maternal nucellar tissues along with a single zygotic embryo (Asker and Jerling, 1992). The plants originating from apomictic embryos, also known as nucellar seedlings, are "true-to-type." The polyembryonic genotypes are ideal as rootstocks, as they are uniform owing to their "true-to-type" nature. However, the use of these genotypes in breeding programme is often limited by their narrow genetic base. Hence, creating variability in these genotypes for various desirable traits, *viz.*, plant stature and salinity tolerance, would make them highly suitable as rootstocks. Induced mutations have been widely employed for creating variability in heterozygous crops like mango (Rossetto et al., 1997; Karsinah et al., 2012; Kumar et al., 2018; Rime et al., 2019).

In polyembryonic mango genotypes, the vigorous and first emerging seedlings, which grow well until maturity, are reported to be of nucellar origin (Srivastava et al., 1988). These nucellar seedlings would be similar to mother plants. The variation observed in the nucellar seedlings upon gamma irradiation can be considered to be due to mutation. Several studies in the past were used to validate mutants including molecular markers like microsatellite markers (Damasco et al., 2019), inter-simple sequence repeats (ISSR) markers (Due et al., 2019), phenotypic characterisation (Atay et al., 2019), and stomatal characters (Yasmeen et al., 2020). Volatile profiling was used as a biochemical marker for the characterisation of germplasm in fig (Oliveira et al., 2010), mango (Li et al., 2017), avocado (Ali et al., 2020), and apple (Roberts and Spadafora, 2020) owing to its species, cultivar specificity, and stability under different environmental conditions. Volatile compounds have also been used as biomarkers for determining susceptibility of different *Mangifera indica* genotypes to mango gall fly (Augustyn et al., 2010) and for distinguishing between the fruit type and the pickling type of mango (Vasugi et al., 2012).

In our previous study, a high level of variability was observed for both morphological and stomatal traits in the putative mutant population of Nekkare (Perveen et al., 2022). Hence, in this study, genetic diversity analysis was carried out in putative mutants of Nekkare exhibiting maximum morphological variability using simple sequence repeat (SSR) markers. Gamma irradiation is likely to cause mutation through deletion and is more likely to induce small deletions between 1 and 10 kbp (Morita et al., 2009). Hence, DNA markers can effectively be used to detect these variations. In this study, putative mutant seedlings generated by gamma irradiation were validated by comparing the leaf volatile profiles of mother plants, control seedlings, and selected putative mutants of polyembryonic mango genotype Nekkare. Our hypotheses were as follows: i) being nucellar in nature, the control seedlings will be similar to mother plants, and any variation observed in the seedlings emerging from gamma irradiation treated kernels could be considered to have been a result of mutation, and ii) SSR markers can be useful in determining whether the morphological diversity in the putative mutant population has manifested at genetic level or not.

# 2 Materials and methods

## 2.1 Experimental material

This study was a part of mango rootstock breeding programme undergoing at ICAR-Indian Institute of Horticultural Research (IIHR), Bengaluru, India. For gamma irradiation, fruits were collected from 30 years old Nekkare mother plants (NMP) being maintained in the Field Gene Bank of IIHR. The putative mutant population was generated by irradiating the seed kernels extracted from these fruits with five doses of gamma irradiation, *viz.*, $T_1$: 15 Gy, $T_2$: 20 Gy, $T_3$: 25 Gy, $T_4$: 30 Gy, and $T_5$: 35 Gy. Polyembryonic genotypes produce more than one seedling per seed. The putative mutant seedlings obtained after sowing the irradiated seed kernels were first evaluated for determining the radio-sensitivity and $LD_{50}$ dose (Perveen et al., 2023a). Higher doses of gamma irradiation resulted in decreased number in seedlings per seed, and only the vigorous seedlings were found to survive (Perveen et al., 2023a). Two months after germination, multiple seedlings emerging from each seed kernel were separated and transplanted in new polybags.

Six months after germination, only one to two seedlings survived per seed, which were considered to be nucellar in origin due to the vigour taking cognisance of the previous study (Srivastava et al., 1988). At this stage, a total of 100 randomly selected putative mutants (20 from each treatment) and 20 control seedlings were screened for morphological and stomatal parameters. On the basis of coefficient of variability (CV), $T_5$: 35

Gy irradiation treatment was found to result in maximum morphological diversity (Perveen et al., 2022). Hence, the putative mutants generated through 35 Gy gamma irradiation were used for the present study. Leaf volatile profiling was carried out for two Nekkare mother plants ($NMP_1$ and $NMP_2$) and 9 months old, 18 control seedlings (NC) along with 18 putative mutants (NM).

## 2.2 HS-SPME extraction of volatiles

Recently matured leaves from NMP, NC, and NM were collected, wrapped separately in aluminium foil after proper labelling, and flash frozen in liquid nitrogen. Owing to the limitation of resources and to reduce the cost of volatile profiling, the samples for analysis were made by mixing leaves from more than one seedling. A total of 18 control seedlings were divided into three samples, *viz.*, $NC_1$, $NC_2$, and $NC_3$, each sample consisting of leaves from six seedlings. A total of 18 putative mutants were divided into six samples, each consisting of leaves from three putative mutant seedlings. These samples were as follows: $NM_1$, consisting seedlings of 10–15 cm (dwarf); $NM_2$, having seedlings of 16–25 cm (moderately vigorous); $NM_3$, comprising seedlings of >26 cm height (vigorous); $NM_4$, comprised of seedlings with narrow leaves (leaf blade width <3 cm); $NM_5$, comprised of seedlings with broad leaves (leaf blade width ≥3 cm); and $NM_6$, comprised of seedlings with dark green leaf.

The volatile compounds were analysed using headspace-solid phase micro-extraction (HS-SPME) method, which involved submerging a thin fused-silica fibre covered with the extracting phase in the headspace of the samples being analysed in order to extract the analytes onto it. It is made of a fused silica fibre that is 1–2 cm long and coated with a stationary phase, such as polydimethylsiloxane (PDMS), divinyl benzene (DVB), carboxen (CAR), or a mixture of all the above three compounds, bonded to a stainless-steel plunger and holder. These fibres are first conditioned at 250°C for 2–3 h in the injector port of GC with a continued flow of helium gas. For extraction of volatiles, 5 g of properly ground leaf sample was taken in a 150-ml conical flask containing a magnetic stirrer, and the mouth of conical flask was properly covered with silicon stopper. This step was followed by insertion of a previously conditioned SPME fibre in the conical flask to adsorb the headspace volatiles for 2 h.

## 2.3 Gas chromatography and mass spectrometry

The SPME fibre was pumped into the gas chromatography–mass spectrometry (GC-MS) injector port after 2 h, and the adsorbed volatiles were allowed to desorb for 10 min. A Varian-3800 gas chromatograph and a Varian-4000 mass spectrometer with an ion trap mass selective detector were used to conduct the GC-MS analysis. The fused-silica capillary column used for the analysis had the following dimensions: 30mm × 0.25mm, 0.25mm film thickness. The column temperature programmes were 40°C for 2 min at an increment of 3°C/min to 190°C with a hold for 1 min, followed by an increment of 5°C/min to 220°C. The injector temperature was set at 250°C, and all injections were made in split-less mode for 0.2 min.

The spectrometer was operating in external electron ionisation mode, with helium serving as the carrier gas (1.5ml/min), the injector temperature being 250°C, the trap temperature being 180°C, the ion source heating being 190°C, the transfer line heating being 260°C, the EI mode being at 70eV, and the full scan range being 50–350amu. The total chromatogram for each sample was obtained by adding all the GC peak areas, and each volatile compound was expressed as relative per cent area. By comparing the collected mass spectra to the spectra found in the Wiley and NIST-2007 libraries, the volatile compounds were identified by their retention periods with reference to standard compounds. The analysis of all the samples was done in triplicate. The results correspond to mean of three readings, generally followed for SPME analysis (Fernandes et al., 2009).

## 2.4 Molecular characterisation of selected putative mutants

Young healthy leaves were taken from 9-month-old, 20 putative mutants (generated through 35Gy gamma irradiation) and 20 untreated (control) seedlings. The collected leaves were wiped with 70% (v/v) alcohol and stored in butter paper envelopes at −10°C until DNA isolation. DNA isolation was done using modified Cetyltrimethylammonium bromide (CTAB) method (Ravishankar et al., 2000). Using Nanodrop, the absorbance at 260 and 280nm was measured to assess the DNA content, and the ratio of the absorbance at 260–280nm ($A_{260}/A_{280}$) was used to quantify the purity of the DNA. The extracted genomic DNA samples were analysed on a 0.8% (w/v) agarose gel using 0.5× Tris-acetate-EDTA (TAE) buffer to perform a qualitative examination of the DNA.

Fluorescence-based PCR method was used for fast, efficient, and precise amplification of microsatellites (Schuelke, 2000), carried out in 20-µl reaction volume. Previously, 90 genomic SSR markers were developed using next-generation sequencing technology (Ravishankar et al., 2015). These markers exhibited high polymorphism information content (PIC) values ranging from 0.738 to 0.960 with a mean of 0.899 and showed high transferability within the *Mangifera* genus (Ravishankar et al., 2015). From these 90 markers, 12 most informative SSR markers as shown by subsequent studies (data not given) were used for this study. The details of SSR primers, components of PCR reaction mixture along with their concentration, and the PCR protocol followed are presented in Supplementary Tables S1.1, S1.2, and S1.3, respectively. The amplification of PCR products was first confirmed by separating them on 3% (w/v) agarose gel. Once the amplification of PCR products was confirmed, four PCR products labelled with four different fluorophores, *viz.*, FAM, VIC, NED, and PET, were mixed to get a single sample. Genotyping of these samples was then performed using an automatic 96-capillary automated DNA sequencer (ABI 3730 DNA Analyser, Applied Biosystems, USA) at ICRISAT facility, Hyderabad, India.

## 2.5 Statistical analysis

### 2.5.1 Volatile profiling

After applying Squared Euclidian Cluster analysis to all of the characters' means, Ward's approach was used to create a dendrogram (Rencher, 1995). From the Euclidean distances, a Pearson correlation matrix was created using PROC CLUSTER and PROC PRINCOMP of SAS V 9.3. Principal components analysis (PCA) was then performed on the correlation matrix (SAS, 2012). A two-dimensional graph was used to plot the first two main principal components.

### 2.5.2 Analysis of molecular data and genetic diversity

Samples were separated on the automatic capillary automated DNA Sequencer once the PCR product's amplification was validated. Peak Scanner V1.0 software (Applied Biosystems) was used to analyse and compile the raw data to determine the allele size (in base pairs). The obtained results were further employed for genetic analysis using CERVUS 3.0.3 software (Kalinowski et al., 2007). Using GenAlEx 6.5, genetic diversity metrics for each group were calculated, including allelic richness, heterozygosity, Shannon's Information Index, and fixation index (Peakall and Smouse, 2006; Peakall and Smouse, 2012). The Gower similarity coefficient served as the input for a dendrogram/phylogenetic tree constructed using the unweighted pair-group method with arithmetic mean (UPGMA) clustering option of the PAST 4.0 software (Hammer et al., 2001).

# 3 Results

## 3.1 Volatile profiling

The compositions and proportions of major volatile compounds (VCs) present in the leaf samples of mother plants, control, and putative mutants determined by GC-MS-MS analysis is presented in Table 1. In this study, monoterpenes and sesquiterpenes were found to be the main VCs present in all the studied samples. α-Pinene was detected in all the selected putative mutant samples except in $NM_2$. Camphene was detected in two putative mutant samples, $NM_2$ (15.82%) and $NM_3$ (22.52%), and trans-Ocimene was detected in $NM_5$ (0.3%) and $NM_6$ (0.84%), while these were absent in all other samples under study. Sabinene, which was present in all the mother plants and control seedlings, was detected only in three of the six putative mutant samples, $NM_4$ (0.41%), $NM_5$ (0.54%), and $NM_6$ (0.88%). Similarly, beta-Ocimene, 3-Carene, γ-Terpinene, and α-Terpinolene were present only in a few putative mutant samples, while they were not detected in either mother plants or control samples. Furthermore, I-Phellandrene was one of the major monoterpenes (more than 20%) detected in all the mother plants and control samples and was also present in higher amount in two of the selected putative mutant samples, $NM_5$ (29.06%) and $NM_6$ (25.47%). Unlike I-Phellandrene, beta-Phellandrene was not detected in any of the mother plants or control seedlings. However, it was present in all the selected putative mutant seedlings (highest in $NM_1$, 29.53%). Furthermore, Cis-Ocimene, which was another most abundant monoterpene ranging from 16.16% to 21.27% in the mother plants and control samples, was detected only in one of the putative mutant samples, ($NM_4$ 17.37%) (Table 1). Many of the sesquiterpenes were detected only in the putative mutants such as alpha-Cubebene, trans-Caryophyllene, Germacrene, alpha-Amorphene, Aromadendrene, delta-Cadinene, alpha-Copaene, alpha-Lonipinene, and (−)-ISOLEDENE (Table 1). In the present study, in general, the concentration of monoterpenes was more than sesquiterpene in all the samples except putative mutant sample $NM_4$, where sesquiterpenes dominated the overall volatile profile (59.14%). Aldehyde (trans-2-Hexenal) was observed to be present only in putative mutant samples $NM_1$, $NM_4$, and $NM_6$ among the studied samples, while alcohol (1-Hexyn-3-ol) was present in the putative mutant sample $NM_2$.

## 3.2 Cluster analysis

Cluster analysis showed high variability among the selected putative mutant samples; $NM_1$, $NM_2$, and $NM_3$ were different from the mother plants and control seedlings but were similar to each other with respect to composition of volatile compounds (Figure 1; Supplementary Table S2). The genetic distance was lowest between samples $NC_1$ and $NC_2$ (0.97) followed by $NMP_1$ and $NC_1$ (1.18), while among the putative mutant samples, $NM_6$ was genetically closest to mother plants and control samples. Using the volatile composition of different samples, a dendogram was generated to understand the relationship between them. The studied samples were divided into two main clusters with two sub-clusters in the first cluster. Cluster 1 comprised of eight samples including mother plants, control, and three putative mutants. Out of these, samples $NMP_1$, $NC_1$, $NC_2$, $NC_3$, $NMP_2$, and $NM_6$ were present in the first sub-cluster, while the second sub-cluster comprised of two putative mutants, *viz.*, $NM_4$ and $NM_5$. Cluster 2 comprised of putative mutants $NM_1$, $NM_2$, and $NM_3$, suggesting that these three putative mutants are more distant from mother plants and control seedlings as compared to the other three putative mutants ($NM_4$, $NM_5$, and $NM_6$).

## 3.3 Principal component analysis

A total of 29 volatile compounds detected in different samples under study were subjected to principal component analysis (PCA) based on a matrix of Pearson correlation coefficients ($p<0.05$) (Supplementary Table S3). PCA results indicated that the total variability is being explained by 29 principal components out of which the components <2.0 eigenvalue were ignored. A principal component loading of more than 0.50 was considered significant for each factor. The correlation matrix, eigenvalues, and factor loadings are provided as Supplementary Tables S3–S5. The first four principal components with eigenvalue >2 together explained

10.3389/fpls.2023.1168947

TABLE 1 Compositions and mean relative content (area %) of leaf volatile compounds of mother plants (NMP1, NMP2), control samples (NC1, NC2, and NC3), and selected putative mutant samples (NM1, NM2, NM3, NM4, NM5, and NM6) of Nekkare (data are mean of three biological replicates; ND, not detected).

| Volatile Compound | Mother plants | | Control | | | Mutants | | | | | |
|---|---|---|---|---|---|---|---|---|---|---|---|
| | NMP1 | NMP2 | NC1 | NC2 | NC3 | NM1 | NM2 | NM3 | NM4 | NM5 | NM6 |
| **Alcohols** | | | | | | | | | | | |
| 1-Hexyn-3-l | ND | ND | ND | ND | ND | ND | 1.38 | ND | ND | ND | ND |
| **Aldehydes** | | | | | | | | | | | |
| trans-2-Hexenal | ND | ND | ND | ND | ND | 0.13 | ND | ND | 0.44 | ND | 0.34 |
| **Mono-terpenoids** | | | | | | | | | | | |
| α-Pinene | ND | 18.48 | 13.80 | 17.31 | 19.15 | 32.83 | ND | 0.09 | 8.15 | 8.80 | 13.23 |
| Camphene | ND | ND | ND | ND | ND | ND | 15.83 | 22.52 | ND | ND | ND |
| Sabinene | 1.04 | 1.06 | 1.35 | 1.15 | 1.83 | ND | ND | ND | 0.42 | 0.55 | 0.89 |
| trans-Ocimene | ND | ND | ND | ND | ND | ND | ND | ND | ND | 0.31 | 0.85 |
| beta-Ocimene | ND | ND | ND | ND | ND | 4.19 | 1.68 | 2.08 | ND | ND | ND |
| I-Phellandrene | 20.45 | 21.86 | 23.32 | 24.95 | 24.88 | ND | 1.54 | ND | 0.34 | 29.06 | 25.48 |
| 3-Carene | ND | ND | ND | ND | ND | 2.25 | ND | 1.76 | ND | ND | ND |
| beta-Phellandrene | ND | ND | ND | ND | ND | 29.53 | 22.62 | 29.13 | 2.34 | 13.06 | 22.20 |
| Cis-Ocimene | 21.27 | 16.17 | 20.44 | 20.81 | 18.95 | ND | ND | ND | 17.37 | ND | ND |
| trans-Ocimene | ND | ND | 2.44 | ND | ND | 21.71 | 21.56 | 21.59 | 6.14 | ND | ND |
| γ-Terpinene | ND | ND | ND | ND | ND | 0.65 | 0.56 | ND | ND | ND | ND |
| α-Terpinolene | ND | ND | ND | ND | ND | 0.25 | 0.19 | ND | ND | ND | ND |
| **Total Monoterpenoids (%)** | **42.76** | **57.57** | **61.35** | **64.22** | **64.80** | **91.41** | **63.98** | **77.17** | **34.76** | **51.78** | **62.64** |
| **Sesqui-terpenoids** | | | | | | | | | | | |
| alpha-Gurjunene | 18.92 | 17.93 | 17.07 | 16.62 | 16.03 | 0.51 | 6.98 | 2.07 | 5.78 | 0.24 | 6.73 |
| alpha-Cubebene | ND | ND | ND | ND | ND | 0.15 | 0.32 | ND | ND | ND | ND |
| trans-Caryophyllene | ND | ND | ND | ND | ND | 0.10 | ND | 0.82 | 30.18 | 18.28 | ND |
| Germacrene | ND | ND | ND | ND | ND | ND | ND | ND | 0.11 | 0.15 | ND |
| alpha-Amorphene | ND | ND | ND | ND | ND | 6.98 | ND | ND | ND | ND | ND |
| Aromadendrene | ND | ND | ND | ND | ND | ND | ND | ND | 0.09 | 0.12 | ND |
| α-Guaiene | ND | ND | ND | ND | ND | 0.16 | ND | ND | 3.86 | 6.01 | 0.75 |
| beta-Cadinene | 1.42 | 1.72 | 1.97 | 1.68 | 1.28 | ND | 1.87 | 1.14 | ND | ND | 1.64 |
| delta-Cadinene | ND | ND | ND | ND | ND | 0.55 | ND | ND | ND | ND | 0.59 |
| alpha-Copaene | ND | ND | ND | ND | ND | ND | 24.09 | 17.41 | 0.26 | 0.83 | 23.29 |
| alpha-Humulene | 11.89 | 10.84 | 9.20 | 10.37 | 9.29 | ND | ND | ND | 16.46 | 10.50 | 0.41 |
| beta-Selinene | 12.79 | ND | 10.40 | 7.11 | 8.61 | ND | ND | 1.21 | ND | 9.08 | 1.19 |
| Valencene | ND | ND | ND | ND | ND | ND | ND | ND | 2.32 | 2.91 | 1.97 |
| alpha-Lonipinene | ND | ND | ND | ND | ND | ND | 1.24 | 0.18 | ND | ND | 0.44 |
| (−)-ISOLEDENE | ND | ND | ND | ND | ND | ND | 0.13 | ND | 0.06 | 0.10 | ND |
| **Total Sesqui-terpenoids (%)** | **45.01** | **30.48** | **38.65** | **35.78** | **35.20** | **8.46** | **34.64** | **22.83** | **59.14** | **48.22** | **37.01** |

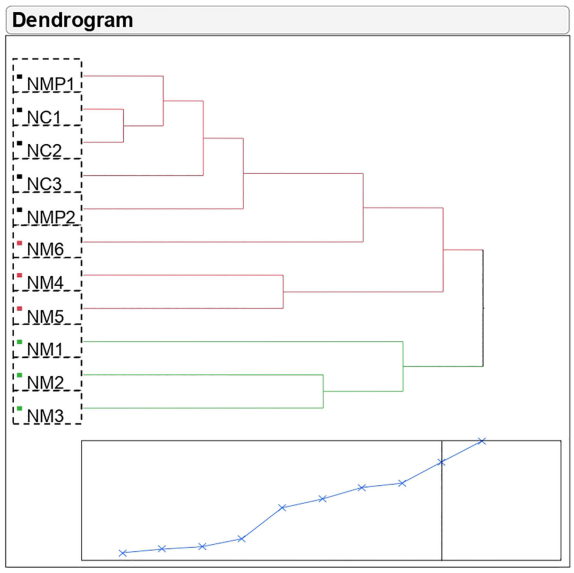


FIGURE 1
Cluster analysis of Nekkare mother plants ($NMP_1$ and $NMP_2$), control sample ($NC_1$, $NC_2$, and $NC_3$), and selected putative mutant samples ($NM_1$, $NM_2$, $NM_3$, $NM_4$, $NM_5$, and $NM_6$).

85.29% of the total variability in VC. The first two principal components that collectively explained 59.60% of the total variability was depicted as two-dimensional biplot (Figure 2). Out of these, 35.9% of total variation was explained by the first principal component, which had an eigenvalue of 10.78. A total of 17 volatile compounds (with loading of >0.5) significantly contributed to the variation in this principal component. Among these, 11 volatile compounds showed positive loadings wherein highest positive loading (>0.8) was exhibited by monoterpenes, *viz.*, beta-Ocimene, gamma terpinene, and alpha-Terpinolene. The second principal component with an eigenvalue of 7.11 explained 23.71% of total variation. Sesquiterpenes like Germacrene, Aromadendrene, trans-Caryophyllene, and alpha-Guaiene with positive loading of >0.9 contributed largely to the variation of this principal component.

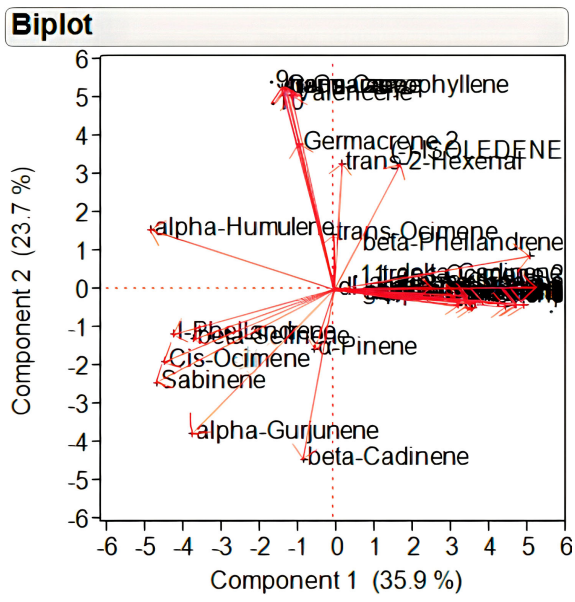


FIGURE 2
Two-dimensional principal component analysis biplot of individual volatile compounds in Nekkare mother plants ($NMP_1$ and $NMP_2$), control sample ($NC_1$, $NC_2$, and $NC_3$), and selected putative mutant samples ($NM_1$, $NM_2$, $NM_3$, $NM_4$, $NM_5$, and $NM_6$).

## 3.4 Characterisation of putative mutant progenies using SSR markers

### 3.4.1 Genetic diversity parameters on population level

The level of genetic divergence in the putative mutant population was determined using 12 SSR markers, out of which eight showed polymorphism and were thus used for further analysis. The analysis of molecular variance (AMOVA) showed that most of the variance in the sample was attributable to the variation within individuals being 58% (Table 2).

Genetic diversity parameters of eight loci for each population are presented in Table 3. In the treated population, for different loci, the mean value for number of alleles (Na) was 7 ranging from 4 to 12 (Table 3) where the highest number of alleles (12) was recorded for locus MiMRD80. The total number of alleles for the control population was less than that of treated population ranging from 3 for locus MiKVR71 to 12 for locus MiMRD80 with a mean of 6.25. Mean number of effective alleles (Ne) was found to be 3.77 and 3.61 for treated and control populations, respectively. The mean Shannon's Information Index (I), an important measure of genetic diversity, was maximum (1.50) for the treated population followed by control (1.42). In the treated population, out of eight loci, for five loci, *viz.*, MiIIHR99, MiKVR98, MiMRD88, MiIIHR78, and 21478, Ho was found to be lower than He, while for other three loci, Ho was found to be higher than He. Contrarily, in the control population for all the loci, Ho was lower than He, except locus MiKVR71 where Ho (0.95) was higher than He (0.596). However, irrespective of the samples, Ho was lower than He, and mean Ho was recorded to be 0.48 and 0.46, while mean He was 0.72 and 0.68 for treated and control plants, respectively. In the treated population, negative fixation index was recorded for three loci, and contrastingly, in the control population, negative fixation index was recorded only for one locus, *viz.*, MiKVR71 (−0.593) (Table 3). Phylogenetic analysis resulted in the separation of studied samples into two main clusters, *viz.*, I and II (Figure 3). Cluster I comprised of only one putative mutant, while cluster II separated into various sub-clusters forming specific groups. A clear separation between clustering of putative mutants and control plants was observed (Figure 3), suggesting that mutation could bring about changes in the treated population.

TABLE 2 Summary AMOVA table.

| Source | Df | SS | MS | Est. Var. | % |
|---|---|---|---|---|---|
| **Among Population** | 1 | 8.741 | 8.741 | 0.097 | 3% |
| **Among Individuals** | 46 | 193.957 | 4.216 | 1.202 | 39% |
| **Within Individuals** | 48 | 87.000 | 1.813 | 1.813 | 58% |
| **Total** | 95 | 289.698 | | 3.111 | 100% |

# 4 Discussion

## 4.1 Volatile profiling

Volatile organic compounds including aldehydes, ketones, esters, and terpenes conferring aroma are among the major determinant of fruit quality. Terpene hydrocarbons including terpinolene, 3-carene, caryophyllene, and α-Pinene are reported to be the major volatiles (depending upon the cultivars) in the pulp of mango fruit (Li et al., 2017). The analysis of volatile compounds in the leaves of polyembryonic mango genotype Nekkare showed the differences between gamma irradiation-derived and untreated plants. Mango volatile profile has been reported to be contributed by volatile compounds like monoterpenes, sesquiterpenes, alcohols, lactones, aldehydes, esters, ketones, fatty acids, and carotenoid compounds (Pandit et al., 2009; Li et al., 2017). In this study, monoterpenes and sesquiterpenes were found to be the main volatile compounds present in the studied samples. However, significant differences were observed in the compositions and proportions of terpenes in the studied samples. On the basis of abundance of different terpenes, Andrade et al. (2000) classified mango genotypes into terpinolene, 3-carene, and myrcene genotypes. In the selected putative mutant samples, the number of monoterpenes was more ranging from 5 (in $NM_5$ and $NM_6$) to 7 (in $NM_1$ and $NM_2$) as compared to mother plants and control seedlings where it ranged from 3 (in $NMP_1$) to 5 (in $NC_1$). Earlier studies have also confirmed terpenes as the most abundant volatile constituent of mango (Pino et al., 2005; Li et al., 2017). The number of sesquiterpenes detected in the selected putative mutants was more ranging from 6 (in $NM_1$, $NM_2$ and $NM_3$) to 10 ($NM_5$) in comparison to mother plants and control samples where it ranged from 3 ($NMP_2$) to 4 ($NMP_1$, $NC_1$, $NC_2$, and $NC_3$). Among the sesquiterpenes, only alpha-Gurjunene was found to be present in all the samples under study including mother plants, control samples, and selected putative mutants. However, the amount detected in mother plants and control samples was more than in the putative mutants. In a study, all the sesquiterpene-dominated mango cultivars were found to be of Indian origin (Pandit et al., 2009). Oliveira et al. (2010) reported differences in volatile composition of white and dark varieties of fig and found sesquiterpenes, Germacrene D, beta-caryophyllene, and s-elemene to be the main volatile compounds in the leaves of the studied fig cultivars. Furthermore, in the present study, aldehyde (trans-2-Hexenal) was found to be present only in putative mutant samples $NM_1$, $NM_4$, and $NM_6$ among all the studied samples. Although present in lower concentrations, aldehydes and alcohols contribute significantly towards flavour and aroma to mangoes (Pino et al., 2005). A very little concentration of aldehyde was detected in two of 25 cultivars studied being 0.38% in Chinese cultivar Renong No.1 and 0.01% in Indonesian cultivar Gleck (Li et al. 2017). Aldehydes

TABLE 3 Number of alleles (Na), number of effective alleles (Ne), Shannon's Information Index (I), observed heterozygosity (Ho), expected heterozygosity (He), and fixation index (F) for different loci in treated (35Gy gamma irradiation) and control (untreated) seedlings of polyembryonic mango genotype Nekkare (n=20).

| Population | | 8095 | MiIlHR78 | MiKVR71 | MiMRD80 | MiKVR99 | MiKVR98 | MiMRD88 | 21478 | Mean |
|---|---|---|---|---|---|---|---|---|---|---|
| **Treated** | **Na** | 4 | 7 | 4 | 12 | 7 | 6 | 6 | 10 | 7.00 |
| | **Ne** | 3.941 | 2.061 | 2.834 | 3.547 | 4.614 | 4.364 | 4.226 | 4.579 | 3.77 |
| | **I** | 1.379 | 1.105 | 1.153 | 1.667 | 1.684 | 1.583 | 1.577 | 1.861 | 1.50 |
| | **Ho** | 0.815 | 0.077 | 0.962 | 0.852 | 0.5 | 0.083 | 0.5 | 0.08 | 0.48 |
| | **He** | 0.746 | 0.515 | 0.647 | 0.718 | 0.783 | 0.771 | 0.763 | 0.782 | 0.72 |
| | **F** | -0.092 | 0.851 | -0.486 | -0.186 | 0.362 | 0.892 | 0.345 | 0.898 | 0.32 |
| **Control** | **Na** | 4 | 6 | 3 | 12 | 5 | 6 | 6 | 8 | 6.25 |
| | **Ne** | 2.711 | 1.77 | 2.477 | 5.674 | 3.88 | 4.73 | 4.762 | 2.893 | 3.61 |
| | **I** | 1.101 | 0.934 | 0.988 | 2.079 | 1.452 | 1.652 | 1.656 | 1.489 | 1.42 |
| | **Ho** | 0.278 | 0.158 | 0.95 | 0.6 | 0.611 | 0.167 | 0.6 | 0.333 | 0.46 |
| | **He** | 0.631 | 0.435 | 0.596 | 0.824 | 0.742 | 0.789 | 0.79 | 0.654 | 0.68 |
| | **F** | 0.56 | 0.637 | –0.593 | 0.272 | 0.177 | 0.789 | 0.241 | 0.491 | 0.32 |

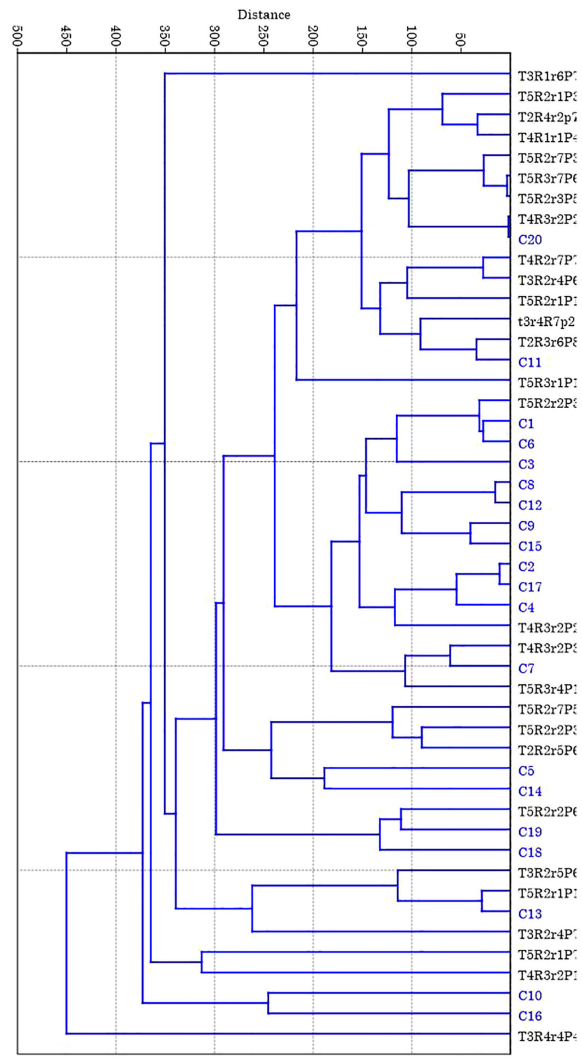


FIGURE 3
Dendogram of 20 putative mutants (35 Gy gamma irradiation) and 20 control seedlings of polyembryonic mango genotype Nekkare cultivars based on SSR data. The phylogenetic tree obtained from unweighted pair-group method with arithmetic mean (UPGMA) clustering option of the PAST 4.0 software.

break down to alcohols and lactones, which further contribute to fruit aroma. In this study, no lactones were detected, but alcohol (1-Hexyn-3-ol) was present in the putative mutant sample $NM_2$.

## 4.1 Characterisation of putative mutant progenies using SSR markers

High level of morphological and stomatal diversity was observed in the irradiated population of polyembryonic mango genotype Nekkare (Perveen et al., 2022). Genetic divergence in the putative mutant population was estimated by using 12 SSR markers. Out of the 12 markers, eight showed polymorphism and were thus used for further analysis. The mean total number of alleles for the treated population was found to be more than that of control population. The high allelic richness observed suggests that mutation treatment could bring about variability in the treated population. An increase in the mean number of alleles with increase in dosage of irradiation has previously been reported (Taheri et al., 2016). The mean Shannon's Information Index (I), an important measure of genetic diversity, was also recorded and was highest for treated population as compared to control. The higher value of I reflects the effectiveness of SSR markers used to identify the variation created by irradiation treatment. Several reports of utilisation of molecular markers for the detection of genetic diversity in mutant population are available in different fruit crops like citrus (Sülü et al., 2020), grapes (Dev et al., 2021), olive (Tekin et al., 2022), and pomegranate (Perveen et al., 2023b). SSR markers have been widely preferred for germplasm characterisation and phylogenetic studies in mango (Azam et al., 2018; Azam et al., 2019; Arogundade et al., 2022). Hitherto, reports on molecular characterisation of mutant population of mango are very few, and results of this study showed the effectiveness of SSR markers for determining the variability in putative mutant population of Nekkare. However, further research using more number of polymorphic SSR markers is paramount to validate the findings of the present study before using these results in devising mango rootstock breeding programme. The selected putative mutants are being maintained and will be evaluated in ensuing studies.

# 5 Conclusion

The studied samples of polyembryonic mango genotype Nekkare, including mother plants, control, and selected putative mutants differed in total concentration and compositions of major volatile compounds, allowing us to distinguish between gamma radiation-treated and untreated plants. Monoterpenes and sesquiterpene hydrocarbons were found to be the major volatile compounds of these samples, wherein untreated samples (control and mother plants) were found to be rich in monoterpenes, while an abundance of sesquiterpenes was detected in the putative mutants. Mother plants and control seedlings grouped together, suggesting the similarity between them while the genetically distant putative mutants grouped apart from the mother plants and control seedlings; this could be the result of mutation. High allelic richness and mean Shannon's Information Index observed in the putative mutant population suggest that mutation created variability in the treated population. Hence, volatile profiling and molecular characterisation using SSR markers could be an effective tool to detect variation in mutated population, and the former can be used to validate putative mutants in polyembryonic mango genotypes where the seedlings are similar to mother plants due to their origin from nucellar region.

# Data availability statement

The original contributions presented in the study are included in the article/Supplementary Material. Further inquiries can be directed to the corresponding authors.

## Author contributions

NP, MD, MS, KS, and KR designed the research. NP performed the experimental work under the supervision of KS and KR. RV and HM provided the required software and conducted the statistical analysis. NP wrote the manuscript. NP, MD and HM reviewed and edited the manuscript. All authors contributed to the article and approved the submitted version.

## Funding

The Department of Science & Technology, Ministry of Science & Technology, Government of India is gratefully acknowledged by the authors for its financial assistance, Grant number DST/INSPIRE Fellowship/2017/IF170480 provided to NP. Furthermore, the financial and technical support provided by ICAR-Indian Institute of Horticultural Research, Bengaluru, India is highly acknowledged.

## Conflict of interest

The authors declare that the research was conducted in the absence of any commercial or financial relationships that could be construed as a potential conflict of interest.

## Publisher's note

All claims expressed in this article are solely those of the authors and do not necessarily represent those of their affiliated organizations, or those of the publisher, the editors and the reviewers. Any product that may be evaluated in this article, or claim that may be made by its manufacturer, is not guaranteed or endorsed by the publisher.

## Supplementary material

The Supplementary Material for this article can be found online at: https://www.frontiersin.org/articles/10.3389/fpls.2023.1168947/full#supplementary-material

## References

Ali, S., Plotto, A., Scully, B. T., Wood, D., Stover, E., Owens, N., et al. (2020). Fatty acid and volatile organic compound profiling of avocado germplasm grown under East-Central Florida conditions. *Sci. Hortic.* 261, 109008. doi: 10.1016/j.scienta.2019.109008

Andrade, E. H. A., Maia, J. G. S., and Maria das Graças, B. Z. (2000). Aroma volatile constituents of Brazilian varieties of mango fruit. *J. Food Compos. Anal.* 13 (1), 27–33. doi: 10.1006/jfca.1999.0841

Arogundade, O., Matthew, J. O., Akinyoola, O. I., Akin-Idowu, P. E., and Akinyemi, S. O. S. (2022). Phenotypic and molecular characterization of mango cultivars in Southwest Nigeria. *Int. J. Fruit Sci.* 22 (1), 151–159. doi: 10.1080/15538362.2021.2019652

Asker, S., and Jerling, L. (1992). Apomixis in plants. Boca Raton. *Ann. Arbor London Tokyo* 1, 285.

Atay, N. A., Atay, E., Kunter, B., Kantoglu, Y. K., and Kaplan, N. (2019). Determination of optimal mutagen dosage and its effects on morpho-agronomic traits in putative mutants of 'Amasya'apple. *Genetika* 51 (2), 629–639. doi: 10.2298/GENSR1902629A

Augustyn, W. A., Botha, B. M., Combrinck, S., and Du Plooy, W. (2010). Correlation of volatile profiles of twenty mango cultivars with their susceptibilities to mango gall fly infestation. *S. Afr. J. Bot.* 76 (4), 710–716. doi: 10.1016/j.sajb.2010.07.005

Azam, K., Mir, H., Prasad, B. D., and Ahmad, F. (2018). Identification of microsatellite markers associated with the horticultural traits in elite mango cultivars. *J. Pharmacogn. Phytochem.* 7 (2), 2830–2834.

Azam, K., Mir, H., Prasad, B. D., Ahmed, F., Kumari, A., and Sinha, A. (2019). Microsatellite marker based characterization of mango cultivars. *Indian J. Hortic.* 76 (4), 561–565. doi: 10.5958/0974-0112.2019.00091.4

Damasco, O. P., Cueva, F. M. D., Descalsota, J. C., and Tayobong, R. R. P. (2019). Gamma radiation and in *vitro* induced Banana Bunchy Top Virus (BBTV) resistant mutant lines of Banana cv 'Lakatan' (Musa sp., AA). *Philipp J. Sci.* 149 (S1), 159–173.

Dev, R., Singh, S. K., Singh, R., Singh, A. K., Patel, V. B., Alizadeh, M., et al. (2021). Assessment of genetic diversity of grape mutants based on RAPD and SSR markers. *Indian J. Hortic.* 78 (1), 17–24. doi: 10.5958/0974-0112.2021.00003.7

Due, M. S., Susilowati, A., and Yunus, A. (2019). The effect of gamma ray's irradiation on diversity of *Musa paradisiaca* var. sapientum as revealed by ISSR molecular marker. *Biodiversitas J. Biol. Diversity* 20 (5), 1416–1422. doi: 10.13057/biodiv/d200534

Fernandes, F., Guedes de Pinho, P., Valentão, P., Pereira, J. A., and Andrade, P. B. (2009). Volatile constituents throughout *Brassica oleracea* L. var. acephala germination. *J. Agric. Food Chem.* 57, 6795–6802. doi: 10.1021/jf901532m

Hammer, Ø., Harper, D. A. T., and Ryan, P. D. (2001). PAST: paleontological statistics software package for education and data analysis. *Palaeontol. Electron.* 4, 9.

Kalinowski, S. T., Taper, M. L., and Marshall, T. C. (2007). Revising how the computer program CERVUS accommodates genotyping error increases success in paternity assignment. *Mol. Ecol.* 16, 1099–1106. doi: 10.1111/j.1365-294X.2007.03089.x

Karsinah,, Indriyani, N. L. P., and Sukartini, (2012). The effect of gamma irradiation on the growth of mango grafted material. *ARPN J. Agric. Biol. Sci.* 7 (10), 840–844. doi: Chttp://www.arpnjournals.com/jabs/rese

Kumar, M. K., Dinesh, M. R., Srivastav, M., Singh, S. K., and Singh, A. K. (2018). Mutagenic sensitivity of scions and seed kernels of polyembryonic mango cultivars Peach and Bappakai to gamma irradiation. *Int. J. Chem. Stud.* 6 (3), 3335–3339.

Li, L., Ma, X. W., Zhan, R. L., Wu, H. X., Yao, Q. S., Xu, W. T., et al. (2017). Profiling of volatile fragrant components in a mini-core collection of mango germplasms from seven countries. *PloS One* 12 (12), e0187487. doi: 10.1371/journal.pone.0187487

Morita, R., Kusaba, M., Iida, S., Yamaguchi, H., Nishio, T., and Nishimura, M. (2009). Molecular characterization of mutations induced by gamma irradiation in rice. *Genes Genetic Syst.*, 84 (5), 361–370. doi: 10.1266/ggs.84.361

Oliveira, A. P., Silva, L. R., de Pinho, P. G., Gil-Izquierdo, A., Valentão, P., Silva, B. M., et al. (2010). Volatile profiling of Ficus carica varieties by HS-SPME and GC–IT-MS. *Food Chem.* 123 (2), 548–557. doi: 10.1016/j.foodchem.2010.04.064

Pandit, S. S., Chidley, H. G., Kulkarni, R. S., Pujari, K. H., Giri, A. P., and Gupta, V. S. (2009). Cultivar relationships in mango based on fruit volatile profiles. *Food Chem.* 114 (1), 363–372. doi: 10.1016/j.foodchem.2008.09.107

Peakall, R., and Smouse, P. E. (2006). GenAlEx 6: genetic analysis in Excel. Population genetic software for teaching and research. *Mol. Ecol. Notes* 6, 288–295. doi: 10.1111/j.1471-8286.2005.01155.x

Peakall, R., and Smouse, P. E. (2012). GenAlEx 6.5: genetic analysis in Excel. Population genetic software for teaching and research—an update. *Bioinformatics* 28 (19), 2537–2539. doi: 10.1093/bioinformatics/bts460

Perveen, N., Cholin, S. S., Hipparagi, K., Prabhuling, G., Murthy, B. N. S., and Peerjade, D. (2023b). Molecular diversity assessment among the pomegranate genotypes belonging to diverse genetic background using microsatellite markers. *Acta Physiol. Plant* 45 (7), 92. doi: 10.1007/s11738-023-03568-x

Perveen, N., Dinesh, M. R., Sankaran, M., Shivashankara, K. S., and Venugopalan, R. (2022). Characterization and evaluation of putative mutant populations of polyembryonic mango genotype Nekkare for dwarfing rootstock traits. *J. Hortic. Sci.* 17 (2), 261–271. doi: 10.24154/jhs.v17i2.1456

Perveen, N., Dinesh, M. R., Sankaran, M., and Venugopalan, R. (2023a). Mutagenic-sensitivity and variability in the putative mutants of polyembryonic mango genotypes. *Indian J. Hort* 80 (1), 3–9. doi: 10.58993/ijh/2023.80.1.1

Pino, J. A., Mesa, J., Muñoz, Y., Martí, M. P., and Marbot, R. (2005). Volatile components from mango (*Mangifera indica* L.) cultivars. *J. Agric. Food Chem.* 53 (6), 2213–2223. doi: 10.1021/jf0402633

Ravishankar, K. V., Anand, L., and Dinesh, M. R. (2000). Assessment of genetic relatedness among mango cultivars of India using RAPD markers. *J. Horti. Sci. Bio.* 75, 198–201. doi: 10.1080/14620316.2000.11511223

Ravishankar, K. V., Dinesh, M. R., Nischita, P., and Sandya, B. S. (2015). Development and characterization of microsatellite markers in mango (*Mangifera indica*) using next-generation sequencing technology and their transferability across species. *Mol. Breed.* 35, 1–13. doi: 10.1007/s11032-015-0289-2

Rencher, A. C. (1995). *Methods of Multivariate Analysis* (New York: Wiley).

Rime, J., Dinesh, M. R., Sankaran, M., Shivashankara, K. S., Rekha, A., and Ravishankar, K. V. (2019). Evaluation and characterization of EMS derived mutant populations in mango. *Sci. Hortic.* 254, 55–60. doi: 10.1016/j.scienta.2019.04.015

Roberts, G., and Spadafora, N. D. (2020). Analysis of apple flavours: The use of volatile organic compounds to address cultivar differences and the correlation between consumer appreciation and aroma Profiling. *J. Food Qual.* 2020, 8497259. doi: 10.1155/2020/8497259

Rossetto, C. J., Ribeiro, I. J. A., Gallo, P. B., Soares, N. B., Sabino, J. C., Martins, A. L. M., et al. (1997). Mango breeding for resistance to diseases and pests. *Acta Hortic. (ISHS)* 455, 299–304. doi: 10.17660/ActaHortic.1997.455.39

Schuelke, M. (2000). An economic method for the fluorescent labelling of PCR fragments. *Nat. Biotechnol.* 18, 233–234. doi: 10.1038/72708

Srivastava, K. C., Rajput, M. S., Singh, N. P., and Lal, B. (1988). Rootstock studies in mango cv. Dashehari. *Acta Hortic.* 231, 216–219.

Sülü, G., Kacar, Y.I.L.D.I.Z., Polat, I., KİTAPCI, A., Turgutoğlu, E., Şimşek, Ö.Z.H.A.N., et al. (2020). Identification of genetic diversity among mutant lemon and mandarin varieties usingdifferent molecular markers. *Turk. J. Agric. For.* 44 (5), 465–478. doi: 10.3906/tar-1909-67

Taheri, S., Abdullah, T. L., Ahmad, Z., Sahebi, M., and Azizi, P. (2016). Phenotypic and molecular effects of chronic gamma irradiation on *Curcuma alismatifolia*. *Eur. J. Hortic. Sci.* 81, 137–147. doi: 10.17660/eJHS.2016/81.3.1

Tekin, A., Dumlupinar, Z., and Bardak, A. (2022). Molecular characterization of mutant lines of Ayvalik olive cultivar obtained by chemical mutation. *Genetika* 54 (2), 717–728. doi: 10.2298/GENSR2202717T

Vasugi, C., Dinesh, M. R., Sekar, K., Shivashankara, K. S., Padmakar, B., and Ravishankar, K. V. (2012). Genetic diversity in unique indigenous mango accessions (Appemidi) of the Western Ghats for certain fruit characteristics. *Curr. Sci.* 103 (2), 199–207. doi: https://www.jstor.org/stable/24085000

Yasmeen, S., Khan, M. T., and Khan, I. A. (2020). Revisiting the physical mutagenesis for sugarcane improvement: a stomatal prospective. *Sci. Rep.* 10 (1), 1–14. doi: 10.1038/s41598-020-73087-z

# Frontiers in
# Plant Science

**Cultivates the science of plant biology and its applications**

The most cited plant science journal, which advances our understanding of plant biology for sustainable food security, functional ecosystems and human health.

---

## Discover the latest Research Topics

See more →

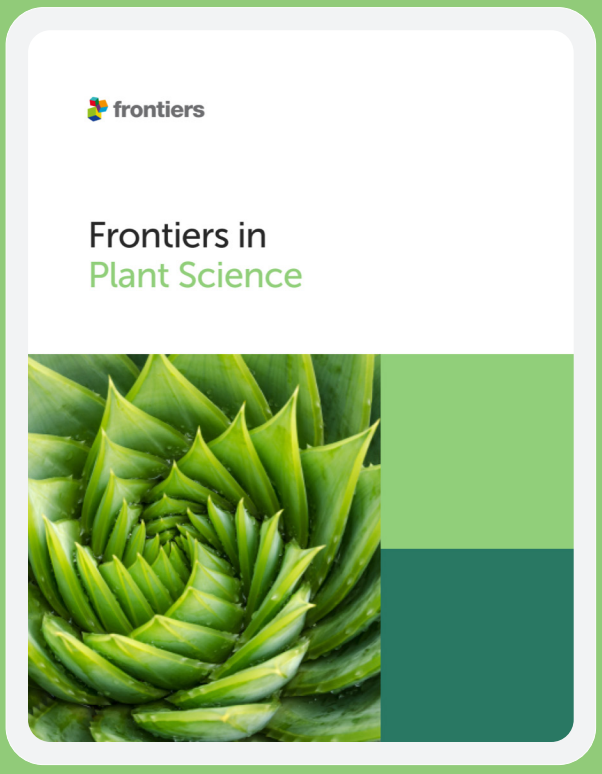


**Frontiers**

Avenue du Tribunal-Fédéral 34
1005 Lausanne, Switzerland
frontiersin.org

**Contact us**

+41 (0)21 510 17 00
frontiersin.org/about/contact